NEURODEGENERATION EDITORS' PICK 2021

EDITED BY: Wendy Noble, Mark P. Burns and Einar M. Sigurdsson
PUBLISHED IN: Frontiers in Neuroscience

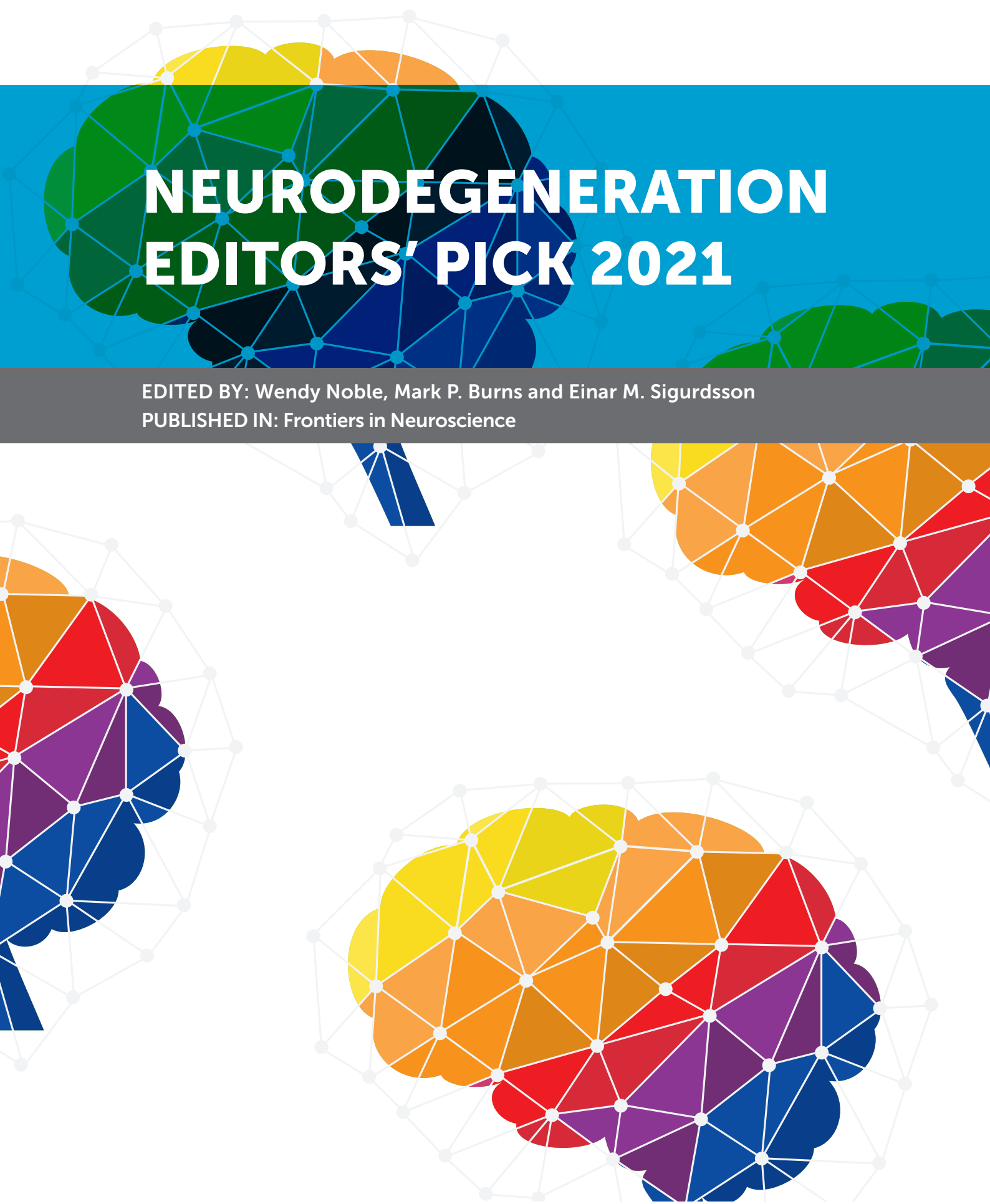

frontiers Research Topics

ISSN 1664-8714
ISBN 978-2-88971-108-6
DOI 10.3389/978-2-88971-108-6

About Frontiers

Frontiers is more than just an open-access publisher of scholarly articles: it is a pioneering approach to the world of academia, radically improving the way scholarly research is managed. The grand vision of Frontiers is a world where all people have an equal opportunity to seek, share and generate knowledge. Frontiers provides immediate and permanent online open access to all its publications, but this alone is not enough to realize our grand goals.

Frontiers Journal Series

The Frontiers Journal Series is a multi-tier and interdisciplinary set of open-access, online journals, promising a paradigm shift from the current review, selection and dissemination processes in academic publishing. All Frontiers journals are driven by researchers for researchers; therefore, they constitute a service to the scholarly community. At the same time, the Frontiers Journal Series operates on a revolutionary invention, the tiered publishing system, initially addressing specific communities of scholars, and gradually climbing up to broader public understanding, thus serving the interests of the lay society, too.

Dedication to Quality

Each Frontiers article is a landmark of the highest quality, thanks to genuinely collaborative interactions between authors and review editors, who include some of the world's best academicians. Research must be certified by peers before entering a stream of knowledge that may eventually reach the public - and shape society; therefore, Frontiers only applies the most rigorous and unbiased reviews.
Frontiers revolutionizes research publishing by freely delivering the most outstanding research, evaluated with no bias from both the academic and social point of view. By applying the most advanced information technologies, Frontiers is catapulting scholarly publishing into a new generation.

What are Frontiers Research Topics?

Frontiers Research Topics are very popular trademarks of the Frontiers Journals Series: they are collections of at least ten articles, all centered on a particular subject. With their unique mix of varied contributions from Original Research to Review Articles, Frontiers Research Topics unify the most influential researchers, the latest key findings and historical advances in a hot research area! Find out more on how to host your own Frontiers Research Topic or contribute to one as an author by contacting the Frontiers Editorial Office: frontiersin.org/about/contact

NEURODEGENERATION EDITORS' PICK 2021

Topic Editors:
Wendy Noble, King's College London, United Kingdom
Mark P. Burns, Georgetown University, United States
Einar M. Sigurdsson, New York University, United States

Citation: Noble, W., Burns, M. P., Sigurdsson, E. M., eds. (2021). Neurodegeneration Editors' Pick 2021. Lausanne: Frontiers Media SA. doi: 10.3389/978-2-88971-108-6

Table of Contents

frontiers in Neuroscience

ORIGINAL RESEARCH
published: 16 April 2019
doi: 10.3389/fnins.2019.00319

Exosomes Derived From Pericytes Improve Microcirculation and Protect Blood–Spinal Cord Barrier After Spinal Cord Injury in Mice

Xiaochen Yuan[1†], Qingbin Wu[1†], Peng Wang[2†], Yingli Jing[3], Haijiang Yao[4], Yinshan Tang[5], Zhigang Li[6*], Honggang Zhang[1*] and Ruijuan Xiu[1]*

[1] Key Laboratory of Microcirculation, Ministry of Health, Institute of Microcirculation, Chinese Academy of Medical Sciences & Peking Union Medical College, Beijing, China, [2] Orthopedics Department, Hebei Provincial Hospital of Traditional Chinese Medicine, Shijiazhuang, China, [3] China Rehabilitation Science Institute, China Rehabilitation Research Center, Center of Neural Injury and Repair, Beijing Institute for Brain Disorders, Beijing Key Laboratory of Neural Injury and Rehabilitation, Beijing, China, [4] Treatment Center of TCM, Beijing Bo'ai Hospital, China Rehabilitation Research Center, School of Rehabilitation, Capital Medical University, Beijing, China, [5] Department of Rehabilitation in Traditional Chinese Medicine, The Second Affiliated Hospital, Zhejiang University School of Medicine, Hangzhou, China, [6] School of Acupuncture, Moxibustion and Tuina, Beijing University of Chinese Medicine, Beijing, China

Spinal cord injury (SCI) often leads to severe and permanent paralysis and places a heavy burden on individuals, families, and society. Until now, the therapy of SCI is still a big challenge for the researchers. Transplantation of mesenchymal stem cells (MSCs) is a hot spot for the treatment of SCI, but many problems and risks have not been resolved. Some studies have reported that the therapeutic effect of MSCs on SCI is related to the paracrine secretion of cells. The exosomes secreted by MSCs have therapeutic potential for many diseases. There are abundant pericytes which possess the characteristics of stem cells in the neurovascular unit. Due to the close relationship between pericytes and endothelial cells, the exosomes of pericytes can be taken up by endothelial cells more easily. There are fewer studies about the therapeutic potential of the exosomes derived from pericytes on SCI now. In this study, exosomes of pericytes were transplanted into the mice with SCI to study the restoration of motor function and explore the underlying mechanism. We found that the exosomes derived from pericytes could reduce pathological changes, improve the motor function, the blood flow and oxygen deficiency after SCI. In addition, the exosomes could improve the endothelial ability to regulate blood flow, protect the blood-spinal cord barrier, reduce edema, decrease the expression of HIF-1α, Bax, Aquaporin-4, and MMP2, increase the expression of Claudin-5, bcl-2 and inhibit apoptosis. The experiments *in vitro* proved that exosomes derived from pericytes could protect the barrier of spinal cord microvascular endothelial cells under hypoxia condition, which was related to PTEN/AKT pathway. In summary, our study showed that exosomes of pericytes had therapeutic prospects for SCI.

Keywords: pericytes, exosomes, spinal cord injury, microcirculation, microvascular

OPEN ACCESS

Edited by:
Federico Benetti, Scuola Internazionale Superiore di Studi Avanzati (SISSA), Italy

Reviewed by:
Ye Xiong, Henry Ford Health System, United States
Varun Kesherwani, University of Nebraska Medical Center, United States

***Correspondence:**
Qingbin Wu
wuqingbin@imc.pumc.edu.cn; 519706@163.com
Zhigang Li
lizhigang620620@163.com
Honggang Zhang
zhanghg1966126@163.com

† These authors have contributed equally to this work

Specialty section:
This article was submitted to Neurodegeneration, a section of the journal Frontiers in Neuroscience

Received: *29 January 2019*
Accepted: *20 March 2019*
Published: *16 April 2019*

Citation:
Yuan X, Wu Q, Wang P, Jing Y, Yao H, Tang Y, Li Z, Zhang H and Xiu R (2019) Exosomes Derived From Pericytes Improve Microcirculation and Protect Blood–Spinal Cord Barrier After Spinal Cord Injury in Mice. Front. Neurosci. 13:319. doi: 10.3389/fnins.2019.00319

INTRODUCTION

Spinal cord injury (SCI) refers to the most common and destructive injuries in spinal surgery which affects about 180,000 patients all over the world every year (Chopp et al., 2000). SCI often leads to severe and permanent paralysis, accompanied by a significant decline in the quality of life, placing a heavy burden on individuals and their families. SCI is characterized by rapid triggering of secondary damage after primary mechanical damage. Ischemia, hypoxia, inflammatory reactions, apoptosis of neurons, and oligodendrocytes appear in the damage area. Over time, astrocyte scarring and spinal cord voids form which inhibit nerve axon regeneration and result in the motor and sensory dysfunction below the damage plane (Schwab and Bartholdi, 1996). At present, SCI treatment is still the biggest challenge for researchers (Carlson and Gorden, 2002).

With the development of stem cell technology, stem cell transplantation has become a hot topic for the treatment of SCI. MSCs possess the multipotency and can be induced into many kinds of cells, such as osteoblasts (bone cells), chondrocytes (cartilage cells), myocytes (muscle cells), and adipocytes (Ho et al., 2008). Some studies have proved that transplantation of MSCs after SCI may be a promising strategy to improve the functions of motor, sensory and/or autonomic nerves (Chopp et al., 2000; Feron et al., 2005; Cizkova et al., 2011; Mothe and Tator, 2012; Nakajima et al., 2012; Neirinckx et al., 2015). However, several studies have shown that the stem cells have lower survival rates in tissues and there are some risks such as cell de-differentiation, immune rejection and malignant tumor formation after transplantation (Balsam et al., 2004; Rubio et al., 2005; Jeong et al., 2011; Rodriguez et al., 2012). Recently, the increasing evidence has proved that the curative effects of MSCs are mostly due to paracrine mechanism, with exosomes taking a great part in this process (Katsuda et al., 2013; Ratajczak et al., 2014). Many kinds of cells can produce exosomes which are small membrane vesicles of internal origin about 30–120 nm in diameter (Stoorvogel et al., 2002). and contain functional mRNA and microRNA, as well as proteins (Record et al., 2011). Exosomes are important for cell communication and suitable to deliver small RNA and proteins (Mathivanan et al., 2010; Zomer et al., 2010). The specific surface ligands of the exosomes allow them to bind the target cells, transmit biological information and related genetic proteins to the target cells, and eventually regulate specific biological functions of cells (Breakefield et al., 2011; Chaput and Théry, 2011). Some studies have shown that exosomes and microvesicles of MSCs can be used for the treatment of liver, cardiovascular, and kidney injury (Gatti et al., 2011; Lai et al., 2011; Li et al., 2012). Studies have shown that the exosomes of MSCs have therapeutic effect on SCI in rats (Huang et al., 2017; Liu et al., 2018).

Pericytes (also known as Rouget cells) are contractile. They encircle the endothelial cells that line the capillaries and venules throughout the body (Simonavicius et al., 2012). They are also important ingredients of the neurovascular unit containing neurons, endothelial cells and astrocytes (Dore-Duffy and Cleary, 2011). Pericytes and endothelial cells establish a close link by multiple intercellular connection and sharing the same basement membrane. Pericytes participate in the control of pressure of microcirculation, integrity and permeability of microvascular, and take part in angiogenesis and differentiation regulation of endothelial cells by direct physical contact and paracrine signaling (Bergers and Song, 2005; Orekhov et al., 2014). Pericytes are heterogeneous, which express MSCs specific markers including CD44, CD73, CD90, CD105, and CD146, platelet-derived growth factor receptor-β (PDGFR-β), stromal precursor antigen-1 (STRO-1), neural glial antigen (NG2), and alpha smooth muscle actin (α-SMA). Due to the special relationship between pericytes and endothelial cells, endothelial cells are able to take up exosomes of pericytes which participate in the mediation of endothelial function. There are fewer studies about therapeutic potential of the exosomes derived from pericytes on SCI. In this study, pericytes exosomes were transplanted into the mice with SCI in order to study their functional recovery and explore the underlying mechanism.

MATERIALS AND METHODS

Experimental Animals

Male ICR mice (License No. SCXK2014-0004) of 8-week-old were bought from the Institute of Laboratory Animal Science, Chinese Academy of Medical Sciences (CAMS) & Peking Union Medical College (PUMC). The mice were bred at 26°C, 38.5% humidity, with a 12-hr light, 12-hr dark cycle (7:30 a.m–7:30 p.m light).

Animal Welfare

The protocols of animal experiments were approved by the Experimental Animal Care and Ethics Committee of the Institute of Microcirculation, CAMS & PUMC.

Experimental Design

In vivo

A total of 90 mice. 30 mice were randomly selected as sham group (Sham group) without SCI. 60 mice were randomly divided into two groups after successful building SCI model: a phosphate-buffered saline (PBS) treatment group (SCI group) and a pericytes exosomes treatment group (Exosomes group). Mice were subjected to SCI and then followed by tail vein injection of exosomes (20 μg of exosomes in 0.3 mL PBS or 0.3 mL PBS) starting an hour after contusion SCI was induced. After 48 h of surgery, 5 mice from each group were detected by Laser Doppler and then the spinal cord was taken out for WB assay. 20 mice in each of the three groups were arranged to immune- histochemistry (n = 5), assessment of microvascular permeability of spinal cord (n = 10), evaluation of spinal cord edema (n = 5). The remaining 5 mice in each group were performed a behavioral study on the 14th day after the injury.

In vitro

Isolation and culture of primary ICR mouse spinal cord microvascular endothelial cells (SCMECs). Cells were cultured under three conditions: Normal conditions, hypoxic conditions,

hypoxia + exosomes (20 μg/ml final concentration). The permeability of monolayer endothelial cells was detected by Transwell system (Corning, Union City, CA, United States). The cultured cells were collected for further experiments.

The experiment was conducted under double-blind condition to avoid potential biases of performance and detection.

Isolation of Micro-Vessels, Culture and Identification of Pericytes

Mice were anesthetized using pentobarbital sodium (100 mg/kg body weight). The brains of the ICR mice were removed and immersed in ice-cold isolation buffer, micro-vessels were isolated as previously reported (Yuan et al., 2018). After removal of the vessels. the gray matter of the brain was isolated and minced in ice-cold Dulbecco's modified Eagle's medium (DMEM), under a dissecting microscope. Then the tissues were digested in DMEM containing collagenase type II (1 mg/ml), DNase I (15 μg/ml) and gentamicin (50 μg/ml) at 37°C for 1.5 h and centrifugated in 20% bovine serum albumin (BSA)/DMEM (1000 × *g*, 20 min). Then they were further digested with collagenase/dispase (1 mg/ml; Roche, Switzerland) and DNaseI (6.7 μg/ml) in DMEM at 37°C for 1 h. The micro-vessel clusters were separated using 33% continuous Percoll (GE Healthcare, United Kingdom) gradient (1000 × *g*, 10 min), and washed twice in DMEM. The microvessel fragments were cultured in DMEM supplemented with 10% fetal bovine serum (FBS), 100 U/ml penicillin, and 100 μg/ml streptomycin. After microvessel adherence (48 h), fresh medium (DMEM supplemented with 10% FBS, 100 U/ml penicillin, and 100 μg/ml streptomycin) was replaced, floating dead cells and other impurities were removed, and then medium was replaced every 2 days. The pericytes were used for subsequent experiments when they reached 80–90% confluence. Pericytes were identified by surface markers desmin (1:250; ab15200; Abcam) and α-SMA (1:250; ab21027; Abcam). Immunocytochemistry with Von Willebrand Factor (vWF, 1:200; ab11713; Abcam) was carried out as previously described (Wu et al., 2015) to determine whether there was endothelial cell contamination.

Isolation of Micro-Vessels and Culture of SCMECs

Mice were anesthetized using pentobarbital sodium (100 mg/kg body weight). The spinal cord of the mice was removed from canalis vertebralis and placed in ice-cold isolation buffer. The micro-vessel fragments were isolated as above described and cultured in DMEM supplemented with 10% FBS, 100 U/ml penicillin, 100 μg/ml streptomycin and 4 μg/mL Puromycin. After 48 h, culture medium without purinomycin was replaced. Then the culture medium was changed every 2 days. The endothelial cells were used for subsequent experiments when they reached 80–90% confluence. The cells that did not express permeability glycoprotein (P-gp) should be killed by puromycin after treatment for 48 h while endothelial cells expressed P-gp, so endothelial cells with high purity could be obtained.

Pericytes Exosomes Generation and Collection

When pericytes reached 60–80% confluence, they were cultured in an exosomes depleted FBS-contained (EXO-FBS-250 A-1; System Biosciences, Mountain View, CA, United States) medium, for an additional 48 h. Then the medium weas gathered and exosomes were isolated by multi-step centrifugation, as previously reported (Xin et al., 2012; Villarroya-Beltri et al., 2013). Briefly, supernatants collected from cultured pericytes were centrifuged at 2000 *g* for 30 min to get rid of the large debris and dead cells, at 10,000 *g* for 30 min to remove the small-cell debris and then at 100,000 *g* for 70 min. At last, contaminating proteins was removed by centrifugation at 100,000 *g* for 70 min. Exosomes were saved at -80°C or utilized for another series of experiments. Exosomes protein content was examined using a bicinchoninic acid assay (BCA). Western blotting was used to examine the specific exosome surface markers which was encapsulated into exosomes including CD9 (1:1000; ab92726; Abcam) and CD81 (1:1000; ab109201; Abcam).

Transmission Electron Microscopy of Pericytes Exosomes

The morphology of pericytes exosomes was observed by transmission electron microscopy (TEM). Exosomes pellets were fixed in 2% paraformaldehyde (PFA) -cacodylate buffer and then they were loaded to copper grids covered with formvar for 20 min. Then exosomes were fixed in 1% (w/v) glutaraldehyde for 5 min. Grids were washed and contrasted in 4% uranyl acetate for 5 min, dried, and observed by TEM (FEI TECNAI G2,120 KV).

Size Distribution Analysis of Pericytes Exosomes

The suspensions with vesicles were analyzed by Nano-Sight LM10 instrument (Malvern, Worcestershire, United Kingdom). A monochromatic laser beam lightened the diluted samples at 405 nm to record a 60 s video taken with a mean frame rate of 25 frames/s. EVs samples were analyzed by the NTA software (version 3.0, Nano-Sight) to distinguish firstly and then followed up each particle on a frame-by-frame basis optimally, and Brownian movement of it was tracked and measured from frame to frame. The size of particle was determined with the two-dimensional Stokes-Einstein equation on basis of the velocity of particle movement. The mean, mode, and median EVs size from each video was used to calculate samples concentration expressed in nanoparticles/mL.

Building of SCI Models

Animals were anesthetized by inhalation of 1.5% isoflurane and performed laminectomy at thoracic vertebra level 10 (T10) on a calorstat heating pad at the prone position. Briefly, a laminectomy was carried out at the T10 level, and we clamped the spinous processes of T8 and T11 in order to stabilize the spine. 50-kd spinal contusion injury was made in mice with the Infinite Horizons Impactor (Precision Systems and Instrumentation, Lexington, KY, United States) (Allen, 1911; Yuan et al., 2017). Mice in the sham group were only performed laminectomy

without impact. Then the animals were put in a warming chamber at about 38.5°C until they woke up completely. The bladders of mice were manually emptied twice a day until the mice were able to recover autonomic bladder function during this period. After surgery, buprenorphine (0.05 mg/kg, ip) was administered at once and then every 6 h for 1 day to reduce pain.

Behavioral Study

Functional recovery after SCI was determined by the Basso Mouse Scale (BMS) scores (Basso et al., 2006). Mice were tested on postoperative days 1, 3, 5, 7, 10, and 14 for the duration of the experiments. Then the scores were recorded in an open-field environment by trained investigators under double-blind conditions.

Tissue Processing

After 48 h of injury, mice were anesthetized and perfused transcardially with 0.9% saline (containing 50 U/mL heparin), followed by 4% PFA in phosphate buffer. 10 mm spinal cord segments were taken with the injured site as the center and placed in the same fixative for 48 h at room temperature. The specimens were embedded into paraffin for production of 5-μm-thick transverse sections at the sites 500 μm rostral to the lesion epicenter. There were three sections used for each immunostaining per mice.

Immunohistochemistry

The sections were incubated in 0.3% hydrogen peroxide for 30 min and in 0.1% Triton X-100 for 20 min. Then they were incubated with anti-Aquaporin-4 (AQP4) antibody (1:100; ab9512; Abcam), with anti-MMP-2 antibody (1:200; ab86607; Abcam), or with anti-claudin-5 antibody (1:200; ab15106; Abcam) overnight at 4°C and washed with PBS, incubated with secondary antibody, at 37°C for 60 min. At last, the slices were washed with PBS and sealed with the coverslip.

Luxol Fast Blue (LFB) Staining

The slices were placed in a Luxol fast blue solution (Servicebio®, China), incubated overnight at 57°C, rinsed with 95% ethanol and distilled water for 3 min, respectively, differentiated in 0.05% lithium carbonate solution for 15 s, and placed in 70% ethanol to continue to differentiate for 30 s until the gray matter was clearly identifiable.

Nissl Staining

The sections were de-paraffinized in xylene 2 or 3 for 10 min each. Then they were hydrated in 100% alcohol for 2 × 5 min followed by 95% alcohol for 3 min, 70% alcohol for 3 min. Next, the sections were rinsed in tap water and then in distilled water. At last they were stained in 0.1% cresyl violet solution for 3–10 min, rinsed quickly in distilled water, differentiated in 95% ethyl alcohol for 2–30 min and checked microscopically for best result. The sections were dehydrated in 100% alcohol for 2 × 5 min, and cleared in xylene for 2 × 5 min and mounted with permanent mounting medium.

Terminal Deoxynucleotidyl Transferase-Mediated dUTP-Biotin Nick End Labeling (TUNEL) Staining

As for apoptosis detection on injury site, terminal deoxynucleotidyl transferase-mediated dUTP nick end labeling (TUNEL) staining was applied using the *in situ* Cell Death Detection Kit (Roche, Mannheim, Germany). The process was done according to manufacturer's instructions. The sections were dewaxed, rehydrated, and washed. Then the sections were pre-treated with proteinase-K for 30 min and incubated with TUNEL reaction mixture for 60 min at 37°C. The converter POD was added and incubated for 30 min at 37°C. The sections were washed with PBS and incubated with diaminobenzidine for 10 min. For quantitative analysis, the sum of the positively stained cells from five random visual fields of the anterior horn of the gray matter were calculated.

Laser Doppler Imaging (LDI) Measurement of Spinal Cord Blood Perfusion

Microvascular blood flow (MVBF) of spinal cord was examined using the Laser Doppler Line Scanner® (LDLS; Moor Instruments, Axminster, United Kingdom) at a stable temperature (24 ± 1°C) and 60% relative humidity. A line of 785 ± 10 nm laser light was used to scan over spinal cord of anesthetized mice. A scanning mirror along with optics on a 64-element linear array could direct the doppler shifted or non-shifted light from the moving blood cells or fixed tissue, respectively, and then establish a two-dimensional color-coded perfusion image. Data was computerized and recorded as image and numerical data (perfusion units, PU). For LDI analysis, three flux images were obtained through continuous scan. Thereafter, in moor LDI Image Review, version 5.3 (Moor Instruments Ltd.), the images were averaged to minimize any disturbance caused by movements (Rendell et al., 1999).

Detection of Vasomotion of Spinal Cord and Spectral Analysis of Laser Doppler Flowmetry (LDF) Signal

After survey of blood perfusion, we measured the vasomotion by dual channel Laser Doppler monitor (Moor – VMS – LDF2) instrument (Moor Instrument, Ltd., Axminster, United Kingdom) and a fiberoptic probe (Moor Instruments) with a calculated penetration depth of 2.5 mm. The electrode was placed within 1 mm to the detection site. After each run, the probes were replaced to shun additive effects and partial exhaustion of contractive and relaxative ability. A specific device containing colloidal latex particles was used to calibrate data before each test session. The normalized values were supplied by brownian motion of these particles The LDF signal was documented consecutively by the interfaced computer equipped Moor software for Windows version (Moor VMS – PC 2.0, Moor Instrument) as previously described (Rendell et al., 1999). Briefly, as for the analysis of LDF, a 5 min consecutive data were filtered by a built-in noise filter in the software to remove any

noise spikes and frequencies above 10 Hz, which were used for subsequent wavelet analysis. The wavelet analysis was performed by means of the Moor software. A three-dimensional (3D) plot was produced from the wavelet transformations of perfusion signals, which linked representation of vasomotor outputs with the time and frequency domain. Then 3D plot was projected in two dimensions as averaged over time. According to previous reports (Li et al., 2007; Pavlov et al., 2014; Neganova et al., 2017), 0.01–5 Hz was detected and slower contributions (0.01–0.25 Hz) were recognized caused by endothelial factors. The relative value of endothelial factors was recorded as the ratio between the value of endothelial amplitude and the sum amplitudes for total frequency range.

Assessment of Microvascular Permeability of Spinal Cord

Evan's Blue (EB) leakage was evaluated using a protocol as described previously (Yuan et al., 2017). EB dye (2% (w/v) in saline; Sigma-Aldrich, St Louis, United States) was infused intraperitoneally. After 3 h, animals were narcotized and infused transcardially with saline. The spinal cord was removed, dried and weighed. The samples were cut into pieces and soaked in a 50% trichloroacetic acid solution for 72 h at room temperature and centrifuged at 10,000 *g* for 10 min. Then we measured the fluorescence of the supernatants using excitation wavelength at 620 nm and emission wavelength at 680 nm. A standard curve with EB dye (0, 50, 100, 200, 400, 800, 1600, 3200, and 6400 ug in trichloacetic acid) was produced and fluorescence intensity was assessed with a spectrophotometer using excitation wavelength at 620 nm and emission wavelength at 680 nm. All data were within the range of detection built by the standard curve. The concentration of dye was qualified as the ratio of absorbance relative to the amount of tissue. Dye of samples was recorded as μg/mg of tissue.

To qualify the EB extravasation, mice were inundated with saline and subsequently with 4% PFA. The spinal cords were sectioned into 20-μm thick with a cryostat. The fluorescence of EB in spinal tissue was observed with a fluorescence microscope and the relative fluorescence intensity was assessed by Image Pro Plus 7.0.

Evaluation of Spinal Cord Edema

To evaluate edema formation, mice were anesthetized, and T9 (rostral cord, approximately 2 mm), T10 (epicenter, approximately 2 mm), and T11 (caudal cord, approximately 2 mm) segments were immediately removed. The samples (size, 5–15 mg) were quantified at once and put into an oven at 90°C for 72 h to get their dry weights. Edema formation was accounted by water content decided from the difference between the wet and dry weights of the samples, as reported before (Sharma and Olsson, 1990).

Establishment of Hypoxic Model to Cells

The SCMECs were seeded in 6-well plates or Transwell system (Yuan et al., 2011). When the cells kept a good state and reached 90%, the old mediums were abandoned, and new mediums were added. The cells were divided into three groups: (1) Hypoxic + Exosomes group: the exosomes were added into the medium at concentration of 20 μg/ml, and the cells were cultured in a 37°C tri-gas hypoxic incubator. The culture condition was 5% CO_2, 94% of N_2, and 1% of O_2. (2) Hypoxic group: The cells were cultured in a 37°C tri-gas hypoxic incubator with a culture condition of 5% CO_2, 94% of N_2, and 1% of O_2. (3) Control group: cells were cultured in normal incubator, with a culture condition of 5% CO_2, 37°C. The culture time was 6 h (Nohda et al., 2007).

Endothelial Permeability Assay

We assessed the paracellular permeability with a *trans*-well system by measuring the flux of FITC–dextran across the endothelial monolayer. FITC-conjugated dextran (40 kDa, 2 mg/mL; Sigma, St Louis, MO, United States) was put in the upper chamber of the Transwell system. Ten microliters of aliquots was taken away from the lower chamber at 0, 5, 15, 30, 60, or 90 min and changed with fresh medium. At last, the fluorescence that passed through the cell-covered inserts was determined with a fluorescence multiwell plate reader.

Western Blot Analysis

Total protein was extracted from spinal cord (epicenter ± 5 mm) with a lysis buffer (Beyotime, China). Briefly, at 4°C, tissue homogenates were lysed for 1 h and then centrifuged at 14,000 *g* for 8 min. The protein was qualified by BCA TM assay kit (Pierce, Rockford, IL, United States). Membrane Protein Extraction Kit (Thermo Scientific, Waltham, MA, United States) was used to extract the proteins from SCMECs. 50 μg total protein was separated by 10% SDS–PAGE and transferred to PVDF membranes (Pall Life Sciences, Port Washington, NY, United States). We incubated the membranes with diluted primary antibodies overnight at 4°C. The primary antibodies included Bax (1:1000; ab32503; Abcam), Bcl-2 (1:2000; ab196495; Abcam), HIF-1 (1:1000; ab82832; Abcam), β-actin (1:1000; ab5694; Abcam), PTEN (1:800; ab31392; Abcam), p-akt (1:1000; ab38449; Abcam), ZO-1 (1:1000; ab96587; Abcam). The membranes were washed it with TBST for three times, and then incubated with appropriate horseradish peroxidase-conjugated secondary antibodies for 1 h at 37°C. The bands were detected using enhanced chemiluminescence (ECL).

Quantitative Measurement of Image and Statistical Analyses

We assessed fluorescence intensity of EB dye, expressions of proteins and the number of apoptosis cells quantitatively with Image Pro Plus 7.0 (Media Cybernetics, Silver Spring, MD, United States). Images of each analytical group were taken from anterior horn of the gray matter or canalis centralis medulla spinalis and acquired using identical exposure settings. The data was analyzed by SPSS version 17.0 statistic software package (Chicago, IL, United States). Significance between SCI and exosomes treated groups was assessed by Student's *t*-test. Significance in three or more groups was determined by one-way analysis of variance (ANOVA) followed by *post hoc* Tukey's

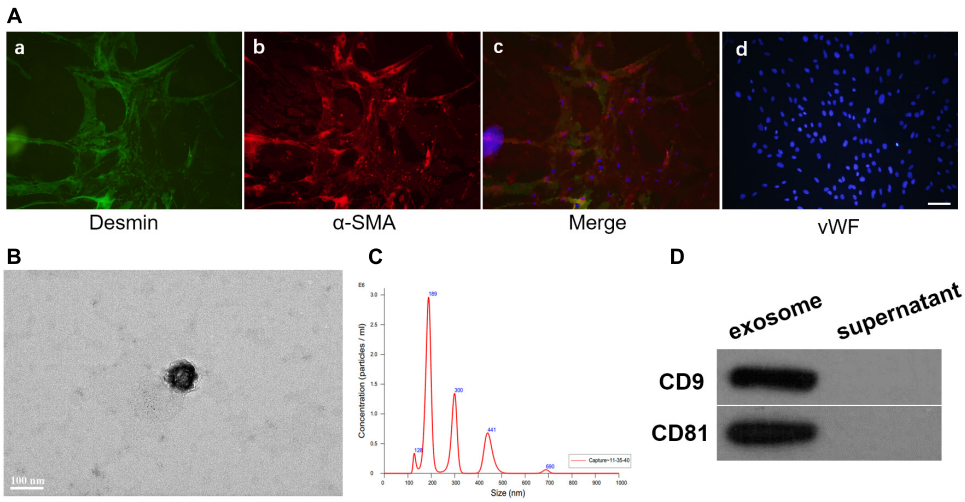

FIGURE 1 | Identification of the pericytes from cerebral micro-vessels and the pericytes exosomes. **(A)** Pericytes were double labeled with desmin and α-SMA, and identified by fluorescence. Pericytes were stained with desmin (a). Pericytes were stained with α-SMA (b). The two types of fluorescence with dapi were merged (c). Pericytes were stained with vWF and dapi (d). Bar = 100 μm. **(B)** Morphology of exosomes was observed by TEM. **(C)** Nanoparticle size distribution was analyzed by Nano-Sight LM10 instrument. **(D)** The surface markers of the exosomes, CD9 and CD81, were analyzed by Western blot.

analysis. All data was presented as mean ± SD, and values of $P < 0.05$ were considered significant.

RESULTS

Morphology of Pericytes and Expression of Generic Markers

After 7 days of culture, pericytes climbed out of the brain micro-vessels, and achieved 80–90% confluence. Then the isolated cells were identified for desmin and α-SMA, the markers of pericytes by immuno-fluorescence (**Figure 1A**).

Characterization of Pericytes Exosomes

Exosomes derived from pericytes were analyzed by TEM, Nano-Sight particle size analysis and western blotting. Transmission electron microscopic observation showed that pericytes exosomes had the presence of spherical vesicles, with a typical cup shape. Nano-Sight particle size analysis revealed that the diameter size distribution of these nanoparticles varied from 30 to 200 nm. The specific exosomes surface markers including CD9 and CD81 were positive in pericytes exosomes according to western blotting results, which further confirmed the exosomes (**Figures 1B–D**).

Pericytes Exosomes Improved Function Recovery of Mice After SCI

The functional recovery was observed over the next 2 weeks in all groups to determine whether exosomes treatment had rescuing effects on locomotion. As a result, exosomes treatment significantly promoted the locomotor function of hind limb from 14 days after injury when compared with that in SCI group.

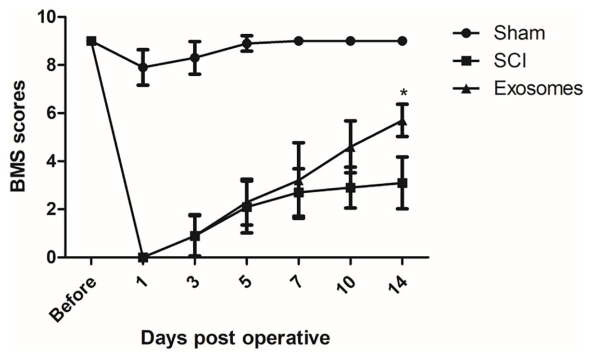

FIGURE 2 | Pericytes exosomes improved functional recovery after SCI in mice. The function of hindlimb recovery was accessed from 1 day to 14 day post-operation by Basso Mouse Scale (BMS) scores. The hindlimb dysfunction was ameliorated with treatment of exosomes. Data are presented as mean ± standard deviation, $n = 5$ in each group. $^*p < 0.05$ compared with SCI group.

These results indicated that pericytes exosomes could improve the movement of mice with SCI (**Figure 2**).

Pericytes Exosomes Reduces Lesion After Spinal Cord Injury

The results from HE staining showed that the structure of spinal cord was complete and the morphology of neural cell was normal, the neurons were polygonal and the nuclear was large and with clear outline and there was no inflammatory cell infiltration, in the sham group. In the SCI group, spinal cord morphology was incomplete and the tissue structure was disordered. Cell nuclear split and even disappeared. The space of cells and vascular was expanded, and inflammatory cell infiltration was obvious.

There was less inflammatory cell infiltration and more complete tissue structure in the exosomes group than that in the SCI group (**Figure 3A**).

The results from LFB showed that in the sham group, the myelin sheath was arranged neatly and with complete structure. In the SCI group, the myelin arrangement was disordered, the myelin gap was large, and the some myelin was lost. The disorder and loss of myelin sheath was improved in exosomes group compared with SCI group (**Figure 3B**).

The results from Nissl staining showed that in the sham group, Nissl body was neatly, well-distributed, tight and deep staining. In the SCI group, Nissl was decomposed into granules and dyed is shallow. The morphology and number of Nissl were significantly improved in exosomes group compared with SCI group (**Figure 3C**).

Pericytes Exosomes Attenuated Cell Apoptosis After Spinal Cord Injury

At 48 h post-injury, TUNEL assays were applied to assess neuronal cell apoptosis in the traumatic area of the spinal cord *in vivo*. The number of TUNEL-positive cells in exosomes treated group decreased obviously when compared with that in the SCI group (**Figures 3D,E**). According to western blot

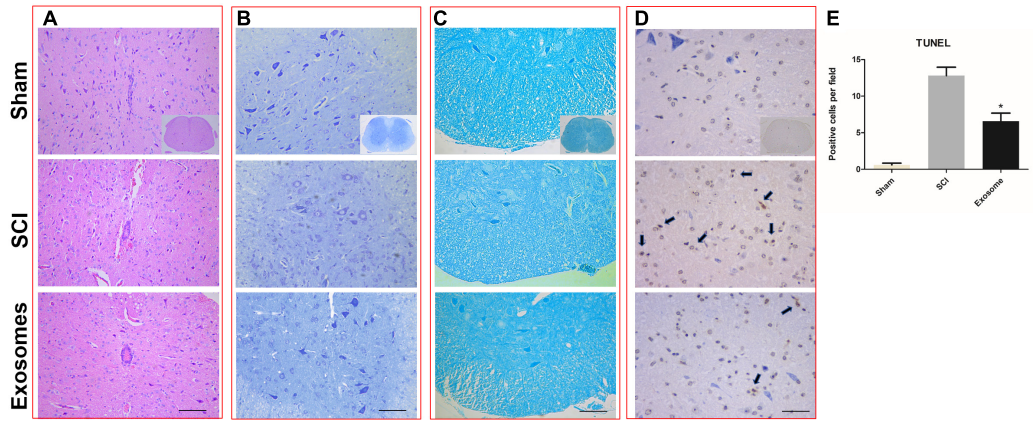

FIGURE 3 | Pericytes exosomes reduced lesion after SCI. **(A)** HE staining in the three groups: Sham, SCI, exosomes. **(B)** Nissl staining in the three groups: Sham, SCI, exosomes. **(C)** LFB staining and **(D)** TUNEL staining in the three groups: Sham, SCI, exosomes. The apoptosis cells was indicated by dark color the arrow pointed. $n = 5$ in each group. Bar = 50 μm. **(E)** The number of TUNEL+ cells (cell apoptosis) in the anterior horn of the gray matter of the transverse spinal cord sections. $n = 5$ in each group. $^*p < 0.05$ compared with SCI group.

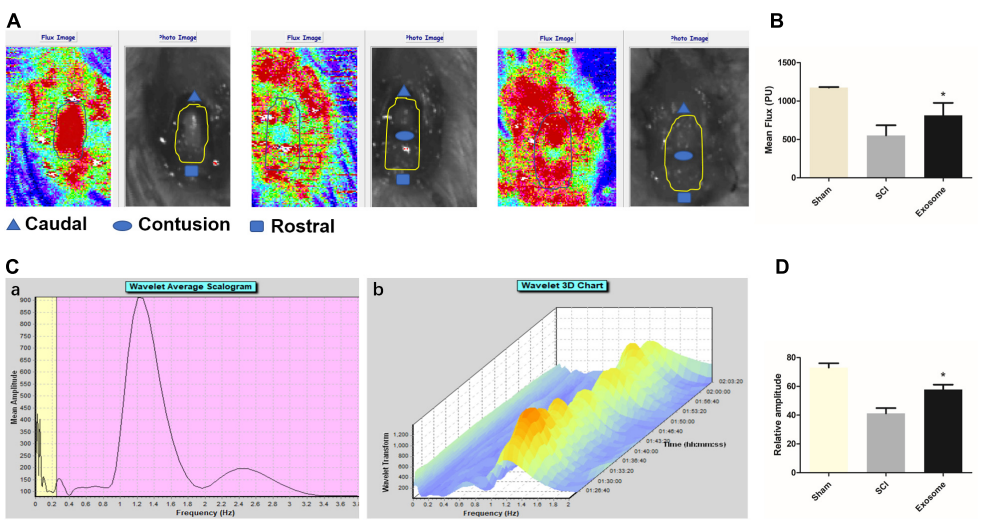

FIGURE 4 | Pericytes exosomes promoted blood flow and improved endothelial function after SCI. **(A)** The blood flow of organs was detected by the Laser Doppler Line Scanner. The video image and flux image of spinal cord in the three groups: Sham, SCI, exosomes. The area of interest is circled by a yellow curve. **(B)** Quantification of blood flow in the three groups. **(C)** The vasomotion of spinal cord was measured by dual channel laser doppler monitor, and the LDF signal was analyzed by wavelet analysis. The wavelet analysis was performed by means of the Moor software. Corresponding vasomotor amplitude during study period (a). A three-dimensional (3D) plot was produced from the wavelet transformations of perfusion signals (b). **(D)** The values of the relative amplitudes of oscillatory LDF signal in the endothelial factor. $n = 5$ in each group. $^*p < 0.05$ compared with SCI group.

results, treatment with exosomes attenuated Bax expression and upregulated Bcl-2 expression compared to the SCI groups (**Figures 7A,B**).

Pericytes Exosomes Meliorated Microcirculation of the Spinal Cord After SCI

Blood flow (BF) in the spinal cord was assessed using LDPI. A loss of microcirculation flux was observed after injury, and the reduction of perfusion signal was pronounced at the contusion site as shown in **Figures 4A,B**. Exosomes treatment significantly increased in perfusion at regions rostral and caudal. Additionally, the LDF investigation of microcirculation was performed by the spectral analysis of spinal cord BF oscillation (**Figure 4C**). The data showed that the relative value of endothelial factors decreased at the contusion site, and exosomes treatment mitigated the trend, suggesting that exosomes improved local microvascular disturbances might be related to the alteration of endothelial function (**Figure 4D**). The results from western blot, confirmed that the expression level of ischemia hypoxia-associated markers, HIF-1α, was obviously reduced in the exosomes group compared with that in the SCI group (**Figures 7A,B**).

Pericytes Exosomes Prevented the Disruption of Blood–Spinal Cord Barrier (BSCB) and Edema Formation

As shown in **Figures 5A,B**, after SCI, the fluorescence intensity of EB dye extravasation in damaged regions increase greatly and it reduced after exosomes treatment. In addition, exosomes effectively inhibited the increase of water content of the contusion site (**Figure 5C**). These results suggested that pericytes exosomes could protect against an early increase in the BSCB permeability and edema formation.

The Effect of Exosomes on the BSCB and Edema Associated Proteins

It was well known that the tight junction (TJ) proteins of endothelia and extracellular matrix were critical for the BSCB. Besides, aquaporins were very important in maintaining the water balance in spinal cord. The effect of exosomes on claudin-5, MMP2 and AQP4 was determined by immune-histochemistry assay. The results showed expression of claudin-5 at 48 h after SCI showed a significant disruption. However, exosomes alleviated the abnormal disruption of claudin-5. In addition, the expression of MMP2 and AQP4 in exosomes treated group decreased obviously when compared with that in the SCI group (**Figures 6**, **7**).

Pericytes Exosomes Protected Endothelial Cells Under Hypoxic Conditions

Endothelial cells from spinal cord microvessel were identified by labeled with vWF (**Figure 8A**). The permeability of endothelial monolayer was tested using *trans*-well assay. As shown in **Figure 8B**, the permeability of the endothelial monolayers increased greatly under hypoxic conditions. It was found that exosomes decreased the permeability induced by hypoxia. These results were in accordance with western blot results, in which TJ proteins of endothelia zonula occludens-1 (ZO-1) was alleviated by exosomes treatment. Moreover, pericytes exosomes can inhibit PTEN expression and promote p-Akt expression in endothelial cells under hypoxia (**Figures 8C,D**), suggesting exosomes therapy can protect the endothelial cells under hypoxia.

DISCUSSION

Spinal cord injury is the most serious complication of spinal trauma, which not only causes physical and mental harm to the patient, but also imposes a heavy burden on the family and society (Alilain et al., 2011). After SCI, a series of dynamic and complex pathophysiological changes occur in the injured area. It causes turbulence of microcirculation including ischemia, hemorrhage, and destruction of the blood-spinal barrier, edema and disorders of micro-hemodynamics. All these factors may affect the functional recovery by promoting apoptosis and necrosis, inflammatory cell infiltration and preventing reformation of functional synapses (Hausmann, 2003). We firstly demonstrated that exosomes from pericytes could improve blood supply, ameliorate endothelial function, protect the BSCB and reduce edema, thus leading to functional behavioral recovery in mice. Notably, our *in vitro* experiments demonstrated that exosomes can improve endothelial barrier function in hypoxic conditions, protect endothelial cells via the PTEN/Akt pathway.

The treatment of SCI was still one of the challenges in the medical field. In recent years, stem cell transplantation became more and more intensive and showed good application prospects (Wyatt and Keirstead, 2012). MSCs were a kind of pluripotent stem cells with self-renewal ability which were ideal donor cells for transplantation, because they owned neuroprotective properties and could promote functional recovery after acute SCI (Chopp et al., 2000; Varma et al., 2013). However, it showed that <1% of transplanted MSCs migrated to injured tissue. A large percentage of MSCs trapped in the lung and liver during the circulation (Phinney and Prockop, 2007).

In the past, it was thought that the repair mechanism of stem cells lies in homing and differentiation, and the replacement of damaged cells. Recently, it was considered that the extracellular vesicles secreted by transplanted cells may be more important for repairment (Ratajczak et al., 2014). Exosomes secreted by MSCs became an important active component. Studies demonstrate that exosomes of MSCs could lessen tissue damage and improve the function in various injury disease models (Théry et al., 2002; Lai et al., 2010; Camussi et al., 2013). Besides the therapeutic effects, administration of exosomes had the advantage that it could avoid limitations caused by direct stem cells transplantation (Camussi et al., 2013). Pericytes owned the characteristics of MSCs and constituted an important component of neurovascular units. They interacted with endothelial cells and took part in keeping the stability of endothelial barriers. There was no literature report on the

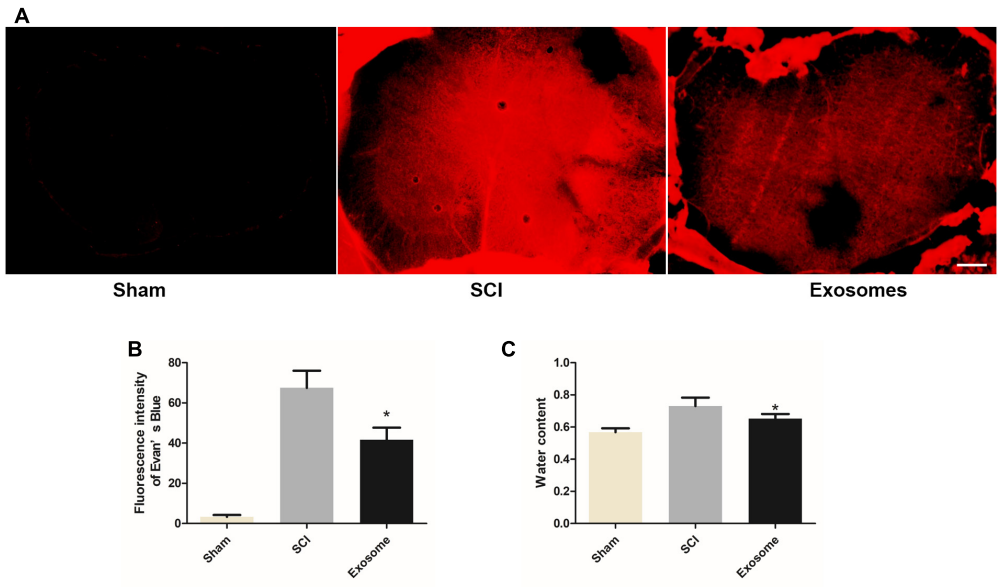

FIGURE 5 | Pericytes exosomes repaired the permeability of the blood–spinal cord barrier (BSCB) and reduced edema after SCI. **(A)** Representative fluorescent image of an Evan's Blue dye extravasation at the spinal parenchyma at 2 days after SCI. **(B)** Quantification of the fluorescence intensity of Evan's Blue. **(C)** The water content of spinal cord in different groups. $n = 15$ in each group. $^*p < 0.05$ compared with SCI group. Scale bar = 200 μm.

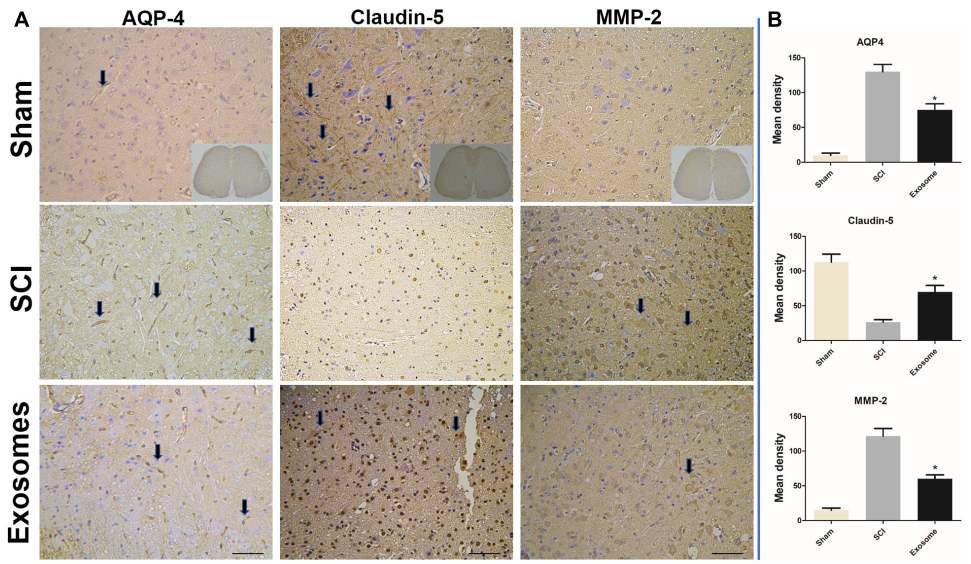

FIGURE 6 | The expression of AQP-4, claudin-5, and MMP2 s was detected in sham, SCI, and Exosomes groups. **(A)** For all immunostained sections, detection of specific proteins was indicated by dark color the arrow pointed. $n = 5$ in each group. Bar = 50 μm. **(B)** Quantitative statistical analysis of protein expression of AQP-4, claudin-5, and MMP2. $^*p < 0.05$ compared with SCI group.

treatment of SCI with pericytes exosomes. In the present study, we applied a series of experiments *in vivo* and *in vitro* to study exosomes treatment in the contusion SCI model. Exosomes derived from pericytes were isolated and identified with a range from 30 to 200 nm in diameter using Nano-Sight particle size analysis. They expressed the specific exosomes surface markers including CD9 and CD81. At the same time, they were confirmed by TEM.

Here, we found that traumatic injury to the spinal cord led to reduced BF and disrupted endothelial BF regulation at the contusion site. Lack of blood flow, resulting in ischemia and hypoxia, were recognized as important reasons for the failure of nervous tissue repair (Oudega, 2012). It was shown that hypoxia resulted in barrier disruptions including increased permeability, vasogenic edema, and tissue damage (Kaur and Ling, 2008), which were related with the up-regulation of HIF-1α. HIF-1α,

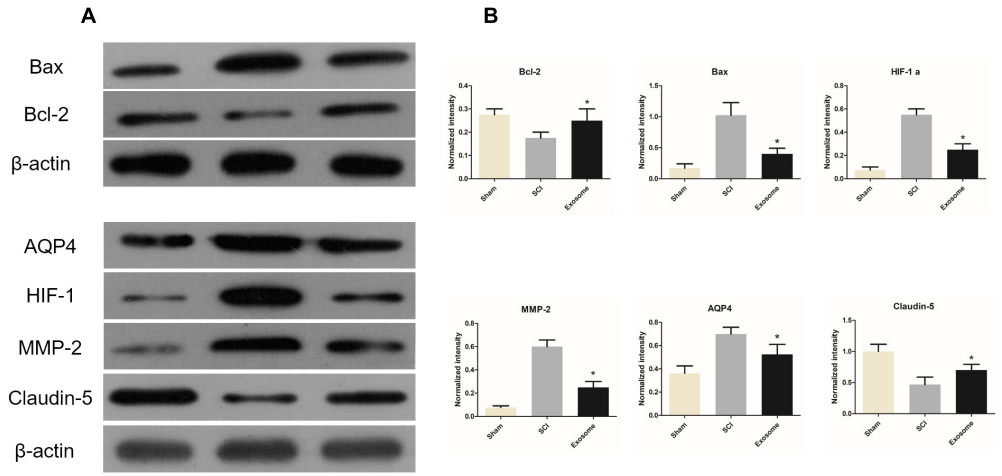

FIGURE 7 | The expressions of Bax / Bcl-2 / HIF-1α / claudin-5 /MMP2 / AQP4 in three groups were determined by WB. **(A)** The expression of Bax / Bcl-2 / HIF-1α / claudin-5 / MMP2 / AQP4 in three different groups were determined by WB. **(B)** The relative expression intensity of Bax / Bcl-2/ HIF-1α / claudin-5 / MMP2 / AQP4 in three different groups. $n = 5$ in each group. $^*p < 0.05$ compared with SCI group.

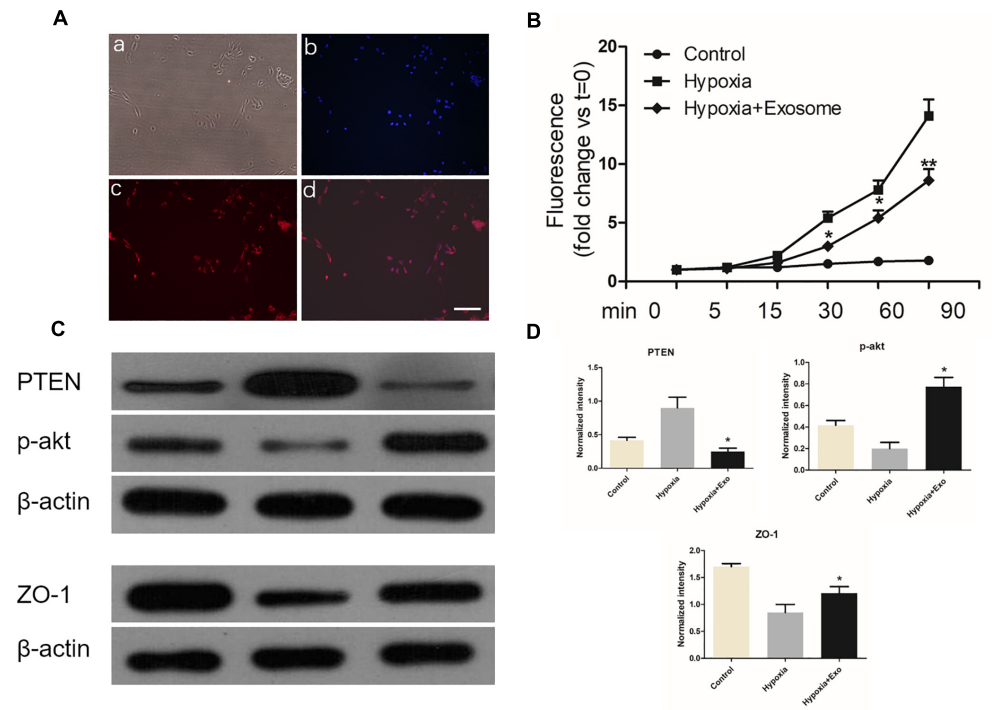

FIGURE 8 | Pericytes exosomes protected endothelial cells under hypoxic conditions. **(A)** Endothelial cells were labeled with vWF, and identified by fluorescence. Bright light (a), dapi (b), vWF (c), merged (d), Bar = 100 μm. **(B)** Transwell assay was used to examine permeability of the endothelial monolayer. $n = 5$ in each group. $^*p < 0.05$ compared with hypoxia group. $^{**}p < 0.01$ compared with hypoxia group. **(C)** The expression of ZO-1 / PTEN / p-akt in three different groups. **(D)** The relative expression intensity of ZO-1 / PTEN / p-akt in three different groups. $n = 3$ in each group. $^*p < 0.05$ compared with hypoxia group.

a transcription factor, was activated by hypoxic conditions and gathered in endothelial cells. It was bound to vascular endothelial growth factor (VEGF) gene promoter and induced the expression of VEGF. The increased expression of HIF-1α were important in the adaptation of tissues and cells in hypoxic environment. In this study, our observation of blood perfusion loss and endothelium BF dysregulation after SCI suggested that the chaos of microcirculation might have contributed to delayed ischemic hypoxic tissue loss. However, the microcirculatory dysfunction was partly meliorated by pericytes exosomes treatment, which was also confirmed by our western blot results. HIF-1α levels were significantly down-regulated by pericytes exosomes. An

important neuroprotective effect of pericytes exosomes may be the promotion of nervous tissue survival through the restoration of blood perfusion.

In addition, the loss of spinal cord blood perfusion following injury was mainly caused by rupture of blood vessels, which increased the permeability of BSCB with subsequent development of tissue edema. The disruption of BSCB resulted in the exchange of the harmful elements from blood and tissue and caused cell death and permanent neurological disability (Lee et al., 2012; Fan et al., 2013). Endothelial cells, pericytes, extracellular matrix, and TJs played key roles for the integrity of BSCB (Wolburg and Lippoldt, 2002). It was shown that a reduction in the permeability of BSCB attenuates edema formation after experimental contusive SCI and It was reported that reduction of edema formation after traumatic spinal injury improved functional recovery in acute and chronic phases after injury (Sharma, 2007; Fukuda et al., 2013).

Spinal cord edema can be divided into vasogenic edema and cytotoxic edema. Vasogenic edema was mainly caused by the destruction of junctions between endothelial cells, increased permeability of the BSCB, and the fluid in the blood entering the extracellular space of the parenchyma. The cytotoxic edema was mainly caused by the astrocyte metabolic disorder affecting the function of the sodium potassium pump on the membrane, which caused a large amount of water molecules to enter the cell and caused cell edema (Borgens and Liu-Snyder, 2012).

TJs around the apical end of the inter-endothelial space, were connected to adherens junctions near the basal end of the inter-endothelial space (Oudega, 2012). They were made up of zonula occludens, occludins, and claudins (Liebner et al., 2011). Claudin 5, the major claudin expressed by endothelial cell, was especially present in the BSCB (Strazielle and Ghersi-Egea, 2013). Alteration in the expression and distribution of TJs proteins was closely due to the permeability of BSCB during SCI (Liebner et al., 2011). In this study, we examined the expression of claudin-5 and found that the expression of claudin-5 was significantly enhanced in exosomes treated group when compared with that in SCI group. This implied that pericytes exosomes could promote BSCB integrity during SCI through the regulation of TJs proteins.

Matrix Metalloproteinases (MMPs) were located in the cell-surface. They were soluble and bound zinc-dependent endopeptidases that could regulate cellular infiltration, extracellular matrix degradation, release of growth factors and cytokines from the matrix, cell migration, tissue damage, remodeling, and repair (De Luca and Papa, 2017). MMPs activity was needed for the inflammatory cell infiltration and early barrier disruption after SCI. Each of these inflammatory cells expressed MMPs including MMP2. Increases of MMP2 were associated with decreases in claudin-5 in the blood vessels. MMP2 decomposed extracellular matrix (ECM), which deteriorated blood vessel damage (Noble et al., 2002). Studies demonstrated a significant up-regulation of MMPs in mouse SCI compression model (Wells et al., 2003). Moreover, it clearly showed that the pharmacological blockade of MMPs improved locomotor recovery after SCI (Hsu et al., 2006). The results also showed that pericytes exosomes treatment was involved with the decrease of MMP2 expression. It implied that the expression of MMPs in SCI might be down-regulated after treatment with pericytes exosomes, which was known to induce BSCB disruption.

Anti-Aquaporin-4 had a key role in keeping the water balance. AQP4 is widely distributed in various organs, especially in the brain and spinal cord. AQP4 was expressed on many types of cells, including glial cells, endothelial cells, and a subset of neuronal cells (Nielsen et al., 1997; Oshio et al., 2004). AQP4 has an effect on vasogenic edema and cytotoxic edema. Although AQP4 is not directly related to the formation of vasogenic edema it was essential for the removal of vasogenic edema (Fukuda et al., 2013; Hubbard et al., 2016). The high expression of AQP4 promoted the entry of liquid into cells, causing cytotoxic edema. Studies observed that a significantly better neurological recovery in AQP4 knockout mice than that in wild-type mice after SCI (Saadoun et al., 2008; Liang et al., 2015). We found that immune-reactivity of AQP4 at the injury site increased in gray and white matter at 48 h. Up-regulation of AQP4 may enhance water flow from the vasculature into spinal cord parenchyma and raise cord swelling after injury. Thus up-regulation of AQP4 represented a maladaptive response following SCI, which was also found in multiple other brain pathologies (Sun et al., 2003). We observed that pericytes exosomes could significantly alleviate the

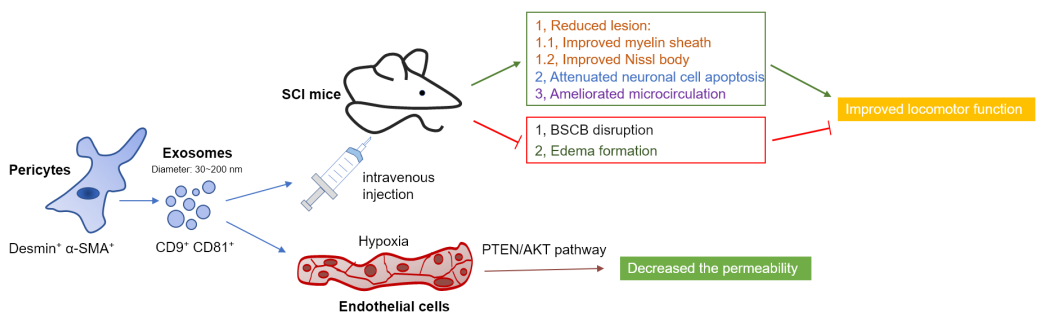

FIGURE 9 | Diagram illustrated the proposed mechanism of treatment of pericytes exosomes after traumatic SCI in mice. Pericytes exosomes improved myelin sheath and Nissl body, attenuated cell apoptosis, ameliorated microcirculation, suppressed BSCB disruption and edema formation and eventually improved functional behavioral recovery after SCI. Especially, treatment of pericytes exosomes protected the barrier of spinal cord microvascular endothelial cells under hypoxia condition, which was related to PTEN/AKT pathway.

level of edema after SCI. At the same time, the expression of AQP4 also decreased.

Apoptosis was a physiological or pathological process of cells that often happened following the alteration of environmental conditions (Hengartner, 2000). Malfunction of apoptosis may be related to a large number of diseases of the CNS (Cavallucci and D'Amelio, 2011). Apoptosis affected functional recovery, nerve cell survival and axon regeneration after SCI (Zhang et al., 2015). Bax and Bcl-2 were the important molecular components about cell apoptosis. Bcl-2 was an anti-apoptotic protein and the expression of Bax represented the occurrence of apoptosis (Adams and Cory, 1998). After neuronal injury, the pro-apoptotic proteins Bax was shown to be upregulated, while the anti-apoptotic protein Bcl-2 was down-regulated (Seki et al., 2003). TUNEL assay demonstrated that treatment with pericytes exosomes could alleviate the apoptosis of neuronal cells in the SCI model, which was also confirmed by the results from western blot. The level of Bax was significantly repressed by pericytes exosomes, whereas the level of Bcl-2 was up-regulated. Both results indicated that administration of pericytes exosomes could protect neuronal cells from injury-induced apoptosis.

To further explore this barrier protection mechanism, we evaluated the extent of permeability of endothelial cells by Transwell system in the hypoxia model *in vitro*. As expected, the *trans*-well assay confirmed that pericytes exosomes could effectively prevent endothelial barrier and up-regulate the expression level of junction protein ZO-1 in the hypoxia condition, which further confirmed our results *in vivo*.

Phosphatase and tensin homolog deleted on chromosome 10 (PTEN) was a tumor suppressor gene. PTEN was considered as a negative regulator of PI3K/AKT pathway. PI3K/AKT pathway has been extensively studied as a regulator of cell survival and apoptosis. p-Akt is phosphorylated protein kinase B (p-PKB), an important signal protein molecule, which can inhibit cell apoptosis and promote cell survival (Bsibsi et al., 2006; Farina et al., 2007). In this article, western blot results showed pericytes exosomes could inhibit PTEN expression and promote p-Akt expression in SMECs, which suggested exosomes therapy could promote the survival of endothelial cells under hypoxia and reduce cell apoptosis.

CONCLUSION

In conclusion, the present study we demonstrated that treatment with pericytes exosomes could promote blood flow, improve endothelial function, protect the BSCB, alleviate the apoptotic response, and thus promote functional and behavioral recovery after SCI (**Figure 9**). In particular, one of the underlying mechanisms may be the protection of the endothelial cells in hypoxia condition. These findings suggested that pericytes-derived exosomes is a potential new therapeutic interventions for SCI.

ETHICS STATEMENT

The procedures of animal experiments were approved by the Experimental Animal Care and Ethics Committee of the Institute of Microcirculation, Chinese Academy of Medical Sciences (CAMS) and Peking Union Medical College (PUMC).

AUTHOR CONTRIBUTIONS

XY, QW, and PW substantial contributions to the conception or design of the work, acquired, analyzed, or interpreted the data for the work. YJ, HY, and YT drafted the work or revised it critically for the important intellectual content. All authors approved the final version to be published. ZL, HZ, and RX agreed to be accountable for all the aspects of the work in ensuring that questions related to the accuracy or integrity of any part of the work are appropriately investigated and resolved.

FUNDING

This study was supported by the National Natural Science Foundation of China (No. 81603678), the innovation fund of the Chinese Academy of Medical Sciences & Peking Union Medical College (Nos. 3332014006 and 3332015123), the Special Fund for Basic Scientific Research of the Central Public Research Institutes (Nos. 2016CZ-1 and 2018CZ-8), and the CAMS Initiative for Innovative Medicine (CAMS-I2M) (No. 2016-I2M-3-006).

REFERENCES

Adams, J. M., and Cory, S. J. S. (1998). The Bcl-2 protein family: arbiters of cell survival. *Science* 281, 1322–1326. doi: 10.1126/science.281.5381.1322

Alilain, W. J., Horn, K. P., Hu, H., Dick, T. E., and Silver, J. J. N. (2011). Functional regeneration of respiratory pathways after spinal cord injury. *Nature* 475, 196–200. doi: 10.1038/nature10199

Allen, A. R. (1911). Surgery of experimental lesion of spinal cord equivalent to crush injury of fracture dislocation of spinal column: a preliminary report. *JAMA* 57, 878–880.

Balsam, L. B., Wagers, A. J., Christensen, J. L., Kofidis, T., Weissman, I. L., and Robbins, R. C. J. N. (2004). Haematopoietic stem cells adopt mature haematopoietic fates in ischaemic myocardium. *Nature* 428, 668–673. doi: 10.1038/nature02460

Basso, D. M., Fisher, L. C., Anderson, A. J., Jakeman, L. B., Mctigue, D. M., and Popovich, P. G. (2006). Basso Mouse Scale for locomotion detects differences in recovery after spinal cord injury in five common mouse strains. *J. Neurotrauma* 23, 635–659. doi: 10.1089/neu.2006.23.635

Bergers, G., and Song, S. (2005). The role of pericytes in blood-vessel formation and maintenance. *Neuro Oncol.* 7, 452–464. doi: 10.1215/s1152851705000232

Borgens, R. B., and Liu-Snyder, P. (2012). Understanding secondary injury. *Q. Rev. Biol.* 87, 89–127.

Breakefield, X. O., Frederickson, R. M., and Simpson, R. J. (2011). Gesicles: microvesicle "cookies" for transient information transfer between cells. *Mol. Ther.* 19, 1574–1576. doi: 10.1038/mt.2011.169

Bsibsi, M., Persoon-Deen, C., Verwer, R. W., Meeuwsen, S., Ravid, R., and Van Noort, J. M. J. G. (2006). Toll-like receptor 3 on adult human astrocytes triggers production of neuroprotective mediators. *Glia* 53, 688–695. doi: 10.1002/glia.20328

Camussi, G., Deregibus, M. C., and Cantaluppi, V. (2013). Role of stem-cell-derived microvesicles in the paracrine action of stem cells. *Biochem. Soc. Trans.* 41, 283–287. doi: 10.1042/BST20120192

Carlson, G. D., and Gorden, C. (2002). Current developments in spinal cord injury research. *Spine J.* 2, 116–128. doi: 10.1016/s1529-9430(01)00029-8

Cavallucci, V., and D'Amelio, M. J. C. P. D. (2011). Matter of life and death: the pharmacological approaches targeting apoptosis in brain diseases. *Curr. Pharm. Des.* 17, 215–229. doi: 10.2174/138161211795049705

Chaput, N., and Théry, C. (2011). Exosomes: immune properties and potential clinical implementations. *Semin. Immunopathol.* 33, 419–440. doi: 10.1007/s00281-010-0233-9

Chopp, M., Zhang, X. H., Li, Y., Wang, L., Chen, J., Lu, D., et al. (2000). Spinal cord injury in rat: treatment with bone marrow stromal cell transplantation. *Neuroreport* 11, 3001–3005. doi: 10.1097/00001756-200009110-00035

Cizkova, D., Novotna, I., Slovinska, L., Vanicky, I., Jergova, S., Rosocha, J., et al. (2011). Repetitive intrathecal catheter delivery of bone marrow mesenchymal stromal cells improves functional recovery in a rat model of contusive spinal cord injury. *J. Neurotrauma* 28, 1951–1961. doi: 10.1089/neu.2010.1413

De Luca, C., and Papa, M. (2017). Matrix metalloproteinases, neural extracellular matrix, and central nervous system pathology. *Prog. Mol. Biol. Transl. Sci.* 148, 167–202. doi: 10.1016/bs.pmbts.2017.04.002

Dore-Duffy, P., and Cleary, K. (2011). Morphology and properties of pericytes. *Methods Mol. Biol.* 686, 49–68. doi: 10.1007/978-1-60761-938-3_2

Fan, Z.-K., Cao, Y., Lv, G., Wang, Y.-S., and Guo, Z.-P. (2013). The effect of cigarette smoke exposure on spinal cord injury in rats. *J. Neurotrauma* 30, 473–479. doi: 10.1089/neu.2012.2574

Farina, C., Aloisi, F., and Meinl, E. (2007). Astrocytes are active players in cerebral innate immunity. *Trends Immunol.* 28, 138–145. doi: 10.1016/j.it.2007.01.005

Feron, F., Perry, C., Cochrane, J., Licina, P., Nowitzke, A., Urquhart, S., et al. (2005). Autologous olfactory ensheathing cell transplantation in human spinal cord injury. *Brain* 128, 2951–2960. doi: 10.1093/brain/awh657

Fukuda, A. M., Adami, A., Pop, V., Bellone, J. A., Coats, J. S., Hartman, R. E., et al. (2013). Posttraumatic reduction of edema with aquaporin-4 RNA interference improves acute and chronic functional recovery. *J. Cereb. Blood Flow Metab.* 33, 1621–1632. doi: 10.1038/jcbfm.2013.118

Gatti, S., Bruno, S., Deregibus, M. C., Sordi, A., Cantaluppi, V., Tetta, C., et al. (2011). Microvesicles derived from human adult mesenchymal stem cells protect against ischaemia–reperfusion-induced acute and chronic kidney injury. *Nephrol. Dial. Transplant.* 26, 1474–1483. doi: 10.1093/ndt/gfr015

Hausmann, O. N. (2003). Post-traumatic inflammation following spinal cord injury. *Spinal Cord* 41, 369–378. doi: 10.1038/sj.sc.3101483

Hengartner, M. O. (2000). The biochemistry of apoptosis. *Nature* 407, 770–776.

Ho, A., Wagner, W., and Franke, W. J. C. (2008). Heterogeneity of mesenchymal stromal cell preparations. *Cytotherapy* 10, 320–330. doi: 10.1080/14653240802217011

Hsu, J.-Y. C., McKeon, R., Goussev, S., Werb, Z., Lee, J.-U., Trivedi, A., et al. (2006). Matrix metalloproteinase-2 facilitates wound healing events that promote functional recovery after spinal cord injury. *J. Neurosci.* 26, 9841–9850. doi: 10.1523/jneurosci.1993-06.2006

Huang, J.-H., Yin, X.-M., Xu, Y., Xu, C.-C., Lin, X., Ye, F.-B., et al. (2017). Systemic administration of exosomes released from mesenchymal stromal cells attenuates apoptosis, inflammation, and promotes angiogenesis after spinal cord injury in rats. *J. Neurotrauma* 34, 3388–3396. doi: 10.1089/neu.2017.5063

Hubbard, J. A., Szu, J. I., Yonan, J. M., and Binder, D. K. (2016). Regulation of astrocyte glutamate transporter-1 (GLT1) and aquaporin-4 (AQP4) expression in a model of epilepsy. *Exp. Neurol.* 283, 85–96. doi: 10.1016/j.expneurol.2016.05.003

Jeong, J.-O., Han, J. W., Kim, J.-M., Cho, H.-J., Park, C., Lee, N., et al. (2011). Malignant tumor formation after transplantation of short-term cultured bone marrow mesenchymal stem cells in experimental myocardial infarction and diabetic neuropathy. *Circ. Res.* 108, 1340–1347. doi: 10.1161/CIRCRESAHA.110.239848

Katsuda, T., Kosaka, N., Takeshita, F., and Ochiya, T. J. P. (2013). The therapeutic potential of mesenchymal stem cell-derived extracellular vesicles. *Proteomics* 13, 1637–1653. doi: 10.1002/pmic.201200373

Kaur, C., and Ling, E. A. (2008). Blood brain barrier in hypoxic-ischemic conditions. *Curr. Neurovasc. Res.* 5, 71–81. doi: 10.2174/156720208783565645

Lai, R. C., Arslan, F., Lee, M. M., Sze, N. S. K., Choo, A., Chen, T. S., et al. (2010). Exosome secreted by MSC reduces myocardial ischemia/reperfusion injury. *Stem Cell Res.* 4, 214–222. doi: 10.1016/j.scr.2009.12.003

Lai, R. C., Chen, T. S., and Lim, S. K. (2011). Mesenchymal stem cell exosome: a novel stem cell-based therapy for cardiovascular disease. *Regen. Med.* 6, 481–492. doi: 10.2217/rme.11.35

Lee, J. Y., Kim, H. S., Choi, H. Y., Oh, T. H., Ju, B. G., and Yune, T. Y. (2012). Valproic acid attenuates blood–spinal cord barrier disruption by inhibiting matrix metalloprotease-9 activity and improves functional recovery after spinal cord injury. *J. Neurochem.* 121, 818–829. doi: 10.1111/j.1471-4159.2012.07731.x

Li, T., Yan, Y., Wang, B., Qian, H., Zhang, X., Shen, L., et al. (2012). Exosomes derived from human umbilical cord mesenchymal stem cells alleviate liver fibrosis. *Stem Cells Dev.* 22, 845–854. doi: 10.1089/scd.2012.0395

Li, Z., Tam, E. W., Mak, A. F., and Lau, R. Y. (2007). Wavelet analysis of the effects of static magnetic field on skin blood flowmotion: investigation using an in vivo rat model. *In Vivo* 21, 61–68.

Liang, F., Luo, C., Xu, G., Su, F., He, X., Long, S., et al. (2015). Deletion of aquaporin-4 is neuroprotective during the acute stage of micro traumatic brain injury in mice. *Neurosci. Lett.* 598, 29–35. doi: 10.1016/j.neulet.2015.05.006

Liebner, S., Czupalla, C. J., and Wolburg, H. (2011). Current concepts of blood-brain barrier development. *Int. J. Dev. Biol.* 55, 467–476. doi: 10.1387/ijdb.103224sl

Liu, W., Wang, Y., Gong, F., Rong, Y., Luo, Y., Tang, P., et al. (2018). Exosomes derived from bone mesenchymal stem cells repair traumatic spinal cord injury via suppressing the activation of A1 neurotoxic reactive astrocytes. *J. Neurotrauma* 36, 469–484.

Mathivanan, S., Ji, H., and Simpson, R. J. (2010). Exosomes: extracellular organelles important in intercellular communication. *J. Proteomics* 73, 1907–1920. doi: 10.1016/j.jprot.2010.06.006

Mothe, A. J., and Tator, C. H. (2012). Advances in stem cell therapy for spinal cord injury. *J. Clin. Invest.* 122, 3824–3834.

Nakajima, H., Uchida, K., Guerrero, A. R., Watanabe, S., Sugita, D., Takeura, N., et al. (2012). Transplantation of mesenchymal stem cells promotes an alternative pathway of macrophage activation and functional recovery after spinal cord injury. *J. Neurotrauma* 29, 1614–1625. doi: 10.1089/neu.2011.2109

Neganova, A. Y., Postnov, D. D., Sosnovtseva, O., and Jacobsen, J. C. B. (2017). Rat retinal vasomotion assessed by laser speckle imaging. *PLoS One* 12:e0173805. doi: 10.1371/journal.pone.0173805

Neirinckx, V., Agirman, G., Coste, C., Marquet, A., Dion, V., Rogister, B., et al. (2015). Adult bone marrow mesenchymal and neural crest stem cells are chemoattractive and accelerate motor recovery in a mouse model of spinal cord injury. *Stem Cell Res. Ther.* 6:211. doi: 10.1186/s13287-015-0202-2

Nielsen, S., Nagelhus, E. A., Amiry-Moghaddam, M., Bourque, C., Agre, P., and Ottersen, O. P. (1997). Specialized membrane domains for water transport in glial cells: high-resolution immunogold cytochemistry of aquaporin-4 in rat brain. *J. Neurosci.* 17, 171–180. doi: 10.1523/jneurosci.17-01-00171.1997

Noble, L. J., Donovan, F., Igarashi, T., Goussev, S., and Werb, Z. (2002). Matrix metalloproteinases limit functional recovery after spinal cord injury by modulation of early vascular events. *Spine* 22, 7526–7535. doi: 10.1523/jneurosci.22-17-07526.2002

Nohda, K., Nakatsuka, T., Takeda, D., Miyazaki, N., Nishi, H., Sonobe, H., et al. (2007). Selective vulnerability to ischemia in the rat spinal cord: a comparison between ventral and dorsal horn neurons. *Spine* 32, 1060–1066. doi: 10.1097/01.brs.0000261560.53428.90

Orekhov, A. N., Bobryshev, Y. V., and Chistiakov, D. A. (2014). The complexity of cell composition of the intima of large arteries: focus on pericyte-like cells. *Cardiovasc. Res.* 103, 438–451. doi: 10.1093/cvr/cvu168

Oshio, K., Binder, D., Yang, B., Schecter, S., Verkman, A., and Manley, G. J. N. (2004). Expression of aquaporin water channels in mouse spinal cord. *Neuroscience* 127, 685–693. doi: 10.1016/j.neuroscience.2004.03.016

Oudega, M. (2012). Molecular and cellular mechanisms underlying the role of blood vessels in spinal cord injury and repair. *Cell Tissue Res.* 349, 269–288. doi: 10.1007/s00441-012-1440-6

Pavlov, A., Semyachkina-Glushkovskaya, O., Zhang, Y., Bibikova, O., Pavlova, O., Huang, Q., et al. (2014). Multiresolution analysis of pathological changes in cerebral venous dynamics in newborn mice with intracranial hemorrhage:

adrenorelated vasorelaxation. *Physiol. Meas.* 35, 1983–1999. doi: 10.1088/0967-3334/35/10/1983

Phinney, D. G., and Prockop, D. J. (2007). Concise review: mesenchymal stem/multipotent stromal cells: the state of transdifferentiation and modes of tissue repair—current views. *Stem Cells* 25, 2896–2902. doi: 10.1634/stemcells.2007-0637

Ratajczak, M. Z., Jadczyk, T., Pêdziwiatr, D., and Wojakowski, W. (2014). New advances in stem cell research: practical implications for regenerative medicine. *Pol. Arch. Med. Wewn.* 124, 417–426. doi: 10.20452/pamw.2355

Record, M., Subra, C., Silvente-Poirot, S., and Poirot, M. (2011). Exosomes as intercellular signalosomes and pharmacological effectors. *Biochem. Pharmacol.* 81, 1171–1182. doi: 10.1016/j.bcp.2011.02.011

Rendell, M. S., Finnegan, M. F., Pisarri, T., Healy, J. C., Lind, A., Milliken, B. K., et al. (1999). A comparison of the cutaneous microvascular properties of the spontaneously hypertensive rat and the Wistar-Kyoto rat. *Comp. Biochem. Physiol. A Mol. Integr. Physiol.* 122, 399–406. doi: 10.1016/s1095-6433(99)00022-7

Rodriguez, R., Rubio, R., and Menendez, P. (2012). Modeling sarcomagenesis using multipotent mesenchymal stem cells. *Cell Res.* 22, 62–77. doi: 10.1038/cr.2011.157

Rubio, D., Garcia-Castro, J., Martín, M. C., de la Fuente, R., Cigudosa, J. C., Lloyd, A. C., et al. (2005). Spontaneous human adult stem cell transformation. *Cancer Res.* 65, 3035–3039. doi: 10.1158/0008-5472.can-04-4194

Saadoun, S., Bell, B. A., Verkman, A., and Papadopoulos, M. C. (2008). Greatly improved neurological outcome after spinal cord compression injury in AQP4-deficient mice. *Brain* 131, 1087–1098. doi: 10.1093/brain/awn014

Schwab, M. E., and Bartholdi, D. (1996). Degeneration and regeneration of axons in the lesioned spinal cord. *Physiol. Rev.* 76, 319–370. doi: 10.1152/physrev.1996.76.2.319

Seki, T., Hida, K., Tada, M., Koyanagi, I., and Iwasaki, Y. J. N. (2003). Role of the bcl-2 gene after contusive spinal cord injury in mice. *Neurosurgery* 53, 192–198. doi: 10.1227/01.neu.0000068988.28788.2c

Sharma, H., and Olsson, Y. (1990). Edema formation and cellular alterations following spinal cord injury in the rat and their modification with p-chlorophenylalanine. *Acta Neuropathol.* 79, 604–610. doi: 10.1007/bf00294237

Sharma, H. S. (2007). A select combination of neurotrophins enhances neuroprotection and functional recovery following spinal cord injury. *Ann. N. Y. Acad. Sci.* 1122, 95–111. doi: 10.1196/annals.1403.007

Simonavicius, N., Ashenden, M., Van Weverwijk, A., Lax, S., Huso, D. L., Buckley, C. D., et al. (2012). Pericytes promote selective vessel regression to regulate vascular patterning. *Blood* 120, 1516–1527. doi: 10.1182/blood-2011-01-332338

Stoorvogel, W., Kleijmeer, M. J., Geuze, H. J., and Raposo, G. J. T. (2002). The biogenesis and functions of exosomes. *Traffic* 3, 321–330. doi: 10.1034/j.1600-0854.2002.30502.x

Strazielle, N., and Ghersi-Egea, J. F. (2013). Physiology of blood–brain interfaces in relation to brain disposition of small compounds and macromolecules. *Mol. Pharm.* 10, 1473–1491. doi: 10.1021/mp300518e

Sun, M.-C., Honey, C. R., Berk, C., Wong, N. L., and Tsui, J. K. (2003). Regulation of aquaporin-4 in a traumatic brain injury model in rats. *J. Neurosurg.* 98, 565–569. doi: 10.3171/jns.2003.98.3.0565

Théry, C., Zitvogel, L., and Amigorena, S. (2002). Exosomes: composition, biogenesis and function. *Nat. Rev. Immunol.* 2, 569–579. doi: 10.1038/nri855

Varma, A. K., Das, A., Wallace, G., Barry, J., Vertegel, A. A., Ray, S. K., et al. (2013). Spinal cord injury: a review of current therapy, future treatments, and basic science frontiers. *Neurochem. Res.* 38, 895–905. doi: 10.1007/s11064-013-0991-6

Villarroya-Beltri, C., Gutiérrez-Vázquez, C., Sánchez-Madrid, F., and Mittelbrunn, M. (2013). Analysis of microRNA and protein transfer by exosomes during an immune synapse. *Methods Mol. Biol.* 1024, 41–51. doi: 10.1007/978-1-62703-453-1_4

Wells, J. E., Rice, T. K., Nuttall, R. K., Edwards, D. R., Zekki, H., Rivest, S., et al. (2003). An adverse role for matrix metalloproteinase 12 after spinal cord injury in mice. *J. Neurosci.* 23, 10107–10115. doi: 10.1523/jneurosci.23-31-10107.2003

Wolburg, H., and Lippoldt, A. (2002). Tight junctions of the blood–brain barrier: development, composition and regulation. *Vascul. Pharmacol.* 38, 323–337.

Wu, Q., Jing, Y., Yuan, X., Li, B., Wang, B., Liu, M., et al. (2015). The distinct abilities of tube-formation and migration between brain and spinal cord microvascular pericytes in rats. *Clin. Hemorheol. Microcirc.* 60, 231–240. doi: 10.3233/CH-141856

Wyatt, L. A., and Keirstead, H. S. (2012). Stem cell-based treatments for spinal cord injury. *Prog. Brain Res.* 201, 233–252. doi: 10.1016/B978-0-444-59544-7.00012-3

Xin, H., Li, Y., Buller, B., Katakowski, M., Zhang, Y., Wang, X., et al. (2012). Exosome-mediated transfer of miR-133b from multipotent mesenchymal stromal cells to neural cells contributes to neurite outgrowth. *Stem Cells* 30, 1556–1564. doi: 10.1002/stem.1129

Yuan, X., Li, B., Li, H., and Xiu, R. (2011). Melatonin inhibits IL-1β-induced monolayer permeability of human umbilical vein endothelial cells via Rac activation. *J. Pineal Res.* 51, 220–225. doi: 10.1111/j.1600-079x.2011.00882.x

Yuan, X., Wu, Q., Liu, X., Zhang, H., and Xiu, R. (2018). Transcriptomic profile analysis of brain microvascular pericytes in spontaneously hypertensive rats by RNA-Seq. *Am. J. Transl. Res.* 10, 2372–2386.

Yuan, X. C., Wang, P., Li, H. W., Wu, Q. B., Zhang, X. Y., Li, B. W., et al. (2017). Effects of melatonin on spinal cord injury-induced oxidative damage in mice testis. *Andrologia* 49:e12692. doi: 10.1111/and.12692

Zhang, J., Cui, Z., Feng, G., Bao, G., Xu, G., Sun, Y., et al. (2015). RBM5 and p53 expression after rat spinal cord injury: implications for neuronal apoptosis. *Int. J. Biochem. Cell Biol.* 60, 43–52. doi: 10.1016/j.biocel.2014.12.020

Zomer, A., Vendrig, T., Hopmans, E. S., van Eijndhoven, M., Middeldorp, J. M., Pegtel, D. M., et al. (2010). Exosomes: fit to deliver small RNA. *Commun. Integr. Biol.* 3, 447–450. doi: 10.4161/cib.3.5.12339

Conflict of Interest Statement: The authors declare that the research was conducted in the absence of any commercial or financial relationships that could be construed as a potential conflict of interest.

frontiers in Neuroscience

REVIEW
published: 18 April 2019
doi: 10.3389/fnins.2019.00381

The Roles of Post-translational Modifications on α-Synuclein in the Pathogenesis of Parkinson's Diseases

*Jiaming Zhang[1], Xiaoping Li[1] and Jia-Da Li[2,3]**

[1] Center for Reproductive Medicine, The First Affiliated Hospital, University of South China, Hengyang, China, [2] Hunan Key Laboratory of Animal Models for Human Diseases, School of Life Sciences, Central South University, Changsha, China, [3] Hunan Key Laboratory of Medical Genetics, Center for Medical Genetics, Central South University, Changsha, China

Parkinson's disease is the second most common neurodegenerative disorder. Although the pathogenesis of Parkinson's disease is not entirely clear, the aberrant aggregation of α-synuclein has long been considered as an important risk factor. Elucidating the mechanisms that influence the aggregation of α-synuclein is essential for developing an effective diagnostic, preventative and therapeutic strategy to treat this devastating disease. The aggregation of α-synuclein is influenced by several post-translational modifications. Here, we summarized the major post-translational modifications (phosphorylation, ubiquitination, truncation, nitration, *O*-GlcNAcylation) of α-synuclein and the effect of these modifications on α-synuclein aggregation, which may provide potential targets for future therapeutics.

Keywords: Parkinson's disease, α-synuclein, toxicity, post-translational modifications, aggregation

OPEN ACCESS

Edited by:
Andrei Surguchov, University of Kansas Medical Center, United States

Reviewed by:
George K. Tofaris, University of Oxford, United Kingdom
Matthew Robert Pratt, University of Southern California, United States
Kunikazu Tanji, Hirosaki University, Japan

***Correspondence:**
Jia-Da Li
lijiada@sklmg.edu.cn

Specialty section:
This article was submitted to Neurodegeneration, a section of the journal Frontiers in Neuroscience

Received: *24 January 2019*
Accepted: *02 April 2019*
Published: *18 April 2019*

Citation:
Zhang J, Li X and Li J-D (2019) The Roles of Post-translational Modifications on α-Synuclein in the Pathogenesis of Parkinson's Diseases. Front. Neurosci. 13:381. doi: 10.3389/fnins.2019.00381

INTRODUCTION

Parkinson's disease (PD), the second most common neurodegenerative disorder, manifests with resting tremor, bradykinesia, rigidity, postural instability, and gait impairment (Auluck et al., 2010; Tysnes and Storstein, 2017). PD is characterized by loss of dopaminergic neuronal cells in the substantia nigra pars compacta (SNpc) and cytoplasmic deposition of amyloid-like aggregates termed Lewy Bodies (LB) (Forno, 1996; Braak et al., 2003; Shulman et al., 2011).

The major component of LB is α-synuclein aggregates (Spillantini et al., 1997). Furthermore, duplications, triplications, or point mutations in α-synuclein also contribute to some autosomal dominant early-onset PDs and sporadic PDs (Golbe et al., 1990; Polymeropoulos et al., 1997; Kruger et al., 1998; Singleton et al., 2003, 2004; Farrer et al., 2004; Zarranz et al., 2004; Hoffman-Zacharska et al., 2013; Proukakis et al., 2013; Pasanen et al., 2014; Ysselstein et al., 2017). Golbe et al. (1990) identified the α-synuclein A53T mutation in a PD patient. Several other mutations have been identified since then, such as A30P, A18T, A29S, E46K, H50Q, G51D, and A53E.

The contribution of α-synuclein in the pathogenesis of PD has been extensively studied in a variety of animal models, including mice, Drosophila, and *Caenorhabditis elegans*. Transgenic mice or flies overexpressing WT, A30P or A53T α-synuclein show motor deficits and neuronal inclusions (Feany and Bender, 2000; Kahle et al., 2000; Masliah et al., 2000; van der Putten et al., 2000; Maguire-Zeiss et al., 2005; Lelan et al., 2011; Lin et al., 2012). The α-synuclein aggregates in dopaminergic neurons are found in WT, A30P, or A53T human α-synuclein transgenic nematodes *C. elegans*

(Kuwahara et al., 2006). Overexpression of human α-synuclein in *C. elegans* causes age- and dose-dependent dopaminergic neurodegeneration (Cao et al., 2005; Hamamichi et al., 2008).

α-Synuclein also undergoes extensive post-translational modification (PTM), which influence the aggregation and/or cytotoxicity. PTMs may mediate the environmental factors on the pathogenesis. In this review, we will summarize physiological and pathological roles of α-synuclein, emphasizing the involvement of PTMs.

STRUCTURE OF α-SYNUCLEIN

In humans, α-synuclein is a member of synuclein family, which includes α-synuclein, β-synuclein, and γ-synuclein (Lashuel et al., 2013). α-Synuclein, a 140-amino acid protein, is composed of three distinct domains. The N-terminus (1–60 residues) contains four imperfect KTKEGV motif repeats. The central hydrophobic domain of α-synuclein (61–95 residues), also known as the non-amyloid component (NAC), is crucial for its aggregation (Giasson et al., 2001). The C-terminus (96–140 residues) is enriched in acidic residues and is the major phosphorylation site (Uversky and Eliezer, 2009).

α-Synucleins purified from bacterial or mouse tissues under denaturing conditions are 'natively unfolded' monomers of about 14 kDa (Weinreb et al., 1996). It may acquire α-helical secondary structure upon binding to lipid vesicles (Davidson et al., 1998; Eliezer et al., 2001). Bartels et al. (2011) found that endogenous α-synuclein under non-denaturing conditions form a folded tetramer and non-crosslinked monomer in all cells, plus some putative dimers in the HeLa, HEK, and red blood cells. They further showed that very few native human α-synuclein tetramers form aggregation, whereas recombinantly expressed monomers readily aggregated into amyloid-like fibrils *in vitro* (Bartels et al., 2011).

FUNCTION OF α-SYNUCLEIN

α-Synuclein is mainly expressed at presynaptic terminals and has been implicated in numerous cellular processes (Adamczyk et al., 2005). However, the exact physiological function of α-synuclein is still unclear. Under physiological conditions, α-synuclein may be involved in the compartmentalization, storage, and recycling of neurotransmitters (Allen Reish and Standaert, 2015).

Soluble *N*-ethylmaleimide-sensitive factor attachment protein receptor (SNARE) proteins are crucial for release of neurotransmitters at the neuronal synapse, vesicle recycling, and synaptic integrity (Goda, 1997; Gerst, 1999). Burre et al. (2010) demonstrated that α-synuclein acts as a molecular chaperone to assist the folding and refolding of SNARE proteins. α-Synuclein directly binds to the SNARE protein synaptobrevin-2 and promote the formation of SNARE-complex (Burre et al., 2010). Moreover, α-synuclein is also involved in the dynamics of synaptic vesicles (SVs) trafficking to control the amount of vesicles docked at the synapses during neurotransmitter release (Burre, 2015). As a result, α-synuclein null mice exhibit accelerated recovery of neurotransmitter release when presented with multiple stimuli. Depletion of α-synuclein from rodent hippocampal neurons also induces a significant loss of undocked SVs (Cabin et al., 2002).

AGGREGATION OF α-SYNUCLEIN

Aggregates of α-synuclein are the major component of Lewy body, the pathological marker of PD, dementia with Lewy bodies and Lewy body variant of Alzheimer's disease (Spillantini et al., 1997, 1998). The aggregation of α-synuclein is formed in three steps. The first step is the rate-limiting step, in which the soluble unstructured monomeric species were converted into partially soluble oligomers when nucleation-dependent chain polymerization occurs. Then, the oligomers aggregate into insoluble mature fibrils. At last, the amyloid fibrillar aggregates are formed (Harper et al., 1997; Walsh et al., 1997; Lambert et al., 1998). Miake et al. (2002) have shown that α-synuclein filaments assembled *in vitro* or extracted from multiple system atrophy (MSA) brains are insoluble to detergents and partially resistant to proteinase K (PK) digestion. Variable amounts of neuritic PK-resistant α-synuclein have been detected in the striatum of all the LB disease cases. PK resistance of α-synuclein may be useful for the development of biomarkers of LB diseases (Neumann et al., 2004).

Both fibrils and oligomers have been shown to display toxicity. Peelaerts et al. (2015) showed that α-synuclein fibrils can lead to progressive motor impairment and cell death. Lots of studies have suggested that amyloids associated with neurodegenerative diseases spread in a prion-like fashion. Fibrillar α-synuclein assemblies seed the aggregation of monomeric α-synuclein *in vitro* and spread from one cell to another in cell cultures and animal models (Wood et al., 1999; Desplats et al., 2009; Hansen et al., 2011). Multiple lines of evidence have also suggested that oligomeric species of α-synuclein are toxic. In this review, we mainly summarized the evidence supporting the toxicity of α-synuclein oligomers in PD and possible mechanisms for this toxicity.

TOXICITY OF α-SYNUCLEIN

α-Synuclein aggregates may cause cytotoxicity through several pathways, such as mitochondrial dysfunction, endoplasmic reticulum (ER) stress, proteasome system dysfunction, phagocytosis and inflammatory response in microglia, membrane damage, and synaptic dysfunction.

Mitochondrial Dysfunction

The loss of dopaminergic neurons is a major pathological feature of PD patient. Dopaminergic neurons are particularly sensitive to mitochondrial dysfunction due to their high energy demands and increased oxidative stress (Ryan et al., 2015). Both the monomer and oligomer of α-synuclein show toxicity to mitochondria. The translocase of the outer membrane (TOM) 20 receptors are important for the mitochondrial protein import. α-Synuclein

can inhibit the protein import of mitochondria by binding to TOM20 (Di Maio et al., 2016). The voltage-dependent anion channel (VDAC) is the major channel of the mitochondrial outer membrane, which controls most of the metabolite fluxes in and out of the mitochondria. Rostovtseva et al. (2015) showed that monomeric α-synuclein reversibly block VDAC in a highly voltage-dependent manner.

α-Synuclein oligomers cause mitochondria fragmentation in a dopaminergic cell line SH-SY5Y (Plotegher et al., 2014). α-Synuclein oligomers decreased the retention time of exogenously added calcium, promoted calcium-induced mitochondrial swelling and depolarization. α-Synuclein oligomers also accelerated cytochrome C release, which cause the apoptosis of dopaminergic neurons (Luth et al., 2014).

Endoplasmic Reticulum Stress

Endoplasmic reticulum is responsible for the synthesis, modification, and delivery of proteins to their target sites within the secretory pathway and the extracellular space. Disruption of any of these processes may cause ER stress (Hampton, 2000). The folding-incompetent proteins can cause ER stress and an ER stress response, called unfolded protein response (UPR). UPR is the biochemical basis for many ER storage diseases (Schroder and Kaufman, 2005). Castillo-Carranza et al. (2012) showed that α-synuclein oligomers induced ER stress in SH-SY5Y cells. Colla et al. (2012) found that accumulation of the toxic α-synuclein oligomers are temporally and spatially linked to the induction of chronic ER stress in the α-synuclein transgenic mice.

Proteasome System Dysfunction

Ubiquitin proteasome system is a highly regulated mechanism of intracellular protein degradation and turnover (Tanaka and Chiba, 1998). PD patients have a vulnerable proteasomal function in the substantia nigra, which may be due to the inhibition of α-synuclein oligomers on the proteasomal system (McNaught and Jenner, 2001; McNaught et al., 2001, 2002, 2003). Indeed, α-synuclein is co-localized with ubiquitin and 20S proteasomal components in Lewy bodies. The α-synuclein oligomers may directly bind to the 20S proteasome. Binding of α-synuclein oligomers to the proteasome inhibits the chymotrypsin-like proteasomal activity of the 20S proteolytic particle (Lindersson et al., 2004). Interestingly, A53T α-synuclein oligomers impaired the proteasomal activity in PC12 cells, which can be reversed by Congo Red, an inhibitor of α-synuclein oligomerization (Emmanouilidou et al., 2010).

Phagocytosis and Inflammatory Response in Microglia

Microglia are the resident macrophage cells in the central nervous system (CNS), involved in chemotaxis, phagocytosis, and secretion of a variety of cytokines and proteases. Microglia have a close relationship with the pathogenesis of PD (Sanchez-Guajardo et al., 2015; Ferreira and Romero-Ramos, 2018). Park et al. (2008) found that microglial phagocytosis is enhanced by extracellular monomeric α-synuclein but inhibited by the aggregated α-synuclein. The inflammatory response in microglia is activated by Toll-like receptor 2 (TLR2) (Stirling et al., 2014). Kim et al. (2013) showed that extracellular α-synuclein released from neuronal cells is an endogenous agonist for TLR2.

Membrane Damage

The cell membrane is an important barrier to prevent extracellular substances from entering the cell, which ensures the relative stability of the intracellular environment and enables various biochemical reactions to run in an orderly manner. Membrane integrity is essential for the basic function of all cell types. Dysfunctional membranes can also lead to abnormal calcium homeostasis. α-Synuclein has been shown to undergo accelerated aggregation at membrane surfaces when incubated with synthetic or natural phospholipid vesicles or supported lipid bilayers, presumably because the two dimensional surface of the membrane increases the probability of molecular interactions needed for oligomerization (Haque et al., 2010). Danzer et al. (2007) showed some types of α-synuclein oligomers induced cell death via disruption of cellular calcium influx by a presumably pore-forming mechanism. Angelova et al. (2016) further confirmed that α-synuclein interacts with membranes to affect Ca2+ signaling in a structure-specific manner and the oligomeric β-sheet-rich α-synuclein species ultimately leads to Ca2+ dysregulation.

Several approaches have been developed to alleviate the α-synuclein-induced membrane damage. Endosulfine-α, which can bind specifically to membrane-associated α-synuclein, alleviates dopaminergic cell death by interfering with the formation of neurotoxic α-synuclein oligomers at the membrane surface (Ysselstein et al., 2017). A novel compound NPT100-18A, which can displace α-synuclein from the membrane, can also reduce a-synuclein toxicity (Wrasidlo et al., 2016).

Synaptic Dysfunction

Synaptic dysfunction is an early pathological feature of PD (Schulz-Schaeffer, 2010). SNARE complex is required for SV fusion. α-Synuclein oligomers prevent the formation of the SNARE complex by binding to synaptobrevin (Choi et al., 2013).

Axonal transport, which relies on the microtubule (MT) network, is fundamental for the maintenance of neuronal homeostasis (Goldstein et al., 2008). Prots et al. (2013) showed that α-synuclein oligomers significantly inhibited MT assembly. 3,4-Dihydroxyphenylacetaldehyde (DOPAL) is a catabolite generated from dopamine by monoamine oxidase (Burke et al., 2003; Goldstein et al., 2011). It has been shown that DOPAL can cause α-synuclein oligomerization *in vitro* and in cell models (Burke et al., 2008; Lima et al., 2018). Plotegher et al. (2017) showed that this kind of α-synuclein-DOPAL oligomers can permeabilize cholesterol-containing lipid membranes mimicking SVs *in vitro*, which suggests that the synergistic effect of α-synuclein and DOPAL accumulation in DA neurons may lead to the formation of oligomers, negatively impacting the structure and function of SVs.

Vesicles for synaptic release are produced by the Golgi apparatus. The dysfunction of Golgi can lead to abnormity

of synaptic function. Gosavi et al. (2002) showed that over-expression of α-synuclein in COS-7 cells caused Golgi fragmentation. As mentioned previously, pore-like oligomers of α-synuclein could also rupture SVs, leading to decreased neurotransmitter release, as well as permeabilization of cell membranes, which could result in Ca2+ influx and excitotoxicity (Danzer et al., 2007).

POST-TRANSLATIONAL MODIFICATIONS OF α-SYNUCLEIN

α-Synuclein is subjected to extensive post-transcriptional modifications (PTMs), including phosphorylation, ubiquitination, nitration, truncation, and *O*-GlcNAcylation. PTMs of α-synuclein may influence its toxicity and aggregation.

Phosphorylation

α-Synuclein within LB can be phosphorylated at serine 129 and 87 (S129-P, S87-P) (Hasegawa et al., 2002; Anderson et al., 2006; Paleologou et al., 2010). S129-P has emerged as a defining hallmark of PD and related synucleinopathies. Feany and Bender (2000) showed that α-synuclein is also phosphorylated at tyrosine 125, 133, and 136 (Y125-P, Y133-P, and Y136-P) (Ellis et al., 2001; Nakamura et al., 2001; Ahn et al., 2002; Negro et al., 2002; Takahashi et al., 2003). The kinases that mediate phosphorylation at Y125 of α-synuclein are still unknown. Hejjaoui et al. (2011) have developed a semi-synthetic strategy that enables the site-specific introduction of single phosphorylation at Y125. They showed that phosphorylation at Y125 does not affect the fibrillization of α-synuclein (Burai et al., 2015). The impact of the phosphorylation at tyrosine 133 and 135 on α-synuclein aggregation is still unknown.

A number of kinases have been shown to phosphorylate α-synuclein at S129 *in vitro*, including casein kinase I (CKI), casein kinase II (CKII), the G protein-coupled receptor kinases (GRK), LRRK2, and polo-like kinases (PLK) (Okochi et al., 2000; Pronin et al., 2000; Inglis et al., 2009).

Fujiwara et al. (2002) showed that phosphorylation of S129 in α-synuclein by CKII promotes *in vitro* fibrillation. Smith et al. (2005) indicated that phosphorylation at S-129 by CKII promotes the formation of cytoplasmic inclusions in some cell culture models.

Phosphorylation of α-synuclein at S-129 by GRK2 was reported to be toxic. Feany and Bender (2000) have studied the phosphorylation of α-synuclein in Drosophila. They showed that co-expression of Drosophila GRK2 with α-synuclein enhances the formation of α-synuclein oligomers and accelerates neuronal loss, as compared to the Drosophila expressing α-synuclein alone (Feany and Bender, 2000).

α-Synuclein phosphorylation at S129 is largely reduced in PLK2-/- transgenic mice, supporting the involvement of PLK in α-synuclein phosphorylation *in vivo* (Inglis et al., 2009). PLK2-induced phosphorylation has no effect on the aggregation of α-synuclein. Nevertheless, Oueslati et al. (2013) showed that PLK2 binds directly to α-synuclein in an ATP-dependent manner and regulates α-synuclein selective clearance via the lysosome–autophagic degradation pathway, which suggests a neuroprotective role of PLK2 against PD pathology.

Ubiquitination and Sumoylation

The core of LBs is immunoreactive for both α-synuclein and ubiquitin proteins and is surrounded by a rim of α-synuclein (Gomez-Tortosa et al., 2000). However, the major α-synuclein species in LBs is mono-, di-, and tri-ubiquitinated, suggesting the involvement of ubiquitination in the pathophysiologic properties of α-synuclein (Hasegawa et al., 2002; Sampathu et al., 2003; Tofaris et al., 2003; Nonaka et al., 2005). The ubiquitination of α-synuclein is correlated with three E3 ubiquitin-protein ligases: C-terminal U-box domain of co-chaperone Hsp70-interacting protein (CHIP), seven in absentia homolog (SIAH) and neuronal precursor cell-expressed, developmentally down-regulated gene 4 (Nedd4) (Liani et al., 2004; Shin et al., 2005; Tofaris et al., 2011).

The mammalian homologs of Drosophila seven in absentia (SIAH-1 and SIAH-2) gene have been characterized as a family of RING-type E3 ligases (Wheeler et al., 2002). Both *in vivo* and *in vitro* data showed that ubiquitination of α-synuclein by SIAH promotes the formation of inclusions. Rott et al. (2008) showed that ubiquitination of α-synuclein *in vitro* by SIAH promotes the formation of higher molecular weight α-synuclein. They then used electron microscopy to show that α-synuclein ubiquitinated by SIAH formed more aggregates (Rott et al., 2008). Lee et al. (2008) also showed that SIAH-1 or SIAH-2-mediated ubiquitination enhances the aggregation of α-synuclein and formation of α-synuclein-positive inclusion in PC12 cells and SH-SY5Y human neuroblastoma (Lee et al., 2008).

CHIP is a multidomain chaperone, utilizing both a tetratricopeptide/Hsp70 binding domain and a U-box/ubiquitin ligase domain to recognize misfolded proteins (Demand et al., 2001; Murata et al., 2001). CHIP is able to mono- and poly-ubiquitinate α-synuclein (Kalia et al., 2011). Shin et al. (2005) showed that CHIP colocalizes with α-synuclein in Lewy bodies and also in a cell culture model of α-synuclein inclusions. Overexpression of CHIP inhibits α-synuclein aggregation and increases α-synuclein degradation in cell culture. Interestingly, they also indicated that CHIP can regulate α-synuclein degradation both via the proteasomal degradation pathway and the lysosomal degradation pathway (Shin et al., 2005). A study from Tetzlaff et al. (2008) showed that CHIP selectively reduced α-synuclein oligomerization and toxicity in a tetratricopeptide domain-dependent, U-box independent manner by specifically degrading toxic α-synuclein oligomers.

Nedd4 is a HECT-domain E3 that functions at the plasma membrane in the turnover of a number of membrane-associated proteins. Tofaris et al. (2011) showed that Nedd4 can act as an E3 for α-synuclein. They demonstrated that Nedd4 directly binds to α-synuclein in brain and cell extracts and promotes the degradation of endogenous α-synuclein by lysosomes (Tofaris et al., 2011). They further found that Nedd4-mediated degradation protects against α-synuclein-induced toxicity in the Drosophila and rodent models of Parkinson's disease (Davies et al., 2014). Nedd4-1-linked

Lys-63 ubiquitination was demonstrated to specify the fate of extrinsic and *de novo* synthesized α-synuclein by facilitating their targeting to endosomes (Sugeno et al., 2014). In yeast ubiquitin ligase, the Nedd4 ortholog Rsp5 is a key enzyme involved in the degradation of abnormal or unfavorable proteins. Wijayanti et al. (2015) have isolated novel hyperactive forms of Rsp5 that alleviate α-synuclein toxicity, by enhancing the clearance of α-synuclein, including the processes of interaction, ubiquitination, and degradation.

The site-specific effects of ubiquitination on aggregation and clearance have been studied using a semi-synthetic strategy (Hejjaoui et al., 2011; Abeywardana et al., 2013). Monomeric ubiquitination of α-synuclein at K6 was shown to resist fibril formation when compared to unmodified protein (Hejjaoui et al., 2011); Ubiquitination of α-synuclein at K10 and K23 readily form fibrils; Ubiquitination of α-synuclein at K6, K12, and K21 moderately inhibit the formation of fibrils; Ubiquitination of α-synuclein at K32, K34, K43, and K96 displayed no fibril formation, suggesting a strong inhibitory effect (Meier et al., 2012). Haj-Yahya et al. (2013) have incorporated K48-linked di- or tetra-Ub chains onto the side chain of Lys12 of α-synuclein and demonstrated that the length of the Ub chain plays an important role in regulating α-synuclein fibril formation and clearance.

α-Synuclein is also conjugated to small ubiquitin-like modifier (SUMO) at lysines. Rott et al. (2017) demonstrated that α-synuclein is SUMOylated by PIAS2, and SUMOylated α-synuclein and PIAS2 are markedly elevated in the substantia nigra of PD brains. Further, Lewy bodies are positive for both SUMO1 and PIAS2. They found that SUMOylation increases α-synuclein aggregation by two self-reinforcing mechanisms. First, SUMOylation by PIAS2 directly promotes the aggregation of α-synuclein. Second, SUMOylation impairs α-synuclein ubiquitination and prevents α-synuclein degradation. Therefore, SUMOylation blockers may provide a strategy to prevent intracellular α-synuclein aggregation (Rott et al., 2017). However, Krumova et al. (2011) showed that sumoylation inhibits α-synuclein aggregation and toxicity. *In vitro* study demonstrated that SUMOylation at K102 of α-synuclein results in more pronounced inhibition of aggregation than the corresponding modification at K96 (Abeywardana and Pratt, 2015).

Truncation

Besides full-length α-synuclein, there exist small amounts of various truncated species with apparent molecular masses of 10–15 kDa in the LBs (Baba et al., 1998; Crowther et al., 1998; Campbell et al., 2001). It is estimated that about 15% α-synuclein in LBs is truncated. And the C-terminally truncated α-synuclein may act as effective seeds to accelerate the aggregation of the full-length protein.

The carboxyl-terminal-truncated α-synuclein produced by aberrant proteolysis, is found in association with α-synuclein aggregates (Tofaris et al., 2003). Tofaris et al. (2003) investigated the effects of truncation by generating both transgenic Drosophila and transgenic mice expressing human α-synuclein. They found that the truncated form of α-synuclein (1–120) increased accumulation of high molecular weight α-synuclein species, and enhanced neurotoxicity *in vivo* (Periquet et al., 2007). They showed that the striatal dopamine levels are reduced and the transgenic mice showed a progressive reduction in spontaneous locomotion and an increased response to amphetamine (Tofaris et al., 2006). Hoyer et al. (2004) used recombinant proteins and showed that the fragments (1–110; 1–119; 110–140) promoting nucleation seed the aggregation of full-length α-synuclein. Murray et al. (2003) also showed that the truncated α-synuclein variants, 1–89, 1–102, 1–110, 1–120, and 1–130 aggregated more rapidly than the full-length protein.

Several enzymes have been implicated in the truncation of α-synuclein, including calpain I, Neurosin, Cathepsin D, and Matrix metalloproteinase 3 (Iwata et al., 2003; Mishizen-Eberz et al., 2005; Sevlever et al., 2008; Choi et al., 2011).

Since α-synuclein is predominantly localized to the pre-synaptic terminal, it may be a substrate for soluble or membrane-associated proteases such as the calcium-activated neutral protease calpain I. Mishizen-Eberz et al. (2003) demonstrated that Calpain I cleaves wild-type α-synuclein predominantly after amino acid 57 and within the NAC region (73, 74, and 83). Calpain-mediated processing of soluble α-synuclein inhibits fibrillization, while processing of fibrillar α-synuclein promotes further aggregation (Mishizen-Eberz et al., 2005).

Neurosin, a serine protease predominantly expressed in the CNS, is presumed to play an important role in the degradation of α-synuclein (Iwata et al., 2003). Neurosin cleaves α-synuclein after amino acid 80 and 97. Cleavage of α-synuclein after 80 by neurosin may inhibit the polymerization; however, the fragment cleaved after 97 has a stronger propensity to polymerize than non-processed α-synuclein (Kasai et al., 2008).

Nitration

Oxidative injury has been implicated in the pathogenesis of PD (Schapira and Jenner, 2011; Bose and Beal, 2016). The action of oxygen and nitric oxide and their products, especially peroxynitrite, leads to the nitration of tyrosine residues in proteins. Giasson et al. (2000) first showed that a-synuclein is nitrated when present in the major filamentous and in the insoluble fractions of affected brain regions of synucleinopathies. All four tyrosine residues in α-synuclein (Y39, Y125, Y133, and Y136) are susceptible to nitration (Sevcsik et al., 2011; Burai et al., 2015).

Danielson et al. (2009) showed that nitration of Y-39 accelerates the oligomerization of α-synuclein, and a mutation in this residue leads to high levels of fibrilization.

Hodara et al. (2004) showed that monomeric or dimeric forms of nitrated α-synuclein accelerate the fibril formation and seed the fibrillation of non-modified α-synuclein. On the other hand, nitrated α-synuclein oligomers inhibit the fibril formation (Hodara et al., 2004).

Through site-specific incorporation of 3-nitrotyrosine at different regions of α-synuclein, Burai et al. (2015) indicated that different site-specifically nitrated α-synuclein species exhibit distinct aggregation properties. They further showed that intermolecular interactions between the N- and C-terminal regions of α-synuclein play critical roles in mediating nitration-induced α-synuclein oligomerization (Burai et al., 2015).

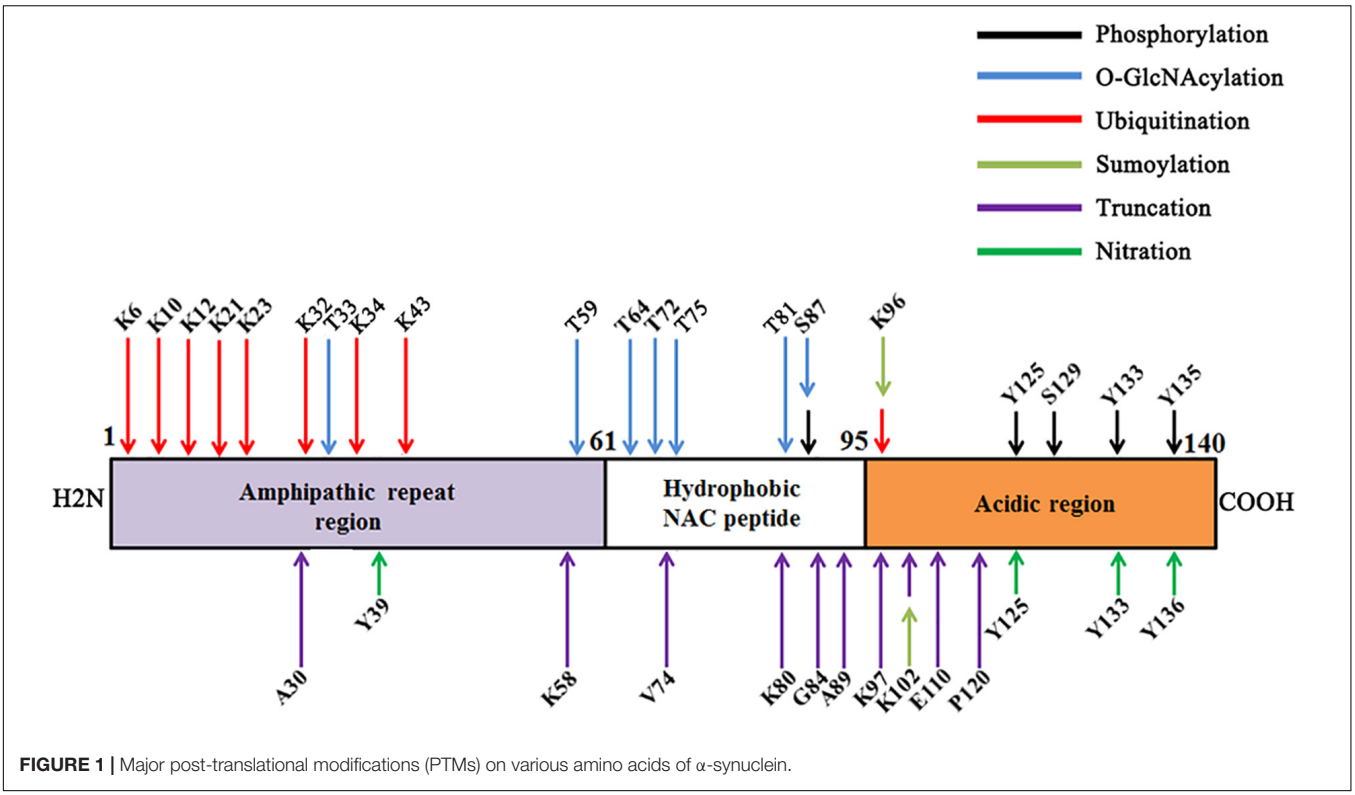

FIGURE 1 | Major post-translational modifications (PTMs) on various amino acids of α-synuclein.

TABLE 1 | Functional consequences of the major PTMs on α-synuclein.

PTM	Amino acid	Enzyme	Effects	References
Phosphorylation	S129	CKII	Promote aggregation	Fujiwara et al., 2002; Smith et al., 2005
	S129	GRK2	Promote oligomerization	Feany and Bender, 2000
	S129	PLK2	Promote degradation	Oueslati et al., 2013
Ubiquitination	K10, 12, 21, 23, 34, 43, 96	SIAH	Promote aggregation	Lee et al., 2008; Rott et al., 2008
		CHIP	Inhibit aggregation	Shin et al., 2005
			Promote degradation	Shin et al., 2005; Tetzlaff et al., 2008
Sumoylation	K96, 102	PIAS2	Promote aggregation	Rott et al., 2017
			Inhibit degradation	
Truncation	K58, V74	Calpain I	Inhibit aggregation	Mishizen-Eberz et al., 2005
	K80	Neurosin	Inhibit polymerization	Kasai et al., 2008
	K97	Neurosin	Promote polymerization	Kasai et al., 2008
Nitration	Y39, 125, 133, 136	–	Promote aggregation	Hodara et al., 2004
O-GlcNAcylation	T72, 75, 81, S87	OGT	Inhibit aggregation	Lewis et al., 2017; Levine et al., 2019

O-GlcNAcylation

O-GlcNAcylation is a dynamic biochemical process, in which *N*-acetylglucosamine (GlcNAc) from uridine 5′-diphospho-*N*-acetylglucosamine (UDP-GlcNAc) is transferred to the serine and threonine residues of proteins by *O*-GlcNAc transferase (OGT) and removed by *O*-GlcNAcase (OGA) (Hart et al., 2007). More than 1,000 proteins can be modified by *O*-GlcNAc, including molecular chaperones, transcription factors, RNA polymerase II, nucleoporin, RNA binding proteins, kinases, and cytoskeletal proteins (Hardiville and Hart, 2014). *O*-GlcNAcylation has identified threonine (T) residue 33, 34, 54, 59, 64, 72, 75, 81, and 87 of α-synuclein isolated from mouse and human samples (Wang et al., 2009, 2010, 2017; Alfaro et al., 2012; Morris et al., 2015).

To understand the effect of *O*-GlcNAcylation on the aggregation of α-synuclein, Marotta et al. (2015) synthesized a peptide of α-synuclein comprising residues 68–77, in which the T72 is *O*-GlcNAcylated. As compared with the unmodified peptide, the *O*-GlcNAcylated peptide inhibits full-length α-synuclein fibrillization. They further synthesized a full-length α-synuclein, with *O*-GlcNAcylation at T72. *O*-GlcNAcylation at T72 completely blocks the formation of both fiber and oligomer aggregates *in vitro*. They synthesized a full-length α-synuclein with *O*-GlcNAcylation at S87, which still aggregates but with

slower kinetics than the unmodified protein (Lewis et al., 2017). Recently, Levine et al. (2019) showed that several of the *O*-GlcNAc sites inhibit the toxicity of extracellular α-synuclein fibers that are likely culprits in the spread of PD. They also demonstrated that *O*-GlcNAcylation can inhibit the aggregation of an aggressive mutant of α-synuclein.

To study the functional consequences of enzymatic *O*-GlcNAcylation of α-synuclein, we co-expressed a shorter form of OGT (sOGT) and α-synuclein in bacteria and got enzymatically *O*-GlcNAcylated α-synuclein. The enzymatic *O*-GlcNAcylation also significantly blocked α-synuclein aggregation (Zhang et al., 2017).

CONCLUSION AND PERSPECTIVE

In this review, we have summarized the major PTMs of α-synuclein (**Figure 1**). Since the presence of PTMs in α-synuclein is able to influence its aggregation and toxicity (**Table 1**), targeting PTMs may be used to develop novel therapeutic approaches for PD. However, it should be noted that most of the effect of PTMs on the α-synuclein aggregation are carried out *in vitro*; the *in vivo* effect is still elusive. Furthermore, α-synuclein may have multiple different PTMs at the same time *in vivo*; however, the current researches regarding PTMs of α-synuclein are studied individually. The interaction of PTMs of α-synuclein has been widely studied. Phosphorylated α-synuclein has been reported to be one of the target proteins for ubiquitination in synucleinopathies (Hasegawa et al., 2002). Shahpasandzadeh et al. (2014), for the first time, demonstrated an interplay between α-synuclein sumoylation and phosphorylation to control protein turnover. They showed that sumoylation exhibits a protective role against α-synuclein toxicity and inclusion formation in yeast cells (Shahpasandzadeh et al., 2014). There is a complex and dynamic interplay between *O*-GlcNAcylation and phosphorylation (Hart et al., 2007). The interplay between α-synuclein *O*-GlcNAcylation and phosphorylation is still unknown. As mentioned before, neurosin is one enzyme that mediates the truncation of α-synuclein. Kasai et al. (2008) showed that phosphorylated α-synuclein was more resistant to degradation by neurosin than non-phosphorylated α-synuclein. A reciprocal reaction may also occur between other PTMs, which still need further study. Third, it is interesting that, in some cases, the same modification may have a different effect. For instance, phosphorylation at S129 by CKII may promote aggregation, but phosphorylation at S129 by PLK2 promotes degradation. More studies are required to understand the underlying mechanisms for the discrepancy. Lastly, although it is well known that PTMs are regulated by the environmental stimuli, few studies have attempted to use PTMs to link environmental factors and α-synuclein toxicity. Thus, future studies on the PTMs of α-synuclein *in vivo* will help to address these concerns, and improve our understanding surrounding the role of the gene-environment interaction in PD pathogenesis.

AUTHOR CONTRIBUTIONS

All authors participated in designing the concept of this manuscript.

FUNDING

This project was financially supported by National Natural Science Foundation of China (Grant Nos. 81770780 and 81728013), the Key Research and Development Programs from Hunan Province (Grant Nos. 2018DK2010 and 2018DK2013).

ACKNOWLEDGMENTS

We apologize to the authors whose work could not be cited in this review due to space limitations but appreciate all of the many contributions to the large body of literature we have tried to summarize here.

REFERENCES

Abeywardana, T., Lin, Y. H., Rott, R., Engelender, S., and Pratt, M. R. (2013). Site-specific differences in proteasome-dependent degradation of monoubiquitinated alpha-synuclein. *Chem. Biol.* 20, 1207–1213. doi: 10.1016/j.chembiol.2013.09.009

Abeywardana, T., and Pratt, M. R. (2015). Extent of inhibition of alpha-synuclein aggregation in vitro by SUMOylation is conjugation site- and SUMO isoform-selective. *Biochemistry* 54, 959–961. doi: 10.1021/bi501512m

Adamczyk, A., Solecka, J., and Strosznajder, J. B. (2005). Expression of alpha-synuclein in different brain parts of adult and aged rats. *J. Physiol. Pharmacol.* 56, 29–37.

Ahn, S., Kim, J., Lucaveche, C. L., Reedy, M. C., Luttrell, L. M., Lefkowitz, R. J., et al. (2002). Src-dependent tyrosine phosphorylation regulates dynamin self-assembly and ligand-induced endocytosis of the epidermal growth factor receptor. *J. Biol. Chem.* 277, 26642–26651. doi: 10.1074/jbc.M201499200

Alfaro, J. F., Gong, C. X., Monroe, M. E., Aldrich, J. T., Clauss, T. R., Purvine, S. O., et al. (2012). Tandem mass spectrometry identifies many mouse brain O-GlcNAcylated proteins including EGF domain-specific O-GlcNAc transferase targets. *Proc. Natl. Acad. Sci. U.S.A.* 109, 7280–7285. doi: 10.1073/pnas.1200425109

Allen Reish, H. E., and Standaert, D. G. (2015). Role of alpha-synuclein in inducing innate and adaptive immunity in Parkinson disease. *J. Parkinsons Dis.* 5, 1–19. doi: 10.3233/JPD-140491

Anderson, J. P., Walker, D. E., Goldstein, J. M., de Laat, R., Banducci, K., Caccavello, R. J., et al. (2006). Phosphorylation of Ser-129 is the dominant pathological modification of alpha-synuclein in familial and sporadic Lewy body disease. *J. Biol. Chem.* 281, 29739–29752. doi: 10.1074/jbc.M600933200

Angelova, P. R., Ludtmann, M. H., Horrocks, M. H., Negoda, A., Cremades, N., Klenerman, D., et al. (2016). Ca2+ is a key factor in alpha-synuclein-induced neurotoxicity. *J. Cell Sci.* 129, 1792–1801. doi: 10.1242/jcs.180737

Auluck, P. K., Caraveo, G., and Lindquist, S. (2010). alpha-Synuclein: membrane interactions and toxicity in Parkinson's disease. *Annu. Rev. Cell Dev. Biol.* 26, 211–233. doi: 10.1146/annurev.cellbio.042308.113313

Baba, M., Nakajo, S., Tu, P. H., Tomita, T., Nakaya, K., Lee, V. M., et al. (1998). Aggregation of alpha-synuclein in Lewy bodies of sporadic Parkinson's disease and dementia with Lewy bodies. *Am. J. Pathol.* 152, 879–884.

Bartels, T., Choi, J. G., and Selkoe, D. J. (2011). alpha-Synuclein occurs physiologically as a helically folded tetramer that resists aggregation. *Nature* 477, 107–110. doi: 10.1038/nature10324

Bose, A., and Beal, M. F. (2016). Mitochondrial dysfunction in Parkinson's disease. *J. Neurochem.* 139(Suppl. 1), 216–231. doi: 10.1111/jnc.13731

Braak, H., Del Tredici, K., Rub, U., de Vos, R. A., Jansen Steur, E. N., and Braak, E. (2003). Staging of brain pathology related to sporadic Parkinson's disease. *Neurobiol. Aging* 24, 197–211. doi: 10.1016/S0197-4580(02)00065-9

Burai, R., Ait-Bouziad, N., Chiki, A., and Lashuel, H. A. (2015). Elucidating the role of site-specific nitration of alpha-synuclein in the pathogenesis of Parkinson's disease via protein semisynthesis and mutagenesis. *J. Am. Chem. Soc.* 137, 5041–5052. doi: 10.1021/ja5131726

Burke, W. J., Kumar, V. B., Pandey, N., Panneton, W. M., Gan, Q., Franko, M. W., et al. (2008). Aggregation of alpha-synuclein by DOPAL, the monoamine oxidase metabolite of dopamine. *Acta Neuropathol.* 115, 193–203. doi: 10.1007/s00401-007-0303-9

Burke, W. J., Li, S. W., Williams, E. A., Nonneman, R., and Zahm, D. S. (2003). 3,4-Dihydroxyphenylacetaldehyde is the toxic dopamine metabolite in vivo: implications for Parkinson's disease pathogenesis. *Brain Res.* 989, 205–213. doi: 10.1016/S0006-8993(03)03354-7

Burre, J. (2015). The synaptic function of alpha-synuclein. *J. Parkinsons Dis.* 5, 699–713. doi: 10.3233/JPD-150642

Burre, J., Sharma, M., Tsetsenis, T., Buchman, V., Etherton, M. R., and Sudhof, T. C. (2010). Alpha-synuclein promotes SNARE-complex assembly in vivo and in vitro. *Science* 329, 1663–1667. doi: 10.1126/science.1195227

Cabin, D. E., Shimazu, K., Murphy, D., Cole, N. B., Gottschalk, W., McIlwain, K. L., et al. (2002). Synaptic vesicle depletion correlates with attenuated synaptic responses to prolonged repetitive stimulation in mice lacking alpha-synuclein. *J. Neurosci.* 22, 8797–8807. doi: 10.1523/JNEUROSCI.22-20-08797.2002

Campbell, B. C., McLean, C. A., Culvenor, J. G., Gai, W. P., Blumbergs, P. C., Jakala, P., et al. (2001). The solubility of alpha-synuclein in multiple system atrophy differs from that of dementia with Lewy bodies and Parkinson's disease. *J. Neurochem.* 76, 87–96. doi: 10.1046/j.1471-4159.2001.00021.x

Cao, S., Gelwix, C. C., Caldwell, K. A., and Caldwell, G. A. (2005). Torsin-mediated protection from cellular stress in the dopaminergic neurons of *Caenorhabditis elegans*. *J. Neurosci.* 25, 3801–3812. doi: 10.1523/JNEUROSCI.5157-04.2005

Castillo-Carranza, D. L., Zhang, Y., Guerrero-Munoz, M. J., Kayed, R., Rincon-Limas, D. E., and Fernandez-Funez, P. (2012). Differential activation of the ER stress factor XBP1 by oligomeric assemblies. *Neurochem. Res.* 37, 1707–1717. doi: 10.1007/s11064-012-0780-7

Choi, B. K., Choi, M. G., Kim, J. Y., Yang, Y., Lai, Y., Kweon, D. H., et al. (2013). Large alpha-synuclein oligomers inhibit neuronal SNARE-mediated vesicle docking. *Proc. Natl. Acad. Sci. U.S.A.* 110, 4087–4092. doi: 10.1073/pnas.1218424110

Choi, D. H., Kim, Y. J., Kim, Y. G., Joh, T. H., Beal, M. F., and Kim, Y. S. (2011). Role of matrix metalloproteinase 3-mediated alpha-synuclein cleavage in dopaminergic cell death. *J. Biol. Chem.* 286, 14168–14177. doi: 10.1074/jbc.M111.222430

Colla, E., Coune, P., Liu, Y., Pletnikova, O., Troncoso, J. C., Iwatsubo, T., et al. (2012). Endoplasmic reticulum stress is important for the manifestations of alpha-synucleinopathy in vivo. *J. Neurosci.* 32, 3306–3320. doi: 10.1523/JNEUROSCI.5367-11.2012

Crowther, R. A., Jakes, R., Spillantini, M. G., and Goedert, M. (1998). Synthetic filaments assembled from C-terminally truncated alpha-synuclein. *FEBS Lett.* 436, 309–312. doi: 10.1016/S0014-5793(98)01146-6

Danielson, S. R., Held, J. M., Schilling, B., Oo, M., Gibson, B. W., and Andersen, J. K. (2009). Preferentially increased nitration of alpha-synuclein at tyrosine-39 in a cellular oxidative model of Parkinson's disease. *Anal. Chem.* 81, 7823–7828. doi: 10.1021/ac901176t

Danzer, K. M., Haasen, D., Karow, A. R., Moussaud, S., Habeck, M., Giese, A., et al. (2007). Different species of alpha-synuclein oligomers induce calcium influx and seeding. *J. Neurosci.* 27, 9220–9232. doi: 10.1523/JNEUROSCI.2617-07.2007

Davidson, W. S., Jonas, A., Clayton, D. F., and George, J. M. (1998). Stabilization of alpha-synuclein secondary structure upon binding to synthetic membranes. *J. Biol. Chem.* 273, 9443–9449. doi: 10.1074/jbc.273.16.9443

Davies, S. E., Hallett, P. J., Moens, T., Smith, G., Mangano, E., Kim, H. T., et al. (2014). Enhanced ubiquitin-dependent degradation by NEDD4 protects against alpha-synuclein accumulation and toxicity in animal models of Parkinson's disease. *Neurobiol. Dis.* 64, 79–87. doi: 10.1016/j.nbd.2013.12.011

Demand, J., Alberti, S., Patterson, C., and Hohfeld, J. (2001). Cooperation of a ubiquitin domain protein and an E3 ubiquitin ligase during chaperone/proteasome coupling. *Curr. Biol.* 11, 1569–1577. doi: 10.1016/S0960-9822(01)00487-0

Desplats, P., Lee, H. J., Bae, E. J., Patrick, C., Rockenstein, E., Crews, L., et al. (2009). Inclusion formation and neuronal cell death through neuron-to-neuron transmission of alpha-synuclein. *Proc. Natl. Acad. Sci. U.S.A.* 106, 13010–13015. doi: 10.1073/pnas.0903691106

Di Maio, R., Barrett, P. J., Hoffman, E. K., Barrett, C. W., Zharikov, A., Borah, A., et al. (2016). alpha-Synuclein binds to TOM20 and inhibits mitochondrial protein import in Parkinson's disease. *Sci. Transl. Med.* 8:342ra78. doi: 10.1126/scitranslmed.aaf3634

Eliezer, D., Kutluay, E., Bussell, R. Jr., and Browne, G. (2001). Conformational properties of alpha-synuclein in its free and lipid-associated states. *J. Mol. Biol.* 307, 1061–1073. doi: 10.1006/jmbi.2001.4538

Ellis, C. E., Schwartzberg, P. L., Grider, T. L., Fink, D. W., and Nussbaum, R. L. (2001). alpha-synuclein is phosphorylated by members of the Src family of protein-tyrosine kinases. *J. Biol. Chem.* 276, 3879–3884. doi: 10.1074/jbc.M010316200

Emmanouilidou, E., Stefanis, L., and Vekrellis, K. (2010). Cell-produced alpha-synuclein oligomers are targeted to, and impair, the 26S proteasome. *Neurobiol. Aging* 31, 953–968. doi: 10.1016/j.neurobiolaging.2008.07.008

Farrer, M., Kachergus, J., Forno, L., Lincoln, S., Wang, D. S., Hulihan, M., et al. (2004). Comparison of kindreds with parkinsonism and alpha-synuclein genomic multiplications. *Ann. Neurol.* 55, 174–179. doi: 10.1002/ana.10846

Feany, M. B., and Bender, W. W. (2000). A *Drosophila* model of Parkinson's disease. *Nature* 404, 394–398. doi: 10.1038/35006074

Ferreira, S. A., and Romero-Ramos, M. (2018). Microglia response during Parkinson's disease: alpha-synuclein intervention. *Front. Cell. Neurosci.* 12:247. doi: 10.3389/fncel.2018.00247

Forno, L. S. (1996). Neuropathology of Parkinson's disease. *J. Neuropathol. Exp. Neurol.* 55, 259–272. doi: 10.1097/00005072-199603000-00001

Fujiwara, H., Hasegawa, M., Dohmae, N., Kawashima, A., Masliah, E., Goldberg, M. S., et al. (2002). alpha-Synuclein is phosphorylated in synucleinopathy lesions. *Nat. Cell Biol.* 4, 160–164. doi: 10.1038/ncb748

Gerst, J. E. (1999). SNAREs and SNARE regulators in membrane fusion and exocytosis. *Cell. Mol. Life Sci.* 55, 707–734. doi: 10.1007/s000180050328

Giasson, B. I., Duda, J. E., Murray, I. V., Chen, Q., Souza, J. M., Hurtig, H. I., et al. (2000). Oxidative damage linked to neurodegeneration by selective alpha-synuclein nitration in synucleinopathy lesions. *Science* 290, 985–989. doi: 10.1126/science.290.5493.985

Giasson, B. I., Murray, I. V., Trojanowski, J. Q., and Lee, V. M. (2001). A hydrophobic stretch of 12 amino acid residues in the middle of alpha-synuclein is essential for filament assembly. *J. Biol. Chem.* 276, 2380–2386. doi: 10.1074/jbc.M008919200

Goda, Y. (1997). SNAREs and regulated vesicle exocytosis. *Proc. Natl. Acad. Sci. U.S.A.* 94, 769–772. doi: 10.1073/pnas.94.3.769

Golbe, L. I., Di Iorio, G., Bonavita, V., Miller, D. C., and Duvoisin, R. C. (1990). A large kindred with autosomal dominant Parkinson's disease. *Ann. Neurol.* 27, 276–282. doi: 10.1002/ana.410270309

Goldstein, A. Y., Wang, X., and Schwarz, T. L. (2008). Axonal transport and the delivery of pre-synaptic components. *Curr. Opin. Neurobiol.* 18, 495–503. doi: 10.1016/j.conb.2008.10.003

Goldstein, D. S., Sullivan, P., Holmes, C., Kopin, I. J., Basile, M. J., and Mash, D. C. (2011). Catechols in post-mortem brain of patients with Parkinson disease. *Eur. J. Neurol.* 18, 703–710. doi: 10.1111/j.1468-1331.2010.03246.x

Gomez-Tortosa, E., Newell, K., Irizarry, M. C., Sanders, J. L., and Hyman, B. T. (2000). alpha-Synuclein immunoreactivity in dementia with Lewy bodies: morphological staging and comparison with ubiquitin immunostaining. *Acta Neuropathol.* 99, 352–357. doi: 10.1007/s004010051135

Gosavi, N., Lee, H. J., Lee, J. S., Patel, S., and Lee, S. J. (2002). Golgi fragmentation occurs in the cells with prefibrillar alpha-synuclein aggregates and precedes the formation of fibrillar inclusion. *J. Biol. Chem.* 277, 48984–48992. doi: 10.1074/jbc.M208194200

Haj-Yahya, M., Fauvet, B., Herman-Bachinsky, Y., Hejjaoui, M., Bavikar, S. N., Karthikeyan, S. V., et al. (2013). Synthetic polyubiquitinated alpha-Synuclein

reveals important insights into the roles of the ubiquitin chain in regulating its pathophysiology. *Proc. Natl. Acad. Sci. U.S.A.* 110, 17726–17731. doi: 10.1073/pnas.1315654110

Hamamichi, S., Rivas, R. N., Knight, A. L., Cao, S., Caldwell, K. A., and Caldwell, G. A. (2008). Hypothesis-based RNAi screening identifies neuroprotective genes in a Parkinson's disease model. *Proc. Natl. Acad. Sci. U.S.A.* 105, 728–733. doi: 10.1073/pnas.0711018105

Hampton, R. Y. (2000). ER stress response: getting the UPR hand on misfolded proteins. *Curr. Biol.* 10, R518–R521. doi: 10.1016/S0960-9822(00)00583-2

Hansen, C., Angot, E., Bergstrom, A. L., Steiner, J. A., Pieri, L., Paul, G., et al. (2011). alpha-Synuclein propagates from mouse brain to grafted dopaminergic neurons and seeds aggregation in cultured human cells. *J. Clin. Invest.* 121, 715–725. doi: 10.1172/JCI43366

Haque, F., Pandey, A. P., Cambrea, L. R., Rochet, J. C., and Hovis, J. S. (2010). Adsorption of alpha-synuclein on lipid bilayers: modulating the structure and stability of protein assemblies. *J. Phys. Chem. B* 114, 4070–4081. doi: 10.1021/jp1006704

Hardiville, S., and Hart, G. W. (2014). Nutrient regulation of signaling, transcription, and cell physiology by O-GlcNAcylation. *Cell Metab.* 20, 208–213. doi: 10.1016/j.cmet.2014.07.014

Harper, J. D., Lieber, C. M., and Lansbury, P. T. Jr. (1997). Atomic force microscopic imaging of seeded fibril formation and fibril branching by the Alzheimer's disease amyloid-beta protein. *Chem. Biol.* 4, 951–959. doi: 10.1016/S1074-5521(97)90303-3

Hart, G. W., Housley, M. P., and Slawson, C. (2007). Cycling of O-linked beta-N-acetylglucosamine on nucleocytoplasmic proteins. *Nature* 446, 1017–1022. doi: 10.1038/nature05815

Hasegawa, M., Fujiwara, H., Nonaka, T., Wakabayashi, K., Takahashi, H., Lee, V. M., et al. (2002). Phosphorylated alpha-synuclein is ubiquitinated in alpha-synucleinopathy lesions. *J. Biol. Chem.* 277, 49071–49076. doi: 10.1074/jbc.M208046200

Hejjaoui, M., Haj-Yahya, M., Kumar, K. S., Brik, A., and Lashuel, H. A. (2011). Towards elucidation of the role of ubiquitination in the pathogenesis of Parkinson's disease with semisynthetic ubiquitinated alpha-synuclein. *Angew. Chem. Int. Ed. Engl.* 50, 405–409. doi: 10.1002/anie.201005546

Hodara, R., Norris, E. H., Giasson, B. I., Mishizen-Eberz, A. J., Lynch, D. R., Lee, V. M., et al. (2004). Functional consequences of alpha-synuclein tyrosine nitration: diminished binding to lipid vesicles and increased fibril formation. *J. Biol. Chem.* 279, 47746–47753. doi: 10.1074/jbc.M408906200

Hoffman-Zacharska, D., Koziorowski, D., Ross, O. A., Milewski, M., Poznanski, J. A., Jurek, M., et al. (2013). Novel A18T and pA29S substitutions in alpha-synuclein may be associated with sporadic Parkinson's disease. *Parkinsonism Relat. Disord.* 19, 1057–1060. doi: 10.1016/j.parkreldis.2013.07.011

Hoyer, W., Cherny, D., Subramaniam, V., and Jovin, T. M. (2004). Impact of the acidic C-terminal region comprising amino acids 109-140 on alpha-synuclein aggregation in vitro. *Biochemistry* 43, 16233–16242. doi: 10.1021/bi048453u

Inglis, K. J., Chereau, D., Brigham, E. F., Chiou, S. S., Schobel, S., Frigon, N. L., et al. (2009). Polo-like kinase 2 (PLK2) phosphorylates alpha-synuclein at serine 129 in central nervous system. *J. Biol. Chem.* 284, 2598–2602. doi: 10.1074/jbc.C800206200

Iwata, A., Maruyama, M., Akagi, T., Hashikawa, T., Kanazawa, I., Tsuji, S., et al. (2003). Alpha-synuclein degradation by serine protease neurosin: implication for pathogenesis of synucleinopathies. *Hum. Mol. Genet.* 12, 2625–2635. doi: 10.1093/hmg/ddg283

Kahle, P. J., Neumann, M., Ozmen, L., Muller, V., Jacobsen, H., Schindzielorz, A., et al. (2000). Subcellular localization of wild-type and Parkinson's disease-associated mutant alpha -synuclein in human and transgenic mouse brain. *J. Neurosci.* 20, 6365–6373. doi: 10.1523/JNEUROSCI.20-17-06365.2000

Kalia, L. V., Kalia, S. K., Chau, H., Lozano, A. M., Hyman, B. T., and McLean, P. J. (2011). Ubiquitinylation of alpha-synuclein by carboxyl terminus Hsp70-interacting protein (CHIP) is regulated by Bcl-2-associated athanogene 5 (BAG5). *PLoS One* 6:e14695. doi: 10.1371/journal.pone.0014695

Kasai, T., Tokuda, T., Yamaguchi, N., Watanabe, Y., Kametani, F., Nakagawa, M., et al. (2008). Cleavage of normal and pathological forms of alpha-synuclein by neurosin in vitro. *Neurosci. Lett.* 436, 52–56. doi: 10.1016/j.neulet.2008.02.057

Kim, C., Ho, D. H., Suk, J. E., You, S., Michael, S., Kang, J., et al. (2013). Neuron-released oligomeric alpha-synuclein is an endogenous agonist of TLR2 for paracrine activation of microglia. *Nat. Commun.* 4:1562. doi: 10.1038/ncomms2534

Kruger, R., Kuhn, W., Muller, T., Woitalla, D., Graeber, M., Kosel, S., et al. (1998). Ala30Pro mutation in the gene encoding alpha-synuclein in Parkinson's disease. *Nat. Genet.* 18, 106–108. doi: 10.1038/ng0298-106

Krumova, P., Meulmeester, E., Garrido, M., Tirard, M., Hsiao, H. H., Bossis, G., et al. (2011). Sumoylation inhibits alpha-synuclein aggregation and toxicity. *J. Cell Biol.* 194, 49–60. doi: 10.1083/jcb.201010117

Kuwahara, T., Koyama, A., Gengyo-Ando, K., Masuda, M., Kowa, H., Tsunoda, M., et al. (2006). Familial Parkinson mutant alpha-synuclein causes dopamine neuron dysfunction in transgenic *Caenorhabditis elegans*. *J. Biol. Chem.* 281, 334–340. doi: 10.1074/jbc.M504860200

Lambert, M. P., Barlow, A. K., Chromy, B. A., Edwards, C., Freed, R., Liosatos, M., et al. (1998). Diffusible, nonfibrillar ligands derived from Abeta1-42 are potent central nervous system neurotoxins. *Proc. Natl. Acad. Sci. U.S.A.* 95, 6448–6453. doi: 10.1073/pnas.95.11.6448

Lashuel, H. A., Overk, C. R., Oueslati, A., and Masliah, E. (2013). The many faces of alpha-synuclein: from structure and toxicity to therapeutic target. *Nat. Rev. Neurosci.* 14, 38–48. doi: 10.1038/nrn3406

Lee, J. T., Wheeler, T. C., Li, L., and Chin, L. S. (2008). Ubiquitination of alpha-synuclein by Siah-1 promotes alpha-synuclein aggregation and apoptotic cell death. *Hum. Mol. Genet.* 17, 906–917. doi: 10.1093/hmg/ddm363

Lelan, F., Boyer, C., Thinard, R., Remy, S., Usal, C., Tesson, L., et al. (2011). Effects of human alpha-synuclein A53T-A30P mutations on SVZ and local olfactory bulb cell proliferation in a transgenic rat model of Parkinson disease. *Parkinsons Dis.* 2011:987084. doi: 10.4061/2011/987084

Levine, P. M., Galesic, A., Balana, A. T., Mahul-Mellier, A. L., Navarro, M. X., De Leon, C. A., et al. (2019). alpha-Synuclein O-GlcNAcylation alters aggregation and toxicity, revealing certain residues as potential inhibitors of Parkinson's disease. *Proc. Natl. Acad. Sci. U.S.A.* 116, 1511–1519. doi: 10.1073/pnas.1808845116

Lewis, Y. E., Galesic, A., Levine, P. M., De Leon, C. A., Lamiri, N., Brennan, C. K., et al. (2017). O-GlcNAcylation of alpha-synuclein at serine 87 reduces aggregation without affecting membrane binding. *ACS Chem. Biol.* 12, 1020–1027. doi: 10.1021/acschembio.7b00113

Liani, E., Eyal, A., Avraham, E., Shemer, R., Szargel, R., Berg, D., et al. (2004). Ubiquitylation of synphilin-1 and alpha-synuclein by SIAH and its presence in cellular inclusions and Lewy bodies imply a role in Parkinson's disease. *Proc. Natl. Acad. Sci. U.S.A.* 101, 5500–5505. doi: 10.1073/pnas.0401081101

Lima, V. A., do Nascimento, L. A., Eliezer, D., and Follmer, C. (2018). Role of Parkinson's disease-linked mutations and N-terminal acetylation on the oligomerization of alpha-synuclein induced by 3,4-dihydroxyphenylacetaldehyde. *ACS Chem. Neurosci.* doi: 10.1021/acschemneuro.8b00498 [Epub ahead of print].

Lin, X., Parisiadou, L., Sgobio, C., Liu, G., Yu, J., Sun, L., et al. (2012). Conditional expression of Parkinson's disease-related mutant alpha-synuclein in the midbrain dopaminergic neurons causes progressive neurodegeneration and degradation of transcription factor nuclear receptor related 1. *J. Neurosci.* 32, 9248–9264. doi: 10.1523/JNEUROSCI.1731-12.2012

Lindersson, E., Beedholm, R., Hojrup, P., Moos, T., Gai, W., Hendil, K. B., et al. (2004). Proteasomal inhibition by alpha-synuclein filaments and oligomers. *J. Biol. Chem.* 279, 12924–12934. doi: 10.1074/jbc.M306390200

Luth, E. S., Stavrovskaya, I. G., Bartels, T., Kristal, B. S., and Selkoe, D. J. (2014). Soluble, prefibrillar alpha-synuclein oligomers promote complex I-dependent, Ca2+-induced mitochondrial dysfunction. *J. Biol. Chem.* 289, 21490–21507. doi: 10.1074/jbc.M113.545749

Maguire-Zeiss, K. A., Short, D. W., and Federoff, H. J. (2005). Synuclein, dopamine and oxidative stress: co-conspirators in Parkinson's disease? *Brain Res. Mol. Brain Res.* 134, 18–23. doi: 10.1016/j.molbrainres.2004.09.014

Marotta, N. P., Lin, Y. H., Lewis, Y. E., Ambroso, M. R., Zaro, B. W., Roth, M. T., et al. (2015). O-GlcNAc modification blocks the aggregation and toxicity of the protein alpha-synuclein associated with Parkinson's disease. *Nat. Chem.* 7, 913–920. doi: 10.1038/nchem.2361

Masliah, E., Rockenstein, E., Veinbergs, I., Mallory, M., Hashimoto, M., Takeda, A., et al. (2000). Dopaminergic loss and inclusion body formation in alpha-synuclein mice: implications for neurodegenerative disorders. *Science* 287, 1265–1269. doi: 10.1126/science.287.5456.1265

McNaught, K. S., Belizaire, R., Isacson, O., Jenner, P., and Olanow, C. W. (2003). Altered proteasomal function in sporadic Parkinson's disease. *Exp. Neurol.* 179, 38–46. doi: 10.1006/exnr.2002.8050

McNaught, K. S., Belizaire, R., Jenner, P., Olanow, C. W., and Isacson, O. (2002). Selective loss of 20S proteasome alpha-subunits in the substantia nigra pars compacta in Parkinson's disease. *Neurosci. Lett.* 326, 155–158. doi: 10.1016/S0304-3940(02)00296-3

McNaught, K. S., and Jenner, P. (2001). Proteasomal function is impaired in substantia nigra in Parkinson's disease. *Neurosci. Lett.* 297, 191–194. doi: 10.1016/S0304-3940(00)01701-8

McNaught, K. S., Olanow, C. W., Halliwell, B., Isacson, O., and Jenner, P. (2001). Failure of the ubiquitin-proteasome system in Parkinson's disease. *Nat. Rev. Neurosci.* 2, 589–594. doi: 10.1038/35086067

Meier, F., Abeywardana, T., Dhall, A., Marotta, N. P., Varkey, J., Langen, R., et al. (2012). Semisynthetic, site-specific ubiquitin modification of alpha-synuclein reveals differential effects on aggregation. *J. Am. Chem. Soc.* 134, 5468–5471. doi: 10.1021/ja300094r

Miake, H., Mizusawa, H., Iwatsubo, T., and Hasegawa, M. (2002). Biochemical characterization of the core structure of alpha-synuclein filaments. *J. Biol. Chem.* 277, 19213–19219. doi: 10.1074/jbc.M110551200

Mishizen-Eberz, A. J., Guttmann, R. P., Giasson, B. I., Day, G. A. III, Hodara, R., Ischiropoulos, H., et al. (2003). Distinct cleavage patterns of normal and pathologic forms of alpha-synuclein by calpain I in vitro. *J. Neurochem.* 86, 836–847. doi: 10.1046/j.1471-4159.2003.01878.x

Mishizen-Eberz, A. J., Norris, E. H., Giasson, B. I., Hodara, R., Ischiropoulos, H., Lee, V. M., et al. (2005). Cleavage of alpha-synuclein by calpain: potential role in degradation of fibrillized and nitrated species of alpha-synuclein. *Biochemistry* 44, 7818–7829. doi: 10.1021/bi047846q

Morris, M., Knudsen, G. M., Maeda, S., Trinidad, J. C., Ioanoviciu, A., Burlingame, A. L., et al. (2015). Tau post-translational modifications in wild-type and human amyloid precursor protein transgenic mice. *Nat. Neurosci.* 18, 1183–1189. doi: 10.1038/nn.4067

Murata, S., Minami, Y., Minami, M., Chiba, T., and Tanaka, K. (2001). CHIP is a chaperone-dependent E3 ligase that ubiquitylates unfolded protein. *EMBO Rep.* 2, 1133–1138. doi: 10.1093/embo-reports/kve246

Murray, I. V., Giasson, B. I., Quinn, S. M., Koppaka, V., Axelsen, P. H., Ischiropoulos, H., et al. (2003). Role of alpha-synuclein carboxy-terminus on fibril formation in vitro. *Biochemistry* 42, 8530–8540. doi: 10.1021/bi027363r

Nakamura, T., Yamashita, H., Takahashi, T., and Nakamura, S. (2001). Activated Fyn phosphorylates alpha-synuclein at tyrosine residue 125. *Biochem. Biophys. Res. Commun.* 280, 1085–1092. doi: 10.1006/bbrc.2000.4253

Negro, A., Brunati, A. M., Donella-Deana, A., Massimino, M. L., and Pinna, L. A. (2002). Multiple phosphorylation of alpha-synuclein by protein tyrosine kinase Syk prevents eosin-induced aggregation. *FASEB J.* 16, 210–212. doi: 10.1096/fj.01-0517fje

Neumann, M., Muller, V., Kretzschmar, H. A., Haass, C., and Kahle, P. J. (2004). Regional distribution of proteinase K-resistant alpha-synuclein correlates with Lewy body disease stage. *J. Neuropathol. Exp. Neurol.* 63, 1225–1235. doi: 10.1093/jnen/63.12.1225

Nonaka, T., Iwatsubo, T., and Hasegawa, M. (2005). Ubiquitination of alpha-synuclein. *Biochemistry* 44, 361–368. doi: 10.1021/bi0485528

Okochi, M., Walter, J., Koyama, A., Nakajo, S., Baba, M., Iwatsubo, T., et al. (2000). Constitutive phosphorylation of the Parkinson's disease associated alpha-synuclein. *J. Biol. Chem.* 275, 390–397. doi: 10.1074/jbc.275.1.390

Oueslati, A., Schneider, B. L., Aebischer, P., and Lashuel, H. A. (2013). Polo-like kinase 2 regulates selective autophagic alpha-synuclein clearance and suppresses its toxicity in vivo. *Proc. Natl. Acad. Sci. U.S.A.* 110, E3945–E3954. doi: 10.1073/pnas.1309991110

Paleologou, K. E., Oueslati, A., Shakked, G., Rospigliosi, C. C., Kim, H. Y., Lamberto, G. R., et al. (2010). Phosphorylation at S87 is enhanced in synucleinopathies, inhibits alpha-synuclein oligomerization, and influences synuclein-membrane interactions. *J. Neurosci.* 30, 3184–3198. doi: 10.1523/JNEUROSCI.5922-09.2010

Park, J. Y., Paik, S. R., Jou, I., and Park, S. M. (2008). Microglial phagocytosis is enhanced by monomeric alpha-synuclein, not aggregated alpha-synuclein: implications for Parkinson's disease. *Glia* 56, 1215–1223. doi: 10.1002/glia.20691

Pasanen, P., Myllykangas, L., Siitonen, M., Raunio, A., Kaakkola, S., Lyytinen, J., et al. (2014). Novel alpha-synuclein mutation A53E associated with atypical multiple system atrophy and Parkinson's disease-type pathology. *Neurobiol. Aging* 35, 2180.e1–2180.e5. doi: 10.1016/j.neurobiolaging.2014.03.024

Peelaerts, W., Bousset, L., Van der Perren, A., Moskalyuk, A., Pulizzi, R., Giugliano, M., et al. (2015). alpha-Synuclein strains cause distinct synucleinopathies after local and systemic administration. *Nature* 522, 340–344. doi: 10.1038/nature14547

Periquet, M., Fulga, T., Myllykangas, L., Schlossmacher, M. G., and Feany, M. B. (2007). Aggregated alpha-synuclein mediates dopaminergic neurotoxicity in vivo. *J. Neurosci.* 27, 3338–3346. doi: 10.1523/JNEUROSCI.0285-07.2007

Plotegher, N., Berti, G., Ferrari, E., Tessari, I., Zanetti, M., Lunelli, L., et al. (2017). DOPAL derived alpha-synuclein oligomers impair synaptic vesicles physiological function. *Sci. Rep.* 7:40699. doi: 10.1038/srep40699

Plotegher, N., Gratton, E., and Bubacco, L. (2014). Number and Brightness analysis of alpha-synuclein oligomerization and the associated mitochondrial morphology alterations in live cells. *Biochim. Biophys. Acta* 1840, 2014–2024. doi: 10.1016/j.bbagen.2014.02.013

Polymeropoulos, M. H., Lavedan, C., Leroy, E., Ide, S. E., Dehejia, A., Dutra, A., et al. (1997). Mutation in the alpha-synuclein gene identified in families with Parkinson's disease. *Science* 276, 2045–2047. doi: 10.1126/science.276.5321.2045

Pronin, A. N., Morris, A. J., Surguchov, A., and Benovic, J. L. (2000). Synucleins are a novel class of substrates for G protein-coupled receptor kinases. *J. Biol. Chem.* 275, 26515–26522. doi: 10.1074/jbc.M003542200

Prots, I., Veber, V., Brey, S., Campioni, S., Buder, K., Riek, R., et al. (2013). alpha-Synuclein oligomers impair neuronal microtubule-kinesin interplay. *J. Biol. Chem.* 288, 21742–21754. doi: 10.1074/jbc.M113.451815

Proukakis, C., Dudzik, C. G., Brier, T., MacKay, D. S., Cooper, J. M., Millhauser, G. L., et al. (2013). A novel alpha-synuclein missense mutation in Parkinson disease. *Neurology* 80, 1062–1064. doi: 10.1212/WNL.0b013e31828727ba

Rostovtseva, T. K., Gurnev, P. A., Protchenko, O., Hoogerheide, D. P., Yap, T. L., Philpott, C. C., et al. (2015). alpha-synuclein shows high affinity interaction with voltage-dependent anion channel, suggesting mechanisms of mitochondrial regulation and toxicity in Parkinson disease. *J. Biol. Chem.* 290, 18467–18477. doi: 10.1074/jbc.M115.641746

Rott, R., Szargel, R., Haskin, J., Shani, V., Shainskaya, A., Manov, I., et al. (2008). Monoubiquitylation of alpha-synuclein by seven in absentia homolog (SIAH) promotes its aggregation in dopaminergic cells. *J. Biol. Chem.* 283, 3316–3328. doi: 10.1074/jbc.M704809200

Rott, R., Szargel, R., Shani, V., Hamza, H., Savyon, M., Abd Elghani, F., et al. (2017). SUMOylation and ubiquitination reciprocally regulate alpha-synuclein degradation and pathological aggregation. *Proc. Natl. Acad. Sci. U.S.A.* 114, 13176–13181. doi: 10.1073/pnas.1704351114

Ryan, B. J., Hoek, S., Fon, E. A., and Wade-Martins, R. (2015). Mitochondrial dysfunction and mitophagy in Parkinson's: from familial to sporadic disease. *Trends Biochem. Sci.* 40, 200–210. doi: 10.1016/j.tibs.2015.02.003

Sampathu, D. M., Giasson, B. I., Pawlyk, A. C., Trojanowski, J. Q., and Lee, V. M. (2003). Ubiquitination of alpha-synuclein is not required for formation of pathological inclusions in alpha-synucleinopathies. *Am. J. Pathol.* 163, 91–100. doi: 10.1016/S0002-9440(10)63633-4

Sanchez-Guajardo, V., Tentillier, N., and Romero-Ramos, M. (2015). The relation between alpha-synuclein and microglia in Parkinson's disease: recent developments. *Neuroscience* 302, 47–58. doi: 10.1016/j.neuroscience.2015.02.008

Schapira, A. H., and Jenner, P. (2011). Etiology and pathogenesis of Parkinson's disease. *Mov. Disord.* 26, 1049–1055. doi: 10.1002/mds.23732

Schroder, M., and Kaufman, R. J. (2005). ER stress and the unfolded protein response. *Mutat. Res.* 569, 29–63. doi: 10.1016/j.mrfmmm.2004.06.056

Schulz-Schaeffer, W. J. (2010). The synaptic pathology of alpha-synuclein aggregation in dementia with Lewy bodies, Parkinson's disease and Parkinson's disease dementia. *Acta Neuropathol.* 120, 131–143. doi: 10.1007/s00401-010-0711-0

Sevcsik, E., Trexler, A. J., Dunn, J. M., and Rhoades, E. (2011). Allostery in a disordered protein: oxidative modifications to alpha-synuclein act distally to regulate membrane binding. *J. Am. Chem. Soc.* 133, 7152–7158. doi: 10.1021/ja2009554

Sevlever, D., Jiang, P., and Yen, S. H. (2008). Cathepsin D is the main lysosomal enzyme involved in the degradation of alpha-synuclein and generation of

its carboxy-terminally truncated species. *Biochemistry* 47, 9678–9687. doi: 10.1021/bi800699v

Shahpasandzadeh, H., Popova, B., Kleinknecht, A., Fraser, P. E., Outeiro, T. F., and Braus, G. H. (2014). Interplay between sumoylation and phosphorylation for protection against alpha-synuclein inclusions. *J. Biol. Chem.* 289, 31224–31240. doi: 10.1074/jbc.M114.559237

Shin, Y., Klucken, J., Patterson, C., Hyman, B. T., and McLean, P. J. (2005). The co-chaperone carboxyl terminus of Hsp70-interacting protein (CHIP) mediates alpha-synuclein degradation decisions between proteasomal and lysosomal pathways. *J. Biol. Chem.* 280, 23727–23734. doi: 10.1074/jbc.M503326200

Shulman, J. M., De Jager, P. L., and Feany, M. B. (2011). Parkinson's disease: genetics and pathogenesis. *Annu. Rev. Pathol.* 6, 193–222. doi: 10.1146/annurev-pathol-011110-130242

Singleton, A., Gwinn-Hardy, K., Sharabi, Y., Li, S. T., Holmes, C., Dendi, R., et al. (2004). Association between cardiac denervation and parkinsonism caused by alpha-synuclein gene triplication. *Brain* 127(Pt 4), 768–772. doi: 10.1093/brain/awh081

Singleton, A. B., Farrer, M., Johnson, J., Singleton, A., Hague, S., Kachergus, J., et al. (2003). alpha-Synuclein locus triplication causes Parkinson's disease. *Science* 302:841. doi: 10.1126/science.1090278

Smith, W. W., Margolis, R. L., Li, X., Troncoso, J. C., Lee, M. K., Dawson, V. L., et al. (2005). Alpha-synuclein phosphorylation enhances eosinophilic cytoplasmic inclusion formation in SH-SY5Y cells. *J. Neurosci.* 25, 5544–5552. doi: 10.1523/JNEUROSCI.0482-05.2005

Spillantini, M. G., Crowther, R. A., Jakes, R., Hasegawa, M., and Goedert, M. (1998). alpha-Synuclein in filamentous inclusions of Lewy bodies from Parkinson's disease and dementia with Lewy bodies. *Proc. Natl. Acad. Sci. U.S.A.* 95, 6469–6473. doi: 10.1073/pnas.95.11.6469

Spillantini, M. G., Schmidt, M. L., Lee, V. M., Trojanowski, J. Q., Jakes, R., and Goedert, M. (1997). Alpha-synuclein in Lewy bodies. *Nature* 388, 839–840. doi: 10.1038/42166

Stirling, D. P., Cummins, K., Mishra, M., Teo, W., Yong, V. W., and Stys, P. (2014). Toll-like receptor 2-mediated alternative activation of microglia is protective after spinal cord injury. *Brain* 137(Pt 3), 707–723. doi: 10.1093/brain/awt341

Sugeno, N., Hasegawa, T., Tanaka, N., Fukuda, M., Wakabayashi, K., Oshima, R., et al. (2014). Lys-63-linked ubiquitination by E3 ubiquitin ligase NEDD4-1 facilitates endosomal sequestration of internalized alpha-synuclein. *J. Biol. Chem.* 289, 18137–18151. doi: 10.1074/jbc.M113.529461

Takahashi, M., Kanuka, H., Fujiwara, H., Koyama, A., Hasegawa, M., Miura, M., et al. (2003). Phosphorylation of alpha-synuclein characteristic of synucleinopathy lesions is recapitulated in alpha-synuclein transgenic *Drosophila*. *Neurosci. Lett.* 336, 155–158. doi: 10.1016/S0304-3940(02)01258-2

Tanaka, K., and Chiba, T. (1998). The proteasome: a protein-destroying machine. *Genes Cells* 3, 499–510. doi: 10.1046/j.1365-2443.1998.00207.x

Tetzlaff, J. E., Putcha, P., Outeiro, T. F., Ivanov, A., Berezovska, O., Hyman, B. T., et al. (2008). CHIP targets toxic alpha-Synuclein oligomers for degradation. *J. Biol. Chem.* 283, 17962–17968. doi: 10.1074/jbc.M802283200

Tofaris, G. K., Garcia Reitbock, P., Humby, T., Lambourne, S. L., O'Connell, M., Ghetti, B., et al. (2006). Pathological changes in dopaminergic nerve cells of the substantia nigra and olfactory bulb in mice transgenic for truncated human alpha-synuclein(1-120): implications for Lewy body disorders. *J. Neurosci.* 26, 3942–3950. doi: 10.1523/JNEUROSCI.4965-05.2006

Tofaris, G. K., Kim, H. T., Hourez, R., Jung, J. W., Kim, K. P., and Goldberg, A. L. (2011). Ubiquitin ligase NEDD4 promotes alpha-synuclein degradation by the endosomal-lysosomal pathway. *Proc. Natl. Acad. Sci. U.S.A.* 108, 17004–17009. doi: 10.1073/pnas.1109356108

Tofaris, G. K., Razzaq, A., Ghetti, B., Lilley, K. S., and Spillantini, M. G. (2003). Ubiquitination of alpha-synuclein in Lewy bodies is a pathological event not associated with impairment of proteasome function. *J. Biol. Chem.* 278, 44405–44411. doi: 10.1074/jbc.M308041200

Tysnes, O. B., and Storstein, A. (2017). Epidemiology of Parkinson's disease. *J. Neural Transm.* 124, 901–905. doi: 10.1007/s00702-017-1686-y

Uversky, V. N., and Eliezer, D. (2009). Biophysics of Parkinson's disease: structure and aggregation of alpha-synuclein. *Curr. Protein Pept. Sci.* 10, 483–499. doi: 10.2174/138920309789351921

van der Putten, H., Wiederhold, K. H., Probst, A., Barbieri, S., Mistl, C., Danner, S., et al. (2000). Neuropathology in mice expressing human alpha-synuclein. *J. Neurosci.* 20, 6021–6029. doi: 10.1523/JNEUROSCI.20-16-06021.2000

Walsh, D. M., Lomakin, A., Benedek, G. B., Condron, M. M., and Teplow, D. B. (1997). Amyloid beta-protein fibrillogenesis. Detection of a protofibrillar intermediate. *J. Biol. Chem.* 272, 22364–22372. doi: 10.1074/jbc.272.35.22364

Wang, S., Yang, F., Petyuk, V. A., Shukla, A. K., Monroe, M. E., Gritsenko, M. A., et al. (2017). Quantitative proteomics identifies altered O-GlcNAcylation of structural, synaptic and memory-associated proteins in Alzheimer's disease. *J. Pathol.* 243, 78–88. doi: 10.1002/path.4929

Wang, Z., Park, K., Comer, F., Hsieh-Wilson, L. C., Saudek, C. D., and Hart, G. W. (2009). Site-specific GlcNAcylation of human erythrocyte proteins: potential biomarker(s) for diabetes. *Diabetes* 58, 309–317. doi: 10.2337/db08-0994

Wang, Z., Udeshi, N. D., O'Malley, M., Shabanowitz, J., Hunt, D. F., and Hart, G. W. (2010). Enrichment and site mapping of O-linked N-acetylglucosamine by a combination of chemical/enzymatic tagging, photochemical cleavage, and electron transfer dissociation mass spectrometry. *Mol. Cell. Proteomics* 9, 153–160. doi: 10.1074/mcp.M900268-MCP200

Weinreb, P. H., Zhen, W., Poon, A. W., Conway, K. A., and Lansbury, P. T. Jr. (1996). NACP, a protein implicated in Alzheimer's disease and learning, is natively unfolded. *Biochemistry* 35, 13709–13715. doi: 10.1021/bi961799n

Wheeler, T. C., Chin, L. S., Li, Y., Roudabush, F. L., and Li, L. (2002). Regulation of synaptophysin degradation by mammalian homologues of seven in absentia. *J. Biol. Chem.* 277, 10273–10282. doi: 10.1074/jbc.M107857200

Wijayanti, I., Watanabe, D., Oshiro, S., and Takagi, H. (2015). Isolation and functional analysis of yeast ubiquitin ligase Rsp5 variants that alleviate the toxicity of human alpha-synuclein. *J. Biochem.* 157, 251–260. doi: 10.1093/jb/mvu069

Wood, S. J., Wypych, J., Steavenson, S., Louis, J. C., Citron, M., and Biere, A. L. (1999). alpha-synuclein fibrillogenesis is nucleation-dependent. Implications for the pathogenesis of Parkinson's disease. *J. Biol. Chem.* 274, 19509–19512. doi: 10.1074/jbc.274.28.19509

Wrasidlo, W., Tsigelny, I. F., Price, D. L., Dutta, G., Rockenstein, E., Schwarz, T. C., et al. (2016). A de novo compound targeting alpha-synuclein improves deficits in models of Parkinson's disease. *Brain* 139(Pt 12), 3217–3236. doi: 10.1093/brain/aww238

Ysselstein, D., Dehay, B., Costantino, I. M., McCabe, G. P., Frosch, M. P., George, J. M., et al. (2017). Endosulfine-alpha inhibits membrane-induced alpha-synuclein aggregation and protects against alpha-synuclein neurotoxicity. *Acta Neuropathol. Commun.* 5:3. doi: 10.1186/s40478-016-0403-7

Zarranz, J. J., Alegre, J., Gomez-Esteban, J. C., Lezcano, E., Ros, R., Ampuero, I., et al. (2004). The new mutation, E46K, of alpha-synuclein causes Parkinson and Lewy body dementia. *Ann. Neurol.* 55, 164–173. doi: 10.1002/ana.10795

Zhang, J., Lei, H., Chen, Y., Ma, Y. T., Jiang, F., Tan, J., et al. (2017). Enzymatic O-GlcNAcylation of alpha-synuclein reduces aggregation and increases SDS-resistant soluble oligomers. *Neurosci. Lett.* 655, 90–94. doi: 10.1016/j.neulet.2017.06.034

Conflict of Interest Statement: The authors declare that the research was conducted in the absence of any commercial or financial relationships that could be construed as a potential conflict of interest.

frontiers in Neuroscience

REVIEW
published: 16 May 2019
doi: 10.3389/fnins.2019.00463

S100 Proteins in Alzheimer's Disease

Joana S. Cristóvão[1,2] *and Cláudio M. Gomes*[1,2]*

[1] Biosystems and Integrative Sciences Institute, Faculdade de Ciências, Universidade de Lisboa, Lisbon, Portugal,
[2] Departamento de Química e Bioquímica, Universidade de Lisboa, Lisbon, Portugal

S100 proteins are calcium-binding proteins that regulate several processes associated with Alzheimer's disease (AD) but whose contribution and direct involvement in disease pathophysiology remains to be fully established. Due to neuroinflammation in AD patients, the levels of several S100 proteins are increased in the brain and some S100s play roles related to the processing of the amyloid precursor protein, regulation of amyloid beta peptide (Aβ) levels and Tau phosphorylation. S100 proteins are found associated with protein inclusions, either within plaques or as isolated S100-positive puncta, which suggests an active role in the formation of amyloid aggregates. Indeed, interactions between S100 proteins and aggregating Aβ indicate regulatory roles over the aggregation process, which may either delay or aggravate aggregation, depending on disease stage and relative S100 and Aβ levels. Additionally, S100s are also known to influence AD-related signaling pathways and levels of other cytokines. Recent evidence also suggests that metal-ligation by S100 proteins influences trace metal homeostasis in the brain, particularly of zinc, which is also a major deregulated process in AD. Altogether, this evidence strongly suggests a role of S100 proteins as key players in several AD-linked physiopathological processes, which we discuss in this review.

Keywords: neuroinflammation and neurodegeneration, amyloid-β, tau, metal ions, protein misfolding, aggregation

OPEN ACCESS

Edited by:
Natalia N. Nalivaeva, University of Leeds, United Kingdom

Reviewed by:
Estelle Leclerc, North Dakota State University, United States
Wieslawa Lesniak, Nencki Institute of Experimental Biology (PAS), Poland
Fabrizio Michetti, Catholic University of the Sacred Heart, Italy

***Correspondence:**
Cláudio M. Gomes
cmgomes@fc.ul.pt

Specialty section:
This article was submitted to Neurodegeneration, a section of the journal Frontiers in Neuroscience

Received: *07 January 2019*
Accepted: *24 April 2019*
Published: *16 May 2019*

Citation:
Cristóvão JS and Gomes CM (2019) S100 Proteins in Alzheimer's Disease. Front. Neurosci. 13:463. doi: 10.3389/fnins.2019.00463

PATHOLOGICAL FEATURES OF ALZHEIMER'S DISEASE

Alzheimer's disease (AD) is a chronic and progressive neurodegenerative disorder that affects wide areas of the cerebral cortex and hippocampus. Most AD patients (>95%) are idiopathic and disease is characterized by late onset (80–90 years of age) with failure in the clearance of amyloid-β peptide (Aβ) from the brain (Masters et al., 2015). The main symptoms of the disease are progressive memory deficits, cognitive impairment, and personality changes. The neuropathological and neurochemical hallmarks of AD include selective neuronal death, synaptic loss and the presence of proteinaceous deposits in the extracellular space (known as diffuse and neuritic plaques) as well as inside neurons [known as neurofibrillary tangles (NFTs)]. Neuroinflammation, oxidative stress, and calcium dysregulation are also important features implicated in AD pathology (Wang X. et al., 2014).

Diffuse and neuritic plaques, most commonly known as amyloid plaques, are mainly constituted by Aβ deposits, surrounded by degenerative presynaptic endings, astrocytes and microglial cells (Weiner and Frenkel, 2006). Aβ peptides are formed from proteolytic cleavage of the amyloid precursor protein (APP) by the γ- and β-secretases (BACE1). Even though the normal function of APP is not known, it is possibly related to regulation of neurite outgrowth, cell adhesion, and neuron migration (Turner et al., 2003). APP processing can involve non-amyloidogenic or

amyloidogenic pathways. When APP is cleaved by α-secretase and subsequently by γ-secretase, sAPPα is predominantly formed, which has an important role in neuronal plasticity and survival. However, in the amyloidogenic pathway, APP is cleaved by β- and γ-secretase producing sAPPβ, C-terminal fragments and Aβ peptides, which promote a range of detrimental effects in neurons and in the brain (Ling et al., 2003). Aβ40 and Aβ42 are the predominant accumulating peptides, whose aggregation into fibrillar cross-β structures is a central feature in AD pathogenesis. Aβ aggregation is naturally heterogeneous and monomers assemble and polymerize into structurally distinct forms, including protofibers, polymorphic oligomers and amyloid fibrils, all found within plaques. Extracellular accumulation of Aβ fibrils is not necessarily intrinsically cytotoxic and emerging evidence suggests precursor oligomers as the key toxic agents, also because of their seeding potential (Dahlgren et al., 2002; Walsh et al., 2002). Moreover, Aβ peptides can also be deposited intracellularly (Gouras et al., 2005).

The presence of neurofibrillar tangles, formed by neuronal intracellular deposition of hyperphosphorylated tau protein, is also a major AD hallmark. It has also been suggested that NFT may not be the major player in neurotoxicity, and that tau oligomers are in fact the major toxic forms promoting synaptic impairment (Tai et al., 2014; Fa et al., 2016). In agreement, it has been described that propagation of tau pathology occurs trans-synaptically (Liu et al., 2012). Other factors that contribute to tauophaties, besides tau hyperphosphorylation, are tau truncation, glycosylation, glycation, nitration, and ubiquitination (Chong et al., 2018).

Additionally, metal ion homeostasis and calcium signaling are also implicated in disease pathogenesis. In the early stages of AD, calcium imbalance promotes Aβ formation and tau hyperphosphorylation, as reviewed previously in LaFerla (2002). Aβ destabilizes neuronal calcium homeostasis generally leading to an increase in cytosolic calcium levels and formation of calcium-permeable pores. Calcium alterations lead to cytoskeletal modifications, triggering neuronal apoptosis and formation of free radicals through mitochondrial dysfunction. Moreover, familial AD mutations in presenilins are linked to altered synaptic Ca^{2+} signaling that imbalance the activities of Ca^{2+}-calmodulin-dependent kinase II (CaMKII) and Ca^{2+}-dependent phosphatase calcineurin (CaN), increasing the long-term depression and causing memory loss (Popugaeva et al., 2017). Transition metals such as Zn^{2+}, Cu^{2+}, and Fe^{2+} have well-established roles as chemical modulators of protein folding, amyloid aggregation and toxicity and are found to accumulate at protein deposits (Leal et al., 2012; Barnham and Bush, 2014; Cristovao et al., 2016).

Neuroinflammation is another cellular process linked to AD pathogenesis. Senile plaques are often closely associated with activated microglial cells and surrounded by activated astrocytes that have abundant filaments (Weiner and Frenkel, 2006). In response to Aβ deposition, activated microglia upregulate the expression of cell-surface proteins and cytokines such as the tumor-necrosis factor (TNF), interleukine-6 (IL-6), interleukine-1 (IL-1), S100 proteins, and chemokines. The presence of Aβ activates different cell receptors and intracellular signaling pathways, mainly those related to the receptor of advanced glycation end products (RAGE)/nuclear factor kappa-light-chain-enhancer of activated B cells (NF-κB) pathway, that is responsible for the transcription of pro-inflammatory cytokines and chemokines in astrocytes (Gonzalez-Reyes et al., 2017). Additionally, astrogliosis appears as an early manifestation of AD. The migration of astrocytes into Aβ plaques is promoted by chemokines CCL2 and CCL3, that are released by activated microglial cells surrounding amyloid plaques. Astrocytes recruited to Aβ plaques have the potential to mediate both neurotoxicity and participate in the clearance of Aβ (Weiner and Frenkel, 2006). S100 proteins are among the alarmins that are upregulated and are highly secreted by astrocytes during this process (Venegas and Heneka, 2017), which results in their accumulation within Aβ deposits and brain tissues, as overviewed in the following sections.

THE S100 PROTEIN FAMILY

S100 proteins are a family of low-molecular weight EF-hand Ca^{2+} proteins that are expressed in distinct organs and tissues. They are involved in multiple intracellular functions, including cell proliferation, differentiation, protein phosphorylation, cytoskeletal assembly, and disassembly and intracellular calcium homeostasis (Mrak and Griffinbc, 2001; Donato et al., 2009, 2013). In pathological conditions S100 proteins can be expressed in a cell type where they are not expressed under normal conditions. Additionally, some S100 proteins are secreted and regulate cell functions in an autocrine or paracrine manner by activation of surface receptors, such as the RAGE receptor, thereby promoting NF-κB signaling, an important trigger of inflammatory processes, recruiting and activating cellular pro-inflammatory effectors (Hofmann et al., 1999; Leclerc et al., 2009). Albeit S100 proteins are not cytokines in *stricto sensu*, in these cases, they have such functions, and act as extracellular alarmins or as damage-associated molecular pattern (DAMP) factors, that can either be beneficial or detrimental depending on concentration and molecular and cellular moiety (Donato et al., 2009, 2013). From the 25 S100 proteins described so far, several are present in the brain and from those, seven have been implicated in AD pathways: S100B, S100A1, S100A6, S100A7, S100A8, S100A9, and S100A12.

S100 proteins occur mainly as homodimers (Barger et al., 1992; Giannakopoulos et al., 1996; Matsui Lee et al., 2000; Cunden et al., 2017). Specifically, it is known that calcium binding to S100 proteins triggers conformational changes that expose a hydrophobic cleft that is crucial to interaction with partners to their activation, regulation and signaling functions. Several S100 proteins also bind zinc and copper, which interestingly are highly abundant in senile plaques (Heizmann et al., 2002; Senior et al., 2003; Maynard et al., 2005). A few S100 proteins are also found as heterodimers, including S100A8/A9 (Teigelkamp et al., 1991), S100B/A1 (Garbuglia et al., 1999) and S100A6/B (Yang et al., 1999). S100 proteins interconvert into functional oligomers, including tetramers, hexamers, and octamers and formation of these species can be promoted by Ca^{2+} or Zn^{2+}

binding (Botelho et al., 2012). The functions described for these S100 oligomers involve a tighter interaction with RAGE, assistance in microtubule formation, neurite outgrowth, and tumor suppression.

S100 proteins influence cognitive processes in the healthy brain and play roles in development and neuronal maintenance. Depending on the study, antisera to neurospecific S100 protein (Gromov et al., 1992; O'Dowd et al., 1997; Epstein et al., 2006) and antibodies directed against S100A1 and S100B (Gromov et al., 1992; O'Dowd et al., 1997; Epstein et al., 2006) either impair or improve learning and memory functions in rat brains (Gromov et al., 1992; O'Dowd et al., 1997; Epstein et al., 2006). Recent studies suggested that elevated S100B levels have deleterious effects during the neurodevelopmental period through RAGE-dependent processes (Santos et al., 2018). Additionally, S100B has been associated with Down Syndrome, a genetic variation where the most profound neurological features are mental retardation, seizures and early onset AD. Levels of S100B are increased in neuronal progenitor cells of patients with Down Syndrome (Esposito et al., 2008a) and in human induced pluripotent stem cells derived from Down Syndrome patients (Chen et al., 2014). S100B overexpression causes toxicity to neurons, reduces neurogenesis, and increases the production of reactive oxygen species (Esposito et al., 2008a; Lu et al., 2011; Chen et al., 2014).

There are several studies using clinical specimens and animal models implicating S100 proteins in AD pathophysiology (Marshak et al., 1992; Akiyama et al., 1994; Sheng et al., 1994; Gerlai et al., 1995; Mrak et al., 1996; Boom et al., 2004; Shepherd et al., 2006; Chaves et al., 2010; Ha et al., 2010; Mori et al., 2010; Roltsch et al., 2010; Chang et al., 2012; Afanador et al., 2014; Cirillo et al., 2015; Horvath et al., 2016; Gruden et al., 2017; Lodeiro et al., 2017; Iashchishyn et al., 2018; Wang et al., 2018). As overviewed in the following sections, different S100 proteins seem to be involved in several processes related to APP processing, influencing Aβ levels, tau post-translational modifications, formation of protein inclusions, and multiple signaling pathways. The ability of acting as Ca^{2+} sensors, regulating the activity of channels/pumps involved in Ca^{2+} release/uptake also provide feedback and feedforward mechanisms for sustaining aberrant Ca^{2+} signaling in AD. Therefore, involvement in all these processes makes a strong case for the importance of the S100 protein family in AD development (**Table 1**).

S100B

S100B is the most studied S100 protein in the scope of AD, as reviewed in Steiner et al. (2011) and Yardan et al. (2011). S100B acts as a pro-inflammatory cytokine and a DAMP molecule depending on its concentration. S100B secreted from astrocytes can have trophic and toxic effect on neurons. At nanomolar concentration, S100B displays neurotrophic effects, leading to promotion of neuronal survival and neurite outgrowth. At micromolar concentrations S100B has deleterious effects inducing neuronal apoptosis (Mrak and Griffinbc, 2001). Upregulation of S100B leads to behavioral abnormalities and loss of dendritic density in mice (Gerlai et al., 1995). S100B

TABLE 1 | Distribution, levels, and implication of brain S100 proteins in AD pathways.

	S100A1	S100A6	S100A7	S100A8	S100A9	S100A12	S100B
Expression	Neurons (Isobe et al., 1984)	Astrocytes (Boom et al., 2004; Yamada and Jinno, 2012); Neurons (Yamada and Jinno, 2014)	Neurons (Qin et al., 2009)	Microglia (Akiyama et al., 1994; Kummer et al., 2012); Neurons (Wang et al., 2018)	Microglia (Akiyama et al., 1994; Kummer et al., 2012); Neurons (Shepherd et al., 2006; Wang C. et al., 2014)	Neurons (Shepherd et al., 2006); Glia (Shepherd et al., 2006)	Astrocytes (Van Eldik and Griffin, 1994; Mrak et al., 1996; Shepherd et al., 2006); Oligodendrocytes (Shepherd et al., 2006); Neurons (Yang et al., 1995; Ichikawa et al., 1997); Microglia (Adami et al., 2001).
APP processing	n/a	n/a	- S100A7 ↑ α-secretase activity via ADAM-10 (Qin et al., 2009).	n/a	- S100A9 knockdown in Tg2576 ↓APP-CT (Chang et al., 2012); - S100A9 knockout in APP/PS1 transgenic mice ↓ BACE expression and activity (Kummer et al., 2012); - S100A9 knockdown in Tg2576 ↑neprilysin and ↓BACE activity (Chang et al., 2012). - Inhibitor of γ-Secretase ↓ S100A9 in BV2 cells (Li et al., 2014). - C-terminal fragments of APLP2 ↑ S100A9 in BV2 cells (Li et al., 2014).	n/a	- S100B ↑APP levels in rat retinal neurons (Anderson et al., 2009); - Tg2576-huS100B mice ↑ soluble APPβ and ↑BACE1 (Mori et al., 2010).

(Continued)

TABLE 1 | Continued

	S100A1	S100A6	S100A7	S100A8	S100A9	S100A12	S100B
Aβ levels	n/a	- Exogenous S100A6 treatment ↓Aβ levels (Tian et al., 2019)	- S100A7 inhibits Aβ42 and Aβ40 generation in primary neurons from Tg2576 transgenic embryos (Qin et al., 2009).	- Treatment with Aβ ↑S100A8 in glia and astrocytes (Lodeiro et al., 2017); - Treatment of SH-SY5Y cells with S100A8: ↑Aβ42 and ↓Aβ40 production (Lodeiro et al., 2017); - Aβ ↑S100A8 mRNA expression (Walker et al., 2006); - S100A8/A9 interacts with Aβ40 (ESI-MS) (Lee et al., 2018); - S100A8/A9 ↓Aβ40 amyloid level (Lee et al., 2018).	- Aβ induces S100A9 expression in the microglial cell line BV-2 (Ha et al., 2010); - S100A9 knockdown in Tg2576 ↓Aβ (Chang et al., 2012); - Aβ42 monomers ↓release of S100A9 in human THP-1 monocytes (Lee et al., 2013); - S100A9 interacts with Aβ40 and promotes the formation of amyloid structures (Zhang et al., 2012; Zhao et al., 2013); - S100A9 interacts with Aβ40 (NMR) (Wang C. et al., 2014); - Cytotoxicity of S100A9 is suppressed by Aβ40 (Zhang et al., 2012); - Coaggregation of S100A9 with Aβ40 and Aβ42 (Wang C. et al., 2014).	n/a	- Aβ injection on rat retinal neurons ↑S100B expression (Anderson et al., 2009); - Overexpressing S100B in Tg2576 mice ↑Aβ levels and amyloid deposits (Mori et al., 2010); - Nanomolar concentration of S100B protect against Aβ-mediated cytotoxicity (Businaro et al., 2006; Clementi et al., 2013, 2016); - S100B interacts with Aβ42 (NMR, ITC, SAXS) (Cristovao et al., 2018); - S100B suppresses Aβ42 aggregation and cellular toxicity in a calcium-tuned manner (Cristovao et al., 2018).
Amyloid plaques	- S100A1 knockout in PS/APP mice ↓plaque load (cortical and hippocampal regions) (Afanador et al., 2014); - S100A1 in amyloid plaques of murine and human AD specimens (Afanador et al., 2014).	- Associated with amyloid plaques (Boom et al., 2004; Tian et al., 2019); - Exogenous S100A6 treatment ↓plaque burden (Tian et al., 2019) - S100A6 is co-localized with S100B and GFAP near amyloid plaques (Boom et al., 2004).	n/a	- S100A8 aggregates observed prior to formation of Aβ plaques (Lodeiro et al., 2017); - ↑S100A8 in microglial cells around amyloid plaques (Kummer et al., 2012);	- Associated with amyloid plaques (Shepherd et al., 2006); - ↑S100A9 in microglial cells around amyloid plaques (Kummer et al., 2012); - S100A9 knockout ↑phagocytosis of fibrillar amyloids in microglia cells and ↓Aβ deposition (Kummer et al., 2012); - Isolated plaques of S100A9 and Aβ (Horvath et al., 2016); - S100A9 knockdown ↓amyloid plaque burden (Ha et al., 2010).	- Associated with amyloid plaques (Shepherd et al., 2006).	- Associated with amyloid plaques (Shepherd et al., 2006); - Present in diffuse (non-neuritic) amyloid deposits (Mrak et al., 1996); - Overexpression of S100B ↑large plaques (Mori et al., 2010); - PSAPP/S100B$^{-/-}$ ↓cortical amyloid plaque load and number (Roltsch et al., 2010); - S100B-positive astrocytes surround neuritic plaques (Van Eldik and Griffin, 1994).
Tau	- Ablation of S100A1 expression ↑tubulin/ microtubules levels in PC12 cells (Zimmer et al., 1998); - S100A1 causes disassembly of microtubules in U251 glioma cells and rat L6 myoblasts (Sorci et al., 2000).	- ↑S100A6 interferes with CacyBP/SIP complex and inhibits its activity and ↓Tau dephosphorylation in NB2a cells (Wasik et al., 2013).	n/a	n/a	- Associated with neurons with neurofibrillary-tangle morphology (Shepherd et al., 2006).	n/a	- ↑ S100B leads to hyperphosphorylated Tau in human neural stem cells (Esposito et al., 2008b); - DKK-1 inhibition abolish S100B-induced tau hyperphosphorylation (Esposito et al., 2008b); - S100B binds Tau through kinase II and inhibits Tau phosphorylation (Baudier and Cole, 1988); - S100B levels are correlated to Tau plaques (Sheng et al., 1994); - Neurofibrillar tangles of parahippocampal cortex of AD patients are correlated to S100B positive astrocytes (Sheng et al., 1997); - PSAPP/S100B$^{-/-}$ ↓phospho-tau positive dystrophic neurons (Roltsch et al., 2010); - S100B causes disassembly of microtubules in U251 glioma cells and rat L6 myoblasts (Sorci et al., 2000).

(Continued)

TABLE 1 | Continued

	S100A1	S100A6	S100A7	S100A8	S100A9	S100A12	S100B
CSF levels	n/a	n/a	- ↑ S100A7 in AD patients (Qin et al., 2009).	n/a	- ↓S100A9 and Aβ42 levels in AD patients (Horvath et al., 2016).	n/a	- ↑ S100B in AD patients (Petzold et al., 2003); - ↑ S100B in mild/moderate AD patients (Peskind et al., 2001).
Inflammation	- S100A1 knockout in PSAPP AD mouse ↓ astrocytosis, microgliosis (Afanador et al., 2014).	n/a	n/a	n/a	n/a	n/a	- Astrocytosis and neurite proliferation in transgenic mice expressing elevated levels of S100B (Reeves et al., 1994); - Astrocytosis and microgliosis in Tg2576 mice overexpressing S100B (Mori et al., 2010); - PSAPP/S100B $^{-/-}$ ↓cortical gliosis (Roltsch et al., 2010); - S100B inhibitor ↓ reactive gliosis, ↓ astrocyte infiltration and rescues neuronal loss in Aβ-injected mice (Cirillo et al., 2015).
Signaling pathways	- S100A1 inhibits Akt/GS3β signaling (Afanador et al., 2014).		- S100A7 promotes Erk1/2 and PKC phosphorylation (Qin et al., 2009).	n/a		n/a	- 3XTg-AD mice with an IL-1 inhibitor ↓S100B levels and suppress Wnt/β-catenin (Kitazawa et al., 2011); - ↑ IL-1β and IL-6 mRNA expression in Tg2576-huS100B mice (Mori et al., 2010); - ↑ S100B activates JNK, degrades β-catenin, and disrupts Wnt pathway in human neural stem cells (Esposito et al., 2008b); - Inhibition of S100B causes ↓ GFAP, ↓ p-p38 MAPK, ↓COX-2, ↓ IL-1β and ↓RAGE expression in C57BL/6J mice (Cirillo et al., 2015); - TNFα ↓S100B expression in astrocytes and ↑S100B extracellular levels in primary astrocytes (Edwards and Robinson, 2006).
S100 conformers	Found in extracellular deposits (Afanador et al., 2014).	Found in clusters around amyloid plaques (Boom et al., 2004).	n/a	Found isolated S100A8 clusters in the hippocampi of Tg2576 and TgAPPartic AD mice models (Lodeiro et al., 2017).	- Found as dimers and as S100A9 multimers in AD brain patients (Shepherd et al., 2006); - Found isolated S100A9 clusters in AD brain tissues (Horvath et al., 2016; Wang et al., 2018).	- Found hexameric S100A12 in AD brain patients (Shepherd et al., 2006).	- Found as native dimers and as higher order multimers in AD brain patients (Shepherd et al., 2006); - Found isolated S100B clusters around tau plaques (Sheng et al., 1994; Mrak et al., 1996).
Brain region	n/a	- ↑ S100A6 in white matter; in gray matter is concentrated in amyloid plaques of AD patients (Boom et al., 2004); - S100A6 in amygdala and hippocampus in APP/London mice (Boom et al., 2004); - ↑ S100A6 expression in APP/PS1KI mice (Wirths et al., 2010; Weissmann et al., 2016).	- ↑ S100A7 in amygdala and hippocampus of AD brain patients (Qin et al., 2009); - ↑ S100A7 in serum of mild cognitively impaired patients (Mueller et al., 2010).	- ↑ S100A8 in hippocampus of Tg2576 and TgAPPartic mice (Lodeiro et al., 2017); - ↑ S100A8 in serum of AD patients (Shen et al., 2017).	- ↑S100A9 in familial and sporadic AD patients (Shepherd et al., 2006); - ↑S100A9 expression in brain lysates of AD patients (Kummer et al., 2012); - ↑S100A9 expression in Tg2576 mice and AD patients (Chang et al., 2012); - ↑S100A9 expression in cortex and hippocampus of CT-Tg and Tg2576 mice model and in AD brain patients (Ha et al., 2010); - S100A9 in plaques of hippocampal and neocortical areas of AD patents in Braak stages III to VI (Wang C. et al., 2014).	n/a	- S100B in cortical and white matter of PS-1 and sporadic AD brains (Shepherd et al., 2006); - S100B in layer I cortex of AD brains (Simpson et al., 2010); - ↑ S100B hippocampus, temporal lobe, frontal lobe and pons in AD brains (Van Eldik and Griffin, 1994).

n/a, no data available.

also regulates the intracellular levels of free calcium in several central nervous system cell types, such as neurons and astrocytes. Recently we demonstrated that S100B acts as a sensor and regulator of elevated zinc levels in the brain and that this metal-buffering activity is tied to a neuroprotective role, through an indirect effect on calcium levels and in inhibition of excitotoxicity (Hagmeyer et al., 2017).

Several studies point to high levels of S100B in AD patients (Marshak et al., 1992; Van Eldik and Griffin, 1994; Peskind et al., 2001; Petzold et al., 2003; Chaves et al., 2010) and in AD mouse models (Yeh et al., 2015). The largest increase in S100B levels is observed in the hippocampus, temporal lobe (Van Eldik and Griffin, 1994) and in the layer I of the cortex (Simpson et al., 2010). It is demonstrated that sera of AD patients with moderate and severe dementia have a 60- and 37-fold increase in S100B, respectively. In AD patients with moderate dementia, the increase of S100B levels is followed by a 10-fold increase in auto-antibodies: however, in AD patients with severe dementia the levels of auto-antibodies remain identical to controls (Gruden et al., 2007), indicating that there is no immune-protection against elevated S100B levels in AD patients with severe dementia. S100B is also elevated in the cerebrospinal fluid (CSF) of AD patients (Peskind et al., 2001; Petzold et al., 2003). S100B is involved in APP cleavage processes: high levels of S100B increase BACE1 activity resulting in higher levels of toxic APPβ and C-terminal fragments, including the amyloidogenic β-CTF (C99) (Anderson et al., 2009; Mori et al., 2010).

S100B surrounding amyloid plaques is mostly produced by astrocytes (Van Eldik and Griffin, 1994; Mrak et al., 1996; Shepherd et al., 2006; Roltsch et al., 2010), but can also originate from oligodendrocytes (Simpson et al., 2010) and microglia (Roltsch et al., 2010). It was also observed that S100B positive astrocytes are present in the diffuse non-neuritic amyloid plaques (Mrak et al., 1996), suggesting an early, yet unclear, action of S100B in the formation of senile plaques. Evidence suggests that S100B may regulate plaque formation as the knockout of S100B in the PS/APP AD mouse model selectively decreases plaque load in the cortical region (Roltsch et al., 2010) and the overexpression of S100B increases Aβ levels and deposits, at early stages (Mori et al., 2010). Even though, it is established that elevated levels of S100B have deleterious effects that promote AD features, nanomolar concentrations of S100B effectively protect cells against Aβ-mediated cytotoxicity (Businaro et al., 2006; Clementi et al., 2013, 2016). Additionally, we have recently found that, *in vitro*, S100B binds to Aβ42 monomers, oligomers, and fibrils resulting in a calcium-tuned suppression of Aβ42 aggregation and cellular toxicity in SH-SY5Y cells (Cristovao et al., 2018). S100B was found both in normal and in AD brains in various oligomeric states (Shepherd et al., 2006); however, the protective or pathological functions of S100B oligomers are still unclear.

Overexpression of S100B in Tg2576 AD transgenic mice is also linked with neuroinflammation, promoting astrogliosis, microgliosis, and neurite proliferation (Reeves et al., 1994; Mori et al., 2010). However, knockout of S100B in PS/APP mouse model decreases cortical gliosis (Roltsch et al., 2010). IL-1 regulates the expression and secretion of S100B from astrocytes (de Souza et al., 2009). Treatment of the 3XTg-AD mice with an antibody against IL-1 reduces S100B levels and results in attenuation of tau pathology and in partial reduction of certain fibrillar and oligomeric forms of Aβ (Kitazawa et al., 2011) Therefore, S100B seems to be tied to different processes related to AD pathology as in addition to its ability to promote brain inflammatory response and tau pathology (Esposito et al., 2008b) it may play roles in directly promoting amyloidogenic APP processing, as proposed by Mori et al. (2010).

Inhibition of S100B using pentamidine in AD mouse models, lead to a reduction in the levels of proinflammatory mediators such as nitrite, MDA, PGE2 and IL-1, followed by an inhibition of Aβ-induced gliosis (Cirillo et al., 2015). Indeed, S100B-overexpressing mice that were infused with oligomeric Aβ exhibited enhanced glial activation. Neuroinflammation and loss of synaptic markers were noted, however there was no difference in the amyloid plaque burden, in comparison to controls (Craft et al., 2005). These results suggest a relationship between S100B and other cytokines that are also implicated in AD pathways. Indeed, the TNF-α cytokine, which is present at high levels in the AD brain, decreases both GFAP and S100B intracellular levels in astrocytes, while increasing their extracellular levels (Edwards and Robinson, 2006). This crosstalk suggests a relationship between TNF-α and the increase of these two proteins in CSF and sera of AD patients. Other reports showed that S100B enhances IL-6 mRNA (Mori et al., 2010; Yeh et al., 2015) and IL-1 mRNA levels in microglia and in neurons (Mori et al., 2010), via Sp1 and NF-κB signaling pathways (Liu et al., 2005). Additionally, knockout of S100B in the Tg2576 AD mouse model background results in a decrease in GFAP-positive astrocytes and in Iba-1 positive microglia (Roltsch et al., 2010), while its overexpression has opposite effects (Mori et al., 2010). Overall, these results suggest that S100B can influence and be influenced by the levels of other cytokines involved in AD pathogenesis.

Regarding tau pathology, high S100B levels in AD patients positively correlate to tau tangles with which S100B was found to be clustered (Sheng et al., 1994, 1997). Knockout of S100B in the PS/APP mouse model decreases phosphorylated-tau positive dystrophic neurons (Roltsch et al., 2010) and in mouse models expressing tau, S100B levels are upregulated (Sidoryk-Wegrzynowicz et al., 2017). Indeed, it has been demonstrated, *in vitro,* that S100B directly binds tau inhibiting its phosphorylation by yet unclear non-covalent interactions in a process that is Ca^{2+} or Zn^{2+}-dependent (Baudier and Cole, 1988). However, contradictory results show that S100B promotes tau hyperphosphorylation by inducing GSK-3β activation and disrupting Wnt signaling (Esposito et al., 2008b), an important pathway to regulate synaptic transmission and plasticity. Indeed, S100B promotes the expression of the Dickkopf-related protein 1 (Dkk1), an antagonist of Wnt signaling that has previously been suggested to play a role in AD (Guo et al., 2016).

As previously mentioned, calcium dysregulation contributes to AD pathology and S100B is a key factor in the Ca^{2+} homeostasis of astrocytes. It was demonstrated that S100B knockout leads to a decrease of induced-Ca^{2+} transients (Xiong et al., 2000) such as those induced by Aβ. In what could be a potentially protective mechanism, S100B levels were found to be

up-regulated in astrocytes upon Aβ induced Ca^{2+} intracellular waves (Chow et al., 2010).

S100A1

The investigation of the role of S100A1 in AD is encouraged by the fact that some of its targets are altered in the disease, such as the ryanodine receptor (RyR), an intracellular calcium release channel, tau and RAGE. S100A1 is primarily expressed in neurons and, as reviewed in Zimmer et al. (2005) is implicated in tau phosphorylation, neuronal cell sensitivity to Aβ and in the regulation of APP expression. In respect to the latter, available data indicates that βAPP steady-state mRNA and intracellular protein levels are down-regulated in response to ablation of S100A1 expression (Zimmer et al., 2005). In the PS/APP mouse model, knockout of S100A1 decreases inflammatory processes, such as astrocytosis and microgliosis, diminishing 3.7-fold the number of cortical plaques and 1.5-fold the number of hippocampal plaques (Afanador et al., 2014). Decreased S100A1 levels in PC12 cells increase tubulin levels and the number of neurites (Zimmer et al., 1998). Additionally, knockout of S100A1 in PC12 cells increases the resistance to Aβ-induced cell death (Zimmer et al., 2005).

S100A1 induces Glycogen synthase kinase 3 (GSK3) phosphorylation (Afanador et al., 2014), that is involved in several processes such as glycogen metabolism and gene transcription. GSK3 over-activation is also related to memory impairment and other AD related features (Hooper et al., 2008). In human and mouse AD brain tissue, S100A1:RyR complexes are present and their formation is Ca^{2+}-dependent. RyR is a receptor with altered levels in AD that is associated with APP processing and Aβ production, however it is not known if it exerts a protective or pathogenic role in AD (Del Prete et al., 2014). S100A1 also binds to stress-inducible phosphoprotein 1 (STIP1) (Maciejewski et al., 2017), a Hsp90 cochaperone that is reported to be present in the vicinity of Aβ oligomers, preventing Aβ-induced synaptic loss and neuronal death in primary neurons (Ostapchenko et al., 2013). S100A1 and S100B also have the ability to cause microtubule disassembly in glioma cells and myoblasts in a Ca^{2+}-dependent manner, suggesting a possible role of S100A1 in tau pathology (Sorci et al., 2000). Moreover, in human AD patients and in the PS/APP mouse model, extracellular S100A1 has been observed in plaque-like deposits (Afanador et al., 2014).

S100A6

S100A6 was identified in the AD gene signature as one of the most significantly positively correlated proteins with AD phenotype (Wruck et al., 2016). As other S100 proteins, S100A6 is upregulated in AD patients and in AD mouse models (Boom et al., 2004; Wirths et al., 2010; Weissmann et al., 2016) and is found in astrocyte-positive clusters that surround Aβ amyloid deposits in the brain's gray matter (Boom et al., 2004). In PS/APP mouse brains, S100A6 localizes in the peripheral region of amyloid plaques and exogenous S100A6 treatment in mouse brain sections reduces Aβ levels and plaque burden (Tian et al., 2019).

Zinc ions are colocalized with senile plaques in AD patients and there is evidence that AD related-cognitive decline is dependent on extracellular zinc levels (Lovell et al., 1998; Takeda and Tamano, 2016). In particular, one study suggested that zinc-binding S100A6 exerts a zinc sequestering function, identical to what has been proposed for S100B (Hagmeyer et al., 2017), thus preventing zinc-induced toxicity in COS-7 cells (Tian et al., 2019). Additionally, PS/APP mice treated with a high-zinc diet have increased S100A6 levels and Aβ deposits. These studies point to a correlation between S100A6, zinc ions and decrease in Aβ plaque load.

The heterodimer S100A6/B is also implicated in pathological signal transduction in melanoma (Yang et al., 1999). It is possible that the formation of the heterodimer also occurs in AD since S100A6 is colocalized with S100B and astrocytic glial fibrillary acidic protein (GFAP), a marker of astrogliosis, near amyloid plaques (Boom et al., 2004). Additionally, it is reported that S100A6 binds to the CacyBP/SIP complex, a complex known to participate in the organization of microtubules. Overexpression of S100A6 in neuroblastoma NB2a cells inhibits CacyBP/SIP complex activity, and consequently lowers the rate of tau dephosphorylation (Wasik et al., 2013).

S100A7

There is scarce evidence regarding the role of S100A7 on AD pathways. It is reported that S100A7 is increased in mildly cognitively impaired patients (Mueller et al., 2010) and in the brain and CSF of AD dementia patients (Qin et al., 2009). S100A7 mRNA expression is regulated in the brain as a function of AD dementia and amyloid neuropathology (Qin et al., 2009). Exogenous S100A7 in primary hippocampal neurons of Tg2576 AD transgenic embryos inhibits the generation of Aβ42 and Aβ40 peptides and promotes the activity of "non- amyloidogenic" α-secretase, via upregulation of ADAM-10 (a disintegrin and metalloproteinase) and phosphorylation of Erk1/2 and PKC (Qin et al., 2009). Therefore, a beneficial role of S100A7 on APP processing is suggested, albeit other studies are required to more extensively support this possibility.

S100A8

S100A8 was found to be upregulated in the sera of AD patients (Shen et al., 2017) and in the hippocampus of Tg2576 and TgAPParc AD mice (Lodeiro et al., 2017). Indeed, several studies establish a correlation between Aβ and S100A8 expression. An increase in S100A8 mRNA levels was induced when aggregated Aβ was added to a microglia culture isolated from post-mortem AD brain tissues. Subsequent culture growth suggested that chronic secretion of S100A8 can lead to chronic activation of microglia (Walker et al., 2006). In rat primary astrocytes, Aβ42 treatment induces a significant increase in S100A8 mRNA levels. Treatment of SH-SY5Y neuroblastoma cells with recombinant S100A8 increased Aβ42 and decreased Aβ40 production (Lodeiro et al., 2017). In PS/APP mice, the S100A8/A9 heterodimer is found to be upregulated in microglial cells surrounding amyloid plaques (Kummer et al., 2012). Additionally, it is reported that S100A8/A9 binds directly to Aβ40 and that it interferes with amyloid formation but

no effect was observed over Aβ42 aggregation (Lee et al., 2018). There is also a link between S100A8/A9 and the "non-amyloidogenic" α-secretase ADAM-10, since S100A8/A9 has lower expression in AD mice models overexpressing ADAM-10 (Prinzen et al., 2009).

S100A8 assemblies were found in the hippocampus of Tg2576 and TgAPParc AD mice brains, distinct from corpora amylacea, that are formed independently of Aβ plaques (Lodeiro et al., 2017). These S100A8 aggregates are likely not amyloidogenic as no staining was observed with thioflavin-S (Lodeiro et al., 2017).

S100A9

S100A9 was found to be strongly increased in brain lysates of AD patients and AD mice compared to healthy, age-matched controls (Ha et al., 2010; Chang et al., 2012; Kummer et al., 2012) and in familial PS-1 AD tissues (Shepherd et al., 2006). S100A9 is present in activated glia and neurons positive for tau neurofibrillary tangles (Shepherd et al., 2006). Additionally, there is a strong correlation between S100A9 and Aβ. In *in vitro* cell assays, Aβ42 reduces extracellular release of S100A9 in human THP-1 monocytes (Lee et al., 2013) and induces S100A9 expression in microglia BV2 cells (Ha et al., 2010). However, in CSF from AD patients with mild cognitive impairment and vascular dementia, the levels of S100A9 and Aβ42 are decreased (Horvath et al., 2016). Knockdown of S100A9 decreases cognition decline on Tg2576 mice and reduces amyloid plaque burden (Ha et al., 2010; Chang et al., 2012). S100A9 was found within amyloid plaques of sporadic and familial PS-1 AD brains (Shepherd et al., 2006; Wang et al., 2018) with distinct Braak stages from III to VI (Kummer et al., 2012; Wang C. et al., 2014). Indeed, in some studies it was possible to observe Aβ42 plaques and also isolated S100A9 plaques that are not colocalized, forming separate tissue deposits (Horvath et al., 2016; Wang et al., 2018).

Regarding the formation of S100A9 puncta in AD brain, a recent study reported that, *in vitro*, S100A9 is able to form polymeric structures that resemble amyloid structures and bind amyloid fluorophores. The polymerization reaction occurs through a two-step nucleation with initial misfolding of S100A9 and β-sheet formation (Iashchishyn et al., 2017). The impact of S100A9 oligomers on memory was studied through intranasal administration of S100A9 (dimers, oligomers, and fibrillar states) in aged mice. S100A9 oligomers and fibrils, but not dimers, evoked amnestic activity which is correlated with disruption of dopaminergic and glutamate neurochemistry in the prefrontal cortical and hippocampal regions (Gruden et al., 2016, 2018). Additionally, intranasal administration of S100A9 induces cellular stress in the frontal lobe, hippocampus, and cerebellum of aged mice, as well as impaired learning. However, co-treatment with S100A9 fibrillar species and glutamate antibodies increases locomotor activity (Gruden et al., 2017; Iashchishyn et al., 2018). In Tg2576 AD mice, knockdown or knockout of S100A9 significantly reduced the neuropathology and greatly improved learning and memory (Chang et al., 2012), suggesting a link between S100A9 and AD pathology. Indeed, knockout of S100A9 in the PS/APP AD mouse model led to increased phagocytosis of fibrillar Aβ and to decreased Aβ deposition (Kummer et al., 2012).

However, several studies focused on the relationship between S100A9 and Aβ42. *In vitro* biophysical approaches showed that S100A9 binds to Aβ40 through hydrophobic interactions (Zhang et al., 2012; Zhao et al., 2013; Wang C. et al., 2014). Kinetic assays suggested that S100A9 co-aggregates with Aβ40, promoting the formation of amyloid fibrils. The co-aggregation of S100A9 with Aβ42 was also referred to inhibit Aβ42 cytotoxicity (Wang C. et al., 2014).

Regarding APP processing, it was found that C-terminal fragments of amyloid precursor-like protein 2 (APLP2) upregulate S100A9 protein and mRNA expression in BV2 cell and that inhibitor of γ-secretase promotes downregulation of S100A9 protein levels (Li et al., 2014). AD mice deficient in S100A9 have decreased levels of key cytokines involved in APP processing and a reduction of BACE1 expression and activity (Kummer et al., 2012). S100A9 knockout also reduced overall levels of Aβ and APP C-terminal fragments in Tg2576 AD mice, due to increase in neprilysin levels and decreased BACE activity (Chang et al., 2012). Knockdown of S100A9 significantly attenuated the increase of Ca^{2+} levels provoked by C-terminals of APP or by Aβ treatment (Ha et al., 2010); however, others observed that a reduction of S100A9 extracellular release is followed by an increase in intracellular Ca^{2+} levels (Lee et al., 2013), evidencing a correlation between S100A9 and calcium dysregulation in AD. In the AD brain and in mouse models, S100A9 is present in its native form but also as large complexes ranging from 90 to 190 kDa (Shepherd et al., 2006). Indeed, after intranasal administration of S100A9 fibrils in aged mice, S100A9 plaques were observed in the brain which resulted in an exacerbation of cell stress (Iashchishyn et al., 2018). Overall there are solid evidences regarding S100A9 as a potential regulator of AD pathways.

S100A12

S100A12 is the least studied S100 protein in the context of AD. To date, a single study reported S100A12 hexamers associated with senile plaques, reactive glia and neurons in brains of sporadic and PS-1 AD patients (Shepherd et al., 2006).

OUTLOOK

Considering the involvement of S100 proteins in multiple regulatory functions in the brain, the fact that they have age- and damage- related expression, and a direct involvement in neuroinflammation, it is not surprising that they are implicated in molecular processes associated with AD pathogenesis (**Figure 1**).

Most of the available studies report essentially deleterious effects of S100 proteins in AD pathological processes. Indeed, elevated levels of S100 proteins around amyloid plaques and neurofibrillary tangles, exacerbate neuroinflammation and interfere with APP processing and with several AD-related proteins and signaling pathways. This scenario is compatible with an aggravating role as part of downstream inflammatory processes in later stages of AD neurodegeneration. However, some protective roles of S100 proteins are emerging as equally important. Indeed, it is now proposed that early inflammatory

responses start at very early stages of the AD neurodegenerative process, most likely before amyloid plaques are formed (Cuello, 2017). This process would involve an elevation of inflammatory molecules, including S100, at the earliest stages of amyloid pathology, even before the onset of the disease phenotypes. Interestingly, several recent studies suggest that low levels of

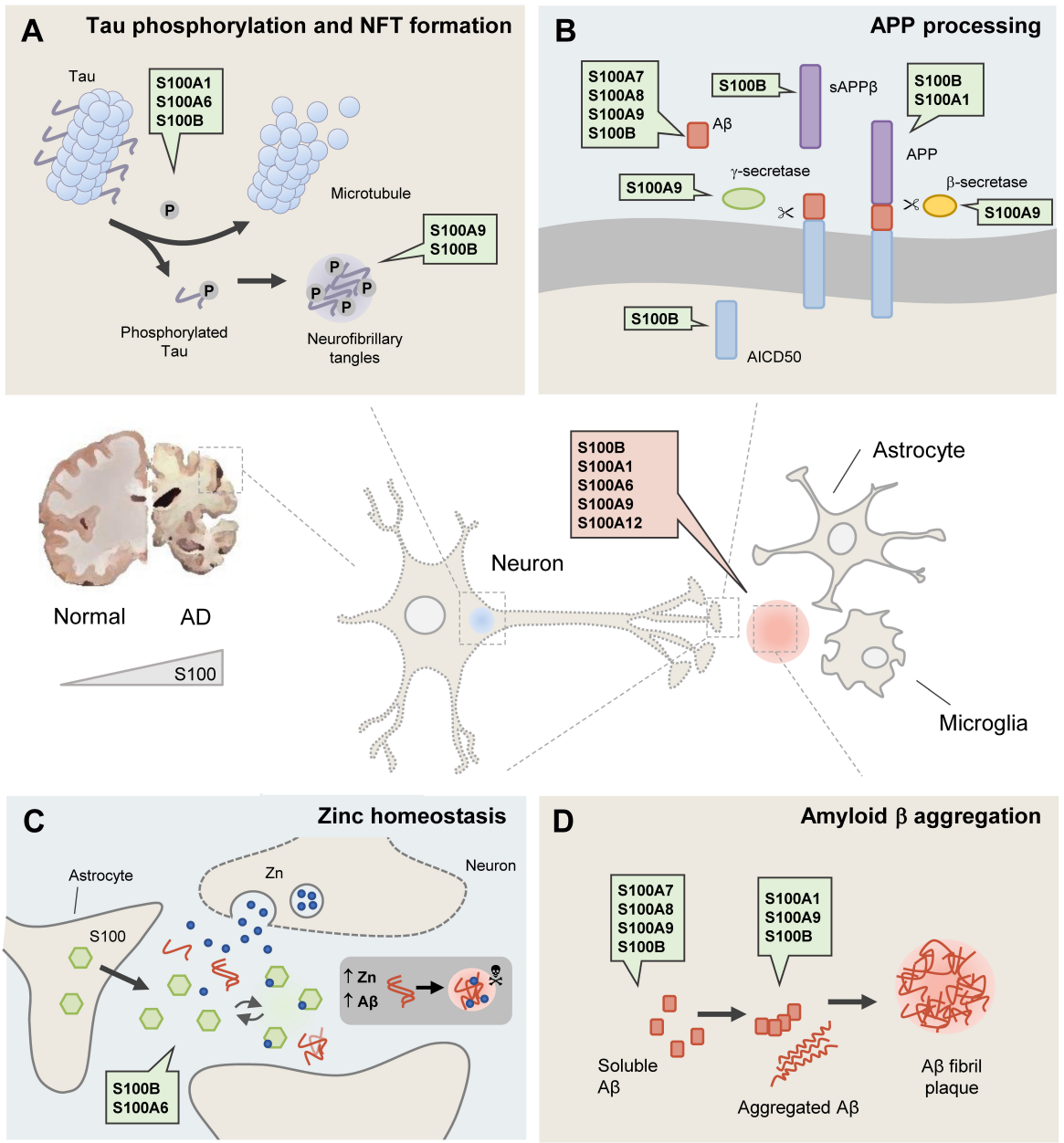

FIGURE 1 | S100 proteins are involved in the main processes associated with Alzheimer's disease (AD). In the AD brain, affected neurons (central panel) are damaged due to the formation of intracellular neurofibrillary tangles (represented by the blue dot) and extracellular amyloid species including an ensemble of low molecular weight aggregates, protofibrils and fibrils (represented by the red dot). As a result of astrocyte and microglia over-activation, some S100 proteins become upregulated, being implicated in several molecular processes altered in AD **(A–D)**. **(A)** Tau phosphorylation and NFT formation. S100A1, S100A6 and S100B are involved in the disassembly of microtubules and Tau release, while S100A9 and S100B are found within neurofibrillary tangles. **(B)** APP processing. Several S100 proteins are implicated in APP cleavage and its amyloidogenic processing. S100A9 regulates γ- and β-secretase expression and activity and S100B and S100A1 regulate APP levels. Moreover, S100A7, S100A8, S100A9 and S100B influence Aβ levels (**Table 1**). **(C)** Zinc homeostasis. Due to their zinc-binding properties, S100B and S100A6 have zinc-buffering activities that are related to neuroprotective roles; and S100A6 reduces zinc levels and senile plaque load in PS/APP mouse brains. **(D)** Amyloid β aggregation. S100A1, S100A9, and S100B proteins can interact, modulate the aggregation and co-aggregate with the Aβ peptide. Several S100 proteins (S100B, S100A1, S100A6, S100A8, S100A9, and S100A12), are found within amyloid plaques and in astrocytes and/or microglia around amyloid deposits. Further details and references can be found in the text and in **Table 1**.

S100B protect cells against Aβ42-mediated cytotoxicity and that low levels of S100A9 inhibit Aβ42 cytotoxicity. This has led to the recent proposal of a new chaperone-like function for S100B (Cristovao et al., 2018), which seems to be extensible to a metal buffering activity (Hagmeyer et al., 2017), both of which are certainly relevant in the context of AD. Therefore, also in AD, S100 proteins may exert different functions according to their (extra)cellular concentrations. At early inflammatory stages and relatively low concentrations they play protective roles, while later in pathology, at higher concentrations, they play essentially disease aggravating roles. This is in line with prior evidence that suggests that decreasing the levels of S100 proteins may be a strategy to mitigate AD progression. The development of S100 neutralizing antibodies and small molecules is already a current therapeutic approach in cancer, autoimmune diseases and chronic inflammatory disorders, as reviewed in Bresnick (2018), and could present a promising strategy for AD as well. Ongoing research in our laboratory will shed light into this subject in the near future.

AUTHOR CONTRIBUTIONS

All authors listed have made a substantial, direct and intellectual contribution to the work, and approved it for publication.

FUNDING

This work was supported by Fundação para a Ciência e a Tecnologia through grants UID/Multi/04046/2013 (to BioISI), PTDC/NEU-NMC/2138/2014 (to CG), IF/01046/2014 (to CG), Ph.D. fellowship SFRH/BD/101171/2014 (to JC) and by Bial Foundation through grant PT/FB/BL-2014-343 (to CG).

REFERENCES

Adami, C., Sorci, G., Blasi, E., Agneletti, A. L., Bistoni, F., and Donato, R. (2001). S100B expression in and effects on microglia. *Glia* 33, 131–142. doi: 10.1002/1098-1136(200102)33%3A2%3C131%3A%3Aaid-glia1012%3E3.0.co%3B2-d

Afanador, L., Roltsch, E. A., Holcomb, L., Campbell, K. S., Keeling, D. A., Zhang, Y., et al. (2014). The Ca2+ sensor S100A1 modulates neuroinflammation, histopathology and Akt activity in the PSAPP Alzheimer's disease mouse model. *Cell Calcium* 56, 68–80. doi: 10.1016/j.ceca.2014.05.002

Akiyama, H., Ikeda, K., Katoh, M., Mcgeer, E. G., and Mcgeer, P. L. (1994). Expression of MRP14, 27E10, interferon-alpha and leukocyte common antigen by reactive microglia in postmortem human brain tissue. *J. Neuroimmunol.* 50, 195–201. doi: 10.1016/0165-5728(94)90046-9

Anderson, P. J., Watts, H. R., Jen, S., Gentleman, S. M., Moncaster, J. A., Walsh, D. T., et al. (2009). Differential effects of interleukin-1beta and S100B on amyloid precursor protein in rat retinal neurons. *Clin. Ophthalmol.* 3, 235–242.

Barger, S. W., Wolchok, S. R., and Van Eldik, L. J. (1992). Disulfide-linked S100 beta dimers and signal transduction. *Biochim. Biophys. Acta* 1160, 105–112. doi: 10.1016/0167-4838(92)90043-d

Barnham, K. J., and Bush, A. I. (2014). Biological metals and metal-targeting compounds in major neurodegenerative diseases. *Chem. Soc. Rev.* 43, 6727–6749. doi: 10.1039/c4cs00138a

Baudier, J., and Cole, R. D. (1988). Interactions between the microtubule-associated Pi-Proteins and S100b regulate Pi-Phosphorylation by the Ca-2+ calmodulin-dependent protein kinase-Ii. *J. Biol. Chem.* 263, 5876–5883.

Boom, A., Pochet, R., Authelet, M., Pradier, L., Borghgraef, P., Van Leuven, F., et al. (2004). Astrocytic calcium/zinc binding protein S100A6 over expression in Alzheimer's disease and in PS1/APP transgenic mice models. *Biochim. Biophys. Acta* 1742, 161–168. doi: 10.1016/j.bbamcr.2004.09.011

Botelho, H. M., Fritz, G., and Gomes, C. M. (2012). Analysis of S100 oligomers and amyloids. *Methods Mol. Biol.* 849, 373–386. doi: 10.1007/978-1-61779-551-0_25

Bresnick, A. R. (2018). S100 proteins as therapeutic targets. *Biophys. Rev* 10, 1617–1629. doi: 10.1007/s12551-018-0471-y

Businaro, R., Leone, S., Fabrizi, C., Sorci, G., Donato, R., Lauro, G. M., et al. (2006). S100B protects LAN-5 neuroblastoma cells against Abeta amyloid-induced neurotoxicity via RAGE engagement at low doses but increases Abeta amyloid neurotoxicity at high doses. *J. Neurosci. Res.* 83, 897–906. doi: 10.1002/jnr.20785

Chang, K. A., Kim, H. J., and Suh, Y. H. (2012). The role of S100a9 in the pathogenesis of Alzheimer's disease: the therapeutic effects of S100a9 knockdown or knockout. *Neurodegener. Dis.* 10, 27–29. doi: 10.1159/000333781

Chaves, M. L., Camozzato, A. L., Ferreira, E. D., Piazenski, I., Kochhann, R., Dall'igna, O., et al. (2010). Serum levels of S100B and NSE proteins in Alzheimer's disease patients. *J. Neuroinflam.* 7:6. doi: 10.1186/1742-2094-7-6

Chen, C., Jiang, P., Xue, H., Peterson, S. E., Tran, H. T., Mccann, A. E., et al. (2014). Role of astroglia in down's syndrome revealed by patient-derived human-induced pluripotent stem cells. *Nat. Commun.* 5:4430. doi: 10.1038/ncomms5430

Chong, F. P., Ng, K. Y., Koh, R. Y., and Chye, S. M. (2018). Tau Proteins and tauopathies in Alzheimer's disease. *Cell Mol. Neurobiol.* 38, 965–980. doi: 10.1007/s10571-017-0574-1

Chow, S. K., Yu, D., Macdonald, C. L., Buibas, M., and Silva, G. A. (2010). Amyloid beta-peptide directly induces spontaneous calcium transients, delayed intercellular calcium waves and gliosis in rat cortical astrocytes. *ASN Neuro* 2:e00026. doi: 10.1042/AN20090035

Cirillo, C., Capoccia, E., Iuvone, T., Cuomo, R., Sarnelli, G., Steardo, L., et al. (2015). S100B inhibitor pentamidine attenuates reactive gliosis and reduces neuronal loss in a mouse model of alzheimer's disease. *Biomed. Res. Int.* 2015:508342. doi: 10.1155/2015/508342

Clementi, M. E., Sampaolese, B., Triggiani, D., Tiezzi, A., and Giardia, B. (2013). S100b protects IMR-32 cells against Ab(1-42) induced neurotoxicity via modulation of apoptotic genes expression. *Adv. Alzh. Dis.* 2, 99–108. doi: 10.4236/aad.2013.23013

Clementi, M. E., Sampaolese, B., and Giardina, B. (2016). S100b induces expression of myoglobin in apbeta treated neuronal cells in vitro: a possible neuroprotective mechanism. *Curr. Aging Sci.* 9, 279–283. doi: 10.2174/1874609809666160222112850

Craft, J. M., Watterson, D. M., Marks, A., and Van Eldik, L. J. (2005). Enhanced susceptibility of S-100B transgenic mice to neuroinflammation and neuronal dysfunction induced by intracerebroventricular infusion of human beta-amyloid. *Glia* 51, 209–216. doi: 10.1002/glia.20194

Cristovao, J. S., Morris, V. K., Cardoso, I., Leal, S. S., Martinez, J., Botelho, H. M., et al. (2018). The neuronal S100B protein is a calcium-tuned suppressor of amyloid-beta aggregation. *Sci. Adv.* 4:eaaq1702. doi: 10.1126/sciadv.aaq1702

Cristovao, J. S., Santos, R., and Gomes, C. M. (2016). Metals and neuronal metal binding proteins implicated in alzheimer's disease. *Oxid. Med. Cell Longev.* 2016:9812178. doi: 10.1155/2016/9812178

Cuello, A. C. (2017). Early and late CNS inflammation in alzheimer's disease: two extremes of a continuum? *Trends Pharmacol. Sci.* 38, 956–966. doi: 10.1016/j.tips.2017.07.005

Cunden, L. S., Brophy, M. B., Rodriguez, G. E., Flaxman, H. A., and Nolan, E. M. (2017). Biochemical and functional evaluation of the intramolecular disulfide bonds in the zinc-chelating antimicrobial protein human

S100A7 (Psoriasin). *Biochemistry* 56, 5726–5738. doi: 10.1021/acs.biochem.7b00781

Dahlgren, K. N., Manelli, A. M., Stine, W. B., Baker, L. K., Krafft, G. A., and Ladu, M. J. (2002). Oligomeric and fibrillar species of amyloid-β peptides differentially affect neuronal viability. *J. Biol. Chem.* 277, 32046–32053. doi: 10.1074/jbc.m201750200

de Souza, D. F., Leite, M. C., Quincozes-Santos, A., Nardin, P., Tortorelli, L. S., Rigo, M. M., et al. (2009). S100B secretion is stimulated by IL-1beta in glial cultures and hippocampal slices of rats: likely involvement of MAPK pathway. *J. Neuroimmunol.* 206, 52–57. doi: 10.1016/j.jneuroim.2008.10.012

Del Prete, D., Checler, F., and Chami, M. (2014). Ryanodine receptors: physiological function and deregulation in Alzheimer disease. *Mol. Neurodegener.* 9:21. doi: 10.1186/1750-1326-9-21

Donato, R., Cannon, B. R., Sorci, G., Riuzzi, F., Hsu, K., Weber, D. J., et al. (2013). Functions of S100 proteins. *Curr. Mol. Med.* 13, 24–57. doi: 10.2174/1566524011307010024

Donato, R., Sorci, G., Riuzzi, F., Arcuri, C., Bianchi, R., Brozzi, F., et al. (2009). S100B's double life: Intracellular regulator and extracellular signal. *Biochim. Biophys. Acta Mol. Cell Res.* 1793, 1008–1022. doi: 10.1016/j.bbamcr.2008.11.009

Edwards, M. M., and Robinson, S. R. (2006). TNF alpha affects the expression of GFAP and S100B: implications for Alzheimer's disease. *J. Neural Transm.* 113, 1709–1715. doi: 10.1007/s00702-006-0479-5

Epstein, O. I., Pavlov, I. F., and Shtark, M. B. (2006). Improvement of memory by means of ultra-low doses of antibodies to S-100B antigen. *Evid. Based Compl. Alternat. Med.* 3, 541–545. doi: 10.1093/ecam/nel073

Esposito, G., Imitola, J., Lu, J., De Filippis, D., Scuderi, C., Ganesh, V. S., et al. (2008a). Genomic and functional profiling of human down syndrome neural progenitors implicates S100B and aquaporin 4 in cell injury. *Hum. Mol. Genet.* 17, 440–457. doi: 10.1093/hmg/ddm322

Esposito, G., Scuderi, C., Lu, J., Savani, C., De Filippis, D., Iuvone, T., et al. (2008b). S100B induces tau protein hyperphosphorylation via Dickopff-1 up-regulation and disrupts the Wnt pathway in human neural stem cells. *J. Cell Mol. Med.* 12, 914–927. doi: 10.1111/j.1582-4934.2008.00159.x

Fa, M., Puzzo, D., Piacentini, R., Staniszewski, A., Zhang, H., Baltrons, M. A., et al. (2016). Extracellular tau oligomers produce an immediate impairment of LTP and memory. *Sci. Rep.* 6:19393. doi: 10.1038/srep19393

Garbuglia, M., Verzini, M., Sorci, G., Bianchi, R., Giambanco, I., Agneletti, A. L., et al. (1999). The calcium-modulated proteins, S100A1 and S100B, as potential regulators of the dynamics of type III intermediate filaments. *Braz. J. Med. Biol. Res.* 32, 1177–1185. doi: 10.1590/s0100-879x1999001000001

Gerlai, R., Wojtowicz, J. M., Marks, A., and Roder, J. (1995). Overexpression of a calcium-binding protein, S100 beta, in astrocytes alters synaptic plasticity and impairs spatial learning in transgenic mice. *Learn. Mem.* 2, 26–39. doi: 10.1101/lm.2.1.26

Giannakopoulos, P., Hof, P. R., Kovari, E., Vallet, P. G., Herrmann, F. R., and Bouras, C. (1996). Distinct patterns of neuronal loss and alzheimer's disease lesion distribution in elderly individuals older than 90 years. *J. Neuropathol. Exp. Neurol.* 55, 1210–1220. doi: 10.1097/00005072-199612000-00004

Gonzalez-Reyes, R. E., Nava-Mesa, M. O., Vargas-Sanchez, K., Ariza-Salamanca, D., and Mora-Munoz, L. (2017). Involvement of astrocytes in alzheimer's disease from a neuroinflammatory and oxidative stress perspective. *Front. Mol. Neurosci.* 10:427. doi: 10.3389/fnmol.2017.00427

Gouras, G. K., Almeida, C. G., and Takahashi, R. H. (2005). Intraneuronal abeta accumulation and origin of plaques in Alzheimer's disease. *Neurobiol. Aging* 26, 1235–1244. doi: 10.1016/j.neurobiolaging.2005.05.022

Gromov, L. A., Syrovatskaya, L. P., and Ovinova, G. V. (1992). Functional role of the neurospecific S-100 protein in the processes of memory. *Neurosci. Behav. Physiol.* 22, 25–29. doi: 10.1007/bf01186664

Gruden, M. A., Davidova, T. B., Malisauskas, M., Sewell, R. D., Voskresenskaya, N. I., Wilhelm, K., et al. (2007). Differential neuroimmune markers to the onset of Alzheimer's disease neurodegeneration and dementia: autoantibodies to Abeta(25-35) oligomers, S100b and neurotransmitters. *J. Neuroimmunol.* 186, 181–192. doi: 10.1016/j.jneuroim.2007.03.023

Gruden, M. A., Davydova, T. V., Fomina, V. G., Vetrile, L. A., Morozova-Roche, L. A., and Sewell, R. D. E. (2017). Antibodies to glutamate reversed the amnesic effects of proinflammatory S100A9 protein fibrils in aged C57Bl/6 Mice. *Bull. Exp. Biol. Med.* 162, 430–432. doi: 10.1007/s10517-017-3632-2

Gruden, M. A., Davydova, T. V., Kudrin, V. S., Wang, C., Narkevich, V. B., Morozova-Roche, L. A., et al. (2018). S100A9 protein aggregates boost hippocampal glutamate modifying monoaminergic neurochemistry: a glutamate antibody sensitive outcome on alzheimer-like memory decline. *ACS Chem. Neurosci.* 9, 568–577. doi: 10.1021/acschemneuro.7b00379

Gruden, M. A., Davydova, T. V., Wang, C., Narkevich, V. B., Fomina, V. G., Kudrin, V. S., et al. (2016). The misfolded pro-inflammatory protein S100A9 disrupts memory via neurochemical remodelling instigating an Alzheimer's disease-like cognitive deficit. *Behav. Brain Res.* 306, 106–116. doi: 10.1016/j.bbr.2016.03.016

Guo, X., Tang, P., Liu, P., Liu, Y., Chong, L., and Li, R. (2016). Dkk1: a promising molecule to connect Alzheimer's disease and osteoporosis. *Med. Hypoth.* 88, 30–32. doi: 10.1016/j.mehy.2015.12.023

Ha, T. Y., Chang, K. A., Kim, J., Kim, H. S., Kim, S., Chong, Y. H., et al. (2010). S100a9 knockdown decreases the memory impairment and the neuropathology in Tg2576 mice, AD animal model. *PLoS One* 5:e8840. doi: 10.1371/journal.pone.0008840

Hagmeyer, S., Cristóvão, J. S., Mulvihill, J. J., Boeckers, T. M., Gomes, C. M., and Grabrucker, A. M. (2017). Zinc binding to S100B affords regulation of trace metal homeostasis and excitotoxicity in the brain. *Front. Mol. Neurosci.* 10:456. doi: 10.3389/fnmol.2017.00456

Heizmann, C. W., Fritz, G., and Schafer, B. W. (2002). S100 proteins: structure, functions and pathology. *Front. Biosci.* 7, d1356–d1368.

Hofmann, M. A., Drury, S., Fu, C., Qu, W., Taguchi, A., Lu, Y., et al. (1999). RAGE mediates a novel proinflammatory axis: a central cell surface receptor for S100/calgranulin polypeptides. *Cell* 97, 889–901. doi: 10.1016/s0092-8674(00)80801-6

Hooper, C., Killick, R., and Lovestone, S. (2008). The GSK3 hypothesis of Alzheimer's disease. *J. Neurochem.* 104, 1433–1439. doi: 10.1111/j.1471-4159.2007.05194.x

Horvath, I., Jia, X., Johansson, P., Wang, C., Moskalenko, R., Steinau, A., et al. (2016). Pro-inflammatory S100A9 protein as a robust biomarker differentiating early stages of cognitive impairment in alzheimer's disease. *ACS Chem. Neurosci.* 7, 34–39. doi: 10.1021/acschemneuro.5b00265

Iashchishyn, I. A., Gruden, M. A., Moskalenko, R. A., Davydova, T. V., Wang, C., Sewell, R. D. E., et al. (2018). Intranasally Administered S100A9 Amyloids Induced Cellular Stress, Amyloid Seeding, and Behavioral Impairment in Aged Mice. *ACS Chem Neurosci.* 9, 1338–1348 doi: 10.1021/acschemneuro.7b00512

Iashchishyn, I. A., Sulskis, D., Nguyen Ngoc, M., Smirnovas, V., and Morozova-Roche, L. A. (2017). Finke-Watzky Two-Step Nucleation-Autocatalysis Model of S100A9 Amyloid Formation: Protein Misfolding as "Nucleation" Event. *ACS Chem Neurosci* 8, 2152–2158. doi: 10.1021/acschemneuro.7b00251

Ichikawa, H., Jacobowitz, D. M., and Sugimoto, T. (1997). S100 protein-immunoreactive primary sensory neurons in the trigeminal and dorsal root ganglia of the rat. *Brain Res* 748, 253–257. doi: 10.1016/s0006-8993(96)01364-9

Isobe, T., Takahashi, K., and Okuyama, T. (1984). S100a0 (alpha alpha) protein is present in neurons of the central and peripheral nervous system. *J. Neurochem.* 43, 1494–1496. doi: 10.1111/j.1471-4159.1984.tb05415.x

Kitazawa, M., Cheng, D., Tsukamoto, M. R., Koike, M. A., Wes, P. D., Vasilevko, V., et al. (2011). Blocking IL-1 signaling rescues cognition, attenuates tau pathology, and restores neuronal beta-catenin pathway function in an Alzheimer's disease model. *J. Immunol.* 187, 6539–6549. doi: 10.4049/jimmunol.1100620

Kummer, M. P., Vogl, T., Axt, D., Griep, A., Vieira-Saecker, A., Jessen, F., et al. (2012). Mrp14 deficiency ameliorates amyloid beta burden by increasing microglial phagocytosis and modulation of amyloid precursor protein processing. *J. Neurosci.* 32, 17824–17829. doi: 10.1523/JNEUROSCI.1504-12.2012

LaFerla, F. M. (2002). Calcium dyshomeostasis and intracellular signalling in Alzheimer's disease. *Nat. Rev. Neurosci.* 3, 862–872. doi: 10.1038/nrn960

Leal, S. S., Botelho, H. M., and Gomes, C. M. (2012). Metal ions as modulators of protein conformation and misfolding in neurodegeneration. *Coord. Chem. Rev.* 256, 2253–2270. doi: 10.1016/j.ccr.2012.04.004

Leclerc, E., Fritz, G., Vetter, S. W., and Heizmann, C. W. (2009). Binding of S100 proteins to RAGE: an update. *Biochim. Biophys. Acta Mol. Cell Res.* 1793, 993–1007. doi: 10.1016/j.bbamcr.2008.11.016

Lee, E. O., Yang, J. H., Chang, K. A., Suh, Y. H., and Chong, Y. H. (2013). Amyloid-beta peptide-induced extracellular S100A9 depletion is associated with decrease

of antimicrobial peptide activity in human THP-1 monocytes. *J. Neuroinflam.* 10:68. doi: 10.1186/1742-2094-10-68

Lee, H. J., Savelieff, M. G., Kang, J., Brophy, M. B., Nakashige, T. G., Lee, S. J. C., et al. (2018). Calprotectin influences the aggregation of metal-free and metal-bound amyloid-beta by direct interaction. *Metallomics* 10, 1116–1127. doi: 10.1039/c8mt00091c

Li, G., Chen, H., Cheng, L., Zhao, R., Zhao, J., and Xu, Y. (2014). Amyloid precursor-like protein 2 C-terminal fragments upregulate S100A9 gene and protein expression in BV2 cells. *Neural Regen. Res.* 9, 1923–1928. doi: 10.4103/1673-5374.145362

Ling, Y., Morgan, K., and Kalsheker, N. (2003). Amyloid precursor protein (APP) and the biology of proteolytic processing: relevance to Alzheimer's disease. *Int. J. Biochem. Cell Biol.* 35, 1505–1535. doi: 10.1016/s1357-2725(03)00133-x

Liu, L., Drouet, V., Wu, J. W., Witter, M. P., Small, S. A., Clelland, C., et al. (2012). Trans-synaptic spread of tau pathology in vivo. *PLoS One* 7:e31302. doi: 10.1371/journal.pone.0031302

Liu, L., Li, Y. K., Van Eldik, L. J., Griffin, W. S. T., and Barger, S. W. (2005). S100B-induced microglial and neuronal IL-1 expression is mediated by cell type-specific transcription factors. *J. Neurochem.* 92, 546–553. doi: 10.1111/j.1471-4159.2004.02909.x

Lodeiro, M., Puerta, E., Ismail, M. A., Rodriguez-Rodriguez, P., Ronnback, A., Codita, A., et al. (2017). Aggregation of the inflammatory S100A8 precedes a beta plaque formation in transgenic APP mice: positive feedback for S100A8 and a beta productions. *J. Gerontol. Ser. Biol. Sci. Med. Sci.* 72, 319–328. doi: 10.1093/gerona/glw073

Lovell, M. A., Robertson, J. D., Teesdale, W. J., Campbell, J. L., and Markesbery, W. R. (1998). Copper, iron and zinc in Alzheimer's disease senile plaques. *J. Neurol. Sci.* 158, 47–52. doi: 10.1016/s0022-510x(98)00092-6

Lu, J., Esposito, G., Scuderi, C., Steardo, L., Delli-Bovi, L. C., Hecht, J. L., et al. (2011). S100B and APP promote a gliocentric shift and impaired neurogenesis in down syndrome neural progenitors. *PLoS One* 6:e22126. doi: 10.1371/journal.pone.0022126

Maciejewski, A., Prado, V. F., Prado, M. A. M., and Choy, W. Y. (2017). Molecular basis for the interaction between stress-inducible phosphoprotein 1 (STIP1) and S100A1. *Biochem. J.* 474, 1853–1866. doi: 10.1042/BCJ20161055

Marshak, D. R., Pesce, S. A., Stanley, L. C., and Griffin, W. S. (1992). Increased S100 beta neurotrophic activity in Alzheimer's disease temporal lobe. *Neurobiol. Aging* 13, 1–7. doi: 10.1016/0197-4580(92)90002-f

Masters, C. L., Bateman, R., Blennow, K., Rowe, C. C., Sperling, R. A., and Cummings, J. L. (2015). Alzheimer's disease. *Nat. Rev. Dis. Primers* 1:15056. doi: 10.1038/nrdp.2015.56

Matsui Lee, I. S., Suzuki, M., Hayashi, N., Hu, J., Van Eldik, L. J., Titani, K., et al. (2000). Copper-dependent formation of disulfide-linked dimer of S100B protein. *Arch. Biochem. Biophys.* 374, 137–141. doi: 10.1006/abbi.1999.1595

Maynard, C. J., Bush, A. I., Masters, C. L., Cappai, R., and Li, Q. X. (2005). Metals and amyloid-beta in Alzheimer's disease. *Int. J. Exp. Pathol.* 86, 147–159.

Mori, T., Koyama, N., Arendash, G. W., Horikoshi-Sakuraba, Y., Tan, J., and Town, T. (2010). Overexpression of human S100B exacerbates cerebral amyloidosis and gliosis in the Tg2576 mouse model of Alzheimer's disease. *Glia* 58, 300–314. doi: 10.1002/glia.20924

Mrak, R. E., and Griffinbc, W. S. (2001). The role of activated astrocytes and of the neurotrophic cytokine S100B in the pathogenesis of Alzheimer's disease. *Neurobiol. Aging* 22, 915–922. doi: 10.1016/s0197-4580(01)00293-7

Mrak, R. E., Sheng, J. G., and Griffin, W. S. (1996). Correlation of astrocytic S100 beta expression with dystrophic neurites in amyloid plaques of Alzheimer's disease. *J. Neuropathol. Exp. Neurol.* 55, 273–279. doi: 10.1097/00005072-199603000-00002

Mueller, C., Zhou, W. D., Vanmeter, A., Heiby, M., Magaki, S., Ross, M. M., et al. (2010). The heme degradation pathway is a promising serum biomarker source for the early detection of alzheimer's disease. *J. Alzh. Dis.* 19, 1081–1091. doi: 10.3233/jad-2010-1303

O'Dowd, B. S., Zhao, W. Q., Ng, K. T., and Robinson, S. R. (1997). Chicks injected with antisera to either S-100 alpha or S-100 beta protein develop amnesia for a passive avoidance task. *Neurobiol. Learn. Mem.* 67, 197–206. doi: 10.1006/nlme.1997.3766

Ostapchenko, V. G., Beraldo, F. H., Mohammad, A. H., Xie, Y. F., Hirata, P. H., Magalhaes, A. C., et al. (2013). The prion protein ligand, stress-inducible phosphoprotein 1, regulates amyloid-beta oligomer toxicity. *J. Neurosci.* 33, 16552–16564. doi: 10.1523/JNEUROSCI.3214-13.2013

Peskind, E. R., Griffin, W. S. T., Akama, K. T., Raskind, M. A., and Van Eldik, L. J. (2001). Cerebrospinal fluid S100B is elevated in the earlier stages of Alzheimer's disease. *Neurochem. Int.* 39, 409–413. doi: 10.1016/s0197-0186(01)00048-1

Petzold, A., Jenkins, R., Watt, H. C., Green, A. J., Thompson, E. J., Keir, G., et al. (2003). Cerebrospinal fluid S100B correlates with brain atrophy in Alzheimer's disease. *Neurosci. Lett.* 336, 167–170. doi: 10.1016/s0304-3940(02)01257-0

Popugaeva, E., Pchitskaya, E., and Bezprozvanny, I. (2017). Dysregulation of neuronal calcium homeostasis in Alzheimer's disease – A therapeutic opportunity? *Biochem. Biophys. Res. Commun.* 483, 998–1004. doi: 10.1016/j.bbrc.2016.09.053

Prinzen, C., Trumbach, D., Wurst, W., Endres, K., Postina, R., and Fahrenholz, F. (2009). Differential gene expression in ADAM10 and mutant ADAM10 transgenic mice. *BMC Genomics* 10:66. doi: 10.1186/1471-2164-10-66

Qin, W., Ho, L., Wang, J., Peskind, E., and Pasinetti, G. M. (2009). S100A7, a novel alzheimer's disease biomarker with non-amyloidogenic alpha-secretase activity acts via selective promotion of ADAM-10. *PLoS One* 4:e4183. doi: 10.1371/journal.pone.0004183

Reeves, R. H., Yao, J., Crowley, M. R., Buck, S., Zhang, X., Yarowsky, P., et al. (1994). Astrocytosis and axonal proliferation in the hippocampus of S100b transgenic mice. *Proc. Natl. Acad. Sci. U.S.A.* 91, 5359–5363. doi: 10.1073/pnas.91.12.5359

Roltsch, E., Holcomb, L., Young, K. A., Marks, A., and Zimmer, D. B. (2010). PSAPP mice exhibit regionally selective reductions in gliosis and plaque deposition in response to S100B ablation. *J. Neuroinflam.* 7:78. doi: 10.1186/1742-2094-7-78

Santos, G., Barateiro, A., Gomes, C. M., Brites, D., and Fernandes, A. (2018). Impaired oligodendrogenesis and myelination by elevated S100B levels during neurodevelopment. *Neuropharmacology* 129, 69–83. doi: 10.1016/j.neuropharm.2017.11.002

Senior, S. Z., Mans, L. L., Vanguilder, H. D., Kelly, K. A., Hendrich, M. P., and Elgren, T. E. (2003). Catecholase activity associated with copper-S100B. *Biochemistry* 42, 4392–4397. doi: 10.1021/bi0205799

Shen, L. M., Liao, L. P., Chen, C., Guo, Y., Song, D. L., Wang, Y., et al. (2017). Proteomics analysis of blood serums from alzheimer's disease patients using iTRAQ labeling technology. *J. Alzh. Dis.* 56, 361–378. doi: 10.3233/JAD-160913

Sheng, J. G., Mrak, R. E., and Griffin, W. S. (1994). S100 beta protein expression in Alzheimer disease: potential role in the pathogenesis of neuritic plaques. *J. Neurosci. Res.* 39, 398–404. doi: 10.1002/jnr.490390406

Sheng, J. G., Mrak, R. E., and Griffin, W. S. (1997). Glial-neuronal interactions in Alzheimer disease: progressive association of IL-1alpha+ microglia and S100beta+ astrocytes with neurofibrillary tangle stages. *J. Neuropathol. Exp. Neurol.* 56, 285–290. doi: 10.1097/00005072-199703000-00007

Shepherd, C. E., Goyette, J., Utter, V., Rahimi, F., Yang, Z., Geczy, C. L., et al. (2006). Inflammatory S100A9 and S100A12 proteins in Alzheimer's disease. *Neurobiol. Aging* 27, 1554–1563. doi: 10.1016/j.neurobiolaging.2005.09.033

Sidoryk-Wegrzynowicz, M., Gerber, Y. N., Ries, M., Sastre, M., Tolkovsky, A. M., and Spillantini, M. G. (2017). Astrocytes in mouse models of tauopathies acquire early deficits and lose neurosupportive functions. *Acta Neuropathol. Commun.* 5:89. doi: 10.1186/s40478-017-0478-9

Simpson, J. E., Ince, P. G., Lace, G., Forster, G., Shaw, P. J., Matthews, F., et al. (2010). Astrocyte phenotype in relation to Alzheimer-type pathology in the ageing brain. *Neurobiol. Aging* 31, 578–590. doi: 10.1016/j.neurobiolaging.2008.05.015

Sorci, G., Agneletti, A. L., and Donato, R. (2000). Effects of S100A1 and S100B on microtubule stability. An in vitro study using triton-cytoskeletons from astrocyte and myoblast cell lines. *Neuroscience* 99, 773–783. doi: 10.1016/s0306-4522(00)00238-4

Steiner, J., Bogerts, B., Schroeter, M. L., and Bernstein, H. G. (2011). S100B protein in neurodegenerative disorders. *Clin. Chem. Lab. Med.* 49, 409–424. doi: 10.1515/CCLM.2011.083

Tai, H. C., Wang, B. Y., Serrano-Pozo, A., Frosch, M. P., Spires-Jones, T. L., and Hyman, B. T. (2014). Frequent and symmetric deposition of misfolded tau oligomers within presynaptic and postsynaptic terminals in Alzheimer's disease. *Acta Neuropathol. Commun.* 2:146. doi: 10.1186/s40478-014-0146-2

Takeda, A., and Tamano, H. (2016). Insight into cognitive decline from Zn(2+) dynamics through extracellular signaling of glutamate and

glucocorticoids. *Arch. Biochem. Biophys.* 611, 93–99. doi: 10.1016/j.abb.2016.06.021

Teigelkamp, S., Bhardwaj, R. S., Roth, J., Meinardus-Hager, G., Karas, M., and Sorg, C. (1991). Calcium-dependent complex assembly of the myeloic differentiation proteins MRP-8 and MRP-14. *J. Biol. Chem.* 266, 13462–13467.

Tian, Z.-Y., Wang, C.-Y., Wang, T., Li, Y.-C., and Wang, Z. Y. (2019). Glial S100A6 Degrades beta-amyloid aggregation through targeting competition with zinc ions. *Aging Dis.* 10:14.

Turner, P. R., O'connor, K., Tate, W. P., and Abraham, W. C. (2003). Roles of amyloid precursor protein and its fragments in regulating neural activity, plasticity and memory. *Prog. Neurobiol.* 70, 1–32. doi: 10.1016/s0301-0082(03)00089-3

Van Eldik, L. J., and Griffin, W. S. (1994). S100 beta expression in Alzheimer's disease: relation to neuropathology in brain regions. *Biochim. Biophys. Acta* 1223, 398–403.

Venegas, C., and Heneka, M. T. (2017). Danger-associated molecular patterns in Alzheimer's disease. *J. Leukoc. Biol.* 101, 87–98. doi: 10.1189/jlb.3MR0416-204R

Walker, D. G., Link, J., Lue, L. F., Dalsing-Hernandez, J. E., and Boyes, B. E. (2006). Gene expression changes by amyloid beta peptide-stimulated human postmortem brain microglia identify activation of multiple inflammatory processes. *J. Leukoc. Biol.* 79, 596–610. doi: 10.1189/jlb.0705377

Walsh, D. M., Klyubin, I., Fadeeva, J. V., Cullen, W. K., Anwyl, R., Wolfe, M. S., et al. (2002). Naturally secreted oligomers of amyloid β protein potently inhibit hippocampal long-term potentiation in vivo. *Nature* 416, 535–539. doi: 10.1038/416535a

Wang, C., Iashchishyn, I. A., Pansieri, J., Nystrom, S., Klementieva, O., Kara, J., et al. (2018). S100A9-Driven amyloid-neuroinflammatory cascade in traumatic brain injury as a precursor state for alzheimer's disease. *Sci. Rep.* 8:12836. doi: 10.1038/s41598-018-31141-x

Wang, C., Klechikov, A. G., Gharibyan, A. L., Warmlander, S. K., Jarvet, J., Zhao, L., et al. (2014). The role of pro-inflammatory S100A9 in Alzheimer's disease amyloid-neuroinflammatory cascade. *Acta Neuropathol.* 127, 507–522. doi: 10.1007/s00401-013-1208-4

Wang, X., Wang, W., Li, L., Perry, G., Lee, H. G., and Zhu, X. (2014). Oxidative stress and mitochondrial dysfunction in Alzheimer's disease. *Biochim. Biophys. Acta* 1842, 1240–1247.

Wasik, U., Schneider, G., Mietelska-Porowska, A., Mazurkiewicz, M., Fabczak, H., Weis, S., et al. (2013). Calcyclin binding protein and Siah-1 interacting protein in Alzheimer's disease pathology: neuronal localization and possible function. *Neurobiol. Aging* 34, 1380–1388. doi: 10.1016/j.neurobiolaging.2012.11.007

Weiner, H. L., and Frenkel, D. (2006). Immunology and immunotherapy of Alzheimer's disease. *Nat. Rev. Immunol.* 6, 404–416.

Weissmann, R., Huttenrauch, M., Kacprowski, T., Bouter, Y., Pradier, L., Bayer, T. A., et al. (2016). Gene expression profiling in the APP/PS1KI mouse model of familial alzheimer's disease. *J. Alzh. Dis.* 50, 397–409. doi: 10.3233/JAD-150745

Wirths, O., Breyhan, H., Marcello, A., Cotel, M. C., Bruck, W., and Bayer, T. A. (2010). Inflammatory changes are tightly associated with neurodegeneration in the brain and spinal cord of the APP/PS1KI mouse model of Alzheimer's disease. *Neurobiol. Aging* 31, 747–757. doi: 10.1016/j.neurobiolaging.2008.06.011

Wruck, W., Schroter, F., and Adjaye, J. (2016). Meta-analysis of transcriptome data related to hippocampus biopsies and iPSC-derived neuronal cells from alzheimer's disease patients reveals an association with FOXA1 and FOXA2 gene regulatory networks. *J. Alzh. Dis.* 50, 1065–1082. doi: 10.3233/JAD-150733

Xiong, Z., O'hanlon, D., Becker, L. E., Roder, J., Macdonald, J. F., and Marks, A. (2000). Enhanced calcium transients in glial cells in neonatal cerebellar cultures derived from S100B null mice. *Exp. Cell Res.* 257, 281–289. doi: 10.1006/excr.2000.4902

Yamada, J., and Jinno, S. (2012). Upregulation of calcium binding protein, S100A6, in activated astrocytes is linked to glutamate toxicity. *Neuroscience* 226, 119–129. doi: 10.1016/j.neuroscience.2012.08.068

Yamada, J., and Jinno, S. (2014). S100A6 (Calcyclin) is a novel marker of neural stem cells and astrocyte precursors in the subgranular zone of the adult mouse hippocampus. *Hippocampus* 24, 89–101. doi: 10.1002/hipo.22207

Yang, Q., Hamberger, A., Hyden, H., Wang, S., Stigbrand, T., and Haglid, K. G. (1995). S-100 beta has a neuronal localisation in the rat hindbrain revealed by an antigen retrieval method. *Brain Res.* 696, 49–61. doi: 10.1016/0006-8993(95)00755-f

Yang, Q., O'hanlon, D., Heizmann, C. W., and Marks, A. (1999). Demonstration of heterodimer formation between S100B and S100A6 in the yeast two-hybrid system and human melanoma. *Exp. Cell Res.* 246, 501–509. doi: 10.1006/excr.1998.4314

Yardan, T., Erenler, A. K., Baydin, A., Aydin, K., and Cokluk, C. (2011). Usefulness of S100B protein in neurological disorders. *J. Pak. Med. Assoc.* 61, 276–281.

Yeh, C. W., Yeh, S. H., Shie, F. S., Lai, W. S., Liu, H. K., Tzeng, T. T., et al. (2015). Impaired cognition and cerebral glucose regulation are associated with astrocyte activation in the parenchyma of metabolically stressed APPswe/PS1dE9 mice. *Neurobiol. Aging* 36, 2984–2994. doi: 10.1016/j.neurobiolaging.2015.07.022

Zhang, C., Liu, Y., Gilthorpe, J., and Van Der Maarel, J. R. (2012). MRP14 (S100A9) protein interacts with Alzheimer beta-amyloid peptide and induces its fibrillization. *PLoS One* 7:e32953. doi: 10.1371/journal.pone.0032953

Zhao, L. N., Zhang, T., Zhang, C., Wang, C., Morozova-Roche, L. A., Chew, L. Y., et al. (2013). S100A9 induces aggregation-prone conformation in abeta peptides: a combined experimental and simulation study. *RSC Adv.* 3, 24081–24089.

Zimmer, D. B., Chaplin, J., Baldwin, A., and Rast, M. (2005). S100-mediated signal transduction in the nervous system and neurological diseases. *Cell Mol Biol.* 51, 201–214.

Zimmer, D. B., Cornwall, E. H., Reynolds, P. D., and Donald, C. M. (1998). S100A1 regulates neurite organization, tubulin levels, and proliferation in PC12 cells. *J. Biol. Chem.* 273, 4705–4711. doi: 10.1074/jbc.273.8.4705

Conflict of Interest Statement: The authors declare that the research was conducted in the absence of any commercial or financial relationships that could be construed as a potential conflict of interest.

frontiers in Neuroscience

ORIGINAL RESEARCH
published: 16 May 2019
doi: 10.3389/fnins.2019.00419

The Extent of Human Apolipoprotein A-I Lipidation Strongly Affects the β-Amyloid Efflux Across the Blood-Brain Barrier *in vitro*

Roberta Dal Magro[1†], Sara Simonelli[2†], Alysia Cox[1], Beatrice Formicola[1], Roberta Corti[1], Valeria Cassina[1], Luca Nardo[1], Francesco Mantegazza[1], Domenico Salerno[1], Gianvito Grasso[3], Marco Agostino Deriu[3], Andrea Danani[3], Laura Calabresi[2] and Francesca Re[1]*

[1] School of Medicine and Surgery, Nanomedicine Center NANOMIB, University of Milano-Bicocca, Monza, Italy, [2] Dipartimento di Scienze Farmacologiche e Biomolecolari, Centro Grossi Paoletti, Università degli Studi di Milano, Milan, Italy, [3] Istituto Dalle Molle di Studi sull'Intelligenza Artificiale, Scuola Universitaria Professionale della Svizzera Italiana, Università della Svizzera Italiana, Manno, Switzerland

OPEN ACCESS

Edited by:
Irving E. Vega, Michigan State University, United States

Reviewed by:
Ling Li, University of Minnesota, United States
Baiba Kurins Gillard, Houston Methodist Research Institute, United States
Cheryl Wellington, University of British Columbia, Canada

***Correspondence:**
Alysia Cox
a.cox1@campus.unimib.it

† These authors have contributed equally to this work

Specialty section:
This article was submitted to Neurodegeneration, a section of the journal Frontiers in Neuroscience

Received: *23 January 2019*
Accepted: *11 April 2019*
Published: *16 May 2019*

Citation:
Dal Magro R, Simonelli S, Cox A, Formicola B, Corti R, Cassina V, Nardo L, Mantegazza F, Salerno D, Grasso G, Deriu MA, Danani A, Calabresi L and Re F (2019) The Extent of Human Apolipoprotein A-I Lipidation Strongly Affects the β-Amyloid Efflux Across the Blood-Brain Barrier in vitro. Front. Neurosci. 13:419. doi: 10.3389/fnins.2019.00419

Much evidence suggests a protective role of high-density lipoprotein (HDL) and its major apolipoprotein apoA-I, in Alzheimer's disease (AD). The biogenesis of nascent HDL derived from a first lipidation of apoA-I, which is synthesized by the liver and intestine but not in the brain, in a process mediated by ABCA1. The maturation of nascent HDL in mature spherical HDL is due to a subsequent lipidation step, LCAT-mediated cholesterol esterification, and the change of apoA-I conformation. Therefore, different subclasses of apoA-I-HDL simultaneously exist in the blood circulation. Here, we investigated if and how the lipidation state affects the ability of apoA-I-HDL to target and modulate the cerebral β-amyloid (Aβ) content from the periphery, that is thus far unclear. In particular, different subclasses of HDL, each with different apoA-I lipidation state, were purified from human plasma and their ability to cross the blood-brain barrier (BBB), to interact with Aβ aggregates, and to affect Aβ efflux across the BBB was assessed *in vitro* using a transwell system. The results showed that discoidal HDL displayed a superior capability to promote Aβ efflux *in vitro* (9×10^{-5} cm/min), when compared to apoA-I in other lipidation states. In particular, no effect on Aβ efflux was detected when apoA-I was in mature spherical HDL, suggesting that apoA-I conformation, and lipidation could play a role in Aβ clearance from the brain. Finally, when apoA-I folded its structure in discoidal HDL, rather than in spherical ones, it was able to cross the BBB *in vitro* and strongly destabilize the conformation of Aβ fibrils by decreasing the order of the fibril structure (−24%) and the β-sheet content (−14%). These data suggest that the extent of apoA-I lipidation, and consequently its conformation, may represent crucial features that could exert their protective role in AD pathogenesis.

Keywords: HDL, apoA-I, β-amyloid, Alzheimer's disease, blood-brain barrier

INTRODUCTION

Apolipoprotein A-I (apoA-I) is involved in the generation and metabolism of high-density lipoproteins (HDL) (Zannis et al., 2006). The 28 kDa protein is synthesized in the small intestine and liver, and lipidated with cholesterol and phospholipids by the membrane-bound ATP-binding cassette transporter A1 (ABCA1) to create different subclasses of plasma HDL particles, including discoidal ones. Subsequently, a second lipidation step, mediated by LCAT, is required for maturation of nascent HDL into mature spherical lipid-rich HDL (Oram and Heinecke, 2005; Curtiss et al., 2006). During the HDL maturation process the secondary structure of apoA-I slightly changes (Sevugan Chetty et al., 2012). Therefore, in humans, HDL consist of heterogeneous subclasses, characterized according to charge, size, density, protein, and/or lipid composition. HDL are involved in removing excess cholesterol from peripheral tissues, e.g., the arterial wall, and transporting it to the liver for secretion by reverse cholesterol transport. HDL exert other protective effects, including anti-oxidative, anti-inflammatory, anti-apoptotic, and anti-infective actions (Kingwell et al., 2014).

It is well established that plasma levels of HDL cholesterol (HDL-c) and apoA-I, the major protein component of plasma HDL, inversely correlate with the development of many disorders, including cardiovascular diseases, diabetes, obesity, cancer, and infectious diseases. Dysregulated HDL metabolism has also been linked to brain disorders: a decrease in plasma levels of HDL-c and/or apoA-I are risk factors for memory decline and neurodegenerative diseases, such as Alzheimer's disease (AD) (Vitali et al., 2014).

Alzheimer's disease is the most common type of dementia and affects tens of millions of people worldwide. The amyloid hypothesis (Haass and Selkoe, 1993; Glenner and Wong, 2012; Selkoe and Hardy, 2016) proposes that β-amyloid peptide (Aβ), the main component of senile plaques, is the key player in AD pathogenesis. Aβ monomers, derived from the proteolytic cleavage of the larger glycoprotein amyloid precursor protein, if not efficiently cleared from the brain can aggregate into different assemblies, which can then form regular fibrils and plaques.

Some evidence suggests that apoA-I might be involved in the pathogenesis of AD, but its role has not yet been elucidated. In a recent publication, Robert et al. (2017a) suggest that the risk to develop AD could be reduced when supported by high concentrations of plasma levels of HDL and apoA-I. It has also been shown that higher plasma levels of HDL and apoA-I are directly correlated with an increased MMSE and a lower risk of developing AD (Merched et al., 2000). Moreover, a reduction of hippocampal and whole brain volume and of cortical thickness has been detected in AD patients, along with lower plasma levels of apoA-I (Hye et al., 2014). In another study, reduced serum apoA-I has been detected in AD, contrarily to non-demented age-matched patients (Shih et al., 2014). This body of evidence suggests that apoA-I could play a protective role in AD pathogenesis, possibly by promoting the clearance of Abeta from the brain. In favor of this hypothesis are also *in vivo* studies on AD mouse animal models, showing that cognitive deficit is prevented by apoA-I overexpression (Lewis et al., 2010), while it is worsened by its deletion (Lefterov et al., 2010), and i.v., administration of HDL reduces soluble Aβ brain levels (Robert et al., 2016).

However, more research is needed to clarify its implications and no information is available concerning the possible role of distinct HDL subclasses. In this study, we investigate *in vitro* the ability of apoA-I in different lipidation states to affect Aβ efflux across the BBB, using a transwell system made by immortalized human brain capillary endothelial cells.

Moreover, it is known that apoA-I is present in the brain (Elliott et al., 2010), but its mRNA has not been detected (Mahley et al., 1984; Harr et al., 1996; Huang et al., 2008). Thus, brain apoA-I is believed to be plasma derived from peripheral HDL that cross the blood-brain barrier (BBB) (Roheim et al., 1979; Pitas et al., 1987; Stukas et al., 2014; Fung et al., 2017).

Therefore, within the present study we have also investigated how the extent of apoA-I lipidation (giving rise to different HDL subclasses) affects the traversing of the BBB and the interaction with Aβ aggregates; an issue that, to the best of our knowledge, has never been investigated before.

MATERIALS AND METHODS

Human Samples

Human plasma samples from healthy donors were provided by the Immunohematology and Transfusion Medicine Service (SIMT) of ASST Grande Ospedale Metropolitano Niguarda, Milan. All experimental protocols were approved by license 446-092014 CE from Ospedale Niguarda Ca' Granda and carried out in accordance with these guidelines and regulations. Informed consent was obtained from all donors. Plasma was prepared by low speed centrifugation at 4°C and lipoprotein isolation started within 6 h of blood collection.

Purification of apoA-I-HDL From Human Plasma

High-density lipoprotein (d = 1.063–1.21 g/mL) were purified from human plasma of healthy blood donors by sequential ultracentrifugation. Purified lipoproteins were dialyzed against saline immediately before use and were representative of the total HDL pool of human plasma. This sample was treated with chymase, which degrades small discoidal HDL particles, to obtain a fraction containing only spherical apoA-I-HDL (Favari et al., 2004). Briefly, apoA-I-HDL plasma pool was incubated with granule remnants isolated from rat mast cells (30°μg/ml of granule remnant total protein, equal to 40 BTEE Units/ml) for 2 h at 37°C. After incubation, tubes were placed on ice and centrifuged at 4°C, 12,000 rpm, for 5 min to remove the granule remnant-bound chymase, and the chymase-free supernatants were collected. The lack of discoidal, apoA-I-containing HDL was verified by non-denaturing two-dimensional (2-D) electrophoresis, in which agarose gel electrophoresis was followed by non-denaturing gradient gel electrophoresis (GGE), and immunoblotting against apoA-I. Spherical apoA-I-HDL were characterized by AFM, as described below.

Preparation of Discoidal HDL

Apolipoprotein A-I was purified from human plasma by gel-filtration chromatography (Bernini et al., 1996) and its purity (>95%) was confirmed by SDS-polyacrylamide gel electrophoresis (SDS-PAGE) using Coomassie protein staining, as previously described (Schägger and von Jagow, 1987). This sample represents lipid-poor apoA-I, having few bound phospholipid molecules. Discoidal apoA-I-HDL were prepared by the cholate dialysis method using palmitoyl-oleoyl-phosphatidylcholine (POPC) and apoA-I in the weight ratio of 2.5:1 (Calabresi et al., 1997). Their size was estimated by non-denaturing GGE using precast 4–30% gels and the Pharmacia Phast System (Franceschini et al., 2013). Phospholipid content of lipid-poor apoA-I and discoidal HDL was measured by an enzymatic method and apoA-I concentration was measured by Lowry method. The final preparation of discoidal HDL contained 2 apoA-I and 205 POPC molecules. Discoidal HDL were characterized by AFM, as described below.

Atomic Force Microscopy Imaging of apoA-I-HDL

Atomic force microscopy (AFM) imaging was performed using a Nanowizard II (JPK Instruments, Berlin) scanning probe microscope operating in tapping and contact mode in air. In tapping mode imaging of $A\beta_{1-42}$ fibrils, RTESP-300 (Bruker, United States) cantilevers were used with a nominal force constant of 40 N/m, a resonance frequency of 300 kHz, and a nominal tip radius 8 nm. For contact mode imaging of HDL subtypes, DNPS-10 (Bruker, United States) cantilevers were used with a nominal force constant of 0.06 N/m, and a nominal tip radius 10 nm. A detailed protocol used for the apoA-I-HDL characterization is supplied as Supplementary Information (see section "Characterization of HDL by AFM Imaging"). A wide range of areas of AFM images were analyzed using the commercial JPK image processing software and a customized image-analysis software (Matlab, MathWorks Inc, United States).

Preparation and Characterization of Aβ Aggregates

$A\beta_{1-42}$ (Sigma–Aldrich, Milan, Italy) fibrils were prepared as described (Gregori et al., 2010; Bana et al., 2014; Mancini et al., 2016). Briefly, the peptide (1 mg/mL) was solubilized in 1,1,3,3,3-hexafluoro-2-propanol (HFIP; Sigma–Aldrich, Milan, Italy), dried, resuspended in DMSO at a concentration of 5 mM, and bath sonicated for 10 min. To obtain a fibril-enriched preparation, samples were diluted to 200μM in 10 mM HCl and incubated at 37°C for 72 h. Aβ fibrils were characterized by AFM (Gregori et al., 2010). For the fibrillation process, samples were diluted to 100μM in 10 mM HCl and incubated at 37°C. In the reported images, Aβ was diluted to a final concentration of 10°μM in 10 mM HCl and deposited on freshly cleaved mica. Images were acquired in air in tapping mode.

Preparation and Characterization of the *in vitro* Model of Blood-Brain Barrier

The *in vitro* BBB model was prepared and characterized as previously described (Mancini et al., 2016), using immortalized human brain endothelial cells (hCMEC/D3 cells) from Institut National de la Sante et de la Recherche Medicale, Paris, France. Briefly, hCMEC/D3 were seeded (60,000 cells/cm^2) onto collagen-coated (8°μg/cm^2 rat tail collagen type 1; Gibco, Thermo Fisher Scientific) transwell filters (polycarbonate 12-well, pore size 0.4°μm, translucent membrane inserts 1.12 cm^2; Costar) to establish a polarized monolayer. The cell monolayer separates two compartments, an apical one (0.5 ml) representing the blood and a basolateral one (1 ml) representing the brain. Cells were grown for 3 days in complete EBM-2 medium (1.4°μM hydrocortisone, 10 mM HEPES, 1% penicillin-streptomycin, 5°μg.mL^{-1} ascorbic acid, and 1% chemically defined lipid concentrate) supplemented with 1 ng.mL^{-1} basic fibroblast growth factor and 10% fetal bovine serum (FBS). After 3 days *in vitro* (DIV), medium was changed to complete EBM-2 medium supplemented with 5% FBS, and 10 mM LiCl and grown for a further 3 days. *Trans*-endothelial electrical resistance (TEER) was monitored with STX2 electrode Epithelial Volt-Ohm meter (World Precision Instruments, Sarasota, FL, United States). The formation of junctions was evaluated by confocal microscopy (LSM710, Carl Zeiss, Oberkochen, Germany) and by measuring the endothelial permeability (EP) to [^{14}C-sucrose] (0.5°μCi) and [^{3}H]-propranolol (0.5°μCi), as described (Bana et al., 2014). Cell viability was assessed by MTT assay (Bana et al., 2014).

Effect of apoA-I Lipidation on *in vitro* Aβ Efflux Across the BBB

Five hundred nanomolar of Aβ fibrils dissolved in 1 ml of complete culture medium were placed in the basolateral compartment of the transwell system, as previously described (Mancini et al., 2016). The impact of this treatment on the cell monolayer was evaluated by monitoring TEER, EP to radiolabeled probes, and cell viability, following the procedure described above. 5 nmol/ml of apoA-I in discoidal HDL, spherical HDL, or total HDL plasma pool (Merino-Zamorano et al., 2016) dissolved in 500°μl of PBS was added to the apical compartment of the transwell. The impact on hCMEC/D3 monolayers of the treatments was determined by measuring the TEER after 3–24 h of incubation with apoA-I-HDL in the apical side of transwells. After different incubation times (up to 3 h) at 37°C, aliquots from the apical compartment were collected and the Aβ content was measured by ELISA assay (IBL International, Italy). The Aβ EP across the cell monolayer from the basolateral to the apical compartment (defined as Aβ efflux) was calculated as described (Bana et al., 2014; Mancini et al., 2016). As controls, 5 nmol/ml of commercially available apoA-I (Sigma-Aldrich, Milano, Italy) was dissolved in PBS and added

to the apical compartment. The Aβ efflux was determined as previously described.

Effect of Lipidation of apoA-I on Its Ability to Cross the BBB *in vitro*

A total of 5 nmol/ml of apoA-I in discoidal HDL, spherical HDL, or total HDL plasma pool dissolved in 500°μl of PBS was added to the apical compartment of the transwell and incubated at 37°C. After different times (up to 3 h) of incubation, the amount of apoA-I in the basolateral compartment was measured by ELISA assay (IBL International, Italy), and EP was calculated as described (Bana et al., 2014; Mancini et al., 2016).

Effect of apoA-I Lipidation on Preformed Aβ Fibrils

Fifty micromolar $A\beta_{1-42}$ fibrils were incubated at 37°C in buffer B (PBS 15 mM and NaCl 20 mM, pH 7.4) with discoidal HDL, spherical HDL, or apoA-I-HDL plasma pool, containing 0.18 nmol/ml of apoA-I in order to mimic its low brain concentration (Roheim et al., 1979; Fagan et al., 2000). After different times of incubation an aliquot from each sample was immobilized on a freshly cleaved mica substrate, rinsed with Milli-Q water, dried under a gentle stream of nitrogen, and analyzed by AFM.

The effect of apoA-I lipidation on preformed Aβ fibrils was also monitored by ThT assay (Quan et al., 2016). Briefly, 2°μM of Aβ fibrils were added with 5°μM ThT (Sigma-Aldrich, Milan, Italy), 10 mM glycine buffer pH 8.5 in 1 cm^2 × 1 cm^2 fluorimeter quartz cuvettes equipped with hermetic tips to prevent evaporation. 0.0036 nmol/ml of apoA-I in discoidal HDL, spherical HDL, or total HDL plasma pool were added to the sample and the ThT fluorescence (ex. 450 nm; em. 485 nm) was monitored at 37°C under stirring with a FP8500 fluorimeter (Jasco) equipped with a 4-cells peltier-thermostated sample holder. Low Aβ and apoA-I concentrations (25-fold less than in the AFM experiments) were utilized for ThT experiments since fibrils produce sizeable scattering of the fluorescence excitation light, and in order to maintain the Aβ:apoA-I molar ratio as in the AFM experiments.

Molecular Modeling of apoA-I

The recently obtained discoidal HDL with apoA-I (Bibow et al., 2017) without helix-5 was considered the starting point for this work (PDB ID: 2N5E). It was demonstrated by chemical shift comparison and lipid paramagnetic relaxation enhancement experiments (Bibow et al., 2017) that apoA-I with and without helix 5 are structurally similar, strongly indicating that the overall structure of apoaA-I is preserved in the shortened construct considered in the present study. One hundred 1,2-dimyristoyl-sn-glycero-3-phosphocholine (DMPC) lipid molecules were inserted as previously described (Bibow et al., 2017). This model was solvated and neutralized by adding 0.15 M Na and Cl ions. CHARMM36 force field (Huang and MacKerell, 2013) was used to define protein and lipids topologies, and TIP3P model (Jorgensen et al., 1983) was used for the water molecules. The obtained system was minimized by applying 1,000 steps of steepest descent energy minimization algorithm, followed by preliminary NVT of 200 ps. V-rescale thermostat was applied to maintain the temperature at 300 K with a time constant of 0.1 ps (Bussi et al., 2007). An NPT of 200 ps was carried out at 300 K (τ = 1 ps) and 1 atm (τ = 5 ps). V-rescale (Bussi et al., 2007) and Berendsen (Berendsen et al., 1984) coupling methods were used as temperature and pressure coupling. Finally, molecular dynamics (MD) equilibration of 100 ns was performed to optimize the DMPC/apoA-I complex.

Computational Docking and MD of apoA-I in Complex With Aβ Fibril

To determine the initial orientation of Aβ fibrils on DMPC/apoA-I complex, a pentamer of $A\beta_{17-42}$ was extracted from the PDB model 2BEG (Lührs et al., 2005), and considered for docking experiments (Yu and Zheng, 2012). In this NMR model, each peptide monomer has the disordered N-terminal residues 1–16 missing. However, the remaining residues 17–42 were suggested to contribute the stability of the mature fibril mostly and were included in the simulation models here, as described in previous computational studies (Fan et al., 2015; Grasso et al., 2018). The $A\beta_{17-42}$ model was first docked on apoA-I using Patchdock (Schneidman-Duhovny et al., 2005). The top-scored 100 conformations were subjected to Firedock (Andrusier et al., 2007; Mashiach et al., 2008) to refine and rescore docking solutions. The top ranked molecular system was solvated in a cubic box of 13 nm^3× 11 nm^3× 8 nm^3 and neutralized by counterions. Each system consisted of approximately 120,000 interacting particles. CHARMM36 force field (Huang and MacKerell, 2013) was used to define protein and lipids topologies, while TIP3P model (Jorgensen et al., 1983) was used for water molecules. The system was first minimized by applying the steepest descent energy minimization algorithm. Three different replicas of the same system were generated with different initial velocities to increase the statistics of MD data. A preliminary MD simulation of 100 ps was performed in NPT ensemble at 300 K (τ = 1 ps) and 1 atm (τ = 5 ps) by applying position restraints on the heavy atoms of the solute. V-rescale (Bussi et al., 2007) and Berendsen (Berendsen et al., 1984) coupling methods were used as temperature and pressure coupling. Finally, three production simulations were performed at 300K for 100 ns. For comparison, $A\beta_{17-42}$ alone in water was also simulated. Principal component analysis (PCA) was applied to reduce the dimensionality of the system (Deriu et al., 2016a; Grasso et al., 2016), elucidating large-scale and low-frequency modes, thus yielding collective motions related to the destabilization of the $A\beta_{17-42}$ fibril (Maisuradze et al., 2009). After the alignment of $A\beta_{17-42}$ C-α Cartesian coordinates, the covariance matrix was calculated and diagonalized. To estimate the structural order of the $A\beta_{17-42}$ model and to what extent fibrils chains are aligned, an order parameter was calculated for each MD snapshot using equation (1):

$$(1) ordP = \frac{1}{N_r}\sum_{r=17}^{42}\frac{\langle v_r, z\rangle}{\|v_r\|\cdot\|z\|} = \frac{1}{N_r}\sum_{r=17}^{42}\cos\alpha$$

where N, is the number of residues along the peptide chain; v_r is the vector joining each of the Cα-atoms pertaining to chain A with the corresponding Cα-atom (same residue number) of chain E; and z is the fibril axis. Values of ordP close to 1 indicate the amyloid-like shape alignment, whereas values of ordP < 1 are typical of a distorted structure.

Statistical Analysis

Data are expressed as mean ± SEM or SD obtained from three independent experiments, each of them in triplicate. Data were analyzed with one-tailed Student's t test for MD analysis. Data from *in vitro* transwell assays were analyzed with one-way ANOVA and the Tukey's *post hoc* test was applied. p-value < 0.05 was considered significant.

RESULTS

Characterization of apoA-I-HDL

Plasma derived HDL were analyzed by 2D-GGE (**Figure 1A**). Left smear represents the subclass of discoidal apoA-I-HDL and right smear represents the subclass of spherical apoA-I-HDL, as previously described (Didichenko et al., 2016). About 10–14% of apoA-I-HDL plasma pool is represented by discoidal apoA-I-HDL. This sample was treated with chymase in order to selectively degrade discoidal apoA-I-HDL, obtaining a preparation containing mature spherical apoA-I-HDL. In **Figure 1B**, the complete degradation of discoidal particles is evident, indicated by the disappearance of their smear. Synthetic discoidal apoA-I-HDL were also characterized by 2D-GGE (**Figure 1C**). As expected, the discoidal particles migrate in the pre-beta region. The estimated diameter of HDL by 2D-GGE is 11 ± 2 nm for spherical HDL and 8.8 ± 0.2 nm for synthetic discoidal HDL.

Spherical and discoidal apoA-I-HDL were also characterized by AFM imaging (**Supplementary Figure 2**). Both HDL subclasses displayed visual homogeneity in size distribution and morphology (**Figures 2A,B**). The height statistical distributions of AFM imaging allowed discrimination between the spherical and discoidal shapes (**Figure 2C**) and showed that the average dimensions of the two HDL subclasses were comparable (spherical apoA-I-HDL diameter $2R_S$ 12.7 nm, discoidal apoA-I-HDL size 12.9 nm). It should be noted that the HDL sizes obtained by using 2D-GGE and AFM techniques agree qualitatively, even if there are inherent technical differences between the two methods, which do not allow direct comparison of the results.

The extent of apoA-I lipidation, determined by measuring the phospholipid content, was 92:1 mmol lipids/mmol apoA-I for synthetic discoidal apoA-I and 15:1 mmol lipids/mmol apoA-I for lipid-poor apoA-I, as calculated from our own and previously published data (Jayaraman et al., 2012).

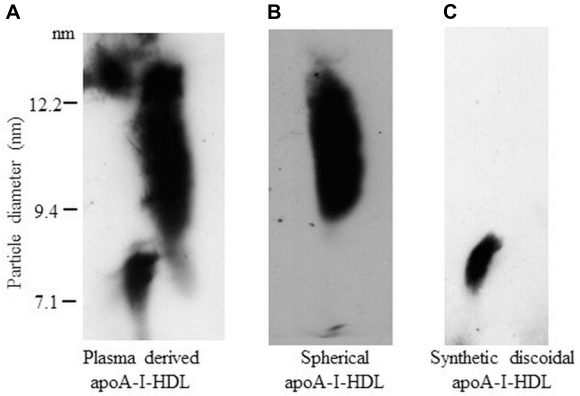

FIGURE 1 | Characterization of HDL by 2D-GGE. Total HDL, purified from human plasma, were separated by two-dimensional electrophoresis and transferred onto a nitrocellulose membrane, on which different HDL subclasses were detected by immunoblotting using anti-human apoA-I antibody. **(A)** Plasma derived apoA-I-HDL (total plasma HDL). **(B)** Spherical apoA-I-HDL, derived from plasma HDL preparation after incubation for 2 h at 37°C with chymase-containing granule remnants, which degrades small discoidal HDL particles. **(C)** Synthetic discoidal apoA-I-HDL, prepared by the cholate dialysis method.

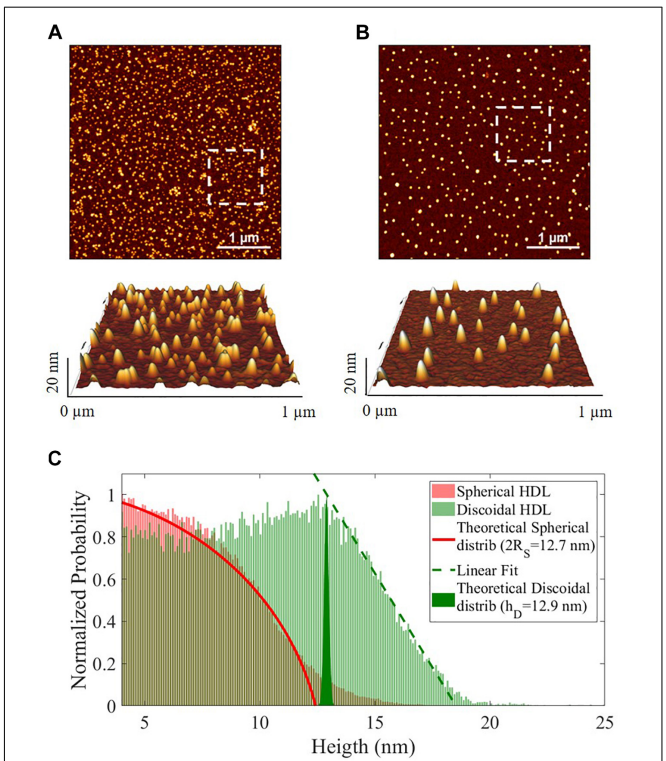

FIGURE 2 | Representative images of the morphology of HDL subclasses obtained by AFM imaging. **(A)** Discoidal and **(B)** spherical HDL on APTES functionalized mica (4 μm^2 × 4 μm^2, 1024 × 1024-pixel, Z-scale 20 nm), with 3-dimensional projections of a 1 μm^2 × 1 μm^2 region (white squares in the images). **(C)** Normalized height statistical distributions of spherical (red) and discoidal (green) HDL in the range 4–25 nm. The red fit is the theoretical distribution for a sphere ($2R_S$ = 12.7 nm), the green filled area represents the δ-function (hD = 12.9 nm) and the green dotted line is the linear regression for the final part of the distribution.

Characterization of Aβ Fibrillation

The aggregation process of Aβ from monomers to fibrils was followed and characterized by AFM imaging. Several images were acquired at the beginning of the fibrillation (t = 0h) and at successive fixed times (t = 4, 8, 24, and 48 h). Representative images are illustrated in **Figure 3A**. The results showed that long fibrils were formed over time, as previously observed (Gregori et al., 2010). The aggregation is characterized by progressive formation of unbranched fibrils of constant diameter and increasing length.

The process of fibril growth can be quantitatively evaluated by considering the time evolution of the number of pixels above a fixed height threshold in the AFM images of fibril morphology (**Supplementary Figures 1**, **2**). **Figure 3B** shows AFM images of Aβ fibrils at different incubation times with a height threshold of 1.5 nm. The percentage of pixels above a certain threshold increases with fibril extension and density, and it can be considered as a quantitative index of the aggregation process. Threshold pixel percentages over time (**Figure 3C**) show that there is continuous Aβ fibril growth in length up to 48 h.

Characterization of *in vitro* BBB Model

The *in vitro* BBB model was prepared and characterized (**Figure 4**). The TEER was monitored over time and the results showed that the maximum value (116.37 ± 4.37 Ω/cm^2) was registered 6 days after seeding (**Figure 4B**). At this time point, the formation of junctions was checked by confocal microscopy and by measuring the paracellular and transcellular EP of radiolabeled sucrose and propranolol, respectively. The results showed that Claudin-5 (**Figure 4C**, stained in green) and VE-Cadherin (**Figure 4C**, stained in red), two key components of tight and adherens endothelial junctions, are formed in

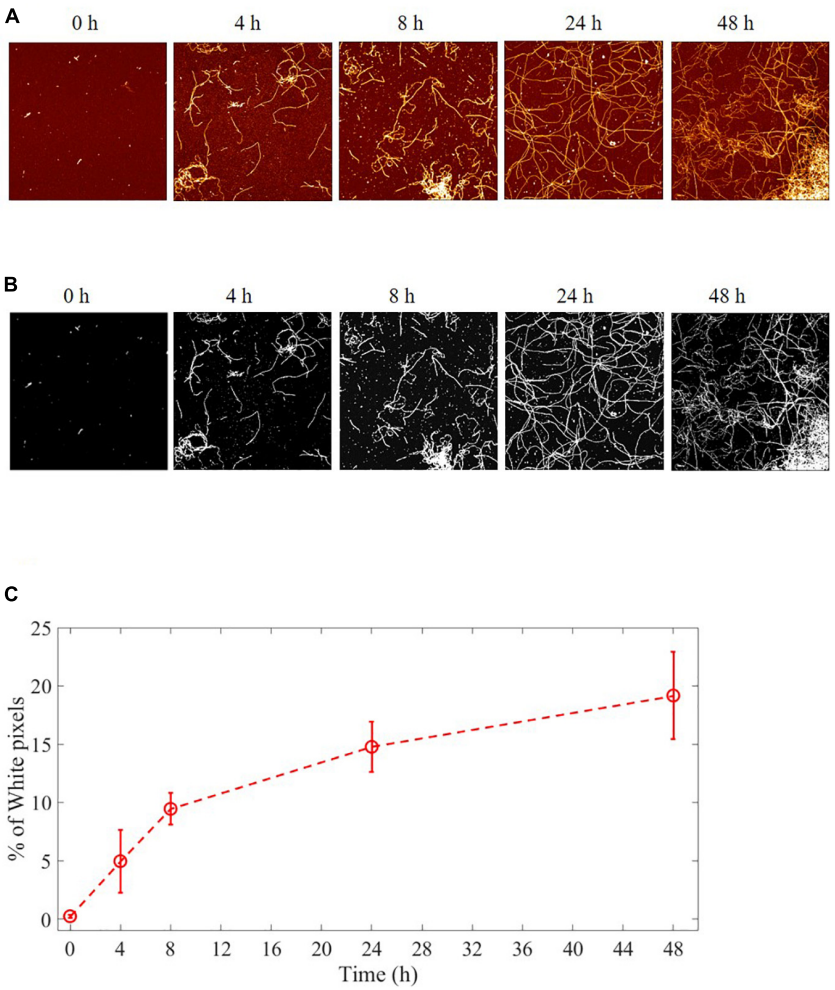

FIGURE 3 | Aggregation process of Aβ from monomers to fibrils studied by AFM. Representative images of Aβ at different fibrillation stages (t = 0, 4, 8, 24, and 48 h) of incubation at 37°C. **(A)** AFM images: 4 μm^2 × 4 μm^2, 1024 × 1024-pixel, Z-scale 10 nm. **(B)** A fixed height threshold (here 1.5 nm) is applied to the AFM images in order to quantify the number of pixels above this threshold, expressed in terms of percentage with respect the total number of pixels. The number of such pixels is proportional to the total length of the fibril i.e., to the sum of the lengths of all the deposited fibrils. In this way, it is possible to quantify the fibril growth. **(C)** Quantification of the fibrillation. Percentage of pixel above a height threshold (1.5 nm) as obtained from AFM images, plotted as a function of the incubation time at 37°C.

the hCMEC/D3 monolayer 6 days after seeding. The EP of [^{3}H]-propranolol and [^{14}C]-sucrose was 1.56 ± 0.13 × 10^{-5} and 3.83 ± 0.84 × 10^{-5} cm/min, respectively, suggesting that tight junctions had formed (**Figure 4D**). At 6 days after seeding, 500 nM of Aβ fibrils (characterized by AFM images, see **Figure 3**) were added to the basolateral compartment of the transwell system and the impact of fibrils on cell monolayer properties was checked. After 3h of hCMEC/D3 monolayer exposure to fibrils, TEER did not significantly change (114.10 ± 4.82 Ω cm^2) nor did EP of *trans*- and para-cellular probes (**Figure 4D**). Moreover, the treatment did not affect cell viability (>95% cells viability with respect to untreated cells), as assessed by MTT assay.

The impact on hCMEC/D3 monolayers of the different subclasses of apoA-I-HDL was determined by measuring the TEER after 3 and 24 h of incubation with particles in the apical side of transwells. The results showed that the treatments of cell monolayers with HDL did not affect their bioelectrical properties, with TEER values of 114 ± 11 Ω·cm^2 after treatment (**Supplementary Table 1**).

Effect of apoA-I Lipidation on *in vitro* Aβ Efflux Across the BBB

The Aβ efflux from the basolateral compartment of the transwell when apoA-I in different lipidation states were present in the apical compartment was measured by ELISA assay (**Supplementary Figure 5**).

The presence of apoA-I in the apical compartment significantly increased Aβ efflux from the basolateral side

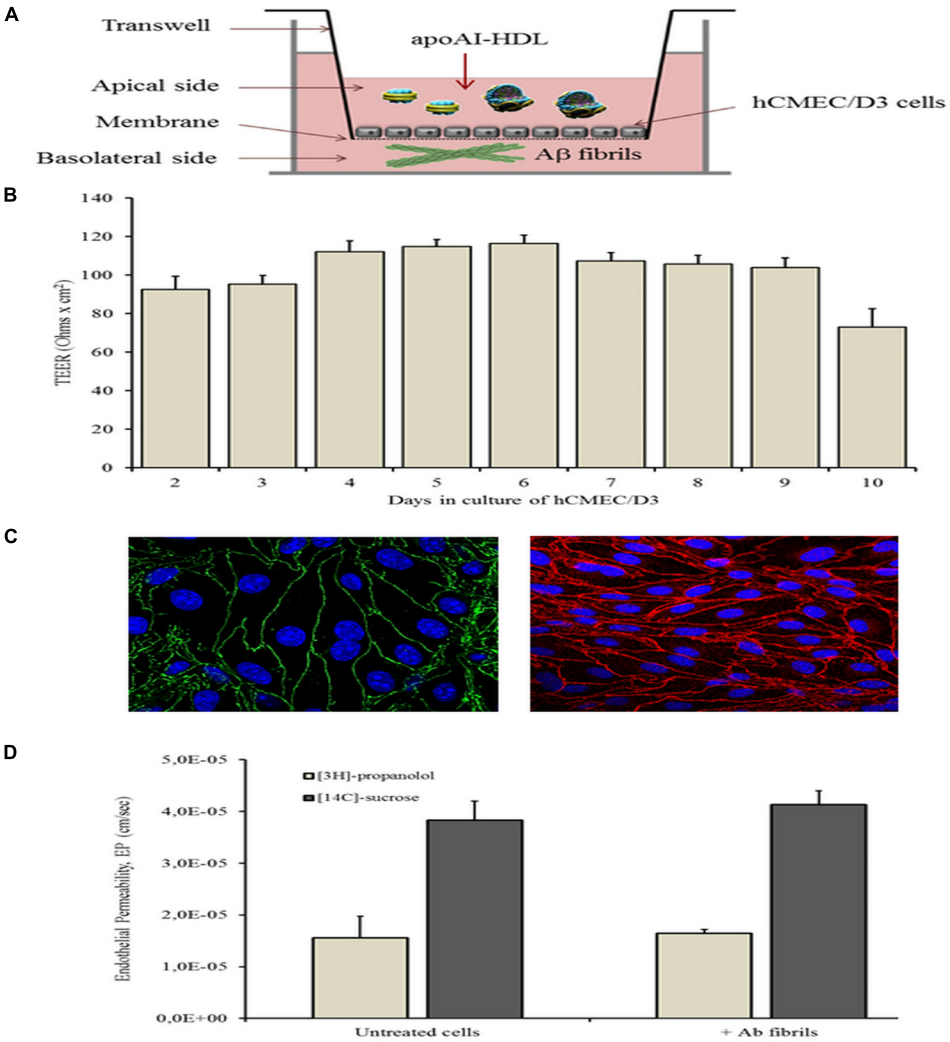

FIGURE 4 | *In vitro* BBB model. The *in vitro* BBB model, made in a transwell system by culturing hCMEC/D3 cells was characterized by monitoring the TEER values over time, by probing the formation of tight junctions and by measuring the para- and transcellular passage of radioactively labeled probes. **(A)** Graphical representation of BBB model. **(B)** TEER values monitored from 2 to 10 days in culture. **(C)** confocal microscopy visualization of tight and adherens junctions (blue, nuclei; green, ZO-1; and red, VE-cadherin). **(D)** endothelial permeability of [^{14}C]-sucrose, as probe for paracellular permeability, and [^{3}H]-propranolol, as probe for transcellular permeability, before and after incubation with Aβ fibrils in the basolateral compartment of the transwell system.

of the BBB model (**Figure 5A**). In particular, the ability of apoA-I to enhance the Aβ efflux increased with the increase of its lipidation state, reaching maximum Aβ efflux when discoidal apoA-I-HDL were present in the apical compartment.

The discoidal apoA-I-HDL significantly increased Aβ efflux from the basolateral side of the BBB model, compared to the apoA-I-HDL plasma pool ($p = 0.0016$) and spherical apoA-I-HDL ($p = 0.011$) (**Figure 5B**).

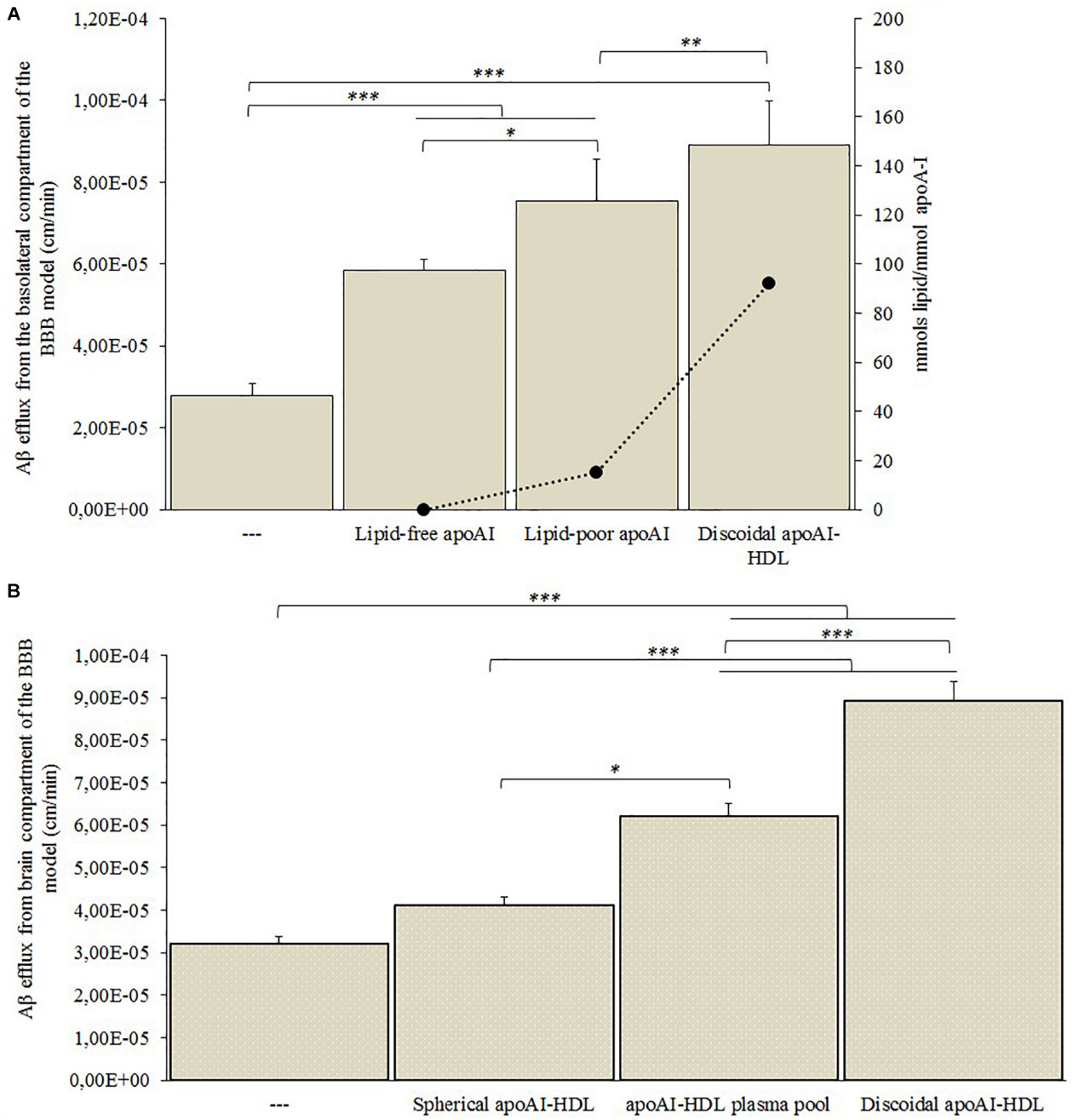

FIGURE 5 | Aβ efflux across the BBB model in the presence of human plasma-derived HDL. hCMEC/D3 cells were cultured on a transwell system and 500 nM of Aβ fibrils was added to the medium in the basolateral compartment. Different subclasses of HDL or Aβ-binding proteins were added to the apical compartment and the Aβ efflux from the basolateral compartment was measured by ELISA assay. **(A)** Endothelial permeability (EP) values of Aβ in the presence of lipid-free, lipid-poor or discoidal apoA-I, and the ratio of lipids to apoA-I in each sample. PBS alone in the apical compartment was used as a control (—). **(B)** EP values of Aβ in the presence of spherical apoA-I-HDL, apoA-I-HDL plasma pool or discoidal apoA-I-HDL. PBS alone in the apical compartment was used as a control (—). Data were expressed as endothelial permeability (EP), reported as the mean ± SEM of triplicate experiments. One-way ANOVA found significant differences **(A)** $F_{(3,32)} = 87.47$; $p = 0.00001$; **(B)** $F_{(3,32)} = 120.61$; $p = 0.00001$. $^*p < 0.05$, $^{**}p < 0.01$, $^{***}p < 0.01$ by Tukey's *post hoc* test.

In vitro BBB Crossing of apoA-I-HDL

Different subclasses of apoA-I-HDL were added to the apical compartment of the transwell system and their EP across the cell monolayer was estimated by measuring the apoA-I content in the basolateral compartment by ELISA assay for up to 3 h. The results (**Figure 6**) showed that discoidal HDL displayed higher EP values (with a passage of 1.8 ± 0.6% of apical apoA-I), compared to spherical ones ($p = 0.004$), and lipid-free apoA-I ($p = 0.048$).

Effect of apoA-I Lipidation on Preformed Aβ Fibrils

The effect of apoA-I lipidation on the disaggregation of preformed Aβ fibrils was assessed by AFM and thioflavine T (ThT) assay (Quan et al., 2016). Aβ fibrils were incubated with apoA-I in different lipidation states for up to 24 h and changes in the morphology of fibrils were followed by AFM imaging (**Figure 7**). The results showed that, starting from mature Aβ fibrils of comparable length (**Figure 7A**, row 1), the incubation with spherical apoA-I HDL did not induce significant changes in fibril morphology, and concentration (**Figure 7A**, column 2) compared to Aβ fibrils alone (**Figure 7A**, column 1). On the contrary, incubation with both the apoA-I-HDL plasma pool (**Figure 7**, column 3) and discoidal apoA-I-HDL (**Figure 7A**, column 4) induced a strong time-dependent reduction of fibril concentration and extension.

The percentage of pixels above the 1.5 nm threshold (determined as reported in **Supplementary Figure 1**) normalized with respect to the starting point (value at $t = 0$ h) is reported for each sample at different times to obtain a quantitative analysis of AFM images. The results (**Figure 7B**) demonstrate the superior capability (1.6-fold increase) of discoidal apoA-I-HDL in disassembling preformed Aβ fibrils compared to spherical apoA-I-HDL.

The β-sheet content of Aβ fibril samples were analyzed using a ThT fluorescence assay and the results (**Figure 7C**) showed that when fibrils are in incubation alone or with spherical apoA-I-HDL, their β-sheet content did not significantly change. On the contrary, the presence of apoA-I-HDL plasma pool induced a 40% reduction in β-sheet content after 18 h, and there is an almost complete disruption of β-sheet structures within 4 h in the presence of discoidal apoA-I-HDL.

Discoidal apoA-I-HDL Induce a Structural Destabilization of Aβ

The interaction between discoidal apoA-I-HDL and $A\beta_{17-42}$ was evaluated using MD simulations. Protein structural stability was analyzed by monitoring the time evolution of the root mean square deviation (RMSD) of $A\beta_{17-42}$ in water and $A\beta_{17-42}$ in complex with apoA-I. Three different replicas of the $A\beta_{17-42}$ alone in water and in complex with apoA-I were examined to increase the statistics of the MD data. It was observed that protein conformational stability was reasonably reached in the last 20 ns of the simulations (**Supplementary Figure 3**). The apoA-I-$A\beta_{17-42}$ contact surface, characterized by protein-lipid (Aβ-1,2-dimyristoyl-sn-glycero-3-phosphocholine) and protein-protein (Aβ-apoA-I) interactions, covers 6.3 ± 2 nm^2 of solvent accessible surface. The hydrophobic interaction plays a pivotal role in the contact area (**Supplementary Figure 4**). The visual inspection of the apoA-I-$A\beta_{17-42}$ complex through the MD simulation is reported in **Figure 8A** and highlights the conformational destabilization of the $A\beta_{17-42}$ due to the interaction with apoA-I.

The previously highlighted conformational instability can be quantified by analyzing the fibril order parameter (*ordP*), as reported in **Figure 8B**. A significantly decreased *ordP* value (ordP < 1 are typical of a distorted structure) was found in the case of apoA-I-$A\beta_{17-42}$ ($ordP = 0.60 \pm 0.02$) compared

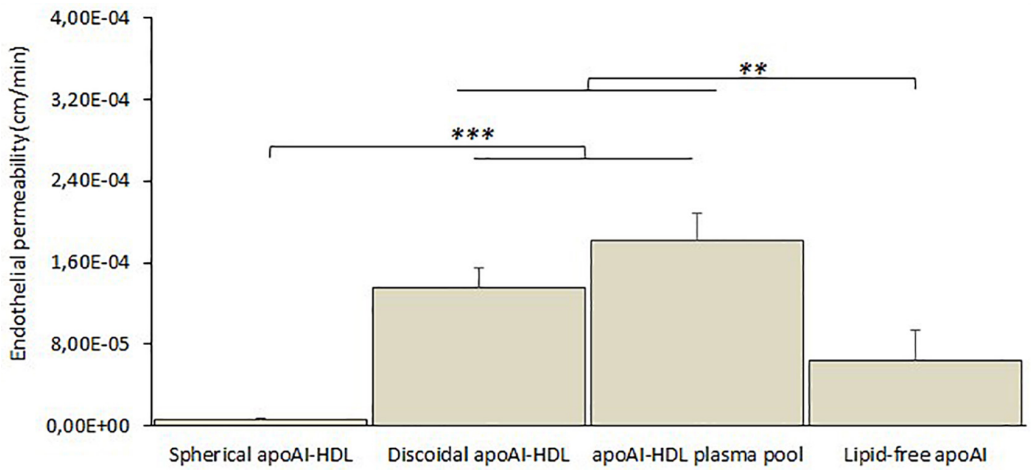

FIGURE 6 | *In vitro* BBB crossing of different subclasses of human plasma HDL. The passage of apoA-I in different lipidation states (spherical apoA-I-HDL, discoidal apoA-I-HDL, apoA-I-HDL plasma pool, or lipid-free apoA-I) across the hCMEC/D3 monolayer was determined by measuring apoA-I in the lower compartment of the transwell system at different incubation times (up to 3 h) by ELISA assay. Data were expressed as endothelial permeability (EP), reported as the mean ± SEM of triplicate experiments. One-way ANOVA found a significant difference [$F_{(3,32)} = 75.14$; $p = 0.00001$]. $^{**}p < 0.01$, $^{***}p < 0.01$ by Tukey's *post hoc* test.

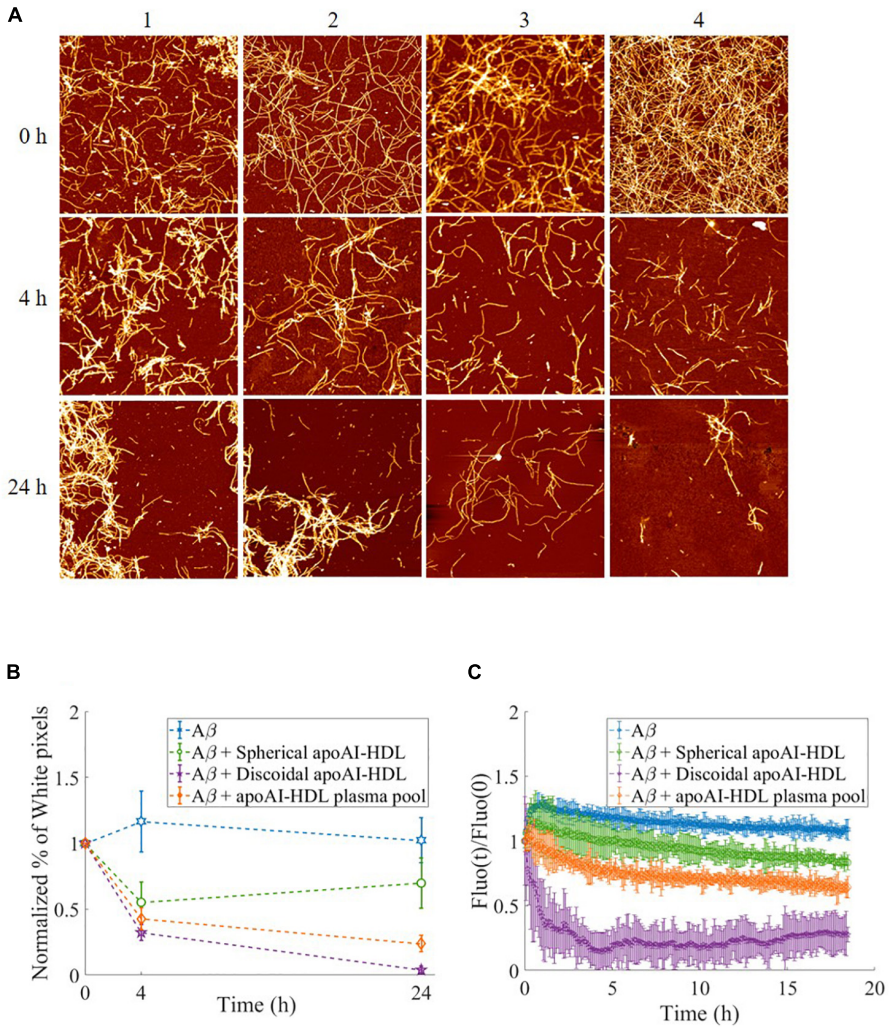

FIGURE 7 | Disaggregation of preformed Aβ fibrils in the presence of HDL. **(A)** Representative AFM images of Aβ fibrils over time, incubated at 37°C either alone (column 1) or with different HDL subclasses: spherical HDL (column 2), total HDL plasma pool (column 3), discoidal HDL (column 4). Images are 4 μm^2 × 4 μm^2, 1024 × 1024-pixel, Z-scale 10 nm. **(B)** The normalized percentage of pixels with a height above a threshold of 1.5 nm (white pixel percentage) is reported for Aβ in the presence of the different HDL subclasses at different incubation times. Values are the average of pixels higher than the threshold over several images acquired on the same sample. Error bars represent SD Each sample is normalized to its respective starting point (value at t = 0 h). **(C)** Thioflavine T fluorescence as a function of time in samples containing 2 μM Aβ fibrils alone (blue dotted) or incubated with spherical HDL (green dotted), total HDL pool (orange dotted), or discoidal HDL (purple dotted). The intensities were normalized to the respective zero-time intensity.

to $A\beta_{17-42}$ alone in water (*ordP* = 0.79 ± 0.02). The PCA provides another image, which highlights the large-scale and low frequency modes mainly related to the distortion of the Aβ fibril. After the alignment of the Aβ C-α atoms, the covariance matrix was calculated, and diagonalized for each simulated system ($A\beta_{17-42}$ in water and $A\beta_{17-42}$ in complex with apoA-I). The amplitude of the first Principal Component Vector, which takes into account more than 50% of the total variance of the protein motion, is reported in **Figure 8C**, highlighting a marked increase of conformational fluctuations when $A\beta_{17-42}$ is in complex with apoA-I ($eigval_{PCA1}$ = 17) compared to $A\beta_{17-42}$ alone in water ($eigval_{PCA1}$ = 5). Finally, a decreased β-sheet content was observed by computing the secondary structures probabilities (**Figure 8D**) along the Aβ fibril chains at the equilibrium, as previously described (Deriu et al., 2014, 2016b; Grasso et al., 2015, 2016, 2017; Janaszewska et al., 2017). Despite the beta-sheet percentage decreases only by 14%, this is a statistically significant molecular event observed only in the apoAI-Aβ molecular system in the simulated time-scale of 100 ns. Moreover, the marked loss of structural order, quantified by fibril order parameter, will further affect the beta-sheet percentage in longer time-scale. Within this framework, our results clearly show a molecular event not observed in the Aβ system in water environment, i.e., the ability of apoA-I protein to affect the conformational stability of Aβ in the investigated time-scale of 100 ns.

We note that, notwithstanding the different experimental and simulative approaches, the ThT and simulation techniques

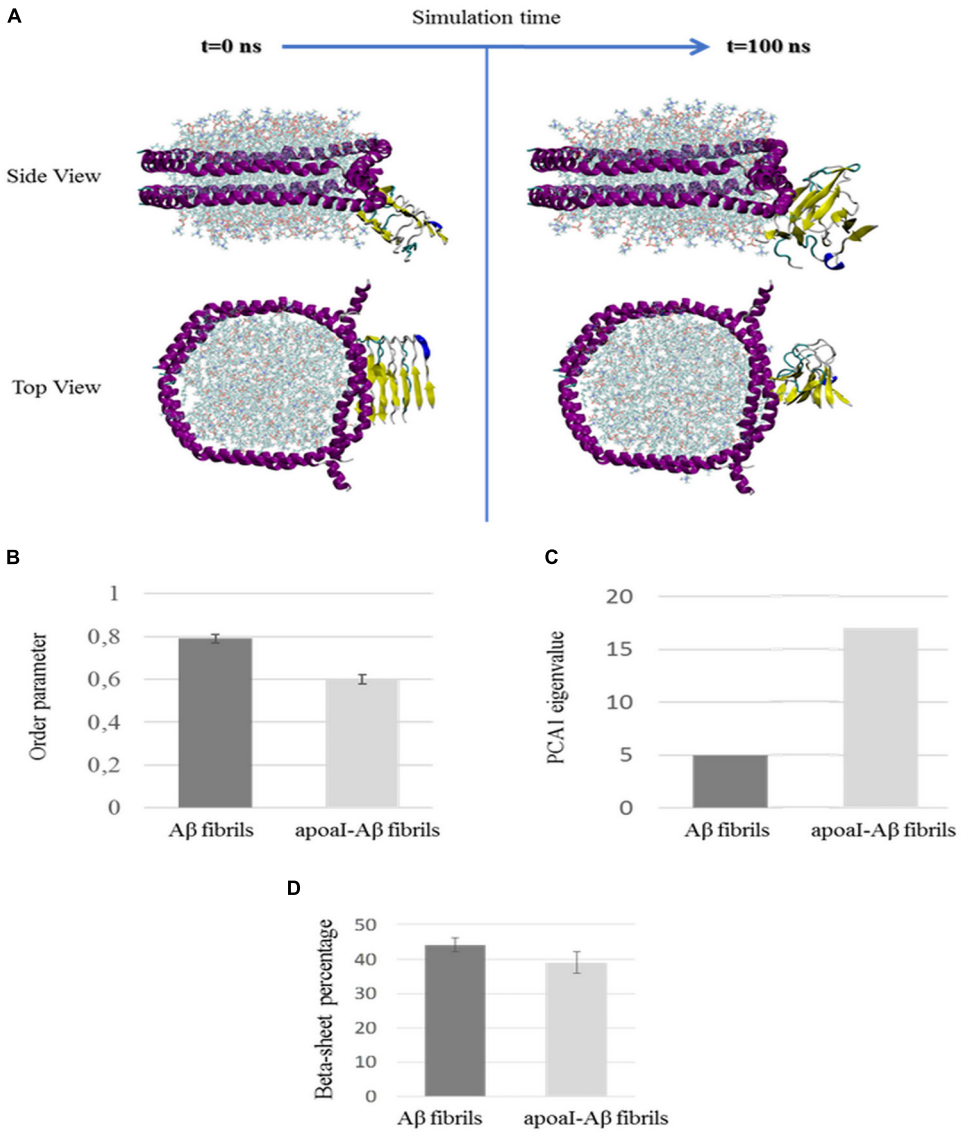

FIGURE 8 | Molecular dynamic simulation analysis. **(A)** Visual inspection of the apoA-I interaction with Aβ fibril at the beginning (t = 0 ns) and at the end (t = 100 ns) of the MD simulation. The side-view and top-view representations are reported in the upper and lower panels, respectively. Yellow represents $A\beta_{17-42}$ and magenta represents apoA-I. **(B–D)** The destabilization of Aβ fibril by discoidal apoA-I-HDL obtained by MD simulations is shown. **(B)** the order parameter calculated at the equilibrium, **(C)** the eigenvalue of the first PCA vector, and **(D)** the β-sheet content of Aβ fibril alone in water and in complex with apoA-I.

both suggest a relevant role in Aβ destabilization induced by discoidal HDL.

DISCUSSION

Considerable evidence suggests that plasma HDL, as well as having vasoprotective functions, could exert a protective role in AD (Kingwell et al., 2014; Vitali et al., 2014), and but the mechanisms involved have not been thoroughly investigated. Since Aβ clearance from the brain, a way to counteract the onset or progression of AD, partially occurs across the brain vasculature (Bates et al., 2009), and it is essential to understand if and how circulating HDL might affect Aβ passage across the BBB.

Considering previously published data about the ability of HDL and apoA-I to bind Aβ *in vitro* (Koldamova et al., 2001; Paula-Lima et al., 2009; Shih et al., 2014) and reduce Aβ levels in the brain of AD animal models (Robert et al., 2016), we hypothesized that plasma-derived HDL acts by accelerating the Aβ egress from the brain to the blood via "sink effect," as already speculated for different Aβ binding molecules or particles (Golabek et al., 1995; Mancini et al., 2016).

To investigate this issue, we used a simple BBB model consisting of an hCMEC/D3 monolayer that separates a basolateral compartment containing Aβ fibrils to mimic the

AD brain from an apical one containing different human HDL subclasses, and mimicking the blood. We chose to carry out the experiments on fibrils, since we have already shown, using the same BBB model system utilized in the present investigation, that oligomers are able to exit from the brain side either spontaneously or by "sink effect" induced by Aβ-binding liposomes (Mancini et al., 2016).

The results showed that the presence of apoA-I in the apical compartment of the transwell system strongly enhanced the Aβ egress from the basolateral one. This effect is dependent on the lipidation of apoA-I, reaching the maximum Aβ efflux when apoA-I is folded in discoidal HDL. Actually, no effect on Aβ efflux was detected when apoA-I was contained in mature spherical HDL. It should be noted that other lipid-based nanoparticles functionalized with Aβ ligands (Mancini et al., 2016) showed the ability to promote Aβ clearance, however with a lower efficiency compared to discoidal HDL.

Our results suggest the possibility that the apoA-I conformation, which depends on its lipidation state, may be also involved. In fact, the flexible apoA-I molecule adapts its structural motif to stabilize the different HDL subclasses (Silva et al., 2008; Phillips, 2013).

Therefore, we theorize that the plasma profile of HDL subclasses could differ between healthy and AD patients, thus affecting Aβ clearance from the brain. A recent study showed that HDL from AD patients were less functional compared to HDL from healthy subjects (Camponova et al., 2017), supporting this idea. Since only small soluble Aβ assemblies, and not fibrils, are able to cross the endothelial monolayer (Mancini et al., 2016), and since apoA-I is not synthetized in the brain (Demeester et al., 2000; Koch et al., 2001), the herein shown ability of apoA-I-HDL to promote the Aβ clearance across the BBB should assume their ability to cross the barrier and to disaggregate fibrils.

To verify this speculation, we tested the ability of HDL subclasses to cross the BBB *in vitro*.

Our results show that when apoA-I folded its structure in discoidal HDL, rather than in spherical particles, it was able to cross the BBB *in vitro*, suggesting that the lipidation state of apoA-I could be a key determinant affecting these features. Moreover, we found that the apical/basolateral ratio of apoA-I in our model system is comparable with the plasma/CSF ratio. Concerning the mechanism of apoA-I crossing, it should be noted that previous work suggests that the SR-BI receptor is highly selective for lipid uptake, and excludes apoAI and apoAII (Acton et al., 1996; Gillard et al., 2017). Therefore, our speculation is that apoA-I crosses the BBB through a mechanism involving the LDL receptor-related protein family, as previously suggested (Merino-Zamorano et al., 2016), and that the shape and size of HDL could be additional determining factors (Fernández-de-Retana et al., 2017).

To the best of our knowledge, the data about the ability of different HDL subclasses to cross the BBB reported in this investigation have never been published before.

Finally, we investigated the effect of different apoA-I-HDL subclasses on pre-formed Aβ fibrils by AFM imaging, ThT assay, and MD simulation. AFM imaging showed that the presence of discoidal apoA-I-HDL strongly reduced the amount and concentration of long fibrils. This was confirmed by ThT assay, where a strong, and rapid reduction of the β-sheet content of fibrils was detected. The molecular modeling results highlighted the conformational destabilization of Aβ upon its interaction with apoA-I when associated to discoidal HDL. A significant distortion of the fibril order and a decrease in the β-sheet content was identified, clearly suggesting a key role played by discoidal apoA-I-HDL in destabilizing the Aβ fibrils.

Taken all together the data reported in present investigation, suggest that apoA-I-HDL action is not only peripheral via "sink effect," but also central after BBB crossing.

In summary, we can speculate that at earliest stages of AD, discoidal apoA-I-HDL species in plasma, more than alternatively lipidated HDL species, may be involved in synergic activity with brain discoidal apoA-I-HDL pool: the central HDL pool maintains Aβ in a soluble form, while the peripheral HDL pool enhances its efflux from the brain. These results add new information to previously published knowledge (Robert et al., 2016, 2017b; Slot et al., 2017), suggesting that the lipidation state of apoA-I, and its conformation may be an important determinant for its role in preventing β-amyloidosis, and therefore may influence the pathogenesis of AD.

Our results are also in agreement with a previously published study about the ability of apoA-I-HDL to promote clearance of Aβ through the cerebral vessel (Robert et al., 2017b) in a more advanced 3D cerebrovascular model. Our data adds new insights about the potential ability of discoidal HDL to cross the BBB and to destroy Aβ aggregates enhancing its clearance from the brain.

Considering that the main brain apoprotein, apoE, promotes Aβ aggregation (Dafnis et al., 2016), we can speculate that the ratio with brain apoA-I, promoting disaggregation, may be an important key point in modulating the peptide aggregation/disaggregation paradigm. Moreover, considering that apoE in the blood is able to promote Aβ clearance from the brain (Robert et al., 2017b) its coupling with the disaggregating activity of brain apoA-I could play an important role in brain Aβ clearance. Finally, considering that Aβ cleared into the blood interacts with circulating apoA-I, preventing its aggregation and reducing its accumulation in the vasculature (Handattu et al., 2009; Lefterov et al., 2010; Lewis et al., 2010; Robert et al., 2016, 2017a; Fernández-de-Retana et al., 2017) depicts a complex interplay among these apolipoproteins in the brain and in the blood.

However, the synergic action between different lipoproteins in modulating Aβ aggregation/disaggregation and transport across the BBB will be an important issue to be investigated.

As a final consideration, it should be pointed out that the results herein reported have been obtained using an *in vitro* model. Evidently, the neurovascular unit (NVU), the area where these processes naturally occur, is considerably more complex than endothelial cells alone (Sagare et al., 2012). Indeed, the brain capillary endothelial cells of the BBB do not function alone, but they work in synergy within a context of a multicellular NVU, which includes neurons, astrocytes, pericytes, and microglia and the blood vessels themselves (McConnell et al., 2017). The NVU components cooperate to regulate cerebrovascular function and permeability

through the vasculature, which has unique structure along the vascular tree in the brain (Andreone et al., 2017). Thus, different structures can contribute to Aβ exchange across the BBB. Accordingly, our results should be taken as an indication that will deserve confirmation on a model closer to the physiological state (Robert et al., 2017a) or *in vivo* in animal models.

ETHICS STATEMENT

Human plasma samples from healthy donors were provided by the Immunohematology and Transfusion Medicine Service (SIMT) of ASST Grande Ospedale Metropolitano Niguarda, Milan, Italy. All experimental protocols were approved by license 446-092014 CE from Ospedale Niguarda Ca' Granda and carried out in accordance with these guidelines and regulations. Written informed consent was obtained from each donor and all donors were over the age of 18.

AUTHOR CONTRIBUTIONS

RD performed *in vitro* experiments on the blood-brain barrier model. SS purified, prepared, and characterized the different subtypes of HDL from human plasma. AC performed *in vitro* experiments with beta-amyloid peptide. BF prepared and characterized beta-amyloid aggregates. RC and VC performed AFM imaging experiments. LN performed ThT fluorescence assays. DS performed statistical analysis of data. GG, MD, and AD performed the molecular modeling analysis. LC, FM, and FR contributed to the data interpretation and participated in the drafting of the manuscript. FR coordinated the study, designed the experiments, and analyzed the data. All authors contributed to the manuscript revision, read and approved the submitted version, and agreed to be accountable for all the aspects of the work.

FUNDING

This work was supported by the Grant JPND-COFUND_FP-829-031 (2016–2019) to FR.

SUPPLEMENTARY MATERIAL

The Supplementary Material for this article can be found online at: https://www.frontiersin.org/articles/10.3389/fnins.2019.00419/full#supplementary-material

REFERENCES

Acton, S., Rigotti, A., Landschulz, K. T., Xu, S., Hobbs, H. H., and Krieger, M. (1996). Identification of scavenger receptor SR-BI as a high density lipoprotein receptor. *Science* 271, 518–520. doi: 10.1126/science.271.5248.518

Andreone, B. J., Chow, B. W., Tata, A., Lacoste, B., Ben-Zvi, A., Bullock, K., et al. (2017). Blood-brain barrier permeability is regulated by lipid transport-dependent suppression of caveolae-mediated transcytosis. *Neuron* 94, 581–594.e5. doi: 10.1016/j.neuron.2017.03.043

Andrusier, N., Nussinov, R., and Wolfson, H. J. (2007). FireDock: fast interaction refinement in molecular docking. *Proteins* 69, 139–159. doi: 10.1002/prot.21495

Bana, L., Minniti, S., Salvati, E., Sesana, S., Zambelli, V., Cagnotto, A., et al. (2014). Liposomes bi-functionalized with phosphatidic acid and an ApoE-derived peptide affect Aβ aggregation features and cross the blood-brain-barrier: implications for therapy of Alzheimer disease. *Nanomedicine* 10, 1583–1590. doi: 10.1016/j.nano.2013.12.001

Bates, K. A., Verdile, G., Li, Q. X., Ames, D., Hudson, P., Masters, C. L., et al. (2009). Clearance mechanisms of Alzheimer's amyloid-beta peptide: implications for therapeutic design and diagnostic tests. *Mol. Psychiatry* 14, 469–486. doi: 10.1038/mp.2008.96

Berendsen, H. J. C., Postma, J. P. M., Gunsteren, W. F. V., DiNola, A., and Haak, J. R. (1984). Molecular dynamics with coupling to an external bath. *J. Chem. Phys.* 81, 3684–3690. doi: 10.1063/1.448118

Bernini, F., Calabresi, L., Bonfadini, G., and Franceschini, G. (1996). The molecular structure of apolipoprotein A-II modulates the capacity of HDL to promote cell cholesterol efflux. *Biochim. Biophys. Acta* 1299, 103–109. doi: 10.1016/0005-2760(95)00200-6

Bibow, S., Polyhach, Y., Eichmann, C., Chi, C. N., Kowal, J., Albiez, S., et al. (2017). Solution structure of discoidal high-density lipoprotein particles with a shortened apolipoprotein A-I. *Nat. Struct. Mol. Biol.* 24, 187–193. doi: 10.1038/nsmb.3345

Bussi, G., Donadio, D., and Parrinello, M. (2007). Canonical sampling through velocity rescaling. *J Chem. Phys.* 126:014101. doi: 10.1063/1.2408420

Calabresi, L., Vecchio, G., Frigerio, F., Vavassori, L., Sirtori, C. R., and Franceschini, G. (1997). Reconstituted high-density lipoproteins with a disulfide-linked apolipoprotein A-I dimer: evidence for restricted particle size heterogeneity. *Biochemistry* 36, 12428–12433. doi: 10.1021/bi970505a

Camponova, P., Le Page, A., Berrougui, H., Lamoureux, J., Pawelec, G., Witkowski, M. J., et al. (2017). Alteration of high-density lipoprotein functionality in Alzheimer's disease patients. *Can. J. Physiol. Pharmacol.* 95, 894–903. doi: 10.1139/cjpp-2016-0710

Curtiss, L. K., Valenta, D. T., Hime, N. J., and Rye, K. A. (2006). What is so special about apolipoprotein AI in reverse cholesterol transport? *Arterioscler. Thromb. Vasc. Biol.* 26, 12–19. doi: 10.1161/01.atv.0000194291.94269.5a

Dafnis, I., Argyri, L., Sagnou, M., Tzinia, A., Tsilibary, E. C., Stratikos, E., et al. (2016). The ability of apolipoprotein E fragments to promote intraneuronal accumulation of amyloid beta peptide 42 is both isoform and size-specific. *Sci. Rep.* 6:30654. doi: 10.1038/srep30654

Demeester, N., Castro, G., Desrumaux, C., De Geitere, C., Fruchart, J. C., Santens, P., et al. (2000). Characterization and functional studies of lipoproteins, lipid transfer proteins, and lecithin:cholesterol acyltransferase in CSF of normal individuals and patients with Alzheimer's disease. *J. Lipid Res.* 41, 963–974.

Deriu, M. A., Grasso, G., Licandro, G., Danani, A., Gallo, D., Tuszynski, J. A., et al. (2014). Investigation of the Josephin domain protein-protein interaction by molecular dynamics. *PLoS One* 9:e108677. doi: 10.1371/journal.pone.0108677

Deriu, M. A., Grasso, G., Tuszynski, J. A., Gallo, D., Morbiducci, U., and Danani, A. (2016a). Josephin domain structural conformations explored by metadynamics in essential coordinates. *PLoS Comput. Biol.* 12:e1004699. doi: 10.1371/journal.pcbi.1004699

Deriu, M. A., Grasso, G., Tuszynski, J. A., Massai, D., Gallo, D., Morbiducci, U., et al. (2016b). Characterization of the AXH domain of Ataxin-1 using enhanced sampling and functional mode analysis. *Proteins* 84, 666–673. doi: 10.1002/prot.25017

Didichenko, S. A., Navdaev, A. V., Cukier, A. M., Gille, A., Schuetz, P., Spycher, M. O., et al. (2016). Enhanced HDL functionality in small HDL species produced upon remodeling of HDL by reconstituted HDL, CSL112: effects on cholesterol efflux, anti-inflammatory and antioxidative activity. *Circ. Res.* 2, 751–763. doi: 10.1161/CIRCRESAHA.116.308685

Elliott, D. A., Weickert, C. S., and Garner, B. (2010). Apolipoproteins in the brain: implications for neurological and psychiatric disorders. *Clin. Lipidol.* 51, 555–573. doi: 10.2217/CLP.10.37

Fagan, A. M., Younkin, L. H., Morris, J. C., Fryer, J. D., Cole, T. G., Younkin, S. G., et al. (2000). Differences in the Abeta40/Abeta42 ratio associated with cerebrospinal fluid lipoproteins as a function of apolipoprotein E genotype. *Ann. Neurol.* 48, 201–210. doi: 10.1002/1531-8249(200008)48:2<201::aid-ana10>3.0.co;2-x

Fan, H. M., Gu, R. X., Wang, Y. J., Pi, Y. L., Zhang, Y. H., Xu, Q., et al. (2015). Destabilization of Alzheimer's Abeta42 protofibrils with a novel drug candidate wgx-50 by molecular dynamics simulations. *J. Phys. Chem. B* 27, 11196–11202. doi: 10.1021/acs.jpcb.5b03116

Favari, E., Lee, M., Calabresi, L., Franceschini, G., Zimetti, F., Bernini, F., et al. (2004). Depletion of pre-beta-high density lipoprotein by human chymase impairs ATP-binding cassette transporter A1- but not scavenger receptor class B type I-mediated lipid efflux to high density lipoprotein. *J. Biol. Chem.* 279, 9930–9936. doi: 10.1074/jbc.m312476200

Fernández-de-Retana, S., Cano-Sarabia, M., Marazuela, P., Sánchez-Quesada, J. L., Garcia-Leon, A., Montañola, A., et al. (2017). Characterization of ApoJ-reconstituted high-density lipoprotein (rHDL) nanodisc for the potential treatment of cerebral β-amyloidosis. *Sci. Rep.* 7:14637. doi: 10.1038/s41598-017-15215-w

Franceschini, G., Favari, E., Calabresi, L., Simonelli, S., Bondioli, A., Adorni, M. P., et al. (2013). Differential effects of fenofibrate and extended-release niacin on high-density lipoprotein particle size distribution and cholesterol efflux capacity in dyslipidemic patients. *J. Clin. Lipidol.* 7, 414–422. doi: 10.1016/j.jacl.2013.06.007

Fung, K. Y., Wang, C., Nyegaard, S., Heit, B., Fairn, G. D., and Lee, W. L. (2017). SR-BI mediated transcytosis of HDL in brain microvascular endothelial cells is independent of caveolin, clathrin, and PDZK1. *Front. Physiol.* 8:841. doi: 10.3389/fphys.2017.00841

Gillard, B. K., Bassett, G. R., Gotto, A. M., Rosales, C., and Pownall, H. J. (2017). Scavenger receptor B1 (SR-B1) profoundly excludes high density lipoprotein (HDL) apolipoprotein AII as it nibbles HDL-cholesteryl ester. *J. Biol. Chem.* 292, 8864–8873. doi: 10.1074/jbc.M117.781963

Glenner, G. G., and Wong, C. W. (2012). Alzheimer's disease: initial report of the purification and characterization of a novel cerebrovascular amyloid protein. 1984. *Biochem. Biophys. Res. Commun.* 425, 534–539. doi: 10.1016/j.bbrc.2012.08.020

Golabek, A., Marques, M. A., Lalowski, M., and Wisniewski, T. (1995). Amyloid beta binding proteins in vitro and in normal human cerebrospinal fluid. *Neurosci. Lett.* 191, 79–82. doi: 10.1016/0304-3940(95)11565-7

Grasso, G., Deriu, M. A., Prat, M., Rimondini, L., Vernè, E., Follenzi, A., et al. (2015). Cell penetrating peptide adsorption on magnetite and silica surfaces: a computational investigation. *J Phys. Chem. B* 119, 8239–8246. doi: 10.1021/jp512782e

Grasso, G., Deriu, M. A., Tuszynski, J. A., Gallo, D., Morbiducci, U., and Danani, A. (2016). Conformational fluctuations of the AXH monomer of Ataxin-1. *Proteins* 84, 52–59. doi: 10.1002/prot.24954

Grasso, G., Rebella, M., Muscat, S., Morbiducci, U., Tuszynski, J., Danani, A., et al. (2018). Conformational dynamics and stability of U-shaped and S-shaped amyloid beta assemblies. *Int. J. Mol. Sci.* 14:19. doi: 10.3390/ijms19020571

Grasso, G., Tuszynski, J. A., Morbiducci, U., Licandro, G., Danani, A., and Deriu, M. A. (2017). Thermodynamic and kinetic stability of the Josephin Domain closed arrangement: evidences from replica exchange molecular dynamics. *Biol. Direct* 12:2. doi: 10.1186/s13062-016-0173-y

Gregori, M., Cassina, V., Brogioli, D., Salerno, D., De Kimpe, L., Scheper, W., et al. (2010). Stability of Aβ (1-42) peptide fibrils as consequence of environmental modifications. *Eur. Biophys. J.* 39, 1613–1623. doi: 10.1007/s00249-010-0619-6

Haass, C., and Selkoe, D. J. (1993). Cellular processing of beta-amyloid precursor protein and the genesis of amyloid beta-peptide. *Cell.* 75, 1039–1042. doi: 10.1016/0092-8674(93)90312-e

Handattu, S. P., Garber, D. W., Monroe, C. E., van Groen, T., Kadish, I., Nayyar, G., et al. (2009). Oral apolipoprotein A-I mimetic peptide improves cognitive function and reduces amyloid burden in a mouse model of Alzheimer's disease. *Neurobiol. Dis.* 34, 525–534. doi: 10.1016/j.nbd.2009.03.007

Harr, S. D., Uint, L., Hollister, R., Hyman, B. T., and Mendez, A. J. (1996). Brain expression of apolipoproteins E, J, and A-I in Alzheimer's disease. *J. Neurochem.* 66, 2429–2435.

Huang, J., and MacKerell, A. D. (2013). CHARMM36 all-atom additive protein force field: validation based on comparison to NMR data. *J. Comput. Chem.* 34, 2135–2145. doi: 10.1002/jcc.23354

Huang, J. T., Wang, L., Prabakaran, S., Wengenroth, M., Lockstone, H. E., Koethe, D., et al. (2008). Independent protein-profiling studies show a decrease in apolipoprotein A1 levels in schizophrenia CSF, brain and peripheral tissues. *Mol. Psychiatry.* 13, 1118–1128. doi: 10.1038/sj.mp.4002108

Hye, A., Riddoch-Contreras, J., Baird, A. L., Ashton, N. J., Bazenet, C., Leung, R., et al. (2014). Plasma proteins predict conversion to dementia from prodromal disease. *Alzheimers Dement.* 10, 799–807.e2. doi: 10.1016/j.jalz.2014.05.1749

Janaszewska, A., Klajnert-Maculewicz, B., Marcinkowska, M., Duchnowicz, P., Appelhans, D., Grasso, G., et al. (2017). Multivalent interacting glycodendrimer to prevent amyloid-peptide fibril formation induced by Cu(II): a multidisciplinary approach. *Nano Res.* 11, 1204–1226. doi: 10.1007/s12274-017-1734-9

Jayaraman, S., Cavigiolio, G., and Gursky, O. (2012). Folded functional lipid-poor apolipoprotein A–I obtained by heating of high-density lipoproteins: relevance to high-density lipoprotein biogenesis. *Biochem. J.* 442, 703–712. doi: 10.1042/BJ20111831

Jorgensen, W. L., Chandrasekhar, J., Madura, J. D., Impey, R. W., and Klein, M. L. (1983). Comparison of simple potential functions for simulating liquid water. *J. Chem. Phys.* 79, 926–935. doi: 10.1063/1.445869

Kingwell, B. A., Chapman, M. J., Kontush, A., and Miller, N. E. (2014). HDL-targeted therapies: progress, failures and future. *Nat. Rev. Drug Discov.* 13, 445–464. doi: 10.1038/nrd4279

Koch, S., Donarski, N., Goetze, K., Kreckel, M., Stuerenburg, H. J., Buhmann, C., et al. (2001). Characterization of four lipoprotein classes in human cerebrospinal fluid. *J. Lipid Res.* 42, 1143–1151.

Koldamova, R. P., Lefterov, I. M., Lefterova, M. I., and Lazo, J. S. (2001). Apolipoprotein A-I directly interacts with amyloid precursor protein and inhibits A beta aggregation and toxicity. *Biochemistry* 40, 3553–3560. doi: 10.1021/bi002186k

Lefterov, I., Fitz, N. F., Cronican, A. A., Fogg, A., Lefterov, P., Kodali, R., et al. (2010). Apolipoprotein A-I deficiency increases cerebral amyloid angiopathy and cognitive deficits in APP/PS1DeltaE9 mice. *J. Biol. Chem.* 285, 36945–36957. doi: 10.1074/jbc.M110.127738

Lewis, T. L., Cao, D., Lu, H., Mans, R. A., Su, Y. R., Jungbauer, L., et al. (2010). Overexpression of human apolipoprotein A-I preserves cognitive function and attenuates neuroinflammation and cerebral amyloid angiopathy in a mouse model of Alzheimer disease. *J. Biol. Chem.* 285, 36958–36968. doi: 10.1074/jbc.M110.127829

Lührs, T., Ritter, C., Adrian, M., Riek-Loher, D., Bohrmann, B., Döbeli, H., et al. (2005). 3D structure of Alzheimer's amyloid-beta(1-42) fibrils. *Proc. Natl. Acad. Sci. U.S.A.* 102, 17342–17347.

Mahley, R. W., Innerarity, T. L., Rall, S. C., and Weisgraber, K. H. (1984). Plasma lipoproteins: apolipoprotein structure and function. *J. Lipid Res.* 25, 1277–1294.

Maisuradze, G. G., Liwo, A., and Scheraga, H. A. (2009). Principal component analysis for protein folding dynamics. *J. Mol. Biol.* 385, 312–329. doi: 10.1016/j.jmb.2008.10.018

Mancini, S., Minniti, S., Gregori, M., Sancini, G., Cagnotto, A., Couraud, P. O., et al. (2016). The hunt for brain Aβ oligomers by peripherally circulating multi-functional nanoparticles: potential therapeutic approach for Alzheimer disease. *Nanomedicine* 12, 43–52. doi: 10.1016/j.nano.2015.09.003

Mashiach, E., Schneidman-Duhovny, D., Andrusier, N., Nussinov, R., and Wolfson, H. J. (2008). FireDock: a web server for fast interaction refinement in molecular docking. *Nucleic Acids Res.* 36, W229–W232. doi: 10.1093/nar/gkn186

McConnell, H. L., Kersch, C. N., Woltjer, R. L., and Neuwelt, E. A. (2017). The translational significance of the neurovascular unit. *J. Biol. Chem.* 292, 762–770. doi: 10.1074/jbc.r116.760215

Merched, A., Xia, Y., Visvikis, S., Serot, J. M., and Siest, G. (2000). Decreased high-density lipoprotein cholesterol and serum apolipoprotein AI concentrations are highly correlated with the severity of Alzheimer's disease. *Neurobiol. Aging* 21, 27–30. doi: 10.1016/s0197-4580(99)00103-7

Merino-Zamorano, C., Fernández-de Retana, S., Montañola, A., Batlle, A., Saint-Pol, J., Mysiorek, C., et al. (2016). Modulation of amyloid-β1-40 transport by ApoA1 and ApoJ across an in vitro model of the blood-brain barrier. *J. Alzheimers Dis.* 53, 677–691. doi: 10.3233/JAD-150976

Oram, J. F., and Heinecke, J. W. (2005). ATP-binding cassette transporter A1: a cell cholesterol exporter that protects against cardiovascular disease. *Physiol. Rev.* 85, 1343–1372. doi: 10.1152/physrev.00005.2005

Paula-Lima, A. C., Tricerri, M. A., Brito-Moreira, J., Bomfim, T. R., Oliveira, F. F., Magdesian, M. H., et al. (2009). Human apolipoprotein A-I binds amyloid-beta and prevents Abeta-induced neurotoxicity. *Int. J. Biochem. Cell Biol.* 41, 1361–1370. doi: 10.1016/j.biocel.2008.12.003

Phillips, M. C. (2013). New insights into the determination of HDL structure by apolipoproteins: thematic review series: high density lipoprotein structure, function, and metabolism. *J. Lipid Res.* 54, 2034–2048. doi: 10.1194/jlr.R034025

Pitas, R. E., Boyles, J. K., Lee, S. H., Hui, D., and Weisgraber, K. H. (1987). Lipoproteins and their receptors in the central nervous system. Characterization of the lipoproteins in cerebrospinal fluid and identification of apolipoprotein B,E(LDL) receptors in the brain. *J. Biol. Chem.* 262, 14352–14360.

Quan, L., Wu, J., Lane, L. A., Wang, J., Lu, Q., Gu, Z., et al. (2016). Enhanced detection specificity and sensitivity of Alzheimer's disease using Amyloid-β-Targeted quantum dots. *Bioconjug. Chem.* 27, 809–814. doi: 10.1021/acs.bioconjchem.6b00019

Robert, J., Button, E. B., Stukas, S., Boyce, G. K., Gibbs, E., Cowan, C. M., et al. (2017a). High-density lipoproteins suppress Aβ-induced PBMC adhesion to human endothelial cells in bioengineered vessels and in monoculture. *Mol. Neurodegener.* 12:60. doi: 10.1186/s13024-017-0201-0

Robert, J., Button, E. B., Yuen, B., Gilmour, M., Kang, K., Bahrabadi, A., et al. (2017b). Clearance of beta-amyloid is facilitated by apolipoprotein E and circulating high-density lipoproteins in bioengineered human vessels. *eLife* 6:e29595. doi: 10.7554/eLife.29595

Robert, J., Stukas, S., Button, E., Cheng, W. H., Lee, M., Fan, J., et al. (2016). Reconstituted high-density lipoproteins acutely reduce soluble brain Aβ levels in symptomatic APP/PS1 mice. *Biochim. Biophys. Acta* 1862, 1027–1036. doi: 10.1016/j.bbadis.2015.10.005

Roheim, P. S., Carey, M., Forte, T., and Vega, G. L. (1979). Apolipoproteins in human cerebrospinal fluid. *Proc. Natl. Acad. Sci. U.S.A.* 76, 4646–4649. doi: 10.1073/pnas.76.9.4646

Sagare, A. P., Bell, R. D., and Zlokovic, B. V. (2012). Neurovascular dysfunction and faulty amyloid β-peptide clearance in Alzheimer disease. *Cold Spring Harb. Perspect. Med.* 2:a011452. doi: 10.1101/cshperspect.a011452

Schägger, H., and von Jagow, G. (1987). Tricine-sodium dodecyl sulfate-polyacrylamide gel electrophoresis for the separation of proteins in the range from 1 to 100 kDa. *Anal. Biochem.* 166, 368–379. doi: 10.1016/0003-2697(87)90587-2

Schneidman-Duhovny, D., Inbar, Y., Nussinov, R., and Wolfson, H. J. (2005). PatchDock and SymmDock: servers for rigid and symmetric docking. *Nucleic Acids Res.* 33, W363–W367.

Selkoe, D. J., and Hardy, J. (2016). The amyloid hypothesis of Alzheimer's disease at 25 years. *EMBO Mol. Med.* 8, 595–608. doi: 10.15252/emmm.201606210

Sevugan Chetty, P., Mayne, L., Kan, Z. Y., Lund-Katz, S., Englander, S. W., and Phillips, M. C. (2012). Apolipoprotein A-I helical structure and stability in discoidal high-density lipoprotein (HDL) particles by hydrogen exchange and mass spectrometry. *Proc. Natl. Acad. Sci. U.S.A.* 109, 11687–11692. doi: 10.1073/pnas.1209305109

Shih, Y. H., Tsai, K. J., Lee, C. W., Shiesh, S. C., Chen, W. T., Pai, M. C., et al. (2014). Apolipoprotein C-III is an amyloid-β-binding protein and an early marker for Alzheimer's disease. *J. Alzheimers. Dis.* 41, 855–865. doi: 10.3233/JAD-140111

Silva, R. A., Huang, R., Morris, J., Fang, J., Gracheva, E. O., Ren, G., et al. (2008). Structure of apolipoprotein A-I in spherical high density lipoproteins of different sizes. *Proc. Natl. Acad. Sci. U.S.A.* 105, 12176–12181. doi: 10.1073/pnas.0803626105

Slot, R. E., Van Harten, A. C., Kester, M. I., Jongbloed, W., Bouwman, F. H., Teunissen, C. E., et al. (2017). Apolipoprotein A1 in cerebrospinal fluid and plasma and progression to Alzheimer's disease in non-demented elderly. *J. Alzheimers Dis.* 56, 687–697. doi: 10.3233/JAD-151068

Stukas, S., Robert, J., Lee, M., Kulic, I., Carr, M., Tourigny, K., et al. (2014). Intravenously injected human apolipoprotein A-I rapidly enters the central nervous system via the choroid plexus. *J. Am. Heart Assoc.* 3:e001156. doi: 10.1161/JAHA.114.001156

Vitali, C., Wellington, C. L., and Calabresi, L. (2014). HDL and cholesterol handling in the brain. *Cardiovasc. Res.* 103, 405–413. doi: 10.1093/cvr/cvu148

Yu, X., and Zheng, J. (2012). Cholesterol promotes the interaction of Alzheimer β-amyloid monomer with lipid bilayer. *J. Mol. Biol.* 421, 561–571. doi: 10.1016/j.jmb.2011.11.006

Zannis, V. I., Chroni, A., and Krieger, M. (2006). Role of apoA-I, ABCA1, LCAT, and SR-BI in the biogenesis of HDL. *J. Mol. Med.* 84, 276–294. doi: 10.1007/s00109-005-0030-4

Conflict of Interest Statement: The authors declare that the research was conducted in the absence of any commercial or financial relationships that could be construed as a potential conflict of interest.

frontiers in Neuroscience

REVIEW
published: 18 June 2019
doi: 10.3389/fnins.2019.00552

Prion-Like Mechanisms in Parkinson's Disease

Jiangnan Ma, Jing Gao, Jing Wang and Anmu Xie**

Department of Neurology, Affiliated Hospital of Qingdao University, Qingdao, China

Formation and aggregation of misfolded proteins in the central nervous system (CNS) is a key hallmark of several age-related neurodegenerative diseases, including Parkinson's disease (PD), Alzheimer's disease (AD), and amyotrophic lateral sclerosis (ALS). These diseases share key biophysical and biochemical characteristics with prion diseases. It is believed that PD is characterized by abnormal protein aggregation, mainly that of α-synuclein (α-syn). Of particular importance, there is growing evidence indicating that abnormal α-syn can spread to neighboring brain regions and cause aggregation of endogenous α-syn in these regions as seeds, in a "prion-like" manner. Abundant studies *in vitro* and *in vivo* have shown that α-syn goes through a templated conformational change, propagates from the original region to neighboring regions, and eventually cause neuron degeneration in the substantia nigra and striatum. The objective of this review is to summarize the mechanisms involved in the aggregation of abnormal intracellular α-syn and its subsequent cell-to-cell transmission. According to these findings, we look forward to effective therapeutic perspectives that can block the progression of neurodegenerative diseases.

Keywords: Parkinson's disease, prion-like mechanisms, α-synuclein, templated conformational change, transcellular propagation

OPEN ACCESS

Edited by:
Andrei Surguchov, University of Kansas Medical Center, United States

Reviewed by:
Fredric P. Manfredsson, Michigan State University, United States
Holger Wille, University of Alberta, Canada
Giuseppe Legname, Scuola Internazionale Superiore di Studi Avanzati (SISSA), Italy

****Correspondence:***
Jing Wang
hebgdwj@163.com
Anmu Xie
xieanmu@163.com

Specialty section:
This article was submitted to Neurodegeneration, a section of the journal Frontiers in Neuroscience

Received: *09 November 2018*
Accepted: *13 May 2019*
Published: *18 June 2019*

Citation:
Ma J, Gao J, Wang J and Xie A (2019) Prion-Like Mechanisms in Parkinson's Disease. Front. Neurosci. 13:552. doi: 10.3389/fnins.2019.00552

INTRODUCTION

Parkinson's disease (PD) is the most prevalent neurodegenerative motor disorder worldwide, characterized by motor symptoms, such as bradykinesia, resting tremor, rigidity, and postural instability. However, a myriad of non-motor symptoms, such as constipation, dementia, anosmia, depression, and sleep disturbances, regularly manifest prior to the motor symptoms and affect quality of life (Dehay and Fernagut, 2016; Tyson et al., 2016). The primary pathological manifestation of PD is the relative selective loss of dopaminergic neurons in the substantia nigra pars compacta (SN), which results in a significant decrease in the dopamine (DA) content of the striatum. The exact cause of this pathological change is still unclear. Genetic and environmental factors, aging, and oxidative stress may be involved in the degenerative death of dopaminergic neurons. Lewy bodies (LBs) and Lewy neurites (LNs) are the morphological markers of neuron degeneration. LBs, which are intraneuronal proteinaceous cytoplasmic inclusions, are composed primarily of misfolded α-syn (Sian-Hulsmann et al., 2015). The degeneration of dopaminergic neurons underlie the motor symptoms of PD, however, the causes of cell degeneration and the occurrence of more complicated non-motor symptoms have attracted more and more attention. Not only that, many observations support the "prion-like" behavior of α-syn, which postulates that misfolded α-syn is capable of transferring between interconnected neuron networks and acting

as a template to induce further aggregation of intracellularly transferred α-syn.

PRION DISEASES AND PRION-LIKE MECHANISM

Prion diseases are fatal transmissible neurodegenerative disorders with genetic, sporadic, and acquired forms (Acquatella-Tran Van Ba et al., 2013). Prions are the infectious agents responsible for the transmissible spongiform encephalopathies (TSEs), a group of lethal neurodegenerative diseases (Le et al., 2015). These diseases also include Kuru, Creutzfeldt-Jakob disease (CJD), Gerstmann–Sträussler–Scheinker disease (GSS), and fatal familial insomnia in human, bovine spongiform encephalopathy (BSE) in cattle, and scrapie in sheep (Goedert et al., 2010; Costanzo and Zurzolo, 2013; Tamguney and Korczyn, 2018).

Prion protein (PrP), is capable of resisting chemical therapy or physical prevention that inhibits ordinary infectious agents. PrP is encoded by the endogenous gene-*PRNP* and expressed in a variety of cells whether infected or not. PrP^{C}, a glycosylphosphatidylinositol (GPI) anchored protease-sensitive protein of 33–35 kDa, is the normal product of *PRNP* gene (Le et al., 2015; Quek and Hill, 2017). PrP^{C} is commonly detected on the surface of cell membranes and dominantly located in neurons, though it is ubiquitously expressed. However, the specific biological functions of PrP^{C} are still unknown. It is believed that PrP^{C} participates in many physiological processes, including signal transduction, maintaining copper or zinc homeostasis, and acting as a receptor (Halliday et al., 2014; Quek and Hill, 2017; Tamguney and Korczyn, 2018). The crucial role of copper-binding sites in maintaining the neuritogenesis function in PrP^{C} has been proven (Nguyen et al., 2019). The central causative event in neurodegeneration is the conversion of the normal form PrP^{C} into a protease-resistant, disease-associated form PrP^{Sc}, which is known as templated conformation change. These two isoforms of PrP share an identical composition of polypeptide chain but differ in secondary and tertiary structure. The α-helices of native PrP^{C} transform into β-sheet conformation to form the pathological PrP^{Sc}. The configuration of PrP^{Sc} is quite stable and equipped to interact with molecules in a similar state. The misfolded protein can proliferate via templated conformational change. Exogenous PrP^{Sc} interacts with endogenous PrP^{C} and induces it to pathological conformational transition. The unstable oligomeric species grow by recruiting and integrating PrP^{C} and PrP^{Sc} constantly until forming stable prion aggregates (Acquatella-Tran Van Ba et al., 2013; Renner and Melki, 2014). PrP^{Sc} aggregates result in cell rupture, and shed PrP^{Sc} acts as seeds which propagate into other cells indefinitely (**Figure 1**). Both PrP^{C} and PrP^{Sc} are detected in exosomes from diverse sources including neuronal cells, blood, and cerebrospinal fluid (CSF). (Yin et al., 2014; Quek and Hill, 2017) Coupled application of immunogold labeling and electron microscopy imaging confirmed the presence of PrP on exosome membranes, showing that exosomes may play a crucial role in transferring prion infectivity. Beyond that, it has been verified that exosomes are able to spread along tunneling nanotubes (TNTs), suggesting a function in cell-to-cell propagation of infectious prions (Costanzo and Zurzolo, 2013; Kaufman and Diamond, 2013; Yin et al., 2014). Propagating prions cause devastating neurodegeneration cell by cell, but it is still under debate how infectious prions induce TSEs and eventually neuronal death.

Emerging research highlights that many neurodegenerative diseases share key prion-like similarities with the progress of prion diseases. α-Syn is a typical pathogenic agent for PD and exhibits properties of self-aggregation and propagation, just like prions do.

In addition to the templated misfolding, the transmission between cells is also a central feature of prions. Under normal conditions, infection of prions gives rise to dissemination through the peripheral and central nervous system (CNS) by distal neuronal spreading. Prions induce epidemics due to the transmission between individuals and species (Goedert et al., 2010). However, there is no epidemiological data to show that PD is infectious. Therefore, an extended definition of "seeding" is used to describe the transmissibility of misfolded proteins in neurodegenerative diseases *in vivo* (Fernandez-Borges et al., 2013; Halliday et al., 2014; Diack et al., 2016).

THE PRION-LIKE MECHANISM OF PD

Basic α-Synuclein Biology

α-Synuclein is a 14 kDa protein composed of 140 amino acids and encoded by *SNCA* (the coding gene) (Tamguney and Korczyn, 2018). High concentrations of α-syn are present in presynaptic terminals, where it associates with vesicular membranes (Volpicelli-Daley et al., 2011; Narkiewicz et al., 2014; Renner and Melki, 2014). Abundant evidence suggests that the normal physiological functions of α-syn include direct interaction with cell membrane phospholipids (especially referring to vesicles), neurotransmitter release, and enhancement of microtubule formation (Recasens and Dehay, 2014; Hasegawa et al., 2016; Burre et al., 2018). A study by Cali et al., using organelle-targeting Ca^{2+}-sensitive aequorin probes, demonstrates that physiological levels of α-syn are required to maintain normal mitochondrial function and morphological integrity. Consequently, α-syn overexpression and/or changes in its aggregation properties induce the redistribution of α-syn and the loss of modulation on mitochondrial function (Cali et al., 2012). In addition, the accumulation of α-syn can impair synaptic dopamine release and cause the death of nigrostriatal neurons (Longhena et al., 2017). Insights into the localization and function of α-syn in subcellular compartments would facilitate the understanding of the pathology of α-syn.

Accumulation of oligomers and larger aggregates of misfolded α-syn is detected in multiple neurodegenerative diseases called synucleinopathies, including Parkinson's disease (PD), dementia with Lewy bodies (DLB), and multiple system atrophy (MSA) (Tamguney and Korczyn, 2018). The initial pathogenesis of synucleinopathies is still considered involving the conversion of soluble α-syn into insoluble aggregates via spontaneous nucleation. This pathological conversion could be

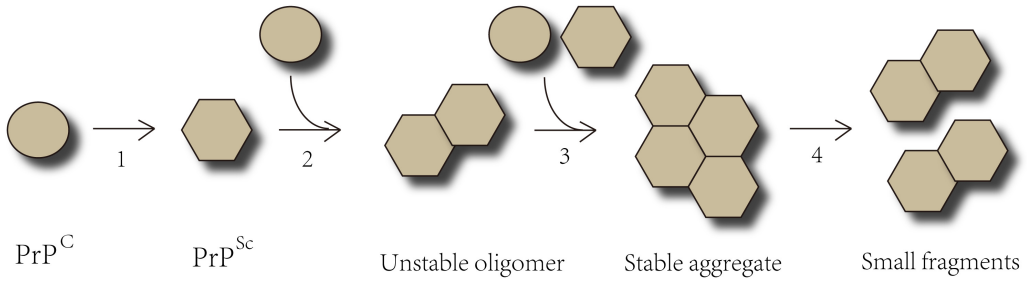

FIGURE 1 | The Templated Conformation Change of Prions. Step 1- The α-helices of PrP^{C} transform into the β-sheets conformation to form pathological PrP^{Sc}. Step 2- PrP^{Sc} interacts with PrP^{C} and converts them into pathological form. Step 3- PrP^{Sc} binds to the cognate prion molecules. Unstable oligomeric species grow by recruiting additional unfolded or oligomeric species of the same protein until forming a stable nucleus. Step 4- The prion aggregates break into small fragments that act as seeds and spread indefinitely from the point of infection to the CNS.

caused by countless environmental or genetic factors, and is quite likely the result of interaction among diverse factors (Karpowicz et al., 2019).

α-syn is composed of three domains: an amino terminus with α-helix, a non-amyloid component (NAC), and an unstructured carboxy terminus. Soluble α-syn is natively unstructured and monomeric. These three domains are essential for the pathogenic progress observed in PD and other synucleinopathies. The amino terminus of α-syn forms an α-helical structure upon binding to protein interactors or lipid membranes (Kim et al., 2014; Narkiewicz et al., 2014; Lawand et al., 2015). Accumulating biophysical and biochemical studies have demonstrated that interactions between α-syn and lipids influence α-syn oligomerization and aggregation, both *in vitro* and *in vivo*. Mainly three kinds of lipids are associated with pathological interactions with α-syn, i.e., fatty acids, sterols and sphingolipids. Both the chemical properties of lipids and the lipid-to-protein-ratio could modulate the aggregation propensity of α-syn. Lipid vesicles interacting with monomeric and fibrillar α-syn are possible to affect the initiation of the amyloid formation and the amplification of the toxic aggregates. Measurements of the kinetics of amyloid formation *in vitro* in the presence of different lipid systems allow for the study of mechanistic details of the effects of lipids on α-syn aggregation and toxicity, and open a new therapeutic road to attenuate or prevent crucial events (Galvagnion, 2017; Suzuki et al., 2018).

A technique called cryo-electron microscopy (cryo-EM) was applied to capture the structure of full-length α-syn fibril. Two protofilaments intertwining along an approximate 21 screw axis into a left-handed helix form a polar fibril composed of stacked β-strands. The backbone of residues 38–95, including the fibril core and the NACore, is well illustrated in the EM map. Residues 50–57, containing three mutation sites linked to familial PD, form the interface between the two protofilaments and are associated with fibril stability. A hydrophobic cleft at one end of the fibril may have an impact on fibril elongation, and has implications for diagnosis and treatment of PD (Dillard et al., 2018; Guerrero-Ferreira et al., 2018; Li et al., 2018a,b).

α-Syn turns into oligomeric and/or fibrillar conformations in particular pathological conditions, including gene mutations of *SNCA*, decreased rate of clearance, possible alteration of α-syn (such as truncations), oxidative stress, iron concentration, or posttranslational modifications (Lawand et al., 2015; Sian-Hulsmann et al., 2015). In particular, posttranslational modifications of α-syn, such as phosphorylation, ubiquitination, acetylation, sumoylation, and nitration, have been observed to alter the structure and function of α-syn, and are related to α-syn aggregation and neurotoxicity (Hodara et al., 2004; Kim et al., 2014; Hasegawa et al., 2017). Most cases of PD are sporadic, and rare familial PD is induced by missense mutations of *SNCA* or multiplications of the gene. Other genetic mutations, including *PARK-LRRK2* and *PARK-VPS35*, are also related to the pathogenesis of α-syn (Hyun et al., 2013; Chan et al., 2017). The N-terminal region of α-syn contains pathogenic gene mutation sites A53T, A53E, A30P, E46K, H50Q, and G51D, and six imperfectly conserved repeats (KTKEGV) that promote protein interaction (Hasegawa et al., 2016; Rey et al., 2016; Burre et al., 2018). Recent studies with animal and cell models, as well as autopsy studies of PD patients, provide abundant evidences for "prion-like" behavior of α-syn.

Evidence for the Prion-Like Properties of α-Synuclein

Abnormal Aggregation of α-Syn

The primary component of the proteinaceous filaments of LBs and LNs is α-syn. A slight accumulation of LBs or LNs is capable of reducing striatal tyrosine hydroxylase (TH) levels, which implies the preclinical prodromal phase of PD (Chan et al., 2017). Because dopamine neurons are invariably compromised in PD, Perez and Hastings have been exploring the functions of α-syn with particular relevance to dopamine neurons. TH, the rate limiting enzyme in dopamine synthesis, converts tyrosine to L-dihydroxyphenylalanine (L-DOPA), which is then converted into dopamine by aromatic amino acid decarboxylase (AADC). In several rodent models overexpressing α-syn, reduced TH activity and/or diminished dopamine synthesis are observed. It was also confirmed that α-syn significantly reduced AADC activity and phosphorylation in cells (Perez et al., 2002; Peng et al., 2005; Tehranian et al., 2006).

In vitro studies indicate that recombinant α-syn can polymerize into amyloidogenic fibrils with similar morphologies

and staining as those obtained from extracts of disease-affected brains (Narkiewicz et al., 2014). *In vitro* aggregation assays are feasible tools for studying the mechanisms responsible for the formation of different α-syn species, their structural properties and functions, as well as for the development of new drug capable of restraining from the aggregation of α-syn. However, recombinant preformed α-syn fibrils (PFFs) are not naturally toxic to cultured neurons, as neurons in the absence of α-syn (α-syn KO) display no toxicity following transduction with the same concentration of α-syn PFFs that could produce robust pathologic α-syn inclusions and cause eventual cell death in wild type (WT) neurons (Volpicelli-Daley et al., 2011).

When α-syn is incubated *in vitro* at a high concentration under shaking conditions, it undergoes a conformational change and turns into fibrils within a few days. In contrast, little or no fibrils form at a lower α-syn concentration without shaking, and the protein needs more time to assemble. However, the number of fibrils would increase upon adding preformed fibrils into the monomer, suggesting that the conformational conversion of α-syn is facilitated by accretion of misfolded α-syn. In cultured cell models, when preformed α-syn fibrils are added by lipofection, a large number of phosphorylated and partially ubiquitinated α-syn aggregations similar to LBs, both morphologically and biochemically, are detected in few days. Cultured cells with α-syn aggregates show signs of slow degeneration, with a noticeable impairment of proteasome activity, which resembles disease progression in patients with PD (Hasegawa et al., 2017). These studies indicate that the mechanism underlying the pathological aggregation of α-syn is as follows: exogenous abnormal α-syn acts on the endogenous natural α-syn of recipient cells and causes pathological aggregation of α-syn.

It was observed that treating SH-SY5Y cell lines with recombinant human α-syn short amyloid fibrils resulted in sustained aggregation and accumulation of endogenous α-syn. This approach provides an excellent tool for potential therapeutic screening of pathogenic α-syn aggregates in cell culture (Aulic et al., 2014). Peelaerts et al. injected structurally well-defined human α-syn strains (including oligomers, ribbons, and fibrils) into mice brain, then reported that distinct α-syn strains show differential seeding capacities, inducing strain-specific pathology and neurotoxic phenotypes. These results point to α-syn short amyloid fibrils as the pathological species of α-syn aggregates involved in the transmission of α-syn pathology (Peelaerts et al., 2015; Braak and Del Tredici, 2016; Hasegawa et al., 2017). Tarutani et al. examined the seeding properties of various forms of α-syn *in vitro*, cells, and mice experimental models, and eventually, a consistent conclusion with Peelaerts was reached (Tarutani et al., 2016).

Several studies have reported that α-syn aggregation is induced by environmental and other exogenous factors, including pesticides, herbicides, heavy metals, polycations, histones, organic solvents, heat shock proteins (Hsp) and some small chemical compounds (Uversky, 2007; Narkiewicz et al., 2014). Recently, some studies, that have characterized the microscopic process in the mechanism of aggregation of α-syn, show that solution conditions may play an important role. For example, at faintly acidic pH values (such as those present intracellularly, including within endosomes and lysosomes), the expansion of α-syn aggregation is faster than at normal physiological pH values (Buell et al., 2014). Additional factors destabilizing the native fold of α-syn, such as point mutations, denaturants, and higher temperature, have been shown to enhance fibril formation (Rochet and Lansbury, 2000; Narkiewicz et al., 2014). The factors responsible for the kinetics of α-syn fibrillization include initial protein concentration, molecular crowding, agitation, pH, temperature, and ionic strength (Narkiewicz et al., 2014). These findings provide new directions for the prevention and treatment of PD, but these ideas need further development.

Under physiological conditions, normal nerve cells, for the lifetime of an individual, are capable of degrading and eliminating errant proteins and/or toxic metabolites. Intracellular homeostasis of α-syn depends on proper degradation mechanisms. Autophagic impairment has been reported in a donor recipient co-culture cell model to increase intercellular transfer of α-syn. Although, it is unknown whether if impaired autophagy in donor cells leads to increased release, or increased deposition and retention of transferred α-syn (Lee et al., 2013). There are three pathways currently involved in PD: chaperone-mediated autophagy, microautophagy, and macroautophagy (Karabiyik et al., 2017). The first process is carried out through the ubiquitination of the misfolded α-syn and their subsequent treatment by chaperones. When the function of the chaperones is altered, this option cannot be performed (Van Bulck et al., 2019). The other two autophagy methods are also altered in most neurodegenerative diseases for various reasons including the biogenesis of autophagosomes or lysosomal function (Menzies et al., 2017). Exosomal secretion of α-syn aggregates has been observed in response to knockdown of macroautophagy component ATG5 (Fussi et al., 2018). It has been demonstrated, by utilizing cell models, that α-syn inclusions cannot be effectively degraded and can impair overall macroautophagy by reducing autophagosome clearance, which may contribute to increased cell death (Tanik et al., 2013). In brief, perturbations in these degradation pathways may create an environment that leads to the formation and propagation of misfolded α-syn (Lee et al., 2010; Tanik et al., 2013; Lopes da Fonseca et al., 2015; Victoria and Zurzolo, 2015).

Transcellular Propagation of α-Synuclein

Braak and colleagues first revealed that LBs and LNs are enriched in the dorsal motor nucleus of the vagal nerve (dmX) and olfactory bulb prior to the appearance of classic motor symptoms in PD by post-mortem histopathological studies; afterward, they are present in interconnected brain regions with the development of disease (Braak et al., 2003; Braak and Del Tredici, 2016). They describe the assumption of active retrograde transport of α-syn for stages 1–6. In stage 1, α-syn is present within the olfactory bulb, dmX, and the intermediate reticular zone. In this stage, loss of smell is reported in patients. In stage 2, the level-setting nuclei of the lower brainstem are involved, followed by a group of non-thalamic nuclei that project widely to the cerebral cortex. In stage 2, patients may suffer from disturbance of sleep and wakefulness,

movement problems, lowered blood pressure, constipation, and emotional disorders. In stage 3, the α-syn pathology reaches the midbrain nuclei (including substantia nigra pars compacta) and the central subnucleus of the amygdala. Patients in this stage manifest thermoregulation disorder, and cognitive impairment. In stage 4, Lewy pathology invades additional subnuclei of the amygdala and the cerebral cortex. Clinically, four major symptoms, these being bradykinesia, resting tremor, rigidity, and postural instability, can be observed. During stages 5 and 6, the deep layers of the neocortex are involved, and patients may suffer motion fluctuations, frequent fatigue, visual hallucination, dementia, and psychiatric symptoms (Goedert et al., 2010, 2014; Dunning et al., 2012; Braak and Del Tredici, 2016). The former three stages compose the pre-symptomatic phase, and the latter stages the symptomatic phase (Braak et al., 2003). This pathological propagation describes the symptomatic progression of patients with PD. These observations provide the basis for the prion-like hypothesis of α-syn.

The propagation of PD among different organs

Braak et al. argue that the olfactory bulb and enteric plexus of the stomach may be starting points of pathology in many neurodegenerative diseases including PD (Acquatella-Tran Van Ba et al., 2013; Renner and Melki, 2014; Rey et al., 2018). The presence of Lewy pathology in the enteric nervous system (ENS) led to the hypothesis that α-syn pathology starts in the peripheral nervous system (PNS) with α-syn serving as a direct seed (Goedert et al., 2014). In order to test this hypothesis, Manfredsson et al. used two distinct models of rodents and non-human primates (NHP): the α-syn viral overexpression model and the preformed fibril (PFF) model. Their data suggest that α-syn can be transported from ENS to the CNS brainstem in both rodents and NHPs, however, the pathology was neither sustained, nor did it spread (Manfredsson et al., 2018).

A recent study by Takahashi and colleagues indicates that α-syn PFF inoculation into the mouse gastrointestinal tract induces α-syn pathology resembling that at early stage of PD, which supports the "gut-to-brain" hypothesis (Uemura et al., 2018). According to Braak's hypothesis, abnormal α-syn is spread between anatomically interconnected systems (Recasens and Dehay, 2014; Braak and Del Tredici, 2016). However, this hypothesis is merely confined to snapshots of degeneration mechanisms in independent post-mortem PD patients after diagnosis. A separate, alternative hypothesis proposed by Engelender and Isacson is that selective vulnerability underlies pathogenesis, which better accounts for the current neurobiology of PD symptoms progression compared to the hypothesis proposed by Braak that the pathology ascends from the PNS to the CNS. According to this assumption, less-resistant nerve cells suffer attack earlier; conversely, more-resistant cells can survive by benefiting from cellular compensation. The "threshold theory" explains that signs from the PNS and brainstem appear earlier than motor signs. The symptoms of PD only show signs when the functional reserve of neurons (and their connecting brain regions) is undercompensated. In conclusion, early symptoms of PD reflect loss of function in the least compensated tissues, such as the GI tract, olfactory system, and brainstem (Engelender and Isacson, 2017).

Svensson et al. used data from the Danish National Patient Registry (DNPR) and reported that patients who had undergone full truncal vagotomy had a clear reduced risk for PD compared to both super-selective vagotomies and the general population, suggesting that the vagal nerve was critically involved in the pathogenesis of PD (Svensson et al., 2015; Tysnes et al., 2015). Holmqvist et al. (2014) provided the first experimental evidence with injecting brain lysate containing different α-syn forms (monomeric, oligomeric, and fibrillar) and distinct recombinant α-syn into the intestinal wall. They demonstrated that different α-syn forms spread from the gut to the brain via the vagal nerve in a time-dependent manner (Holmqvist et al., 2014). In addition, α-syn is particularly abundant in the Appendix, which makes it an anatomical candidate for the initiation of PD pathology. Two independent epidemiological datasets showed that appendectomy decades before PD onset was associated with a reduced risk for PD and delayed the age of PD onset. Possible mechanisms were studied when it was observed that Appendix lysates induce the rapid cleavage and oligomerization of full-length α-syn (Killinger et al., 2018). The Appendix has been recently shown to contain an abundance of α-syn and PD pathology-associated α-syn truncation products that accumulate in LBs in neurologically intact individuals. α-syn is detected in the whole ENS of healthy people and PD patients, suggesting that the discovery of α-syn alone is not sufficient to explain the progress of PD. The removal of the Appendix is possibly not sufficient to inhibit the exposure of CNS to α-syn via vagal retrograde transport. However, whether the Appendix, as a GI tract lymphoid organ, has an enhanced capacity to generate truncated α-syn amylogenic seeds is unknown. Further studies are required to elucidate the role of Appendix in PD (Marras et al., 2016; Svensson et al., 2016; Yilmaz et al., 2017; Palacios et al., 2018).

Experiments *in vivo* by DiMonte were carried out to clarify the relation between α-syn accumulation in the brain and in peripheral organs, and to explore potential mechanisms involved in long-distance transmission of α-syn. These studies revealed a route-specific transmission of α-syn from the brain to the stomach of rats, following targeted midbrain overexpression of human α-syn. A specific tendency of vagal motor neurons and efferent fibers to accrue α-syn and transfer it to peripheral organs has also been studied. The significant work by DiMonte suggests a potential for two-way spread between the ENS and CNS (Ulusoy et al., 2017). Another study by DiMonte emphasized that rapid long-distance diffusion and accumulation of monomeric and oligomeric α-syn might result in a fatal neuronal burden and contribute to the development of PD. However, the field of α-syn staining in peripheral tissues is not mature right now, hence we have insufficient knowledge about the pathology in this area (Helwig et al., 2016; Ulusoy et al., 2017; Borghammer, 2018).

The host-to-graft transmission of PD

The first tentative evidence for the transcellular propagation of α-syn was in the autopsy of patients with PD who had had embryonic brain tissue transplanted into the striatum to

replace degenerated dopaminergic neurons (Kordower et al., 2008; Hansen et al., 2011). Over 10–16 years after injection of the graft, when examining the brain tissues of these patients post-mortem, it was found that pathologic α-syn inclusions, similar to those in the host brain, appeared in the cells generated from the grafted embryonic tissue (Kaufman and Diamond, 2013; Goedert et al., 2014). One possibility is that pathological α-syn spread from the degenerated host brain tissue to the healthy young brain tissue, recruited further α-syn from the recipient cells and generated α-syn inclusions. Another study found that patients with PD who survived for only 4–9 years after transplantation did not manifest pathological progress. These studies indicate that the prion-like pathological process develops at a slow rate (Kordower et al., 2008).

Consequently, numerous research programs were launched to explore the "host-to-graft transmission" hypothesis in animal models, such as mice and NHP. Seven distinct experimental categories have been used to investigate the spreading of α-syn:

(1) Mougenot and colleagues extracted insoluble α-syn aggregates from the cerebral homogenate of gerontic pathogenetic mice (12–18 months) overexpressing α-syn or expressing mutated A53T α-syn and injected the extract into the brain of younger transgenic mice (7–9 weeks). They found that α-syn aggregation appeared in the brain of the young mice, who showed early symptoms of PD. In grafts, LBs could be observed in up to 5% dopaminergic neurons, similar to the proportion of LB-containing neurons in the substantia nigra of patients with PD patients (Mougenot et al., 2012). On the contrary, after injection of identical extract to mice with *SNCA* gene knockout, the pathologic progress and PD manifestations could not be observed (Luk et al., 2012b; Recasens et al., 2014; Fernandez-Borges et al., 2015; Peelaerts et al., 2015).

(2) When synthetic α-syn PFF were injected into the striatum or substantia nigra of rat brain over time, α-syn inclusions spreading over the brain were observed by immunohistochemistry, while mice injected with soluble α-syn did not exhibit pathological symptoms, suggesting that inoculation of PFF causes spreading in anatomically interconnected brain regions (Masuda-Suzukake et al., 2013; Recasens and Dehay, 2014; Paumier et al., 2015).

(3) Injection of PFF into wild-type mice can generate the same results with transgenic mice (Luk et al., 2012a,b; Masuda-Suzukake et al., 2013, 2014; Recasens and Dehay, 2014).

(4) When injecting recombinant monomeric and oligomeric α-syn into the olfactory bulb of wild-type mice, the formation of α-syn aggregates is observed in interconnected regions (Rey et al., 2013; Recasens and Dehay, 2014).

(5) Injection of LB extracts containing α-syn from the brain tissues of post-mortem patients with PD into the striatum or substantia nigra of wild-type mice triggers neurodegeneration and the aggregation of α-syn in nigral neurons and anatomically interconnected areas. However, this was not observed when injecting the LB extract into mice lacking α-syn expression (Recasens and Dehay, 2014; Recasens et al., 2014; Fernandez-Borges et al., 2015; Dehay and Fernagut, 2016).

(6) Intramuscular injection of PFF into the hind limbs of mice expressing either wild-type or A53T mutated α-syn, causes α-syn pathology swiftly in the brain and a rapid-onset motor phenotype. Injection of α-syn fibrils via intravenous and intraperitoneal routes in α-syn-overexpressing mice can also induce the above pathological process. These findings reveal that α-syn can give rise to neuro-invasion from peripheral exposures (Sacino et al., 2014; Ayers et al., 2017).

(7) The significant discoveries of intra-nigral injections of recombinant adeno-associated viral vectors (AAVs), encoding either human wild-type or mutated α-syn, include: (1) the production of cytoplasmic α-syn inclusions and α-syn-loaded dystrophic neurites like PD; (2) the generation of post-translationally modified α-syn; (3) the accumulation of high-molecular-weight α-syn detectable both biochemically and also immunohistochemically; (4) synaptic dysfunction; (5) the reduction of striatal dopamine. In 2013, Ulusoy and colleagues developed a new AAV model that targeted the vagal system, which demonstrated inter-neuronal transmission of α-syn *in vivo* and a direct relationship between α-syn overexpression and efficient CNS protein propagation for the first time. The animal model with vagal injections of α-syn-carrying AAVs is characterized by a caudo-rostral pattern of spread that shares similarities with the pattern of the anatomical distribution of α-syn pathology in PD (Fernandez-Borges et al., 2015; Ulusoy et al., 2015, 2017; Helwig et al., 2016; Recasens et al., 2018).

With time, α-syn aggregates spread through the brain following axonal projections. The strongest evidence for α-syn propagation is the early work where microfluidic devices were utilized, which effectively separates somata from axonal projections in fluidically isolated microenvironments. It was demonstrated that α-syn fibrils are internalized, anterogradely transported within axons, released, and subsequently taken up by additional neurons. The findings by Freundt et al. suggested that transmission can occur in the absence of synapses, because their formation in mixed E17 murine neuron/astrocyte cultures requires 2–3 weeks, whereas the second-order neurons had been cultivated for only 1 or 4 days. If axon-to-somata transmission of misfolded α-syn occurs in a similar pathway in the CNS, the extracellular progresses may offer an opportunity to block fibrillar α-syn (Freundt et al., 2012). Brahic et al. (2016) observed that α-syn fibrils are transported along axons, both in the anterograde and retrograde direction and secreted by axons after anterograde transport, in the absence of axonal lysis, hinting that trans-neuronal transfer can occur in intact healthy neurons. The kinetics of transport suggests that α-syn fibrils are part of the slow component b of axonal transport (Freundt et al., 2012;

Bieri et al., 2018). It was verified that accumulation of pathologic α-syn led to selective reduction in synaptic proteins, progressive impairments in neuronal network function, and excitability that all culminate in neuron death. However, data in rodents is still equivocal, as much of the published data can be explained simply via retrograde transport of protein (Taylor et al., 2005; Volpicelli-Daley et al., 2011).

All the experimental findings clearly illustrate that misfolded α-syn is the "spreading agent," and is characterized by a "prion-like" behavior of transcellular propagation.

There have been recent studies on the methods that allow for monitoring prion-like propagation of the pathogenic protein between diverse cells in the *Drosophila melanogaster* model. This experimental paradigm can be useful for investigating and identifying molecular mechanisms underlying α-syn pathology in PD (McGurk et al., 2015; Donnelly and Pearce, 2018).

Cellular Release of α-Synuclein

In 2003, the first evidence that demonstrated α-syn present outside the cells was the discovery of α-syn in cultured neuroblastoma cells, CSF, and plasma, and this was observed earlier than the concept that α-syn would act as prions do. These observations showed multiple molecular species of α-syn in the extracellular space of the human CNS regardless of disease conditions. However, the relevant regulatory mechanism of secretion, the correlation of α-syn aggregation, and their localization are unknown (Tyson et al., 2016).

It is generally believed that α-syn can be transferred by classic exocytosis and endocytosis pathways (including micropinocytosis), tunneling nanotubes (TNTs), synapses or synapse-like structures, and several receptors (Goedert et al., 2010; Dunning et al., 2012; De Cecco and Legname, 2018).

Recent studies indicate that α-syn exists in secretory vesicles of neurons and multifarious biological fluids such as CSF and plasma, implying that α-syn may be secreted via exocytosis (Goedert et al., 2010; Lee et al., 2010; Tyson et al., 2016). There is growing evidence supporting that α-syn could be transferred by two ways. The first is through an exosome-associated mechanism in a calcium-dependent manner, further exacerbated after lysosomal inhibition. Because of their nanometric size, exosomes can pass through the endothelial cells of the blood-brain barrier by receptor-mediated endocytosis. Exosomes are regarded as an indispensable means of transport in CNS. Exosomes are rich in RNA transcripts, especially in small RNAs. When exosomes are ingested by cells, the embedded RNAs can regulate the expression of their target genes. The presence of misfolded α-syn and unique RNA profiles can provide effective biomarkers that favor the diagnosis and treatment of PD (Quek and Hill, 2017). The other mechanism through which α-syn can be transferred is vesicle-mediated exocytosis. Extracellular vesicles containing α-syn are released by primary neurons under stress induced by the lipid peroxidation product 4-hydroxynonenal, internalized into by secondary neurons and trafficked within axons. These results suggest that α-syn transfer via extracellular vesicles may be at least partially involved in the spread of PD (Zhang et al., 2018). More studies hint that the mechanism of release may be non-classical ER-Golgi–independent exocytosis (Kaufman and Diamond, 2013). Moreover, Jang and colleagues demonstrated that inhibition of mitochondrial complex I, as well as proteasomal and lysosomal activities, could affect exocytotic α-syn release (Sian-Hulsmann et al., 2015; Tyson et al., 2016).

Tunneling nanotubes (TNTs) containing F-actin, whose diameter is < 200 nm, are an important mechanism for α-syn propagation in a similar manner as prions. By using quantitative fluorescence microscopy with co-cultured neurons, α-syn fibrils efficiently transfer from donor to acceptor cells through TNTs inside lysosomal vesicles (Abounit et al., 2016a). TNTs allow direct physical connections of remote cell membranes. Theirs physiological role is to transfer cellular components, but under pathological conditions TNTs can facilitate the spreading of viruses and pathogenic proteins (Sherer and Mothes, 2008; Dunning et al., 2012). It is postulated that misfolded protein aggregates can promote the formation of TNTs and thereby their own intercellular transfer, contributing to the propagation of pathology. Because intracellular accumulation of misfolded α-syn induces lysosomal impairments, neurons try to dispose of impaired material through TNTs, which enhances their formation. The accumulation of α-syn in lysosomes may change organelle signaling and positioning, making them have a stronger tendency to enter the new TNTs. Proteolytic degradation of misfolded α-syn in the lysosome prevents neurons from α-syn seeding pathogenicity (Sacino et al., 2017). Moreover, truncated species of α-syn show higher seeding propensity, suggesting that tuning of lysosomal protease activity under different conditions may modulate pathogenicity of the α-syn seeds (Karpowicz et al., 2019). Furthermore, lysosomal impairment can directly or indirectly influence mitochondrial health and function, which may ultimately mediate toxicity in PD. As a result of lysosomal damage, the rate of aggregate growth in neurons increases, suggesting that decreased α-syn seed degradation, increased escape from damaged lysosomes, or both, can potentiate recruitment of α-syn into aggregates (Abounit et al., 2016b; Victoria and Zurzolo, 2017; Karpowicz et al., 2019). Astrocytes, as the major cell type of the brain, may actively transfer α-syn aggregates to healthy astrocytes by direct contact or TNTs. This finding reveals astrocytes as a potential target for PD therapy (Bukoreshtliev et al., 2009; Rostami et al., 2017). Although these structures are known to be present in cultured cells, their formation in tissue is still controversial and uncharacterized.

Another approach for α-syn spreading is necrotic neurons death, which releases intracellular contents. Nonetheless, many studies show that the majority of monomeric α-syn outside the cells originates from active release instead of passive release from neuron death (Costanzo and Zurzolo, 2013).

Subsequently, several studies showed that α-syn may be actively secreted and this process can be constitutive and regulated. In induced pluripotent stem cell (iPSC)-derived cells that express a triplicate of the gene encoding α-syn, high levels of the protein can be found in their extracellular medium. These results indicate that there is an interrelation between the amount of α-syn in the cell and its secretion to the extracellular space. This finding may be applicable during aging in PD, where there are higher levels of cytoplasmic α-syn in neural cells,

and therefore greater secretion of α-syn (Woodard et al., 2014; Tyson et al., 2016).

Cellular Uptake of α-Synuclein

Following intracortical injection of recombinant α-syn in rats, the cellular uptake was attenuated with co-injection of an endocytosis inhibitor. This fact demonstrates the significant role of endocytosis (Hansen et al., 2011). In primary neurons transduced with recombinant α-syn PFFs labeled with environmentally-responsive fluorophores, the vast majority of PFFs are acidified along the endocytic pathway and remain there for a week or more (Karpowicz et al., 2017). The ability to uptake extracellular α-syn, and subsequent degradation, is in connection with the α-syn species with different dimensions. The entry of larger aggregates requires specific entry pathways, including dynamin-dependent endocytosis. Oligomeric and fibrillar α-syn are taken up by cold temperature and dynamin K44A-sensitive endocytosis (Kaufman and Diamond, 2013; Chan et al., 2017). Diffusion through the cell membrane is one of the simplest pathways for cellular uptake. Monomeric α-syn is capable of readily diffusing through the cell membrane, because its uptake cannot be inhibited by low temperature or blocked as in typical pathways like endocytosis.

Most classical endocytosis requires receptors to mediate internalization. Different studies report the existence of α-syn receptors that may mediate the cell-to-cell transmission of α-syn pathology. The first specific mediator of α-syn was a class of glycosylated extracellular matrix proteins known as heparan sulfate proteoglycans (HSPGs) (Holmes et al., 2013; Karpowicz et al., 2019). HSPGs are capable of mediating macropinocytosis related to α-syn and other aggregation-prone proteins (Holmes et al., 2013; Stopschinski et al., 2018). The α3 subunit of the Na^+/K^+-ATPase can interact with both oligomeric and fibrillar α-syn at the cell surface. The Fc gamma receptor IIb is described as a receptor for α-syn fibrils. The lymphocyte-activation gene 3 (LAG3) binds misfolded α-syn built-in in PFFs with high selectivity but does not interact with monomeric α-synuclein (Mao et al., 2016). The proposed pathway for LAG3-dependent uptake is clathrin-mediated endocytosis (CME), which may participate in α-syn monomer uptake (Konno et al., 2012; Karpowicz et al., 2019). Similar specificity to aggregated, but not monomeric α-synuclein, is described for toll-like receptor-2 (TLR2) and transmembrane ion channels receptor P2X7. Neurexin 1α is described as a cell surface receptor for both α-syn PFFs and fibrils. α-syn fibrils were also shown to interact with amyloid-β precursor-like protein 1 and heparin sulfate proteoglycans that mediate endocytosis. Interestingly, PrP^C is reported as a possible receptor for α-syn amyloid fibrils, facilitating their internalization through and endocytic pathway (Urrea et al., 2017; De Cecco and Legname, 2018). The *in vitro* data confirmed that the presence of PrP^C facilitates the higher and faster uptake of α-syn fibrils, which was also shown *in vivo* in wild type (*Prnp*+/+) compared to PrP knock-out (*Prnp*−/−) mice (Aulic et al., 2017; Urrea et al., 2018). This cooperation fosters the transmission of α-syn between cells and causes synaptic dysfunction via a signaling cascade acting through phosphorylation of Fyn kinase and activation of the N-methyl-D-aspartate receptor (NMDAR). α-syn-PrP^C binding induces cofilin/actin rods formation, which changes actin dynamics, resulting in rearrangements of cytoskeleton and eventual synaptic dysfunction (Clavaguera et al., 2015; Bras et al., 2018; Surguchev et al., 2019). Equally, α-syn amyloids blocked the replication of PrP^{Sc} *in vitro* and *ex vivo* (Aulic et al., 2017). Deciphering the mechanisms involved in sensing diverse forms of extracellular α-syn may prove invaluable in our quest to devise novel diagnostic and therapeutic approaches in PD. The internalized fibrils and oligomeric α-syn are trafficked via the endosomal pathway and degraded by the lysosome. In contrast, the monomer of α-syn rapidly pass through the plasma membrane before being degraded by the proteolytic systems (Lee et al., 2008; Chan et al., 2017).

Introduction of α-syn aggregates by PFFs generated from truncated recombinant human wild-type α-syn into primary hippocampal neurons, cause adsorptive-mediated endocytosis promoting soluble α-syn into insoluble LBs and LNs (Volpicelli-Daley et al., 2011; Jellinger, 2012). When a GTPase-deficient Rab5A was introduced into the cells, α-syn uptake and cell degeneration decreased. This indicates that α-syn could be taken up through Rab5A-dependent endocytosis (Tyson et al., 2016) (**Figure 2**).

Ultimately, internalized α-syn proteins act as amplification seeds by recruiting endogenous native proteins and leading to formation of toxic LBs.

There are key factors that dramatically modulate the prion-like propensities of α-syn, including the concentration of nuclei, the presence of oligomers, and the toxicity, resistance, and localization of α-syn aggregates. In brief, these mentioned factors which favor the high concentration of extracellular nuclei or oligomers, characterized by small size, with a low toxicity would effectively enhance prion propensity; in contrast, low concentrations of highly toxic intracellular aggregates, with a larger size, would obviously prevent spreading (Espargaro et al., 2016).

In addition to α-syn aggregation, inflammation also plays a key role in the progression of PD. Chemical or viral exposure may give rise to immune activation in the gastrointestinal tract or olfactory system, triggering misfolding, aggregation, and subsequent propagation of α-syn. The dysregulated action of glial cells and astrocytes triggered by the neurotoxic α-syn can induce inflammation in the brain. It is proposed that neuroinflammation can prompt the prion-like pathology of α-syn by increasing its release, uptake, or both. But this hypothesis has not been fully confirmed. However, further studies about the relation between inflammation and prion-like behavior is required to support the hypothesis (Lema Tome et al., 2013; Lawand et al., 2015; Chandra et al., 2017).

IMPLICATIONS FOR THERAPEUTIC STRATEGIES

There is no cure for PD and available palliative treatments only focus on restoring dopamine deficits and controlling the symptoms. Present efforts for therapies of PD focus mainly on restraint for the templated conformation change and transcellular

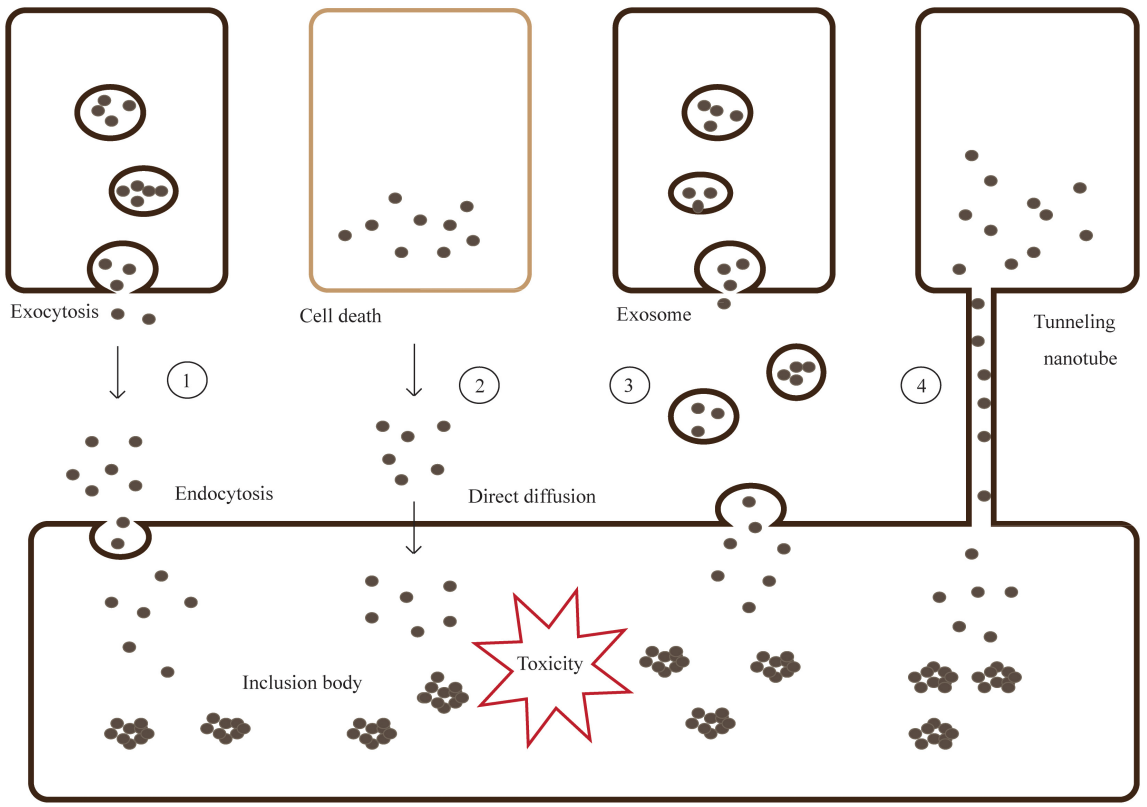

FIGURE 2 | Models for cell-to-cell transmission of misfolded and aggregated proteins. Step 1- Misfolded and aggregated proteins are released from neurons by vesicle-mediated exocytosis, then taken into the neighboring cells via endocytosis. Step 2- Proteins are spilled from dead cells and enter the neighboring cells through direct diffusion. Step 3,4- Proteins can transmit by packaging into exosomes or tunneling nanotubes (TNTs).

propagation. The former includes stabilizing the physiological conformation of synuclein, decreasing its expression, preventing aggregation of α-syn, and increasing intracellular clearance of the aggregates; and the latter consists of preventing the release, decreasing uptake by cells, and increasing extracellular clearance (Kaufman and Diamond, 2013; Hasegawa et al., 2017). In view of the normal physiological function of α-syn, Benskey and colleagues proposed the hypothesis that loss of a-syn function within nigrostriatal neurons initiates a neuronal-mediated neuroinflammatory cascade, ultimately resulting in the death of affected dopaminergic neurons. Therefore, more studies are needed for reasonable intervention of α-syn clearance (Benskey et al., 2018). Beyond that, anti-inflammation approaches may be used as new therapeutic methods. Considerable research is currently directed on targeting proinflammatory mediators, such as cytokines and the transcription factors that regulate their expression, trying to identify a novel treatment of PD (Lawand et al., 2015). Small molecular compounds that are capable of blocking aggregation of intracellular α-syn have remarkable application prospects for pharmacotherapy of PD. These compounds firstly enter the brain, then specifically bind to the abnormal α-syn and inhibits its action (Lawand et al., 2015; Hasegawa et al., 2017).

For the treatment of PD, the most effective therapy to inhibit the propagation of α-syn is knock-out of the related gene or inhibiting protein expression via gene or RNAi therapy. However, as mentioned earlier, it is still unknown whether gene therapy will affect α-syn normal function. Further studies are needed to evaluate the relevant efficacy before the approach can be used for clinical treatment (Kaufman and Diamond, 2013; Nielsen and Nielsen, 2013; Braak and Del Tredici, 2016; Hasegawa et al., 2017).

Furthermore, immunotherapy targeting extracellular α-syn is showing great promise. Experiments in PD models indicate that active vaccination against recombinant α-syn leads to ameliorated pathology (Sian-Hulsmann et al., 2015). Similarly, passive immunotherapy also produced positive effects. Antibodies produced by immunotherapy are expected to block the spreading of pathological α-syn (Lawand et al., 2015). Moreover, the spreading of α-syn in wild-type mice after intracerebral inoculation of α-syn fibrils was prevented by monoclonal antibodies (mAbs) against abnormal α-syn. α-Syn mAbs reduce α-syn PFF-induced LBs/LNs formation and rescue synapse/neuron loss in primary neuronal cultures by preventing both uptake and subsequent cell-to-cell transmission of pathology (Tran et al., 2014).

Existing symptomatic therapeutic strategies for treating PD include L-DOPA and monoamine oxidase (MAO) inhibitors. On the other hand, more attention has been paid to the experimental disease modifying treatments such as neurotrophic factors, neuroprotective factors and stem cell regeneration.

Neurotrophic factors are a family of secreted proteins that participate in neuronal survival and neuroplasticity. These proteins can be upregulated together with their receptors under pathogenic conditions which corresponds with the notion that they are protective and enhance brain plasticity, thus avoiding brain damage (Ibanez and Andressoo, 2017). One of the most studied is glial cell line-derived neurotrophic factor (GDNF), which has neuroprotective and neurorestorative effects in PD animal models, however, it is challenging to achieve such neuroprotection in clinical trials on PD patients (Francardo et al., 2017). Another widely studied neuroprotective factor is Brain-derived neurotrophic factor (BDNF), which is a ubiquitous neurotrophin in the adult brain, maintaining dopaminergic neuronal survival, promoting synaptic plasticity, dendritic morphogenesis and arborization, and even neurogenesis (Rahmani et al., 2019). Moreover, α-syn effectively blocks neurotrophic activity of BDNF in SN, first by downregulating BDNF expression (Yuan et al., 2010), and second by competitive inhibition of BDNF signaling at receptor level (Kang et al., 2017). Most studies have a consensus that exogenous introduction of BDNF is able to mitigate dopaminergic neuronal loss in neuronal culture and in animal models of PD (Sadan et al., 2009; Zhao et al., 2014; Goldberg et al., 2015). It was also reported that anti-PD drugs, even dopamine replacement treatments, performed part of functions by upregulating BDNF (Rahmani et al., 2019). Another treatment strategy is DA neuron restoration in damaged regions by neurogenesis stimulation or iPSCs. One way of stimulating neurogenesis is through the activation of the transcription factors, such as nuclear receptor related 1 (Nurr1) (Kim et al., 2015). Furthermore, a PD animal model with iPSC-derived neuronal stem cells transplanted into the striatum showed improvement in functional defects of rotational asymmetry. Moreover, the neuronal stem cells survived and integrated into the brains of transplanted PD animals and differentiated into neurons, including DA neurons. Clinical application of the experimental treatments for PD may become an attractive strategy in the future (Han et al., 2015; Van Bulck et al., 2019).

However, these treatments rely on discriminating the correct α-syn species for intervention and a deeper understanding of the interrelation between the degradation and propagation of α-syn. Because of the variety of pathogeneses, combination therapies receive increasing attention compared to single-target agents (Valera and Masliah, 2016). Further studies on underlying influencing factors are expected to reveal the best targets for the treatment for PD.

Although the inoculation of α-syn aggregates may induce neuronal damage and clinical abnormalities (e.g., motor impairments) in wild-type mice, none of available studies provided evidence for a transmission of PD between individuals. The findings published so far on the effects of experimentally transmitted α-syn seeds do not indicate specific precautionary measures in the context of hemotherapy, but call for vigilance in transfusion medicine and other medical areas. This suggests that patients may possibly get medical security by a thorough decontamination from the α-syn aggregates in surgical instruments, blood or blood products and medical services (Beekes et al., 2014; Recasens et al., 2014).

A novel real-time quaking-induced conversion (RT-QuIC) based assay is able to detect α-syn aggregation in brain and CSF from PD patients with a sensitivity of 95%, and with a specificity of 100% (Le et al., 2015; Fairfoul et al., 2016). It is demonstrated that α-syn can be rapidly detected and quantitated, even in early symptomatic stages of synucleinopathy (Groveman et al., 2018). By this token, RT-QuiC analysis of CSF is potentially useful for the early clinical assessment of PD patients (Fairfoul et al., 2016).

Several diagnostic imaging probes were reported to monitor cerebral amyloid lesions in neurodegenerative disorders. Florbetapir is the first radioactive dye for brain imaging of amyloid plaques approved by the FDA in AD. The importance of further studies for their practical implications in therapy and diagnostics should be highlighted (Aulic et al., 2013).

DISSENTING OPINIONS

In this review we described the prion-like hypothesis in PD from a biophysical point of view and discussed the literature in support of the hypothesis. Pathological α-syn is known as prion-like or prionoid, which describes the dominating properties that PrP^{Sc} and pathological α-syn have in common: seeding/templating, propagation, structurally differentiated conformations, and subsequent neurodegeneration. While it is evident that PrP^{Sc} and pathological α-syn share properties, not all experimental observations can be entirely explained by this fact. The most significant difference between pathological α-syn and PrP^{Sc} is that PrP^{Sc} is transmissible between humans and PD-associated α-syn is not. However, human-to-human transmission of prion diseases is nowadays restricted to iatrogenic incidents. The presence of amyloid-β protein (Aβ) deposits have been reported in patients with CJD who had been treated with human cadaveric pituitary derived growth hormone (c-hGH) contaminated with prions during childhood with short stature. Purro et al. verified the presence of Aβ seeds in archived c-hGH vials and proposed a hypothesis about the iatrogenic human transmission of Aβ pathology. Doubts should be raised regarding whether transmission of α-syn may occur under special circumstances (Purro et al., 2018).

In terms of the potential propagation of α-syn, the staging for PD is an indirect measure. All information on α-syn propagation are rooted in experimental animals, primarily rodents, but not from humans. Another point of difference is that PD is not rapidly progressive like prions. Neurodegenerative diseases are generally considered to be chronic diseases, and the rate of disease progression is also one of their differences.

CONCLUSION

It is believed that self-aggregation and transmission of α-syn contribute to the gradual spreading of pathological degeneration in PD. Misfolded aggregates escape from clearance and are released into the extracellular space via synapse, exosome, vesicle,

cell death, or tunneling nanotubes. Afterward, α-syn aggregates are internalized by the recipient cells and induce endogenous α-syn to misfold and assemble in some unclear manner. All the studies mentioned in this review support the fact that misfolded α-syn have much in common with prions in their mode of action: (i) α-syn and prions both mainly exist either without a defined structure or in an α-helix, however, they tend to misfold when the conformation is rich in β-sheets under certain circumstances. (ii) Misfolded proteins lead to further accumulation of normal proteins and acts as template to change their conformation. (iii) Misfolded proteins are capable of being taken in by and transferred from cell to cell. However, there are still plenty of unanswered questions regarding the pathogenesis of α-syn: (i) the specific molecular mechanisms of misfolding, release, uptake, and transmission of the aggregates; (ii) whether the misfolded protein in a cell can induce protein misfolding in the neighboring cells directly; (iii) the physicochemical and environmental factors that affect the pathological process; (iv) whether the diversity of species and conformations has an impact on clinical manifestations; and (v) whether PD has the same infectivity as prion diseases. By asking these questions, we are witnessing the beginning of a new field of research in PD and other neurodegenerative disorders.

AUTHOR CONTRIBUTIONS

JW and AX planned the study. JM, JG, and JW analyzed the data and edited the manuscript. JM wrote the manuscript.

FUNDING

This work was supported by grants from the Natural Science Foundation of China (81571225).

ACKNOWLEDGMENTS

We would like to acknowledge the investigators for their helpful comments on this manuscript.

REFERENCES

Abounit, S., Bousset, L., Loria, F., Zhu, S., de Chaumont, F., Pieri, L., et al. (2016a). Tunneling nanotubes spread fibrillar alpha-synuclein by intercellular trafficking of lysosomes. *EMBO J.* 35, 2120–2138. doi: 10.15252/embj.201593411

Abounit, S., Wu, J. W., Duff, K., Victoria, G. S., and Zurzolo, C. (2016b). Tunneling nanotubes: a possible highway in the spreading of tau and other prion-like proteins in neurodegenerative diseases. *Prion* 10, 344–351. doi: 10.1080/19336896.2016.1223003

Acquatella-Tran Van Ba, I., Imberdis, T., and Perrier, V. (2013). From prion diseases to prion-like propagation mechanisms of neurodegenerative diseases. *Int. J. Cell Biol.* 2013:975832. doi: 10.1155/2013/975832

Aulic, S., Bolognesi, M. L., and Legname, G. (2013). Small-molecule theranostic probes: a promising future in neurodegenerative diseases. *Int. J. Cell Biol.* 2013:150952. doi: 10.1155/2013/150952

Aulic, S., Le, T. T., Moda, F., Abounit, S., Corvaglia, S., Casalis, L., et al. (2014). Defined alpha-synuclein prion-like molecular assemblies spreading in cell culture. *BMC Neurosci.* 15:69. doi: 10.1186/1471-2202-15-69

Aulic, S., Masperone, L., Narkiewicz, J., Isopi, E., Bistaffa, E., Ambrosetti, E., et al. (2017). alpha-synuclein amyloids hijack prion protein to gain cell entry, facilitate cell-to-cell spreading and block prion replication. *Sci. Rep.* 7:10050. doi: 10.1038/s41598-017-10236-x

Ayers, J. I., Brooks, M. M., Rutherford, N. J., Howard, J. K., Sorrentino, Z. A., Riffe, C. J., et al. (2017). Robust central nervous system pathology in transgenic mice following peripheral injection of alpha-synuclein fibrils. *J. Virol.* 91:e2095-16. doi: 10.1128/JVI.02095-16

Beekes, M., Thomzig, A., Schulz-Schaeffer, W. J., and Burger, R. (2014). Is there a risk of prion-like disease transmission by Alzheimer- or Parkinson-associated protein particles? *Acta Neuropathol.* 128, 463–476. doi: 10.1007/s00401-014-1324-9

Benskey, M. J., Sellnow, R. C., Sandoval, I. M., Sortwell, C. E., Lipton, J. W., and Manfredsson, F. P. (2018). Silencing alpha synuclein in mature nigral neurons results in rapid neuroinflammation and subsequent toxicity. *Front. Mol. Neurosci.* 11:36. doi: 10.3389/fnmol.2018.00036

Bieri, G., Gitler, A. D., and Brahic, M. (2018). Internalization, axonal transport and release of fibrillar forms of alpha-synuclein. *Neurobiol. Dis.* 109(Pt B), 219–225. doi: 10.1016/j.nbd.2017.03.007

Borghammer, P. (2018). How does parkinson's disease begin? Perspectives on neuroanatomical pathways, prions, and histology. *Mov. Disord.* 33, 48–57. doi: 10.1002/mds.27138

Braak, H., and Del Tredici, K. (2016). Potential Pathways of abnormal tau and alpha-synuclein dissemination in sporadic Alzheimer's and Parkinson's diseases. *Cold Spring Harb. Perspect Biol.* 8:a023630. doi: 10.1101/cshperspect.a023630

Braak, H., Del Tredici, K., Rub, U., de Vos, R. A., Jansen Steur, E. N., and Braak, E. (2003). Staging of brain pathology related to sporadic Parkinson's disease. *Neurobiol. Aging* 24, 197–211.

Brahic, M., Bousset, L., Bieri, G., Melki, R., and Gitler, A. D. (2016). Axonal transport and secretion of fibrillar forms of alpha-synuclein, Abeta42 peptide and HTTExon 1. *Acta Neuropathol.* 131, 539–548. doi: 10.1007/s00401-016-1538-0

Bras, I. C., Lopes, L. V., and Outeiro, T. F. (2018). Sensing alpha-synuclein from the outside via the prion protein: implications for neurodegeneration. *Mov. Disord.* 33, 1675–1684. doi: 10.1002/mds.27478

Buell, A. K., Galvagnion, C., Gaspar, R., Sparr, E., Vendruscolo, M., Knowles, T. P., et al. (2014). Solution conditions determine the relative importance of nucleation and growth processes in alpha-synuclein aggregation. *Proc. Natl. Acad. Sci. U.S.A.* 111, 7671–7676. doi: 10.1073/pnas.1315346111

Bukoreshtliev, N. V., Wang, X., Hodneland, E., Gurke, S., Barroso, J. F., and Gerdes, H. H. (2009). Selective block of tunneling nanotube (TNT) formation inhibits intercellular organelle transfer between PC12 cells. *FEBS Lett.* 583, 1481–1488. doi: 10.1016/j.febslet.2009.03.065

Burre, J., Sharma, M., and Sudhof, T. C. (2018). Cell biology and pathophysiology of alpha-synuclein. *Cold Spring Harb. Perspect. Med.* 8:a024091. doi: 10.1101/cshperspect.a024091

Cali, T., Ottolini, D., Negro, A., and Brini, M. (2012). alpha-synuclein controls mitochondrial calcium homeostasis by enhancing endoplasmic reticulum-mitochondria interactions. *J. Biol. Chem.* 287, 17914–17929. doi: 10.1074/jbc.M111.302794

Chan, D. K. Y., Xu, Y. H., Chan, L. K. M., Braidy, N., and Mellick, G. D. (2017). Mini-review on initiatives to interfere with the propagation and clearance of alpha-synuclein in Parkinson's disease. *Transl. Neurodegener.* 6:33. doi: 10.1186/s40035-017-0104-6

Chandra, R., Hiniker, A., Kuo, Y. M., Nussbaum, R. L., and Liddle, R. A. (2017). alpha-Synuclein in gut endocrine cells and its implications for Parkinson's disease. *JCI Insight* 2:92295. doi: 10.1172/jci.insight.92295

Clavaguera, F., Hench, J., Goedert, M., and Tolnay, M. (2015). Invited review: prion-like transmission and spreading of tau pathology. *Neuropathol. Appl. Neurobiol.* 41, 47–58. doi: 10.1111/nan.12197

Costanzo, M., and Zurzolo, C. (2013). The cell biology of prion-like spread of protein aggregates: mechanisms and implication in neurodegeneration. *Biochem. J.* 452, 1–17. doi: 10.1042/BJ20121898

De Cecco, E., and Legname, G. (2018). The role of the prion protein in the internalization of alpha-synuclein amyloids. *Prion* 12, 23–27. doi: 10.1080/19336896.2017.1423186

Dehay, B., and Fernagut, P. O. (2016). Alpha-synuclein-based models of Parkinson's disease. *Rev. Neurol.* 172, 371–378. doi: 10.1016/j.neurol.2016.04.003

Diack, A. B., Alibhai, J. D., Barron, R., Bradford, B., Piccardo, P., and Manson, J. C. (2016). Insights into mechanisms of chronic neurodegeneration. *Int. J. Mol. Sci.* 17:E82. doi: 10.3390/ijms17010082

Dillard, R. S., Hampton, C. M., Strauss, J. D., Ke, Z., Altomara, D., Guerrero-Ferreira, R. C., et al. (2018). Biological applications at the cutting edge of cryo-electron microscopy. *Microsc. Microanal.* 24, 406–419. doi: 10.1017/s1431927618012382

Donnelly, K. M., and Pearce, M. M. P. (2018). Monitoring cell-to-cell transmission of prion-like protein aggregates in drosophila melanogaster. *J. Vis. Exp.* 133:e56906. doi: 10.3791/56906

Dunning, C. J., Reyes, J. F., Steiner, J. A., and Brundin, P. (2012). Can Parkinson's disease pathology be propagated from one neuron to another? *Prog. Neurobiol.* 97, 205–219. doi: 10.1016/j.pneurobio.2011.11.003

Engelender, S., and Isacson, O. (2017). The threshold theory for Parkinson's disease. *Trends Neurosci.* 40, 4–14. doi: 10.1016/j.tins.2016.10.008

Espargaro, A., Busquets, M. A., Estelrich, J., and Sabate, R. (2016). Key points concerning amyloid infectivity and prion-like neuronal invasion. *Front. Mol. Neurosci.* 9:29. doi: 10.3389/fnmol.2016.00029

Fairfoul, G., McGuire, L. I., Pal, S., Ironside, J. W., Neumann, J., Christie, S., et al. (2016). Alpha-synuclein RT-QuIC in the CSF of patients with alpha-synucleinopathies. *Ann. Clin. Transl. Neurol.* 3, 812–818. doi: 10.1002/acn3.338

Fernandez-Borges, N., Erana, H., Elezgarai, S. R., Harrathi, C., Gayosso, M., and Castilla, J. (2013). Infectivity versus seeding in neurodegenerative diseases sharing a prion-like mechanism. *Int. J. Cell Biol.* 2013:583498. doi: 10.1155/2013/583498

Fernandez-Borges, N., Erana, H., Venegas, V., Elezgarai, S. R., Harrathi, C., and Castilla, J. (2015). Animal models for prion-like diseases. *Virus Res.* 207, 5–24. doi: 10.1016/j.virusres.2015.04.014

Francardo, V., Schmitz, Y., Sulzer, D., and Cenci, M. A. (2017). Neuroprotection and neurorestoration as experimental therapeutics for Parkinson's disease. *Exp. Neurol.* 298(Pt B), 137–147. doi: 10.1016/j.expneurol.2017.10.001

Freundt, E. C., Maynard, N., Clancy, E. K., Roy, S., Bousset, L., Sourigues, Y., et al. (2012). Neuron-to-neuron transmission of alpha-synuclein fibrils through axonal transport. *Ann. Neurol.* 72, 517–524. doi: 10.1002/ana.23747

Fussi, N., Hollerhage, M., Chakroun, T., Nykanen, N. P., Rosler, T. W., Koeglsperger, T., et al. (2018). Exosomal secretion of alpha-synuclein as protective mechanism after upstream blockage of macroautophagy. *Cell Death Dis.* 9:757. doi: 10.1038/s41419-018-0816-2

Galvagnion, C. (2017). The role of lipids interacting with alpha-synuclein in the pathogenesis of Parkinson's disease. *J. Parkinsons Dis.* 7, 433–450. doi: 10.3233/JPD-171103

Goedert, M., Clavaguera, F., and Tolnay, M. (2010). The propagation of prion-like protein inclusions in neurodegenerative diseases. *Trends Neurosci.* 33, 317–325. doi: 10.1016/j.tins.2010.04.003

Goedert, M., Falcon, B., Clavaguera, F., and Tolnay, M. (2014). Prion-like mechanisms in the pathogenesis of tauopathies and synucleinopathies. *Curr. Neurol. Neurosci. Rep.* 14:495. doi: 10.1007/s11910-014-0495-z

Goldberg, N. R. S., Caesar, J., Park, A., Sedgh, S., Finogenov, G., Masliah, E., et al. (2015). Neural stem cells rescue cognitive and motor dysfunction in a transgenic model of dementia with lewy bodies through a BDNF-dependent mechanism. *Stem Cell Reports* 5, 791–804. doi: 10.1016/j.stemcr.2015.09.008

Groveman, B. R., Orru, C. D., Hughson, A. G., Raymond, L. D., Zanusso, G., Ghetti, B., et al. (2018). Rapid and ultra-sensitive quantitation of disease-associated alpha-synuclein seeds in brain and cerebrospinal fluid by alphaSyn RT-QuIC. *Acta Neuropathol. Commun.* 6:7. doi: 10.1186/s40478-018-0508-2

Guerrero-Ferreira, R., Taylor, N. M. I., Mona, D., Ringler, P., Lauer, M. E., Riek, R., et al. (2018). Cryo-EM structure of alpha-synuclein fibrils. *eLife* 7:e36402. doi: 10.7554/eLife.36402

Halliday, M., Radford, H., and Mallucci, G. R. (2014). Prions: generation and spread versus neurotoxicity. *J. Biol. Chem.* 289, 19862–19868. doi: 10.1074/jbc.R114.568477

Han, F., Wang, W., Chen, B., Chen, C., Li, S., Lu, X., et al. (2015). Human induced pluripotent stem cell-derived neurons improve motor asymmetry in a 6-hydroxydopamine-induced rat model of Parkinson's disease. *Cytotherapy* 17, 665–679. doi: 10.1016/j.jcyt.2015.02.001

Hansen, C., Angot, E., Bergstrom, A. L., Steiner, J. A., Pieri, L., Paul, G., et al. (2011). alpha-synuclein propagates from mouse brain to grafted dopaminergic neurons and seeds aggregation in cultured human cells. *J. Clin. Invest.* 121, 715–725. doi: 10.1172/JCI43366

Hasegawa, M., Nonaka, T., and Masuda-Suzukake, M. (2016). alpha-synuclein: experimental pathology. *Cold Spring Harb. Perspect. Med.* 6:a024273. doi: 10.1101/cshperspect.a024273

Hasegawa, M., Nonaka, T., and Masuda-Suzukake, M. (2017). Prion-like mechanisms and potential therapeutic targets in neurodegenerative disorders. *Pharmacol. Ther.* 172, 22–33. doi: 10.1016/j.pharmthera.2016.11.010

Helwig, M., Klinkenberg, M., Rusconi, R., Musgrove, R. E., Majbour, N. K., El-Agnaf, O. M., et al. (2016). Brain propagation of transduced alpha-synuclein involves non-fibrillar protein species and is enhanced in alpha-synuclein null mice. *Brain* 139(Pt 3), 856–870. doi: 10.1093/brain/awv376

Hodara, R., Norris, E. H., Giasson, B. I., Mishizen-Eberz, A. J., Lynch, D. R., Lee, V. M., et al. (2004). Functional consequences of alpha-synuclein tyrosine nitration: diminished binding to lipid vesicles and increased fibril formation. *J. Biol. Chem.* 279, 47746–47753. doi: 10.1074/jbc.M408906200

Holmes, B. B., DeVos, S. L., Kfoury, N., Li, M., Jacks, R., Yanamandra, K., et al. (2013). Heparan sulfate proteoglycans mediate internalization and propagation of specific proteopathic seeds. *Proc. Natl. Acad. Sci. U.S.A.* 110, E3138–E3147. doi: 10.1073/pnas.1301440110

Holmqvist, S., Chutna, O., Bousset, L., Aldrin-Kirk, P., Li, W., Bjorklund, T., et al. (2014). Direct evidence of Parkinson pathology spread from the gastrointestinal tract to the brain in rats. *Acta Neuropathol.* 128, 805–820. doi: 10.1007/s00401-014-1343-6

Hyun, C. H., Yoon, C. Y., Lee, H. J., and Lee, S. J. (2013). LRRK2 as a potential genetic modifier of synucleinopathies: interlacing the two major genetic factors of Parkinson's disease. *Exp. Neurobiol.* 22, 249–257. doi: 10.5607/en.2013.22.4.249

Ibanez, C. F., and Andressoo, J. O. (2017). Biology of GDNF and its receptors - Relevance for disorders of the central nervous system. *Neurobiol. Dis.* 97(Pt B), 80–89. doi: 10.1016/j.nbd.2016.01.021

Jellinger, K. A. (2012). Interaction between pathogenic proteins in neurodegenerative disorders. *J. Cell Mol. Med.* 16, 1166–1183. doi: 10.1111/j.1582-4934.2011.01507.x

Kang, S. S., Zhang, Z., Liu, X., Manfredsson, F. P., Benskey, M. J., Cao, X., et al. (2017). TrkB neurotrophic activities are blocked by alpha-synuclein, triggering dopaminergic cell death in Parkinson's disease. *Proc. Natl. Acad. Sci. U.S.A.* 114, 10773–10778. doi: 10.1073/pnas.1713969114

Karabiyik, C., Lee, M. J., and Rubinsztein, D. C. (2017). Autophagy impairment in Parkinson's disease. *Essays Biochem.* 61, 711–720. doi: 10.1042/EBC20170023

Karpowicz, R. J., Haney, C. M., Mihaila, T. S., Sandler, R. M., Petersson, E. J., and Lee, V. M. Y. (2017). Selective imaging of internalized proteopathic α-synuclein seeds in primary neurons reveals mechanistic insight into transmission of synucleinopathies. *J. Biol. Chem.* 292, 13482–13497. doi: 10.1074/jbc.M117.780296

Karpowicz, R. J., Trojanowski, J. Q., and Lee, V. M. Y. (2019). Transmission of α-synuclein seeds in neurodegenerative disease: recent developments. *Lab. Invest.* doi: 10.1038/s41374-019-0195-z [Epub ahead of print].

Kaufman, S. K., and Diamond, M. I. (2013). Prion-like propagation of protein aggregation and related therapeutic strategies. *Neurotherapeutics* 10, 371–382. doi: 10.1007/s13311-013-0196-3

Killinger, B. A., Madaj, Z., Sikora, J. W., Rey, N., Haas, A. J., Vepa, Y., et al. (2018). The vermiform appendix impacts the risk of developing Parkinson's disease. *Sci. Transl. Med.* 10:aar5280. doi: 10.1126/scitranslmed.aar5280

Kim, C. H., Han, B. S., Moon, J., Kim, D. J., Shin, J., Rajan, S., et al. (2015). Nuclear receptor Nurr1 agonists enhance its dual functions and improve behavioral deficits in an animal model of Parkinson's disease. *Proc. Natl. Acad. Sci. U.S.A.* 112, 8756–8761. doi: 10.1073/pnas.1509742112

Kim, W. S., Kagedal, K., and Halliday, G. M. (2014). Alpha-synuclein biology in Lewy body diseases. *Alzheimers Res. Ther.* 6:73. doi: 10.1186/s13195-014-0073-2

Konno, M., Hasegawa, T., Baba, T., Miura, E., Sugeno, N., Kikuchi, A., et al. (2012). Suppression of dynamin GTPase decreases alpha-synuclein uptake by neuronal and oligodendroglial cells: a potent therapeutic target for synucleinopathy. *Mol. Neurodegener.* 7:38. doi: 10.1186/1750-1326-7-38

Kordower, J. H., Chu, Y., Hauser, R. A., Freeman, T. B., and Olanow, C. W. (2008). Lewy body-like pathology in long-term embryonic nigral transplants in Parkinson's disease. *Nat. Med.* 14, 504–506. doi: 10.1038/nm1747

Lawand, N., Saadé, N., El-Agnaf, O., and Safieh-Garabedian, B. (2015). Targeting α-synuclein as a therapeutic strategy for Parkinson's disease. *Expert Opin. Ther. Targets* 19, 1351–1360. doi: 10.1517/14728222.2015.1062877

Le, N. T., Narkiewicz, J., Aulic, S., Salzano, G., Tran, H. T., Scaini, D., et al. (2015). Synthetic prions and other human neurodegenerative proteinopathies. *Virus Res.* 207, 25–37. doi: 10.1016/j.virusres.2014.10.020

Lee, H. J., Cho, E. D., Lee, K. W., Kim, J. H., Cho, S. G., and Lee, S. J. (2013). Autophagic failure promotes the exocytosis and intercellular transfer of alpha-synuclein. *Exp. Mol. Med.* 45:e22. doi: 10.1038/emm.2013.45

Lee, H. J., Suk, J. E., Bae, E. J., Lee, J. H., Paik, S. R., and Lee, S. J. (2008). Assembly-dependent endocytosis and clearance of extracellular alpha-synuclein. *Int. J. Biochem. Cell Biol.* 40, 1835–1849. doi: 10.1016/j.biocel.2008.01.017

Lee, S. J., Desplats, P., Sigurdson, C., Tsigelny, I., and Masliah, E. (2010). Cell-to-cell transmission of non-prion protein aggregates. *Nat. Rev. Neurol.* 6, 702–706. doi: 10.1038/nrneurol.2010.145

Lema Tome, C. M., Tyson, T., Rey, N. L., Grathwohl, S., Britschgi, M., and Brundin, P. (2013). Inflammation and alpha-synuclein's prion-like behavior in Parkinson's disease–is there a link? *Mol. Neurobiol.* 47, 561–574. doi: 10.1007/s12035-012-8267-8

Li, B., Ge, P., Murray, K. A., Sheth, P., Zhang, M., Nair, G., et al. (2018a). Cryo-EM of full-length alpha-synuclein reveals fibril polymorphs with a common structural kernel. *Nat. Commun.* 9:3609. doi: 10.1038/s41467-018-05971-2

Li, Y., Zhao, C., Luo, F., Liu, Z., Gui, X., Luo, Z., et al. (2018b). Amyloid fibril structure of alpha-synuclein determined by cryo-electron microscopy. *Cell Res.* 28, 897–903. doi: 10.1038/s41422-018-0075-x

Longhena, F., Faustini, G., Missale, C., Pizzi, M., Spano, P., and Bellucci, A. (2017). The contribution of alpha-synuclein spreading to Parkinson's disease synaptopathy. *Neural Plast* 2017:5012129. doi: 10.1155/2017/5012129

Lopes da Fonseca, T., Villar-Pique, A., and Outeiro, T. F. (2015). The interplay between alpha-synuclein clearance and spreading. *Biomolecules* 5, 435–471. doi: 10.3390/biom5020435

Luk, K. C., Kehm, V., Carroll, J., Zhang, B., O'Brien, P., Trojanowski, J. Q., et al. (2012a). Pathological alpha-synuclein transmission initiates Parkinson-like neurodegeneration in nontransgenic mice. *Science* 338, 949–953. doi: 10.1126/science.1227157

Luk, K. C., Kehm, V. M., Zhang, B., O'Brien, P., Trojanowski, J. Q., and Lee, V. M. (2012b). Intracerebral inoculation of pathological alpha-synuclein initiates a rapidly progressive neurodegenerative alpha-synucleinopathy in mice. *J. Exp. Med.* 209, 975–986. doi: 10.1084/jem.20112457

Manfredsson, F. P., Luk, K. C., Benskey, M. J., Gezer, A., Garcia, J., Kuhn, N. C., et al. (2018). Induction of alpha-synuclein pathology in the enteric nervous system of the rat and non-human primate results in gastrointestinal dysmotility and transient CNS pathology. *Neurobiol. Dis.* 112, 106–118. doi: 10.1016/j.nbd.2018.01.008

Mao, X., Ou, M. T., Karuppagounder, S. S., Kam, T. I., Yin, X., Xiong, Y., et al. (2016). Pathological alpha-synuclein transmission initiated by binding lymphocyte-activation gene 3. *Science* 353:aah3374. doi: 10.1126/science.aah3374

Marras, C., Lang, A. E., Austin, P. C., Lau, C., and Urbach, D. R. (2016). Appendectomy in mid and later life and risk of Parkinson's disease: a population-based study. *Mov. Disord.* 31, 1243–1247. doi: 10.1002/mds.26670

Masuda-Suzukake, M., Nonaka, T., Hosokawa, M., Kubo, M., Shimozawa, A., Akiyama, H., et al. (2014). Pathological alpha-synuclein propagates through neural networks. *Acta Neuropathol. Commun.* 2:88. doi: 10.1186/s40478-014-0088-8

Masuda-Suzukake, M., Nonaka, T., Hosokawa, M., Oikawa, T., Arai, T., Akiyama, H., et al. (2013). Prion-like spreading of pathological alpha-synuclein in brain. *Brain* 136(Pt 4), 1128–1138. doi: 10.1093/brain/awt037

McGurk, L., Berson, A., and Bonini, N. M. (2015). Drosophila as an *in vivo* Model for human neurodegenerative disease. *Genetics* 201, 377–402. doi: 10.1534/genetics.115.179457

Menzies, F. M., Fleming, A., Caricasole, A., Bento, C. F., Andrews, S. P., Ashkenazi, A., et al. (2017). Autophagy and neurodegeneration: pathogenic mechanisms and therapeutic opportunities. *Neuron* 93, 1015–1034. doi: 10.1016/j.neuron.2017.01.022

Mougenot, A. L., Nicot, S., Bencsik, A., Morignat, E., Verchere, J., Lakhdar, L., et al. (2012). Prion-like acceleration of a synucleinopathy in a transgenic mouse model. *Neurobiol. Aging* 33, 2225–2228. doi: 10.1016/j.neurobiolaging.2011.06.022

Narkiewicz, J., Giachin, G., and Legname, G. (2014). In vitro aggregation assays for the characterization of α-synuclein prion-like properties. *Prion* 8, 19–32. doi: 10.4161/pri.28125

Nguyen, X. T. A., Tran, T. H., Cojoc, D., and Legname, G. (2019). Copper binding regulates cellular prion protein function. *Mol. Neurobiol.* doi: 10.1007/s12035-019-1510-9 [Epub ahead of print],

Nielsen, T. T., and Nielsen, J. E. (2013). Antisense gene silencing: therapy for neurodegenerative disorders? *Genes* 4, 457–484. doi: 10.3390/genes4030457

Palacios, N., Hughes, K. C., Cereda, E., Schwarzschild, M. A., and Ascherio, A. (2018). Appendectomy and risk of Parkinson's disease in two large prospective cohorts of men and women. *Mov. Disord.* 33, 1492–1496. doi: 10.1002/mds.109

Paumier, K. L., Luk, K. C., Manfredsson, F. P., Kanaan, N. M., Lipton, J. W., Collier, T. J., et al. (2015). Intrastriatal injection of pre-formed mouse alpha-synuclein fibrils into rats triggers alpha-synuclein pathology and bilateral nigrostriatal degeneration. *Neurobiol. Dis.* 82, 185–199. doi: 10.1016/j.nbd.2015.06.003

Peelaerts, W., Bousset, L., Van der Perren, A., Moskalyuk, A., Pulizzi, R., Giugliano, M., et al. (2015). alpha-Synuclein strains cause distinct synucleinopathies after local and systemic administration. *Nature* 522, 340–344. doi: 10.1038/nature14547

Peng, X., Tehranian, R., Dietrich, P., Stefanis, L., and Perez, R. G. (2005). Alpha-synuclein activation of protein phosphatase 2A reduces tyrosine hydroxylase phosphorylation in dopaminergic cells. *J. Cell Sci.* 118(Pt 15), 3523–3530. doi: 10.1242/jcs.02481

Perez, R. G., Waymire, J. C., Lin, E., Liu, J. J., Guo, F., and Zigmond, M. J. (2002). A role for alpha-synuclein in the regulation of dopamine biosynthesis. *J. Neurosci.* 22, 3090–3099.

Purro, S. A., Farrow, M. A., Linehan, J., Nazari, T., Thomas, D. X., Chen, Z., et al. (2018). Transmission of amyloid-beta protein pathology from cadaveric pituitary growth hormone. *Nature* 564, 415–419. doi: 10.1038/s41586-018-0790-y

Quek, C., and Hill, A. F. (2017). The role of extracellular vesicles in neurodegenerative diseases. *Biochem. Biophys. Res. Commun.* 483, 1178–1186. doi: 10.1016/j.bbrc.2016.09.090

Rahmani, F., Saghazadeh, A., Rahmani, M., Teixeira, A. L., Rezaei, N., Aghamollaii, V., et al. (2019). Plasma levels of brain-derived neurotrophic factor in patients with Parkinson disease: a systematic review and meta-analysis. *Brain Res.* 1704, 127–136. doi: 10.1016/j.brainres.2018.10.006

Recasens, A., and Dehay, B. (2014). Alpha-synuclein spreading in Parkinson's disease. *Front. Neuroanat.* 8:159. doi: 10.3389/fnana.2014.00159

Recasens, A., Dehay, B., Bove, J., Carballo-Carbajal, I., Dovero, S., Perez-Villalba, A., et al. (2014). Lewy body extracts from Parkinson disease brains trigger alpha-synuclein pathology and neurodegeneration in mice and monkeys. *Ann. Neurol.* 75, 351–362. doi: 10.1002/ana.24066

Recasens, A., Ulusoy, A., Kahle, P. J., Di Monte, D. A., and Dehay, B. (2018). In vivo models of alpha-synuclein transmission and propagation. *Cell Tissue Res.* 373, 183–193. doi: 10.1007/s00441-017-2730-9

Renner, M., and Melki, R. (2014). Protein aggregation and prionopathies. *Pathol. Biol.* 62, 162–168. doi: 10.1016/j.patbio.2014.01.003

Rey, N. L., George, S., and Brundin, P. (2016). Review: spreading the word: precise animal models and validated methods are vital when evaluating prion-like behaviour of alpha-synuclein. *Neuropathol. Appl. Neurobiol.* 42, 51–76. doi: 10.1111/nan.12299

Rey, N. L., Petit, G. H., Bousset, L., Melki, R., and Brundin, P. (2013). Transfer of human alpha-synuclein from the olfactory bulb to interconnected brain regions in mice. *Acta Neuropathol.* 126, 555–573. doi: 10.1007/s00401-013-1160-3

Rey, N. L., Wesson, D. W., and Brundin, P. (2018). The olfactory bulb as the entry site for prion-like propagation in neurodegenerative diseases. *Neurobiol. Dis.* 109(Pt B), 226–248. doi: 10.1016/j.nbd.2016.12.013

Rochet, J. C., and Lansbury, P. T. Jr. (2000). Amyloid fibrillogenesis: themes and variations. *Curr. Opin. Struct. Biol.* 10, 60–68.

Rostami, J., Holmqvist, S., Lindstrom, V., Sigvardson, J., Westermark, G. T., Ingelsson, M., et al. (2017). Human astrocytes transfer aggregated alpha-synuclein via tunneling nanotubes. *J. Neurosci.* 37, 11835–11853. doi: 10.1523/JNEUROSCI.0983-17.2017

Sacino, A. N., Brooks, M., Thomas, M. A., McKinney, A. B., Lee, S., Regenhardt, R. W., et al. (2014). Intramuscular injection of alpha-synuclein induces CNS alpha-synuclein pathology and a rapid-onset motor phenotype in transgenic mice. *Proc. Natl. Acad. Sci. U.S.A.* 111, 10732–10737. doi: 10.1073/pnas.1321785111

Sacino, A. N., Brooks, M. M., Chakrabarty, P., Saha, K., Khoshbouei, H., Golde, T. E., et al. (2017). Proteolysis of alpha-synuclein fibrils in the lysosomal pathway limits induction of inclusion pathology. *J. Neurochem.* 140, 662–678. doi: 10.1111/jnc.13743

Sadan, O., Bahat-Stromza, M., Barhum, Y., Levy, Y. S., Pisnevsky, A., Peretz, H., et al. (2009). Protective effects of neurotrophic factor-secreting cells in a 6-OHDA rat model of Parkinson disease. *Stem Cells Dev.* 18, 1179–1190. doi: 10.1089/scd.2008.0411

Sherer, N. M., and Mothes, W. (2008). Cytonemes and tunneling nanotubules in cell-cell communication and viral pathogenesis. *Trends Cell Biol.* 18, 414–420. doi: 10.1016/j.tcb.2008.07.003

Sian-Hulsmann, J., Monoranu, C., Strobel, S., and Riederer, P. (2015). Lewy bodies: a spectator or salient killer? *CNS Neurol. Disord. Drug Targets* 14, 947–955.

Stopschinski, B. E., Holmes, B. B., Miller, G. M., Manon, V. A., Vaquer-Alicea, J., Prueitt, W. L., et al. (2018). Specific glycosaminoglycan chain length and sulfation patterns are required for cell uptake of tau versus alpha-synuclein and beta-amyloid aggregates. *J. Biol. Chem.* 293, 10826–10840. doi: 10.1074/jbc.RA117.000378

Surguchev, A. A., Emamzadeh, F. N., and Surguchov, A. (2019). Cell responses to extracellular alpha-synuclein. *Molecules* 24:E305. doi: 10.3390/molecules24020305

Suzuki, M., Sango, K., Wada, K., and Nagai, Y. (2018). Pathological role of lipid interaction with alpha-synuclein in Parkinson's disease. *Neurochem. Int.* 119, 97–106. doi: 10.1016/j.neuint.2017.12.014

Svensson, E., Horvath-Puho, E., Stokholm, M. G., Sorensen, H. T., Henderson, V. W., and Borghammer, P. (2016). Appendectomy and risk of Parkinson's disease: a nationwide cohort study with more than 10 years of follow-up. *Mov. Disord.* 31, 1918–1922. doi: 10.1002/mds.26761

Svensson, E., Horvath-Puho, E., Thomsen, R. W., Djurhuus, J. C., Pedersen, L., Borghammer, P., et al. (2015). Vagotomy and subsequent risk of Parkinson's disease. *Ann. Neurol.* 78, 522–529. doi: 10.1002/ana.24448

Tamguney, G., and Korczyn, A. D. (2018). A critical review of the prion hypothesis of human synucleinopathies. *Cell Tissue Res.* 373, 213–220. doi: 10.1007/s00441-017-2712-y

Tanik, S. A., Schultheiss, C. E., Volpicelli-Daley, L. A., Brunden, K. R., and Lee, V. M. (2013). Lewy body-like alpha-synuclein aggregates resist degradation and impair macroautophagy. *J. Biol. Chem.* 288, 15194–15210. doi: 10.1074/jbc.M113.457408

Tarutani, A., Suzuki, G., Shimozawa, A., Nonaka, T., Akiyama, H., Hisanaga, S., et al. (2016). The effect of fragmented pathogenic alpha-synuclein seeds on prion-like propagation. *J. Biol. Chem.* 291, 18675–18688. doi: 10.1074/jbc.M116.734707

Taylor, A. M., Blurton-Jones, M., Rhee, S. W., Cribbs, D. H., Cotman, C. W., and Jeon, N. L. (2005). A microfluidic culture platform for CNS axonal injury, regeneration and transport. *Nat. Methods* 2, 599–605. doi: 10.1038/nmeth777

Tehranian, R., Montoya, S. E., Van Laar, A. D., Hastings, T. G., and Perez, R. G. (2006). Alpha-synuclein inhibits aromatic amino acid decarboxylase activity in dopaminergic cells. *J. Neurochem.* 99, 1188–1196. doi: 10.1111/j.1471-4159.2006.04146.x

Tran, H. T., Chung, C. H., Iba, M., Zhang, B., Trojanowski, J. Q., Luk, K. C., et al. (2014). Alpha-synuclein immunotherapy blocks uptake and templated propagation of misfolded alpha-synuclein and neurodegeneration. *Cell Rep.* 7, 2054–2065. doi: 10.1016/j.celrep.2014.05.033

Tysnes, O. B., Kenborg, L., Herlofson, K., Steding-Jessen, M., Horn, A., Olsen, J. H., et al. (2015). Does vagotomy reduce the risk of Parkinson's disease? *Ann. Neurol.* 78, 1011–1012. doi: 10.1002/ana.24531

Tyson, T., Steiner, J. A., and Brundin, P. (2016). Sorting out release, uptake and processing of alpha-synuclein during prion-like spread of pathology. *J. Neurochem.* 139(Suppl. 1), 275–289. doi: 10.1111/jnc.13449

Uemura, N., Yagi, H., Uemura, M. T., Hatanaka, Y., Yamakado, H., and Takahashi, R. (2018). Inoculation of alpha-synuclein preformed fibrils into the mouse gastrointestinal tract induces Lewy body-like aggregates in the brainstem via the vagus nerve. *Mol. Neurodegener.* 13:21. doi: 10.1186/s13024-018-0257-5

Ulusoy, A., Musgrove, R. E., Rusconi, R., Klinkenberg, M., Helwig, M., Schneider, A., et al. (2015). Neuron-to-neuron alpha-synuclein propagation in vivo is independent of neuronal injury. *Acta Neuropathol. Commun.* 3:13. doi: 10.1186/s40478-015-0198-y

Ulusoy, A., Phillips, R. J., Helwig, M., Klinkenberg, M., Powley, T. L., and Di Monte, D. A. (2017). Brain-to-stomach transfer of alpha-synuclein via vagal preganglionic projections. *Acta Neuropathol.* 133, 381–393. doi: 10.1007/s00401-016-1661-y

Urrea, L., Ferrer, I., Gavin, R., and Del Rio, J. A. (2017). The cellular prion protein (PrP(C)) as neuronal receptor for alpha-synuclein. *Prion* 11, 226–233. doi: 10.1080/19336896.2017.1334748

Urrea, L., Segura-Feliu, M., Masuda-Suzukake, M., Hervera, A., Pedraz, L., Garcia-Aznar, J. M., et al. (2018). Involvement of cellular prion protein in alpha-synuclein transport in neurons. *Mol. Neurobiol.* 55, 1847–1860. doi: 10.1007/s12035-017-0451-4

Uversky, V. N. (2007). Neuropathology, biochemistry, and biophysics of alpha-synuclein aggregation. *J. Neurochem.* 103, 17–37. doi: 10.1111/j.1471-4159.2007.04764.x

Valera, E., and Masliah, E. (2016). Combination therapies: the next logical Step for the treatment of synucleinopathies? *Mov. Disord.* 31, 225–234. doi: 10.1002/mds.26428

Van Bulck, M., Sierra-Magro, A., Alarcon-Gil, J., Perez-Castillo, A., and Morales-Garcia, J. A. (2019). Novel approaches for the treatment of Alzheimer's and Parkinson's disease. *Int. J. Mol. Sci.* 20:E719. doi: 10.3390/ijms20030719

Victoria, G. S., and Zurzolo, C. (2015). Trafficking and degradation pathways in pathogenic conversion of prions and prion-like proteins in neurodegenerative diseases. *Virus Res.* 207, 146–154. doi: 10.1016/j.virusres.2015.01.019

Victoria, G. S., and Zurzolo, C. (2017). The spread of prion-like proteins by lysosomes and tunneling nanotubes: implications for neurodegenerative diseases. *J. Cell Biol.* 216, 2633–2644. doi: 10.1083/jcb.201701047

Volpicelli-Daley, L. A., Luk, K. C., Patel, T. P., Tanik, S. A., Riddle, D. M., Stieber, A., et al. (2011). Exogenous alpha-synuclein fibrils induce Lewy body pathology leading to synaptic dysfunction and neuron death. *Neuron* 72, 57–71. doi: 10.1016/j.neuron.2011.08.033

Woodard, C. M., Campos, B. A., Kuo, S. H., Nirenberg, M. J., Nestor, M. W., Zimmer, M., et al. (2014). iPSC-derived dopamine neurons reveal differences between monozygotic twins discordant for Parkinson's disease. *Cell Rep.* 9, 1173–1182. doi: 10.1016/j.celrep.2014.10.023

Yilmaz, R., Bayram, E., Ulukan, C., Altinok, M. K., and Akbostanci, M. C. (2017). Appendectomy history is not related to Parkinson's disease. *J. Parkinsons Dis.* 7, 347–352. doi: 10.3233/JPD-171071

Yin, R. H., Tan, L., Jiang, T., and Yu, J. T. (2014). Prion-like mechanisms in Alzheimer's disease. *Curr. Alzheimer Res.* 11, 755–764.

Yuan, Y., Sun, J., Zhao, M., Hu, J., Wang, X., Du, G., et al. (2010). Overexpression of alpha-synuclein down-regulates BDNF expression. *Cell Mol. Neurobiol.* 30, 939–946. doi: 10.1007/s10571-010-9523-y

Zhang, S., Eitan, E., Wu, T. Y., and Mattson, M. P. (2018). Intercellular transfer of pathogenic alpha-synuclein by extracellular vesicles is induced by the lipid peroxidation product 4-hydroxynonenal. *Neurobiol. Aging* 61, 52–65. doi: 10.1016/j.neurobiolaging.2017.09.016

Zhao, L., He, L. X., Huang, S. N., Gong, L. J., Li, L., Lv, Y. Y., et al. (2014). Protection of dopamine neurons by vibration training and up-regulation of brain-derived neurotrophic factor in a MPTP mouse model of Parkinson's disease. *Physiol. Res.* 63, 649–657.

Conflict of Interest Statement: The authors declare that the research was conducted in the absence of any commercial or financial relationships that could be construed as a potential conflict of interest.

frontiers in Neuroscience

ORIGINAL RESEARCH
published: 20 August 2019
doi: 10.3389/fnins.2019.00859

Resveratrol Activates Autophagy via the AKT/mTOR Signaling Pathway to Improve Cognitive Dysfunction in Rats With Chronic Cerebral Hypoperfusion

*Nan Wang[1], Jinting He[1], Chengliang Pan[2], Jiaoqi Wang[1], Ming Ma[1], Xinxiu Shi[1] and Zhongxin Xu[1]**

[1] Department of Neurology, China-Japan Union Hospital of Jilin University, Changchun, China, [2] College of Clinical Medicine, Jilin University, Changchun, China

OPEN ACCESS

Edited by:
Mohammad Badruzzaman Khan, Augusta University, United States

Reviewed by:
Md Suhail Alam, University of Notre Dame, United States
Murali Vijayan, Texas Tech University Health Sciences Center, United States
Mohammad Farhan, Hamad Bin Khalifa University, Qatar

***Correspondence:**
Zhongxin Xu
xuzhongxin9999@163.com

Specialty section:
This article was submitted to Neurodegeneration, a section of the journal Frontiers in Neuroscience

Received: *26 March 2019*
Accepted: *30 July 2019*
Published: *20 August 2019*

Citation:
Wang N, He J, Pan C, Wang J, Ma M, Shi X and Xu Z (2019) Resveratrol Activates Autophagy via the AKT/mTOR Signaling Pathway to Improve Cognitive Dysfunction in Rats With Chronic Cerebral Hypoperfusion. Front. Neurosci. 13:859. doi: 10.3389/fnins.2019.00859

Chronic cerebral hypoperfusion (CCH) is a main cause of vascular dementia and is also an etiological factor of neurological diseases and mental disorders. However, few treatments are available for CCH, and new medications are needed. In the present study, we employed a rat model of CCH that was based on bilateral common carotid artery occlusion and investigated the therapeutic effects of resveratrol and its detailed mechanism of action. We evaluated neurological deficit scores and performed the Morris water maze test, hematoxylin and eosin staining, TUNEL staining, enzyme-linked immunosorbent assays, and Western blot. Resveratrol reduced neurological deficit scores in CCH rats and reduced pathological damage in the frontal cortex and hippocampus. Resveratrol activated autophagy and inhibited the expression of AKT/mechanistic target of rapamycin (mTOR) signaling pathway-related proteins. Treatment with a phosphoinositide-3 kinase inhibitor reversed the protective effect of resveratrol. These findings suggest that resveratrol improves cognitive function in a rat model of CCH and reduces oxidative stress-induced neuronal damage in the frontal cortex and hippocampus by activating autophagy and inhibiting neuronal apoptosis. These effects may be regulated by the AKT/mTOR signaling pathway.

Keywords: resveratrol, AKT, mTOR, cognitive dysfunction, chronic cerebral hypoperfusion

INTRODUCTION

Chronic cerebral hypoperfusion (CCH) can contribute to the development of various neurological diseases and mental disorders, including vascular dementia, Alzheimer's disease, and Binswanger disease (Duncombe et al., 2017; Feng et al., 2018). Early stage CCH is mainly characterized by cognitive impairment that is followed by biological changes, such as energy metabolism disorders, abnormal neuronal electrical activity, oxidative stress, glial cell activation, and inflammatory factor release. These changes can lead to abnormal brain structure and function, including neuronal damage and degeneration of the frontal cortex and hippocampus, resulting in cognitive

impairment (Du et al., 2017). One main factor that is involved in such damage is the transient expression of reactive oxygen species (ROS) that are induced by lower cerebral blood flow. Excessive ROS and free radicals can cause the apoptosis of nerve cells and astrocytes, leading to permanent nerve damage (Su et al., 2017). This process is associated with oxidative stress and mitochondrial dysfunction (Panchal and Tiwari, 2018).

In states of oxidative stress, cells undergo autophagy to remove damaged mitochondria, the endoplasmic reticulum, and proteins to slow the cell death process (Filomeni et al., 2015). Autophagy is a phenomenon of "self-eating" to recirculate molecules within cells. Impairments in autophagy are seen in many diseases, such as neurodegenerative diseases, insulin resistance, and immunity (Deretic et al., 2013; Moloudizargari et al., 2017; Tan et al., 2018). Previous studies have found that autophagy is initiated by inhibition of the rapamycin receptor mechanistic/mammalian target of rapamycin (mTOR), which is involved in various physiological and pathological cell processes and regulates cell growth, proliferation, differentiation, and autophagy by affecting protein synthesis (Dunlop and Tee, 2014; Kim and Guan, 2015; Munson and Ganley, 2015). In Alzheimer's disease, low mTOR levels in peripheral blood lymphocytes may be related to disease progression. The inhibition of mTOR activity may impair memory consolidation, whereas activation of the AKT pathway may prevent the toxic effects of amyloid β (O'Neill, 2013). In epilepsy models, mTOR inhibition has been shown to reduce neuronal death, nerve regeneration, and the development of spontaneous epilepsy (Romero-Leguizamon et al., 2016). Long-lasting high levels of ROS can lead to excessive AKT/mTOR-regulated autophagy, transforming this normally protective pathway into an apoptosis-inducing mechanism (Wang X. et al., 2018).

Resveratrol is a natural polyphenolic phytoalexin with a range of protective physiological functions, including antioxidative and anti-inflammatory effects. It is used for the management of diabetes, neuroprotection and myocardium protection. Several studies reported that resveratrol induced autophagy (Bagul and Banerjee, 2015; Wan et al., 2016; Ling et al., 2017; Chen et al., 2018). Huang et al. (2016) found that resveratrol alleviated the hydrogen peroxide-mediated apoptosis of cardiomyocytes by regulating autophagic flow. Resveratrol was shown to reduce oxidative stress-induced brain damage in an Alzheimer's disease model by inducing autophagy to reduce oxidative stress (Wang H. et al., 2018). Resveratrol was reported to alleviate cerebral ischemia/reperfusion injury in rats by inhibiting NLRP3 inflammasome activation through Sirt1-dependent autophagy induction (He Q. et al., 2017), but the effect of resveratrol on cerebral ischemia/reperfusion injury that is related to the AKT/mTOR pathway has not been reported. Resveratrol has a close relationship with AKT/mTOR. Resveratrol was shown

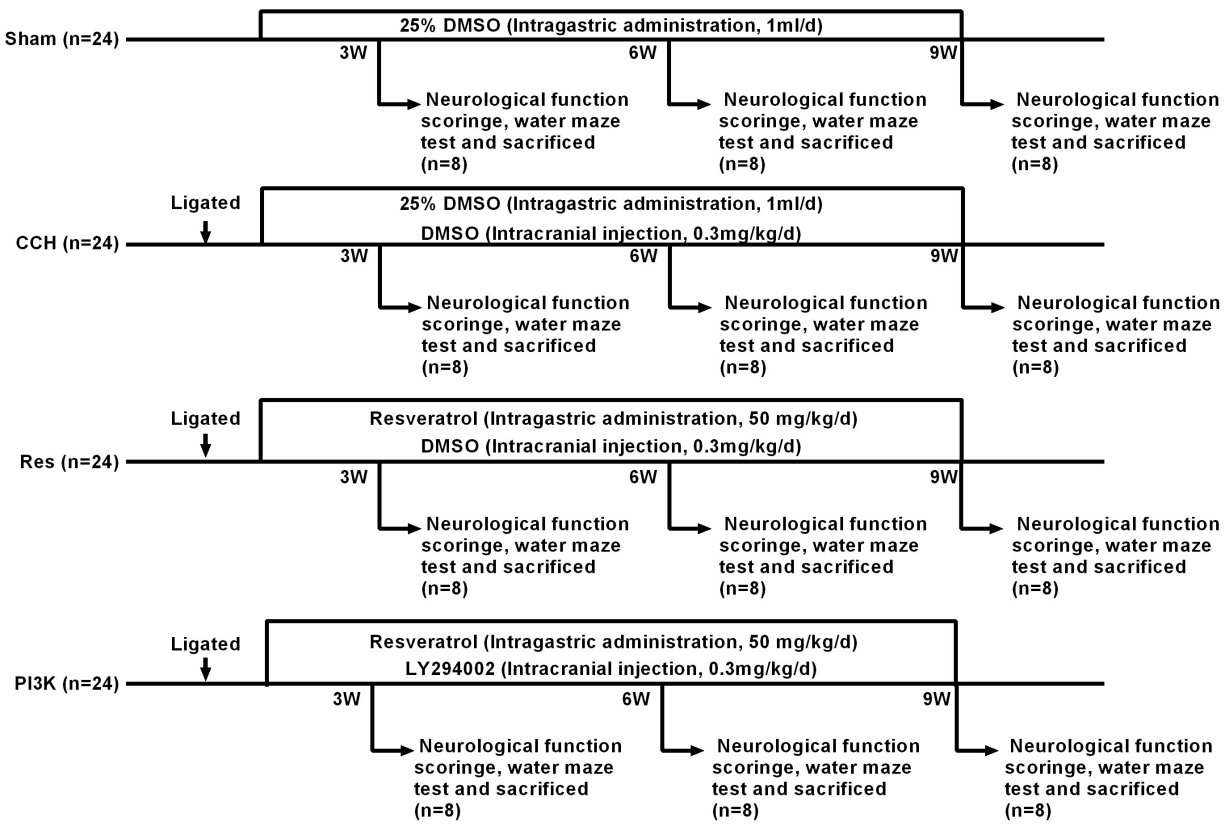

FIGURE 1 | Schematic diagram of the rat groups and treatment regimens. Because the scores were zero in the Sham group, there is no bar-plot for this group.

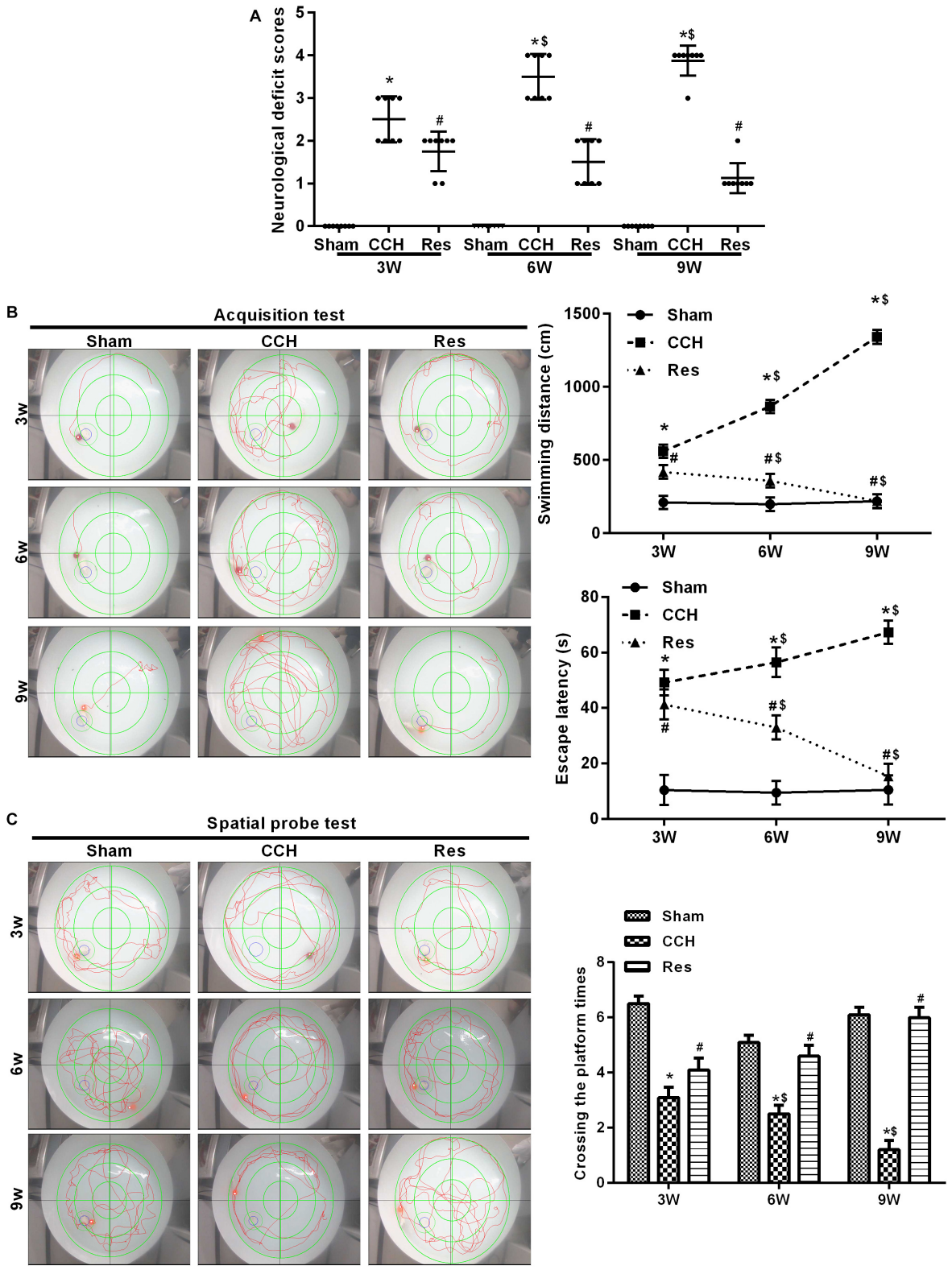

FIGURE 2 | Resveratrol improved neurological damage and cognitive function in CCH rats. Neurological impairment was measured by the Bederson scoring method. Memory performance was measured in the Morris water maze test. **(A)** Neurological deficit scores. **(B,C)** Morris water maze test. $^{*}p < 0.05$, vs. Sham group; $^{\#}p < 0.05$, vs. CCH group; $^{\$}p < 0.05$, vs. 3 weeks. Sham group, treated with an equal volume of vehicle; CCH group, chronic cerebral hypoperfusion and no treatment; CCH + Res group, CCH and treated with resveratrol.

to inhibit the phosphoinositide-3 kinase (PI3K)/AKT pathway to inhibit the proliferation and migration of hepatocellular carcinoma cells (Chai et al., 2017). Resveratrol was also reported to rescue hyperglycemia-induced endothelial dysfunction via the activation of AKT (Li et al., 2017). We hypothesized that resveratrol would ameliorate cognitive dysfunction that is caused by chronic cerebral ischemia, likely by the activation of autophagy through the AKT/mTOR signaling pathway. To test this hypothesis, we established a rat model of CCH that was induced by bilateral common carotid artery occlusion (BCCAO). The rats were treated with resveratrol, and we evaluated cognitive function and brain tissue apoptosis and autophagy. We investigated the possible involvement of the ATK/mTOR signaling pathway in the mechanism of action of resveratrol.

MATERIALS AND METHODS

Laboratory Animals and Experimental Groups

A total of 96 male Sprague-Dawley rats, weighing 260–300 g, were purchased from the Beijing Vital River Laboratory Animal Technology Co., Ltd. The animal experiments were performed in the experimental animal department of China Medical University [experimental animal license no. SYXK (Liao) 20150001] with a 12 h/12 h light/dark cycle, controlled temperature (22°C ± 3°C), and controlled humidity (60% ± 5%). The animals had *ad libitum* access to food and water. The study was approved by the Experimental Animal Welfare and Ethics Committee of China Medical University (IACUC no. 2018097).

The rats were randomly divided into four groups using the random number table method (n = 24/group). The groups received the following treatments daily for 9 weeks: sham surgery and vehicle treatment (Sham group), CCH surgery and no treatment (CCH group), CCH surgery and resveratrol treatment (catalog no. R8350, Solarbio, Beijing, China; Res group), and CCH surgery and treatment with both resveratrol and the PI3K inhibitor LY294002 (PI3K group). After CCH was successfully established, determined by evaluating the rats in the CCH group relative to the Sham group, the Sham group was not used further.

Establishment of Chronic Cerebral Hypoperfusion Model

The animals in each group were fasted for 12 h with water that was provided before surgery. The rats were anesthetized by an intraperitoneal injection of 2% sodium pentobarbital

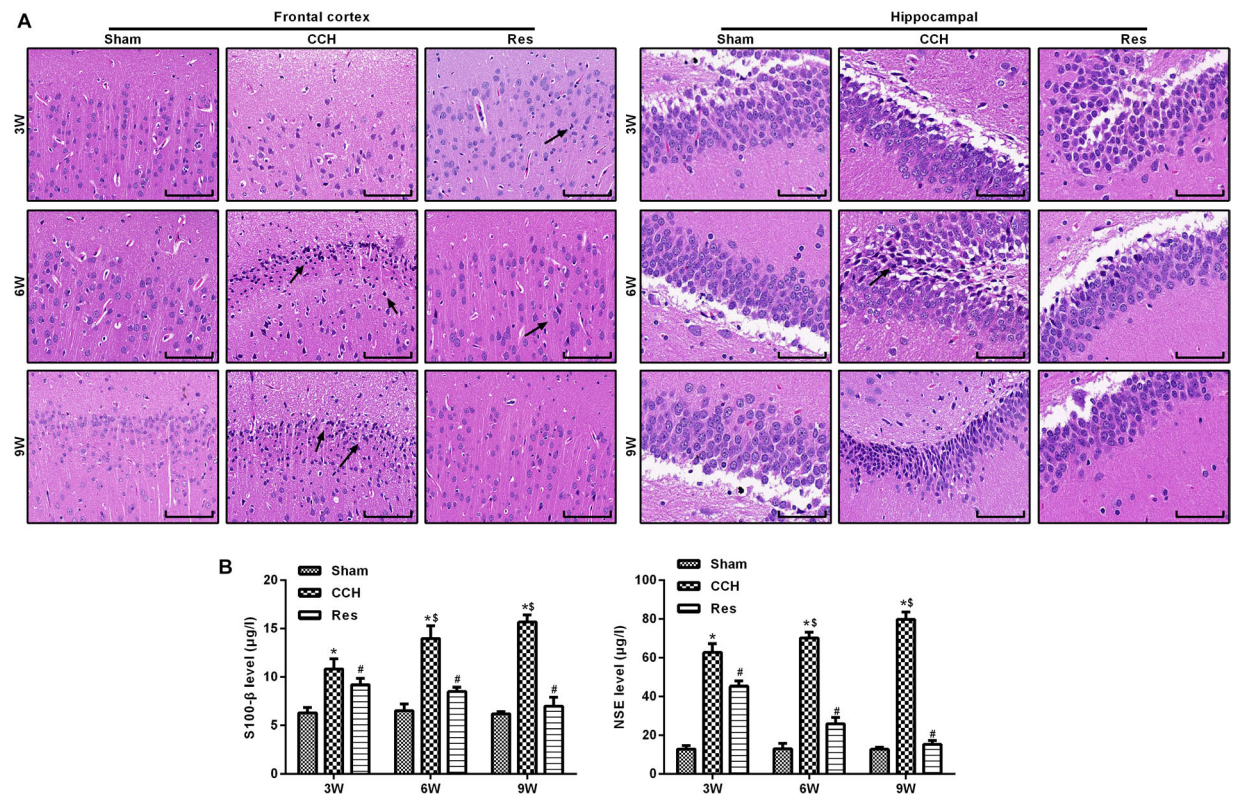

FIGURE 3 | Resveratrol alleviated brain damage in CCH rats. Neuronal pathological changes were detected by HE staining in the frontal cortex and hippocampal CA1 ar ea in each group. ELISA was used to observe the brain damage markers S-100β and NSE. **(A)** Hematoxylin and eosin staining. Scale bar = 50 μm. **(B)** S-100β and NSE levels were detected by ELISA. $^{*}p < 0.05$, vs. control group; $^{\#}p < 0.05$, vs. CCH group; $^{*}p < 0.05$, vs. Sham group; $^{\#}p < 0.05$, vs. CCH group; $^{\$}p < 0.05$, vs. 3 weeks. Sham group, treated with an equal volume of vehicle; CCH group, chronic cerebral hypoperfusion and no treatment; Res group, CCH and treated with resveratrol.

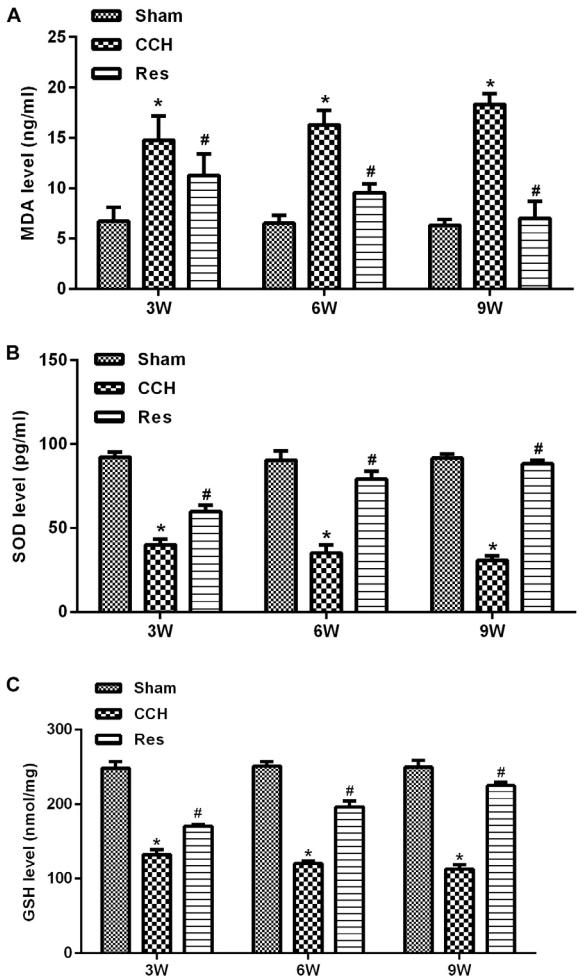

FIGURE 4 | Resveratrol inhibited oxidative stress in CCH rats. ELISA was used to detect oxidative stress factors. **(A)** Levels of MDA. **(B)** Levels of SOD. **(C)** Levels of GSH. $^{*}p < 0.05$, vs. Sham group; $^{\#}p < 0.05$, vs. CCH group. Sham group, treated with an equal volume of vehicle; CCH group, chronic cerebral hypoperfusion and no treatment; Res group, CCH and treated with resveratrol.

(3 mg/kg) and placed in the supine position. The skin on the neck was prepared, and a midline incision was made to separate the bilateral common carotid arteries and vagus nerve. In the groups that were subjected to CCH, the bilateral common carotid arteries were permanently ligated at the distal end of the telecentric end with No. 4 surgical thread. The incision was then closed by layer-by-layer sutures. Gentamicin was injected subcutaneously to prevent infection, and the rats were returned to their home cages for feeding. The Res group was intragastrically administered resveratrol (50 mg/kg/day) after surgery (Fang et al., 2018). After anesthesia with sodium pentobarbital in the PI3K group, a vertical incision was made along the midline to separate the fascia of the skull surface to fully expose the skull surface, which was then disinfected with hydrogen peroxide. The coordinates of the puncture site were 1.0 mm anterior/posterior and 1.5 mm from the center line, and the puncture site was marked with a marker. A dental drill was used to drill into the skull, exposing the dura mater. A stainless-steel injection catheter was then inserted (0.64 mm outer diameter) vertically into the puncture site, and gel was used on the surface of the skull to close the skin. The PI3K inhibitor LY294002 (Sigma-Aldrich, St. Louis, MO, United States; Shen et al., 2019; Zhan et al., 2019) was dissolved in dimethylsulfoxide (DMSO) at a concentration of 0.3 mg/ml and intracranially injected at a dose of 0.3 mg/kg at the beginning of hypoperfusion. In the Sham group, the bilateral common carotid arteries were separated from the nerves but not ligated, and 1 ml of 25% DMSO was intragastrically administered daily. Eight rats from each group were used for neurological function scoring and the Morris water maze test 3, 6, and 9 weeks after surgery. After the experiment, brain tissue samples were harvested. A portion was fixed in 4% paraformaldehyde, and the remainder was stored in a −80°C freezer. Blood was collected from the posterior saphenous vein, centrifuged to separate serum, and stored at −80°C (**Figure 1**).

Detecting Behavioral Impairment in Rats Based on Neurological Deficit Scores

We used the Bederson neurological deficit scoring method (Desland et al., 2014). Symptoms in each group were observed, neurological deficits were recorded, and neurological function was scored. The scoring criteria were the following: 0 (no symptoms of nerve damage), 1 (contralateral forelimb cannot be fully extended when lifting the tail), 2 (the rats turn to the temporal side while walking), 3 (the rats fall to the opposite side of the lesion), and 4 (the rats cannot walk spontaneously).

Testing Cognitive Function in Rats in the Morris Water Maze

Spatial memory function was assessed using the Morris water maze (Institute of Medicine, Chinese Academy of Medical Sciences, Beijing, China). The time spent locating the platform was recorded. The rats were placed in the water from four water inlet points on the pool wall twice daily for 5 days. The latency to find and climb on the platform (escape latency) in a 3 min session and the swimming path during this period (swimming distance) were recorded. The escape latency was used as a memory score for each rat, and average scores were calculated for four consecutive days. Afterward, the platform was removed, a water inlet point was selected to place the rat in the pool, and the number of times the rat crossed the original platform position during a 3 min session was recorded.

Pathological Changes in the Frontal Cortex and Hippocampus Detected by Hematoxylin and Eosin Staining

Hematoxylin and eosin (HE) staining was used to evaluate neuronal damage in the frontal cortex and hippocampus. After behavioral testing, the rats were euthanized by deep anesthesia and bloodletting. Brain tissue was quickly placed on ice, and longitudinal sections of the brain were fixed with 4% paraformaldehyde. The H&E staining kit was purchased from

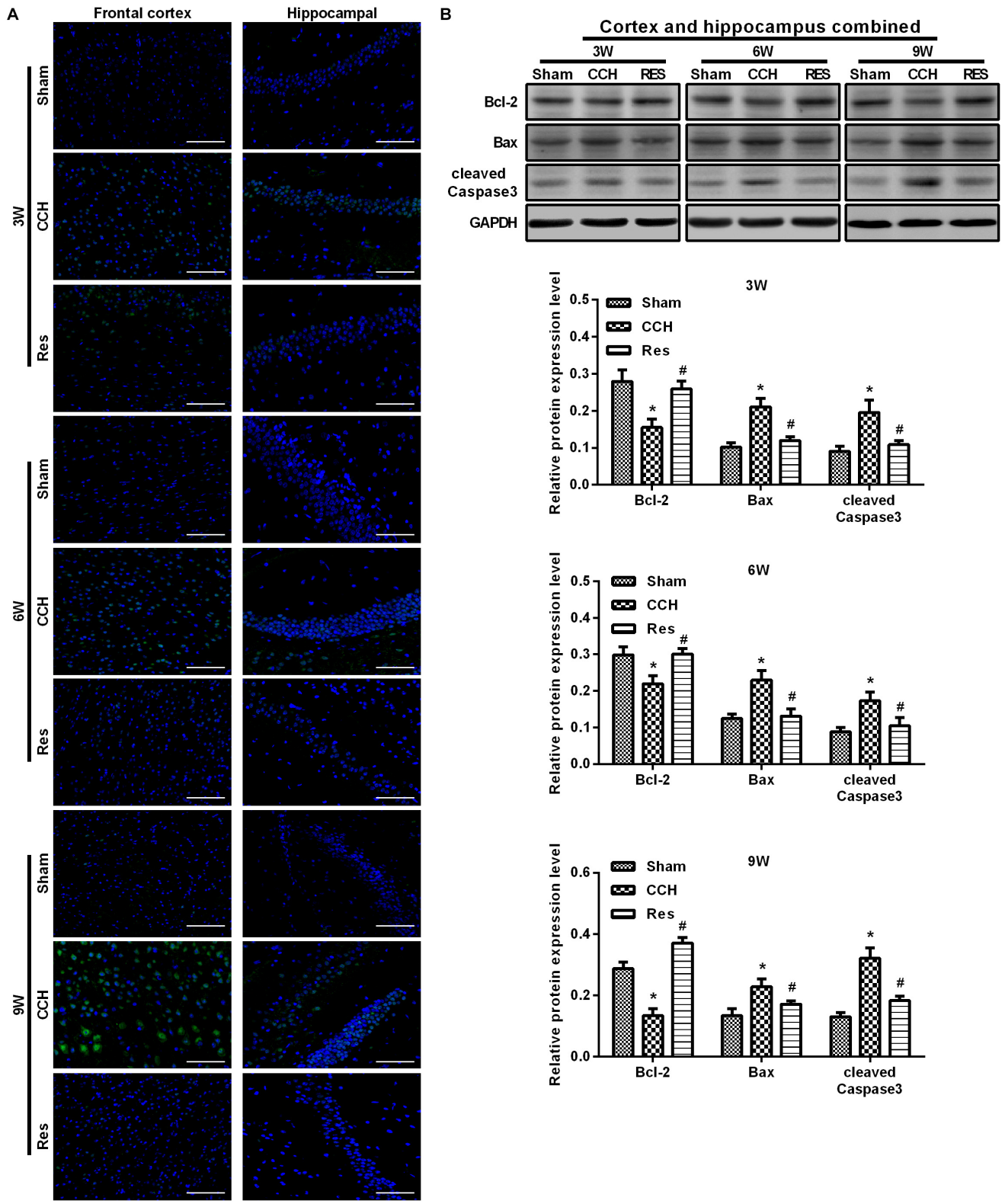

FIGURE 5 | Resveratrol inhibited neuronal apoptosis in CCH rats. TUNEL staining was used to detect neuronal apoptosis in the frontal cortex and hippocampal CA1 area in each group. Apoptosis-related proteins were detected by Western blot. **(A)** TUNEL staining. Scale bar = 50 μm. **(B)** Western blot. $^{*}p < 0.05$, vs. Sham group; $^{\#}p < 0.05$, vs. CCH group. Sham group, treated with an equal volume of vehicle; CCH group, chronic cerebral hypoperfusion and no treatment; Res group, CCH and treated with resveratrol.

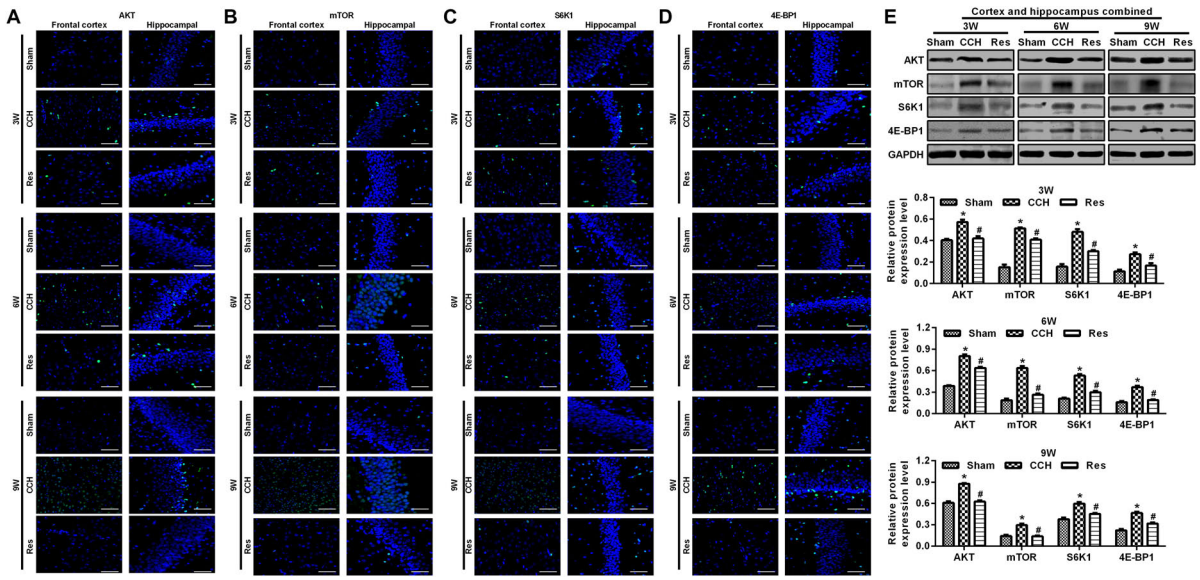

FIGURE 6 | Resveratrol reduced brain damage in CCH rats via the AKT/mTOR signaling pathway. Immunofluorescence staining and Western blot were used to detect the expression of AKT/mTOR signaling pathway-related proteins. **(A–D)** Immunofluorescence staining. Scale bar = 50 μm. **(E)** Western blot. $^{*}p < 0.05$, vs. Sham group; $^{\#}p < 0.05$, vs. CCH group. Sham group, treated with an equal volume of vehicle; CCH group, chronic cerebral hypoperfusion and no treatment; Res group, CCH and treated with resveratrol.

Beyotime (Jiangsu, China), and the experimental procedure was performed according to the manufacturer's instructions.

Apoptosis in the Frontal Cortex and Hippocampus Detected by TUNEL Staining

Neuronal apoptosis in the frontal cortex and hippocampus was examined using a TUNEL staining kit (catalog no. 11684817910, Roche, Basel, Switzerland) according to the manufacturer's instructions. Samples of the hippocampus and cerebral cortex were collected, fixed in paraformaldehyde, routinely dehydrated, paraffin embedding, and sectioned. Based on the number of slides and size of the tissue samples, the appropriate amounts of reagent 1 (TdT) and reagent 2 (dUTP) in the TUNEL kit were mixed in a 1:9 ratio and then added to the tissues. The sections were placed in a humidified 37°C incubator for 2 h and then evenly covered and blocked with 3% bovine serum albumin at room temperature for 30 min. Biotinylated nucleotides and terminal deoxynucleotidyl transferase were added to the sections (1:500 dilution) and incubated overnight at 4°C. The sections were then washed with phosphate-buffered saline (PBS) and covered with horseradish peroxidase (HRP)-labeled streptavidin in the dark for 50 min. DAPI staining solution was added, and the mixture was incubated at room temperature for 10 min in a darkroom, sealed with an anti-fluorescence quenching tablet, and photographed under a fluorescence microscope.

Enzyme-Linked Immunosorbent Assay

The oxidative stress markers superoxide dismutase (SOD; catalog no. SES134Ra, USCN, Wuhan, China), malondialdehyde (MDA; catalog no. CEA597Ge, USCN), and reduced glutathione (GSH; catalog no. CEA294Ge, USCN) and brain damage markers S-100β (catalog no. SEA012Ra, USCN) and neuron-specific enolase (NSE; catalog no. SEA537Ra, USCN) were detected by enzyme-linked immunosorbent assay (ELISA) kits in brain tissues according to the manufacturer's instructions.

Immunofluorescence Assay

The immunofluorescence assay (IFA) was performed as previously described (Jing et al., 2015; Xiong et al., 2017). Briefly, sections were processed with relevant primary antibodies, including Bax (diluted 1:50, catalog no. ab32503, Abcam, Cambridge, United Kingdom), Bcl2 (diluted 1:50, catalog no. ab32124, Abcam, Cambridge, United Kingdom), cleaved caspase-3 (diluted 1:50, catalog no. ab13847, Abcam, Cambridge, United Kingdom), LC3B (diluted 1:50, catalog no. ab48394, Abcam, Cambridge, United Kingdom), Beclin 1 (diluted 1:50, catalog no. ab207612, Abcam, Cambridge, United Kingdom), mTOR (diluted 1:50, catalog no. ab2732, Abcam, Cambridge, United Kingdom), AKT (diluted 1:50, catalog no. ab8805, Abcam, Cambridge, United Kingdom), S6K1 (diluted 1:50, catalog no. ab32529, Abcam, Cambridge, United Kingdom), and 4E-BP1 (diluted 1:50, catalog no. ab2606, Abcam, Cambridge, United Kingdom). The sections were immersed in blocking solution and then incubated with fluorescent isothiocyanate-labeled secondary antibodies for 30 min at 37°C. After washing with PBS, the sections were stained with DAPI (catalog no. D1306, Thermo Fisher Scientific, MMAS, United States) for 10 min at room temperature and washed again with PBS. The sections

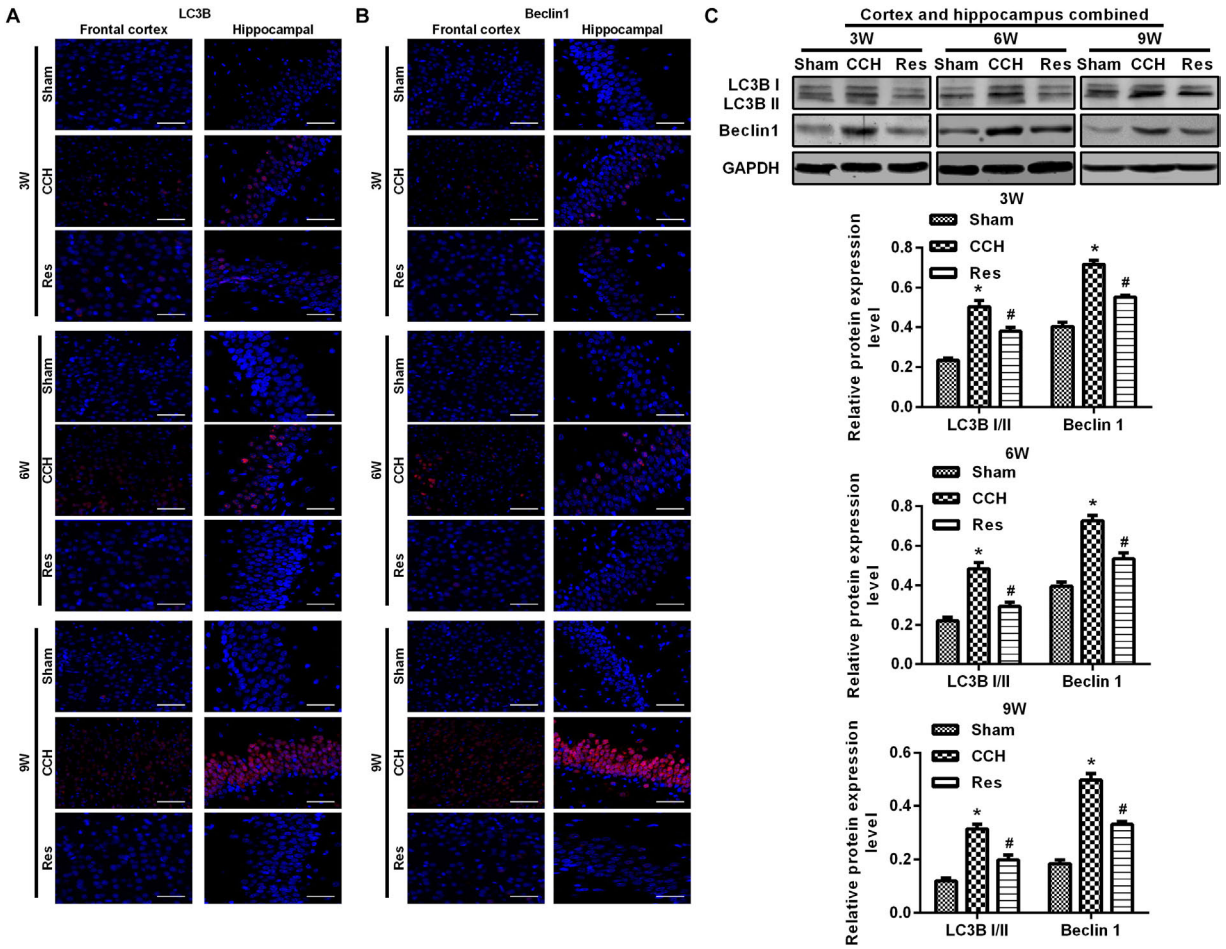

FIGURE 7 | Resveratrol regulated autophagy in CCH rats. Immunofluorescence staining and Western blot were used to detect the expression of LC3B and Beclin 1. **(A,B)** Immunofluorescence staining. Scale bar = 50 μm. **(C)** Western blot. $^{*}p < 0.05$, vs. Sham group; $^{\#}p < 0.05$, vs. CCH group. Sham group, treated with an equal volume of vehicle; CCH group, chronic cerebral hypoperfusion and no treatment; Res group, CCH and treated with resveratrol.

were sealed with neutral resin and observed under a fluorescence microscope.

Western Blot

Tissue samples of the cortex and hippocampus were lysed together in RIPA buffer (Beyotime, Shanghai, China). Supernatants were collected, and proteins were quantified using the BCA Protein Assay kit (Beyotime, Shanghai, China). Denatured protein samples were separated on 10% sodium dodecyl sulfate-polyacrylamide electrophoresis (SDS-PAGE) gels and then transferred to polyvinyl difluoridine (PVDF) membranes. Membranes were blocked with 5% non-fat dry milk for 2 h and incubated with the following primary antibodies overnight at 4°C: Bax (diluted 1:1000, catalog no. ab32503, Abcam, Cambridge, United Kingdom), Bcl2 (diluted 1:1000, catalog no. ab32124, Abcam, Cambridge, United Kingdom), cleaved caspase-3 (diluted 1:500, catalog no. ab13847, Abcam, Cambridge, United Kingdom), LC3B (diluted 1:1000, catalog no. ab48394, Abcam, Cambridge, United Kingdom), Beclin 1 (diluted 1:2000, catalog no. ab207612, Abcam, Cambridge, United Kingdom), AKT (diluted 1:500, catalog no. ab8805, Abcam, Cambridge, United Kingdom), mTOR (diluted 1:2000, catalog no. ab2732, Abcam, Cambridge, United Kingdom), S6K1 (diluted 1:5000, catalog no. ab32529, Abcam, Cambridge, United Kingdom), 4E-BP1 (diluted 1:1000, catalog no. ab2606, Abcam, Cambridge, United Kingdom), or GAPDH (diluted 1:5000, catalog no. ab8245, Abcam, Cambridge, United Kingdom). The membranes were then incubated with goat anti-rabbit IgG H&L (HRP) (diluted 1:5000, catalog no. ab6721, Abcam, Cambridge, United Kingdom) or goat anti-mouse IgG H&L (HRP) (diluted 1:5000, catalog no. ab205719, Abcam, Cambridge, United Kingdom) secondary antibody for 2 h at room temperature. Protein bands were visualized using an enhanced chemiluminescence (ECL) kit (catalog no. 35050, Pierce, MMAS, United States) and quantified by scanning densitometry using ImageJ software.

Statistical Analysis

All of the statistical analyses were performed using SPSS 19.0 software. The data are expressed as mean ± standard deviation.

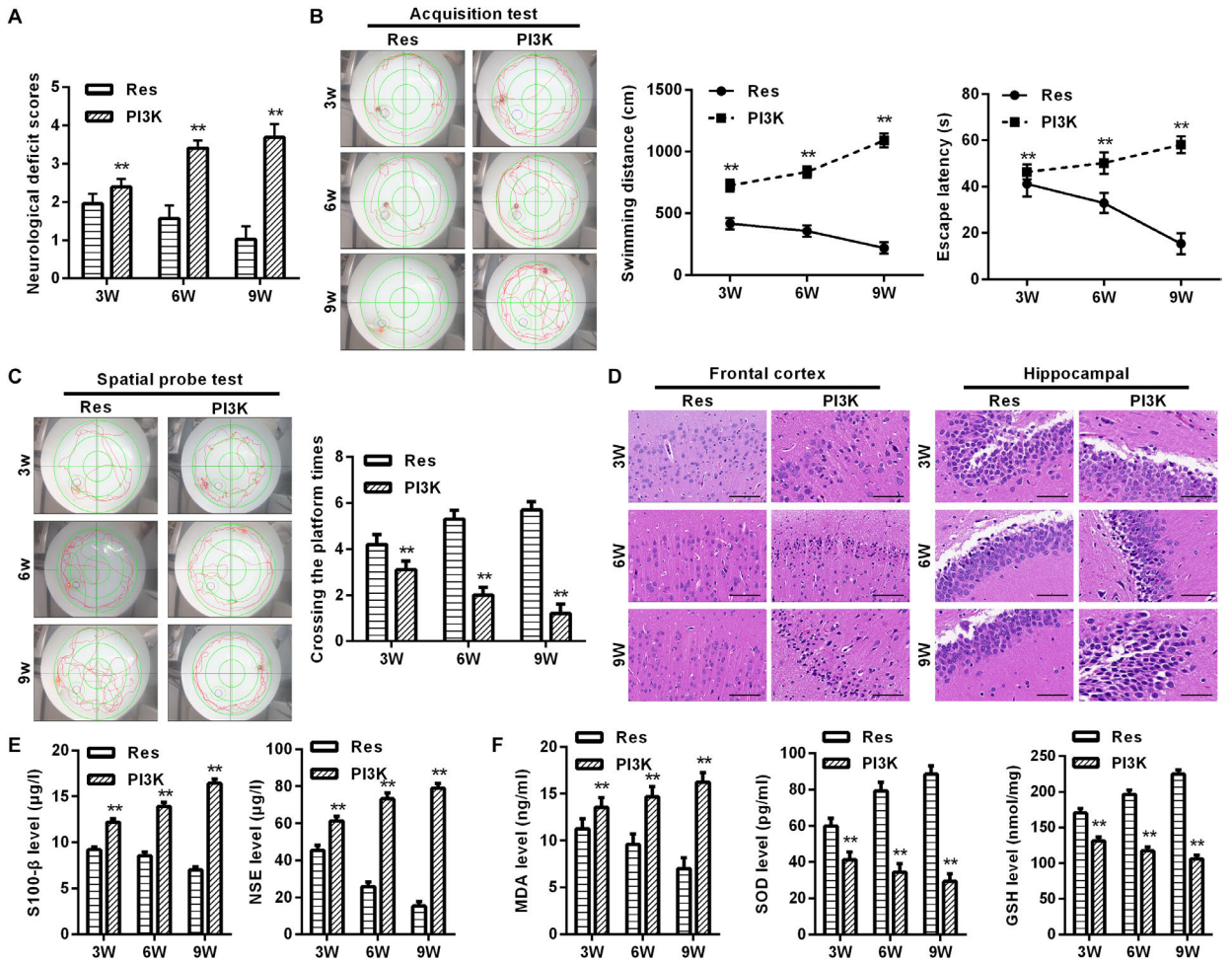

FIGURE 8 | PI3K inhibition reversed the therapeutic effects of resveratrol in CCH rats. Neurological impairment was measured by the Bederson scoring method. Memory performance was measured in the Morris water maze test. Neuronal pathological changes were detected by HE staining in the frontal cortex and hippocampal CA1 area in each group. ELISA was used to observe markers of brain damage and oxidative stress. **(A)** Neurological deficit scores. **(B,C)** Morris water maze test. **(D)** Hematoxylin staining. Scale bar = 50 μm. **(E)** Levels of S-100β and NSE. **(F)** Levels of MDA, SOD, and GSH. $^{**}p < 0.05$, vs. Res group. Res group, CCH and treated with resveratrol; PI3K group, CCH and treated with resveratrol and the PI3K inhibitor LY294002.

Comparisons between groups were performed using one-way analysis of variance. Intra-group comparisons were performed using a repeated measures design. Values of $p < 0.05$ were considered statistically significant.

RESULTS

Resveratrol Significantly Decreased Neurological Deficit Scores in CCH Rats

We first examined the effect of CCH on untreated rat brains. Neurological deficit scores increased after BCCAO, and both spatial cognitive ability and spatial memory decreased in CCH rats compared with the Sham group ($p < 0.05$). Neurological deficit scores gradually increased 3, 6, and 9 weeks after ligation. Repeated resveratrol treatment decreased neurological deficit scores in rats (**Figure 2A**). We then tested memory performance in the Morris water maze test (**Figures 2B,C**). Three weeks after BCCAO, the escape latency and swimming path significantly increased in CCH rats compared with the Sham group ($p < 0.05$), with more pronounced effects at 6 and 9 weeks of ischemia ($p < 0.05$, 9 weeks vs. 3 weeks).

Resveratrol Alleviated Brain Damage in CCH Rats

The retinal cortex and hippocampal CA1 area were monitored in CCH rats that were treated with resveratrol (Res group) at 3, 6, and 9 weeks of ischemia. Ischemia that was induced by CCH gradually improved, and nuclei were large and round with clear nucleoli, indicating that resveratrol improved brain damage that was caused by CCH (**Figure 3A**). Compared with the Sham group, levels of the brain damage markers S-100β and NSE gradually increased in the CCH group at 3, 6, and 9 weeks of ischemia, whereas S-100β and NSE levels significantly decreased

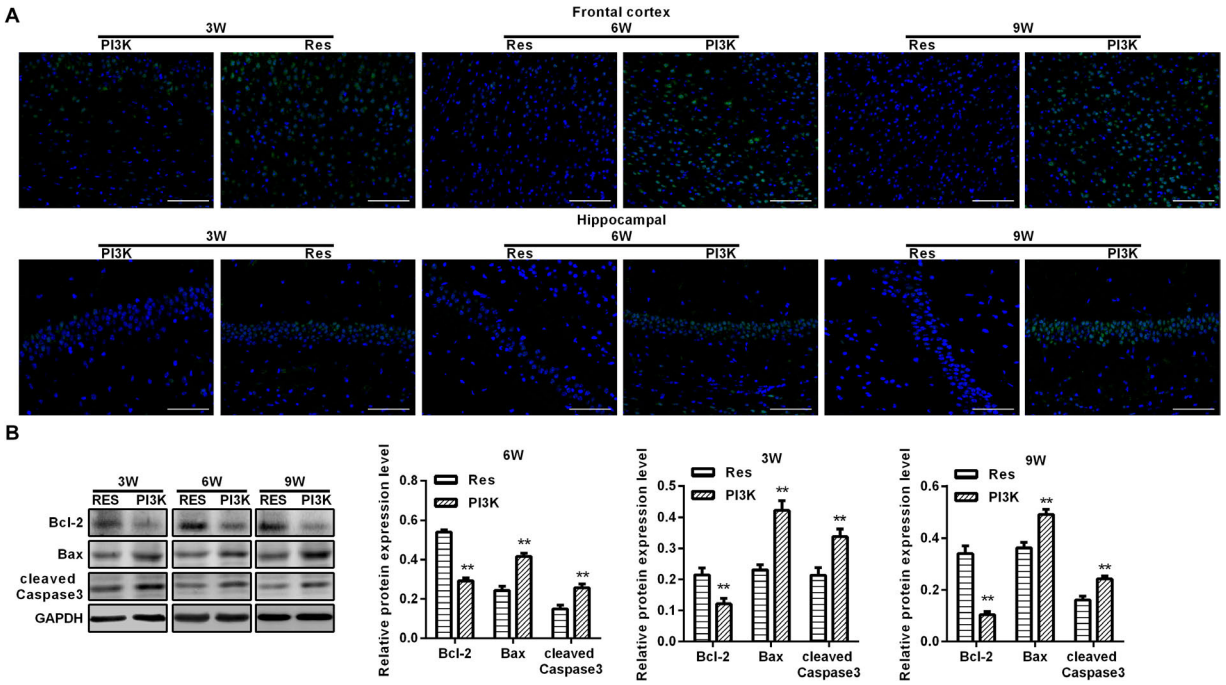

FIGURE 9 | PI3K inhibition reversed the therapeutic effects of resveratrol in CCH rats. TUNEL assays were performed to evaluate neuronal apoptosis in the frontal cortex and hippocampal CA1 area in each group. Apoptosis-related proteins were detected by Western blot. **(A)** TUNEL staining. Scale bar = 50 μm. **(B)** Western blot. $^{**}p < 0.05$, vs. Res group. Res group, CCH and treated with resveratrol; PI3K group, CCH and treated with resveratrol and the PI3K inhibitor LY294002.

in the Res group at the corresponding time points compared with the CCH group ($p < 0.05$), suggesting that resveratrol alleviated brain damage in CCH rats (**Figure 3B**).

To evaluate oxidative stress between experimental groups, we performed ELISAs for several known markers of oxidative stress. After resveratrol treatment, MDA levels gradually decreased in the frontal cortex and hippocampal CA1 area in the Res group, whereas SOD and GSH levels gradually increased (**Figure 4**). Rats that were subjected to CCH exhibited apparent neuronal apoptosis. The rate of apoptosis gradually increased over time and reached its highest point at 9 weeks of ischemia (**Figure 5A**). Bcl-2 expression gradually decreased, whereas cleaved caspase-3 and Bax increased in CCH rats compared with the Sham group ($p < 0.05$) at later timepoints. Repeated resveratrol treatment significantly improved neuronal apoptosis, increased Bcl-2 expression, and decreased cleaved caspase-3 and Bax expression compared with the CCH group ($p < 0.05$; **Figure 5B**).

Resveratrol Protected Against CCH via the PI3K/AKT/mTOR Pathway

To explore the possible mechanism by which these physiological changes occurred, we examined the AKT/mTOR signaling pathway in each experimental group. The expression of AKT, mTOR, S6K1, and 4E-BP1 in the frontal cortex and hippocampal CA1 area increased over time in the CCH group compared with the Sham group ($p < 0.05$; **Figures 6A–D**). After resveratrol treatment for 3, 6, and 9 weeks, the expression of AKT, mTOR, S6K1, and 4E-BP1 gradually decreased in the frontal cortex and hippocampal CA1 area compared with the CCH group ($p < 0.05$; **Figure 6E**). The AKT/mTOR signaling pathway has been linked to autophagy (Heras-Sandoval et al., 2014). Therefore, we evaluated markers of autophagy in the different experimental groups. At extended ligation times, rats in the CCH group exhibited higher LC3B and Beclin 1 expression in the frontal cortex and hippocampal CA1 area compared with the Sham group ($p < 0.05$; **Figures 7A,B**). After resveratrol treatment, the expression of LC3B and Beclin 1 gradually decreased compared with the CCH group ($p < 0.05$; **Figure 7C**).

The Protective Effect of Resveratrol Against CCH Was Blocked by a PI3K Inhibitor

To evaluate whether the protective effects of resveratrol against CCH depend on the PI3K/AKT/mTOR pathway, we treated CCH rats with both the PI3K inhibitor LY294002 and resveratrol. Neurological deficit scores in the PI3K group gradually increased, and their cognitive and spatial memory abilities were poor compared with the Res group ($p < 0.05$; **Figures 8A–C**). Brain tissue in the frontal cortex and hippocampal CA1 area was decrease in the PI3K group, and the hippocampus was atrophied. Neuronal injury was most apparent at 9 weeks of ischemia, with an increase in bubble-like structures in the PI3K group compared with the Res group ($p < 0.05$; **Figure 8D**). The expression of MDA, S-100β, and NSE gradually increased with administration time in the PI3K group compared with the Res group, whereas SOD and GSH expression gradually decreased

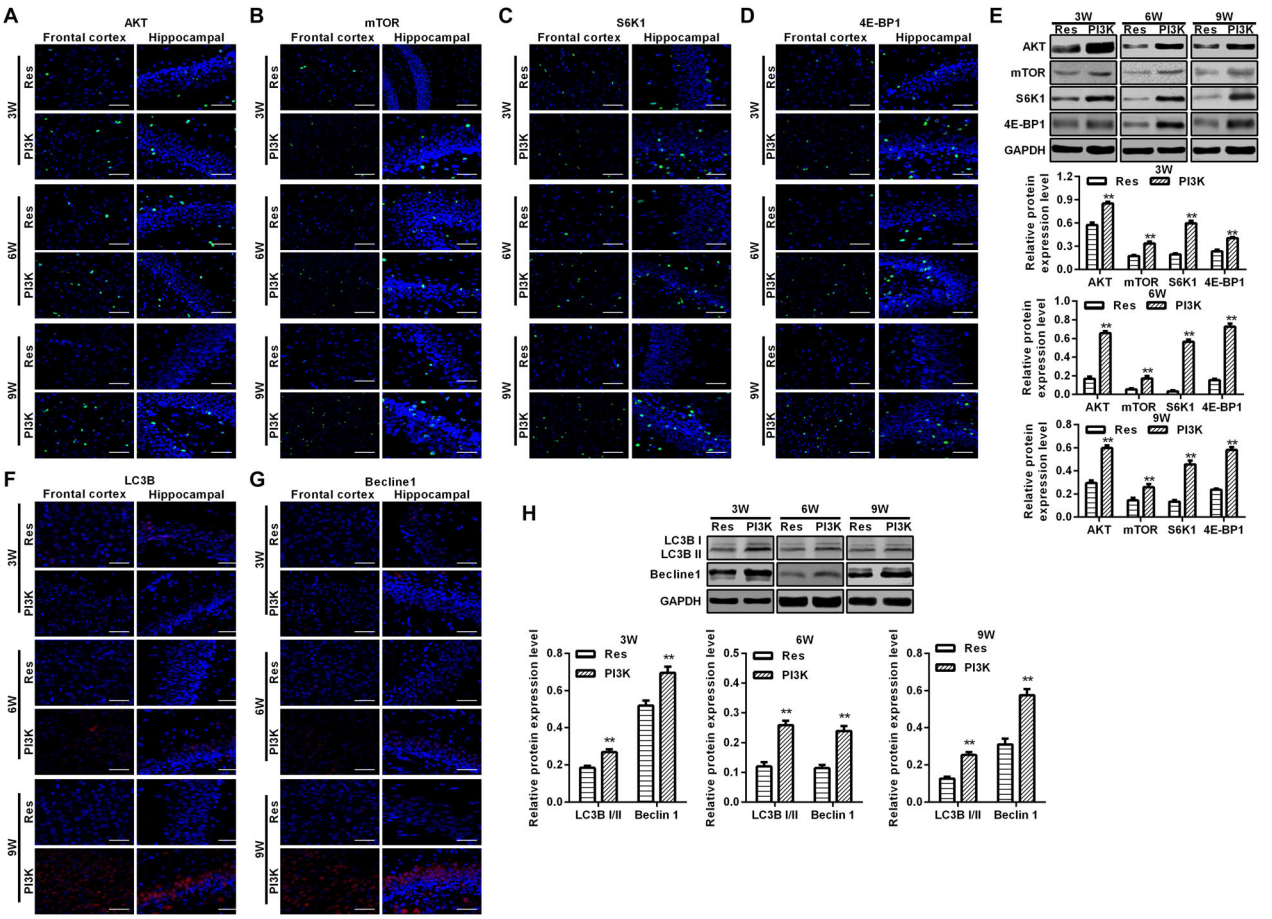

FIGURE 10 | PI3K inhibition reversed the therapeutic effects of resveratrol in CCH rats. Immunofluorescence staining and Western blot were used to detect expression of the AKT/mTOR signaling pathway-related proteins LC3B and Beclin 1. **(A–D,F,G)** Immunofluorescence staining. Scale bar = 50 μm. **(E,H)** Western blot. $^{**}p < 0.05$, vs. Res group. Res group, CCH and treated with resveratrol; PI3K group, CCH and treated with resveratrol and the PI3K inhibitor LY294002.

($p < 0.05$; **Figures 8E,F**). The rate of neuronal apoptosis in the frontal cortex and hippocampal CA1 area increased in the PI3K group, reaching its highest point at 9 weeks (**Figure 9A**). Bcl-2 expression decreased over time in the PI3K group compared with the Res group, and the expression of cleaved caspase-3 and Bax gradually increased ($p < 0.05$; **Figure 9B**). The expression of AKT, mTOR, S6K1, 4E-BP1, LC3B, and Beclin 1 increased in the frontal cortex and hippocampal CA1 area in the PI3K group with prolonged administration compared with the Res group ($p < 0.05$; **Figure 10**). Future studies will investigate the detailed mechanism of action of resveratrol, including its targeted proteins.

DISCUSSION

Chronic cerebral hypoperfusion is a pathological disorder that is known to lead to cognitive dysfunction. To investigate the effect of resveratrol on cognitive function in CCH, a rat model of CCH was established by permanently ligating the bilateral common carotid arteries. After establishing the CCH model, resveratrol was administered for 21 consecutive days. Cognitive function was evaluated in rats in the Morris water maze at 3, 6, and 9 weeks of ischemia. Cognitive function improved in CCH rats after resveratrol administration. We examined pathological damage to the frontal cortex and hippocampus using HE staining and found decreases in markers of oxidative stress and brain injury following resveratrol treatment. The Western blot data showed that resveratrol activated autophagy, decreased LC3B and Beclin 1 expression, and inhibited the expression of AKT/mTOR signaling pathway-related proteins. These results were the most significant at 9 weeks. After the administration of a PI3K inhibitor, the expression of AKT/mTOR signaling pathway-related proteins increased, and autophagy decreased, indicating that the neuroprotective effects of resveratrol were inhibited. However, we did not use quantitative polymerase chain reaction to detect the transcription levels of mTOR-related genes. Thus, we were unable to determine whether resveratrol exerts its functions through transcriptional regulation or an increase in the half-life of mTOR-related proteins. Future studies will seek to unveil the molecular mechanism of action of resveratrol. Previous studies have shown that neuronal cells in the frontal

cortex and hippocampus play important roles in maintaining normal learning and cognitive ability. Therefore, blocking neuronal apoptosis in the frontal cortex and hippocampus is important for improving cognitive dysfunction. The present study showed that resveratrol improved cognitive function in CCH rats and improved neuronal damage in the frontal cortex and hippocampus.

Resveratrol is a non-flavonoid polyphenolic compound that is produced by plants (Pezzuto, 2018). Recent studies reported that polyphenols exert protective effects on many aging-related central nervous system diseases, and the neuroprotective effects of resveratrol have also been confirmed in many animal models (Zhao et al., 2017; Palle and Neerati, 2018). Ghanim et al. (2010) found that a resveratrol extract inhibited ROS production, and Martinez and Moreno (2000) found that resveratrol exerted a strong inhibitory effect on superoxide radicals, indicating that resveratrol can reduce or prevent the occurrence of oxidative stress. Neuronal degeneration that is caused by CCH is a pathological basis for neuronal apoptosis (Jing et al., 2015). Many studies have shown that resveratrol can alleviate axonal degeneration and inhibit hippocampal neuronal apoptosis (Moriya et al., 2011; Zhang et al., 2015; Tian et al., 2016). Resveratrol was shown to protect the nervous system by regulating autophagy and clearing pathological proteins, thus contributing to the treatment of neurological diseases, but its mechanism of action is still unclear (Hu et al., 2017). The present study established a rat model of CCH to explore the mechanism of its neuroprotective effects. Our results showed that CCH rats exhibited the gradual recovery of cognitive and learning abilities, coinciding with improvements in pathological damage in the frontal cortex and hippocampal CA1 area with prolonged resveratrol administration. The present study focused on promoting cognitive function. We did not evaluate changes in dendritic spines. Furthermore, factors that are indicative of oxidative stress and apoptosis gradually decreased with resveratrol treatment, with decreases in AKT, mTOR, S6K1, and 4E-BP1 levels and inhibition of the expression of LC3B and Beclin 1. These findings indicate that resveratrol improves brain tissue damage in the frontal cortex and hippocampal CA1 area by inhibiting oxidative stress, thereby attenuating neuronal apoptosis. This was associated with decreases in the expression of AKT/mTOR signaling pathway-associated proteins and increases in autophagy in the frontal cortex and hippocampal CA1 region.

The AKT/mTOR signaling pathway is a classic anti-apoptosis pathway that is involved in various cellular activities and closely related to cell survival, the cell cycle, cell proliferation, and apoptosis (Wang et al., 2017; Zhang et al., 2018). Several recent studies have shown that regulating this pathway can prevent or improve neurodegenerative diseases (Guillot et al., 2016; Giacoppo et al., 2017). Resveratrol appears to regulate the cell cycle through numerous molecular mechanisms (Medina-Aguilar et al., 2016; He Y. et al., 2017; Singh et al., 2017). In T-ALL cells, resveratrol inhibited the expression of AKT, mTOR, and 4E-BP1 and activated p38 and mitogen-activated protein kinase signals to induce apoptosis (Ge et al., 2013). In addition to controlling the rate of aging of cells and tissues, mTOR signaling is also important for inhibiting autophagy and the formation of lysosomes (Yu et al., 2010). Numerous studies have shown that there may be a common regulatory factor between autophagy and apoptosis. In the model of focal cerebral ischemia and ischemic injury, Beclin 1 may be involved in the activation of caspase-3, and the anti-apoptotic protein Bcl-2 binds to Beclin 1 to block autophagy (Ciechomska et al., 2009; Yang et al., 2017; Ding et al., 2018; Wang J. et al., 2018). In the present study, we established a rat model of CCH and took samples at different timepoints of resveratrol treatment. Our results indicated that resveratrol exerted an inhibitory effect on neuronal apoptosis by increasing the expression of Bcl-2, decreasing the expression of cleaved caspase-3 and Bax, and downregulating the expression of AKT, mTOR, S6K1, and 4E-BP1 in brain tissue. These resveratrol-induced changes were reversed by the PI3K inhibitor LY294002. The present results suggest that resveratrol may activate autophagy via the AKT/mTOR pathway to improve neuronal apoptosis in CCH rats. Thus, inhibiting the AKT/mTOR signaling pathway-mediated activation of autophagy may be important for the treatment of cognitive decline.

CONCLUSION

Resveratrol improved pathological damage and cognitive function in a rat model of CCH by activating autophagy to reduce oxidative stress and inhibiting neuronal apoptosis in the frontal cortex and hippocampus. These beneficial effects of resveratrol may be regulated by the AKT/mTOR signaling pathway.

DATA AVAILABILITY

The raw data supporting the conclusions of this manuscript will be made available by the authors, without undue reservation, to any qualified researcher.

ETHICS STATEMENT

All of the animal experiments conformed to internationally accepted standards and were approved by the Experimental Animal Welfare and Ethics Committee of China Medical University (IACUC No. 2018097).

AUTHOR CONTRIBUTIONS

NW and ZX conceived and designed the experiments. NW, JH, CP, JW, MM, and XS performed the experiments. JW, MM, and XS analyzed the data. NW and ZX wrote the manuscript.

FUNDING

This work was supported by the International Cooperation Program of Science and Technology Development Plan in Jilin Province (Grant No. 20170414014GH).

REFERENCES

Bagul, P. K., and Banerjee, S. K. (2015). Application of resveratrol in diabetes: rationale, strategies and challenges. *Curr. Mol. Med.* 15, 312–330. doi: 10.2174/1566524015666150505155702

Chai, R., Fu, H., Zheng, Z., Liu, T., Ji, S., and Li, G. (2017). Resveratrol inhibits proliferation and migration through SIRT1 mediated posttranslational modification of PI3K/AKT signaling in hepatocellular carcinoma cells. *Mol. Med. Rep.* 16, 8037–8044. doi: 10.3892/mmr.2017.7612

Chen, C. Y., Kao, C. L., and Liu, C. M. (2018). The cancer prevention, anti-inflammatory and anti-oxidation of bioactive phytochemicals targeting the TLR4 signaling pathway. *Int. J. Mol. Sci.* 19:2729. doi: 10.3390/ijms19092729

Ciechomska, I. A., Goemans, C. G., and Tolkovsky, A. M. (2009). Why doesn't Beclin 1, a BH3-only protein, suppress the anti-apoptotic function of Bcl-2? *Autophagy* 5, 880–881. doi: 10.4161/auto.9096

Deretic, V., Saitoh, T., and Akira, S. (2013). Autophagy in infection, inflammation and immunity. *Nat. Rev. Immunol.* 13, 722–737. doi: 10.1038/nri3532

Desland, F. A., Afzal, A., Warraich, Z., and Mocco, J. (2014). Manual versus automated rodent behavioral assessment: comparing efficacy and ease of Bederson and Garcia neurological deficit scores to an open field video-tracking system. *J. Cent. Nerv. Syst. Dis.* 6, 7–14. doi: 10.4137/JCNSD.S13194

Ding, L. Y., Chu, M., Jiao, Y. S., Hao, Q., Xiao, P., Li, H. H., et al. (2018). TFDP3 regulates the apoptosis and autophagy in breast cancer cell line MDA-MB-231. *PLoS One* 13:e0203833. doi: 10.1371/journal.pone.0203833

Du, S. Q., Wang, X. R., Xiao, L. Y., Tu, J. F., Zhu, W., He, T., et al. (2017). Molecular mechanisms of vascular dementia: what can be learned from animal models of chronic cerebral hypoperfusion? *Mol. Neurobiol.* 54, 3670–3682. doi: 10.1007/s12035-016-9915-1

Duncombe, J., Kitamura, A., Hase, Y., Ihara, M., Kalaria, R. N., and Horsburgh, K. (2017). Chronic cerebral hypoperfusion: a key mechanism leading to vascular cognitive impairment and dementia. Closing the translational gap between rodent models and human vascular cognitive impairment and dementia. *Clin. Sci.* 131, 2451–2468. doi: 10.1042/CS20160727

Dunlop, E. A., and Tee, A. R. (2014). mTOR and autophagy: a dynamic relationship governed by nutrients and energy. *Semin. Cell Dev. Biol.* 36, 121–129. doi: 10.1016/j.semcdb.2014.08.006

Fang, W. J., Wang, C. J., He, Y., Zhou, Y. L., Peng, X. D., and Liu, S. K. (2018). Resveratrol alleviates diabetic cardiomyopathy in rats by improving mitochondrial function through PGC-1alpha deacetylation. *Acta Pharmacol. Sin.* 39, 59–73. doi: 10.1038/aps.2017.50

Feng, T., Yamashita, T., Zhai, Y., Shang, J., Nakano, Y., Morihara, R., et al. (2018). Chronic cerebral hypoperfusion accelerates Alzheimer's disease pathology with the change of mitochondrial fission and fusion proteins expression in a novel mouse model. *Brain Res.* 1696, 63–70. doi: 10.1016/j.brainres.2018.06.003

Filomeni, G., De Zio, D., and Cecconi, F. (2015). Oxidative stress and autophagy: the clash between damage and metabolic needs. *Cell Death Differ.* 22, 377–388. doi: 10.1038/cdd.2014.150

Ge, J., Liu, Y., Li, Q., Guo, X., Gu, L., Ma, Z. G., et al. (2013). Resveratrol induces apoptosis and autophagy in T-cell acute lymphoblastic leukemia cells by inhibiting Akt/mTOR and activating p38-MAPK. *Biomed. Environ. Sci.* 26, 902–911. doi: 10.3967/bes2013.019

Ghanim, H., Sia, C. L., Abuaysheh, S., Korzeniewski, K., Patnaik, P., Marumganti, A., et al. (2010). An antiinflammatory and reactive oxygen species suppressive effects of an extract of *Polygonum* cuspidatum containing resveratrol. *.J Clin. Endocrinol Metab.* 95, E1–E8. doi: 10.1210/jc.2010-0482

Giacoppo, S., Bramanti, P., and Mazzon, E. (2017). Triggering of inflammasome by impaired autophagy in response to acute experimental Parkinson's disease: involvement of the PI3K/Akt/mTOR pathway. *Neuroreport* 28, 996–1007. doi: 10.1097/WNR.0000000000000871

Guillot, F., Kemppainen, S., Lavasseur, G., Miettinen, P. O., Laroche, S., Tanila, H., et al. (2016). Brain-specific basal and novelty-induced alternations in PI3K-Akt and MAPK/ERK signaling in a middle-aged AbetaPP/PS1 mouse model of Alzheimer's disease. *J. Alzheimers Dis.* 51, 1157–1173. doi: 10.3233/JAD-150926

He, Q., Li, Z., Wang, Y., Hou, Y., Li, L., and Zhao, J. (2017). Resveratrol alleviates cerebral ischemia/reperfusion injury in rats by inhibiting NLRP3 inflammasome activation through Sirt1-dependent autophagy induction. *Int. Immunopharmacol.* 50, 208–215. doi: 10.1016/j.intimp.2017.06.029

He, Y., Zeng, H., Yu, Y., Zhang, J., Zeng, X., Gong, F., et al. (2017). Resveratrol improves cell cycle arrest in chronic prostatitis rats, by C-kit/SCF suppression. *DNA Cell Biol.* 36, 709–714. doi: 10.1089/dna.2017.3741

Heras-Sandoval, D., Perez-Rojas, J. M., Hernandez-Damian, J., and Pedraza-Chaverri, J. (2014). The role of PI3K/AKT/mTOR pathway in the modulation of autophagy and the clearance of protein aggregates in neurodegeneration. *Cell. Signal.* 26, 2694–2701. doi: 10.1016/j.cellsig.2014.08.019

Hu, J., Han, H., Cao, P., Yu, W., Yang, C., Gao, Y., et al. (2017). Resveratrol improves neuron protection and functional recovery through enhancement of autophagy after spinal cord injury in mice. *Am. J. Transl. Res.* 9, 4607–4616.

Huang, C. Y., Ting, W. J., Huang, C. Y., Yang, J. Y., and Lin, W. T. (2016). Resveratrol attenuated hydrogen peroxide-induced myocardial apoptosis by autophagic flux. *Food Nutr. Res.* 60:30511. doi: 10.3402/fnr.v60.30511

Jing, Z., Shi, C., Zhu, L., Xiang, Y., Chen, P., Xiong, Z., et al. (2015). Chronic cerebral hypoperfusion induces vascular plasticity and hemodynamics but also neuronal degeneration and cognitive impairment. *J. Cereb. Blood Flow Metab.* 35, 1249–1259. doi: 10.1038/jcbfm.2015.55

Kim, Y. C., and Guan, K. L. (2015). mTOR: a pharmacologic target for autophagy regulation. *J. Clin. Invest.* 125, 25–32. doi: 10.1172/JCI73939

Li, J. Y., Huang, W. Q., Tu, R. H., Zhong, G. Q., Luo, B. B., and He, Y. (2017). Resveratrol rescues hyperglycemia-induced endothelial dysfunction via activation of Akt. *Acta Pharmacol. Sin.* 38, 182–191. doi: 10.1038/aps.2016.109

Ling, L., Gu, S., and Cheng, Y. (2017). Resveratrol activates endogenous cardiac stem cells and improves myocardial regeneration following acute myocardial infarction. *Mol. Med. Rep.* 15, 1188–1194. doi: 10.3892/mmr.2017.6143

Martinez, J., and Moreno, J. J. (2000). Effect of resveratrol, a natural polyphenolic compound, on reactive oxygen species and prostaglandin production. *Biochem. Pharmacol.* 59, 865–870. doi: 10.1016/s0006-2952(99)00380-9

Medina-Aguilar, R., Marchat, L. A., Arechaga Ocampo, E., Gariglio, P., Garcia Mena, J., Villegas Sepulveda, N., et al. (2016). Resveratrol inhibits cell cycle progression by targeting Aurora kinase A and Polo-like kinase 1 in breast cancer cells. *Oncol. Rep.* 35, 3696–3704. doi: 10.3892/or.2016.4728

Moloudizargari, M., Asghari, M. H., Ghobadi, E., Fallah, M., Rasouli, S., and Abdollahi, M. (2017). Autophagy, its mechanisms and regulation: implications in neurodegenerative diseases. *Ageing Res. Rev.* 40, 64–74. doi: 10.1016/j.arr.2017.09.005

Moriya, J., Chen, R., Yamakawa, J., Sasaki, K., Ishigaki, Y., and Takahashi, T. (2011). Resveratrol improves hippocampal atrophy in chronic fatigue mice by enhancing neurogenesis and inhibiting apoptosis of granular cells. *Biol. Pharm. Bull* 34, 354–359. doi: 10.1248/bpb.34.354

Munson, M. J., and Ganley, I. G. (2015). MTOR, PIK3C3, and autophagy: signaling the beginning from the end. *Autophagy* 11, 2375–2376. doi: 10.1080/15548627.2015.1106668

O'Neill, C. (2013). PI3-kinase/Akt/mTOR signaling: impaired on/off switches in aging, cognitive decline and Alzheimer's disease. *Exp. Gerontol.* 48, 647–653. doi: 10.1016/j.exger.2013.02.025

Palle, S., and Neerati, P. (2018). Improved neuroprotective effect of resveratrol nanoparticles as evinced by abrogation of rotenone-induced behavioral deficits and oxidative and mitochondrial dysfunctions in rat model of Parkinson's disease. *Naunyn Schmiedebergs Arch. Pharmacol.* 391, 445–453. doi: 10.1007/s00210-018-1474-8

Panchal, K., and Tiwari, A. K. (2018). Mitochondrial dynamics, a key executioner in neurodegenerative diseases. *Mitochondrion* 47, 151–173. doi: 10.1016/j.mito.2018.11.002

Pezzuto, J. M. (2018). Resveratrol: twenty years of growth, development and controversy. *Biomol. Ther.* 27, 1–14. doi: 10.4062/biomolther.2018.176

Romero-Leguizamon, C. R., Ramirez-Latorre, J. A., Mora-Munoz, L., and Guerrero-Naranjo, A. (2016). [Signaling pathways mTOR and AKT in epilepsy]. *Rev. Neurol.* 63, 33–41.

Shen, D., Chen, R., Zhang, L., Rao, Z., Ruan, Y., Li, L., et al. (2019). Sulodexide attenuates endoplasmic reticulum stress induced by myocardial ischaemia/reperfusion by activating the PI3K/Akt pathway. *J. Cell Mol. Med.* 23, 5063–5075. doi: 10.1111/jcmm.14367

Singh, S. K., Banerjee, S., Acosta, E. P., Lillard, J. W., and Singh, R. (2017). Resveratrol induces cell cycle arrest and apoptosis with docetaxel in prostate cancer cells via a p53/p21WAF1/CIP1 and p27KIP1 pathway. *Oncotarget* 8, 17216–17228. doi: 10.18632/oncotarget.15303

Su, S. H., Wu, Y. F., Lin, Q., and Hai, J. (2017). Cannabinoid receptor agonist WIN55,212-2 and fatty acid amide hydrolase inhibitor URB597 ameliorate neuroinflammatory responses in chronic cerebral hypoperfusion model by blocking NF-kappaB pathways. *Naunyn Schmiedebergs Arch. Pharmacol.* 390, 1189–1200. doi: 10.1007/s00210-017-1417-9

Tan, Y., Gong, Y., Dong, M., Pei, Z., and Ren, J. (2018). Role of autophagy in inherited metabolic and endocrine myopathies. *Biochim. Biophys. Acta Mol. Basis Dis.* 1865, 48–55. doi: 10.1016/j.bbadis.2018.10.023

Tian, Z., Wang, J., Xu, M., Wang, Y., Zhang, M., and Zhou, Y. (2016). Resveratrol improves cognitive impairment by regulating apoptosis and synaptic plasticity in streptozotocin-induced diabetic rats. *Cell Physiol. Biochem.* 40, 1670–1677. doi: 10.1159/000453216

Wan, D., Zhou, Y., Wang, K., Hou, Y., Hou, R., and Ye, X. (2016). Resveratrol provides neuroprotection by inhibiting phosphodiesterases and regulating the cAMP/AMPK/SIRT1 pathway after stroke in rats. *Brain Res. Bull* 121, 255–262. doi: 10.1016/j.brainresbull.2016.02.011

Wang, H., Jiang, T., Li, W., Gao, N., and Zhang, T. (2018). Resveratrol attenuates oxidative damage through activating mitophagy in an in vitro model of Alzheimer's disease. *Toxicol Lett.* 282, 100–108. doi: 10.1016/j.toxlet.2017.10.021

Wang, J., Zhang, Y., Song, W., Ma, T., and Wang, K. (2018). microRNA-590-5p targets transforming growth factor beta1 to promote chondrocyte apoptosis and autophagy in response to mechanical pressure injury. *J. Cell Biochem.* 119, 9931–9940. doi: 10.1002/jcb.27315

Wang, X., Fu, Y. F., Liu, X., Feng, G., Xiong, D., Mu, G. F., et al. (2018). ROS promote Ox-LDL-induced platelet activation by up-regulating autophagy through the inhibition of the PI3K/AKT/mTOR pathway. *Cell Physiol. Biochem.* 50, 1779–1793. doi: 10.1159/000494795

Wang, X. Y., Zhang, X. H., Peng, L., Liu, Z., Yang, Y. X., He, Z. X., et al. (2017). Bardoxolone methyl (CDDO-Me or RTA402) induces cell cycle arrest, apoptosis and autophagy via PI3K/Akt/mTOR and p38 MAPK/Erk1/2 signaling pathways in K562 cells. *Am. J. Transl. Res.* 9, 4652–4672.

Xiong, Z., Lu, W., Zhu, L., Zeng, L., Shi, C., Jing, Z., et al. (2017). Dl-3-n-butylphthalide treatment enhances hemodynamics and ameliorates memory deficits in rats with chronic cerebral hypoperfusion. *Front. Aging Neurosci.* 9:238. doi: 10.3389/fnagi.2017.00238

Yang, Y., Chen, S., Zhang, Y., Lin, X., Song, Y., Xue, Z., et al. (2017). Induction of autophagy by spermidine is neuroprotective via inhibition of caspase 3-mediated Beclin 1 cleavage. *Cell Death Dis.* 8:e2738. doi: 10.1038/cddis.2017.161

Yu, L., McPhee, C. K., Zheng, L., Mardones, G. A., Rong, Y., Peng, J., et al. (2010). Termination of autophagy and reformation of lysosomes regulated by mTOR. *Nature* 465, 942–946. doi: 10.1038/nature09076

Zhan, L., Liu, D., Wen, H., Hu, J., Pang, T., Sun, W., et al. (2019). Hypoxic postconditioning activates the Wnt/beta-catenin pathway and protects against transient global cerebral ischemia through Dkk1 inhibition and GSK-3beta inactivation. *FASEB J.* 33, 9291–9307. doi: 10.1096/fj.201802633R

Zhang, T., Ji, D., Wang, P., Liang, D., Jin, L., Shi, H., et al. (2018). The atypical protein kinase RIOK3 contributes to glioma cell proliferation/survival, migration/invasion and the AKT/mTOR signaling pathway. *Cancer Lett.* 415, 151–163. doi: 10.1016/j.canlet.2017.12.010

Zhang, Y., Li, H., Cao, Y., Zhang, M., and Wei, S. (2015). Sirtuin 1 regulates lipid metabolism associated with optic nerve regeneration. *Mol. Med. Rep.* 12, 6962–6968. doi: 10.3892/mmr.2015.4286

Zhao, X., Wang, J., Hu, S., Wang, R., Mao, Y., and Xie, J. (2017). Neuroprotective effect of resveratrol on rotenone-treated C57BL/6 mice. *Neuroreport* 28, 498–505. doi: 10.1097/WNR.0000000000000789

Conflict of Interest Statement: The authors declare that the research was conducted in the absence of any commercial or financial relationships that could be construed as a potential conflict of interest.

frontiers in Neuroscience

REVIEW
published: 06 December 2019
doi: 10.3389/fnins.2019.01310

ALS Genetics, Mechanisms, and Therapeutics: Where Are We Now?

Rita Mejzini[1,2], Loren L. Flynn[1,2,3], Ianthe L. Pitout[1,2,3], Sue Fletcher[1,2,3], Steve D. Wilton[1,2,3] and P. Anthony Akkari[1,2,3]**

[1] Centre for Molecular Medicine and Innovative Therapeutics, Murdoch University, Perth, WA, Australia, [2] The Perron Institute for Neurological and Translational Science, Perth, WA, Australia, [3] Centre for Neuromuscular and Neurological Disorders, The University of Western Australia, Perth, WA, Australia

The scientific landscape surrounding amyotrophic lateral sclerosis (ALS) continues to shift as the number of genes associated with the disease risk and pathogenesis, and the cellular processes involved, continues to grow. Despite decades of intense research and over 50 potentially causative or disease-modifying genes identified, etiology remains unexplained and treatment options remain limited for the majority of ALS patients. Various factors have contributed to the slow progress in understanding and developing therapeutics for this disease. Here, we review the genetic basis of ALS, highlighting factors that have contributed to the elusiveness of genetic heritability. The most commonly mutated ALS-linked genes are reviewed with an emphasis on disease-causing mechanisms. The cellular processes involved in ALS pathogenesis are discussed, with evidence implicating their involvement in ALS summarized. Past and present therapeutic strategies and the benefits and limitations of the model systems available to ALS researchers are discussed with future directions for research that may lead to effective treatment strategies outlined.

Keywords: amyotrophic lateral sclerosis, TDP-43, FUS, missing heritability, disease mechanisms, cell models, therapeutics

OPEN ACCESS

Edited by:
Francesca Trojsi, University of Campania Luigi Vanvitelli, Italy

Reviewed by:
Serena Lattante, Catholic University of the Sacred Heart, Italy
Nicola Ticozzi, University of Milan, Italy

****Correspondence:***
Rita Mejzini
rita.mejzini@murdoch.edu.au
P. Anthony Akkari
anthony.akkari@perron.uwa.edu.au

Specialty section:
This article was submitted to Neurodegeneration, a section of the journal Frontiers in Neuroscience

Received: *10 September 2019*
Accepted: *22 November 2019*
Published: *06 December 2019*

Citation:
Mejzini R, Flynn LL, Pitout IL, Fletcher S, Wilton SD and Akkari PA (2019) ALS Genetics, Mechanisms, and Therapeutics: Where Are We Now? Front. Neurosci. 13:1310. doi: 10.3389/fnins.2019.01310

INTRODUCTION

Amyotrophic lateral sclerosis (ALS) is a fatal motor neuron disease characterized by degenerative changes in both upper and lower motor neurons (Rowland and Shneider, 2001). Onset typically occurs in late middle life and presents as a relentlessly progressive muscle atrophy and weakness, with the effects on respiratory muscles limiting survival to 2–4 years after disease onset in most cases (Chio et al., 2009). ALS is the most common adult motor neuron disease with an incidence of 2 per 100,000 and prevalence of 5.4 per 100,000 individuals (Chiò et al., 2013). Current treatment options are based on symptom management and respiratory support with the only approved medications in widespread use, Riluzole and Edaravone, providing only modest benefits and only in some patients (Petrov et al., 2017; Sawada, 2017). Many factors have contributed to the slow progress in developing effective treatments for this devastating disease. Although ALS is believed to have a large genetic component with high heritability, many of the gene variants that cause or predispose an individual to develop ALS remain unknown. Furthermore, with so many cellular processes implicated in ALS disease progression, determining which are causative remains challenging. The complex nature of the disease and large genetic and phenotypic heterogeneity between patients also complicates matters, making it difficult for studies in genetically similar animal models to translate to success in human clinical trials.

This review discusses the genetic landscape of ALS in the context of ALS research and reviews disease mechanisms and cellular pathways implicated in ALS disease progression. Past and current therapeutic strategies and model systems available to ALS researchers are also explored and the factors contributing to the slow progress in therapeutic development discussed.

GENETICS OF ALS

Evidence from clinical and basic research suggests multiple causes of ALS, with important but varied genetic components. Up to 10% of ALS affected individuals have at least one other affected family member and are defined as having familial ALS (fALS); almost all of these cases have been found to be inherited in an autosomal dominant manner (Kirby et al., 2016). The remaining 90–95% of ALS cases occur in people with no prior family history; these individuals are said to have sporadic ALS (sALS) (Chen et al., 2013).

As technology has advanced, molecular genetic techniques have been increasingly applied to ALS research. Genome-wide association studies and "next-generation" sequencing techniques have supplemented the "first generation" methods, such as genetic linkage analysis, and have allowed the search for ALS-linked genes to be conducted in large sample sets (Boylan, 2015). Such advances have contributed to our understanding of the genetic causes of fALS with approximately 40–55% of cases accounted for by variants in known ALS-linked genes (Zou et al., 2017). Although more than 50 potentially causative or disease-modifying genes have been identified, pathogenic variants in *SOD1*, *C9ORF72*, *FUS*, and *TARDBP* occur most frequently with disease causing variants in other genes being relatively uncommon (Boylan, 2015). The proportion of ALS cases attributed to variants in the most common ALS-linked genes in European and Asian populations can be seen in **Figure 1**. In sALS cases however, diagnostic advancements have only helped in explaining a fraction of cases, with the etiology remaining unexplained in over 90% of patients (Renton et al., 2014). Genetic risk factors are widely considered to contribute to sALS with estimates from twin studies putting heritability at around 60% (Al-Chalabi et al., 2010). Despite many genetic association studies being carried out, the identification of heritable genetic risk factors in sALS remains elusive.

Missing Heritability in ALS

There are several factors that may contribute to the missing heritability in ALS, including limitations due to technical issues as well as the inherently complex nature of the disease(s). One potentially large contributing factor to the missing heritability in ALS has been the limitations of the technologies used in large association studies. ALS association studies have relied extensively upon short read, high throughput sequencing technologies (Fogh et al., 2014; Wouter van et al., 2016). Although useful for detecting single-nucleotide polymorphisms (SNPs), the majority of structural variations (SVs) occurring in the human genome are not well characterized by single short-read platforms. Technical issues involving amplification of repetitive DNA regions, short-read mapping and SV detection algorithms have made SVs difficult to analyze, especially those consisting of long repeats or which occur in repetitive DNA regions (Chaisson et al., 2014; Cameron et al., 2019). Genome-wide association studies now commonly make use of genotyping arrays that cover a million SNPs across the genome and include thousands of clinically diagnosed patients. Although this method has successfully identified several novel and rare ALS-linked genes, a vast gap still exists in identifying heritable genetic traits that contribute to ALS risk. The missing heritability suggests that SNPs are unlikely to account for a substantial proportion of the genetic contribution to ALS and highlights the urgent need for alternative approaches to aid in understanding ALS etiology, including the search for genetic modifiers and risk factors.

Structural variations remain underexplored potential genetic modifiers of ALS and other diseases. Structural variations include all genomic deletions, insertions, inversions and microsatellites, with over 7 million classified in the human genome. Many of these are associated with a simple sequence repeat or tandem repeat in which a short base-pair motif is repeated several times in tandem. Simple sequence repeats have long been known to have a propensity for slippage mutations in which the number of repeats is increased or decreased during replication (Sutherland and Richards, 1994; Kovtun and McMurray, 2008). Simple sequence repeats occur frequently throughout eukaryotic genomes with the polymorphisms they produce being exploited in various applications, including lineage analysis and DNA fingerprinting. Many SVs, including short sequence repeats, are located within introns of genes leading early researchers to believe they were genetic "junk" with no effect on phenotype. The subsequent discovery of at least 20 neurological disorders caused by expanded short sequence repeats (including the *C9ORF72* expansion seen in ALS) has illuminated a pathological extreme that points to a wider influence of short sequence repeats on normal brain function (Fondon et al., 2008).

A recent study has highlighted the extent and cryptic nature of SVs when using high throughput sequencing; by utilizing a suite of long-read and short-read sequencing technologies and several SV calling algorithms, a three to sevenfold increase in the detection of SVs was reported, compared to standard high throughput sequencing, with an average of over 800,000 SVs uncovered per genome (Chaisson et al., 2018). Furthermore, on a per variant basis SVs are 50 times more likely to affect the expression of a gene compared with a SNP (Chiang et al., 2017). Polymorphic structural variants may account for differences between individuals at risk for a specific phenotype, including the risk of disease, disease course, mechanism of pathogenesis and response to treatment, particularly in complex genetic diseases such as ALS (Roses et al., 2016). The characterization of SVs that occur within and around regulatory regions of ALS associated genes may reveal a source of novel sALS heritability or shed light on risk factors or pathogenic mechanisms.

There are several other factors that may contribute to the missing heritability in ALS, including the potential oligogenic nature of the disease. The difficulty in uncovering the genetic determinants of ALS suggests the disease has a complex genetic architecture that may consist of combinations of gene variants

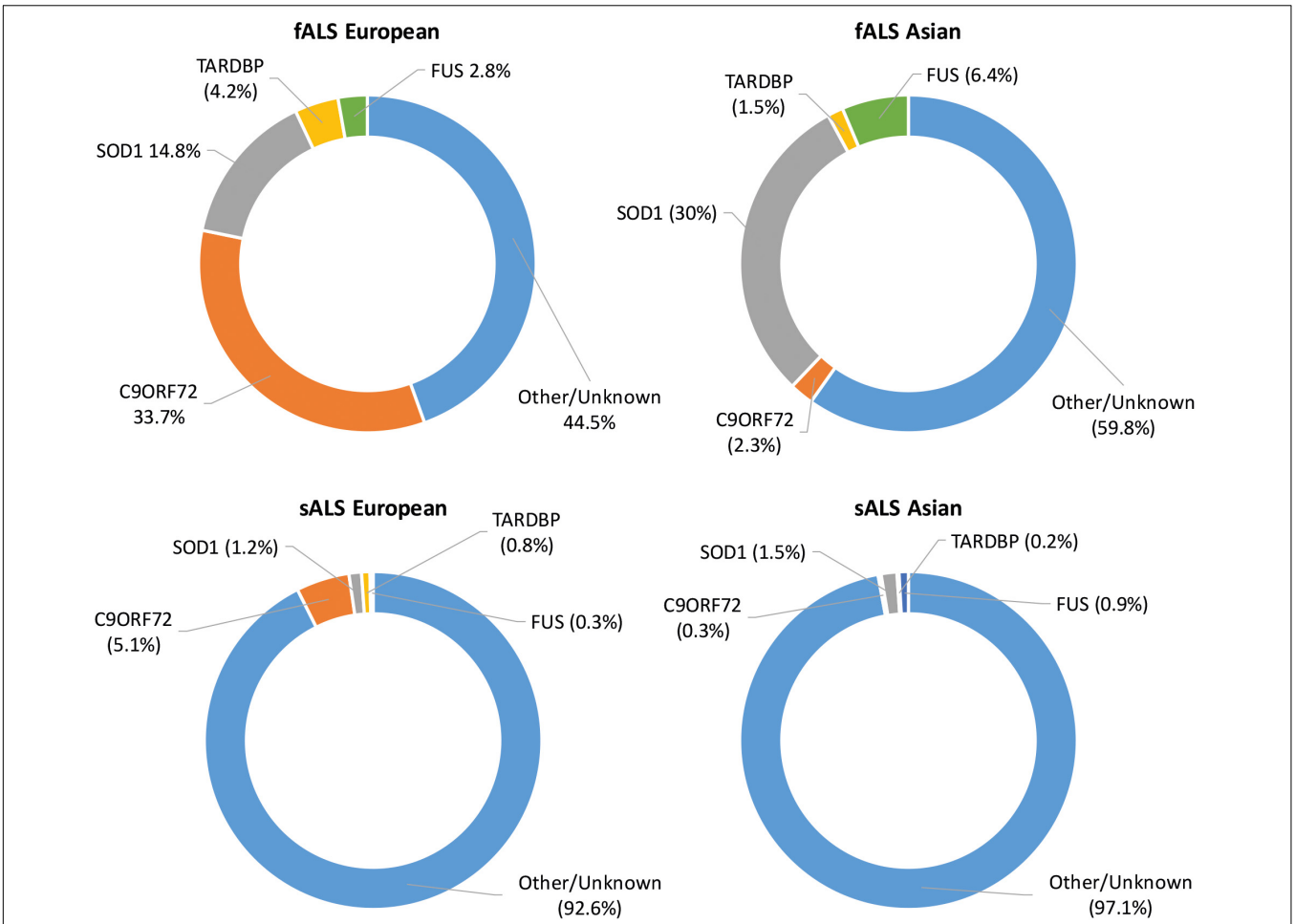

FIGURE 1 | Proportion of ALS explained by the four most commonly mutated genes in Asian and European populations. Data adapted from Zou et al. (2017).

differing in frequency and noxiousness. Interest in the potential oligogenic nature of ALS has recently increased. The number of ALS patients reported to have more than one ALS risk variant varies depending on the study, but has been reported to be between 1 and 4% (Kenna et al., 2013; Cady et al., 2015; Morgan et al., 2017). Some studies have reported that the presence of a second risk variant further increased the risk of ALS and disease progression (Pang et al., 2017). Others have suggested that those with a known highly penetrant risk allele are more likely to be defined as being oligogenic than controls for a given panel of variations, introducing an often uncontrolled bias to these studies. A recent study on oligogenic variation in neurodegenerative disease found that after controlling for the major known variant there was no association between the second likely benign oligogenic variation and neurodegenerative disease (Keogh et al., 2018). Complicating matters further, what counts as a secondary variant is debatable, as many variants are of uncertain significance. Low frequency variants could account for a substantial part of the missing heritability in ALS. Variants of low minor allele frequency may not be captured by current genotyping arrays and effect sizes may not be large enough to be detected by linkage analysis in families (Manolio et al., 2009). Additionally, the small number of patients harboring some potentially deleterious variants can make determining pathogenicity difficult. Substantially larger datasets than those studied to date will be required to resolve this issue.

The way that genetic diagnoses are made may also be contributing to the apparent missing heritability in ALS. Genetic diagnosis is often done by whole exome sequencing, resulting in potentially important intronic and intergenic variants being missed. An increase in rare variants, many of unknown significance, has been found in the untranslated regions of known disease-causing genes including *SOD1, TARDBP, FUS, VCP, OPTN* and *UBQLN2,* highlighting the potential importance of regulatory gene regions when determining disease pathogenesis and making genetic diagnoses (Morgan et al., 2017). Heritability can also be hard to determine in some cases due to the incomplete penetrance of variants in many ALS-associated genes. *C9ORF72* and *ATXN2* variants for example show incomplete penetrance, with symptoms not always manifesting in mutation carriers (Elden et al., 2010; Murphy et al., 2017). This may lead to inherited cases that appear to be sporadic. Monogenic high

penetrance variants may therefore account for a large proportion of those with no apparent family history (Al-Chalabi and Lewis, 2011). Several social and clinical factors come into play when determining whether disease is familial or sporadic, with the distinction looking increasingly artificial.

A large proportion of the genetic risk for sALS remains elusive; this has meant much research to date has focused on understanding how variations and differences in expression of known ALS-linked genes lead to disease. *SOD1*, *TARDBP*, *FUS*, and *C9ORF72* have been most extensively characterized.

ALS ASSOCIATED GENES

SOD1

The *SOD1* gene (encoding superoxide dismutase 1 [Cu/Zn]) was the first to be associated with ALS, in 1993 (Rosen et al., 1993). *SOD1* encodes a 153 amino acid metalloenzyme, one of three superoxide dismutase enzymes found in humans. The protein binds copper and zinc and forms an extremely stable homodimer. SOD1 dimers reside in the cytosol and the intermembrane space of mitochondria, providing an important antioxidant defense mechanism by catalyzing the production of oxygen and hydrogen peroxide from the superoxide species produced during cellular respiration (McCord and Fridovich, 1969). A recent meta-analysis found that pathogenic variants in *SOD1* account for approximately 15–30% of fALS and fewer than 2% of sALS cases (Zou et al., 2017).

Over 185 disease-associated variations in *SOD1* have now been identified and are distributed throughout the gene (Yamashita and Ando, 2015). The majority are missense mutations, with the D90A variant the most common worldwide. Phenotype, disease duration and severity can differ significantly depending on the variants involved. Rapid disease progression and shorter survival times are seen in patients with the A4V, H43R, L84V, G85R N86S, and G93A variants, whilst patients with the G93C, D90A, or H46R variants generally have longer life expectancies (Yamashita and Ando, 2015). Genotype-phenotype correlations in SOD1-ALS are apparent with distinct clinical features manifesting in patients harboring particular variants. The A4V variant, for example, is associated with a limb-onset, aggressive ALS form (Juneja et al., 1997). Patients homozygous for the D90A variant generally display a slowly progressive paresis that starts in the legs and gradually spreads upward, as well as some atypical features such as bladder disturbance (Andersen et al., 1996). In contrast, heterozygous D90A variation is associated with several ALS forms including bulbar, upper limb onset and lower limb onset with a faster progression (Hong-Fu and Zhi-Ying, 2016).

SOD1 Disease Mechanisms

Variations in *SOD1* have been associated with a decrease in enzyme activity of 50–80% (Deng et al., 1993; Rosen et al., 1993), leading to early propositions that disease was conferred through a loss of dismutase activity. However, a later study showed that dismutase activity did not correlate with disease severity, indicating that a toxic gain of function mechanism might be at play (Cleveland et al., 1995). Support for a toxic gain of function mechanism was soon supported by a *Sod1*-knockout mouse model that did not display an ALS phenotype (Siwek et al., 1996). Mutation-induced conformational and functional changes of SOD1 have been proposed to confer toxicity via interactions with many proteins and through several mechanisms. These include excitotoxicity, oxidative stress via upregulation of reactive oxygen species, endoplasmic reticulum stress, mitochondrial dysfunction, and prion-like propagation as reviewed by Hayashi et al. (2016). As in other neurodegenerative diseases involving protein aggregation, debate surrounds whether the soluble or aggregated forms of the protein are responsible for exerting toxicity. Additionally, non-native formations of wild-type SOD1 have been detected in small granular SOD1-immunoreactive inclusions in the motor neurons of sALS patients without pathogenic *SOD1* variants (Forsberg et al., 2010) and in patients carrying the *C9ORF72* repeat expansion and pathogenic variants in other ALS-associated genes (Forsberg et al., 2019). This suggests that misfolding of wild-type SOD1 may be deleterious or be part of a common downstream event in ALS progression.

TDP-43

Histological examinations of spinal cord samples had revealed that neuronal cytoplasmic ubiquitinated inclusions were present in the majority of ALS patients (Leigh et al., 1991). In 2006, a shift in the understanding of ALS pathogenesis occurred with the discovery that the main component of the ubiquitinated protein aggregates found in sALS patients was TAR DNA-binding protein 43 (TDP-43) (Arai et al., 2006; Neumann et al., 2006). Further histological studies have since confirmed that TDP-43 is present in the cytoplasmic aggregates of the majority of ALS patients including sporadic cases without pathogenic variants in the *TARDBP* gene, and in those with *C9ORF72* hexanucleotide repeat expansions (Giordana et al., 2010; Schipper et al., 2016; Takeuchi et al., 2016). The aggregation of TDP-43 in ubiquitin-positive cytoplasmic neuronal inclusions in the brain and spinal cord is now considered a pathological hallmark of ALS.

TDP-43 is a DNA/RNA binding protein composed of 414 amino acids, encoded by the *TARDBP* gene. Although usually concentrated in the nucleus, TDP-43 contains both a nuclear localization signal and a nuclear export signal (**Figure 2A**) and shuttles back and forth between the nucleus and cytoplasm (Ayala et al., 2008). TDP-43 functions as a regulator of gene expression and is involved in several RNA processing steps with roles in pre-mRNA splicing, regulation of mRNA stability, mRNA transport, translation, and the regulation of non-coding RNAs (Buratti and Baralle, 2010; Tollervey et al., 2011; Ratti and Buratti, 2016).

In 2008, dominant mutations in the *TARDBP* gene were identified as a primary cause of ALS, providing evidence that aberrant TDP-43 could be causative of neurodegeneration (Gitcho et al., 2008; Kabashi et al., 2008; Sreedharan et al., 2008; Van Deerlin et al., 2008; Yokoseki et al., 2008). To date, at least 48 variants in *TARDBP* have been associated with ALS (Lattante et al., 2013). The majority of these are missense mutations located in the glycine-rich region at the carboxy-terminal of the transcript. The carboxy-terminal region interacts with other heterogeneous ribonucleoproteins and is involved in pre-mRNA splicing regulation (Buratti et al., 2005; Neumann et al., 2006).

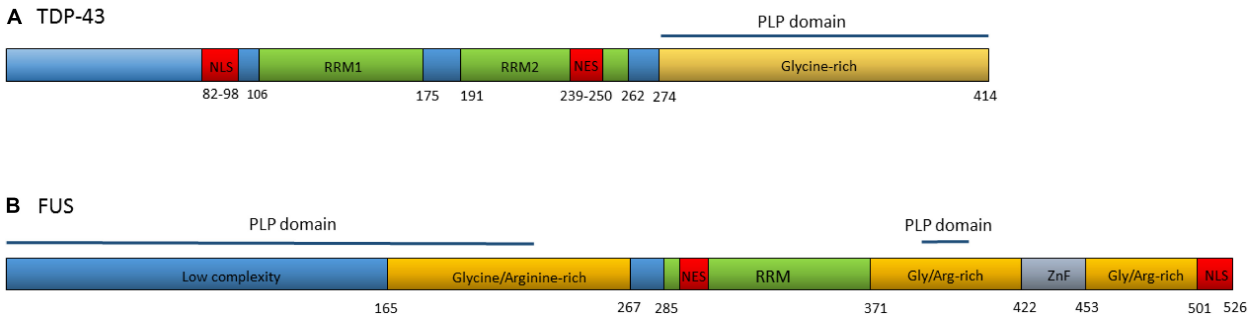

FIGURE 2 | (A) Domain structure of TDP-43. Numbers refer to amino acid positions. NLS is nuclear localization signal, NES is nuclear export signal, RRM1 and RRM2 are RNA recognition motifs. Prion-like protein (PLP) domain spans from amino acids 274–414. ALS associated mutations are clustered in the glycine-rich region. **(B)** Domain structure of the FUS protein. Numbers refer to amino acid positions. NLS is nuclear localization signal, NES is nuclear export signal, RRM is the RNA recognition motif, ZnF is the Zinc-Finger domain. Prion-like protein domains span from amino acids 1–239 and 391–407. A cluster or ALS associated mutations occur within the nuclear localization signal with others spread throughout the gene.

TDP-43 Disease Mechanisms

The cytoplasmic accumulation of TDP-43 is concomitant with a loss of nuclear TDP-43; this has led to proposed mechanisms of disease involving a loss of normal TDP-43 function in the nucleus, a toxic gain of function, or both. Various animal models have been generated to test the loss of function hypotheses. Homozygous TDP-43 null mice are not viable, demonstrating that TDP-43 is vital in embryonic development (Kraemer et al., 2010; Sephton et al., 2010; Wu et al., 2010). An inducible knockout in adult mice also proves lethal (Chiang et al., 2010). Mice heterozygous for *TARDBP* deletion displayed motor deficits but no degeneration of motor neurons and no reduction in TDP-43 protein levels (Kraemer et al., 2010).

Much of the evidence for the gain of function hypothesis comes from overexpression models. TDP-43 overexpression rodent models have consistently found that overexpression of both wild-type and mutant TDP-43 can cause a neurodegenerative phenotype (Ash et al., 2010; Kabashi et al., 2010; Liachko et al., 2010; Stallings et al., 2010; Wils et al., 2010; Xu et al., 2011). Overexpression of normal human TDP-43 in mouse models can cause fragmentation of the protein, resulting in the production of the signature 35 and 25 kDa fragments seen in human ALS cases (Wils et al., 2010).

Both the loss and overexpression of TDP-43 are causative of disease, highlighting the importance of tightly controlled regulation of this protein. There is increasing evidence that ALS may be caused by aberrant TDP-43 regulation. Expression of TDP-43 is autoregulated through a feedback mechanism by which the protein binds to a region within the 3′UTR of its own pre-mRNA when in nuclear excess, triggering the use of alternative polyadenylation signals and splicing events that result in mRNA transcripts that are degraded rather than translated (Avendaño-Vázquez et al., 2012; D'Alton et al., 2015; Koyama et al., 2016). The depletion of TDP-43 from the nucleus is thought to result in the continuous upregulation of TDP-43 synthesis (**Figure 3**) (Koyama et al., 2016). TDP-43 homeostasis is critical for normal cellular function. Excess TDP-43 in the cytoplasm may result in the formation of inclusion bodies leading to cellular dysfunction whilst nuclear depletion may induce widespread dysregulation of mRNA metabolism, with TDP-43 knockdown shown to lead to the differential splicing or expression of hundreds of targets (Highley et al., 2014; Colombrita et al., 2015; Klim et al., 2019).

In addition to the abnormal distribution and aggregation of TDP-43 in ALS, several post-translational modifications are associated with pathologic TDP-43, including ubiquitination, proteolytic cleavage, and phosphorylation. There is also evidence of less well characterized post-translational modifications of TDP-43 that include acetylation, sumoylation, disulfide bridge formation and others, as reviewed by Buratti (2018). The temporal sequence of these post-translational modifications and the role each plays in disease onset remains unclear. There is also accumulating evidence that ALS may share similarities to prion-like disorders in which the accumulation of misfolded proteins is self-propagating. Disease propagation can be seen clinically in ALS as a focal onset of disease that spreads to neighboring sites (Ravits et al., 2007; Brettschneider et al., 2013). Such a mechanism may be operating in ALS aided by the presence of TDP-43's prion-like protein domain (Nonaka et al., 2013; Mompeán et al., 2016).

FUS

In 2009, pathogenic variants in the gene encoding another RNA-binding protein, fused in sarcoma (FUS), were identified in a subset of ALS patients (Kwiatkowski et al., 2009; Vance et al., 2009). *FUS* variants are associated with early onset and juvenile ALS (Zou et al., 2013; Hübers et al., 2015a,b; Gromicho et al., 2017). FUS-ALS is characterized by pathological FUS aggregation, generally reported to occur only in patients with pathogenic variants in the *FUS* gene. TDP-43 aggregation is not commonly seen in FUS-ALS patients suggesting that the FUS disease pathway is independent of TDP-43 (Vance et al., 2009).

FUS encodes a ubiquitously expressed 526 amino acid protein belonging to the FET family of RNA binding proteins. FUS is predominantly localized to the nucleus under normal physiological conditions but crosses over to the cytoplasm, functioning in nucleocytoplasmic transport (Zinszner et al., 1997). FUS shares many physiological roles with TDP-43; playing a role in several aspects of gene expression

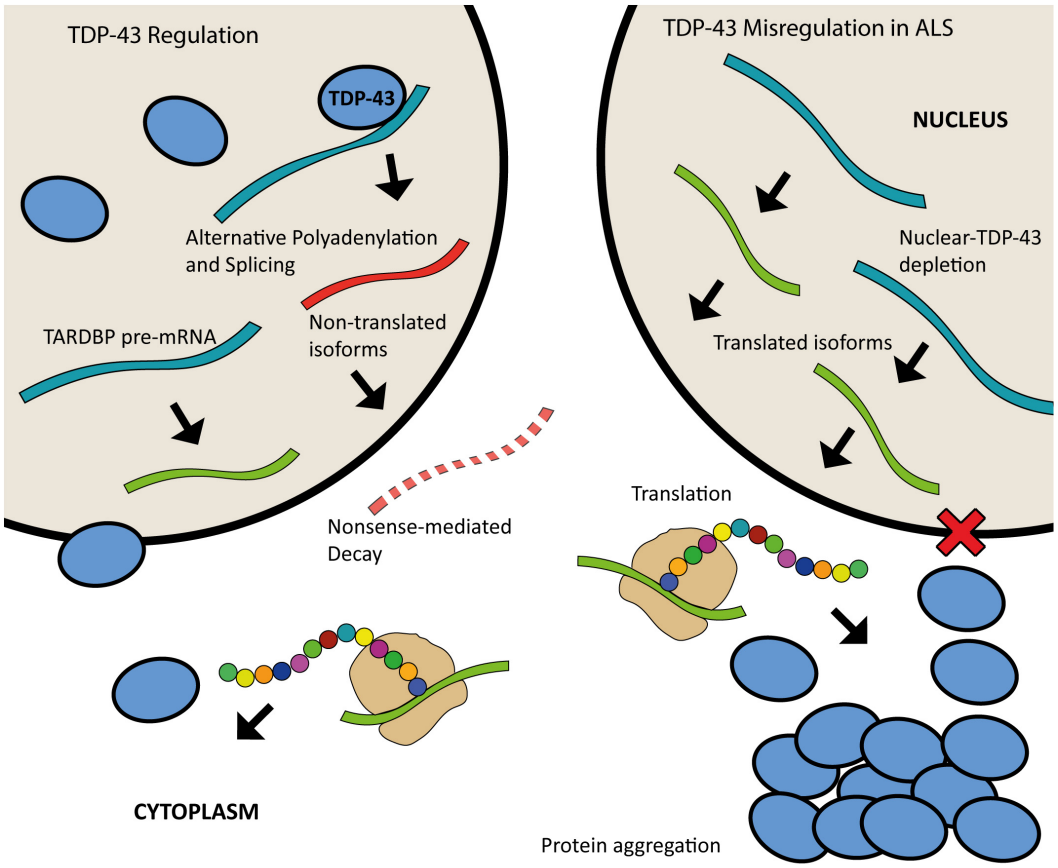

FIGURE 3 | Schematic of TDP-43 autoregulation and misregulation in ALS. When in nuclear excess, TDP-43 binds to a region in the 3′UTR of the TARDBP pre-mRNA leading to alternative polyadenylation and splicing; this produces mature mRNA transcripts that are subject to nonsense mediated decay. Nuclear depletion of TDP-43 as seen in ALS (right) leads to continuous upregulation of TDP-43 synthesis as more of the translated isoforms are produced.

including transcription, pre-mRNA splicing, RNA transport and translation regulation (Ratti and Buratti, 2016). Although they share many similarities, TDP-43 and FUS regulate different RNA targets and show different sequence binding specificity (Lagier-Tourenne et al., 2012; Colombrita et al., 2015). Additionally, FUS is involved in DNA repair mechanisms including both homologous recombination during DNA double-strand break repair and in non-homologous end joining (Baechtold et al., 1999; Mastrocola et al., 2013; Wang W.-Y. et al., 2013). FUS also plays a role in the formation of paraspeckles providing cellular defense against various types of stress (Hennig et al., 2015).

Over 50 autosomal dominant *FUS* variants have now been identified in ALS patients. The majority are missense mutations, although in rare cases insertions, deletions, splicing, and nonsense mutations have been reported (Lattante et al., 2013). Many of the pathogenic variants are clustered within the nuclear localization signal and lead to the redistribution of FUS to the cytoplasm (Niu et al., 2012; Vance et al., 2013). Others occur in the glycine and arginine-rich regions, the prion-like domain and the 3′UTR (**Figure 2B**) (Shang and Huang, 2016). Variants within some regions appear to increase the propensity of the protein to form solid aggregates, pointing to various pathomechanisms operating in FUS related ALS (Nomura et al., 2014).

FUS Disease Mechanisms

As with TDP-43, debate continues as to the extent to which a loss of function or a gain of function mechanism causes disease in FUS-ALS. FUS loss of function theories suppose that the pathologic cytoplasmic redistribution of FUS renders it incapable of carrying out its functions in the nucleus. A homozygous *Fus* knockout mouse model was developed in 2015, and while the mice survived into adulthood, they did not show ALS-like phenotypes, suggesting that loss of FUS is not sufficient to cause ALS (Kino et al., 2015). This result was followed by development of further models in which FUS was conditionally removed from the motor neurons of mice, with no significant loss of motor neurons or denervation (Sharma et al., 2016). However, the findings were contradictory when Drosophila *Fus* knockdown models were used, whereby neuronal degeneration and locomotive defects followed the knockdown of the *FUS* ortholog *Cabeza* (Sasayama et al., 2012).

There is strong evidence for gain of function mechanisms operating in FUS-ALS. A transgenic mouse model overexpressing

wild-type human FUS reportedly developed an aggressive phenotype of motor neurodegeneration and evidence of cytoplasmic FUS accumulation (Mitchell et al., 2013). There is debate as to whether toxicity is primarily mediated by the FUS aggregates directly or via an increase in soluble FUS in the cytoplasm after its redistribution. There is some evidence that toxicity may be caused by FUS aggregates directly. Cytoplasmic FUS accumulation and a severe motor phenotype were observed in transgenic mouse models that express aggregate-prone FUS variants lacking the ability to recognize and bind RNA (Shelkovnikova et al., 2013; Robinson et al., 2015). Additionally, as seen with TDP-43, there are indications of a propagating mechanism of disease in FUS-ALS, possibly mediated by its prion-like protein domain (Lee and Kim, 2015; Feuillette et al., 2017). There is also evidence that soluble cytoplasmic FUS may be toxic. Several rodent models in which neurodegeneration was observed have displayed increased cytoplasmic FUS, without the formation of aggregates (Huang et al., 2011; Scekic-Zahirovic et al., 2016; Sharma et al., 2016). Cytoplasmic FUS distribution also alters stress granule dynamics (Vance et al., 2013; Lenzi et al., 2015). Some have proposed that FUS aggregation may be a compensatory mechanism protecting cells from potentially toxic increases in soluble cytoplasmic FUS. Rather than purely pathologic, the propensity of FUS to aggregate is important in normal cellular functions (Hennig et al., 2015). Impaired cellular function can also be the direct result of pathogenic *FUS* variants that have been reported to cause splicing defects, DNA damage and to compromise FUS autoregulation (Wang W.-Y. et al., 2013; Zhou Y. et al., 2013; Qiu et al., 2014; Rulten et al., 2014).

C9ORF72

In 2011, the most common inherited cause of ALS in European populations, a hexanucleotide repeat expansion (GGGGCC) in the non-coding region of the *C9ORF72* gene, was discovered (DeJesus-Hernandez et al., 2011; Renton et al., 2011). Typically, 5–10 copies of this hexanucleotide repeat expansion are present in the gene, but ALS patients with the expansion may have hundreds to thousands of repeats. This hexanucleotide repeat expansion occurs in approximately 34% of fALS and 5% of sALS cases in European populations, but is less frequent in Asian populations (Zou et al., 2017). The function of the *C9ORF72* product is poorly understood, but recent reports have pointed toward functions in regulating endosomal trafficking and autophagy (Farg et al., 2014; Nassif et al., 2017). Several *C9ORF72* deficient mouse models have shown immune dysregulation pointing to a possible function of C9ORF72 in the immune system (Atanasio et al., 2016; Burberry et al., 2016).

C9ORF72 Disease Mechanisms

The *C9ORF72* mRNA and protein levels were reportedly decreased in ALS patients with repeat expansions, leading to the hypotheses that a loss of the protein may be implicated in disease (Waite et al., 2014; Xiao et al., 2015). A *C9ORF72* conditional knockout mouse model was generated to test this hypothesis but the animals were not found to show evidence of motor neuron degeneration or motor deficits, indicating that a loss of C9ORF72 function alone was insufficient to cause motor neuron disease (Koppers et al., 2015). Furthermore, the targeted knockdown of *C9ORF72* RNA is well tolerated in mice and in ALS patient induced pluripotent stem cell (iPSC) derived neurons (Donnelly et al., 2013; Lagier-Tourenne et al., 2013). It is therefore supposed that loss of *C9ORF72* function alone is not a major cause of C9 related frontotemporal dementia or ALS.

There is evidence for several toxic gain of function mechanisms underpinning C9ORF72-ALS. The G rich nature of the repeats makes the transcript susceptible to the formation of highly stable G-quadruplex secondary structures that trigger abnormal interactions with a range of proteins (Fratta et al., 2012). Although numerous pathways may be misregulated in C9ORF72-ALS, RNA misprocessing has consistently appeared as a key pathway affected. Firstly, processing of the expanded transcript itself is altered. The C9ORF72 transcript contains two alternatively used first exons (1a and 1b) with the repeat expansion residing in the intron between them. The various isoforms produced from the transcript contain one or both of the exons with the presence of the repeat expansion favoring transcription from exon 1a. This leads to an increase in the proportion of transcripts produced that contain the repeat expansion (Sareen et al., 2013). Other misregulated RNA processing events affecting the repeat containing transcripts have also been described including abortive transcription, decreased splicing of the repeat containing intron and nuclear aggregation (Barker et al., 2017). Additionally, a portion of the repeat-containing transcripts are subject to repeat-associated non-ATG (RAN) translation, resulting in the production of abnormal dipeptide repeat proteins that also form neuronal inclusions in the CNS and may contribute to disease pathogenesis via various mechanisms (Ash et al., 2013; Gendron et al., 2013). Furthermore, the expanded repeat causes several downstream effects on RNA processing. RNA transcripts containing the repeat expansion form discrete nuclear structures referred to as RNA foci (DeJesus-Hernandez et al., 2011) that are found in the majority of C9ORF72-ALS patients (Schipper et al., 2016). Toxicity may arise as these RNA foci are able to aberrantly interact with and sequester various RNA-binding proteins, impairing their function and leading to more general effects on RNA expression and splicing (Todd and Petrucelli, 2016). Consensus has not yet been achieved on the extent to which each of these mechanisms contributes to disease progression.

Genes With Minor Involvement in ALS

The increasing use of next-generation sequencing of family pedigrees as well as large cohorts of ALS patients has led to the discovery of rare genetic variants associated with ALS in many other genes, as shown in **Table 1**. These variants have been found primarily in genes that influence RNA processing, protein homeostasis and cytoskeletal dynamics. Although rare, they provide hints as to some of the pathogenic mechanisms underpinning ALS. The link between a particular gene variant and disease is not always clear due to the small number of patients harboring some of the variants, as well as study size limitations leading to inconclusive results. For example, several studies have reported that DNA variants in the paraoxonase locus are associated with sALS (Saeed et al., 2006; Landers et al.,

TABLE 1 | Genes thought to be causative of ALS.

Involved in	Gene	Protein	Functions include	References
RNA processing	TARDBP	TAR DNA-Binding Protein, 43-Kd	Splicing regulation, RNA transport, miRNA biogenesis	Rutherford et al., 2008; Sreedharan et al., 2008; Neumann, 2009
	FUS	Fused in sarcoma	Splicing regulation, RNA transport, maintenance of genomic integrity, miRNA processing	Kwiatkowski et al., 2009; Vance et al., 2009
	ANG	Angiogenin	RNA processing, neurite outgrowth, vascularisation, stress granule formation	Greenway et al., 2006; Wu et al., 2007
	SETX	Senataxin	DNA/RNA metabolism and helicase activity	Chen et al., 2004; Hirano et al., 2011
	MATR3	Matrin 3	RNA processing, chromatin organization	Johnson et al., 2014b
	ATXN2	Ataxin 2	RNA processing (interacts with TDP-43), endocytosis, modulates mTOR signaling	Elden et al., 2010; Sproviero et al., 2016
	TAF15	TATA-binding protein-associated factor 2N	transcription initiation; RNA polymerase II	Couthouis et al., 2011; Ticozzi et al., 2011
	EWSR1	EWS RNA Binding Protein 1	RNA splicing, transcriptional repressor,	Couthouis et al., 2012
	hnRNPa1	Heterogeneous nuclear ribonucleoprotein A1	mRNA processing, splicing, and transport	Kim et al., 2013; Naruse et al., 2018
	hnRNPA2B1	Heterogeneous nuclear ribonucleoproteins A2/B1	mRNA processing, splicing, and transport	Kim et al., 2013; Fifita et al., 2017
	ELP3	Elongator complex protein 3	Protein synthesis, maturation of projection neurons	Simpson et al., 2009
Protein Trafficking and degradation	C9ORF72	Guanine nucleotide exchange C9orf72	Transcription, splicing regulation, endosomal trafficking, autophagy	DeJesus-Hernandez et al., 2011; Renton et al., 2011
	ALS2	Alsin	Endosomal dynamics and trafficking, neurite outgrowth	Hadano et al., 2001; Yang et al., 2001
	VAPB	Vesicle-associated membrane protein-associated protein B/C	Vesicle trafficking	Nishimura et al., 2004; Sanhueza et al., 2013
	CHMP2B	Charged multivesicular body protein 2b	Multivesicular body formation, protein trafficking to lysosomes	Parkinson et al., 2006; Cox et al., 2010
	FIG4	Polyphosphoinositide phosphatase	Endosomal trafficking to Golgi network, autophagy regulation	Chow et al., 2009; Osmanovic et al., 2017; Bertolin et al., 2018
	UBQLN2	Ubiquilin-2	Protein degradation via UPS	Deng et al., 2011; Gellera et al., 2013
	SQSTM1	Sequestosome-1 (p62)	Protein degradation via UPS and autophagy	Fecto et al., 2011; Rubino et al., 2012; Hirano et al., 2013
	SIGMAR1	Sigma non-opioid intracellular receptor 1	Lipid transport from ER, mitochondrial axonal transport, BDNF and EGF signaling	Luty et al., 2010; Al-Saif et al., 2011; Ullah et al., 2015
	OPTN	Optineurin	Golgi maintenance, membrane trafficking, exocytosis, autophagy	Maruyama et al., 2010; Tümer et al., 2012; Pottier et al., 2018
	VCP	Valosin Containing Protein	Protein degradation via UPS, autophagy, membrane fusion	Forman et al., 2006; Johnson et al., 2010
	TBK1	Tank Binding Kinase 1	Autophagy, innate immunity signaling	Borghero et al., 2015; Cirulli et al., 2015; Oakes et al., 2017
Cytoskeletal and axonal dynamics	DCTN1	Dynactin subunit 1	Axonogenesis, microtubule anchoring, ER to Golgi transport, spindle formation, vesicle transport, cilia formation	Münch et al., 2004, 2005; Takahashi et al., 2008; Liu et al., 2014
	PFN1	Profilin 1	Cytoskeletal signaling, regulates actin polymerization	Wu et al., 2012; Smith et al., 2015
	SPG11	Spatacsin	Cytoskeletal stability, regulating synaptic vesicle transport	Orlacchio et al., 2010; Daoud et al., 2012
	TUBA4A	Tubulin α-4A chain	Component of microtubules	Smith et al., 2014; Pensato et al., 2015

(Continued)

TABLE 1 | Continued

Involved in	Gene	Protein	Functions include	References
	NEFH	Neurofilament heavy polypeptide	Maintenance of neuronal caliber, intracellular transport	Figlewicz et al., 1994; Al-Chalabi et al., 1999
	PRPH	Peripherin	Cytoskeletal protein, neurite elongation, axonal regeneration	Gros-Louis et al., 2004; Leung et al., 2004; Corrado et al., 2011
	NEK1	NIMA (Never In Mitosis Gene A)-Related Kinase 1	Cilia formation, DNA-damage response, microtubule stability, neuronal morphology, axonal polarity	Brenner et al., 2016; Kenna et al., 2016; Nguyen et al., 2018; Shu et al., 2018
Mitochondria	CHCHD10	Coiled-Coil-Helix-Coiled-Coil-Helix Domain Containing 10	Mitochondrial protein, cristae morphology, oxidative phosphorylation	Bannwarth et al., 2014; Chaussenot et al., 2014; Johnson et al., 2014a
	C19ORF12	Protein C19orf12	Mitochondrial protein	Deschauer et al., 2012
Other	SOD1	Superoxide dismutase [Cu-Zn]	Cytosolic Antioxidant	Rosen et al., 1993
	ERBB4	Receptor tyrosine-protein kinase erbB-4	Neuronal cell mitogenesis and differentiation	Takahashi et al., 2013
	SS18L1	Calcium-responsive transactivator	Neuron specific chromatin remodeling	Teyssou et al., 2014
	PNPLA6	Neuropathy target esterase	Regulation of neuronal membrane composition	Rainier et al., 2008
	PON1-3	Paraoxonase 1-3	Enzymatic breakdown of nerve toxins	Saeed et al., 2006; Wills et al., 2009; Ticozzi et al., 2010
	DAO	D-amino-acid oxidase	Regulates D-serine levels, N-methyl-D-aspartate receptor regulation	Mitchell et al., 2010; Morgan et al., 2017
	CHRNA3,4,B4	Neuronal acetylcholine receptor subunit α-3, α-4, β-4	Cholinergic Neurotransmission	Sabatelli et al., 2009, 2012
	ALS3	ALS3	Disulfide redox protein	Hand et al., 2002
Unknown	ALS7	Unknown	Unknown	Sapp et al., 2003
	ALS6-21	Unknown	Unknown	Butterfield et al., 2009
	ALS-FTD	Unknown	Unknown	Dobson-Stone et al., 2013

2008; Valdmanis et al., 2008). However, these findings were not replicated when a larger genome wide meta-analysis was undertaken (Wills et al., 2009).

In addition to the large number of gene variants thought to be primary causes of ALS, a number of variants appear to influence ALS phenotype or susceptibility. Common variants of the *UNC13A* gene, for example, have been associated with susceptibility to ALS and shorter survival time of patients (Diekstra et al., 2012). Intermediate length trinucleotide repeat expansions of the both the *ATXN1* and *ATXN2* genes also increase the risk of disease, particularly so for *C9ORF72* expansion carriers in the case of *ATXN1* (Sproviero et al., 2016; Lattante et al., 2018). A copy number variation of the *EPHA3* gene, in contrast, has been flagged as a potential protective factor for ALS (Uyan et al., 2013). Many other potential genetic modifiers of ALS risk have been identified, including variations in genes implicated in detoxification pathways, highlighting the potential interplay of environmental and genetic factors (Dardiotis et al., 2018). As well as gene variants, variations in gene expression can also alter ALS disease susceptibility or phenotype. Although no association was found between any of the 654 SNPs occurring in the *EPHA4* gene and ALS susceptibility, disease onset and survival inversely correlated with EPHA4 expression (Van Hoecke et al., 2012).

PROPOSED MECHANISMS OF DISEASE

Despite decades of research, causative pathogenic mechanisms in ALS still remain unclear, especially in sporadic cases. It is likely that multiple factors, rather than a single initiating event contribute to the development and progression of the disease. Furthermore, genetic and phenotypic variation between patients makes it difficult to uncover and draw conclusions regarding pathogenic mechanisms of ALS in general. The large number of genes and cellular processes implicated in ALS has led to the proposal of many disease mechanisms operating (**Figure 4**). These include disturbances in RNA metabolism, impaired protein homeostasis, nucleocytoplasmic transport defects, impaired DNA repair, excitotoxicity, mitochondrial dysfunction, oxidative stress, axonal transport disruption, neuroinflammation, oligodendrocyte dysfunction, and vesicular transport defects. Clarification is needed on the timing and extent to which each of these mechanisms contributes to disease pathogenesis.

Altered RNA Metabolism

There was a shift in focus to RNA dysregulation as a key pathomechanism in ALS with the identification of disease-causing variations in RNA-binding protein genes, *TARDBP* and

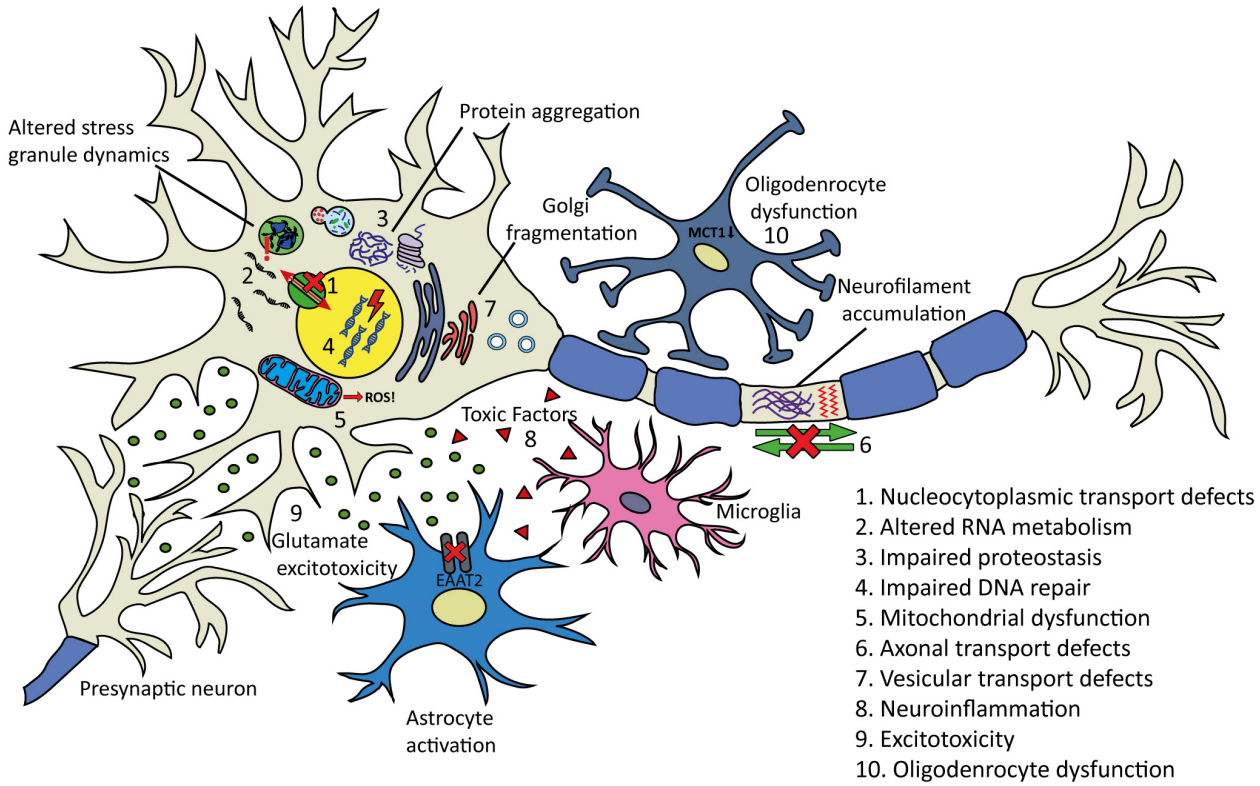

FIGURE 4 | Proposed pathogenic mechanisms and pathology in ALS. (1) Nucleocytoplasmic transport defects including altered transport of RNA molecules and RNA-binding proteins. (2) Altered RNA metabolism. RNA-binding proteins including TDP-43 or FUS may become mislocalized in the cytoplasm leading to altered transcription and splicing. Stress granule dynamics are also affected. (3) Proteostasis is impaired with aggregating proteins including TDP-43 accumulating in the cytoplasm. There is evidence that the two main protein clearance pathways, autophagy and the UPS may be involved. (4) Impaired DNA repair: several ALS-linked genes including *FUS*, *TARDBP*, *TAF15*, *SETX*, and *EWSR1* are involved in DNA repair. (5) Mitochondrial dysfunction resulting in the increased formation of reactive oxygen species (ROS) has been proposed as an initiating factor in ALS. Several ALS-linked proteins including SOD1, TDP-43, and FUS interact with mitochondria. (6) Axonal transport defects have been implicated in ALS pathogenesis. Neuropathological evidence has shown evidence of this including neurofilament accumulation and cytoskeletal disorganization. (7) Several ALS-linked genes including *OPTN*, *VAPB*, *CHMP2B*, and *UNC13A* are involved in vesicular transport. Impaired vesicular trafficking can lead to protein accumulation and golgi fragmentation which has been observed in ALS patients. (8) Neuroinflammation: the secretion of inflammatory proteins by activated microglia leads to the potentially neurotoxic activation of astrocytes, which may contribute to the death of neurons and oligodendrocytes. (9) Excitotoxicity: glutamate receptor overstimulation has been proposed to occur via several mechanisms including increased synaptic glutamate release, alterations to AMPA receptors and reduced clearance of glutamate by astrocytes. (10) Oligodendrocyte dysfunction may lead to reduced support for neurons. Changes in lactate production and transport via MCT1 have been implicated.

FUS. RNA-binding proteins are involved in several aspects of RNA metabolism, including splicing, transcription, transport, translation, and storage in stress granules. The number of RNA-binding proteins directly involved in neurodegeneration has grown to include *EWS* and *TAF15* (involved in FTD) (Neumann et al., 2011) *hnRNPA1* (Kim et al., 2013), and *MATR3* (Johnson et al., 2014b). A variety of RNA binding factors are found sequestered in association with the hexanucleotide repeat expansion in the *C9ORF72* gene transcript (Lee et al., 2013; Mori et al., 2013; Cooper-Knock et al., 2014). These discoveries have led to an increased interest in the role of RNA metabolism in neurodegenerative diseases.

Interestingly, many of the ALS-linked RNA-binding proteins contain prion-like domains that are involved in stress granule formation or dynamics, including TDP-43, FUS, TAF15, ESWR1, hnRNPA1, and hnRNPA2B1. Stress granules are transient RNA/protein complexes formed under cellular stress that are able to sequester specific mRNAs and prevent their translation. These granules facilitate cell survival by the translational arrest of non-essential transcripts and pro-apoptotic proteins when under stress (Protter and Parker, 2016). Prion-like domains are thought to be vital for the reversible assembly of stress granules due to their capacity for forming multiple transient weak interactions (Harrison and Shorter, 2017). Interest in the involvement of stress granules in ALS pathogenesis has recently increased.

Nucleocytoplasmic Transport Defects

The mislocalization to the cytoplasm and nuclear depletion of RNA-binding proteins such as TDP-43 and FUS in ALS pathology suggest nuclear transport defects as a mechanism contributing to ALS pathogenesis. Recent studies into the consequences of the *C9ORF72* hexanucleotide repeat expansion have contributed to the growing evidence of nucleocytoplasmic transport defects in ALS. In a genetic screen in Drosophila to

identify modifiers of C9ORF72 toxicity, 18 genetic modifiers involved in nucleocytoplasmic transport and RNA export were identified, highlighting this system as a primary target of hexanucleotide repeat expansion related toxicity (Freibaum et al., 2015). For a review of the role of nucleocytoplasmic transport in ALS see (Kim and Taylor, 2017).

Impaired Proteostasis

The accumulation of damaged proteins contributes to several neurodegenerative diseases including Alzheimer's, Huntington's and Parkinson's diseases, and has also emerged as a key characteristic in ALS. The most commonly mutated ALS genes (*SOD1*, *C9ORF72*, *TARDBP*, and *FUS*) all give rise to proteins that are found to aggregate in the neurons of ALS patients. Although protein aggregation is central to ALS pathology, questions remain about the formation, role and toxicity of these aggregates.

There is evidence that disruption of the two main protein clearance pathways, autophagy and the Ubiquitin-proteasome system (UPS) are involved in ALS pathogenesis. Autophagy is an intracellular pathway involved in the degradation and recycling of long-lived proteins and cytoplasmic organelles and is important in maintaining homeostasis in multicellular organisms (Kelekar, 2006). In the UPS pathway, proteins are marked for degradation by ubiquitination before being recognized and degraded by the proteasome (Finley, 2009). Several ALS associated genes encode proteins involved in autophagy or the UPS including *C9ORF72*, *OPTN*, *SQSTM1*, *VCP*, and *UBQLN2* (Majcher et al., 2015; Ying and Yue, 2016; Nassif et al., 2017). Given the role of ubiquitination in marking proteins for degradation, it is not surprising that pathological protein inclusions in ALS are ubiquitin-positive. Ubiquitination may be a critical factor in keeping TDP-43 and other protein levels in neurons within a healthy physiological range and the persistence of ubiquitin-positive aggregates is suggestive of impaired or overwhelmed protein clearance systems.

Impaired DNA Repair

Impairment of DNA repair is another suggested mechanism that may contribute to ALS pathogenesis. Two of the best studied ALS linked proteins, TDP-43 and FUS, function in the prevention or repair of transcription-associated DNA damage (Hill et al., 2016). FUS in particular seems to play an important role in this regard and is involved in the repair of double-stranded DNA breaks via both homologous recombination and non-homologous end-joining repair mechanisms (Mastrocola et al., 2013; Wang W.-Y. et al., 2013). Variations in the genes of other ALS-linked RNA-binding proteins, including *TAF15*, *SETX*, and *EWSR1* have also been linked to impaired DNA damage repair, further implicating the breakdown of this process in ALS pathogenesis (Paronetto et al., 2011; Skourti-Stathaki et al., 2011; Izhar et al., 2015).

Mitochondrial Dysfunction and Oxidative Stress

Oxidative stress has been suggested as a primary initiating factor in ALS pathogenesis. Oxidative stress occurs when a cell's antioxidant capacity is superseded by its rate of production of reactive oxygen species. When antioxidants do not neutralize reactive oxygen species, they can seriously damage macromolecules such as DNA, proteins and phospholipids. There is morphological evidence of oxidative damage, including lipid peroxidation and protein glycoxidation in the spinal cords of sALS patients (Shibata et al., 2001).

Mitochondria produce the majority of reactive oxygen species with large amounts of superoxide radicals generated as a by-product of cellular respiration, leading researchers to investigate potential mitochondria-related pathogenic mechanisms in ALS. These have included the disruption of mitochondrial function by aggregated products of ALS related genes, impaired clearance of damaged mitochondria by autophagy and dysfunction and mitochondrial damage due to aberrant RNA processing (Carrì et al., 2017). The role of SOD1 as a cytosolic anti-oxidative enzyme was also suggestive of a role for oxidative stress in ALS pathogenesis. Interestingly, mutant SOD1 is not generally thought to cause disease through loss of its antioxidative function, but rather through interactions that upregulate reactive oxygen species as well as through altered interactions with mitochondria and other proteins (Cozzolino et al., 2009).

Both oxidative stress and RNA misregulation occur in ALS pathogenesis and there are dual views regarding mechanism and causation. One hypothesis is that oxidative stress may cause RNA dysregulation. There is some evidence for this with oxidative stress shown to cause mislocalization and increased aggregation tendency of regulatory RNA proteins TDP-43 and FUS (Vance et al., 2013; Cohen et al., 2015). Others have suggested that RNA dysregulation may be causative of oxidative stress and mitochondrial damage that could occur via several mechanisms. Damage may be induced through direct interaction of ALS associated proteins with mitochondria, leading to increased formation of reactive oxygen species (Pickles et al., 2016). Altered interactions of RNA-binding proteins such as TDP-43 and FUS with non-mitochondrial proteins may also contribute to mitochondrial dysfunction. FUS, for example, is thought to localize in the mitochondria through interactions with the mitochondrial chaperone protein HSP60 (Deng et al., 2015). Yet another possibility is that pathogenic RNA binding proteins in ALS, such as TDP-43 may directly affect the regulation of mRNA coding for proteins involved in mitochondrial physiology. There is evidence for this hypothesis with overexpression, underexpression or mutations in TDP-43 shown to influence mitochondrial dynamics, causing dysfunction (Wang W. et al., 2013).

Axonal Transport Defects

Axonal transport involves the movement and spatiotemporal distribution of intracellular cargo such as lipids, proteins, mRNA, membrane-bound vesicles, and organelles along the axon. It is important in maintaining the structure and function of the cell and in the long-distance communication between the cell body and synaptic terminals. Axonal transport defects are commonly seen in neurodegenerative diseases (Millecamps and Julien, 2013). Early neuropathological evidence consistent with axonal transport defects in ALS came from

post-mortem studies. These revealed abnormal accumulations of neurofilaments, mitochondria and lysosomes as well as spheroids containing vesicles, lysosomes, mitochondria, neurofilaments, and microtubules (Hirano et al., 1984a,b; Corbo and Hays, 1992; Rouleau et al., 1996; Sasaki and Iwata, 1996). Axonal transport was later found to be impaired in several *SOD1* mouse models (Zhang et al., 1997; Williamson and Cleveland, 1999; Ligon et al., 2005; Bilsland et al., 2010). Pathogenic variants in axonal transport machinery and cytoskeletal genes such as those in *TUBA4A* have since been indicated as a primary cause of ALS in rare cases (Smith et al., 2014).

There is evidence to suggest that TDP-43 may be involved in axonal transport defects seen in ALS. TDP-43 facilitates the delivery of mRNA via active axonal transport (Akira et al., 2016), and pathogenic variants in TDP-43 impair this movement in Drosophila, mouse cortical neurons and in ALS patient stem cell-derived neurons (Alami et al., 2014). In mouse models, axonal transport defects were observed early in disease progression, before symptom onset, suggesting a role in pathogenesis (Williamson and Cleveland, 1999).

Vesicular Transport Defects

Several proteins involved in vesicular transport have been linked to ALS and FTD, implicating defective vesicular transport in ALS pathogenesis. These include *OPTN*, *VAPB*, *CHMP2B*, and *UNC13A* (Cox et al., 2010; Urwin et al., 2010; Vidal-Taboada et al., 2015; Chadi et al., 2017; Sundaramoorthy et al., 2017). Prolonged inhibition of vesicular trafficking from the golgi to the plasma membrane can lead to protein accumulation and golgi fragmentation (Zolov and Lupashin, 2005; Zhou Z. et al., 2013; Sundaramoorthy et al., 2015), the latter being a prominent histopathological feature seen in ALS patients (Gonatas et al., 1992; Mourelatos et al., 1994; Fujita and Okamoto, 2005; Fujita et al., 2007). Evidence indicates that fragmentation of the golgi apparatus occurs early in the pathological cascade of disease, suggesting that it may be a trigger of neurodegeneration, rather than a consequence (Gonatas et al., 2006; Dis et al., 2014).

Neuroinflammation

There is increasing evidence that neuroinflammation plays a role in ALS pathophysiology. Neuroinflammation associated with neuronal loss is characterized by microglia and astrocyte activation, overproduction of inflammatory cytokines and infiltration of T lymphocytes (Komine and Yamanaka, 2015). There is strong evidence for the activation of microglia in ALS (Turner et al., 2004; Corcia et al., 2012). Microglia are able to detect insults and injuries that disrupt brain homeostasis, responding with a change in morphology and the release of cytokines and chemokines to clear pathogens or debris. The secretion of inflammatory proteins by activated microglia leads to the potentially neurotoxic activation of astrocytes that may contribute to the death of neurons and oligodendrocytes (Liddelow et al., 2017). Astrocytes provide trophic support for neurons, prune synapses and provide other homeostatic functions in the CNS (Clarke and Barres, 2013). The potential of microglia to play a direct role in ALS pathogenesis was highlighted by the identification of several ALS linked genes that influence the function of, and are highly expressed in microglia, including *C9ORF72*, *TBK1*, and *PGRN* (Irwin et al., 2008; Freischmidt et al., 2015; Lall and Baloh, 2017). Immune cells have been implicated both in protective effects on neuronal survival and in exerting deleterious effects, depending on the stage of disease progression (Liu and Wang, 2017).

Excitotoxicity

Excitotoxicity is a pathological process of glutamate receptor overstimulation resulting in neuronal damage or degeneration (Dong et al., 2017). Glutamate acts as a neurotransmitter and is released from presynaptic terminals to act on post- and pre-synaptic glutamate receptors. In the CNS, extracellular glutamate levels are kept low with intracellular levels being much higher. When the extracellular glutamate level is elevated, neurons are damaged through excessive stimulation of glutamate receptors. Excitotoxicity has long been suspected as a mediator of disease in ALS. Oral intake of excitotoxins is responsible for particular forms of motor neuron disease, suggesting motor neurons may be particularly vulnerable to excitotoxicity (Spencer et al., 1986). Current evidence for altered glutamate levels in ALS patients is contradictory with results varying across studies (Van Cutsem et al., 2006). The evidence for altered glutamatergic signaling in ALS comes primarily from electrophysiological studies (de Carvalho et al., 2017).

There are several mechanisms by which the dysregulation of glutamatergic transmission has been proposed to occur. Direct mechanisms include the increased synaptic release of glutamate or insufficient re-uptake from the synaptic cleft. Alterations in glutamate receptor expression or function including alterations to AMPA receptors leading to increased influx of Ca^{2+} has also been proposed (Kwak et al., 2010). Reduced expression and activity of glutamate receptor EAAT2 on glial astrocytes may also contribute to excitotoxicity via reduced glutamate clearance (Boston-Howes et al., 2006). Other hypotheses of excitotoxic causality include altered regulation by interneuron populations, intrinsic excitability of motor neurons or the release of intracellular glutamate from lethally damaged neurons, astrocytes or microglia. Much research has gone into the study of these mechanisms in ALS with mixed conclusions, as reviewed by King et al. (2016). The question remains as to whether altered glutamatergic signaling in ALS patients is directly pathogenic or whether it is driven by other factors. While the use of Riluzole has shown modest benefit to some ALS patients by addressing excitotoxicity, numerous other drugs targeting glutamatergic transmission have been unsuccessful in clinical trials.

Oligodendrocyte Dysfunction

There is growing evidence supporting the contribution of non-neuronal cells, such as oligodendrocytes, to ALS pathogenesis. Oligodendrocytes are the myelinating cells in the CNS responsible for producing the myelin sheath that insulates the axons of nerves and neurons (Bradl and Lassmann, 2010). Gray matter oligodendrocytes are not involved in myelin sheath formation and are thought to play a role in providing metabolic support to neurons (Nave, 2010; Philips and Rothstein, 2017).

Oligodendrocytes are proposed to contribute to axonal degeneration through changes in the production of the metabolite lactate. There is some evidence for this with the dominant lactate transporter in the brain, MCT1, that is highly enriched within oligodendroglia, reduced in the motor cortex in mouse models of ALS and in ALS patients (Lee et al., 2012). $SOD1^{G93A}$ transgenic mice also have impaired function and extensive degeneration of gray matter oligodendrocytes in the spinal cord, with oligodendrocyte precursors failing to fully differentiate (Kang et al., 2013). It remains unclear whether these changes precede neuronal loss or are a consequence of it. Alterations in myelin structure in the spinal cords of mice occur presymptomatically and early in disease progression indicating possible contributions to causality (Niebroj-Dobosz et al., 2007; Kang et al., 2013).

APPROACHES TO TREATMENT

History

The current standard of care for ALS involves multidisciplinary symptom management including nutritional and respiratory support. The most widely used treatment for ALS is Riluzole. This drug was first approved in 1995 and is only mildly effective, prolonging survival for up to 2–3 months in some patients and exerting a beneficial effect only in the first 6 months of therapy (Bensimon et al., 1994; Cetin et al., 2015). When launched, Riluzole was hypothesized to act via the modulation of glutamatergic transmission (Bensimon et al., 1994). Research into the mechanism of action of Riluzole has consistently shown that its effects on glutamate receptors are limited, and that the mechanisms of action are likely more varied and complex (Bellingham, 2011). This may help to explain why other anti-glutamatergic compounds such as Ceftriaxone, Memantine, and Talampanel have failed to show efficacy in ALS clinical trials (de Carvalho et al., 2010; Pascuzzi et al., 2010; Cudkowicz et al., 2014).

During the years since Riluzole was launched, over 60 other molecules have been investigated as potential treatments for ALS (Petrov et al., 2017). Treatments reaching clinical trials have overwhelmingly been anti-inflammatory, anti-oxidative, anti-glutamatergic, neuroprotective, and neurotrophic compounds. The most commonly used primary outcome measure to evaluate the efficacy of treatments in ALS is the ALSFRS-R scale. Scores on the scale are arrived at through a 12-question form that evaluates the gross motor, fine motor, bulbar, and respiratory function of patients (Cedarbaum et al., 1999). The vast majority of compounds tested have failed to demonstrate efficacy in human clinical trials, most of which measured differences in ALSFRS-R scores or survival time.

In 2017, the first new treatment for ALS in over two decades was approved for use in Japan, South Korea and the United States. Radicava (Edaravone) is an antioxidative compound proposed to function by reducing oxidative stress, although its exact mechanism is unknown. Edaravone was initially approved for use in Japan for the treatment of cerebral embolism. Efficacy of Edaravone for the treatment of ALS was tested in two phase III clinical trials and was determined by the change in ALSFRS-R scores compared to baseline. The first double-blind placebo-controlled trial (MCI-186-16) reported no significant differences between treatment and placebo groups (Abe et al., 2014). After a *post hoc* analysis of the results was carried out, a follow-up study (MCI-186-19) in a more narrowly defined patient population was undertaken. This trial reported a modest but statistically significant difference in ALSFRS-R scores, with Edaravone treated patients showing reduced functional loss when compared to patients receiving a placebo after 6 months of treatment (Sawada, 2017). Concomitant use of Riluzole was allowed during this study. The majority of treatments investigated for ALS thus far have been small molecules. Although success has been limited, there is hope that alternative approaches, including RNA based therapeutics may be more fruitful.

Molecular Approaches to Treat ALS

RNA targeted therapeutics have entered a new phase of growth with the two main strategies investigated being short interfering RNA (siRNA) and antisense oligonucleotides (AOs). siRNA are double-stranded RNA molecules that can be used to downregulate the expression of target genes to which they are complementary through interactions with the RNA-induced silencing complex. Although there have been several preclinical investigations on the use of siRNA to target ALS genes, none have yet reached clinical trials (Ding et al., 2003; Nishimura et al., 2014). This review focuses on potential AO therapeutics for ALS. AOs are short, single-stranded nucleic acids that can bind to RNA through Watson-Crick base pairing and can alter gene expression through several different mechanisms. They can be used to restore or reduce protein expression or to modify protein isoform production through splice switching strategies.

Therapeutic use of many RNA analog drugs has been slowed by inefficient and poorly targeted delivery. Unmodified single-stranded RNA is unable to cross the cell membrane efficiently unaided, due to its size and negative charge and is susceptible to rapid degradation by nucleases. A range of chemical modifications has helped to address some of these issues, as reviewed by Khvorova and Watts (2017). Synthetic RNA-like drugs are commonly delivered to target cells using a nanoparticle delivery platform (usually a cationic polymer or lipid) or through conjugation to a bioactive ligand or cell penetrating peptide (Kaczmarek et al., 2017). Achieving effective concentrations of AOs in the organ or tissue of interest can be challenging, although treatment of neurodegenerative diseases with AOs may be advantageous in this regard as the AOs can be administered directly to the CNS via intrathecal administration. Once in the nervous system, AOs are readily taken up by neurons and glia (Smith et al., 2006). Furthermore, the blood-brain barrier prevents the dispersion into peripheral tissues and subsequent clearance by the kidney and liver, allowing clinically

effective concentrations to be more easily reached. This means smaller doses can be used, minimizing any potential toxicity (Evers et al., 2015) or systemic off-target effects. Several AO drugs have received FDA approval in recent years to treat a variety of conditions, including Eteplirsen (Exondys 51®) for Duchenne muscular dystrophy (Stein, 2016) Nusinersen (Spinraza®) for spinal muscular atrophy (Singh et al., 2017) and Inotersen (Tegsedi®) for hereditary transthyretin-mediated amyloidosis (hATTR) (Keam, 2018). Exploration of AO therapeutics has also begun for the treatment of ALS.

The first AO drug in clinical development for the treatment of ALS was developed by ISIS Pharmaceuticals (now Ionis) and targets the *SOD1* transcript (Miller et al., 2013). This AO exploits RNase H mediated degradation to target both mutant and wild-type *SOD1* mRNA. As the toxicity of SOD1 is proposed to be primarily due to a gain of function rather than a loss of function, knockdown of the protein is not expected to be harmful (Miller et al., 2013). Phase I studies to evaluate the safety, tolerability, and pharmacokinetics are ongoing (NCT02623699). AOs targeting the *SOD1* mRNA that utilize different chemistries and with alternative mechanisms of action are also in preclinical development by several groups.

Pre-clinical studies of AOs targeted to *C9ORF72* transcripts have also begun. In the case of C9ORF72, researchers have been able to exploit the location of the pathogenic hexanucleotide expansion that occurs in an intron between two alternatively used first exons. AOs utilizing RNase H mediated degradation that targets only HRE containing transcripts or all C9ORF72 transcripts have been developed with both methods reported to reduce RNA foci in patient-derived fibroblasts and iPSCs (Donnelly et al., 2013; Lagier-Tourenne et al., 2013; Sareen et al., 2013). HRE targeting AOs have also been able to reduce pathological *C9ORF72* RNA in transgenic mice (Jiang et al., 2016).

There are currently no AOs in clinical development that directly target the *TARDBP* or *FUS* transcripts. AOs that target *ATXN2* transcripts have been tested in TDP-43 transgenic mouse models (Becker et al., 2017). Ataxin-2 is thought to promote the maturation of stress granules (Kaehler et al., 2012), and reduced levels were hypothesized to decrease the recruitment of TDP-43 into these granules, potentially reducing the propensity of TDP-43 to form pathologic inclusions. The AOs reduced TDP-43 aggregation, extended lifespan and reduced pathology in the *TDP-43*$^{Tg/Tg}$ mouse model.

With the scope of RNA therapeutics rapidly expanding and the genetic basis of ALS continuing to be uncovered, AOs may be a promising area for future therapeutic developments for subsets of ALS patients.

MODELS FOR ALS

Determining the mechanisms involved in ALS and other brain disorders has been challenging due to the difficulty in obtaining living tissue or cells from the CNS of patients. A wide variety of model systems have been utilized by researchers to investigate the complex processes occurring in this disease. These models vary widely and include *in vitro* biochemical systems, cell lines and primary cell cultures, various small animal and rodent models. More recently, patient-derived cellular models are being developed and evaluated.

Rodent Models

Nearly all human genes have a homolog in the mouse and rat. Evaluation of drugs in these animals therefore increases the chances of successful translation of results to humans over lower animal models. Rodent models have been used extensively in ALS research since the first *SOD1*$^{(G93A)}$ and *SOD1*$^{(A4V)}$ ALS mouse models were produced in 1994 (Gurney et al., 1994). Yet for therapeutic applications, translation from animal models to successful outcomes in human clinical trials has remained dismal. Several factors have contributed to this outcome; overall, rodents generally display milder ALS phenotypes than humans, with animals in some models showing no signs of neurodegeneration. The shorter lifespan of rodents means that pathological changes have a shorter time to develop when compared to humans and confounding effects may also be conferred by the genetic background of the rodent. These factors may contribute to the differences in pathology and milder symptoms, potentially limiting the usefulness of rodent models in studying the late stages of neurodegenerative disease. There are also significant differences in RNA splicing and metabolism between humans and rodents. Although there is a high rate of conservation for constitutive exons between humans and rodents, for minor forms and tissue specific transcripts, only about a quarter of alternatively spliced exons are conserved between human and rodents (Modrek and Lee, 2003). The significance of this difference in regard to ALS pathogenesis remains unexplored. Physiological differences between humans and rodents also exist including differences in cellular and molecular functionality, as well as gross neuroanatomy and circuitry (Bodenreider et al., 2005). These factors have likely contributed to the overwhelming failure of translation from pre-clinical animal studies to effective clinical therapies for ALS. Comparisons of pathology between human ALS and some ALS rodent models are reviewed below.

Several transgenic *SOD1* rodent models have been developed in the past 25 years, most of which overexpress missense, mutant or truncated human *SOD1*. The *SOD1*$^{(G93A)}$ model however remains the most widely utilized. *SOD1* rodent lines generally develop adult-onset motor neuron disease, reminiscent of the human disease with hallmarks of human disease such as SOD1 aggregation, excitotoxic cell death of neurons, neuroinflammatory reactions and altered oligodendrocyte biology replicated in *SOD1* mouse models (Philips and Rothstein, 2015). These models have been used to characterize ALS biology and in preclinical evaluation for potential therapeutics. Although several potential therapeutics have been able to affect disease and show benefit in *SOD1* mouse models, translation to benefit in human clinical trials has been poor. Minocycline, for example, was able to slow disease in *SOD1*$^{(G37R)}$ mice (Kriz et al., 2002) but was shown to accelerate disease in

human clinical trials involving a diverse ALS patient group (Gordon et al., 2007).

TDP-43 rodent models, in contrast, often show significant differences in disease phenotype from that in humans. Most TDP-43 mouse models do not appear to develop ALS symptoms similar in severity to humans (Philips and Rothstein, 2015) and in low-level overexpression models, loss of cortical or spinal motor neurons is modest compared to that in human ALS patients (Philips and Rothstein, 2015). Another notable lack or correlation between rodent models and humans is the presence of TDP-43 positive cytoplasmic inclusions that, while widely reported in human ALS, are not regularly seen in rodent models of disease (Arnold et al., 2013).

FUS rodent models have been developed that include knockout, knockdown and overexpression models of both wild-type and mutated FUS proteins. While providing clues as to the pathomechanism of FUS-ALS, no models to date have been able to reproduce the distinct neuropathological features seen in humans (Nolan et al., 2016). Furthermore, phenotypic discrepancies between models are common; several transgenic models using the same R521C mutation, for example, have been produced with a range of phenotypes reported (Huang et al., 2011; Verbeeck et al., 2012; Qiu et al., 2014; Sharma et al., 2016).

Rodents modeling the *C9ORF72* hexanucleotide repeat expansion have recently been developed. A C9ORF72 mouse model that expresses 66 repeats in the CNS, mediated by adeno-associated virus was established, with mice developing histopathological and clinical symptoms of ALS, including motor deficits (Chew et al., 2015). In contrast, two independent mouse models that express the human hexanucleotide repeat expansion from a bacterial artificial chromosome were generated (O'Rourke et al., 2015; Peters et al., 2015); in both cases, mice developed the distinctive histopathological features seen in human ALS, including widespread RNA foci and dipeptide repeat proteins, however, no behavioral changes or neurodegeneration were observed. This supports the hypotheses that RNA foci and dipeptides are not sufficient to drive degeneration, although it is possible that these results are specific to these models and are not representative of human disease.

Another mouse model widely used in ALS research is the "wobbler" mouse. The wobbler mouse arose spontaneously in a C57BL/Fa strain and was first described by Falconer in 1956 (Falconer, 1956). These mice display phenotypic features similar to human ALS including muscle weakness, motor defects and a marked loss of motor neurons. Wobbler mouse motor neurons share many of the characteristics described in human ALS including vesicle transport defects, mitochondrial dysfunction, enlarged endosomes, vacuolization, impaired axonal transport, cortical excitotoxicity, ubiquitin-positive protein aggregates and neurofilament aggregation (Moser et al., 2013). TDP-43 pathology in the wobbler mouse resembles that seen in sporadic human ALS, including elevated TDP-43 levels, abnormal distribution to the cytoplasm, the presence of carboxy-terminal fragments and co-localization with ubiquitin-positive inclusions (Dennis and Citron, 2009). The variant responsible for this phenotype was uncovered in 2005 as a point mutation in the *VPS54* gene (Drepper et al., 2005). The VPS54 protein is part of the Golgi-associated retrograde protein complex with variations in this gene resulting in impairment of retrograde vesicle transport (Pérez-Victoria et al., 2010). Although no ALS-linked variants in the homologous human gene have yet been described, this model has been used to test a variety of potential ALS therapeutics over the years, including trophic neuroprotective factors, anti-inflammatory agents, anti-glutamatergic agents, mitochondrial support agents, antioxidants, steroids and stem cell therapies as reviewed by Moser et al. (2013).

Higher Mammal Models

Although not widely used, alternative animal models for ALS, including pigs and primates, are being explored. The similarities between pigs and humans make pigs a valuable model in disease characterization and therapy development and they have, therefore, been used to model TDP-43 and SOD1-ALS. Transgenic pigs expressing the TDP-43 M337V variant show a severe ALS like phenotype and the cytoplasmic mislocalization of TDP-43, but not the formation of aggregates (Wang et al., 2015). *SOD1*$^{(G93A)}$ pigs showed nuclear accumulation of SOD1 (Yang et al., 2014) with both TDP-43 and SOD1 models uncovering protein interactions not seen in rodent models of the disease. Primate models are also shedding light on disease pathomechanisms. In a TDP-43 overexpression model that closely recapitulates ALS phenotypes seen in humans, TDP-43 was found to be mislocalized early in disease progression. In this model, TDP-43 phosphorylation was only detected in the later stage of disease and the signature 25-kDa C-terminal fragment was not detected, indicating these may not be necessary to initiate TDP-43 induced neuronal dysfunction in monkeys (Uchida et al., 2012). In a recent study that compared transgenic monkeys and mice expressing the TDP-43 M337V variant, species dependent localization and cleavage of TDP-43 was apparent. Interestingly, the C-terminal fragments were abundant in the monkeys' brains in this model, in contrast to the TDP-43 overexpression monkey model (Yin et al., 2019).

There is no doubt that animal models have been useful in helping uncover mechanisms of pathogenesis in ALS, but it is important to also recognize their limitations. No animal model is able to fully replicate the entire spectrum of phenotypes seen in human ALS. The heterogeneity of ALS may lead to varied responses to similar treatments in different patients. This makes it difficult to assess how a therapeutic effect may translate from animal models to efficacy in humans. Animal models clearly need to be supplemented with pre-clinical models that can capture the heterogeneity of disease seen in humans.

iPSCs

Recently, the use of patient-derived stem cell models has emerged in ALS research; many of the first investigations have used iPSC derived motor neurons. iPSCs are reprogrammed from somatic cells by the introduction of key pluripotency factors. This was first achieved in mouse fibroblasts in 2006 (Takahashi and Yamanaka, 2006) and in human cells the following year (Takahashi et al., 2007). The pluripotent cells can then be guided to differentiate

into the desired cell lineage including neurons, motor neurons or glial cells. This approach provides several advantages over other cellular models for the study of human genetic diseases. Firstly, the need to overexpress transgenes containing pathogenic gene variants is eliminated. Additionally, these cells carry endogenous gene variants within the context of an individual's genetic background making them particularly valuable for the study of sporadic disease in which the causative genetic factors are unknown. iPSC-derived neurons have proved to be a valuable model for ALS, with several aspects of disease neuropathology recapitulated. Motor neurons derived from iPSCs have been utilized to study variants in *TARDBP*, *C9ORF72*, *SOD1*, *FUS* and in models of sporadic disease.

Various ALS-associated *SOD1* variants have been modeled using iPSCs. These models have the capacity to reflect pathology seen in patients, such as SOD1 aggregation and have been used to explore disease mechanisms (Bhinge et al., 2016; Seminary et al., 2018). Whilst iPSC derived motor neurons from patients with pathogenic *TARDBP* variants were reported to show characteristics of TDP-43 proteinopathy, results have not always been consistent. Increased levels of soluble and detergent resistant TDP-43 and decreased cell survival were reported in a *TARDBP* M337V iPSC model for example (Bilican et al., 2012; Egawa et al., 2012), whilst others reported no difference in cytoplasmic TDP-43 aggregation or cell survival between TARDBP mutant iPSC motor neurons and controls, despite the same variant (M337V) (Seminary et al., 2018). iPSC-derived motor neurons from patients with pathogenic *FUS* variants develop typical FUS pathologies, including the cytoplasmic mislocalization of FUS and recruitment into stress granules. These models have also been useful in demonstrating the relationship between specific point mutations and cytosolic FUS mislocalization (Japtok et al., 2015; Lenzi et al., 2015; Ichiyanagi et al., 2016; Guo et al., 2017). iPSC derived motor neurons from *C9ORF72* ALS patients harbor disease-associated characteristics, including aggregation of mRNA containing the hexanucleotide repeat expansion and the formation of RAN translated dipeptides (Almeida et al., 2013). *C9ORF72* iPSC derived motor neurons have revealed other disease characteristics associated with the *C9ORF72* hexanucleotide repeat expansions such as alterations in gene expression, nucleocytoplasmic transport defects and susceptibility to excitotoxicity (Donnelly et al., 2013; Sareen et al., 2013; Freibaum et al., 2015). Although iPSC derived motor neurons have proved valuable in ALS research, there is also valid concern over genetic and epigenetic variations in iPSCs that may compromise their utility (Liang and Zhang, 2013). As aging is the leading risk factor in the development of ALS and other neurodegenerative disorders, it is important to consider the age-related characteristics of the cells being studied. iPSC derived neurons do not maintain the aging and epigenetic signatures of the donor (Hewitt and Garlick, 2013).

Directly Reprogrammed Motor Neurons

Although not yet in widespread use in ALS research, an alternative approach to generating patient derived motor neurons that more acutely model the age-related phenotype is gaining momentum. Fully differentiated somatic cells are now able to be directly reprogramed into functional neurons that may be guided to subtype-specific neurons, based on the addition of specific transcription factors or microRNAs (Pang et al., 2011; Yoo et al., 2011). This method has been used to successfully convert fibroblasts from ALS patients with both pathogenic *FUS* variants and *C9ORF72* expansions to motor neurons that displayed disease specific degeneration (Su et al., 2014; Lim et al., 2016; Liu et al., 2016). It has been shown that directly reprogrammed motor neurons are able to maintain the aging hallmarks of old donors, including heterochromatin loss, DNA damage and nuclear organization (Tang et al., 2017). Although only beginning to be explored in ALS research, directly reprogrammed motor neurons may be more suitable than iPSC derived motor neurons to model late-onset neurodegeneration.

Olfactory Stem Cell Cultures

Another patient-derived stem cell model that has recently emerged in the study of brain diseases uses stem cells derived from the olfactory mucosa of human patients. The olfactory mucosa is a neural tissue that is easily accessible in a clinical setting (Féron et al., 1998) and contains several cell types including a large population of multipotent neural stem cells. These stem cells can be purified from surrounding cells and expanded as neurospheres (clusters of neural progenitor cells) that may then be propagated in neurospheres as neural progenitor cells or dissociated and propagated as olfactory neurosphere-derived stem cells (ONS cells) (Féron et al., 2013). ONS cells may also be differentiated to form neurons or glia for further study.

Recent advances have made less invasive approaches to tissue biopsy available, with olfactory stem cells now readily obtainable from living human subjects (Benítez-King et al., 2011). Improvements in the enrichment of neural cells from biopsied tissue have also occurred (Tajinda et al., 2010), with several advantages in using olfactory mucosa-derived stem cells over iPSCs. Firstly, the reprogramming step from somatic cell to stem cell is bypassed, reducing confounding events such as epigenetic changes that can interfere with accurate assessment of differential gene expression. In addition, elimination of the re-programming step makes the use of olfactory derived cells less time consuming and less costly, making this cell type more suitable for high throughput studies. Furthermore, ONS cells can be easily maintained in culture and are suitable for use in multiwell assays, making them useful for many applications, including understanding disease etiology, diagnostics, and drug screening.

Patient-derived ONS cells have shown disease-specific alterations in gene expression and cell function in several complex neurological disorders including schizophrenia, Parkinson's disease, and dysautonomia (Boone et al., 2010; Cook et al., 2011; Fan et al., 2012; Mackay-Sim, 2012). ONS cells have also demonstrated utility in modeling hereditary spastic paraplegia (Abrahamsen et al., 2013), an adult-onset disease involving axonal degeneration in corticospinal motor

neurons and in ataxia-telangiectasia (Stewart et al., 2013), a rare disorder with varying symptoms including neuropathological features. ONS cells are a promising platform for gene expression studies, drug discovery and diagnostics in neurological disease and may be of utility in ALS research. ONS cells and ONS derived neurons may be particularly useful in modeling early disease processes, before disease onset and in modeling sporadic disease.

Although the use of patient derived motor neurons has been validated for use in exploring the molecular basis of ALS and developing new drug screening platforms, several challenges remain. In order to enable comparison of results across laboratories, it is necessary to develop and define standard criteria for the maturation, molecular characterization and electrical and transcriptional functioning of patient derived motor neurons (Sances et al., 2016). Most studies to date have represented only a few patients; increasing sample sizes in these studies will strengthen the observed ALS related phenotypes.

CHALLENGES AND FUTURE DIRECTIONS

Many challenges remain for researchers in the pursuit of understanding and ultimately providing effective treatments for people living with ALS. Questions regarding unidentified heredity remain unanswered. Single nucleotide polymorphisms account for only a fraction of ALS cases. A shift in focus to genetic disease modifiers, such as copy number variations and structural variants as well as further interrogation of intronic DNA regions during DNA diagnosis may help to fill in the gaps.

It remains difficult to unravel the temporal etiology of ALS with downstream effects and potential causes feeding back into each other. The contribution that each of the proposed disease mechanisms plays in ALS pathogenesis and which of these are initiating factors remains unclear, with conflicting reports from researchers depending on the protocols and model systems used. Models that reflect early and even pre-symptomatic disease pathogenesis may help to discriminate initiating factors causative of disease from follow-on consequences. It is clear that TDP-43 is involved in ALS pathogenesis in most ALS cases. At what stage of disease progression it becomes involved still needs to be determined, as does the role of the various post-translational modifications to TDP-43 seen in ALS. The degree to which aggregation of ALS proteins mediates toxicity also requires further investigation.

Given the large number of genetic variants associated with ALS and the number of cellular pathways affected, there is likely a large amount of heterogeneity between patients. No animal model is able to fully replicate the spectrum of phenotypes seen in human disease making it very difficult to unravel the causes and determine effective treatments. Translation from benefit in animal models to benefit in humans remains poor; this is likely to have multiple causes, however, it is probable that pathophysiologic heterogeneity between patients is a major contributing factor. Utilizing patient-derived cellular models from large numbers of individuals with ALS may help in more accurately determining treatments that may be of broad benefit to patients.

Personalized medicine is a medical scheme that incorporates genetic, clinical diagnostics and environmental information to individualize patient care, and is gradually becoming more commonplace especially in the treatment of cancers. Personalized medicine is an important advancement as subtypes of patients may respond differently to potential disease-modifying therapies. The further identification of ALS patient subtypes according to genetic and non-genetic information and the identification of clinical biomarkers would be most beneficial. Taking complete genetic information into account when assessing clinical trial outcomes may help in determining treatments that are most suitable for particular subgroups of patients. An example demonstrating the benefit of this approach comes from a genetic *post hoc* meta-analysis on the data from three recent trials into the efficacy of lithium carbonate to treat ALS. Although no improvement in 12-month survival was reported in any of these studies, investigators found that those homozygous for a common A > C single nucleotide variant in the *UNC13A* gene had a significant increase in survival probability after 12 months; increasing from 40.1 to 67.7% after treatment (van Eijk et al., 2017).

Gene expression analysis has shown molecular heterogeneity exists in sALS patients with different pathways and genes dysregulated (Aronica et al., 2014). Ultimately, a comprehensive systems biology approach that integrates genomics and other cellular information with bioinformatic analyses could greatly improve our understanding of this complex and multifactorial disease and help in developing a more accurate biomarker-assisted diagnosis, and hopefully more personalized and effective treatment strategies.

AUTHOR CONTRIBUTIONS

RM: conception and initial draft writing. IP, LF, PA, SF and SW: critical editing of the manuscript.

FUNDING

RM was supported by a RTP Scholarship through Murdoch University and a Perron Institute Prestige Scholarship. PA and LF were supported by the Perron Institute. IP was supported by the Giumelli Foundation and the Racing for MNDi Foundation (Western Australia) Fellowship.

ACKNOWLEDGMENTS

PA would like to acknowledge the financial support and mentorship of the Late Prof. Allen Roses and Ann Saunders.

REFERENCES

Abe, K., Itoyama, Y., Sobue, G., Tsuji, S., Aoki, M., Doyu, M., et al. (2014). Confirmatory double-blind, parallel-group, placebo-controlled study of efficacy and safety of edaravone (MCI-186) in amyotrophic lateral sclerosis patients. *Amyotroph. Lateral Scler. Frontotemporal Degener.* 15, 610–617. doi: 10.3109/21678421.2014.959024

Abrahamsen, G., Fan, Y., Matigian, N., Wali, G., Bellette, B., Sutharsan, R., et al. (2013). A patient-derived stem cell model of hereditary spastic paraplegia with SPAST mutations. *Dis. Models Mech.* 6, 489–502. doi: 10.1242/dmm.010884

Akira, I., Nobuyuki, K., Yuto, W., Sumiko, W., and Akira, I. (2016). TDP-43 binds and transports G-quadruplex-containing mRNAs into neurites for local translation. *Genes Cells* 21, 466–481. doi: 10.1111/gtc.12352

Alami, N. H., Smith, R. B., Carrasco, M. A., Williams, L. A., Winborn, C. S., Han, S. S. W., et al. (2014). Axonal transport of TDP-43 mRNA granules is impaired by ALS-Causing mutations. *Neuron* 81, 536–543. doi: 10.1016/j.neuron.2013.12.018

Al-Chalabi, A., Andersen, P. M., Nilsson, P., Chioza, B., Andersson, J. L., Russ, C., et al. (1999). Deletions of the heavy neurofilament subunit tail in amyotrophic lateral sclerosis. *Hum. Mol. Genet.* 8, 157–164. doi: 10.1093/hmg/8.2.157

Al-Chalabi, A., Fang, F., Hanby, M. F., Leigh, P. N., Shaw, C. E., Ye, W., et al. (2010). An estimate of amyotrophic lateral sclerosis heritability using twin data. *J. Neurol. Neurosurg. Psychiatr.* 81:1324. doi: 10.1136/jnnp.2010.207464

Al-Chalabi, A., and Lewis, C. M. (2011). Modelling the effects of penetrance and family size on rates of sporadic and familial disease. *Hum. Hered.* 71, 281–288. doi: 10.1159/000330167

Almeida, S., Gascon, E., Tran, H., Chou, H. J., Gendron, T. F., Degroot, S., et al. (2013). Modeling key pathological features of frontotemporal dementia with C9ORF72 repeat expansion in iPSC-derived human neurons. *Acta Neuropathol.* 126, 385–399. doi: 10.1007/s00401-013-1149-y

Al-Saif, A., Al-Mohanna, F., and Bohlega, S. (2011). A mutation in sigma-1 receptor causes juvenile amyotrophic lateral sclerosis. *Ann. Neurol.* 70, 913–919. doi: 10.1002/ana.22534

Andersen, P. M., Forsgren, L., Binzer, M., Nilsson, P., Ala-Hurula, V., Keränen, M.-L., et al. (1996). Autosomal recessive adult-onset amyotrophic lateral sclerosis associated with homozygosity for Asp90Ala CuZn-superoxide dismutase mutation: a clinical and genealogical study of 36 patients. *Brain* 119, 1153–1172. doi: 10.1093/brain/119.4.1153

Arai, T., Hasegawa, M., Akiyama, H., Ikeda, K., Nonaka, T., Mori, H., et al. (2006). TDP-43 is a component of ubiquitin-positive tau-negative inclusions in frontotemporal lobar degeneration and amyotrophic lateral sclerosis. *Biochem. Biophys. Res. Commun.* 351, 602–611. doi: 10.1016/j.bbrc.2006.10.093

Arnold, E. S., Ling, S.-C., Huelga, S. C., Lagier-Tourenne, C., Polymenidou, M., Ditsworth, D., et al. (2013). ALS-linked TDP-43 mutations produce aberrant RNA splicing and adult-onset motor neuron disease without aggregation or loss of nuclear TDP-43. *Proc. Natl. Acad. Sci. U.S.A.* 110, E736–E745.

Aronica, E., Baas, F., Iyer, A., Ten Asbroek, A. L. M. A., Morello, G., and Cavallaro, S. (2014). Molecular classification of amyotrophic lateral sclerosis by unsupervised clustering of gene expression in motor cortex. *Neurobiol. Dis.* 74, 359–376. doi: 10.1016/j.nbd.2014.12.002

Ash, P. E. A., Bieniek, K. F., Gendron, T. F., Caulfield, T., Lin, W.-L., Dejesus-Hernandez, M., et al. (2013). Unconventional translation of C9ORF72 GGGGCC expansion generates insoluble polypeptides specific to c9FTD/ALS. *Neuron* 77, 639–646. doi: 10.1016/j.neuron.2013.02.004

Ash, P. E. A., Zhang, Y.-J., Roberts, C. M., Saldi, T., Hutter, H., Buratti, E., et al. (2010). Neurotoxic effects of TDP-43 overexpression in *C. elegans*. *Hum. Mol. Genet.* 19, 3206–3218. doi: 10.1093/hmg/ddq230

Atanasio, A., Decman, V., White, D., Ramos, M., Ikiz, B., Lee, H.-C., et al. (2016). C9orf72 ablation causes immune dysregulation characterized by leukocyte expansion, autoantibody production, and glomerulonephropathy in mice. *Sci. Rep.* 6:23204. doi: 10.1038/srep23204

Avendaño-Vázquez, S. E., Dhir, A., Bembich, S., Buratti, E., Proudfoot, N., and Baralle, F. E. (2012). Autoregulation of TDP-43 mRNA levels involves interplay between transcription, splicing, and alternative polyA site selection. *Genes Dev.* 26, 1679–1684. doi: 10.1101/gad.194829.112

Ayala, Y. M., Zago, P., D'ambrogio, A., Xu, Y.-F., Petrucelli, L., Buratti, E., et al. (2008). Structural determinants of the cellular localization and shuttling of TDP-43. *J. Cell Sci.* 121, 3778–3785. doi: 10.1242/jcs.038950

Baechtold, H., Kuroda, M., Sok, J., Ron, D., Lopez, B. S., and Akhmedov, A. T. (1999). Human 75-kDa DNA-pairing protein is identical to the pro-oncoprotein TLS/FUS and is able to promote D-loop formation. *J. Biol. Chem.* 274, 34337–34342. doi: 10.1074/jbc.274.48.34337

Bannwarth, S., Ait-El-Mkadem, S., Chaussenot, A., Genin, E. C., Lacas-Gervais, S., Fragaki, K., et al. (2014). A mitochondrial origin for frontotemporal dementia and amyotrophic lateral sclerosis through CHCHD10 involvement. *Brain* 137, 2329–2345. doi: 10.1093/brain/awu138

Barker, H. V., Niblock, M., Lee, Y.-B., Shaw, C. E., and Gallo, J.-M. (2017). RNA misprocessing in C9orf72-Linked neurodegeneration. *Front. Cell. Neurosci.* 11:195. doi: 10.3389/fncel.2017.00195

Becker, L. A., Huang, B., Bieri, G., Ma, R., Knowles, D. A., Jafar-Nejad, P., et al. (2017). Therapeutic reduction of ataxin-2 extends lifespan and reduces pathology in TDP-43 mice. *Nature* 544:367. doi: 10.1038/nature22038

Bellingham, M. C. (2011). A Review of the neural mechanisms of action and clinical efficiency of Riluzole in treating amyotrophic lateral sclerosis: what have we learned in the last decade? *CNS Neurosci. Therapeut.* 17, 4–31. doi: 10.1111/j.1755-5949.2009.00116.x

Benítez-King, G., Riquelme, A., Ortíz-López, L., Berlanga, C., Rodríguez-Verdugo, M. S., Romo, F., et al. (2011). A non-invasive method to isolate the neuronal linage from the nasal epithelium from schizophrenic and bipolar diseases. *J. Neurosci. Methods* 201, 35–45. doi: 10.1016/j.jneumeth.2011.07.009

Bensimon, G., Lacomblez, L., and Meininger, V. (1994). A controlled trial of Riluzole in amyotrophic Lateral Sclerosis. *New Engl. J. Med.* 330, 585–591. doi: 10.1056/nejm199403033300901

Bertolin, C., Querin, G., Bozzoni, V., Martinelli, I., De Bortoli, M., Rampazzo, A., et al. (2018). New FIG4 gene mutations causing aggressive ALS. *Eur. J. Neurol.* 25, e41–e42. doi: 10.1111/ene.13559

Bhinge, A., Namboori, S. C., Zhang, X., Vandongen, A. M. J., and Stanton, L. W. (2016). Genetic correction of SOD1 mutant iPSCs reveals ERK and JNK activated AP1 as a driver of neurodegeneration in amyotrophic Lateral Sclerosis. *Stem Cell Rep.* 8, 856–869. doi: 10.1016/j.stemcr.2017.02.019

Bilican, B., Serio, A., Barmada, S. J., Nishimura, A. L., Sullivan, G. J., Carrasco, M., et al. (2012). Mutant induced pluripotent stem cell lines recapitulate aspects of TDP-43 proteinopathies and reveal cell-specific vulnerability. *Proc. Natl. Acad. Sci. U.S.A.* 109, 5803–5808. doi: 10.1073/pnas.1202922109

Bilsland, L. G., Sahai, E., Kelly, G., Golding, M., Greensmith, L., and Schiavo, G. (2010). Deficits in axonal transport precede ALS symptoms in vivo. *Proc. Natl. Acad. Sci. U.S.A.* 107, 20523–20528. doi: 10.1073/pnas.1006869107

Bodenreider, O., Hayamizu, T. F., Ringwald, M., De Coronado, S., and Zhang, S. (2005). Of mice and men: aligning mouse and human anatomies. *AMIA Annu. Symp. Proc.* 2005, 61–65.

Boone, N., Loriod, B., Bergon, A., Sbai, O., Formisano-Tréziny, C., Gabert, J., et al. (2010). Olfactory stem cells, a new cellular model for studying molecular mechanisms underlying familial dysautonomia. *PLoS One* 5:e15590. doi: 10.1371/journal.pone.0015590

Borghero, G., Pugliatti, M., Marrosu, F., Marrosu, M. G., Murru, M. R., Floris, G., et al. (2015). TBK1 is associated with ALS and ALS-FTD in Sardinian patients. *Neurobiol. Aging* 43:180.e1-5. doi: 10.1016/j.neurobiolaging.2016.03.028

Boston-Howes, W., Gibb, S. L., Williams, E. O., Pasinelli, P., Brown, R. H., and Trotti, D. (2006). Caspase-3 cleaves and inactivates the glutamate transporter EAAT2. *J. Biol. Chem.* 281, 14076–14084. doi: 10.1074/jbc.m600653200

Boylan, K. (2015). Familial ALS. *Neurol. Clin.* 33, 807–830. doi: 10.1016/j.ncl.2015.07.001

Bradl, M., and Lassmann, H. (2010). Oligodendrocytes: biology and pathology. *Acta Neuropathol.* 119, 37–53. doi: 10.1007/s00401-009-0601-5

Brenner, D., Müller, K., Wieland, T., Weydt, P., Böhm, S., Lulé, D., et al. (2016). *NEK1* mutations in familial amyotrophic lateral sclerosis. *Brain* 139:e28. doi: 10.1093/brain/aww033

Brettschneider, J., Del Tredici, K., Toledo, J. B., Robinson, J. L., Irwin, D. J., Grossman, M., et al. (2013). Stages of pTDP-43 pathology in amyotrophic lateral sclerosis. *Ann. Neurol.* 74, 20–38. doi: 10.1002/ana.23937

Buratti, E. (2018). TDP-43 post-translational modifications in health and disease. *Expert Opin. Ther. Targets* 22, 279–293. doi: 10.1080/14728222.2018.1439923

Buratti, E., and Baralle, F. E. (2010). The multiple roles of TDP-43 in pre-mRNA processing and gene expression regulation. *RNA Biol.* 7, 420–429. doi: 10.4161/rna.7.4.12205

Buratti, E., Brindisi, A., Giombi, M., Tisminetzky, S., Ayala, Y. M., and Baralle, F. E. (2005). TDP-43 Binds Heterogeneous Nuclear Ribonucleoprotein A/B through Its C-terminal Tail: an important region for the inhibition of cystic fibrosis transmembrane conductance regulator exon 9 splicing. *J. Biol. Chem.* 280, 37572–37584. doi: 10.1074/jbc.m505557200

Burberry, A., Suzuki, N., Wang, J.-Y., Moccia, R., Mordes, D. A., Stewart, M. H., et al. (2016). Loss-of-function mutations in the C9ORF72 mouse ortholog cause fatal autoimmune disease. *Sci. Transl. Med.* 8:347ra93. doi: 10.1126/scitranslmed.aaf6038

Butterfield, R. J., Ramachandran, D., Hasstedt, S. J., Otterud, B. E., Leppert, M. F., Swoboda, K. J., et al. (2009). A novel form of juvenile recessive ALS maps to loci on 6p25 and 21q22. *Neuromusc. Disord.* 19, 279–287. doi: 10.1016/j.nmd.2009.02.006

Cady, J., Allred, P., Bali, T., Pestronk, A., Goate, A., Miller, T. M., et al. (2015). Amyotrophic lateral sclerosis onset is influenced by the burden of rare variants in known amyotrophic lateral sclerosis genes. *Ann. Neurol.* 77, 100–113. doi: 10.1002/ana.24306

Cameron, D. L., Leon, Di, S., and Papenfuss, A. T. (2019). Comprehensive evaluation and characterisation of short read general-purpose structural variant calling software. *Nat. Commun.* 10, 1–11. doi: 10.1038/s41467-019-11146-4

Carrì, M. T., D'ambrosi, N., and Cozzolino, M. (2017). Pathways to mitochondrial dysfunction in ALS pathogenesis. *Biochem. Biophys. Res. Commun.* 483, 1187–1193. doi: 10.1016/j.bbrc.2016.07.055

Cedarbaum, J. M., Stambler, N., Malta, E., Fuller, C., Hilt, D., Thurmond, B., et al. (1999). The ALSFRS-R: a revised ALS functional rating scale that incorporates assessments of respiratory function. *J. Neurol. Sci.* 169, 13–21. doi: 10.1016/s0022-510x(99)00210-5

Cetin, H., Rath, J., Füzi, J., Reichardt, B., Fülöp, G., Koppi, S., et al. (2015). Epidemiology of amyotrophic lateral sclerosis and effect of riluzole on disease course. *Neuroepidemiology* 44, 6–15. doi: 10.1159/000369813

Chadi, G., Maximino, J. R., Jorge, F. M. D. H., Borba, F. C. D., Gilio, J. M., Callegaro, D., et al. (2017). Genetic analysis of patients with familial and sporadic amyotrophic lateral sclerosis in a Brazilian Research Center. *Amyotroph. Lateral Scler. Frontotemporal Degener.* 18, 249–255. doi: 10.1080/21678421.2016.1254245

Chaisson, M. J. P., Huddleston, J., Dennis, M. Y., Sudmant, P. H., Malig, M., Hormozdiari, F., et al. (2014). Resolving the complexity of the human genome using single-molecule sequencing. *Nature* 517, 608–611. doi: 10.1038/nature13907

Chaisson, M. J. P., Sanders, A. D., Zhao, X., Malhotra, A., Porubsky, D., Rausch, T., et al. (2018). Multi-platform discovery of haplotype-resolved structural variation in human genomes. *bioRxiv* [Preprint]. doi: 10.1038/s41467-018-08148-z

Chaussenot, A., Le Ber, I., Ait-El-Mkadem, S., Camuzat, A., De Septenville, A., Bannwarth, S., et al. (2014). Screening of CHCHD10 in a French cohort confirms the involvement of this gene in frontotemporal dementia with amyotrophic lateral sclerosis patients. *Neurobiol. Aging* 35:2884.e1–2884.e4. doi: 10.1016/j.neurobiolaging.2014.07.022

Chen, S., Sayana, P., Zhang, X., and Le, W. (2013). Genetics of amyotrophic lateral sclerosis: an update. *Mol. Neurodegener.* 8:28. doi: 10.1186/1750-1326-8-28

Chen, Y.-Z., Bennett, C. L., Huynh, H. M., Blair, I. P., Puls, I., Irobi, J., et al. (2004). DNA/RNA helicase gene mutations in a form of juvenile amyotrophic lateral sclerosis (ALS4). *Am. J. Hum. Genet.* 74, 1128–1135. doi: 10.1086/421054

Chew, J., Gendron, T. F., Prudencio, M., Sasaguri, H., Zhang, Y.-J., Castanedes-Casey, M., et al. (2015). Neurodegeneration. *C*9ORF72 repeat expansions in mice cause TDP-43 pathology, neuronal loss, and behavioral deficits. *Science* 348:1151. doi: 10.1126/science.aaa9344

Chiang, C., Scott, A. J., Davis, J. R., Tsang, E. K., Li, X., Kim, Y., et al. (2017). The impact of structural variation on human gene expression. *Nat. Genet.* 49, 692–699. doi: 10.1038/ng.3834

Chiang, P.-M., Ling, J., Jeong, Y. H., Price, D. L., Aja, S. M., and Wong, P. C. (2010). Deletion of TDP-43 down-regulates Tbc1d1, a gene linked to obesity, and alters body fat metabolism. *Proc. Natl. Acad. Sci. U.S.A.* 107, 16320–16324. doi: 10.1073/pnas.1002176107

Chio, A., Logroscino, G., Hardiman, O., Swingler, R., Mitchell, D., Beghi, E., et al. (2009). Prognostic factors in ALS: a critical review. *Amyotroph. Lateral Scler.* 10, 310–323.

Chiò, A., Logroscino, G., Traynor, B. J., Collins, J., Simeone, J. C., Goldstein, L. A., et al. (2013). Global epidemiology of amyotrophic lateral sclerosis: a systematic review of the published literature. *Neuroepidemiology* 41, 118–130. doi: 10.1159/000351153

Chow, C. Y., Landers, J. E., Bergren, S. K., Sapp, P. C., Grant, A. E., Jones, J. M., et al. (2009). Deleterious variants of FIG4, a phosphoinositide phosphatase, in patients with ALS. *Am. J. Hum. Genet.* 84, 85–88. doi: 10.1016/j.ajhg.2008.12.010

Cirulli, E. T., Lasseigne, B. N., Petrovski, S., Sapp, P. C., Dion, P. A., Leblond, C. S., et al. (2015). Exome sequencing in amyotrophic lateral sclerosis identifies risk genes and pathways. *Science* 347, 1436–1441. doi: 10.1126/science.aaa3650

Clarke, L. E., and Barres, B. A. (2013). Emerging roles of astrocytes in neural circuit development. *Nat. Rev. Neurosci.* 14, 311–321. doi: 10.1038/nrn3484

Cleveland, D. W., Laing, N., Hurse, P. V., and Brown, R. H. Jr. (1995). Toxic mutants in Charcot's sclerosis. *Nature* 378:342. doi: 10.1038/378342a0

Cohen, T. J., Hwang, A. W., Restrepo, C. R., Yuan, C.-X., Trojanowski, J. Q., and Lee, V. M. Y. (2015). An acetylation switch controls TDP-43 function and aggregation propensity. *Nat. Commun.* 6:5845. doi: 10.1038/ncomms6845

Colombrita, C., Onesto, E., Buratti, E., De La Grange, P., Gumina, V., Baralle, F. E., et al. (2015). From transcriptomic to protein level changes in TDP-43 and FUS loss-of-function cell models. *Biochim. Biophys. Acta* 1849, 1398–1410. doi: 10.1016/j.bbagrm.2015.10.015

Cook, A. L., Vitale, A. M., Ravishankar, S., Matigian, N., Sutherland, G. T., Shan, J., et al. (2011). Nrf2 activation restores disease related metabolic deficiencies in olfactory neurosphere-derived cells from patients with sporadic parkinson's disease. *PLoS One* 6:e21907. doi: 10.1371/journal.pone.0021907

Cooper-Knock, J., Walsh, M. J., Higginbottom, A., Highley, J. R., Dickman, M. J., Edbauer, D., et al. (2014). Sequestration of multiple RNA recognition motif-containing proteins by C9orf72 repeat expansions. *Brain* 137, 2040–2051. doi: 10.1093/brain/awu120

Corbo, M., and Hays, A. P. (1992). Peripherin and neurofilament protein coexist in spinal spheroids of motor neuron disease. *J. Neuropathol. Exp. Neurol.* 51, 531–537. doi: 10.1097/00005072-199209000-00008

Corcia, P., Tauber, C., Vercoullie, J., Arlicot, N., Prunier, C., Praline, J., et al. (2012). Molecular imaging of microglial activation in amyotrophic Lateral Sclerosis. *PLoS One* 7:e52941. doi: 10.1371/journal.pone.0052941

Corrado, L., Carlomagno, Y., Falasco, L., Mellone, S., Godi, M., Cova, E., et al. (2011). A novel peripherin gene (PRPH) mutation identified in one sporadic amyotrophic lateral sclerosis patient. *Neurobiol. Aging* 32:552.e1-6. doi: 10.1016/j.neurobiolaging.2010.02.011

Couthouis, J., Hart, M. P., Erion, R., King, O. D., Diaz, Z., Nakaya, T., et al. (2012). Evaluating the role of the FUS/TLS-related gene EWSR1 in amyotrophic lateral sclerosis. *Hum. Mol. Genet.* 21, 2899–2911. doi: 10.1093/hmg/dds116

Couthouis, J., Hart, M. P., Shorter, J., Dejesus-Hernandez, M., Erion, R., Oristano, R., et al. (2011). A yeast functional screen predicts new candidate ALS disease genes. *Proc. Natl. Acad. Sci. U.S.A.* 108, 20881–20890. doi: 10.1073/pnas.1109434108

Cox, L. E., Ferraiuolo, L., Goodall, E. F., Heath, P. R., Higginbottom, A., Mortiboys, H., et al. (2010). Mutations in CHMP2B in lower motor neuron predominant amyotrophic lateral sclerosis (ALS). *PLoS One* 5:e9872. doi: 10.1371/journal.pone.0009872

Cozzolino, M., Pesaresi, M. G., Amori, I., Crosio, C., Ferri, A., Nencini, M., et al. (2009). Oligomerization of mutant SOD1 in mitochondria of motoneuronal cells drives mitochondrial damage and cell toxicity. *Antioxid. Redox Signal.* 11, 1547–1558. doi: 10.1089/ARS.2009.2545

Cudkowicz, M. E. P., Titus, S. M. P. H., Kearney, M. B. A., Yu, H. M. S., Sherman, A. M., Schoenfeld, D. P., et al. (2014). Safety and efficacy of ceftriaxone for amyotrophic lateral sclerosis: a multi-stage, randomised, double-blind, placebo-controlled trial. *Lancet Neurol* 13, 1083–1091. doi: 10.1016/S1474-4422(14)70222-4

D'Alton, S., Altshuler, M., and Lewis, J. (2015). Studies of alternative isoforms provide insight into TDP-43 autoregulation and pathogenesis. *RNA* 21, 1419–1432. doi: 10.1261/rna.047647.114

Daoud, H., Zhou, S., Noreau, A., Sabbagh, M., Belzil, V., Dionne-Laporte, A., et al. (2012). Exome sequencing reveals SPG11 mutations causing juvenile ALS. *Neurobiol. Aging* 33:839.e5-9. doi: 10.1016/j.neurobiolaging.2011.11.012

Dardiotis, E., Siokas, V., Sokratous, M., Tsouris, Z., Michalopoulou, A., Andravizou, A., et al. (2018). Genetic polymorphisms in amyotrophic lateral sclerosis: evidence for implication in detoxification pathways of environmental toxicants. *Environ. Int.* 116, 122–135. doi: 10.1016/j.envint.2018.04.008

de Carvalho, M., Kiernan, M. C., and Swash, M. (2017). Fasciculation in amyotrophic lateral sclerosis: origin and pathophysiological relevance. *J. Neurol. Neurosurg. Psychiatry* 88, 773–779. doi: 10.1136/jnnp-2017-315574

de Carvalho, M., Pinto, S., Costa, J., Evangelista, T., Ohana, B., and Pinto, A. (2010). A randomized, placebo-controlled trial of memantine for functional disability in amyotrophic lateral sclerosis. *Amyotroph. Lateral Scler.* 11, 456–460. doi: 10.3109/17482968.2010.498521

DeJesus-Hernandez, M., Mackenzie, I. R., Boeve, B. F., Boxer, A. L., Baker, M., Rutherford, N. J., et al. (2011). Expanded GGGGCC hexanucleotide repeat in noncoding region of C9ORF72 causes chromosome 9p-Linked FTD and ALS. *Neuron* 72, 245–256. doi: 10.1016/j.neuron.2011.09.011

Deng, H.-X., Chen, W., Hong, S.-T., Boycott, K. M., Gorrie, G. H., Siddique, N., et al. (2011). Mutations in UBQLN2 cause dominant X-linked juvenile and adult-onset ALS and ALS/dementia. *Nature* 477, 211–215. doi: 10.1038/nature10353

Deng, H. X., Hentati, A., Tainer, J. A., Iqbal, Z., Cayabyab, A., Hung, W. Y., et al. (1993). Amyotrophic lateral sclerosis and structural defects in Cu,Zn superoxide dismutase. *Science* 261, 1047–1051.

Deng, J., Yang, M., Chen, Y., Chen, X., Liu, J., Sun, S., et al. (2015). FUS interacts with HSP60 to promote mitochondrial damage: e1005357. *PLoS Genet.* 11:e1005357. doi: 10.1371/journal.pgen.1005357

Dennis, J. S., and Citron, B. A. (2009). Wobbler mice modeling motor neuron disease display elevated transactive response DNA binding protein. *Neuroscience* 158, 745–750. doi: 10.1016/j.neuroscience.2008.10.030

Deschauer, M., Gaul, C., Behrmann, C., Prokisch, H., Zierz, S., and Haack, T. B. (2012). C19orf12 mutations in neurodegeneration with brain iron accumulation mimicking juvenile amyotrophic lateral sclerosis. *J. Neurol.* 259, 2434–2439. doi: 10.1007/s00415-012-6521-7

Diekstra, F. P., Van Vught, P. W. J., Van Rheenen, W., Koppers, M., Pasterkamp, R. J., Van Es, M. A., et al. (2012). UNC13A is a modifier of survival in amyotrophic lateral sclerosis. *Neurobiol. Aging* 33:630.e3-8. doi: 10.1016/j.neurobiolaging.2011.10.029

Ding, H., Schwarz, D. S., Keene, A., Affar el, B., Fenton, L., Xia, X., et al. (2003). Selective silencing by RNAi of a dominant allele that causes amyotrophic lateral sclerosis. *Aging Cell* 2, 209–217. doi: 10.1046/j.1474-9728.2003.00054.x

Dis, V., Kuijpers, M., Haasdijk, E., Teuling, E., Oakes, S. A., Hoogenraad, C., et al. (2014). Golgi fragmentation precedes neuromuscular denervation and is associated with endosome abnormalities in SOD1-ALS mouse motor neurons. *Acta Neuropathol. Commun.* 2:38. doi: 10.1186/2051-5960-2-38

Dobson-Stone, C., Luty, A. A., Thompson, E. M., Blumbergs, P., Brooks, W. S., Short, C. L., et al. (2013). Frontotemporal dementia-amyotrophic lateral sclerosis syndrome locus on chromosome 16p12.1-*q*12.2: genetic, clinical and neuropathological analysis. *Acta Neuropathol.* 125, 523–533. doi: 10.1007/s00401-013-1078-9

Dong, Y. N., Lin, H., Rattelle, A., Panzer, J., Lynch, D. R., et al. (2017). "Excitotoxicity," in *Comprehensive Toxicology,* 3rd edn, ed. C. McQueen (Kidlington: Elsevier Science & Technology), 70. Available at: https://www.elsevier.com/books/comprehensive-toxicology/mcqueen/978-0-08-100601-6 (accessed August 10, 2019).

Donnelly, C. J., Zhang, P.-W., Pham, J. T., Heusler, A. R., Mistry, N. A., Vidensky, S., et al. (2013). RNA toxicity from the ALS/FTD C9ORF72 expansion is mitigated by antisense intervention. *Neuron* 80, 415–428. doi: 10.1016/j.neuron.2013.10.015

Drepper, C., Lengeling, A., Thiel, C., Meisler, M. H., Jockusch, H., Mußmann, A., et al. (2005). Mutation of Vps54 causes motor neuron disease and defective spermiogenesis in the wobbler mouse. *Nat. Genet.* 37, 1213–1215. doi: 10.1038/ng1661

Egawa, N., Kitaoka, S., Tsukita, K., Naitoh, M., Takahashi, K., Yamamoto, T., et al. (2012). Drug screening for ALS using patient-specific induced pluripotent stem cells. *Sci. Transl. Med.* 4:145ra104. doi: 10.1126/scitranslmed.3004052

Elden, A. C., Kim, H.-J., Hart, M. P., Chen-Plotkin, A. S., Johnson, B. S., Fang, X., et al. (2010). Ataxin-2 intermediate-length polyglutamine expansions are associated with increased risk for ALS. *Nature* 466, 1069–1075. doi: 10.1038/nature09320

Evers, M. M., Toonen, L. J. A., and Van Roon-Mom, W. M. C. (2015). Antisense oligonucleotides in therapy for neurodegenerative disorders. *Adv. Drug Deliv. Rev.* 87, 90–103. doi: 10.1016/j.addr.2015.03.008

Falconer, D. S. (1956). Wobbler. *Mouse News Lett.* 15, 23–29.

Fan, Y., Abrahamsen, G., Mcgrath, J. J., and Mackay-Sim, A. (2012). Altered cell cycle dynamics in Schizophrenia. *Biol. Psychiatry* 71, 129–135. doi: 10.1016/j.biopsych.2011.10.004

Farg, M. A., Sundaramoorthy, V., Sultana, J. M., Yang, S., Atkinson, R. A. K., Levina, V., et al. (2014). C9ORF72, implicated in amytrophic lateral sclerosis and frontotemporal dementia, regulates endosomal trafficking. *Hum. Mol. Genet.* 23, 3579–3595. doi: 10.1093/hmg/ddu068

Fecto, F., Yan, J., Vemula, S., Liu, E., Yang, Y., Chen, W., et al. (2011). Sqstm1 mutations in familial and sporadic amyotrophic lateral sclerosis. *Arch. Neurol.* 68, 1440–1446. doi: 10.1001/archneurol.2011.250

Féron, F., Perry, C., Girard, S. D., and Mackay-Sim, A. (2013). Isolation of adult stem cells from the human olfactory mucosa. *Methods Mol. Biol.* 1059, 107–114. doi: 10.1007/978-1-62703-574-3_10

Féron, F., Perry, C., Mcgrath, J. J., and Mackay-Sim, A. (1998). New techniques for biopsy and culture of human olfactory epithelial neurons. *Arch. Otolaryngol.* 124, 861–866.

Feuillette, S., Delarue, M., Riou, G., Gaffuri, A.-L., Wu, J., Lenkei, Z., et al. (2017). Neuron-to-neuron transfer of FUS in drosophila primary neuronal culture is enhanced by ALS-associated mutations. *J. Mol. Neurosci.* 62, 114–122. doi: 10.1007/s12031-017-0908-y

Fifita, J. A., Zhang, K. Y., Galper, J., Williams, K. L., Mccann, E. P., Hogan, A. L., et al. (2017). Genetic and pathological assessment of hnRNPA1, hnRNPA2/B1, and hnRNPA3 in familial and Sporadic Amyotrophic Lateral Sclerosis. *Neuro Degener. Dis.* 17, 304–312. doi: 10.1159/000481258

Figlewicz, D. A., Figlewicz, D. A., Krizus, A., Krizus, A., Martinoli, M. G., Martinoli, M. G., et al. (1994). Variants of the heavy neurofilament subunit are associated with the development of amyotrophic lateral sclerosis. *Hum. Mol. Genet.* 3, 1757–1761. doi: 10.1093/hmg/3.10.1757

Finley, D. (2009). Recognition and processing of ubiquitin-protein conjugates by the proteasome. *Annu. Rev. Biochem.* 78, 477–513. doi: 10.1146/annurev.biochem.78.081507.101607

Fogh, I., Ratti, A., Gellera, C., Lin, K., Tiloca, C., Moskvina, V., et al. (2014). A genome-wide association meta-analysis identifies a novel locus at 17q11.2 associated with sporadic amyotrophic lateral sclerosis. *Hum. Mol. Genet.* 23, 2220–2231. doi: 10.1093/hmg/ddt587

Fondon, J. W., Hammock, E. A., Hannan, A. J., and King, D. G. (2008). Simple sequence repeats: genetic modulators of brain function and behavior. *Trends Neurosci.* 31, 328–334. doi: 10.1016/j.tins.2008.03.006

Forman, M. S., Mackenzie, I. R., Cairns, N. J., Swanson, E., Boyer, P. J., Drachman, D. A., et al. (2006). Novel ubiquitin neuropathology in frontotemporal dementia with valosin-containing protein gene mutations. *J. Neuropathol. Exp. Neurol.* 65, 571–581. doi: 10.1097/00005072-200606000-00005

Forsberg, K., Graffmo, K., Pakkenberg, B., Weber, M., Nielsen, M., Marklund, S., et al. (2019). Misfolded SOD1 inclusions in patients with mutations in ⁢em>C9orf72⁢/em> and other ALS/FTD-associated genes. *J. Neurol. Neurosurg. Psychiatry* 90, 861–869. doi: 10.1136/jnnp-2018-319386

Forsberg, K., Jonsson, P. A., Andersen, P. M., Bergemalm, D., Graffmo, K. S., Hultdin, M., et al. (2010). Novel antibodies reveal inclusions containing non-native SOD1 in sporadic ALS patients. *PLoS One* 5:e11552. doi: 10.1371/journal.pone.0011552

Fratta, P., Mizielinska, S., Nicoll, A. J., Zloh, M., Fisher, E. M. C., Parkinson, G., et al. (2012). C9orf72 hexanucleotide repeat associated with amyotrophic lateral sclerosis and frontotemporal dementia forms RNA G-quadruplexes. *Sci. Rep.* 2:1016. doi: 10.1038/srep01016

Freibaum, B. D., Lu, Y., Lopez-Gonzalez, R., Kim, N. C., Almeida, S., Lee, K.-H., et al. (2015). GGGGCC repeat expansion in C9orf72 compromises nucleocytoplasmic transport. *Nature* 525, 129–133. doi: 10.1038/nature14974

Freischmidt, A., Wieland, T., Richter, B., Ruf, W., Schaeffer, V., Müller, K., et al. (2015). Haploinsufficiency of TBK1 causes familial ALS and fronto-temporal dementia. *Nat. Neurosci.* 18, 631–636. doi: 10.1038/nn.4000

Fujita, Y., Mizuno, Y., Takatama, M., and Okamoto, K. (2007). Anterior horn cells with abnormal TDP-43 immunoreactivities show fragmentation of the Golgi apparatus in ALS. *J. Neurol. Sci.* 269, 30–34. doi: 10.1016/j.jns.2007.12.016

Fujita, Y., and Okamoto, K. (2005). Golgi apparatus of the motor neurons in patients with amyotrophic lateral sclerosis and in mice models of amyotrophic lateral sclerosis. *Neuropathology* 25, 388–394. doi: 10.1111/j.1440-1789.2005.00616.x

Gellera, C., Tiloca, C., Del Bo, R., Corrado, L., Pensato, V., Agostini, J., et al. (2013). Ubiquilin 2 mutations in Italian patients with amyotrophic lateral sclerosis and frontotemporal dementia. *J. Neurol. Neurosurg. Psychiatry* 84, 183–187. doi: 10.1136/jnnp-2012-303433

Gendron, T. F., Bieniek, K. F., Zhang, Y.-J., Jansen-West, K., Ash, P. E. A., Caulfield, T., et al. (2013). Antisense transcripts of the expanded C9ORF72 hexanucleotide repeat form nuclear RNA foci and undergo repeat-associated non-ATG translation in c9FTD/ALS. *Acta Neuropathol.* 126, 829–844. doi: 10.1007/s00401-013-1192-8

Giordana, M. T., Piccinini, M., Grifoni, S., Marco, G. D., Vercellino, M., Magistrello, M., et al. (2010). TDP-43 redistribution is an early event in sporadic Amyotrophic Lateral Sclerosis. *Brain Pathol.* 20, 351–360. doi: 10.1111/j.1750-3639.2009.00284.x

Gitcho, M. A., Baloh, R. H., Chakraverty, S., Mayo, K., Norton, J. B., Levitch, D., et al. (2008). TDP-43 A315T mutation in familial motor Neuron Disease. *Ann. Neurol.* 63, 535–538. doi: 10.1002/ana.21344

Gonatas, J. O., Gonatas, N. K., and Stieber, A. (2006). Fragmentation of the Golgi apparatus in neurodegenerative diseases and cell death. *J. Neurol. Sci.* 246, 21–30. doi: 10.1016/j.jns.2006.01.019

Gonatas, N. K., Stieber, A., Mourelatos, Z., Chen, Y., Gonatas, J. O., Appel, S. H., et al. (1992). Fragmentation of the Golgi apparatus of motor neurons in amyotrophic lateral sclerosis. *Am. J. Pathol.* 140, 731–737.

Gordon, P. H., Moore, D. H., Miller, R. G., Florence, J. M., Verheijde, J. L., Doorish, C., et al. (2007). Efficacy of minocycline in patients with amyotrophic lateral sclerosis: a phase III randomised trial. *Lancet Neurol.* 6, 1045–1053. doi: 10.1016/s1474-4422(07)70270-3

Greenway, M. J., Andersen, P. M., Russ, C., Ennis, S., Cashman, S., Donaghy, C., et al. (2006). ANG mutations segregate with familial and 'sporadic' amyotrophic lateral sclerosis. *Nat. Genet.* 38, 411–413. doi: 10.1038/ng1742

Gromicho, M., Oliveira Santos, M., Pinto, A., Pronto-Laborinho, A., and De Carvalho, M. (2017). Young-onset rapidly progressive ALS associated with heterozygous FUS mutation. *Amyotroph. Lateral Scler. Frontotemporal Degener.* 18, 451–453. doi: 10.1080/21678421.2017.1299762

Gros-Louis, F., Larivière, R., Gowing, G., Laurent, S., Camu, W., Bouchard, J.-P., et al. (2004). A frameshift deletion in peripherin gene associated with amyotrophic Lateral Sclerosis. *J. Biol. Chem.* 279, 45951–45956. doi: 10.1074/jbc.m408139200

Guo, W., Naujock, M., Fumagalli, L., Vandoorne, T., Baatsen, P., Boon, R., et al. (2017). HDAC6 inhibition reverses axonal transport defects in motor neurons derived from FUS-ALS patients. *Nat. Commun.* 8, 1–15. doi: 10.1038/s41467-017-00911-y

Gurney, M. E., Pu, H., Chiu, A. Y., Canto, M. C. D., Polchow, C. Y., Alexander, D. D., et al. (1994). Motor neuron degeneration in mice that express a human Cu, Zn superoxide dismutase mutation. *Science* 264, 1772–1775. doi: 10.1126/science.8209258

Hadano, S., Hand, C. K., Osuga, H., Yanagisawa, Y., Otomo, A., Devon, R. S., et al. (2001). A gene encoding a putative GTPase regulator is mutated in familial amyotrophic lateral sclerosis 2. *Nat. Genet.* 29, 166–173. doi: 10.1038/ng1001-166

Hand, C. K., Khoris, J., Salachas, F., Gros-Louis, F., Lopes, A. A. S., Mayeux-Portas, V., et al. (2002). A novel locus for familial amyotrophic lateral sclerosis, on chromosome 18q. *Am. J. Hum. Genet.* 70, 251–256. doi: 10.1086/337945

Harrison, A. F., and Shorter, J. (2017). RNA-binding proteins with prion-like domains in health and disease. *Biochem. J.* 474, 1417–1438. doi: 10.1042/BCJ20160499

Hayashi, Y., Homma, K., and Ichijo, H. (2016). SOD1 in neurotoxicity and its controversial roles in SOD1 mutation-negative ALS. *Adv. Biol. Regul.* 60, 95–104. doi: 10.1016/j.jbior.2015.10.006

Hennig, S., Kong, G., Mannen, T., Sadowska, A., Kobelke, S., Blythe, A., et al. (2015). Prion-like domains in RNA binding proteins are essential for building subnuclear paraspeckles. *J. Cell Biol.* 210, 529–539. doi: 10.1083/jcb.201504117

Hewitt, K. J., and Garlick, J. A. (2013). Cellular reprogramming to reset epigenetic signatures. *Mol. Aspects Med.* 34, 841–848. doi: 10.1016/j.mam.2012.08.002

Highley, J. R., Kirby, J., Jansweijer, J. A., Webb, P. S., Hewamadduma, C. A., Heath, P. R., et al. (2014). Loss of nuclear TDP-43 in amyotrophic lateral sclerosis (ALS) causes altered expression of splicing machinery and widespread dysregulation of RNA splicing in motor neurones. *Neuropathol. Appl. Neurobiol.* 40, 670–685. doi: 10.1111/nan.12148

Hill, S. J., Mordes, D. A., Cameron, L. A., Neuberg, D. S., Landini, S., Eggan, K., et al. (2016). Two familial ALS proteins function in prevention/repair of transcription-associated DNA damage. *Proc. Natl. Acad. Sci. U.S.A.* 113, E7701–E7709.

Hirano, A., Donnenfeld, H., Sasaki, S., and Nakano, I. (1984a). Fine structural observations of neurofilamentous changes in amyotrophic Lateral Sclerosis. *J. Neuropathol. Exp. Neurol.* 43, 461–470. doi: 10.1097/00005072-198409000-00001

Hirano, A., Nakano, I., Kurland, L. T., Mulder, D. W., Holley, P. W., and Saccomanno, G. (1984b). Fine structural study of neurofibrillary changes in a family with amyotrophic Lateral Sclerosis. *J. Neuropathol. Exp. Neurol.* 43, 471–480. doi: 10.1097/00005072-198409000-00002

Hirano, M., Nakamura, Y., Saigoh, K., Sakamoto, H., Ueno, S., Isono, C., et al. (2013). Mutations in the gene encoding p62 in Japanese patients with amyotrophic lateral sclerosis. *Neurology* 80:458. doi: 10.1212/WNL.0b013e31827f0fe5

Hirano, M., Quinzii, C. M., Mitsumoto, H., Hays, A. P., Roberts, J. K., Richard, P., et al. (2011). Senataxin mutations and amyotrophic lateral sclerosis. *Amyotroph. Lateral Scler.* 12, 223–227. doi: 10.3109/17482968.2010.545952

Hong-Fu, L., and Zhi-Ying, W. (2016). Genotype-phenotype correlations of amyotrophic lateral sclerosis. *Transl. Neurodegener.* 5:3. doi: 10.1186/s40035-016-0050-8

Huang, C., Zhou, H., Tong, J., Chen, H., Liu, Y.-J., Wang, D., et al. (2011). FUS transgenic rats develop the phenotypes of amyotrophic lateral sclerosis and frontotemporal lobar degeneration. *PLoS Genet.* 7:e1002011. doi: 10.1371/journal.pgen.1002011

Hübers, A., Just, W., Rosenbohm, A., Müller, K., Marroquin, N., Goebel, I., et al. (2015a). De novo FUS mutations are the most frequent genetic cause in early-onset German ALS patients. *Neurobiol. Aging* 36, 3117.e1–3117.e6. doi: 10.1016/j.neurobiolaging.2015.08.005

Hübers, A., Volk, A., Just, W., Rosenbohm, A., Bierbaumer, N., Kathrin, M., et al. (2015b). V42. De novo mutations in the FUS gene are a frequent cause of sporadic ALS in very young patients. *Clin. Neurophysiol.* 126:e87. doi: 10.1016/j.clinph.2015.04.120

Ichiyanagi, N., Fujimori, K., Yano, M., Ishihara-Fujisaki, C., Sone, T., Akiyama, T., et al. (2016). Establishment of in vitro FUS-associated familial amyotrophic lateral sclerosis model using human induced pluripotent stem cells. *Stem Cell Rep.* 6, 496–510. doi: 10.1016/j.stemcr.2016.02.011

Irwin, D., Lippa, C. F., and Rosso, A. (2008). Progranulin (PGRN) expression in ALS: an immunohistochemical study. *J. Neurol. Sci.* 276, 9–13. doi: 10.1016/j.jns.2008.08.024

Izhar, L., Adamson, B., Ciccia, A., Lewis, J., Pontano-Vaites, L., Leng, Y., et al. (2015). A Systematic analysis of factors localized to damaged chromatin reveals PARP-dependent recruitment of transcription factors. *Cell Rep.* 11, 1486–1500. doi: 10.1016/j.celrep.2015.04.053

Japtok, J., Lojewski, X., Naumann, M., Klingenstein, M., Reinhardt, P., Sterneckert, J., et al. (2015). Stepwise acquirement of hallmark neuropathology in FUS-ALS iPSC models depends on mutation type and neuronal aging. *Neurobiol. Dis.* 82, 420–429. doi: 10.1016/j.nbd.2015.07.017

Jiang, J., Zhu, Q., Gendron, T. F., Saberi, S., Mcalonis-Downes, M., Seelman, A., et al. (2016). Gain of toxicity from ALS/FTD-linked repeat expansions in C9ORF72 is alleviated by antisense oligonucleotides targeting GGGGCC-containing RNAs. *Neuron* 90, 535–550. doi: 10.1016/j.neuron.2016.04.006

Johnson, J. O., Glynn, S. M., Gibbs, J. R., Nalls, M. A., Sabatelli, M., Restagno, G., et al. (2014a). Mutations in the CHCHD10 gene are a common cause of familial amyotrophic lateral sclerosis. *Brain* 137:e311. doi: 10.1093/brain/awu265

Johnson, J. O., Pioro, E. P., Boehringer, A., Chia, R., Feit, H., Renton, A. E., et al. (2014b). Mutations in the Matrin 3 gene cause familial amyotrophic lateral sclerosis. *Nat. Neurosci.* 17, 664–666.

Johnson, J. O., Mandrioli, J., Benatar, M., Abramzon, Y., Van Deerlin, V. M., Trojanowski, J. Q., et al. (2010). Exome sequencing reveals VCP mutations as a cause of familial ALS. *Neuron* 68, 857–864. doi: 10.1016/j.neuron.2010.11.036

Juneja, T., Pericak-Vance, M. A., Laing, N. G., Dave, S., and Siddique, T. (1997). Prognosis in familial amyotrophic lateral sclerosis: progression and survival in patients with glu100gly and ala4val mutations in Cu,Zn superoxide dismutase. *Neurology* 48, 55–57. doi: 10.1212/wnl.48.1.55

Kabashi, E., Lin, L., Tradewell, M. L., Dion, P. A., Bercier, V., Bourgouin, P., et al. (2010). Gain and loss of function of ALS-related mutations of TARDBP (TDP-43) cause motor deficits in vivo. *Hum. Mol. Genet.* 19, 671–683. doi: 10.1093/hmg/ddp534

Kabashi, E., Valdmanis, P. N., Dion, P., Spiegelman, D., Mcconkey, B. J., Vande Velde, C., et al. (2008). TARDBP mutations in individuals with sporadic and familial amyotrophic lateral sclerosis. *Nat. Genet.* 40, 572–574. doi: 10.1038/ng.132

Kaczmarek, J. C., Kowalski, P. S., and Anderson, D. G. (2017). Advances in the delivery of RNA therapeutics: from concept to clinical reality. *Genome Med.* 9:60. doi: 10.1186/s13073-017-0450-0

Kaehler, C., Isensee, J., Nonhoff, U., Terrey, M., Hucho, T., Lehrach, H., et al. (2012). Ataxin-2-Like is a regulator of stress granules and processing bodies. *PLoS One* 7:e50134. doi: 10.1371/journal.pone.0050134

Kang, S. H., Li, Y., Fukaya, M., Lorenzini, I., Cleveland, D. W., Ostrow, L. W., et al. (2013). Degeneration and impaired regeneration of gray matter oligodendrocytes in amyotrophic lateral sclerosis. *Nat. Neurosci.* 16, 571–579. doi: 10.1038/nn.3357

Keam, S. J. (2018). Inotersen: first global approval. *Drugs* 78, 1371–1376. doi: 10.1007/s40265-018-0968-5

Kelekar, A. (2006). Autophagy. *Ann. N. Y. Acad. Sci.* 1066, 259–271.

Kenna, K. P., Mclaughlin, R. L., Byrne, S., Elamin, M., and Heverin, M. (2013). Delineating the genetic heterogeneity of ALS using targeted high-throughput sequencing. *J.Med. Genet.* 50, 776–783. doi: 10.1136/jmedgenet-2013-101795

Kenna, K. P., Van Doormaal, P. T. C., Dekker, A. M., Ticozzi, N., Kenna, B. J., Diekstra, F. P., et al. (2016). *NEK1* variants confer susceptibility to amyotrophic lateral sclerosis. *Nat. Genet*. 48, 1037–1042. doi: 10.1038/ng.3626

Keogh, M. J., Wei, W., Aryaman, J., Wilson, I., Talbot, K., Turner, M. R., et al. (2018). Oligogenic genetic variation of neurodegenerative disease genes in 980 postmortem human brains. *J.Neurol. Neurosurg. Psychiatry* 89:813. doi: 10.1136/jnnp-2017-317234

Khvorova, A., and Watts, J. K. (2017). The chemical evolution of oligonucleotide therapies of clinical utility. *Nat. Biotechnol.* 35, 238–248. doi: 10.1038/nbt.3765

Kim, H. J., Kim, N. C., Wang, Y.-D., Scarborough, E. A., Moore, J., Diaz, Z., et al. (2013). Mutations in prion-like domains in hnRNPA2B1 and hnRNPA1 cause multisystem proteinopathy and ALS. *Nature* 495, 467–473. doi: 10.1038/nature11922

Kim, H. J., and Taylor, J. P. (2017). Lost in transportation: nucleocytoplasmic transport defects in ALS and other neurodegenerative diseases. *Neuron* 96, 285–297. doi: 10.1016/j.neuron.2017.07.029

King, A. E., Woodhouse, A., Kirkcaldie, M. T. K., and Vickers, J. C. (2016). Excitotoxicity in ALS: overstimulation, or overreaction? *Exp. Neurol.* 275, 162–171. doi: 10.1016/j.expneurol.2015.09.019

Kino, Y., Washizu, C., Kurosawa, M., Yamada, M., Miyazaki, H., Akagi, T., et al. (2015). FUS/TLS deficiency causes behavioral and pathological abnormalities distinct from amyotrophic lateral sclerosis. *Acta Neuropathol. Commun.* 3:24. doi: 10.1186/s40478-015-0202-6

Kirby, J., Al Sultan, A., Waller, R., and Heath, P. (2016). The genetics of amyotrophic lateral sclerosis: current insights. *Degener. Neurol. Neuromusc. Dis.* 6, 49–64. doi: 10.2147/DNND.S84956

Klim, J. R., Williams, L. A., Limone, F., San Juan, G. I., Davis-Dusenbery, B. N., Mordes, D. A., et al. (2019). ALS-implicated protein TDP-43 sustains levels of STMN2, a mediator of motor neuron growth and repair. *Nat. Neurosci.* 22, 167–179. doi: 10.1038/s41593-018-0300-4

Komine, O., and Yamanaka, K. (2015). Neuroinflammation in motor neuron disease. *Nagoya J. Med. Sci.* 77, 537–549.

Koppers, M., Blokhuis, A. M., Westeneng, H. J., Terpstra, M. L., Zundel, C. A., Vieira de Sá, R., et al. (2015). C9orf72 ablation in mice does not cause motor neuron degeneration or motor deficits. *Ann. Neurol.* 78, 426–438. doi: 10.1002/ana.24453

Kovtun, I. V., and McMurray, C. T. (2008). Features of trinucleotide repeat instability in vivo. *Cell Res.* 18, 198–213. doi: 10.1038/cr.2008.5

Koyama, A., Sugai, A., Kato, T., Ishihara, T., Shiga, A., Toyoshima, Y., et al. (2016). Increased cytoplasmic TARDBP mRNA in affected spinal motor neurons in ALS caused by abnormal autoregulation of TDP-43. *Nucleic Acids Res.* 44, 5820–5836. doi: 10.1093/nar/gkw499

Kraemer, B. C., Schuck, T., Wheeler, J. M., Robinson, L. C., Trojanowski, J. Q., Lee, V. M. Y., et al. (2010). Loss of murine TDP-43 disrupts motor function and plays an essential role in embryogenesis. *Acta Neuropathol.* 119, 409–419. doi: 10.1007/s00401-010-0659-0

Kriz, J., Nguyen, M. D., and Julien, J.-P. (2002). Minocycline slows disease progression in a mouse model of amyotrophic Lateral Sclerosis. *Neurobiol. Dis.* 10, 268–278. doi: 10.1006/nbdi.2002.0487

Kwak, S., Hideyama, T., Yamashita, T., and Aizawa, H. (2010). AMPA receptor-mediated neuronal death in sporadic ALS. *Neuropathology* 30, 182–188. doi: 10.1111/j.1440-1789.2009.01090.x

Kwiatkowski, T. J., Bosco, D. A., Leclerc, A. L., Tamrazian, E., Vanderburg, C. R., Russ, C., et al. (2009). Mutations in the FUS/TLS gene on chromosome 16 cause familial amyotrophic Lateral Sclerosis. *Science* 323, 1205–1208.

Lagier-Tourenne, C., Baughn, M., Rigo, F., Sun, S., Liu, P., Li, H.-R., et al. (2013). Targeted degradation of sense and antisense C9orf72 RNA foci as therapy for ALS and frontotemporal degeneration. *Proc. Natl. Acad. Sci. U.S.A.* 110, E4530–E4539. doi: 10.1073/pnas.1318835110

Lagier-Tourenne, C., Polymenidou, M., Hutt, K. R., Vu, A. Q., Baughn, M., Huelga, S. C., et al. (2012). Divergent roles of ALS-linked proteins FUS/TLS and TDP-43 intersect in processing long pre-mRNAs. *Nat. Neurosci.* 15, 1488–1497. doi: 10.1038/nn.3230

Lall, D., and Baloh, R. H. (2017). Microglia and C9orf72 in neuroinflammation and ALS and frontotemporal dementia. *J. Clin. Invest.* 127, 3250–3258. doi: 10.1172/jci90607

Landers, J. E., Shi, L., Cho, T.-J., Glass, J. D., Shaw, C. E., Leigh, P. N., et al. (2008). A common haplotype within the PON1 promoter region is associated with sporadic ALS. *Amyotroph. Lateral Scler.* 9, 306–314. doi: 10.1080/17482960802233177

Lattante, S., Pomponi, M. G., Conte, A., Marangi, G., Bisogni, G., Patanella, A. K., et al. (2018). ATXN1 intermediate-length polyglutamine expansions are associated with amyotrophic lateral sclerosis. *Neurobiol. Aging* 64, 157.e1–157.e5. doi: 10.1016/j.neurobiolaging.2017.11.011

Lattante, S., Rouleau, G. A., and Kabashi, E. (2013). TARDBP and FUS mutations associated with amyotrophic lateral sclerosis: summary and update. *Hum. Mutat.* 34, 812–826. doi: 10.1002/humu.22319

Lee, S., and Kim, H. J. (2015). Prion-like mechanism in amyotrophic lateral Sclerosis: are protein aggregates the key? *Exp. Neurobiol.* 24, 1–7. doi: 10.5607/en.2015.24.1.1

Lee, Y., Morrison, B. M., Li, Y., Lengacher, S., Farah, M. H., Hoffman, P. N., et al. (2012). Oligodendroglia metabolically support axons and contribute to neurodegeneration. *Nature* 487, 443–448. doi: 10.1038/nature11314

Lee, Y.-B., Chen, H.-J., Peres, J. N., Gomez-Deza, J., Attig, J., Štalekar, M., et al. (2013). Hexanucleotide repeats in ALS/FTD form length-dependent RNA Foci. sequester RNA binding proteins, and are neurotoxic. *Cell Rep.* 5, 1178–1186. doi: 10.1016/j.celrep.2013.10.049

Leigh, P. N., Whitwell, H., Garofalo, O., Buller, J., Swash, M., Martin, J., et al. (1991). Ubiquitin-immunoreactive intraneuronal inclusions in amyotrophic lateral sclerosis. Morphology, distribution, and specificity. *Brain* 114(Pt 2), 775–788. doi: 10.1093/brain/114.2.775

Lenzi, J., De Santis, R., De Turris, V., Morlando, M., Laneve, P., Calvo, A., et al. (2015). ALS mutant FUS proteins are recruited into stress granules in induced pluripotent stem cell-derived motoneurons. *DMM Dis. Models Mech.* 8, 755–766. doi: 10.1242/dmm.020099

Leung, C. L., He, C. Z., Kaufmann, P., Chin, S. S., Naini, A., Liem, R. K. H., et al. (2004). A pathogenic peripherin gene mutation in a patient with Amyotrophic Lateral Sclerosis. *Brain Pathol.* 14, 290–296. doi: 10.1111/j.1750-3639.2004.tb00066.x

Liachko, N. F., Guthrie, C. R., and Kraemer, B. C. (2010). Phosphorylation promotes neurotoxicity in a *Caenorhabditis elegans* model of TDP-43

proteinopathy. *J. Neurosci.* 30, 16208–16219. doi: 10.1523/JNEUROSCI.2911-10.2010

Liang, G., and Zhang, Y. (2013). Genetic and epigenetic variations in iPSCS: potential causes and implications for application. *Cell Stem Cell* 13, 149–159. doi: 10.1016/j.stem.2013.07.001

Liddelow, S. A., Guttenplan, K. A., Clarke, L. E., Bennett, F. C., Bohlen, C. J., Schirmer, L., et al. (2017). Neurotoxic reactive astrocytes are induced by activated microglia. *Nature* 541, 481–487. doi: 10.1038/nature21029

Ligon, L. A., Lamonte, B. H., Wallace, K. E., Weber, N., Kalb, R. G., and Holzbaur, E. L. F. (2005). Mutant superoxide dismutase disrupts cytoplasmic dynein in motor neurons. *Neuroreport* 16, 533–536. doi: 10.1097/00001756-200504250-00002

Lim, S. M., Choi, W. J., Oh, K.-W., Xue, Y., Choi, J. Y., Kim, S. H., et al. (2016). Directly converted patient-specific induced neurons mirror the neuropathology of FUS with disrupted nuclear localization in amyotrophic lateral sclerosis. *Mol. Neurodegener.* 11:8. doi: 10.1186/s13024-016-0075-6

Liu, J., and Wang, F. (2017). Role of neuroinflammation in amyotrophic lateral sclerosis: cellular mechanisms and therapeutic implications. *Front. immunol.* 8:1005. doi: 10.3389/fimmu.2017.01005

Liu, M.-L., Zang, T., and Zhang, C.-L. (2016). Direct lineage reprogramming reveals disease-specific phenotypes of motor neurons from human ALS patients. *Cell Rep.* 14, 115–128. doi: 10.1016/j.celrep.2015.12.018

Liu, Z.-J., Li, H.-F., Tan, G.-H., Tao, Q.-Q., Ni, W., Cheng, X.-W., et al. (2014). Identify mutation in amyotrophic lateral sclerosis cases using HaloPlex target enrichment system. *Neurobiol. Aging* 35, 2881.e11–2881.e15. doi: 10.1016/j.neurobiolaging.2014.07.003

Luty, A. A., Kwok, J. B. J., Dobson-Stone, C., Loy, C. T., Coupland, K. G., Karlström, H., et al. (2010). Sigma nonopioid intracellular receptor 1 mutations cause frontotemporal lobar degeneration-motor neuron disease. *Ann. Neurol.* 68, 639–649. doi: 10.1002/ana.22274

Mackay-Sim, A. (2012). Concise review: patient-derived olfactory stem cells: new models for brain diseases. *Stem Cells* 30, 2361–2365. doi: 10.1002/stem.1220

Majcher, V., Goode, A., James, V., and Layfield, R. (2015). Autophagy receptor defects and ALS-FTLD. *Mol. Cell. Neurosci.* 66, 43–52. doi: 10.1016/j.mcn.2015.01.002

Manolio, T. A., Collins, F. S., Cox, N. J., Goldstein, D. B., Hindorff, L. A., Hunter, D. J., et al. (2009). Finding the missing heritability of complex diseases. *Nature* 461, 747–753. doi: 10.1038/nature08494

Maruyama, H., Morino, H., Ito, H., Izumi, Y., Kato, H., Watanabe, Y., et al. (2010). Mutations of optineurin in amyotrophic lateral sclerosis. *Nature* 465, 223–226. doi: 10.1038/nature08971

Mastrocola, A. S., Kim, S. H., Trinh, A. T., Rodenkirch, L. A., and Tibbetts, R. S. (2013). The RNA-binding protein fused in sarcoma (FUS) functions downstream of poly(ADP-ribose) polymerase (PARP) in response to DNA damage. *J. Biol. Chem.* 288, 24731–24741. doi: 10.1074/jbc.M113.497974

McCord, J. M., and Fridovich, I. (1969). Superoxide dismutase: an enzymatic function for erythrocuprein (hemocuprein). *J. Biol. Chem.* 244, 6049–6055.

Millecamps, S., and Julien, J.-P. (2013). Axonal transport deficits and neurodegenerative diseases. *Nat. Rev. Neurosci.* 14, 161–176. doi: 10.1038/nrn3380

Miller, T., Pestronk, A., David, W., Rothstein, J., Simpson, E., Appel, S. H., et al. (2013). A phase I, randomised, first-in-human study of an antisense oligonucleotide directed against SOD1 delivered intrathecally in SOD1-familial ALS patients. *Lancet Neurol.* 12, 435–442. doi: 10.1016/s1474-4422(13)70061-9

Mitchell, J., Paul, P., Chen, H.-J., Morris, A., Payling, M., Falchi, M., et al. (2010). Familial amyotrophic lateral sclerosis is associated with a mutation in D-amino acid oxidase. *Proc. Natl. Acad. Sci. U.S.A.* 107, 7556–7561. doi: 10.1073/pnas.0914128107

Mitchell, J. C., Mcgoldrick, P., Vance, C., Hortobagyi, T., Sreedharan, J., Rogelj, B., et al. (2013). Overexpression of human wild-type FUS causes progressive motor neuron degeneration in an age- and dose-dependent fashion. *Acta Neuropathol.* 125, 273–288. doi: 10.1007/s00401-012-1043-z

Modrek, B., and Lee, C. J. (2003). Alternative splicing in the human, mouse and rat genomes is associated with an increased frequency of exon creation and/or loss. *Nat. Genet.* 34, 177–180. doi: 10.1038/ng1159

Mompeán, M., Baralle, M., Buratti, E., and Laurents, D. V. (2016). An amyloid-like pathological conformation of TDP-43 is stabilized by hypercooperative hydrogen bonds. *Front. Mol. Neurosci.* 9:125.

Morgan, S., Shatunov, A., Sproviero, W., Jones, A. R., Shoai, M., Hughes, D., et al. (2017). A comprehensive analysis of rare genetic variation in amyotrophic lateral sclerosis in the UK. *Brain* 140, 1611–1618.

Mori, K., Lammich, S., Mackenzie, I. R. A., Forné, I., and Zilow, S. (2013). hnRNP A3 binds to GGGGCC repeats and is a constituent of p62-positive/TDP43-negative inclusions in the hippocampus of patients with C9orf72 mutations. *Acta Neuropathol.* 125, 413–423. doi: 10.1007/s00401-013-1088-7

Moser, J. M., Bigini, P., and Schmitt-John, T. (2013). The wobbler mouse, an ALS animal model. *Mol. Genet. Genom.* 288, 207–229. doi: 10.1007/s00438-013-0741-0

Mourelatos, Z., Hirano, A., Rosenquist, A. C., and Gonatas, N. K. (1994). Fragmentation of the golgi apparatus of motor neurons in amyotrophic lateral sclerosis (ALS): clinical studies in ALS of guam and experimental studies in deafferented neurons and in ß,ß′-iminodipropionitrile axonopathy. *Am. J. Pathol.* 144, 1288–1300.

Münch, C., Rosenbohm, A., Sperfeld, A.-D., Uttner, I., Reske, S., Krause, B. J., et al. (2005). Heterozygous R1101K mutation of the DCTN1 gene in a family with ALS and FTD. *Ann. Neurol.* 58, 777–780. doi: 10.1002/ana.20631

Münch, C., Sedlmeier, R., Meyer, T., Homberg, V., Sperfeld, A. D., Kurt, A., et al. (2004). Point mutations of the p150 subunit of ⁢em>dynactin⁢/em> (⁢em>DCTN1⁢/em&gt) gene in ALS. *Neurology* 63, 724–726. doi: 10.1212/01.wnl.0000134608.83927.b1

Murphy, N. A., Arthur, K. C., Tienari, P. J., Houlden, H., Chio, A., and Traynor, B. J. (2017). Age-related penetrance of the C9orf72 repeat expansion. *Sci. Rep.* 7, 1–7. doi: 10.1038/s41598-017-02364-1

Naruse, H., Ishiura, H., Mitsui, J., Date, H., Takahashi, Y., Matsukawa, T., et al. (2018). Molecular epidemiological study of familial amyotrophic lateral sclerosis in Japanese population by whole-exome sequencing and identification of novel HNRNPA1 mutation. *Neurobiol. Aging* 61, 255.e9–255.e16. doi: 10.1016/j.neurobiolaging.2017.08.030

Nassif, M., Woehlbier, U., and Manque, P. A. (2017). The Enigmatic Role of C9ORF72 in Autophagy. *Front. Neurosci.* 11:442. doi: 10.3389/fnins.2017.00442

Nave, K.-A. (2010). Myelination and support of axonal integrity by glia. *Nature* 468, 244–252. doi: 10.1038/nature09614

Neumann, M. (2009). Molecular neuropathology of TDP-43 proteinopathies. *Int. J. Mol. Sci.* 10, 232–246. doi: 10.3390/ijms10010232

Neumann, M., Bentmann, E., Dormann, D., Jawaid, A., Dejesus-Hernandez, M., Ansorge, O., et al. (2011). FET proteins TAF15 and EWS are selective markers that distinguish FTLD with FUS pathology from amyotrophic lateral sclerosis with FUS mutations. *Brain* 134, 2595–2609. doi: 10.1093/brain/awr201

Neumann, M., Sampathu, D. M., Kwong, L. K., Truax, A. C., Micsenyi, M. C., Chou, T. T., et al. (2006). Ubiquitinated TDP-43 in frontotemporal lobar degeneration and amyotrophic Lateral Sclerosis. *Science* 314, 130–133.

Nguyen, H. P., Van Mossevelde, S., Dillen, L., De Bleecker, J. L., Moisse, M., Van Damme, P., et al. (2018). NEK1 genetic variability in a Belgian cohort of ALS and ALS-FTD patients. *Neurobiol. Aging* 61, 255.e251–255.e257. doi: 10.1016/j.neurobiolaging.2017.08.021

Niebroj-Dobosz, I., Rafałowska, J., Fidziańska, A., Gadamski, R., and Grieb, P. (2007). Myelin composition of spinal cord in a model of amyotrophic lateral sclerosis (ALS) in SOD1G93A transgenic rats. *Folia Neuropathol.* 45, 236–241.

Nishimura, A. L., Mitne-Neto, M., Silva, H. C. A., Richieri-Costa, A., Middleton, S., Cascio, D., et al. (2004). A mutation in the vesicle-trafficking protein VAPB causes late-onset spinal muscular atrophy and amyotrophic lateral sclerosis. *Am. J. Hum. Genet.* 75, 822–831. doi: 10.1086/425287

Nishimura, A. L., Shum, C., Scotter, E. L., Abdelgany, A., Sardone, V., Wright, J., et al. (2014). Allele-specific knockdown of ALS-associated mutant TDP-43 in neural stem cells derived from induced pluripotent stem cells. *PLoS One* 9:e91269. doi: 10.1371/journal.pone.0091269

Niu, C., Zhang, J., Gao, F., Yang, L., Jia, M., Zhu, H., et al. (2012). FUS-NLS/Transportin 1 complex structure provides insights into the nuclear targeting mechanism of FUS and the implications in ALS. *PLoS One* 7:e47056. doi: 10.1371/journal.pone.0047056

Nolan, M., Talbot, K., and Ansorge, O. (2016). Pathogenesis of FUS-associated ALS and FTD: insights from rodent models. *Acta Neuropathol. Commun.* 4:99. doi: 10.1186/s40478-016-0358-8

Nomura, T., Watanabe, S., Kaneko, K., Yamanaka, K., Nukina, N., and Furukawa, Y. (2014). Intranuclear aggregation of mutant FUS/TLS as a molecular pathomechanism of amyotrophic lateral sclerosis. *J. Biol. Chem.* 289, 1192–1202. doi: 10.1074/jbc.M113.516492

Nonaka, T., Masuda-Suzukake, M., Arai, T., Hasegawa, M., Hasegawa, Y., Akatsu, H., et al. (2013). Prion-like properties of pathological TDP-43 aggregates from diseased brains. *Cell Rep.* 4, 124–134. doi: 10.1016/j.celrep.2013.06.007

Oakes, J. A., Davies, M. C., and Collins, M. O. (2017). TBK1: a new player in ALS linking autophagy and neuroinflammation. *Mol. Brain* 10:5. doi: 10.1186/s13041-017-0287-x

Orlacchio, A., Babalini, C., Borreca, A., Patrono, C., Massa, R., Basaran, S., et al. (2010). SPATACSIN mutations cause autosomal recessive juvenile amyotrophic lateral sclerosis. *Brain* 133, 591–598. doi: 10.1093/brain/awp325

O'Rourke, J. G., Bogdanik, L., Muhammad, A. K. M. G., Gendron, T. F., Kim, K. J., Austin, A., et al. (2015). C9orf72 BAC Transgenic Mice Display Typical Pathologic Features of ALS/FTD. *Neuron* 88, 892–901. doi: 10.1016/j.neuron.2015.10.027

Osmanovic, A., Rangnau, I., Kosfeld, A., Abdulla, S., Janssen, C., Auber, B., et al. (2017). FIG4 variants in central European patients with amyotrophic lateral sclerosis: a whole-exome and targeted sequencing study. *Eur. J. Hum. Genet.* 25, 324–331. doi: 10.1038/ejhg.2016.186

Pang, S. Y.-Y., Hsu, J. S., Teo, K.-C., Li, Y., Kung, M. H. W., Cheah, K. S. E., et al. (2017). Burden of rare variants in ALS genes influences survival in familial and sporadic ALS. *Neurobiol. Aging* 58, 238.e9–238.e15. doi: 10.1016/j.neurobiolaging.2017.06.007

Pang, Z. P., Yang, N., Vierbuchen, T., Ostermeier, A., Fuentes, D. R., Yang, T. Q., et al. (2011). Induction of human neuronal cells by defined transcription factors. *Nature* 476, 220–223. doi: 10.1038/nature10202

Parkinson, N., Ince, P. G., Smith, M. O., Highley, R., Skibinski, G., Andersen, P. M., et al. (2006). ALS phenotypes with mutations in ⁢em>CHMP2B⁢/em> (charged multivesicular body protein 2B). *Neurology* 67, 1074–1077.

Paronetto, Maria P, Miñana, B., and Valcárcel, J. (2011). The ewing sarcoma protein regulates DNA damage-induced alternative splicing. *Mol. Cell* 43, 353–368. doi: 10.1016/j.molcel.2011.05.035

Pascuzzi, R. M., Shefner, J., Chappell, A. S., Bjerke, J. S., Tamura, R., Chaudhry, V., et al. (2010). A phase II trial of talampanel in subjects with amyotrophic lateral sclerosis. *Amyotroph. Lateral Scler.* 11, 266–271. doi: 10.3109/17482960903307805

Pensato, V., Tiloca, C., Corrado, L., Bertolin, C., Sardone, V., Del Bo, R., et al. (2015). TUBA4A gene analysis in sporadic amyotrophic lateral sclerosis: identification of novel mutations. *J. Neurol.* 262, 1376–1378.

Pérez-Victoria, F. J., Abascal-Palacios, G., Tascón, I., Kajava, A., Magadán, J. G., Pioro, E. P., et al. (2010). Structural basis for the wobbler mouse neurodegenerative disorder caused by mutation in the Vps54 subunit of the GARP complex. *Proc. Natl. Acad. Sci. U.S.A.* 107, 12860–12865. doi: 10.1073/pnas.1004756107

Peters, O. M., Cabrera, G. T., Tran, H., Gendron, T. F., Mckeon, J. E., Metterville, J., et al. (2015). Human C9ORF72 hexanucleotide expansion reproduces RNA foci and dipeptide repeat proteins but not neurodegeneration in BAC transgenic mice. *Neuron* 88, 902–909. doi: 10.1016/j.neuron.2015.11.018

Petrov, D., Mansfield, C., Moussy, A., and Hermine, O. (2017). ALS clinical trials review: 20 years of failure. are we any closer to registering a new treatment?. *Front. Aging Neurosci.* 9:68. doi: 10.3389/fnagi.2017.00068

Philips, T., and Rothstein, J. D. (2015). Rodent models of amyotrophic Lateral Sclerosis. *Curr. Protoc. Pharmacol.* 69:5.67.1-21.

Philips, T., and Rothstein, J. D. (2017). Oligodendroglia: metabolic supporters of neurons. *J. Clin. Invest.* 127, 3271–3280. doi: 10.1172/jci90610

Pickles, S., Semmler, S., Broom, H. R., Destroismaisons, L., Legroux, L., Arbour, N., et al. (2016). ALS-linked misfolded SOD1 species have divergent impacts on mitochondria. *Acta Neuropathol. Commun.* 4:43. doi: 10.1186/s40478-016-0313-8

Pottier, C., Rampersaud, E., Baker, M., Wu, G., Wuu, J., Mccauley, J. L., et al. (2018). Identification of compound heterozygous variants in OPTN in an ALS-FTD patient from the CReATe consortium: a case report. *Amyotroph. Lateral Scler. Frontotemporal Degener.* 19, 469–471. doi: 10.1080/21678421.2018.1452947

Protter, D. S. W., and Parker, R. (2016). Principles and properties of stress granules. *Trends Cell Biol.* 26, 668–679. doi: 10.1016/j.tcb.2016.05.004

Qiu, H., Lee, S., Shang, Y., Wang, W.-Y., Au, K. F., Kamiya, S., et al. (2014). ALS-associated mutation FUS-R521C causes DNA damage and RNA splicing defects. *J. Clin. Invest.* 124, 981–999. doi: 10.1172/JCI72723

Rainier, S., Bui, M., Mark, E., Thomas, D., Tokarz, D., Ming, L., et al. (2008). Neuropathy target esterase gene mutations cause motor neuron disease. *Am. J. Hum. Genet.* 82, 780–785. doi: 10.1016/j.ajhg.2007.12.018

Ratti, A., and Buratti, E. (2016). Physiological functions and pathobiology of TDP-43 and FUS/TLS proteins. *J. Neurochem.* 138, 95–111. doi: 10.1111/jnc.13625

Ravits, J., Paul, P., and Jorg, C. (2007). Focality of upper and lower motor neuron degeneration at the clinical onset of ALS. *Neurology* 68, 1571–1575. doi: 10.1212/01.wnl.0000260965.20021.47

Renton, A. E., Chio, A., and Traynor, B. J. (2014). State of play in amyotrophic lateral sclerosis genetics. *Nat. Neurosci.* 17, 17–23. doi: 10.1038/nn.3584

Renton, A. E., Majounie, E., Waite, A., Simón-Sánchez, J., Rollinson, S., Gibbs, J. R., et al. (2011). A hexanucleotide repeat expansion in C9ORF72 is the cause of chromosome 9p21-linked ALS-FTD. *Neuron* 72, 257–268. doi: 10.1016/j.neuron.2011.09.010

Robinson, H. K., Deykin, A. V., Bronovitsky, E. V., Ovchinnikov, R. K., Ustyugov, A. A., Shelkovnikova, T. A., et al. (2015). Early lethality and neuronal proteinopathy in mice expressing cytoplasm-targeted FUS that lacks the RNA recognition motif. *Amyotroph. Lateral Scler. Frontotemporal Degener.* 16, 402–409. doi: 10.3109/21678421.2015.1040994

Rosen, D. R., Siddique, T., Patterson, D., Figlewicz, D. A., Sapp, P., Hentati, A., et al. (1993). Mutations in Cu/Zn superoxide dismutase gene are associated with familial amyotrophic lateral sclerosis. *Nature* 362:59.

Roses, A. D., Akkari, P. A., Chiba-Falek, O., Lutz, M. W., Gottschalk, W. K., Saunders, A. M., et al. (2016). Structural variants can be more informative for disease diagnostics, prognostics and translation than current SNP mapping and exon sequencing. *Expert Opin. Drug Metab. Toxicol.* 12, 135–147. doi: 10.1517/17425255.2016.1133586

Rouleau, G. A., Clark, A. W., Rooke, K., Pramatarova, A., Krizus, A., Suchowersky, O., et al. (1996). SOD1 mutation is associated with accumulation of neurofilaments in amyotrophic lateral sclerosis. *Ann. Neurol.* 39, 128–131.

Rowland, L. P., and Shneider, N. A. (2001). Amyotrophic lateral sclerosis. *New Engl. J. Med.* 344, 1688–1700.

Rubino, E., Rainero, I., Chiò, A., Rogaeva, E., Galimberti, D., Fenoglio, P., et al. (2012). SQSTM1 mutations in frontotemporal lobar degeneration and amyotrophic lateral sclerosis. *Neurology* 79, 1556–1562. doi: 10.1212/WNL.0b013e31826e25df

Rulten, S. L., Rotheray, A., Green, R. L., Grundy, G. J., Moore, D. A. Q., Gómez-Herreros, F., et al. (2014). PARP-1 dependent recruitment of the amyotrophic lateral sclerosis-associated protein FUS/TLS to sites of oxidative DNA damage. *Nucleic Acids Res.* 42, 307–314. doi: 10.1093/nar/gkt835

Rutherford, N. J., Zhang, Y.-J., Baker, M., Gass, J. M., Finch, N. A., Xu, Y.-F., et al. (2008). Novel mutations in TARDBP (TDP-43) in patients with familial amyotrophic Lateral Sclerosis. *PLoS Genet.* 4:e1000193. doi: 10.1371/journal.pgen.1000193

Sabatelli, M., Eusebi, F., Al-Chalabi, A., Conte, A., Madia, F., Luigetti, M., et al. (2009). Rare missense variants of neuronal nicotinic acetylcholine receptor altering receptor function are associated with sporadic amyotrophic lateral sclerosis. *Hum. Mol Genet.* 18, 3997–4006. doi: 10.1093/hmg/ddp339

Sabatelli, M., Lattante, S., Conte, A., Marangi, G., Luigetti, M., Del Grande, A., et al. (2012). Replication of association of CHRNA4 rare variants with sporadic amyotrophic lateral sclerosis: the Italian multicentre study. *Amyotroph. Lateral Scler.* 13, 580–584. doi: 10.3109/17482968.2012.704926

Saeed, M., Siddique, N., Hung, W. Y., Usacheva, E., Liu, E., Sufit, R. L., et al. (2006). Paraoxonase cluster polymorphisms are associated with sporadic ALS. *Neurology* 67, 771–776. doi: 10.1212/01.wnl.0000227187.52002.88

Sances, S., Bruijn, L. I., Chandran, S., Eggan, K., Ho, R., Klim, J. R., et al. (2016). Modeling ALS with motor neurons derived from human induced pluripotent stem cells. *Nat. Neurosci.* 19, 542–553. doi: 10.1038/nn.4273

Sanhueza, M., Zechini, L., Gillespie, T., and Pennetta, G. (2013). Gain-of-function mutations in the ALS8 causative gene VAPB have detrimental

effects on neurons and muscles. *Biol. Open* 3, 59–71. doi: 10.1242/bio.20137070

Sapp, P. C., Hosler, B. A., Mckenna-Yasek, D., Chin, W., Gann, A., Genise, H., et al. (2003). Identification of two novel loci for dominantly inherited familial amyotrophic lateral sclerosis. *Am. J. Hum. Genet.* 73, 397–403. doi: 10.1086/377158

Sareen, D., O'rourke, J. G., Meera, P., Muhammad, A., Grant, S., Simpkinson, M., et al. (2013). Targeting RNA foci in iPSC-derived motor neurons from ALS patients with C9ORF72 repeat expansion. *Sci. Transl. Med.* 5:ra149-208. doi: 10.1126/scitranslmed.3007529

Sasaki, S., and Iwata, M. (1996). Ultrastructural study of synapses in the anterior horn neurons of patients with amyotrophic lateral sclerosis. *Neurosci. Lett.* 204, 53–56. doi: 10.1016/0304-3940(96)12314-4

Sasayama, H., Shimamura, M., Tokuda, T., Azuma, Y., Yoshida, T., Mizuno, T., et al. (2012). Knockdown of the Drosophila Fused in Sarcoma (FUS) homologue causes deficient locomotive behavior and shortening of motoneuron terminal Branches. *PLoS One* 7:e39483. doi: 10.1371/journal.pone.0039483

Sawada, H. (2017). Clinical efficacy of edaravone for the treatment of amyotrophic lateral sclerosis. *Expert Opin. Pharmacother.* 18, 735–738. doi: 10.1080/14656566.2017.1319937

Scekic-Zahirovic, J., Sendscheid, O., El Oussini, H., Jambeau, M., Sun, Y., Mersmann, S., et al. (2016). Toxic gain of function from mutant FUS protein is crucial to trigger cell autonomous motor neuron loss. *EMBO J.* 35, 1077–1097. doi: 10.15252/embj.201592559

Schipper, L. J., Raaphorst, J., Aronica, E., Baas, F., Haan, R., Visser, M., et al. (2016). Prevalence of brain and spinal cord inclusions, including dipeptide repeat proteins, in patients with the C9ORF72 hexanucleotide repeat expansion: a systematic neuropathological review. *Neuropathol. Appl. Neurobiol.* 42, 547–560. doi: 10.1111/nan.12284

Seminary, E. R., Sison, S. L., and Ebert, A. D. (2018). modeling protein aggregation and the heat shock response in ALS iPSC-derived motor neurons. *Front. Neurosci.* 12:86. doi: 10.3389/fnins.2018.00086

Sephton, C. F., Good, S. K., Atkin, S., Dewey, C. M., Iii, P. M., Herz, J., et al. (2010). TDP-43 is a developmentally regulated protein essential for early embryonic development. *J. Biol. Chem.* 285, 6826–6834. doi: 10.1074/jbc.M109.061846

Shang, Y., and Huang, E. J. (2016). Mechanisms of FUS mutations in familial amyotrophic lateral sclerosis. *Brain Res.* 1647, 65–78. doi: 10.1016/j.brainres.2016.03.036

Sharma, A., Lyashchenko, A. K., Lu, L., Nasrabady, S. E., Elmaleh, M., Mendelsohn, M., et al. (2016). ALS-associated mutant FUS induces selective motor neuron degeneration through toxic gain of function. *Nat. Commun.* 7:10465. doi: 10.1038/ncomms10465

Shelkovnikova, T. A., Peters, O. M., Deykin, A. V., Connor-Robson, N., Robinson, H., Ustyugov, A. A., et al. (2013). Fused in sarcoma (FUS) protein lacking nuclear localization signal (NLS) and major RNA binding motifs triggers proteinopathy and severe motor phenotype in transgenic mice. *J. Biol. Chem.* 288, 25266–25274. doi: 10.1074/jbc.M113.492017

Shibata, N., Nagai, R., Uchida, K., Horiuchi, S., Yamada, S., Hirano, A., et al. (2001). Morphological evidence for lipid peroxidation and protein glycoxidation in spinal cords from sporadic amyotrophic lateral sclerosis patients. *Brain Res.* 917, 97–104. doi: 10.1016/s0006-8993(01)02926-2

Shu, S., Lei, X., Liu, F., Cui, B., Liu, Q., Ding, Q., et al. (2018). Mutation screening of *NEK1* in Chinese ALS patients. *Neurobiol. Aging* 71, 267.e261–267.e264. doi: 10.1016/j.neurobiolaging.2018.06.022

Simpson, C. L., Lemmens, R., Miskiewicz, K., Broom, W. J., Hansen, V. K., Van Vught, P. W. J., et al. (2009). Variants of the elongator protein 3 (ELP3) gene are associated with motor neuron degeneration. *Hum. Mol. Genet.* 18, 472–481. doi: 10.1093/hmg/ddn375

Singh, N. N., Howell, M. D., Androphy, E. J., and Singh, R. N. (2017). How the discovery of ISS-N1 led to the first medical therapy for spinal muscular atrophy. *Gene Ther.* 24, 520–526. doi: 10.1038/gt.2017.34

Siwek, D. R., Beal, M. F., Brown, R. H., Hoffman, E. K., Kowall, N. W., Ferrante, R. J., et al. (1996). Motor neurons in Cu/Zn superoxide dismutase-deficient mice develop normally but exhibit enhanced cell death after axonal injury. *Nat. Genet.* 13, 43–47. doi: 10.1038/ng0596-43

Skourti-Stathaki, K., Proudfoot, N. J., and Gromak, N. (2011). Human senataxin resolves RNA/DNA hybrids formed at transcriptional pause sites to promote Xrn2-dependent termination. *Mol. Cell* 42, 794–805. doi: 10.1016/j.molcel.2011.04.026

Smith, B. N., Ticozzi, N., Fallini, C., Gkazi, A. S., Topp, S., Kenna, K. P., et al. (2014). Exome-wide rare variant analysis identifies tuba4a mutations associated with familial ALS. *Neuron* 84, 324–331. doi: 10.1016/j.neuron.2014.09.027

Smith, B. N., Vance, C., Scotter, E. L., Troakes, C., Wong, C. H., Topp, S., et al. (2015). Novel mutations support a role for Profilin 1 in the pathogenesis of ALS. *Neurobiol. Aging* 36, 1602.e17–1602.e27. doi: 10.1016/j.neurobiolaging.2014.10.032

Smith, R. A., Miller, T. M., Yamanaka, K., Monia, B. P., Condon, T. P., Hung, G., et al. (2006). Antisense oligonucleotide therapy for neurodegenerative disease. *J. Clin. Invest.* 116, 2290–2296. doi: 10.1172/jci25424

Spencer, P. S., Spencer, P., Ludolph, A., Dwivedi, M. P., Roy, D., Roy, D. N., et al. (1986). Lathyrism: evidence for role of the neuroexcitatory aminoacid BOAA. *Lancet* 328, 1066–1067. doi: 10.1016/s0140-6736(86)90468-x

Sproviero, W., Shatunov, A., Stahl, D., Shoai, M., Van Rheenen, W., Jones, A. R., et al. (2016). ATXN2 trinucleotide repeat length correlates with risk of ALS. *Neurobiol. Aging* 51, 178.e1–178.e9. doi: 10.1016/j.neurobiolaging.2016.11.010

Sreedharan, J., Blair, I. P., Tripathi, V. B., Hu, X., Vance, C., Rogelj, B., et al. (2008). TDP-43 mutations in familial and sporadic amyotrophic lateral sclerosis. *Science* 319, 1668–1672. doi: 10.1126/science.1154584

Stallings, N. R., Puttaparthi, K., Luther, C. M., Burns, D. K., and Elliott, J. L. (2010). Progressive motor weakness in transgenic mice expressing human TDP-43. *Neurobiol. Dis.* 40, 404–414. doi: 10.1016/j.nbd.2010.06.017

Stein, C. A. (2016). Eteplirsen approved for duchenne muscular dystrophy: the FDA faces a difficult choice. *Mol. Ther.* 24, 1884–1885. doi: 10.1038/mt.2016.188

Stewart, R., Kozlov, S., Matigian, N., Wali, G., Gatei, M., Sutharsan, R., et al. (2013). A patient-derived olfactory stem cell disease model for ataxia-telangiectasia. *Hum. Mol. Genet.* 22, 2495–2509. doi: 10.1093/hmg/ddt101

Su, Z., Zhang, Y., Gendron, T. F., Bauer, P. O., Chew, J., Yang, W.-Y., et al. (2014). Discovery of a biomarker and lead small molecules to target r(GGGGCC)-associated defects in c9FTD/ALS. *Neuron* 83, 1043–1050. doi: 10.1016/j.neuron.2014.07.041

Sundaramoorthy, V., Sultana, J. M., and Atkin, J. D. (2015). Golgi fragmentation in amyotrophic lateral sclerosis, an overview of possible triggers and consequences. *Front. Neurosci.* 9:400. doi: 10.3389/fnins.2015.00400

Sundaramoorthy, V., Walker, A. K., Tan, V., Fifita, J. A., Mccann, E. P., Williams, K. L., et al. (2017). Defects in optineurin- and myosin VI-mediated cellular trafficking in amyotrophic lateral sclerosis. *Hum. Mol. Genet.* 26:3452. doi: 10.1093/hmg/ddx268

Sutherland, G. R., and Richards, R. I. (1994). Simple repeat DNA is not replicated simply. *Nat. Genet.* 6, 114–116. doi: 10.1038/ng0294-114

Tajinda, K., Ishizuka, K., Colantuoni, C., Morita, M., Winicki, J., Le, C., et al. (2010). Neuronal biomarkers from patients with mental illnesses: a novel method through nasal biopsy combined with laser-captured microdissection. *Mol. Psychiatr.* 15:231. doi: 10.1038/mp.2009.73

Takahashi, K., Tanabe, K., Ohnuki, M., Narita, M., Ichisaka, T., Tomoda, K., et al. (2007). Induction of pluripotent stem cells from adult human fibroblasts by defined factors. *Cell* 131, 861–872. doi: 10.1016/j.cell.2007.11.019

Takahashi, K., and Yamanaka, S. (2006). Induction of pluripotent stem cells from mouse embryonic and adult fibroblast cultures by defined factors. *Cell* 126, 663–676. doi: 10.1016/j.cell.2006.07.024

Takahashi, Y., Fukuda, Y., Yoshimura, J., Toyoda, A., Kurppa, K., Moritoyo, H., et al. (2013). ERBB4 mutations that disrupt the neuregulin-ErbB4 pathway cause amyotrophic lateral sclerosis type 19. *Am. J. Hum. Genet.* 93, 900–905. doi: 10.1016/j.ajhg.2013.09.008

Takahashi, Y., Seki, N., Ishiura, H., Mitsui, J., Matsukawa, T., Kishino, A., et al. (2008). Development of a high-throughput microarray-based resequencing system for neurological disorders and its application to molecular genetics of amyotrophic lateral sclerosis. *Arch. Neurol.* 65, 1326–1332. doi: 10.1001/archneur.65.10.1326

Takeuchi, R., Tada, M., Shiga, A., Toyoshima, Y., Konno, T., Sato, T., et al. (2016). Heterogeneity of cerebral TDP-43 pathology in sporadic amyotrophic lateral sclerosis: evidence for clinico-pathologic subtypes. *Acta Neuropathol. Commun.* 4:61. doi: 10.1186/s40478-016-0335-2

Tang, Y., Liu, M.-L., Zang, T., and Zhang, C.-L. (2017). Direct reprogramming rather than iPSC-based reprogramming maintains aging hallmarks in human motor neurons. *Front. Mol. Neurosci.* 10:359. doi: 10.3389/fnmol.2017.00359

Teyssou, E., Vandenberghe, N., Moigneu, C., Boillée, S., Couratier, P., Meininger, V., et al. (2014). Genetic analysis of SS18L1 in French amyotrophic lateral sclerosis. *Neurobiol. Aging* 35, 1213.e9–1213.e12. doi: 10.1016/j.neurobiolaging.2013.11.023

Ticozzi, N., Leclerc, A. L., Keagle, P. J., Glass, J. D., Wills, A.-M., Van Blitterswijk, M., et al. (2010). Paraoxonase gene mutations in amyotrophic lateral sclerosis. *Ann. Neurol.* 68, 102–107. doi: 10.1002/ana.21993

Ticozzi, N., Vance, C., Leclerc, A. L., Keagle, P., Glass, J. D., Mckenna-Yasek, D., et al. (2011). Mutational analysis reveals the FUS homolog TAF15 as a candidate gene for familial amyotrophic lateral sclerosis. *Am. J. Med. Genet. Part B Neuropsychiatr. Genet.* 156B, 285–290. doi: 10.1002/ajmg.b.31158

Todd, T. W., and Petrucelli, L. (2016). Insights into the pathogenic mechanisms of Chromosome 9 open reading frame 72 (C9orf72) repeat expansions. *J. Neurochem.* 138, 145–162. doi: 10.1111/jnc.13623

Tollervey, J. R., Curk, T., Rogelj, B., Briese, M., Cereda, M., Kayikci, M., et al. (2011). Characterising the RNA targets and position-dependent splicing regulation by TDP-43; implications for neurodegenerative diseases. *Nat. Neurosci.* 14, 452–458. doi: 10.1038/nn.2778

Tümer, Z., Bertelsen, B., Gredal, O., Magyari, M., Nielsen, K. C., Lucamp, G. K., et al. (2012). A novel heterozygous nonsense mutation of the OPTN gene segregating in a Danish family with ALS. *Neurobiol. Aging* 33:208.e1-5. doi: 10.1016/j.neurobiolaging.2011.07.001

Turner, M. R., Cagnin, A., Turkheimer, F. E., Miller, C. C. J., and Shaw, C. E. (2004). Evidence of widespread cerebral microglial activation in amyotrophic lateral sclerosis: an [C-11](R)-PK11195 positron emission tomography study. *Neurobiol. Dis.* 15, 601–609. doi: 10.1016/j.nbd.2003.12.012

Uchida, A., Sasaguri, H., Kimura, N., Tajiri, M., Ohkubo, T., Ono, F., et al. (2012). Non-human primate model of amyotrophic lateral sclerosis with cytoplasmic mislocalization of TDP-43. *Brain* 135, 833–846. doi: 10.1093/brain/awr348

Ullah, M. I., Ahmad, A., Raza, S. I., Amar, A., Ali, A., Bhatti, A., et al. (2015). In silico analysis of SIGMAR1 variant (rs4879809) segregating in a consanguineous Pakistani family showing amyotrophic lateral sclerosis without frontotemporal lobar dementia. *Neurogenetics* 16, 299–306. doi: 10.1007/s10048-015-0453-1

Urwin, H., Authier, A., Nielsen, J. E., Metcalf, D., Powell, C., Froud, K., et al. (2010). Disruption of endocytic trafficking in frontotemporal dementia with CHMP2B mutations. *Hum. Mol. Genet.* 19, 2228–2238. doi: 10.1093/hmg/ddq100

Uyan, Ö, Ömür, Ö, Ağım, Z. S., Özoğuz, A., Li, H., Parman, Y., et al. (2013). Genome-wide copy number variation in sporadic amyotrophic lateral sclerosis in the Turkish population: deletion of EPHA3 is a possible protective factor. *PLoS One* 8:e72381. doi: 10.1371/journal.pone.0072381

Valdmanis, P., Kabashi, E., Dyck, A., Hince, P., Lee, J., Dion, P., et al. (2008). Association of paraoxonase gene cluster polymorphisms with ALS in France. Quebec, and Sweden. *Neurology* 71, 514–520. doi: 10.1212/01.wnl.0000324997.21272.0c

Van Cutsem, P., Dewil, M., Robberecht, W., and Van Den Bosch, L. (2006). Excitotoxicity and Amyotrophic Lateral Sclerosis. *Neurodegener. Dis.* 2, 147–159.

Van Deerlin, V. M., Leverenz, J. B., Bekris, L. M., Bird, T. D., Yuan, W., Elman, L. B., et al. (2008). TARDBP mutations in amyotrophic lateral sclerosis with TDP-43 neuropathology: a genetic and histopathological analysis. *Lancet Neurol.* 7, 409–416. doi: 10.1016/S1474-4422(08)70071-1

van Eijk, R. P. A., Jones, A. R., Sproviero, W., Shatunov, A., Shaw, P. J., Leigh, P. N., et al. (2017). Meta-analysis of pharmacogenetic interactions in amyotrophic lateral sclerosis clinical trials. *Neurology* 89, 1915–1922. doi: 10.1212/WNL.0000000000004606

Van Hoecke, A., Schoonaert, L., Lemmens, R., Timmers, M., Staats, K. A., Laird, A. S., et al. (2012). EPHA4 is a disease modifier of amyotrophic lateral sclerosis in animal models and in humans. *Nat. Med.* 18, 1418–1422.

Vance, C., Rogelj, B., Hortobágyi, T., Kurt, J. D. V., Nishimura, A. L., Sreedharan, J., et al. (2009). Mutations in FUS, an RNA processing protein, cause familial amyotrophic lateral sclerosis type 6. *Science* 323, 1208–1211. doi: 10.1126/science.1165942

Vance, C., Scotter, E. L., Nishimura, A. L., Troakes, C., Mitchell, J. C., Kathe, C., et al. (2013). ALS mutant FUS disrupts nuclear localization and sequesters wild-type FUS within cytoplasmic stress granules. *Hum. Mol. Genet.* 22, 2676–2688. doi: 10.1093/hmg/ddt117

Verbeeck, C., Deng, Q., Dejesus-Hernandez, M., Taylor, G., Ceballos-Diaz, C., Kocerha, J., et al. (2012). Expression of Fused in sarcoma mutations in mice recapitulates the neuropathology of FUS proteinopathies and provides insight into disease pathogenesis. *Mol. Neurodegener.* 7:53. doi: 10.1186/1750-1326-7-53

Vidal-Taboada, J. M., Lopez-Lopez, A., Salvado, M., Lorenzo, L., Garcia, C., Mahy, N., et al. (2015). UNC13A confers risk for sporadic ALS and influences survival in a Spanish cohort. *J. Neurol.* 262, 2285–2292. doi: 10.1007/s00415-015-7843-z

Waite, A. J., Bäumer, D., East, S., Neal, J., Morris, H. R., Ansorge, O., et al. (2014). Reduced C9orf72 protein levels in frontal cortex of amyotrophic lateral sclerosis and frontotemporal degeneration brain with the C9ORF72 hexanucleotide repeat expansion. *Neurobiol. Aging* 35:1779.e5-1779.e13. doi: 10.1016/j.neurobiolaging.2014.01.016

Wang, G., Yang, H., Yan, S., Wang, C.-E., Liu, X., Zhao, B., et al. (2015). Cytoplasmic mislocalization of RNA splicing factors and aberrant neuronal gene splicing in TDP-43 transgenic pig brain. *Mol. Neurodegener.* 10:42. doi: 10.1186/s13024-015-0036-5

Wang, W.-Y., Pan, L., Su, S. C., Quinn, E. J., Sasaki, M., Jimenez, J. C., et al. (2013). Interaction of FUS and HDAC1 regulates DNA damage response and repair in neurons. *Nat. Neurosci.* 16, 1383–1391. doi: 10.1038/nn.3514

Wang, W., Li, L., Lin, W.-L1., Dickson, D. W., Petrucelli, L., Zhang, T., et al. (2013). The ALS disease-associated mutant TDP-43 impairs mitochondrial dynamics and function in motor neurons. *Hum. Mol. Genet.* 22, 4706–4719. doi: 10.1093/hmg/ddt319

Williamson, T. L., and Cleveland, D. W. (1999). Slowing of axonal transport is a very early event in the toxicity of ALS–linked SOD1 mutants to motor neurons. *Nat. Neurosci.* 2, 50–56. doi: 10.1038/4553

Wills, A. M., Cronin, S., Slowik, A., Kasperaviciute, D., Van Es, M. A., Morahan, J. M., et al. (2009). A large-scale international meta-analysis of paraoxonase gene polymorphisms in sporadic ALS. *Neurology* 73, 16–24. doi: 10.1212/WNL.0b013e3181a18674

Wils, H., Kleinberger, G., Janssens, J., Pereson, S., Joris, G., Cuijt, I., et al. (2010). TDP-43 transgenic mice develop spastic paralysis and neuronal inclusions characteristic of ALS and frontotemporal lobar degeneration. *Proc. Natl. Acad. Sci. U.S.A.* 107, 3858–3863. doi: 10.1073/pnas.0912417107

Wouter van, R., Shatunov, A., Dekker, A. M., Mclaughlin, R. L., Diekstra, F. P., Pulit, S. L., et al. (2016). Genome-wide association analyses identify new risk variants and the genetic architecture of amyotrophic lateral sclerosis. *Nat. Genet.* 48, 1043–1408. doi: 10.1038/ng.3622

Wu, C.-H., Fallini, C., Ticozzi, N., Keagle, P. J., Sapp, P. C., Piotrowska, K., et al. (2012). Mutations in the profilin 1 gene cause familial amyotrophic lateral sclerosis. *Nature* 488, 499–503. doi: 10.1038/nature11280

Wu, D., Yu, W., Kishikawa, H., Folkerth, R. D., Iafrate, A. J., Shen, Y., et al. (2007). Angiogenin loss-of-function mutations in amyotrophic lateral sclerosis. *Ann. Neurol.* 62, 609–617.

Wu, L.-S., Cheng, W., Hou, S.-C., Yan, Y.-T., Jiang, S.-T., and Shen, C. K. J. (2010). TDP-43, a neuro-pathosignature factor, is essential for early mouse embryogenesis. *Genesis* 48, 56–62. doi: 10.1002/dvg.20584

Xiao, S., Macnair, L., Mcgoldrick, P., Mckeever, P. M., Mclean, J. R., Zhang, M., et al. (2015). Isoform-specific antibodies reveal distinct subcellular localizations of C9orf72 in amyotrophic lateral sclerosis. *Ann. Neurol.* 78, 568–583. doi: 10.1002/ana.24469

Xu, Y.-F., Zhang, Y.-J., Lin, W.-L., Cao, X., Stetler, C., Dickson, D. W., et al. (2011). Expression of mutant TDP-43 induces neuronal dysfunction in transgenic mice. *Mol. Neurodegener.* 6:73. doi: 10.1186/1750-1326-6-73

Yamashita, S., and Ando, Y. (2015). Genotype-phenotype relationship in hereditary amyotrophic lateral sclerosis. *Transl. Neurodegener.* 4:13. doi: 10.1186/s40035-015-0036-y

Yang, H., Wang, G., Sun, H., Shu, R., Liu, T., Wang, C.-E., et al. (2014). Species-dependent neuropathology in transgenic SOD1 pigs. *Cell Res.* 24, 464–481. doi: 10.1038/cr.2014.25

Yang, Y., Hentati, A., Deng, H.-X., Dabbagh, O., Sasaki, T., Hirano, M., et al. (2001). The gene encoding alsin, a protein with three guanine-nucleotide exchange factor domains, is mutated in a form of recessive amyotrophic lateral sclerosis. *Nat. Genet.* 29, 160–165. doi: 10.1038/ng1001-160

Yin, P., Guo, X., Yang, W., Yan, S., Yang, S., Zhao, T., et al. (2019). Caspase-4 mediates cytoplasmic accumulation of TDP-43 in the primate brains. *Acta Neuropathol.* 137, 919–937. doi: 10.1007/s00401-019-01979-0

Ying, H., and Yue, B. Y. J. T. (2016). Optineurin: the autophagy connection. *Exp. Eye Res.* 144, 73–80. doi: 10.1016/j.exer.2015.06.029

Yokoseki, A., Shiga, A., Tan, C. F., Tagawa, A., Kaneko, H., Koyama, A., et al. (2008). TDP-43 mutation in familial amyotrophic lateral sclerosis. *Ann. Neurol.* 63, 538–542. doi: 10.1002/ana.21392

Yoo, A. S., Sun, A. X., Li, L., Shcheglovitov, A., Portmann, T., Li, Y., et al. (2011). MicroRNA-mediated conversion of human fibroblasts to neurons. *Nature* 476, 228–231. doi: 10.1038/nature10323

Zhang, B., Tu, P.-H., Abtahian, F., Trojanowski, J. Q., and Lee, V. M.-Y. (1997). Neurofilaments and orthograde transport are reduced in ventral root axons of transgenic mice that express human SOD1 with a G93A mutation. *J. Cell Biol.* 139, 1307–1315. doi: 10.1083/jcb.139.5.1307

Zhou, Y., Liu, S., Liu, G., Öztürk, A., and Hicks, G. G. (2013). ALS-associated FUS mutations result in compromised FUS alternative splicing and autoregulation. *PLoS Genet.* 9:e1003895. doi: 10.1371/journal.pgen.1003895

Zhou, Z., Mogensen, M. M., Powell, P. P., Curry, S., and Wileman, T. (2013). Foot-and-mouth disease virus 3C protease induces fragmentation of the Golgi compartment and blocks Intra-Golgi transport. *J. Virol.* 87, 11721–11729. doi: 10.1128/JVI.01355-13

Zinszner, H., Sok, J., Immanuel, D., Yin, Y., and Ron, D. (1997). TLS (FUS) binds RNA in vivo and engages in nucleo-cytoplasmic shuttling. *J. Cell Sci.* 110(Pt 15), 1741–1750.

Zolov, S. N., and Lupashin, V. V. (2005). Cog3p depletion blocks vesicle-mediated golgi retrograde trafficking in hela cells. *J. Cell Biol.* 168, 747–759. doi: 10.1083/jcb.200412003

Zou, Z.-Y., Cui, L.-Y., Sun, Q., Li, X.-G., Liu, M.-S., Xu, Y., et al. (2013). De novo FUS gene mutations are associated with juvenile-onset sporadic amyotrophic lateral sclerosis in China. *Neurobiol. Aging* 34:1312.e1-8. doi: 10.1016/j.neurobiolaging.2012.09.005

Zou, Z.-Y., Zhou, Z.-R., Che, C.-H., Liu, C.-Y., He, R.-L., and Huang, H.-P. (2017). Genetic epidemiology of amyotrophic lateral sclerosis: a systematic review and meta-analysis. *J. Neurol. Neurosurg. Psychiatr.* 88, 540–549.

Conflict of Interest: The authors declare that the research was conducted in the absence of any commercial or financial relationships that could be construed as a potential conflict of interest.

frontiers in Neuroscience

ORIGINAL RESEARCH
published: 21 January 2020
doi: 10.3389/fnins.2019.01434

Experimental Traumatic Brain Injury Induces Chronic Glutamatergic Dysfunction in Amygdala Circuitry Known to Regulate Anxiety-Like Behavior

*Joshua A. Beitchman[1,2,3], Daniel R. Griffiths[1,2], Yerin Hur[1,2], Sarah B. Ogle[1,2,4], Caitlin E. Bromberg[1,2], Helena W. Morrison[5], Jonathan Lifshitz[1,2,6], P. David Adelson[1,2] and Theresa Currier Thomas[1,2,6]**

[1] Barrow Neurological Institute at Phoenix Children's Hospital, Phoenix, AZ, United States, [2] Department of Child Health, University of Arizona College of Medicine-Phoenix, Phoenix, AZ, United States, [3] College of Graduate Studies, Midwestern University, Glendale, AZ, United States, [4] Banner University Medical Center, Phoenix, AZ, United States, [5] College of Nursing, University of Arizona, Tucson, AZ, United States, [6] Phoenix VA Health Care System, Phoenix, AZ, United States

OPEN ACCESS

Edited by:
Antonio Lucio Teixeira, University of Texas Health Science Center at Houston, United States

Reviewed by:
Daniel T. Christian, Des Moines University, United States
Aline Silva Miranda, Federal University of Minas Gerais, Brazil

***Correspondence:**
Theresa Currier Thomas
theresathomas@email.arizona.edu

Specialty section:
This article was submitted to Neurodegeneration, a section of the journal Frontiers in Neuroscience

Received: *30 August 2019*
Accepted: *18 December 2019*
Published: *21 January 2020*

Citation:
Beitchman JA, Griffiths DR, Hur Y, Ogle SB, Bromberg CE, Morrison HW, Lifshitz J, Adelson PD and Currier Thomas T (2020) Experimental Traumatic Brain Injury Induces Chronic Glutamatergic Dysfunction in Amygdala Circuitry Known to Regulate Anxiety-Like Behavior. Front. Neurosci. 13:1434. doi: 10.3389/fnins.2019.01434

Up to 50% of traumatic brain injury (TBI) survivors demonstrate persisting and late-onset anxiety disorders indicative of limbic system dysregulation, yet the pathophysiology underlying the symptoms is unclear. We hypothesize that the development of TBI-induced anxiety-like behavior in an experimental model of TBI is mediated by changes in glutamate neurotransmission within the amygdala. Adult, male Sprague-Dawley rats underwent midline fluid percussion injury or sham surgery. Anxiety-like behavior was assessed at 7 and 28 days post-injury (DPI) followed by assessment of real-time glutamate neurotransmission in the basolateral amygdala (BLA) and central nucleus of the amygdala (CeA) using glutamate-selective microelectrode arrays. The expression of anxiety-like behavior at 28 DPI coincided with decreased evoked glutamate release and slower glutamate clearance in the CeA, not BLA. Numerous factors contribute to the changes in glutamate neurotransmission over time. In two additional animal cohorts, protein levels of glutamatergic transporters (Glt-1 and GLAST) and presynaptic modulators of glutamate release (mGluR2, TrkB, BDNF, and glucocorticoid receptors) were quantified using automated capillary western techniques at 28 DPI. Astrocytosis and microglial activation have been shown to drive maladaptive glutamate signaling and were histologically assessed over 28 DPI. Alterations in glutamate neurotransmission could not be explained by changes in protein levels for glutamate transporters, mGluR2 receptors, astrocytosis, and microglial activation. Presynaptic modulators, BDNF and TrkB, were significantly decreased at 28 DPI in the amygdala. Dysfunction in presynaptic regulation of glutamate neurotransmission may contribute to anxiety-related behavior and serve as a therapeutic target to improve circuit function.

Keywords: diffuse traumatic brain injury, amperometry, glutamate neurotransmission, amygdala, chronic

HIGHLIGHTS

- A single diffuse brain injury induces anxiety-like behavior in an open field environment.
- Altered glutamate neurotransmission occurs following diffuse TBI in the CeA, but not in the BLA.
- The expression of affective symptoms coincides with altered glutamate neurotransmission in the CeA.
- Altered glutamate neurotransmission occurs in the absence of overt neuropathology and gliosis.
- BDNF and TrkB were significantly decreased at 28 DPI in the amygdala.

INTRODUCTION

Affective disorders, including generalized anxiety disorder and post-traumatic stress disorder (PTSD), develop and persist in up to 50% of traumatic brain injury (TBI) survivors, however, few common biological mechanisms between TBI and non-TBI patients have been elucidated (Kessler et al., 2005; Scholten et al., 2016). The incidence of TBI continues to rise, with at least 2.5 million Americans reporting a TBI each year, costing the American health care system 76.5 billion dollars (Hyder et al., 2007; Coronado et al., 2012). Three-quarters of all TBIs are diffuse TBIs (dTBI) in which the signature pathology is multi-focal diffuse axonal injury with no overt pathology detected by CT or MRI (Lee and Newberg, 2005; Grossman et al., 2010; Liu et al., 2014). dTBI subsequently induces secondary sequelae that occur seconds to months following the initial injury, leading to the development of affective, cognitive, and somatic symptoms (McAllister, 1992; Masel and DeWitt, 2010). Despite clinical prevalence, the pathophysiology contributing to affective symptoms following dTBI is poorly understood, resulting in misdiagnosis and ineffective treatments (Van der Kolk, 2002; Collins et al., 2004; Hoge et al., 2014). Ultimately, ineffective treatment impacts a patient's ability to return to work, daily function, and social interactions; severely impairing the quality of life for both the patient and caregivers (Trahan et al., 2001; Guerin et al., 2006; van der Horn et al., 2013).

Clinical and preclinical data demonstrate that dTBI causes profound lasting changes in the amygdala. In Veterans, early amygdala fMRI reactivity post-injury is predictive of the development of PTSD and could contribute to the bilateral reduction of amygdala size observed in patients diagnosed with both TBI and PTSD (Depue et al., 2014; Stevens et al., 2016). A study in collegiate football players report a positive correlation between amygdala shape and mood states (Cho et al., 2018). TBI survivors with major depressive disorder had smaller lateral and dorsal prefrontal cortex, which mediates ventral-limbic and paralimbic pathways and influences amygdala circuitry (Jorge et al., 2004). Preclinically, diffuse and focal experimental models of TBI also identify alterations in amygdala circuitry, including increased neuronal hyperexcitability and GABA production proteins in the absence of overt neuropathology (Hallam et al., 2004; Meyer et al., 2012). In addition, pyramidal and stellate neurons in the basolateral amygdala (BLA) demonstrate increased complexity distal and proximal to the soma as early as 1 day post-injury (DPI) and persisting until at least 28 DPI indicating BLA- central nucleus of the amygdala (CeA) circuit reorganization after dTBI (Hoffman et al., 2017). Together, these data indicate that TBI-induced changes to the amygdala and associated limbic system circuitry could contribute to the development of affective disorders following injury.

Limbic system circuitry influences affective symptoms with evidence that glutamatergic neurons originating in the BLA and projecting into the CeA play a critical role in mediating anxiety-like behavior (Swanson and Petrovich, 1998; Tye et al., 2011; Janak and Tye, 2015; Babaev et al., 2018). BLA neurons are 90% glutamatergic, highlighting the role of glutamate neurotransmission in displays of affective behavior (Carlsen, 1988; Smith and Pare, 1994). Glutamate neurotransmission is regulated by astrocytes and microglia processes surrounding the synapse (Murugan et al., 2013). Glutamate transporters, Glt-1 and GLAST (located on astrocytes), rapidly remove glutamate from the extracellular space, restricting glutamate to the synaptic cleft (Danbolt, 2001; Pal, 2018). When spillover does occur, feedback through the metabotropic glutamate receptor 2 (mGluR2) can reduce presynaptic release of glutamate (Loane et al., 2012). Decreased levels of brain derived neurotropic factor (BDNF), tropomyosin-related kinase B (TrkB) receptors, and glucocorticoid receptors (GluR) – commonly reported with affective disorders – have also been reported to attenuate presynaptic glutamate release (Numakawa et al., 2009; Chiba et al., 2012; Meis et al., 2012). Each of these molecular components contribute to the complex regulation of glutamatergic neurotransmission and work to maintain homeostatic communication.

We hypothesize that TBI-induced anxiety-like behavior is mediated by changes in glutamate neurotransmission within the amygdala. In a well-established model of dTBI that causes diffuse axonal injury (DAI) in rats, we assessed the expression of anxiety-like behavior at 1-week and 1-month post-injury using open field testing (OFT). Immediately following OFT, *in vivo* amperometric recordings in the BLA and CeA evaluated glutamate clearance kinetics and available glutamate stores as an indicator of disrupted glutamate neurotransmission. Pathological and molecular analyses of nuclei-specific changes were used to identify future therapeutic targets to mediate glutamate neurotransmission associated with amygdala circuit function.

MATERIALS AND METHODS

Animals

A total of 69 adult, male Sprague-Dawley rats (weights 279–420 grams; age 3–4 months) (Envigo, Indianapolis, IN, United States) were used in these experiments. (29 rats for amperometry, 22 for histology, and 18 rats for protein assays). Upon arrival, rats were given a 1-week acclimation period, housed in normal 12-h light/dark cycle (Red light: 18:00 to 06:00) and allowed access to food and water *ad libitum* (Teklad 2918, Envigo, Indianapolis, IN). Rats were pair housed according to injury status (i.e., injured housed with injured) throughout the duration

of the study. All procedures and animal care were conducted in compliance with an approved Institutional Animal Care and Use Committee Protocol (13–460) at the University of Arizona College of Medicine-Phoenix which is consistent with the National Institutes of Health (NIH) Guidelines for the Care and Use of Laboratory Animals.

Rats undergoing open field testing (OFT) were exposed to human contact and handled for a total of 50 min over a period of 7 days. Rats aged out to 28 DPI received an additional 30 min of handling by the same investigator over a period of 3 days immediately prior to testing to reacclimate to human contact. Handling of rats ensures that the response to the behavioral paradigm is not confounded by the threat of investigator handling (Costa et al., 2012). At 7/8 DPI or 28/29 DPI, injured and sham rats underwent OFT between 07:00 and 09:00, immediately followed by *in vivo* amperometric recordings by the handling investigator. Time of day and timing between OFT and recordings were held constant throughout all experiments to account for any potential influence of diurnal corticosterone levels and lasting molecular and structural influences from behavior (OFT)-induced stress responses (Zhang et al., 2018). For the remainder of the manuscript, DPI for the amperometric and behavioral outcome measures at 7/8 and 28/29 DPI will be abbreviated as 7 DPI and 28 DPI. For behavioral analysis and subsequent amperometric recordings, a total of 17 rats were aged to the 1-week time point (11 injured; 6 sham) and 17 rats were aged to 1-month (10 injured; 7 sham), based on *a priori* power-calculations from previous electrochemical experiments (Thomas et al., 2012) (experimental design; **Figure 1A**).

Midline Fluid Percussion Injury (mFPI)

Surgical Procedure

Midline FPI surgery was carried out similarly to previously published methods from this laboratory by an investigator who was *not* the handler (Thomas et al., 2012). Rats were randomized into either injured or sham groups following acclimation to the vivarium facility and exposure to human contact. Briefly, rats were anesthetized with 5% isoflurane in 21% O_2 and placed into a stereotaxic frame (Kopf Instruments, Tujunga, CA, United States) with a nose-cone that maintained 2.5% isoflurane for the duration of the procedure. A 4.8 mm circular craniotomy was centered on the sagittal suture midway between bregma and lambda carefully ensuring that the underlying dura and superior sagittal sinus were not disturbed. An injury hub created from the female portion of a 20-gauge Luer-Loc needle hub was cut, beveled and placed directly above and in-line with the craniectomy site. A stainless-steel anchoring screw was then placed into a 1 mm hand-drilled hole into the right frontal bone. The injury hub was affixed over the craniectomy using cyanoacrylate gel and methyl-methacrylate (Hygenic Corp., Akron, OH, United States) and filled with 0.9% sterile saline. The incision was then partially sutured closed on the anterior and posterior edges with 4.0 Ethilon sutures and topical lidocaine and antibiotic ointment were applied. Rats were returned to a warmed holding cage and monitored until ambulatory (approximately 60–90 min).

Injury Induction

Approximately 24 h following surgical procedures and the return of ambulation, rats were re-anesthetized. The hub was filled with 0.9% sterile saline and attached to the male end of a fluid percussion device (Custom Design and Fabrication, Virginia Commonwealth University, Richmond, VA, United States). After return of the pedal withdrawal reflex, an injury averaging 2.19 atm was administered by releasing the pendulum (16.5 degrees) onto the fluid-filled cylinder. Shams were attached to the fluid percussion device, but the pendulum was not released. Immediately after the administration of injury, the injury hub was removed *en bloc* and rats monitored for the presence of apnea, fencing response, and the return of righting reflex. Then, rats were briefly re-anesthetized to inspect the injury site for hematoma, herniation, and dural integrity. The injury site was then stapled closed and topical lidocaine and antibiotic ointment were applied. Inclusion criterion required that injured rats have a righting reflex time ranging from 5 to 12 min (average 7:43 $\pm$ 0:07 min) and a fencing response (McIntosh et al., 1987; Hosseini and Lifshitz, 2009). After regaining the righting reflex, rats were placed in a clean, warmed holding cage, and monitored for at least 1 h following injury before being returned to the vivarium where post-operative evaluations continued for 3 DPI. Staples for rats with a 28-day time point were removed at 7 DPI.

Midline fluid percussion injury in rats have been used for over 25 years, predominantly in the Sprague-Dawley strain. Reproducible pathophysiological and behavioral responses relevant to clinical data have been published (Riess et al., 2002; Thompson et al., 2005; Witgen et al., 2005; Lifshitz et al., 2007; Hosseini and Lifshitz, 2009; Hall and Lifshitz, 2010; McNamara et al., 2010; Alder et al., 2011; Cao et al., 2012; Learoyd and Lifshitz, 2012; Lifshitz and Lisembee, 2012; Thomas et al., 2012; Rowe et al., 2013, 2014; Harrison et al., 2014, 2015; Fenn et al., 2015). mFPI best models closed head injury with decompressive craniectomy by reproducing diffuse axonal injury without contusion or cavitation encompassing the hallmark pathology of clinical diffuse TBI. While craniectomy is a procedure often carried out in more severe clinical cases in which cerebral herniation is a concern, it provides control of increased intracranial pressure here, which when unregulated can induce a more severe injury with worse outcome (Lafrenaye et al., 2014). After regaining reflexive responses (5–12 min), injured rats require little to no medical intervention in the post-operative period, most similar to mild TBI as defined by a Glasgow Coma Score of 13–15. A more detailed discussion in the clinical relevance of mFPI can be found in our recently published review article (Lifshitz et al., 2016).

Open Field Testing

To evaluate for the presence of the development of affective behaviors following diffuse TBI as modeled by mFPI, an open field analysis was performed. Each rat was placed into the center of a novel black open field (measuring 69 cm $\times$ 69 cm) facing the same direction at least 1 h following the light

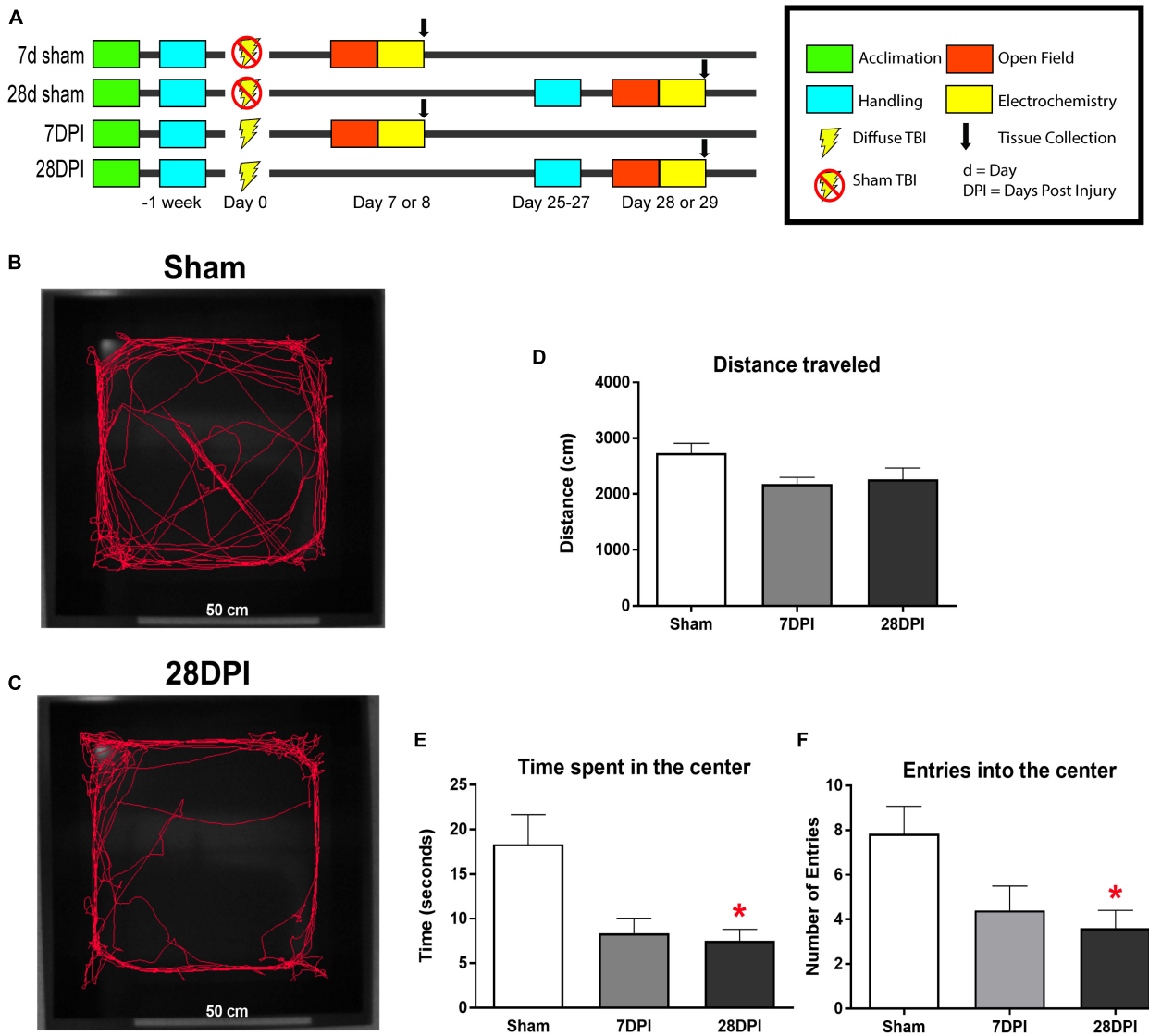

FIGURE 1 | dTBI induces the expression of anxiety-like behavior. **(A)** Study design for behavioral and amperometry studies. **(B)** Representative video tracking data from Ethovision® software during the first 5 min of open field testing from sham. **(C)** Representative video tracking data from Ethovision® software during the first 5 min of open field testing from 28 DPI rats. **(D)** Distance traveled is similar between 7 DPI, 28 DPI, and sham [One-Way ANOVA $F(2,29) = 3.23$; $p = 0.05$]. **(E)** 28 DPI rats spent significantly less time in the center of the open field [Kruskal-Wallis $H = 6.711$; $p < 0.05$; Dunn's *post hoc* comparison $p < 0.05$; Mann-Whitney U *post hoc* $p < 0.05$, $r = 0.48$]. **(F)** 28 DPI rats made significantly fewer entries into the center of the open field when compared to sham [Kruskal-Wallis $H = 6.83$; $p < 0.05$; Dunn's *post hoc* comparison $p < 0.05$; Mann-Whitney U *post hoc* $p < 0.05$, $r = 0.46$]. Bar graphs represents mean ± SEM. $n = 10$–12 for each group. *$p < 0.05$ in comparison to sham.

cycle change from red to white light. White overhead lights ensured equal illumination throughout the container for a total of 15 min. Ambient white noise (60–70 decibels) in the room mitigated any variation in noise levels. Tracking was accomplished by Ethovision® Software which mapped the rat directly overhead. Two regions were defined using Ethovision®, separating the open field into an outer region and an inner region (35 cm × 35 cm). Time spent in each zone was calculated based on the center-point of the rat. Primary outcome measures analyzed total distance traveled, time spent in the center, and entries to the center of the open field for the first 5 min of the task to be more representative of anxiety-like behavior (Gould et al., 2009).

Electrochemistry

Enzyme-Based Microelectrode Arrays

Ceramic-based microelectrode arrays (MEA) encompassing four platinum (Pt) recording surfaces (15 μm × 333 μm) aligned in a dual, paired configuration were prepared to measure glutamate for *in vivo* anesthetized recordings (S2 configuration; Quanteon, Nicholasville, KY, United States). MEAs were fabricated, selected

for recordings, and made glutamate sensitive as previously described (Thomas et al., 2012, 2017). Briefly, Pt sites 1 and 2 were coated with a solution containing glutamate oxidase (GluOx), bovine serum albumin (BSA), and glutaraldehyde, enabling these sites to selectively detect glutamate levels with low limits of detection (Nickell et al., 2005). Pt sites 3 and 4 were coated with only BSA and glutaraldehyde and served as sentinels, recording everything channels 1 and 2 recorded except for glutamate (Burmeister and Gerhardt, 2001). Prior to calibration and *in vivo* recordings, all four Pt recording sites were electroplated with a size exclusion layer of 1,3-phenylendediamine (mPD) (Acros Organics, Morris Plains, NJ, United States). GluOx converts glutamate into α-ketoglutarate and peroxide (H_2O_2). The H_2O_2 functions as a reporter molecule, traversing the mPD layer and is readily oxidized and recorded as current using the FAST-16 mkIII system (Fast Analytical Sensor Technology Mark III, Quanteon, LLC, Nicholasville, KY, United States) (**Supplementary Figure S1**).

Microelectrode Array Calibration

On the morning of *in vivo* recordings, each MEA was calibrated *in vitro* to determine recording parameters: slope (sensitivity to glutamate), limit of detection (LOD; lowest amount of glutamate to be reliably recorded), and selectivity (ratio of glutamate to ascorbic acid). For calibration, aliquots from stock solutions were added to 40 mL of 0.05 M phosphate buffered saline (PBS) (pH 7.1–7.4; stirring; 37°C) in the following sequence: 500 μL of 20 mM ascorbic acid, three additions of 40 μL of 20 mM l-glutamate, and 40 μL of 8.8 mM H_2O_2 to produce a final concentration of 250 μM AA, 20, 40, and 60 μM glutamate, and 8.8 μM H_2O_2. A representative MEA calibration is shown in **Figure 2A**. For the study, a total of 48 MEAs were used with a total of 91 recording sites. Additionally, there was an overall average slope of 6.9 pA/μM, a LOD of 2.4 μM, and a selectivity of 44 to 1.

Microelectrode Array/Micropipette Assembly

Following calibration, a single micropipette was attached to the MEA using the following steps to allow for the local application of solutions during *in vivo* experiments. A single-barreled glass capillary with filament (1.0 mm × 0.58 mm, 6" A-M Systems, Inc., Sequim, WA, United States) was pulled using a Kopf Pipette Puller (David Kopf Instruments, Tujunga, CA, United States). Using a microscope with a calibrated reticle, the pulled micropipette was bumped against a glass rod to have an inner diameter of 7–13 μm (10.5 μm ± 0.2). Clay was used to place the tip of the micropipette between the 4 Pt recording sites. This alignment was secured using Sticky Wax (Kerr Manufacturing Co). The final measurements were the distance between the micropipette tip and the MEA surface (72 ± 3 μm) and the distance between the micropipette tip and the MEA tip (498 ± 4 μm).

Surgery for Amperometric Recordings

Immediately after OFT, sham and brain-injured rats were anesthetized with three or four intraperitoneal injections of 25% urethane in 15-min intervals (1.5 g/Kg; Sigma Aldrich, St. Louis, MO, United States). Following cessation of a pedal withdrawal reflex, each rat was then placed into a stereotaxic frame (David Kopf Instruments) with non-terminal ear bars. Body temperature was maintained at 37°C with isothermal heating pads (Braintree Scientific, Braintree, MA, United States). A midline incision was made and the skin, fascia, and temporal muscles were reflected to expose the skull. A bilateral craniectomy exposed the stereotaxic coordinates for the BLA and CeA. Dura was then removed prior to the implantation of the MEA. Brain tissue was kept moist through the application of saline soaked cotton balls and gauze. Finally, using blunt dissection, an Ag/AgCl coated reference electrode wire was placed in a subcutaneous pocket on the dorsal side of the subject (Moussy and Harrison, 1994; Quintero et al., 2007).

In vivo Amperometric Recording

Amperometric recordings performed here were done similar to previous published methods (Hinzman et al., 2010; Thomas et al., 2012). Briefly, a constant voltage was applied to the MEA using the FAST-16 mkIII recording system. *In vivo* recordings were performed at an applied potential of +0.7 V compared to the Ag/AgCl reference electrode. All data were recorded at a frequency of 10 Hz, amplified by the headstage (2 pA/mV) without signal processing or filtering of the data.

Immediately prior to implantation of the MEA, the pipette was then filled with 120 mM KCl (120 mM KCl, 29mM NaCl, 2.5mM $CaCl_2$ in ddH_2O, and pH 7.2 to 7.5) or 100 μM l-glutamate (100 μM l-glutamate in 0.9% sterile saline pH 7.2–7.6). Concentrations for both solutions have been previously shown to elicit reproducible KCl-evoked glutamate release or exogenous glutamate peaks (Burmeister et al., 2002; Thomas et al., 2012). Solutions were filtered through a 0.20 μm sterile syringe filter (Sarstedt AG & Co., Numbrecht, Germany) and loaded into the affixed micropipette using a 4-inch, 30-gauge stainless steel needle with a beveled tip (Popper and Son, Inc, NY, United States). The open end of the micropipette was connected to a Picospritzer III (Parker-Hannin Corp., General Valve Corporation, Mayfield Heights, OH, United States) with settings to dispense nanoliter quantities of fluid over a 1 s period using the necessary pressure of nitrogen (inert) gas using a dissecting microscope (Meiji Techno, San Jose, CA, United States) with a calibrated reticle in the eyepiece (Cass et al., 1992; Friedemann and Gerhardt, 1992).

The MEA-micropipette was localized in the BLA (A/P: ± 2.4 mm; M/L: ± 5.1 mm; D/V: −8.0 mm) and CeA (A/P: −2.4 mm; M/L: ± 3.9 mm; D/V: −8.0 mm) using coordinates from George Paxinos and Charles Watson Rat Brain Atlas (6th Edition) through use of the Dual Precise Small Animal Stereotaxic Frame (Kopf, model 962). Glutamate and KCl-evoked measures were recorded in both hemispheres in a randomized and balanced experimental design to mitigate possible hemispheric variations or effect of anesthesia duration.

KCl-Evoked Release of Glutamate Analysis Parameters

Once the electrochemical signal had reached baseline, 120 mM KCl was locally applied (BLA: 110 ± 8 nl; CeA: 105 ± 4 nl)

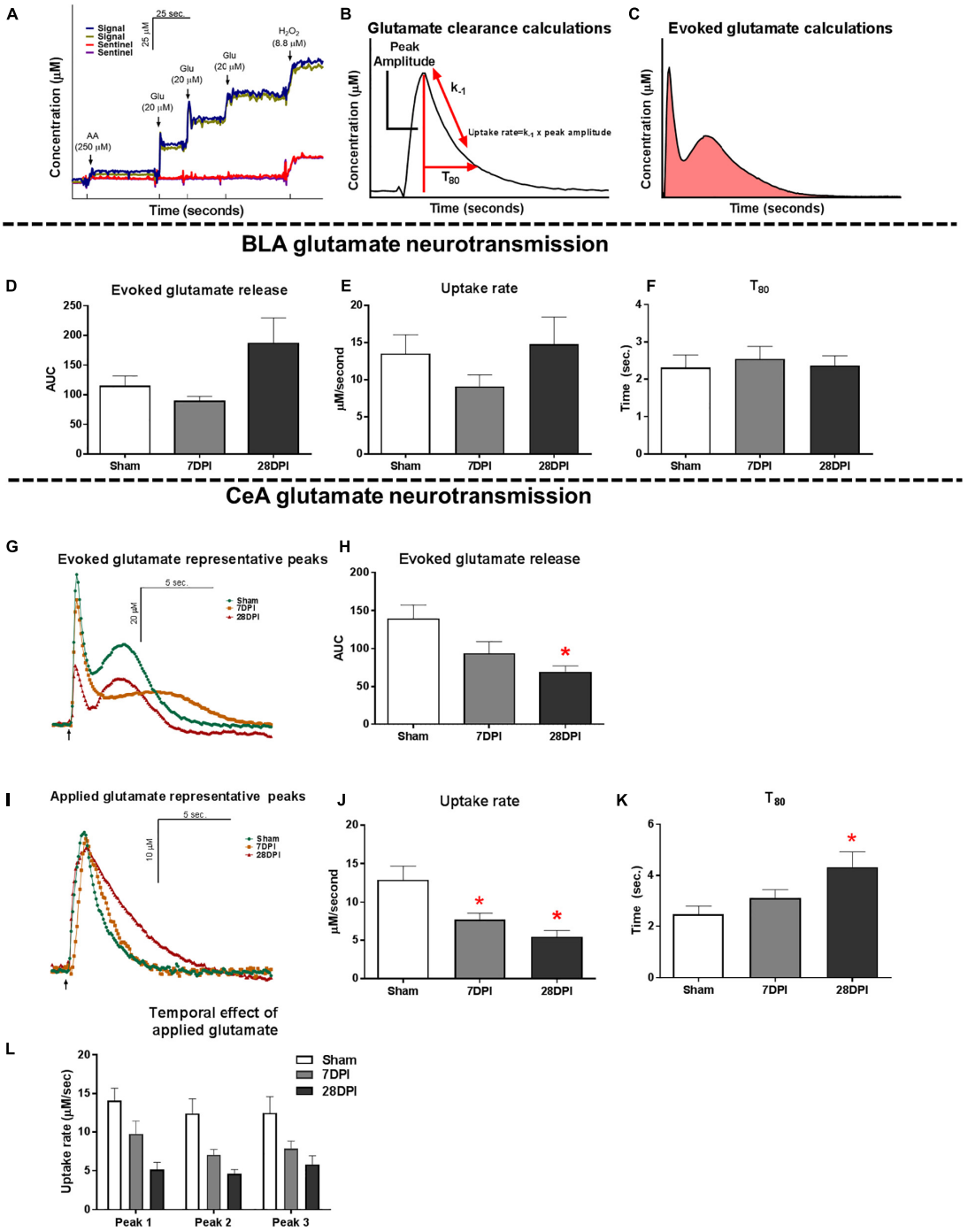

FIGURE 2 | TBI induces altered glutamate neurotransmission in the CeA. **(A)** Representative calibration of glutamate selective MEA. Arrows represent aliquots of solution of either 250 μM ascorbic acid (AA), 20 μM glutamate (Glu), or 8.8 μM H_2O_2. **(B)** Calculations for extracellular clearance of glutamate following local applications of 100 μM glutamate. **(C)** Calculations for total evoked glutamate release following local applications of 120 mM potassium chloride solution (KCl). **(D)** No significant differences were observed in evoked glutamate release in the BLA [Kruskal Wallis $H = 4.63$; $p = 0.10$; $n = 8$–11]. **(E)** No changes in glutamate clearance were observed when assessing the uptake rate [One-way ANOVA $F(2,21) = 1.24$; $p = 0.31$] or **(F)** T_{80} [One-way ANOVA $F(2,21) = 0.14$; $p = 0.87$; $n = 6$–10]. **(G)** Representative traces of KCl-evoked glutamate release. Baseline levels have been adjusted to show comparison amongst the three time points. Arrow represents 120 mM KCl administration. **(H)** 28 DPI rats had 50% less total evoked glutamate when compared to shams [One way ANOVA $F(2,19) = 4.74$ $p < 0.05$ Dunnett's *post hoc* $p < 0.05$, $\eta^2 = 0.33$; $n = 6$–9] in the CeA. **(I)** Representative traces of extracellular glutamate clearance. Baselines levels have been adjusted to show comparison amongst the three time points. Arrow represents 100 μM glutamate administration. **(J)** 7 and 28 DPI rats had 40% and 58% slower uptake rate, respectively [One-way ANOVA $F(2,22) = 7.88$; $p < 0.01$, @ 7 DPI Dunnett's *post hoc* $p < 0.05$, @ 28 DPI Dunnett's *post hoc* $p < 0.01$, $\eta^2 = 0.41$; $n = 7$–10]. **(K)** 28 DPI rats had a 43% increase in T_{80} [One-way ANOVA $F(2,22) = 5.00$; $p < 0.05$, Dunnett's *post hoc* $p < 0.01$, $\eta^2 = 0.33$; $n = 7$–10]. **(L)** Uptake rate remained consistent between subsequent additions of glutamate to the CeA [RM Two-way ANOVA $F(2,21) = 8.16$; $p < 0.01$; $n = 7$–10]. Bar graphs represents mean ± SEM. *$p < 0.05$ in comparison to sham.

to produce an evoked glutamate release. Additional ejections of KCl were completed at 2-min intervals and were volume matched at the time of administration. Criteria for analysis required that the peak with the largest amplitude was acquired from the first local application of KCl. This ensured that the data chosen were most representative of the maximum glutamate released within the surrounding neuronal tissue. Primary outcome measures were area under the curve as a proxy to investigate the total glutamate release capable of the recorded region. For a diagrammatic representation of these calculations, see **Figure 2C**.

Glutamate Clearance Analysis Parameters

Once the baseline was reached and maintained for at least 2 min (10–20 min), 100 μM glutamate was locally applied into the extracellular space (BLA: 73 ± 17 nl; CeA: 78 ± 15 nl). Exogenous glutamate was released at 30 s intervals and amplitude was matched at the time of administration. In analysis, three peaks were selected based on a predetermined amplitude range of 15 to 25 μM to ensure that data chosen were most representative of the glutamate clearance of similar volume and amplitude in accordance with Michaelis-Menton kinetics clearance parameters. The parameters for the 3 peaks were then averaged to create a single representative value per recorded region per rat. Primary outcome measures analyzed the uptake rate and the time taken for 80% of the maximum amplitude of glutamate to clear the extracellular space (T_{80}). The uptake rate was calculated using the uptake rate constant (k_{-1}) multiplied by the peak's maximum amplitude, thus controlling for any variation between the amount of applied glutamate between peaks. For a diagrammatic representation of these calculations, see **Figure 2B**.

MEA Placement Verification

Immediately following *in vivo* anesthetized recordings, rats were transcardially perfused with PBS followed directly by 4% paraformaldehyde (PFA). Brains were cryoprotected and sectioned at 40 μm sections to confirm MEA electrode placement. Of these, 1.96% of electrode tracts were excluded due to inaccurate placement. Representative image shown in **Supplementary Figure S2**.

Microglia Skeleton Analysis

At 1, 7, and 28 DPI, sham and brain-injured rats (n = 3/time point) were administered a lethal dose of Euthasol® (a sodium pentobarbital mixture, 200 mg/kg, i.p., Virbac AH, Inc.) and were transcardially perfused with PBS, followed by a fixative solution containing 4% paraformaldehyde. Brains were then shipped to Neuroscience Associates Inc (Knoxville, TN) where they were embedded into a single gelatin block (MultiBrain® Technology, NeuroScience Associates, Knoxville, TN, United States). Forty-micron thick sections were taken in the coronal plane and wet-mounted on 2%-gelatin-subbed slides before being stained with ionized calcium binding adaptor molecule (Iba1) primary antibody and 3,3′-Diaminobenzidine (DAB) visualization (NeuroScience Associates, Knoxville, TN, United States) to identify all microglia. Images and analysis of alternate regions of the same histology (for all NSA tissue) has been previously described (Cao et al., 2012; Lifshitz and Lisembee, 2012; Miremami et al., 2014; Rowe et al., 2016; Hoffman et al., 2017; Morrison et al., 2017; Thomas et al., 2018).

Photomicrographs of the BLA and CeA were taken using a Zeiss microscope (Imager A2; Carl Zeiss, Jena, Germany) in bright-field mode with a digital camera using a 40× objective. One digital photomicrograph in each region was acquired from the left and right hemisphere, respectively, for each time point across three coronal sections for each mFPI and sham rat, for a total of 6 images per rat. A computer-aided skeletal analysis method was used to quantify morphological remodeling of ramified microglia after experimental diffuse brain injury (Young and Morrison, 2018).

Skeleton Analysis

Microglia were analyzed by an investigator blinded to injury status using computer-aided skeleton analysis as previously published (Young and Morrison, 2018). Briefly, photomicrographs were converted to binary images which were skeletonized using ImageJ software (National Institutes of Health[1]) (**Supplementary Figure S3**). The Analyze Skeleton Plugin (developed by and maintained here[2]) was applied to the skeletonized images, which tags branches and endpoints and provides the total length of branches and total number of endpoints for each photomicrograph. Cell somas were manually counted by 2 investigators and averaged for each photomicrograph. The total branch length and number of process endpoints were normalized to number of microglia cell somas per image. Data from the 6 images were averaged to a single representative measure per animal.

GFAP Analysis

At 7 and 28 DPI, injured and sham rats were given a lethal dose of Euthasol® and transcardially perfused with 4% PFA/PBS (sham = 3, 7 DPI = 3, 28 DPI = 4). The brains were then cryoprotected in graded sucrose solutions (15% and 30%) and cryosectioned (20 μm). Sections were prepared exactly as previously described using rabbit anti-GFAP primary antibody (1:1000; Dako, catalog# Z0334) and biotinylated horse anti-rabbit secondary antibody (1:250; Vector Laboratories, Burlingame, CA, United States; Catalog#Ba-1100) then incubated with DAB (Rowe et al., 2016; Hoffman et al., 2017). The sections were dehydrated with ethanol and cleared in citriSolv before being cover-slipped with DPX.

Montaged images encompassing both hemispheres were taken using a Zeiss microscope (Imager A2; Carl Zeiss, Jena, Germany) in bright-field mode with a digital camera. Quantitative analysis was performed using ImageJ Software (3.1.1v, NIH, Bethesda, MD, United States) on a Macintosh computer (OSX 10.11.6). The CeA was identified and traced based on topographical localization to the optic chiasm, rhinal fissure, and commissural stria terminalis. Grayscale digital images

[1]https://imagej.nih.gov/ij/

[2]http://imagej.net/AnalyzeSkeleton31

were then digitally thresholded to separate positive-stained pixels from unstained pixels. The percentage of argyrophilic (black) stained pixels was calculated for each image using the following formula:

$$\text{Total area measured black/Total area measured} \times 100$$

$$= \text{Percentage area with argyrophilic stain}$$

Five to six rat brain hemispheres were analyzed per rat (n = 3–4/time point), depending on the quality of the section mounted (no folds or tearing within the area of interest). The same image was analyzed three times. The standard deviation between the percent area black was below 10% within each rat.

deOlmos Silver Stain Analysis

Alternating sections of brains prepared by NeuroScience Associates Inc (Knoxville, TN, United States) (see Iba1 staining methods; Thomas et al., 2018) were cryosectioned, mounted, stained using de Olmos aminocupric silver technique, counterstained with Neutral Red, and cover-slipped. Densitometric quantitative analysis was performed identical to GFAP analysis. Four hemispheres per rat (n = 3/time point) were analyzed and each hemisphere was analyzed three times. These 12 statistical numbers indicating the percentage of black pixels were then averaged together to a single value (per rat) and subsequently used in statistical analysis. The standard deviation between the percent area black was below 10% within each rat.

Tissue Dissection and Protein Extraction

At 28 DPI, a new cohort of rats (n = 5/each) were given a lethal dose of Euthasol®. Animals were transcardially perfused with ice-cold PBS for 3 min. The brain was rapidly removed and rinsed with ice-cold PBS. Tissue biopsies (1 mm diameter) taken bilaterally from the BLA and CeA were collected from 2 mm thick coronal sections made using a chilled rat brain matrix. Tissue biopsies were flash frozen and stored at −80°C until protein was extracted for automated capillary western analysis. Total protein was extracted from the BLA and CeA previously stored at −80°C. Tissues were homogenized in 250 μl of ice-cold extraction buffer (pH 8.0) containing 0.24 M Tris, 0.74 M NaCl, 100 μl TritonX100 with a protease inhibitor cocktail (complete, Roche Diagnostics; #11836153001). Tissue was homogenized with the Precellys®24 machine (Bertin Technologies, Montigny le Bretonneux, France) for 40 s bouts until the solution was completely clear (being chilled on iced for 2 min between bouts). Samples were then centrifuged at 3,000 × g for 15 min and the supernatant stored in 10–20 μl aliquots at −80C until analysis. Protein concentrations were determined using the bicinchoninic acid assay (BCA) following manufacturer's instructions (Pierce, Rockford, IL, United States).

Automated Capillary Western – ProteinSimple (Wes)

Protein expression was evaluated using automated capillary western (ProteinSimple™, Biotechne, San Jose, CA, United States). Experiments were run per manufacturer's instructions and using products purchased through ProteinSimple™ (unless otherwise noted), including 12–230 kDA capillary cartridges (SM-W004) and anti-rabbit detection modules (DM001). Proprietary mixtures included a biotinylated ladder and molecular weight standards as internal controls. Technical properties of the Simple Western™ are described by Rustandi et al. and Loughney et al. (2014). Prior to experiments, optimization was carried out for protein concentration, primary antibody concentration, multiplexing with a biological control (GAPDH), denaturing process, and exposure time (**Supplementary Table S1**). Target protein concentration was chosen within the midpoint of the slope (0.125–2.5 μg/capillary). Antibody concentration was based on evidence of antigen saturation at the chosen protein concentration. Target and GAPDH (loading control) were optimized for multiplexing to ensure chemiluminescence was within systems threshold and to ensure no protein-protein interactions. If chemiluminescent detection was above the threshold, secondary antibodies from Jackson ImmunoResearch Laboratories, Inc (West Grove, PA, United States) were used to dilute the manufacturer's secondary antibody to reduce amplification of highly expressed targets (Goat Anti-Rabbit 111-005-045, HRP-Goat Anti-Rabbit 111-035-045, Goat Anti-Mouse 115-005-062, and HRP-Goat Anti-Mouse 115-035-062). Denaturing temperature was chosen based on low signal to noise and baseline. The high-dynamic range of the exposures (algorithm in software) was used for data analysis in all experiments. Every capillary cartridge (25 capillaries) was run with the following controls: the same brain homogenate as a positive control, Erk as a system control, Antibody only, and protein only.

Protein extracts from amygdala samples were combined with sample buffer and master-mix (40 mM DTT, 0.1× ProteinSimple Sample Buffer, and 1× Fluorescent Standards) to achieve the desired protein concentration. Samples were then denatured via heating block at the optimized temperature (37°C × 30 min). Duplicate capillaries of each sample were loaded per manufacturer's instructions, the cartridge was centrifuged at 2500 RPM for 5 min, and placed into the automated capillary western machine where proteins were separated by size (electrophoresis), immobilized, and immunoprobed in individual capillaries. Once loaded into the instrument, the standard default metrics recommended by ProteinSimple were utilized for separation, incubation, and detection. The associated software, Compass (ProteinSimple®), generates an electropherogram with peaks corresponding to the expression of proteins of interest and calculates the area under the curve (AUC) for each peak (**Figure 4E**). To calculate relative protein expression, the AUC for the protein was normalized to the AUC for the biological control (GAPDH). The ratios from duplicate capillaries were averaged. Then, ratios from injured animals were normalized to shams in the same capillary cartridge.

Statistical Analysis

Based on KCl-evoked glutamate release in the thalamus from a previous publication by Thomas *et al* (Thomas et al., 2012), 3–12 rats per group could detect a 100% increase in evoked glutamate release at 80% power at a significance level of 0.05 on a 2-sided test. Statistical analysis was determined by *a priori* planned comparisons, where our primary outcome measure

(OFT, electrochemistry, histology, protein levels) was to detect changes between 7 DPI or 28 DPI and shams. All data were analyzed using a customized Microsoft Excel® spreadsheet and GraphPad® software. Seven day and 28 day shams did not statistically differ from one another for all outcomes of behavior (e.g., time in center: 7D sham 31.3 ± 7.2 s, 28D sham 34.7 ± 6.7 s) and electrochemical measures (e.g., evoked glutamate release (AUC): BLA-7D sham 105.9 ± 33.9, 28D sham 119.1 ± 20.8; and CeA-7D sham 136.4 ± 34.2 and 140 ± 23.6). Therefore, 7D and 28D shams were combined for statistical analysis. When ANOVA assumptions were met and the dependent variable was continuous, data were analyzed using a one-way ANOVA with Dunnet's *post hoc* comparison to sham. All data were assessed for normality and variability. Data not passing Shapiro-Wilks normality tests or Brown-Forsythe variability test were analyzed as non-parametric statistics with a Kruskal-Wallis (KW) analysis and Dunn's *post hoc* comparison to sham. Outliers in the open field test were determined using three standard deviations from the mean. Using these metrics, two rats were excluded from consideration (7-day sham, 7 DPI). Amperometric measures from the paired MEA recording sites for each outcome in each region were averaged and used as a single data point. Outliers for amperometric analysis were determined using a ROUT test with Q = 5% (BLA = 1 of 28; CeA = 4 of 28). Additional analysis of extracellular clearance of glutamate in the CeA assessing for the potential effects of multiple additions of glutamate and differential effects of nuclei-specific microglial activation were conducted with a two-way ANOVA with a Tukey comparison. To be included in the amperometric recordings, the rat had to be included in the in open field testing. Molecular data for glutamate transporters were analyzed using an unpaired, two-tailed Student's *t*-test. Based on our hypothesis of a decrease in protein levels for BDNF, TrkB, and GluR, we used a one-tailed Student's *t*-test. For all instances, statistical significance was defined at $p < 0.05$.

Effect Size

For parametric calculation using the one-way ANOVA, eta squared η^2 was conducted as described by Lakens (2013). η^2 was evaluated and reported such that 0.02 represents a small effect size, 0.13 represents a medium effect size and 0.16 represents a large effect size. Data comparing two means and analyzed using a Student's *t*-test were evaluated using Cohen's d. For non-parametric calculations using the Kruskal-Wallis test, Pearson's r was reported as described by Fritz et al. (2012). To do so, a Mann Whitney U *post hoc* comparison was done between the two groups identified to have a difference as indicated by the Dunn's *post hoc* comparison. Then a Pearson's r effect size calculation was evaluated and reported such that a 0.1 equals a small effect size, 0.3 represents a medium effect size and 0.5 represents a large effect size.

Data Analysis Validation

All outcome measures were evaluated for variability based on cohort membership, cage-mates, cage changes, time/order of open field testing, and time of recordings. Of these, no variables, other than injury status, could explain the variation observed in the presented data sets.

RESULTS

dTBI Induces the Expression of Anxiety-Like Behavior

Representative traces of first 5 min of open field exploration illustrate behavioral performance between brain-injured and sham rats (**Figures 1B,C**). Distances traveled at 7 DPI and 28 DPI did not reach significance when compared to shams [$F(2,29) = 3.23$; $p = 0.054$; **Figure 1D**]. Rats at 7 DPI did not significantly alter their duration in the center of the open field, whereas rats at 28 DPI spent 57% less time in the center when compared to shams (KW = 6.71; $p < 0.05$; Dunn's *post hoc* $p < 0.05$; $r = 0.48$; **Figure 1E**). Rats at 28 DPI also made 54% fewer entries into the center of the open field when compared to shams (KW = 6.83, $p < 0.05$; Dunn's *post hoc* $p < 0.05$; $r = 0.46$; **Figure 1F**). These data indicate that mFPI results in the expression of anxiety-like behavior by 28 DPI.

Glutamate Neurotransmission in the BLA Does Not Change Over 1-Month Following dTBI

As the main sensory nuclei for anxiety-like behavior, the BLA was examined for alterations of glutamate neurotransmission (Pitkanen et al., 1997; Phelps and LeDoux, 2005). BLA tissue was depolarized using a local application of isotonic 120 mM KCl (75–150 nL) to evoke the release of neurotransmitters. Similar volumes of KCl were applied to the extracellular space (**Supplementary Figure S4A**). KCl-evoked glutamate release in the BLA was not significantly different between 7 DPI and 28 DPI brain-injured rats when compared to shams (KW = 4.63 $p = 0.10$; **Figure 2D**).

Evaluation of BLA extracellular glutamate clearance parameters was accomplished through local application of 100 μM exogenous glutamate. Peaks were amplitude-matched to control for Michaelis-Menten kinetics, then analyzed for glutamate clearance parameters (**Supplementary Figure S4B**). Uptake rate was unaltered within the BLA at 7 DPI or 28 DPI following injury when compared to shams [$F(2,21) = 1.24$; $p = 0.31$; **Figure 2E**]. Furthermore, time taken for 80% of maximum applied glutamate to clear (T_{80}) was not altered within the BLA at 7 DPI or 28 DPI when compared to shams [$F(2,21) = 0.140$; $p = 0.870$; **Figure 2F**]. These data indicate that evoked glutamate release and glutamate clearance parameters were not influenced by mFPI at 7 DPI or 28 DPI.

Glutamate Neurotransmission in the CeA Is Significantly Altered Over 1-Month Following dTBI

The CeA is the main amygdaloid nucleus for regulating anxiety-like behavior (Pitkanen et al., 1997; Phelps and LeDoux, 2005;

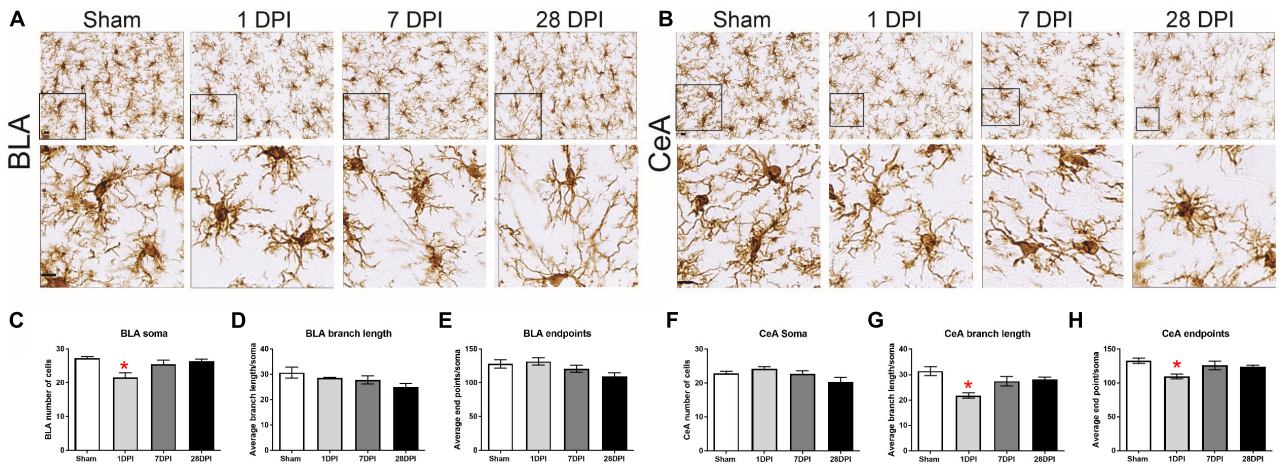

FIGURE 3 | Acute, nuclei-specific microglial alterations occur following dTBI. Representative images of Iba1 staining in the **(A)** BLA and **(B)** CeA. Cropped photomicrographs correspond to the highlighted square (Scale bars = 10 μm). **(C)** In the BLA, the number of microglia changed over time post-injury [One-way ANOVA $F(3,8) = 6.32$; $p < 0.05$; $\eta^2 = 0.70$]. **(D)** Branch length (μm/cell) or **(E)** number of microglia process endpoints per cell did not significantly change over time [One-way ANOVA $F(3,8) = 2.32$; $p = 0.15$ and One-way ANOVA $F(3,8) = 3.18$; $p = 0.09$]. **(F)** In the CeA, the average number of microglia per field did not significantly change over time [One-way ANOVA $F(3,8) = 3.17$; $p = 0.09$]. **(G)** Contrasting to the BLA, branch length (μm/cell) [One-way ANOVA $F(3,8) = 5.27$; $p < 0.05$; $\eta^2 = 0.66$]. **(H)** Number of microglia process endpoints per cell were significantly decreased at 1 DPI in comparison to sham [One-way ANOVA $F(3,8) = 7.32$; $p < 0.05$; $\eta^2 = 0.73$]. Bar graphs represents mean ± SEM. $n = 3$ for each group. *$p < 0.05$ in comparison to sham.

Tye et al., 2011). Surrounding tissues, including pre-synaptic terminals along the BLA-CeA axis, were depolarized to evoke the release of glutamate using local application of 75–150 nL of 120 mM isotonic KCl. There were no statistically significant differences in the volume of applied KCl (**Supplementary Figure S4D**). Representative traces of KCl-evoked glutamate release are shown in **Figure 2G**. Glutamate released in CeA was 50% less at 28 DPI when compared to shams [$F(2,19) = 4.74$; $p < 0.05$; Dunnett's *post hoc* $p < 0.05$; $\eta^2 = 0.33$; **Figure 2H**]. Initial peak amplitude was also significantly less at 28 DPI when compared to shams [$F(2,19) = 4.89$; $p < 0.05$; Dunnett's *post hoc* $p < 0.05$; $\eta^2 = 0.34$; **Supplementary Figures S4C,F**].

Evaluation of CeA extracellular glutamate clearance was accomplished through local application of 100 μM exogenous glutamate. Representative traces of resulting glutamate peaks chosen for analysis are shown in **Figure 2I**. Peaks were amplitude-matched to control for Michaelis-Menten kinetics, then analyzed for glutamate clearance parameters (**Supplementary Figure S4E**). Uptake rate was significantly decreased at 7 DPI and 28 DPI when compared to shams resulting in 40% and 58% decreases, respectively [$F(2,22) = 7.88$; $p < 0.01$; Dunnett's *post hoc* $p < 0.05$ for 7 DPI and $p < 0.01$ for 28 DPI; $\eta^2 = 0.42$; **Figure 2J**]. Further, T_{80} of 28 DPI rats was 43% longer when compared to shams [$F(2,22) = 5.00$; $p < 0.05$; Dunnett's *post hoc* $p < 0.01$; $\eta^2 = 0.31$; **Figure 2K**]. Uptake was independent of subsequent local applications of glutamate to the CeA [RM $F(2,21) = 8.16$; $p < 0.01$; **Figure 2L**]. These data indicate that evoked glutamate release and glutamate clearance parameters in the CeA were significantly influenced by mFPI over 28 DPI.

Nuclei-Specific Microglia Deramification Manifests Acutely Along BLA-CeA Axis Following dTBI

Images of microglia are depicted for BLA (**Figure 3A**) and CeA (**Figure 3B**). In the BLA, microglial cell count significantly changed as a function of time, decreasing at 1 DPI [$F(3,8) = 6.32$; $p < 0.05$; Dunnett's *post hoc* $p < 0.01$ **Figure 3C**]. The branch length per cell (μm/cell) did not significantly change over time [$F(3,8) = 2.32$; $p = 0.15$; $\eta^2 = 0.70$; **Figure 3D**]. Furthermore, the number of microglia process endpoints per cell did not significantly change over time [$F(3,8) = 3.18$; $p = 0.09$; **Figure 3E**].

Identical analysis was performed on microglia in the CeA. The microglial cell count per field did not significantly change over time [$F(3,8) = 3.17$; $p = 0.09$; **Figure 3F**]. The branch length per cell (μm/cell) significantly decreased at 1 DPI [$F(3,8) = 7.32$; $p < 0.05$; $\eta^2 = 0.73$; **Figure 3G**]. The number of microglia process endpoints per cell was also significantly decreased at 1 DPI [$F(3,8) = 5.27$; $p < 0.05$; Dunnett's *post hoc* $p < 0.05$; $\eta^2 = 0.66$; **Figure 3H**].

The same three variables were evaluated with a two-way ANOVA to determine whether the influence of time-post injury was similar in between the BLA and CeA. The number of cells [$F(3,16) = 7.85$; $p < 0.05$], endpoints [$F(3,16) = 5.152$; $p < 0.05$], and process length [$F(3,16) = 3.94$; $p < 0.05$] all differed between regions, indicating that TBI-induced changes in microglial morphology at 1 and 28 DPI are region dependent (**Supplementary Figure S5**). Although there is an acute microglial response in the CeA, similar to other regions in this injury model

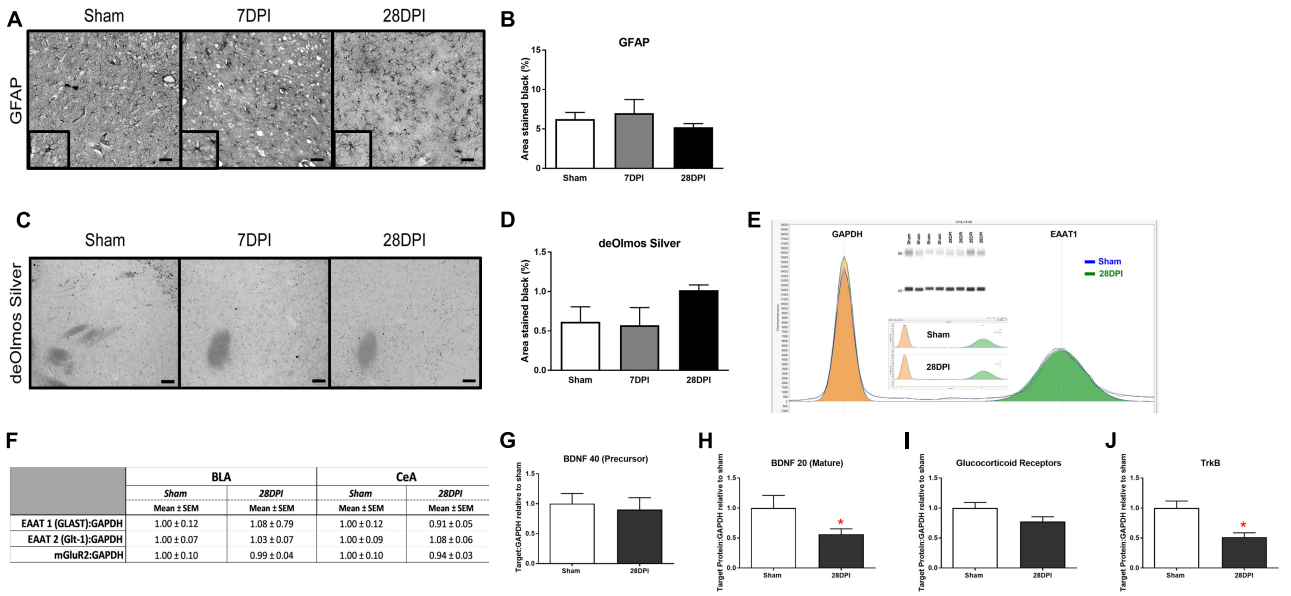

FIGURE 4 | Changes in neurotransmission occur in the absence of neuropathology, astrocytosis and molecular alterations in glutamate transporters and receptor. **(A)** Representative images of GFAP staining of the CeA (40× magnification; scale bar = 50 μm). **(B)** Pixel density analysis of GFAP staining in the CeA revealed no significant differences following diffuse TBI [One-way ANOVA $F(2,7) = 0.80$; $p = 0.49$; $n = 3$–4 per group]. **(C)** de Olmos silver stained sections of the CeA (40× magnification; scale bar = 50 μm). **(D)** Pixel density analysis of aminocupric silver stained tissue revealed that there was no difference following diffuse TBI [One-way ANOVA $F(2,6) = 0.22$; $p = 0.40$; $n = 3$–4 per group]. Automated capillary western blots (in duplicate) were performed to quantify the amount of synaptic glutamate transporters (Glt-1, GLAST) and pre-synaptic glutamate receptors (mGluR2, GluR) at 28 DPI. **(E)** Representative quantification of sham and injured GLAST (EAAT1) shown individually, overlapped and with recreated western blot. **(F)** Levels of GLAST, Glt-1, and mGluR2 were similar to sham indicating an alternative mechanism for observed changes in glutamate neurotransmission ($n = 4$–5 per group). **(G)** The precursor protein to BDNF was similar to sham at 28 DPI. **(H)** Protein levels of mature BDNF were decreased by 43% ($t_{4,5} = 2.07$; $p < 0.05$; $d = 1.33$). **(I)** GluR approached significance with a 20% decrease ($t_{4,5} = 1.854$; $p = 0.053$). **(J)** TrkB receptors were decreased by 49% ($t_{4,5} = 3.68$; $p < 0.01$; $d = 2.41$). $n = 4$–5 per group. Bar graphs represent mean ± SEM.

(Miremami et al., 2014; Morrison et al., 2017; Thomas et al., 2018), and dynamics over time are region-dependent; these data do not provide evidence that microglia have a role in mediating glutamate neurotransmission in BLA-CeA communication at 28 DPI.

Absence of Activated Astrocytes Over 1 Month After dTBI

Robust astrocytosis in the BLA has been previously reported at 7 DPI and resolved by 28 DPI following experimental dTBI using mFPI (Hoffman et al., 2017). Astrocytes are a major contributor to glutamate neurotransmission, where activation indicates a role in glutamate clearance from the extracellular space. GFAP intensity was analyzed as an indicator of astrocytosis in the CeA. There was no evidence that mFPI influenced astrocytosis over time in the CeA [$F(2,7) = 0.80$; $p = 0.49$; **Figures 4A,B**].

Absence of Overt Neuropathology in the CeA Following dTBI

The BLA has been described as lacking overt neuropathology at 7 DPI and 28 DPI (Hoffman et al., 2017), however, the CeA has not been evaluated in a model of mFPI. Using de Olmos silver stain technique, neuropathology in the CeA was assessed at 7 DPI and 28 DPI compared to shams. No overt pathology was identified in the CeA following mFPI [$F(2,6) = 1.99$; $p = 0.22$; **Figures 4C,D**].

Alteration in Glutamate Neurotransmission Are Independent of Glutamate Transporters and Pre-synaptic Receptors

Observed alterations to glutamate neurotransmission could result from altered levels of glutamate transporters or presynaptic metabotropic receptors (Ueda et al., 2001). Proteins involved in glutamate transport [EAAT1 (GLAST) EAAT2 (Glt-1)] were evaluated at 28 DPI for the BLA and CeA. Levels of GLAST and Glt-1 were similar to sham [GLAST (BLA $t_8 = 0.59$ $p = 0.57$; CeA $n = 4$, $t_7 = 0.75$; $p = 0.49$; Glt-1 (BLA $t_7 = 0.25$; $p = 0.81$; CeA $t_6 = 0.81$; $p = 0.45$)] (**Figures 4E,F**). Pre-synaptic metabotropic glutamatergic receptors (mGluR2) levels did not change in comparison to shams (BLA $t_9 = 0.09$; $p = 0.93$; CeA $t_6 = 0.51$; $p = 0.63$) (**Figure 4F**), indicating that observed changes in glutamate neurotransmission were independent of changes in total protein levels of glutamate transporters and mGluR2. **Supplementary Figure S6** depicts a schematic showing localization of these molecules on a presynaptic terminal.

BDNF and TrkB Decreased at 1-Month Post-dTBI

As BDNF, GluR, and TrkB, have been shown to influence presynaptic glutamate release, we tested the hypothesis that dTBI caused decreased levels of BDNF, GluR, and TrkB in the amygdala by 28 DPI (Kunugi et al., 2010). Protein levels of mature BDNF were decreased by 43% ($t_7 = 2.07$; $p < 0.05$; $d = 1.33$; **Figure 4H**) (BDNF precursor was not different; **Figure 4G**) and GluR approached significance with a 20% decrease ($t_7 = 1.854$; $p = 0.053$; **Figure 4I**). TrkB receptors were decreased by 49% ($t_7 = 3.68$; $p > 0.01$; $d = 2.41$; **Figure 4J**). These data indicate that a single dTBI can significantly decrease BDNF and TrkB in the amygdala by 1-month post-injury, coinciding with the changes in evoked glutamate neurotransmission and expression of anxiety-like behavior.

DISCUSSION

Multifactorial mental illnesses are the result of poorly understood pathophysiology that confounds treatment approaches leading to poor symptom control. These are the first experiments that demonstrate dTBI initiates a cascade of molecular events in the amygdala capable of contributing to the expression of anxiety-like behavior. By 1-month post-injury, decreased glutamate release and slower glutamate clearance within the CeA coincided with the expression of anxiety-like behavior. There were no changes in the BLA. Changes in glutamate neurotransmission occurred despite similar protein levels of glutamate transporters, mGluR2, and in the absence of overt neuropathology or glial pathology. BDNF and TrkB protein levels were significantly decreased at 28 DPI, and may be a potential target to modulate glutamate signaling related to anxiety-like behavior. These data indicate novel targets in the quest for understanding chronic TBI pathophysiology associated with TBI-induced affective disorders.

Open field testing is an ethological behavioral-based test for systematic assessment of unconditioned general exploratory drive that can serve as an initial screening of emotional or anxiety-like behavior, locomotor activity, and novel environment exploration. The test can distinguish between the primal drive to survive (aversion to light and innate predatory response) versus exploration (enter the center area) by quantifying thigmotactic variables, distance traveled, entrances and time in the center of the open field as an indicator of emotionality or anxiety-like behavior (Roth and Katz, 1979; Ennaceur, 2014). Specifically, increased time spent alongside the walls of the open field enclosure is indicative of a heighten aversion response and has a high correlation factor with measures of anxiety in the elevated plus maze in rodents (Carola et al., 2002). Characterized by validated metrics reviewed by Gould et al. (2009), we show evidence of late-onset anxiety-like behavior following dTBI. By 28 DPI, rats spent less time and made fewer entries into the center of the open field when compared to shams, indicative of anxiety-like behavior. Distance traveled between sham and brain-injured rats did not reach significance as previously demonstrated in Liu et al. in the same model at the same time point (Liu et al., 2017). While Liu et al. (2017) reports dopamine axonal damage, 25% dopamine neuronal loss and microglia activation the nigrostriatal pathway, a minimum of 50% loss of substantia nigral dopamine neurons is associated with movement symptoms (Grosch et al., 2016), supporting that the loss of DA neurons is not the primary cause of decreased locomotor activity. Morris Water Maze testing at 15 DPI further provides evidence that injured rats were capable of swimming a similar distance at similar swim speed as shams indicating a behavioral response rather than an motor deficit (Clausen et al., 2017). Repeated publications from our lab support that non-noxious sensory stimulation of the whiskers significantly increases freezing, guarding, evasive behaviors and corticosterone levels at 28 DPI in comparison to sham and 7 DPI (McNamara et al., 2010; Thomas et al., 2012), supporting that the observed trends in decreased distance may be associated with a heighten aversion response.

The presence of anxiety and fear-like behavior has been reported at chronic time points in other models of TBI using OFT, elevated plus maze and fear conditioning (Kovesdi et al., 2011; Elder et al., 2012; Shultz et al., 2013; Almeida-Suhett et al., 2014; Hou et al., 2017), however, the presence of affective deficits is inconsistent and varies between experimental models, species, behavioral paradigms and labs. For these experiments, we only used a single behavioral test because repeated stressors (including behavioral tests) can also result in BLA neuronal hypertrophy and enhanced anxiety-like behavior (Vyas et al., 2004), potentially confounding electrochemical experiments. A more thorough independent assessment of anxiety, fear, and depressive behaviors at 1-month post-injury are needed to determine the extent of TBI-induced affective morbidity (Ennaceur, 2014).

Glutamatergic connections between the BLA and CeA have been shown to regulate affective symptomatology during neurological assessment tasks such as open field (Tye et al., 2011; Kim et al., 2013; Janak and Tye, 2015), integrating limbic system circuitry input from numerous regions of the brain (**Figure 5**; Tye et al., 2011; Kim et al., 2013; Janak and Tye, 2015; Tovote et al., 2015). The BLA integrates sensory afferents from the prefrontal cortex (PFC), thalamus, and sensory association cortex and relays this information to the ventral hippocampus, bed nucleus of the stria terminalis (BNST), or CeA by projects that can either promote or diminish the expression of anxiety-like behavior (Phelps and LeDoux, 2005; Janak and Tye, 2015; Tovote et al., 2015; Hrybouski et al., 2016). Reciprocal and interconnections between and within nuclei of the amygdala not shown in our diagram also modulate, in part, the BLA-CeA circuitry and most likely influence the expression of affective behaviors (Pitkanen et al., 1997; Phelps and LeDoux, 2005). While the BLA-CeA circuit plays a known role in mediating affective behaviors (Pitkanen et al., 1997; Phelps and LeDoux, 2005); the functional, structural, and molecular components underlying the development after TBI have never been evaluated.

For real-time recordings of extracellular neurotransmission, *in vivo* amperometry coupled with glutamate selective multielectrode arrays were utilized for their excellent spatial and temporal resolution and the presence of sentinel channels to verify glutamate specificity. Localized KCl administration induced non-specific neurotransmitter release in which glutamate-sensitive MEA's measured synaptic glutamate

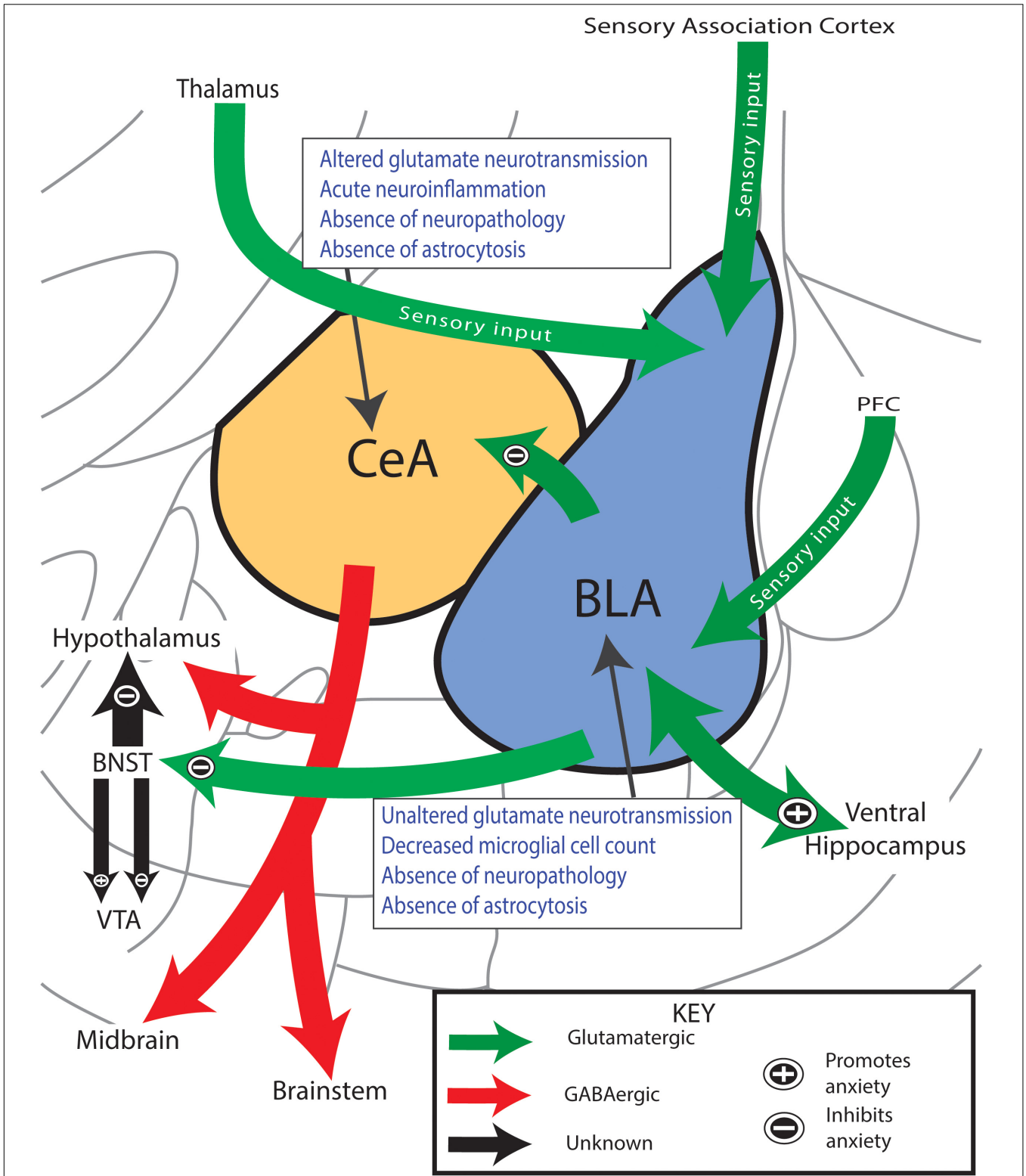

FIGURE 5 | Anxiety-like behavior coincides with altered glutamate neurotransmission in amygdala circuitry. Simplified circuitry of the rat's efferent and afferent projections of the amygdala that are considered to play important roles in the regulation of anxiety-like behavior. Glutamatergic projections enter the BLA from the PFC and thalamus and carry sensory information of the overall anxious state of the rat. The BLA interprets this information and sends efferent outputs to either promote (+) or inhibit (–) the display of anxiety-like behavior. Activation of BLA-CeA circuitry has shown to mediate anxiolytic behavior. Boxes summarize findings. PFC, prefrontal cortex; BLA, basolateral amygdala; CeA, central nucleus of the amygdala; BNST, bed nucleus stria terminalis; VTA, ventral tegmental area. Anatomy modified from Paxinos and Watson, 2007.

overflow. In the BLA, no significant changes were detected, however, in the CeA glutamate release was decreased by 28 DPI compared to uninjured shams. Reduced glutamate release indicates less stores available for potential neuronal communication between those located in presynaptic neurons, interneurons, and astrocytic processes. The second peak within the biphasic profile of KCl-evoked glutamate release (**Figure 2G**) provides evidence that glial transmission could be contributing to glutamate overflow whereas the first peak is thought to primarily be the response of presynaptic neurons (Parpura et al., 1994; Larter and Craig, 2005). While the amplitude of the first peaks was also significantly decreased at 28 DPI compared to shams (**Supplementary Figures S4C,F**), area under the curve was used to evaluate glutamate overflow. Changes in glutamate overflow could arise from impaired vesicular loading (Watt et al., 2000) or secondary to inhibitory GABA-ergic modulation (Jacob et al., 2008). We did not find an injury-induced change in the protein level of mGluR2 in the CeA, indicating that total mGluR2 is not predictive of changes in presynaptic glutamate release. We did not observe astrocytosis or perturbation of microglia at 28 DPI. Decreased BDNF/TrkB/GluR protein levels can reduce presynaptic glutamate release, however, localization, cell type, and functional studies are necessary to identify their role (Numakawa et al., 2009; Meis et al., 2012). As the majority of the CeA is GABAergic in nature, the release of glutamate is hypothesized to be from pre-synaptic neurons originating in the BLA. As Tye et al. (2011) indicates, stimulation of these synapses produces a decrease in the expression of anxiety behavior (McDonald, 1982; Carlsen, 1988; Smith and Pare, 1994). Therefore, decreased glutamate release in the CeA may be indicative of a permissive effect along BLA-CeA circuit such that the ability to suppress an adverse, anxiety-like response is diminished, as indicated by the concurrent expression of anxiety-like behavior. Thus, while novel in TBI, our results parallel the consensus that dysregulation of the CeA may be concomitant with the expression of affective conditions (Kalin et al., 2004; Etkin et al., 2009).

Locally applied glutamate to the BLA and CeA allowed us to calculate glutamate clearance from the extracellular space, primarily mediated by glutamate transporters (Glt-1 and GLAST) located on adjacent astrocytes in the rodent (Danbolt, 2001). The affinity of glutamate transporters can be evaluated using glutamate uptake rate, whereas the number of membrane bound transporters is estimated using T_{80} (Thomas et al., 2017). In the BLA, glutamate clearance parameters did not change as a function of injury over time. In the CeA, the uptake rate was significantly slower at 7 DPI and 28 DPI while glutamate took significantly longer to clear (T_{80}) by 28 DPI. For calculations of glutamate parameters, three consecutive peaks in each region were analyzed. The consecutive peaks were reproducible, and the uptake rate remained significantly different regardless of the repeated applications, confirming that observed alterations to glutamate clearance are not caused by immediate tissue compensation. Changes in glutamate clearance were also not due to changes in the protein levels of glutamate transporters. Slower glutamate clearance could also be caused by surface expression, post-translational modifications, or adaption of glia and adjacent cells (Maragakis and Rothstein, 2004; Hinzman et al., 2012).

No significant alterations were detected in the BLA in anesthetized rats in this study, although studies using focal TBI models indicate that BLA circuitry becomes weakened through altered neuronal excitability, changes in N-methyl-D-aspartate (NMDA) receptors, and changes to GABAergic production proteins (GAD-67), all of which may provide compensatory responses that primarily influence glutamate release in the CeA (Reger et al., 2012; Palmer et al., 2016; Hoffman et al., 2017). Previously, we reported increased neuropathology in the somatosensory cortex and thalamus following dTBI, which could also alter sensory input into the BLA (Lisembee and Lifshitz, 2008; Thomas et al., 2018). Recent publications have also indicated subacute metabolic, and chronic metabolic and structural changes mapped directly to the CeA, and impairments in extinction of contextual fear differences at a chronic time point after experimental TBI (Zhao et al., 2018; Jaiswal et al., 2019; Kulkarni et al., 2019). In accordance with the data in this manuscript, these reports specifically identify the CeA as a vulnerable anatomic locus for future investigations, where FDA approved drugs with affinities for identified targets can be evaluated for new indications on their influence on glutamate signaling in anxiety-like behavior.

No significant differences were measured between 7 DPI and 28 DPI for both OFT and glutamate neurotransmission, however, a trend toward significance was observed over time post-injury. We've previously reported increased dendritic branching of both pyramidal and stellate glutamatergic neurons in the BLA at 1 DPI, continually changing and persisting out to 28 DPI, with evidence of increased distal branching at 28 DPI in comparison to sham (Hoffman et al., 2017). This continuum of increased neuromorphic connection is indicative of increased communication within and beyond the BLA, and could differentially influence behavior and glutamatergic recordings, contributing to less robust responses at 7 DPI. We have previously published a different time course of morphological changes in the ventral posteromedial nucleus of the thalamus (VPM), the thalamic relay of the somatosensory whisker barrel circuit (Thomas et al., 2018). The time course of events in the BLA are different in comparison to the VPM, where dendritic loss peaks and 7 DPI and significantly increases by 28 DPI, coinciding with increased neuropathology (silver stain), glial activation, evoked-glutamate release, and the manifestation of hypersensitivity to whisker stimulation (McNamara et al., 2010; Thomas et al., 2012, 2018). The same archival histology for neuropathology and microglia has also been published for the somatosensory barrel fields of the whisker circuit (Lisembee and Lifshitz, 2008; Cao et al., 2012; Morrison et al., 2017) and replicated in mouse mFPI (Rowe et al., 2019). Together, these data indicate that TBI-induced circuit pathophysiology is dependent on time, region, and likely, circuit connectivity.

Microglia and astrocytes can directly and indirectly contribute to the homeostasis of excitatory neural circuitry through synaptic remodeling, release of soluble molecules, microglia-astrocyte interaction, and scaling excitatory-inhibitory signaling (reviewed in Henstridge et al., 2019). Specifically, activated microglia can

promote neuropathology and synaptic loss that can directly influence glutamate neurotransmission. Morphological analysis of microglia in the BLA and CeA nuclei were evaluated to identify a potential role for microglia in TBI-induced changes in glutamate neurotransmission. At 28 DPI, microglia morphology indicated a ramified state that may not contribute to the changes measured in glutamate neurotransmission. However, nuclei-dependent neuroinflammatory response did preceded changes in glutamatergic neurotransmission along the BLA-CeA circuit. De-ramified microglia were identified in the CeA, but not the BLA, at 1 DPI. In the CeA, microglial cell counts did not change over time, while the summed process length and number of microglial process endpoints per cell were found to be significantly decreased at 1 DPI. These data suggest that microglia become de-ramified in the CeA early and recover to sham levels by 7 DPI, indicative of an acute inflammatory response after injury (Ramlackhansingh et al., 2011). Targeted studies mediating acutely activated microglia are necessary to determine whether early activation influences long-term glutamate neurotransmission.

Subsequently, we analyzed CeA neuropathology to determine if axonal injury and neurodegeneration was coincident with changes in glutamate neurotransmission. However, in accordance with previous results published for the BLA (Hoffman et al., 2017), silver staining had no evidence of neuronal or axonal injury.

Glutamate neurotransmission is primarily mediated by glutamate transporters located on astrocytes. Changes in overflow of glutamate from the tripartite synapse can be attributed to altered astrocytic function. While astrocytes have been implicated in anxiety symptoms, this role is unclear. Studies report that GFAP levels can mediate expression of glutamate transporters, such that low levels of GFAP are associated with mood disorders, activation of astrocytes influence neurotransmission, and microglial activation triggers astrocyte-mediated modulation of excitatory neurotransmission (Pascual et al., 2012). In evaluating GFAP immunohistochemistry, increased levels of GFAP can be interpreted as a presence of activated astrocytes or increased number of astrocytes, whereas decreased levels can indicate a downregulation of GFAP and/or reduced number of astrocyte (reviewed in Hughes et al., 2004; Rajkowska and Miguel-Hidalgo, 2007; Zhou et al., 2019). Analysis of GFAP density in the CeA revealed no differences over time post-injury, in contrast to our previous work in the BLA, where morphology and increased GFAP staining indicated activated astrocytes at 7 DPI (Hoffman et al., 2017). Furthermore, glutamate transporter protein levels were not decreased at 28 DPI, negating a GFAP expression level/glutamate transporter interaction. These data do not support a substantial role for astrocytes in the changes in anxiety-like behavior and glutamate neurotransmission reported in this manuscript. Taking into consideration the microglia results, it is also unlikely that microglia-astrocyte interactions mediate these changes.

Chronologically, dTBI initiates an immediate release of glutamate, a stress response that includes increased circulating corticosterone levels, and a cascade of inflammatory cytokines that could mediate early CeA microglial activation through ionotropic and metabotropic glutamate receptors and glucocorticoid receptors (Murugan et al., 2013; Madalena and Lerch, 2017). We have previously reported a significant decrease in basal plasma corticosterone levels and a blunted stress response at 56 DPI, indicating chronic dysregulation of the HPA axis in this dTBI model (Rowe et al., 2016). Chronic dysregulation of corticosterone in response to stress has also been supported in other TBI models at both earlier and later time points (Griesbach et al., 2011, 2012). The central amygdala mediates the HPA axis response to stress, where changes in circulating corticosterone levels, GR, BDNF, and Trk-B receptor expression have been implicated in the pathology of affective disorders (anxiety-like behavior and posttraumatic stress disorder-like phenotypes) in addition to presynaptic glutamate signaling (Numakawa et al., 2009; Kunugi et al., 2010; Tejeda and Diaz-Guerra, 2017). Further evaluation is necessary to determine whether a role exists for corticosterone dysregulation and corticosterone regulated receptors in the development of anxiety-like behavior and changes in glutamate neurotransmission over time following dTBI.

Clinically, it is difficult to differentiate the initiating insult for patients experiencing affective symptoms, such as anxiety or PTSD, as similar pathophysiology exists between dTBI and chronic stress (Owens et al., 2008; French, 2010; MacGregor et al., 2011; DePalma and Hoffman, 2016). This study provides a novel link between dTBI-induced late-onset anxiety-like behavior and altered glutamate neurotransmission within the CeA, that parallels clinical studies implicating dysfunctional amygdala processing and the expression of affective symptomatology post-injury (Etkin and Wager, 2007; Koenigs and Grafman, 2009; Depue et al., 2014; Buchsbaum et al., 2015; Hrybouski et al., 2016; Stevens et al., 2016). Decreased BDNF/TrkB protein levels implicate one pathway by which dTBI can influence glutamate neurotransmission and thereby anxiety-like symptoms. Identification of common pathways for the development of TBI-induced and non-TBI-induced affective disorders are instrumental in treatment of symptoms, rehabilitation guidelines, and implementation of novel clinical approaches.

DATA AVAILABILITY STATEMENT

The datasets generated for this study are available on request to the corresponding author.

ETHICS STATEMENT

The animal study was reviewed and approved by the Institutional Animal Care and Use Committee Protocol (13–460) at the University of Arizona College of Medicine-Phoenix.

AUTHOR CONTRIBUTIONS

TC conceived and designed the study. JB, TC, YH, SO, CB, and DG performed the experiments, analysis, figure preparation,

and statistics. JB wrote the first draft. JB, PA, JL, HM, and TC interpreted the data. All authors edited the manuscript.

FUNDING

Research reported in this publication was supported in part by the National Institute of Neurological Disorders and Stroke of the National Institutes of Health under Award Number R01NS100793 awarded to TC, the Valley Research Partnership (VRP) P1 (P1201607) awarded to JB, the Phoenix Children's Hospital (PCH) Leadership Circle Grant awarded to TC, the PCH Mission Support Funds awarded to TC, the Arizona Biomedical Research Commission through Arizona Department of Health Services (ADHS14-00003606) awarded to TC, the Director's Research and Education Fund at PCH Foundation awarded to TC, and the Midwestern University ORSP and Midwestern Biomedical Sciences Department Funds awarded to JB. The content is solely the responsibility of the authors and does not necessarily represent the official views of the National Institutes of Health.

ACKNOWLEDGMENTS

The authors would like to thank the following individuals for their assistance on these projects: Dr. Kimbal Cooper at Midwestern University, Dr. Chengcheng Hu from the University of Arizona for statistical guidance, Ms. Katherine R. Giordano for technical assistance and microscopy optimization, and Ms. Carol Haussler, Samantha W. Ridgway, and Dr. Gokul Krishna for valuable editing and feedback.

SUPPLEMENTARY MATERIAL

The Supplementary Material for this article can be found online at: https://www.frontiersin.org/articles/10.3389/fnins.2019.01434/full#supplementary-material

FIGURE S1 | Schematic of glutamate sensitive MEA. Ascorbic acid and other aromatic compounds are repelled from the MEA due to the electroplated 1,3-phenylenediamine (mPD) exclusion layer. Glutamate sensing (bottom pair) and sentinel (top pair) recording sites are coated with BSA and glutaraldehyde. Glutamate oxidase is added to signal sites only to convert glutamate to α-ketoglutarate and peroxide. Peroxide is oxidized on the platinum recording sites as a result of an applied potential of 0.7 V vs. Ag/AgCl reference electrode, thereby producing a current that is correlated with the concentration of glutamate present. Sentinel sites (top pair) are unable to record glutamate due to the lack of glutamate oxidase. Top left corner depicts an MEA. Schematic and MEA are not to scale.

FIGURE S2 | Representative confirmation of MEA placement. Following amperometric experiments, brains were harvested and fixed for MEA placement. Brains were cut coronally at 40 μm. Here, a representative image of MEA placement into the anatomical ventral lateral hemisphere of the rat is shown. The black arrows indicate the outer track (BLA) and the inner track (CeA).

FIGURE S3 | Skeletal Analysis Technique. Individual steps for skeleton analysis of microglia morphologies of Iba1 stained tissue. Original photomicrographs were subjected to a series of uniform ImageJ plugin protocols prior to conversion to binary images which were then skeletonized. An overlay of a resulting skeletonized image (in green) and original photomicrograph shows the relationship between skeleton and photomicrograph. All skeleton analysis was completed on full sized photomicrographs (40× magnification; scale bar = 10 μm).

FIGURE S4 | Controls for applied solutions in amperometric recordings. Anesthetized *in vivo* amperometric recordings of glutamate neurotransmission were conducted in sham, 7 DPI, and 28 DPI rats in the BLA (A/P: −2.4 M/L ± 5.1 D/V −8.0) or CeA (A/P: −2.4 M/L ± 3.9 D/V −8.0). Local applications of 120 mM potassium chloride solution (KCl) were made to depolarize surrounding neurons. No differences in the volume locally applied was observed between sham and brain-injured rats in the **(A)** BLA [One-way ANOVA $F(2,24) = 0.19$; $p = 0.83$; $n = 7$–9] or **(D)** CeA [One-way ANOVA $F(2,19) = 0.68$; $p = 0.52$; $n = 6$–9]. Local applications of exogenous 100 μM were made to measure extracellular glutamate clearance. All applied peaks were amplitude matched prior to analysis in the **(B)** BLA [One-way ANOVA $F(2,21) = 0.23$; $p = 0.79$; $n = 6$–10] and **(E)** CeA[One-way ANOVA $F(2,22) = 1.05$; $p = 0.37$; $n = 7$–10] to control for Michaelis Menten kinetics. The maximum amplitude for evoked glutamate release in the BLA did not differ **(C)** [One-way ANOVA $F(2,24) = 0.11$; $p = 0.90$; $n = 7$–9], but was significantly decreased in the CeA at 28 DPI in comparison to sham **(F)** [One-way ANOVA $F(2,19) = 4.89$; $p < 0.05$; $n = 6$–9]. Bar graphs represent the mean ± SEM.

FIGURE S5 | BLA and CeA microglia respond differently to dTBI over time. Microglial morphology changes as a function of time post-injury and region. **(A)** Microglial cell counts were different than sham after 1, 7, and 28 DPI in the BLA [Two-way ANOVA $F(3,16) = 7.85$; $p < 0.05$] **(B)**. The number of microglial process endpoints/cell was lower than sham after mFPI in the CeA [$(3,16) = 5.152$; $p < 0.05$]. **(C)** The summed process length/cell were lower than sham after mFPI in the CeA [$F(3,16) = 3.94$; $p < 0.05$]. Bar graphs represent mean ± SEM, $n = 3$/group. $^{*}p < 0.05$ in comparison to sham. $^{+}p < 0.05$ in comparison to 1 DPI.

FIGURE S6 | Representation of glutamatergic targets for protein quantification studies. Representation of a glutamatergic synapse and the proteins that regulate glutamate neurotransmission. Diagram modified from Thomas et al. (2012).

TABLE S1 | Optimization parameters for antibodies and protein concentrations.

REFERENCES

Alder, J., Fujioka, W., Lifshitz, J., Crockett, D. P., and Thakker-Varia, S. (2011). Lateral fluid percussion: model of traumatic brain injury in mice. *J. Vis. Exp.* 54:3063.

Almeida-Suhett, C. P., Prager, E. M., Pidoplichko, V., Figueiredo, T. H., Marini, A. M., Li, Z., et al. (2014). Reduced GABAergic inhibition in the basolateral amygdala and the development of anxiety-like behaviors after mild traumatic brain injury. *PLoS One* 9:e102627. doi: 10.1371/journal.pone.0102627

Babaev, O., Piletti Chatain, C., and Krueger-Burg, D. (2018). Inhibition in the amygdala anxiety circuitry. *Exp. Mol. Med.* 50:18.

Buchsbaum, M. S., Simmons, A. N., DeCastro, A., Farid, N., and Matthews, S. C. (2015). Clusters of low (18)F-fluorodeoxyglucose uptake voxels in combat veterans with traumatic brain injury and post-traumatic stress disorder. *J. Neurotrauma* 32, 1736–1750. doi: 10.1089/neu.2014.3660

Burmeister, J. J., and Gerhardt, G. A. (2001). Self-referencing ceramic-based multisite microelectrodes for the detection and elimination of interferences from the measurement of L-glutamate and other analytes. *Anal. Chem.* 73, 1037–1042. doi: 10.1021/ac0010429

Burmeister, J. J., Pomerleau, F., Day, B. K., Huettl, P., and Gerhardt, G. A. (2002). Improved ceramic-based multisite microelectrode for rapid measurements of L-glutamate in the CNS. *J. Neurosci. Methods* 119, 163–171. doi: 10.1016/s0165-0270(02)00172-3

Cao, T., Thomas, T. C., Ziebell, J. M., Pauly, J. R., and Lifshitz, J. (2012). Morphological and genetic activation of microglia after diffuse traumatic brain injury in the rat. *Neuroscience* 225, 65–75. doi: 10.1016/j.neuroscience.2012.08.058

Carlsen, J. (1988). Immunocytochemical localization of glutamate decarboxylase in the rat basolateral amygdaloid nucleus, with special reference to GABAergic innervation of amygdalostriatal projection neurons. *J. Comp. Neurol.* 273, 513–526. doi: 10.1002/cne.902730407

Carola, V., D'Olimpio, F., Brunamonti, E., Mangia, F., and Renzi, P. (2002). Evaluation of the elevated plus-maze and open-field tests for the assessment of anxiety-related behaviour in inbred mice. *Behav. Brain Res.* 134, 49–57. doi: 10.1016/s0166-4328(01)00452-1

Cass, W. A., Gerhardt, G. A., Mayfield, R. D., Curella, P., and Zahniser, N. R. (1992). Differences in dopamine clearance and diffusion in rat striatum and nucleus accumbens following systemic cocaine administration. *J. Neurochem.* 59, 259–266. doi: 10.1111/j.1471-4159.1992.tb08899.x

Chiba, S., Numakawa, T., Ninomiya, M., Richards, M. C., Wakabayashi, C., and Kunugi, H. (2012). Chronic restraint stress causes anxiety- and depression-like behaviors, downregulates glucocorticoid receptor expression, and attenuates glutamate release induced by brain-derived neurotrophic factor in the prefrontal cortex. *Prog. Neuropsychopharmacol. Biol. Psychiatry* 39, 112–119. doi: 10.1016/j.pnpbp.2012.05.018

Cho, H. B., Bueler, C. E., DiMuzio, J., Hicks-Little, C., McGlade, E., Lyoo, I. K., et al. (2018). Negative mood states correlate with laterobasal amygdala in collegiate football players. *Biomed. Res. Int.* 2018:8142631.

Clausen, F., Hansson, H. A., Raud, J., and Marklund, N. (2017). Intranasal administration of the antisecretory peptide AF-16 reduces edema and improves cognitive function following diffuse traumatic brain injury in the rat. *Front. Neurol.* 8:39. doi: 10.3389/fneur.2017.00039

Collins, K. A., Westra, H. A., Dozois, D. J., and Burns, D. D. (2004). Gaps in accessing treatment for anxiety and depression: challenges for the delivery of care. *Clin. Psychol. Rev.* 24, 583–616. doi: 10.1016/j.cpr.2004.06.001

Coronado, V. G., McGuire, L. C., Sarmiento, K., Bell, J., Lionbarger, M. R., Jones, C. D., et al. (2012). Trends in traumatic brain injury in the U.S. and the public health response: 1995-2009. *J. Saf. Res.* 43, 299–307. doi: 10.1016/j.jsr.2012.08.011

Costa, R., Tamascia, M. L., Nogueira, M. D., Casarini, D. E., and Marcondes, F. K. (2012). Handling of adolescent rats improves learning and memory and decreases anxiety. *J. Am. Assoc. Lab. Anim. Sci.* 51, 548–553.

Danbolt, N. C. (2001). Glutamate uptake. *Prog. Neurobiol.* 65, 1–105.

DePalma, R. G., and Hoffman, S. W. (2016). Combat blast related traumatic brain injury (TBI): decade of recognition; promise of progress. *Behav. Brain Res.* 340, 102–105. doi: 10.1016/j.bbr.2016.08.036

Depue, B. E., Olson-Madden, J. H., Smolker, H. R., Rajamani, M., Brenner, L. A., and Banich, M. T. (2014). Reduced amygdala volume is associated with deficits in inhibitory control: a voxel- and surface-based morphometric analysis of comorbid PTSD/mild TBI. *Biomed. Res. Int.* 2014:691505.

Elder, G. A., Dorr, N. P., De Gasperi, R., Gama Sosa, M. A., Shaughness, M. C., Maudlin-Jeronimo, E., et al. (2012). Blast exposure induces post-traumatic stress disorder-related traits in a rat model of mild traumatic brain injury. *J. Neurotrauma* 29, 2564–2575. doi: 10.1089/neu.2012.2510

Ennaceur, A. (2014). Tests of unconditioned anxiety - pitfalls and disappointments. *Physiol. Behav.* 135, 55–71. doi: 10.1016/j.physbeh.2014.05.032

Etkin, A., Prater, K. E., Schatzberg, A. F., Menon, V., and Greicius, M. D. (2009). Disrupted amygdalar subregion functional connectivity and evidence of a compensatory network in generalized anxiety disorder. *Arch. Gen. Psychiatry* 66, 1361–1372.

Etkin, A., and Wager, T. D. (2007). Functional neuroimaging of anxiety: a meta-analysis of emotional processing in PTSD, social anxiety disorder, and specific phobia. *Am. J. Psychiatry* 164, 1476–1488. doi: 10.1176/appi.ajp.2007.07030504

Fenn, A. M., Skendelas, J. P., Moussa, D. N., Muccigrosso, M. M., Popovich, P. G., Lifshitz, J., et al. (2015). Methylene blue attenuates traumatic brain injury-associated neuroinflammation and acute depressive-like behavior in mice. *J. Neurotrauma* 32, 127–138. doi: 10.1089/neu.2014.3514

French, L. M. (2010). Military traumatic brain injury: an examination of important differences. *Ann. N. Y. Acad. Sci.* 1208, 38–45. doi: 10.1111/j.1749-6632.2010.05696.x

Friedemann, M. N., and Gerhardt, G. A. (1992). Regional effects of aging on dopaminergic function in the Fischer-344 rat. *Neurobiol. Aging* 13, 325–332. doi: 10.1016/0197-4580(92)90046-z

Fritz, C. O., Morris, P. E., and Richler, J. J. (2012). Effect size estimates: current use, calculations, and interpretation. *J. Exp. Psychol. Gen.* 141, 2–18. doi: 10.1037/a0024338

Gould, T. D., Dao, D. T., and Kovacsics, C. E. (2009). "The open field test," in *Mood and Anxiety Related Phenotypes in Mice: Characterization Using Behavioral Tests*, ed. T. D. Gould, (Totowa, NJ: Humana Press), 1–20.

Griesbach, G. S., Hovda, D. A., Tio, D. L., and Taylor, A. N. (2011). Heightening of the stress response during the first weeks after a mild traumatic brain injury. *Neuroscience* 178, 147–158. doi: 10.1016/j.neuroscience.2011.01.028

Griesbach, G. S., Vincelli, J., Tio, D. L., and Hovda, D. A. (2012). Effects of acute restraint-induced stress on glucocorticoid receptors and brain-derived neurotrophic factor after mild traumatic brain injury. *Neuroscience* 210, 393–402. doi: 10.1016/j.neuroscience.2012.03.005

Grosch, J., Winkler, J., and Kohl, Z. (2016). Early degeneration of both dopaminergic and serotonergic axons - a common mechanism in Parkinson's disease. *Front. Cell Neurosci.* 10:293. doi: 10.3389/fncel.2016.00293

Grossman, E. J., Inglese, M., and Bammer, R. (2010). Mild traumatic brain injury: is diffusion imaging ready for primetime in forensic medicine? *Top. Magn. Reson. Imaging* 21, 379–386. doi: 10.1097/rmr.0b013e31823e65b8

Guerin, F., Kennepohl, S., Leveille, G., Dominique, A., and McKerral, M. (2006). Vocational outcome indicators in atypically recovering mild TBI: a post-intervention study. *Neurorehabilitation* 21, 295–303.

Hall, K. D., and Lifshitz, J. (2010). Diffuse traumatic brain injury initially attenuates and later expands activation of the rat somatosensory whisker circuit concomitant with neuroplastic responses. *Brain Res.* 1323, 161–173. doi: 10.1016/j.brainres.2010.01.067

Hallam, T. M., Floyd, C. L., Folkerts, M. M., Lee, L. L., Gong, Q. Z., Lyeth, B. G., et al. (2004). Comparison of behavioral deficits and acute neuronal degeneration in rat lateral fluid percussion and weight-drop brain injury models. *J. Neurotrauma* 21, 521–539. doi: 10.1089/089771504774129865

Harrison, J. L., Rowe, R. K., Ellis, T. W., Yee, N. S., O'Hara, B. F., Adelson, P. D., et al. (2015). Resolvins AT-D1 and E1 differentially impact functional outcome, post-traumatic sleep, and microglial activation following diffuse brain injury in the mouse. *Brain Behav. Immun.* 47, 131–140. doi: 10.1016/j.bbi.2015.01.001

Harrison, J. L., Rowe, R. K., O'Hara, B. F., Adelson, P. D., and Lifshitz, J. (2014). Acute over-the-counter pharmacological intervention does not adversely affect behavioral outcome following diffuse traumatic brain injury in the mouse. *Exp. Brain Res.* 232, 2709–2719. doi: 10.1007/s00221-014-3948-3

Henstridge, C. M., Tzioras, M., and Paolicelli, R. C. (2019). Glial contribution to excitatory and inhibitory synapse loss in neurodegeneration. *Front. Cell Neurosci.* 13:63. doi: 10.3389/fncel.2019.00063

Hinzman, J. M., Thomas, T. C., Burmeister, J. J., Quintero, J. E., Huettl, P., Pomerleau, F., et al. (2010). Diffuse brain injury elevates tonic glutamate levels and potassium-evoked glutamate release in discrete brain regions at two days post-injury: an enzyme-based microelectrode array study. *J. Neurotrauma* 27, 889–899. doi: 10.1089/neu.2009.1238

Hinzman, J. M., Thomas, T. C., Quintero, J. E., Gerhardt, G. A., and Lifshitz, J. (2012). Disruptions in the regulation of extracellular glutamate by neurons and glia in the rat striatum two days after diffuse brain injury. *J. Neurotrauma* 29, 1197–1208. doi: 10.1089/neu.2011.2261

Hoffman, A. N., Paode, P. R., May, H. G., Ortiz, J. B., Kemmou, S., Lifshitz, J., et al. (2017). Early and persistent dendritic hypertrophy in the basolateral amygdala following experimental diffuse traumatic brain injury. *J. Neurotrauma* 34, 213–219. doi: 10.1089/neu.2015.4339

Hoge, C. W., Grossman, S. H., Auchterlonie, J. L., Riviere, L. A., Milliken, C. S., and Wilk, J. E. (2014). PTSD treatment for soldiers after combat deployment: low utilization of mental health care and reasons for dropout. *Psychiatr. Serv.* 65, 997–1004. doi: 10.1176/appi.ps.201300307

Hosseini, A. H., and Lifshitz, J. (2009). Brain injury forces of moderate magnitude elicit the fencing response. *Med. Sci. Sports Exerc.* 41, 1687–1697. doi: 10.1249/mss.0b013e31819fcd1b

Hou, J., Nelson, R., Wilkie, Z., Mustafa, G., Tsuda, S., Thompson, F. J., et al. (2017). Mild and mild to moderate traumatic brain injury (TBI)-induced significant progressive and enduring multiple comorbidities. *J. Neurotrauma.* 34, 2456–2466. doi: 10.1089/neu.2016.4851

Hrybouski, S., Aghamohammadi-Sereshki, A., Madan, C. R., Shafer, A. T., Baron, C. A., and Seres, P. (2016). Amygdala subnuclei response and

connectivity during emotional processing. *Neuroimage* 133, 98–110. doi: 10.1016/j.neuroimage.2016.02.056

Hughes, E. G., Maguire, J. L., McMinn, M. T., Scholz, R. E., and Sutherland, M. L. (2004). Loss of glial fibrillary acidic protein results in decreased glutamate transport and inhibition of PKA-induced EAAT2 cell surface trafficking. *Brain Res. Mol. Brain Res.* 124, 114–123. doi: 10.1016/j.molbrainres.2004.02.021

Hyder, A. A., Wunderlich, C. A., Puvanachandra, P., Gururaj, G., and Kobusingye, O. C. (2007). The impact of traumatic brain injuries: a global perspective. *Neurorehabilitation* 22, 341–353.

Jacob, T. C., Moss, S. J., and Jurd, R. (2008). GABA(A) receptor trafficking and its role in the dynamic modulation of neuronal inhibition. *Nat. Rev. Neurosci.* 9, 331–343. doi: 10.1038/nrn2370

Jaiswal, S., Knutsen, A. K., Wilson, C. M., Fu, A. H., Tucker, L. B., and Kim, Y. (2019). Mild traumatic brain injury induced by primary blast overpressure produces dynamic regional changes in [(18)F]FDG uptake. *Brain Res.* 1723:146400. doi: 10.1016/j.brainres.2019.146400

Janak, P. H., and Tye, K. M. (2015). From circuits to behaviour in the amygdala. *Nature* 517, 284–292. doi: 10.1038/nature14188

Jorge, R. E., Robinson, R. G., Moser, D., Tateno, A., Crespo-Facorro, B., and Arndt, S. (2004). Major depression following traumatic brain injury. *Arch. Gen. Psychiatry* 61, 42–50.

Kalin, N. H., Shelton, S. E., and Davidson, R. J. (2004). The role of the central nucleus of the amygdala in mediating fear and anxiety in the primate. *J. Neurosci.* 24, 5506–5515. doi: 10.1523/jneurosci.0292-04.2004

Kessler, R. C., Chiu, W. T., Demler, O., Merikangas, K. R., and Walters, E. E. (2005). Prevalence, severity, and comorbidity of 12-month DSM-IV disorders in the national comorbidity survey replication. *Arch. Gen. Psychiatry* 62, 617–627.

Kim, S. Y., Adhikari, A., Lee, S. Y., Marshel, J. H., Kim, C. K., Mallory, C. S., et al. (2013). Diverging neural pathways assemble a behavioural state from separable features in anxiety. *Nature* 496, 219–223. doi: 10.1038/nature12018

Koenigs, M., and Grafman, J. (2009). Posttraumatic stress disorder: the role of medial prefrontal cortex and amygdala. *Neuroscientist* 15, 540–548. doi: 10.1177/1073858409333072

Kovesdi, E., Gyorgy, A. B., Kwon, S. K., Wingo, D. L., Kamnaksh, A., Long, J. B., et al. (2011). The effect of enriched environment on the outcome of traumatic brain injury; a behavioral, proteomics, and histological study. *Front. Neurosci.* 5:42. doi: 10.3389/fnins.2011.00042

Kulkarni, P., Morrison, T. R., Cai, X., Iriah, S., Simon, N., and Sabrick, J. (2019). Neuroradiological changes following single or repetitive mild TBI. *Front. Syst. Neurosci.* 13:34. doi: 10.3389/fnsys.2019.00034

Kunugi, H., Hori, H., Adachi, N., and Numakawa, T. (2010). Interface between hypothalamic-pituitary-adrenal axis and brain-derived neurotrophic factor in depression. *Psychiatry Clin. Neurosci.* 64, 447–459. doi: 10.1111/j.1440-1819.2010.02135.x

Lafrenaye, A. D., Krahe, T. E., and Povlishock, J. T. (2014). Moderately elevated intracranial pressure after diffuse traumatic brain injury is associated with exacerbated neuronal pathology and behavioral morbidity in the rat. *J. Cereb. Blood Flow Metab.* 34, 1628–1636. doi: 10.1038/jcbfm.2014.122

Lakens, D. (2013). Calculating and reporting effect sizes to facilitate cumulative science: a practical primer for t-tests and ANOVAs. *Front. Psychol.* 4:863. doi: 10.3389/fpsyg.2013.00863

Larter, R., and Craig, M. G. (2005). Glutamate-induced glutamate release: a proposed mechanism for calcium bursting in astrocytes. *Chaos* 15:047511. doi: 10.1063/1.2102467

Learoyd, A. E., and Lifshitz, J. (2012). Comparison of rat sensory behavioral tasks to detect somatosensory morbidity after diffuse brain-injury. *Behav. Brain Res.* 226, 197–204. doi: 10.1016/j.bbr.2011.09.016

Lee, B., and Newberg, A. (2005). Neuroimaging in traumatic brain imaging. *NeuroRx* 2, 372–383. doi: 10.1602/neurorx.2.2.372

Lifshitz, J., Kelley, B. J., and Povlishock, J. T. (2007). Perisomatic thalamic axotomy after diffuse traumatic brain injury is associated with atrophy rather than cell death. *J. Neuropathol. Exp. Neurosci.* 66, 673–673.

Lifshitz, J., and Lisembee, A. M. (2012). Neurodegeneration in the somatosensory cortex after experimental diffuse brain injury. *Brain Struct. Funct.* 217, 49–61. doi: 10.1007/s00429-011-0323-z

Lifshitz, J., Rowe, R. K., Griffiths, D. R., Evilsizor, M. N., Thomas, T. C., Adelson, P. D., et al. (2016). Clinical relevance of midline fluid percussion brain injury: acute deficits, chronic morbidities and the utility of biomarkers. *Brain Inj.* 30, 1293–1301. doi: 10.1080/02699052.2016.1193628

Lisembee, A., and Lifshitz, J. (2008). Neuronal loss and atrophy extends into the somatosensory barrel cortex after midline fluid percussion brain injury. *J. Neurotrauma* 25, 875–875.

Liu, J., Kou, Z., and Tian, Y. (2014). Diffuse axonal injury after traumatic cerebral microbleeds: an evaluation of imaging techniques. *Neural Regen. Res.* 9, 1222–1230.

Liu, M., Bachstetter, A. D., Cass, W. A., Lifshitz, J., and Bing, G. (2017). Pioglitazone attenuates neuroinflammation and promotes dopaminergic neuronal survival in the nigrostriatal system of rats after diffuse brain injury. *J. Neurotrauma* 34, 414–422. doi: 10.1089/neu.2015.4361

Loane, D. J., Stoica, B. A., and Faden, A. I. (2012). Metabotropic glutamate receptor-mediated signaling in neuroglia. Wiley interdisciplinary reviews. *Membr. Transp. Signal.* 1, 136–150. doi: 10.1002/wmts.30

Loughney, J. W., Lancaster, C., Ha, S., and Rustandi, R. R. (2014). Residual bovine serum albumin (BSA) quantitation in vaccines using automated capillary Western technology. *Anal. Biochem.* 461, 49–56. doi: 10.1016/j.ab.2014.05.004

MacGregor, A. J., Dougherty, A. L., and Galarneau, M. R. (2011). Injury-specific correlates of combat-related traumatic brain injury in operation Iraqi freedom. *J. Head Trauma Rehabil.* 26, 312–318. doi: 10.1097/htr.0b013e3181e94404

Madalena, K. M., and Lerch, J. K. (2017). The effect of glucocorticoid and glucocorticoid receptor interactions on brain, spinal cord, and glial cell plasticity. *Neural Plast.* 2017:8640970.

Maragakis, N. J., and Rothstein, J. D. (2004). Glutamate transporters: animal models to neurologic disease. *Neurobiol. Dis.* 15, 461–473. doi: 10.1016/j.nbd.2003.12.007

Masel, B. E., and DeWitt, D. S. (2010). Traumatic brain injury: a disease process, not an event. *J. Neurotrauma* 27, 1529–1540. doi: 10.1089/neu.2010.1358

McAllister, T. W. (1992). Neuropsychiatric sequale of head injuries. *Psychiatr. Clin. North Am.* 15, 395–413.

McDonald, A. J. (1982). Cytoarchitecture of the central amygdaloid nucleus of the rat. *J. Comp. Neurol.* 208, 401–418. doi: 10.1002/cne.902080409

McIntosh, T. K., Noble, L., Andrews, B., and Faden, A. I. (1987). Traumatic brain injury in the rat: characterization of a midline fluid-percussion model. *Cent. Nerv. Syst. Trauma* 4, 119–134. doi: 10.1089/cns.1987.4.119

McNamara, K. C., Lisembee, A. M., and Lifshitz, J. (2010). The whisker nuisance task identifies a late-onset, persistent sensory sensitivity in diffuse brain-injured rats. *J. Neurotrauma* 27, 695–706. doi: 10.1089/neu.2009.1237

Meis, S., Endres, T., and Lessmann, V. (2012). Postsynaptic BDNF signalling regulates long-term potentiation at thalamo-amygdala afferents. *J. Physiol.* 590, 193–208. doi: 10.1113/jphysiol.2011.220434

Meyer, D. L., Davies, D. R., Barr, J. L., Manzerra, P., and Forster, G. L. (2012). Mild traumatic brain injury in the rat alters neuronal number in the limbic system and increases conditioned fear and anxiety-like behaviors. *Exp. Neurol.* 235, 574–587. doi: 10.1016/j.expneurol.2012.03.012

Miremami, J. D., Talauliker, P. M., Harrison, J. L., and Lifshitz, J. (2014). Neuropathology in sensory, but not motor, brainstem nuclei of the rat whisker circuit after diffuse brain injury. *Somatosens. Mot. Res.* 31, 127–135. doi: 10.3109/08990220.2014.897602

Morrison, H., Young, K., Qureshi, M., Rowe, R. K., and Lifshitz, J. (2017). Quantitative microglia analyses reveal diverse morphologic responses in the rat cortex after diffuse brain injury. *Sci. Rep.* 7:13211.

Moussy, F., and Harrison, D. J. (1994). Prevention of the rapid degradation of subcutaneously implanted Ag/AgCl reference electrodes using polymer coatings. *Anal. Chem.* 66, 674–679. doi: 10.1021/ac00077a015

Murugan, M., Ling, E. A., and Kaur, C. (2013). Glutamate receptors in microglia. *CNS Neurol. Disord. Drug Targets* 12, 773–784. doi: 10.2174/18715273113126660174

Nickell, J., Pomerleau, F., Allen, J., and Gerhardt, G. A. (2005). Age-related changes in the dynamics of potassium-evoked L-glutamate release in the striatum of Fischer 344 rats. *J. Neural Transm.* 112, 87–96. doi: 10.1007/s00702-004-0151-x

Numakawa, T., Kumamaru, E., Adachi, N., Yagasaki, Y., Izumi, A., and Kunugi, H. (2009). Glucocorticoid receptor interaction with TrkB promotes BDNF-triggered PLC-gamma signaling for glutamate release via a glutamate

transporter. *Proc. Natl. Acad. Sci. U.S.A.* 106, 647–652. doi: 10.1073/pnas.0800888106

Owens, B. D., Kragh, J. F. Jr., Wenke, J. C., Macaitis, J., Wade, C. E., et al. (2008). Combat wounds in operation Iraqi freedom and operation enduring freedom. *J. Trauma* 64, 295–299.

Pal, B. (2018). Involvement of extrasynaptic glutamate in physiological and pathophysiological changes of neuronal excitability. *Cell Mol. Life Sci.* 75, 2917–2949. doi: 10.1007/s00018-018-2837-5

Palmer, C. P., Metheny, H. E., Elkind, J. A., and Cohen, A. S. (2016). Diminished amygdala activation and behavioral threat response following traumatic brain injury. *Exp. Neurol.* 277, 215–226. doi: 10.1016/j.expneurol.2016.01.004

Parpura, V., Basarsky, T. A., Liu, F., Jeftinija, K., Jeftinija, S., and Haydon, P. G. (1994). Glutamate-mediated astrocyte-neuron signalling. *Nature* 369, 744–747. doi: 10.1038/369744a0

Pascual, O., Ben Achour, S., Rostaing, P., Triller, A., and Bessis, A. (2012). Microglia activation triggers astrocyte-mediated modulation of excitatory neurotransmission. *Proc. Natl. Acad. Sci. U.S.A.* 109, E197–E205.

Paxinos G., and Watson C. (2007). *The Rat Brain In Stereotaxic Coordinates*. New York: Academic Press.

Phelps, E. A., and LeDoux, J. E. (2005). Contributions of the amygdala to emotion processing: from animal models to human behavior. *Neuron* 48, 175–187. doi: 10.1016/j.neuron.2005.09.025

Pitkanen, A., Savander, V., and LeDoux, J. E. (1997). Organization of intra-amygdaloid circuitries in the rat: an emerging framework for understanding functions of the amygdala. *Trends Neurosci.* 20, 517–523. doi: 10.1016/s0166-2236(97)01125-9

Quintero, J. E., Day, B. K., Zhang, Z., Grondin, R., Stephens, M. L., Huettl, P., et al. (2007). Amperometric measures of age-related changes in glutamate regulation in the cortex of rhesus monkeys. *Exp. Neurol.* 208, 238–246. doi: 10.1016/j.expneurol.2007.08.002

Rajkowska, G., and Miguel-Hidalgo, J. J. (2007). Gliogenesis and glial pathology in depression. *CNS Neurol. Disord. Drug Targets* 6, 219–233. doi: 10.2174/187152707780619326

Ramlackhansingh, A. F., Brooks, D. J., Greenwood, R. J., Bose, S. K., Turkheimer, F. E., Kinnunen, K. M., et al. (2011). Inflammation after trauma: microglial activation and traumatic brain injury. *Ann. Neurol.* 70, 374–383. doi: 10.1002/ana.22455

Reger, M. L., Poulos, A. M., Buen, F., Giza, C. C., Hovda, D. A., and Fanselow, M. S. (2012). Concussive brain injury enhances fear learning and excitatory processes in the amygdala. *Biol. Psychiatry* 71, 335–343. doi: 10.1016/j.biopsych.2011.11.007

Riess, P., Zhang, C., Saatman, K. E., Laurer, H. L., Longhi, L. G., Raghupathi, R., et al. (2002). Transplanted neural stem cells survive, differentiate, and improve neurological motor function after experimental traumatic brain injury. *Neurosurgery* 51, 1043–1054. doi: 10.1097/00006123-200210000-00035

Roth, K. A., and Katz, R. J. (1979). Stress, behavioral arousal, and open field activity–a reexamination of emotionality in the rat. *Neurosci. Biobehav. Rev.* 3, 247–263. doi: 10.1016/0149-7634(79)90012-5

Rowe, R. K., Harrison, J. L., Morrison, H. W., Subbian, V., Murphy, S. M., and Lifshitz, J. (2019). Acute post-traumatic sleep may define vulnerability to a second traumatic brain injury in mice. *J. Neurotrauma* 36, 1318–1334. doi: 10.1089/neu.2018.5980

Rowe, R. K., Harrison, J. L., O'Hara, B. F., and Lifshitz, J. (2014). Recovery of neurological function despite immediate sleep disruption following diffuse brain injury in the mouse: clinical relevance to medically untreated concussion. *Sleep* 37, 743–752. doi: 10.5665/sleep.3582

Rowe, R. K., Harrison, J. L., Thomas, T. C., Pauly, J. R., Adelson, P. D., and Lifshitz, J. (2013). Using anesthetics and analgesics in experimental traumatic brain injury. *Lab. Anim.* 42, 286–291. doi: 10.1038/laban.257

Rowe, R. K., Rumney, B. M., May, H. G., Permana, P., Adelson, P. D., Harman, S. M., et al. (2016). Diffuse traumatic brain injury affects chronic corticosterone function in the rat. *Endocr. Connect* 5, 152–166. doi: 10.1530/ec-16-0031

Scholten, A. C., Haagsma, J. A., Cnossen, M. C., Olff, M., van Beeck, E. F., and Polinder, S. (2016). Prevalence of and risk factors for anxiety and depressive disorders after traumatic brain injury: a systematic review. *J. Neurotrauma* 33, 1969–1994. doi: 10.1089/neu.2015.4252

Shultz, S. R., Cardamone, L., Liu, Y. R., Hogan, R. E., Maccotta, L., Wright, D. K., et al. (2013). Can structural or functional changes following traumatic brain injury in the rat predict epileptic outcome? *Epilepsia* 54, 1240–1250. doi: 10.1111/epi.12223

Smith, Y., and Pare, D. (1994). Intra-amygdaloid projections of the lateral nucleus in the cat: PHA-L anterograde labeling combined with postembedding GABA and glutamate immunocytochemistry. *J. Comp. Neurol.* 342, 232–248. doi: 10.1002/cne.903420207

Stevens, J. S., Kim, Y. J., Galatzer-Levy, I. R., Reddy, R., Ely, T. D., Nemeroff, C. B., et al. (2016). Amygdala reactivity and anterior cingulate habituation predict posttraumatic stress disorder symptom maintenance after acute civilian trauma. *Biol. Psychiatry* 81, 1023–1029. doi: 10.1016/j.biopsych.2016.11.015

Swanson, L. W., and Petrovich, G. D. (1998). What is the amygdala? *Trends Neurosci.* 21, 323–331. doi: 10.1016/s0166-2236(98)01265-x

Tejeda, G. S., and Diaz-Guerra, M. (2017). Integral characterization of defective BDNF/TrkB signalling in neurological and psychiatric disorders leads the way to new therapies. *Int. J. Mol. Sci.* 18:268. doi: 10.3390/ijms18020268

Thomas, T. C., Beitchman, J. A., Pomerleau, F., Noel, T., Jungsuwadee, P., Allan Butterfield, D., et al. (2017). Acute treatment with doxorubicin affects glutamate neurotransmission in the mouse frontal cortex and hippocampus. *Brain Res.* 1672, 10–17. doi: 10.1016/j.brainres.2017.07.003

Thomas, T. C., Hinzman, J. M., Gerhardt, G. A., and Lifshitz, J. (2012). Hypersensitive glutamate signaling correlates with the development of late-onset behavioral morbidity in diffuse brain-injured circuitry. *J. Neurotrauma* 29, 187–200. doi: 10.1089/neu.2011.2091

Thomas, T. C., Ogle, S. B., Rumney, B. M., May, H. G., Adelson, P. D., and Lifshitz, J. (2018). Does time heal all wounds? Experimental diffuse traumatic brain injury results in persisting histopathology in the thalamus. *Behav. Brain Res.* 340, 137–146. doi: 10.1016/j.bbr.2016.12.038

Thompson, H. J., Lifshitz, J., Marklund, N., Grady, M. S., Graham, D. I., Hovda, D. A., et al. (2005). Lateral fluid percussion brain injury: a 15-year review and evaluation. *J. Neurotrauma* 22, 42–75. doi: 10.1089/neu.2005.22.42

Tovote, P., Fadok, J. P., and Luthi, A. (2015). Neuronal circuits for fear and anxiety. *Nat. Rev. Neurosci.* 16, 317–331. doi: 10.1038/nrn3945

Trahan, D. E., Ross, C. E., and Trahan, S. L. (2001). Relationships among postconcussional-type symptoms, depression, and anxiety in neurologically normal young adults and victims of mild brain injury. *Arch. Clin. Neuropsychol.* 16, 435–445. doi: 10.1016/s0887-6177(00)00051-2

Tye, K. M., Prakash, R., Kim, S. Y., Fenno, L. E., Grosenick, L., Zarabi, H., et al. (2011). Amygdala circuitry mediating reversible and bidirectional control of anxiety. *Nature* 471, 358–362. doi: 10.1038/nature09820

Ueda, Y., Doi, T., Tokumaru, J., Yokoyama, H., Nakajima, A., Mitsuyama, Y., et al. (2001). Collapse of extracellular glutamate regulation during epileptogenesis: down-regulation and functional failure of glutamate transporter function in rats with chronic seizures induced by kainic acid. *J. Neurochem.* 76, 892–900. doi: 10.1046/j.1471-4159.2001.00087.x

van der Horn, H. J., Spikman, J. M., Jacobs, B., and van der Naalt, J. (2013). Postconcussive complaints, anxiety, and depression related to vocational outcome in minor to severe traumatic brain injury. *Arch. Phys. Med. Rehabil.* 94, 867–874. doi: 10.1016/j.apmr.2012.11.039

Van der Kolk, B. A. (2002). "The assessment and treatment of complex PTSD," in *Treating Trauma Survivors With PTSD*, ed. R. Yehuda, (Philadelphiam, PA: American Psychiatric Press), 127–156.

Vyas, A., Pillai, A. G., and Chattarji, S. (2004). Recovery after chronic stress fails to reverse amygdaloid neuronal hypertrophy and enhanced anxiety-like behavior. *Neuroscience* 128, 667–673. doi: 10.1016/j.neuroscience.2004.07.013

Watt, A. J., van Rossum, M. C. W., MacLeod, K. M., Nelson, S. B., and Turrigiano, G. G. (2000). Activity coregulates quantal AMPA and NMDA currents at neocortical synapses. *Neuron* 26, 659–670. doi: 10.1016/s0896-6273(00)81202-7

Witgen, B. M., Lifshitz, J., Smith, M. L., Schwarzbach, E., Liang, S. L., Grady, M. S., et al. (2005). Regional hippocampal alteration associated with cognitive deficit following experimental brain injury: a systems, network and cellular evaluation. *Neuroscience* 133, 1–15. doi: 10.1016/j.neuroscience.2005.01.052

Young, K., and Morrison, H. (2018). Quantifying microglia morphology from photomicrographs of immunohistochemistry prepared tissue using ImageJ. *J. Vis. Exp.* 136:57648.

Zhang, X., Ge, T. T., Yin, G., Cui, R., Zhao, G., and Yang, W. (2018). Stress-induced functional alterations in amygdala: implications for neuropsychiatric diseases. *Front. Neurosci.* 12:367. doi: 10.3389/fnins.2018.00367

Zhao, J., Huynh, J., Hylin, M. J., O'Malley, J. J., Perez, A., Moore, A. N., et al. (2018). Mild traumatic brain injury reduces spine density of projection neurons in the medial prefrontal cortex and impairs extinction of contextual fear memory. *J. Neurotrauma* 35, 149–156. doi: 10.1089/neu.2016.4898

Zhou, X., Xiao, Q., Xie, L., Yang, F., Wang, L., and Tu, J. (2019). Astrocyte, a promising target for mood disorder interventions. *Front. Mol. Neurosci.* 12:136. doi: 10.3389/fnmol.2019.00136

Conflict of Interest: The authors declare that the research was conducted in the absence of any commercial or financial relationships that could be construed as a potential conflict of interest.

frontiers in Neuroscience

ORIGINAL RESEARCH
published: 28 February 2020
doi: 10.3389/fnins.2020.00098

Abnormality of m6A mRNA Methylation Is Involved in Alzheimer's Disease

Min Han[1], Zhen Liu[1], Yingying Xu[2], Xiangtian Liu[3], Dewei Wang[2], Fan Li[2], Yun Wang[2] and Jianzhong Bi[2]*

[1] Department of General Medicine, The Second Hospital of Shandong University, Jinan, China, [2] Department of Neurology Medicine, Second Hospital of Shandong University, Jinan, China, [3] Medicine School, Shandong University, Jinan, China

Alzheimer's disease (AD), the most common form of dementia, is highly prevalent in older adults. The main clinical feature is the progressive decline of memory function, which eventually leads to the decline of cognitive function. At present, the pathogenesis of AD is unclear. In the disease process, synaptic changes are the key. Recent studies have shown that the dysregulation of RNA methylation is related to many biological processes, including neurodevelopment and neurodegenerative diseases. N6-methyladenosine (m6A) is the most abundant modification in eukaryotic RNA. In this study, RNA m6A methylation was quantified in APP/PS1 transgenic mice, which is an AD mouse model, and C57BL/6 control mice, and data showed that m6A methylation was elevated in the cortex and the hippocampus of APP/PS1 transgenic mice. Next, the alterations of m6A RNA methylation in AD and in C57BL/6 mice were investigated using high-throughput sequencing. Genome-wide maps of m6A mRNA showed that the degrees of m6A methylation were higher in many genes and lower in others in AD mice. Interestingly, the expression of the m6A methyltransferase METTL3 was elevated and that of the m6A demethylase FTO was decreased in AD mice. The data were analyzed by gene ontology (GO) and Kyoto Encyclopedia of Genes and Genomes (KEGG) pathway analyses, and pathways that might be related to synaptic or neuron development and growth were constructed. The related pathways and genes predicted the potential roles of the differentially expressed m6A methylation RNA in AD. Collectively, our findings demonstrate that the m6A methylation of RNA promotes the development of AD.

Keywords: N6-methyladenosine (m6A), AD, synapse, methyltransferase, demethylase, METTL3, FTO

OPEN ACCESS

Edited by:
Patrizia Longone, Santa Lucia Foundation (IRCCS), Italy

Reviewed by:
Daniel Pirici, University of Medicine and Pharmacy of Craiova, Romania
Aline Silva Miranda, Federal University of Minas Gerais, Brazil

****Correspondence:***
Yun Wang
wangyun0531@hotmail.com

Specialty section:
This article was submitted to Neurodegeneration, a section of the journal Frontiers in Neuroscience

Received: *12 October 2019*
Accepted: *23 January 2020*
Published: *28 February 2020*

Citation:
Han M, Liu Z, Xu Y, Liu X, Wang D, Li F, Wang Y and Bi J (2020) Abnormality of m6A mRNA Methylation Is Involved in Alzheimer's Disease. Front. Neurosci. 14:98. doi: 10.3389/fnins.2020.00098

INTRODUCTION

The incidence of Alzheimer's disease (AD) in many countries around the world is very high due to a lack of effective treatments (Bateman et al., 2012). Many reports attempt to detail the pathogenesis of AD; however, the subject is still debated and no definite conclusion has been reached, potentially because there is no single AD pathogenesis. At present, researchers agree that changes in synaptic

function are involved in the pathogenesis of AD, including the dysfunction and loss of the synapse (Mucke and Selkoe, 2012); however, the specific molecular mechanism still remains unresolved, and thus the pathogenesis of AD is still unknown.

The brain is very rich in N6-methyladenosine (m6A). Some studies have shown that m6A is related to the development of the nervous system and to neural degenerative diseases (Meyer et al., 2012; Widagdo et al., 2016; Li et al., 2018), but the role of the regulatory mechanism is still unknown. m6A is a biological marker of dynamic and reversible regulation (Niu et al., 2013), which relies on the combined action of methyltransferase and demethylase. Currently, known methyltransferases include methyltransferase-like protein 3 (METTL3), METTL14, and Wilms tumor 1-associating protein (Liu et al., 2014; Wang and Zhao, 2016; Vu et al., 2017), while demethylases include AlkB homolog 5 and obesity-associated protein (FTO) (Zhou et al., 2015). Among them, METTL3 is the at the center of catalytic methyl reactions, and FTO, which is abundant in rat brains, is related to neurotransmitter delivery and nervous system development (Li et al., 2017, 2018). m6A RNA methylation, regarded as a new frontier in neuroscience, could provide us with a better understanding of neural development and neurological diseases from a novel perspective. In this study, m6A RNA methylation in the brains of AD and of control mice were investigated by high-throughput sequencing and the differences were compared. Further, gene ontology (GO) and Kyoto Encyclopedia of Genes and Genomes (KEGG) pathway analyses were used to predict the function of differentially expressed RNAs.

MATERIALS AND METHODS

Mouse Models

All mice used in this study were male (n = 10 per group). Heterozygous double-transgenic human mice (APP/PS1) at 9 months of age were used as a model for AD, and age-matched C57BL/6 mice were used as controls. All mice were purchased from Beijing HFK Bio-Technology Co., Beijing, China. The mice were housed at 25 ± 2°C in controlled rooms. After 2 weeks, the mice were euthanized using 10% chloral hydrate, and their cerebral cortex, hippocampus, and cerebellum were dissected. All procedures were carried out under the guidelines of the Ethical Committee for Animal Experiments of Shandong University (Jinan, China). Using liquid nitrogen, tissues were immediately frozen after dissection and stored at −80°C until analysis.

RNA Isolation

From frozen mouse cerebral cortex, hippocampus, and cerebellum sections, total RNA was purified using TRI-Reagent (Cat. No.15596026, Thermo Fisher Scientific). The quality of RNA was analyzed using a DeNovix spectrophotometer, and samples with A260/A280 ratios between 1.9 and 2.2 were used for further experiments.

High-Throughput Sequencing

High-throughput sequencing was completed by Shanghai Cloud-seq Biotech Co., Ltd., using mouse hippocampus samples (n = 3 per group). The analysis screened for genes that differentially expressed m6A methylation when comparing the AD and the control groups. GO and KEGG analyses were performed to see if these genes had different physiological functions. $P < 0.05$ was considered as statistically significant.

Quantification of the m6A Modification

The change in global m6A levels in total RNA was measured using an m6A RNA Methylation Quantification Kit (colorimetric; Abcam, ab185912) according to the manufacturer's protocol. For each sample analysis, 200 ng of total RNA was used. The absorbance was measured on a microplate reader at 450 nm, and the m6A horizontal colorimetric value was measured according to the standard curve.

Quantitative Real-Time PCR

One microgram of total RNA from mouse hippocampus samples was used to synthesize cDNA using the PrimeScript First Strand cDNA Synthesis Kit (Takara, RR047A). The cDNA was analyzed to determine the relative RNA levels of target genes by quantitative real-time PCR (qRT-PCR) with the SYBR Green detection method (Takara, RR041A) using the StepOnePlus Real-time PCR System (Eppendorf, Mastercycler, Germany). The procedure was 40 cycles of 95°C for 30 s, 95°C for 15 s, and 55°C for 15 s, and β-actin was used as a normalization control. Genes targeted in qRT-PCR were selected based on the results of the high-throughput sequencing analysis, including two genes with increased methylation in the AD group compared with the control group (AMPA and NMDA) and one with decreased methylation in the AD group (SEMA). The expression levels of METLL3 and FTO were also verified. The following primers were used:

Mouse METTL3 forward: 5′-TTAGCATCTGGTCTGGC CTCTT-3′
Mouse METTL3 reverse: 5′-TGACCTTCTTGCTCTG CTGTTC-3′
Mouse FTO forward: 5′-GACACTTGGCTTCCTT ACCTG-3′
Mouse FTO reverse: 5′-CTCACCACGTCCCGAA ACAA-3′
Mouse AMPA forward: 5′-GGGACAACTCAAGCG TCCAGA-3′
Mouse AMPA reverse: 5′-GCAGCCAGTTCCACG CAGTA-3′
Mouse NMDA forward: 5′-GGCTGACTACCCGAAT GTCCA-3′
Mouse NMDA reverse: 5′-TGTAGACGCGCATCATCT CAAAC-3′
Mouse SEMA forward: 5′-ACAGCTCCAGTTACCACA CCTTC-3′
Mouse SEMA reverse: 5′-TGTAGACGCGCATCATC TCAAAC-3′

Mouse β-actin forward: 5′-CATCCGTAAAGACCTCTAT GCCAAC-3′
Mouse β-actin reverse: 5′-CCCAGTTCCACAGGC ATACA-3′

The real-time PCR reactions were performed in triplicate, and the results were analyzed using the ΔΔCT method (Livak and Schmittgen, 2001).

Western Blot

The cerebral cortex, cerebellum, and hippocampus tissues were stored at −80°C until homogenization and were then used to detect m6A RNA methylase and demethylase. To assess the quantifiable factors of neurodegenerative processes and amyloid burden in these animals, cortical and hippocampal brain tissues were used to measure the expression of synaptophysin and Aβ protein in both groups of mice. The samples were homogenized separately in ice-cold RIPA lysing buffer for 30 min and then were centrifuged at 12,000 × *g* for 15 min at 4°C. Protein concentrations were detected using the bicinchoninic acid method. Briefly, the proteins were separated using SDS-PAGE and transferred to PVDF membranes. Then, the membranes were pretreated with a blocking solution (5% non-fat dry milk) for 1 h and incubated with primary antibodies against METTL3, FTO, beta amyloid, synaptophysin, and β-actin overnight at 4°C. After rinsing with a washing solution (TBST) three times, the membranes were incubated with secondary antibodies for 1 h and washed three times with TBST. The intensity of the protein bands was analyzed using Image J (National Institutes of Health, Bethesda, MD, United States).

The following reagents and antibodies were used: RIPA lysis buffer (Beyotime Biotechnology, P0013B), primary antibody dilution buffer (Beyotime Biotechnology, P0256), protease and phosphatase inhibitor (Beyotime Biotechnology, P1050), anti-METTL3 rabbit IgG (Abcam, ab195352), anti-FTO rabbit IgG (CST, 45980), anti-beta amyloid rabbit polyclone (Abcam, ab2539), anti-synaptophysin rabbit IgG (Abcam, ab32137), anti-actin (CST, 4970), and HRP-labeled goat anti-rabbit IgG secondary antibody (Beyotime Biotechnology, A0208).

Statistical Analysis

All values are expressed as means ± SEM of at least three independent experiments. Student's *t*-test was performed to identify statistical differences among groups. $P < 0.05$ was considered as statistically significant. SPSS17.0 software (SPSS Inc., Chicago, IL, United States) was used for data analysis.

RESULTS

m6A RNA Methylation Level in the Cortex and the Hippocampus of AD

The degree of methylation in the cortex and the hippocampus samples of AD mice were notably higher than that of the control group ($P < 0.05$); however, no difference in the degree of methylation was observed in the cerebellum (**Figure 1**).

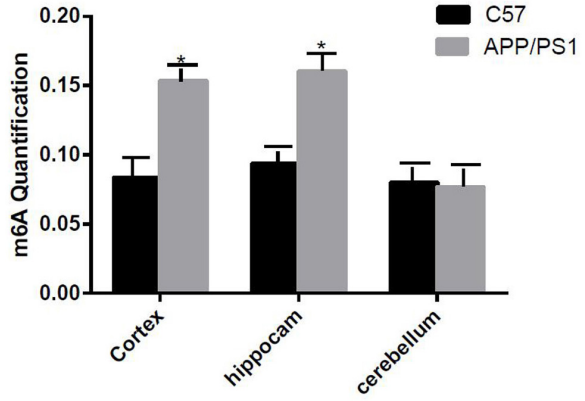

FIGURE 1 | Comparison of methylation content of the cortex, hippocampus, and cerebellum samples between the two groups. Among them, m6A RNA methylation significantly increased in the hippocampus and cortex samples. Student's *t*-test was used to detect differences between the two groups, and data are presented as mean ± SEM; $n = 6$ per group, $^*P < 0.05$.

GO Analysis and KEGG Pathway Analysis of Differentially Expressed m6A RNA Methylation-Derived Genes

When compared to the control group, the degree of methylation in the AD group increased in 659 genes, while the degree of methylation decreased in 991 genes. In order to clarify if m6A RNA methylation was related to specific functional roles in AD, GO term enrichment analyses of target RNAs identified in the AD and in the control groups were performed, revealing increased methylation of m6A in the AD group compared to that in the control group. GO analysis consisted of three parts: biological processes (BP), cell components (CC), and molecular functions (MF). The GO analysis of BP showed that the genes with increased expression of m6A RNA methylation in the AD group were significantly associated with the regulation of dendrite development, transport, positive regulation of cellular components and processes, cellular component organization or biogenesis, positive regulation of BP, nervous system development, and single-organism processes. Significant GO CC terms of differentially expressed RNAs showed that these mRNAs were associated with the cytoplasm, organelles, cell parts, intracellular parts, and intracellular organelles. For MF, these mRNAs were associated with the binding of specific substances, such as proteins, enzymes, metal ions, cations, and heterocyclic compounds, and catalytic activity (**Figures 2A–F**). The KEGG pathway dot-plot revealed the significant enrichment pathways with the top 18 enrichment scores [−log10 (*P*-value)]. KEGG pathway analysis predicted the pathways affected by the variation of mRNAs in the AD brain samples, including synaptic growth at the neuromuscular junction, snRNA transcription, the smoothened signaling pathway involved in dorsal/ventral neural tube patterning, regulation of synapse structural plasticity, regulation of keratinocyte migration, regulation of interleukin-2 secretion, regulation of guanyl-nucleotide exchange factor

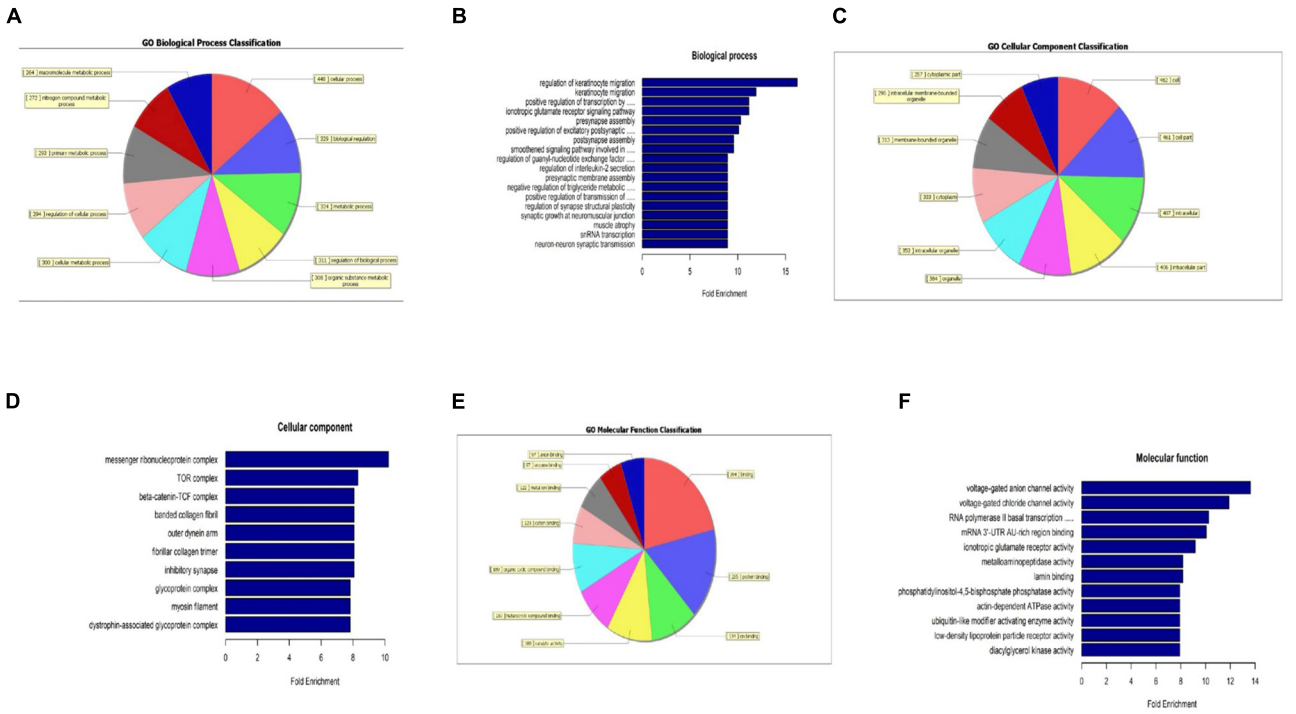

FIGURE 2 | Gene ontology analysis showing that m6A RNA methylation is related to specific functional roles in AD. The analyzed genes with increased m6A RNA methylation expression in the AD group are shown; biological process-specific function **(A,B)**, cell component-specific function **(C,D)**, and molecular function-specific function **(E,F)**.

activity, presynaptic membrane assembly, pre-synapse assembly, post-synapse assembly, positive regulation of transmission of nerve impulse, positive regulation of transcription by RNA polymerase III, positive regulation of excitatory post-synaptic potential, neuron–neuron synaptic transmission, negative regulation of triglyceride metabolic process, muscle atrophy, keratinocyte migration, and ionotropic glutamate receptor signaling pathway (**Figures 3A–C**). Additionally, the four main pathways were associated with synapses, glutamatergic synapse, axon guidance, long-term potentiation, and calcium signaling pathway (**Figures 4A–D**).

Ubiquitous Expression of m6A Methyltransferases and Demethylases Between the Two Groups

The mRNA expression of METTL3 and FTO was examined. The results showed an increased expression of METTL3 ($P < 0.05$) and a decreased expression of FTO genes in the AD group ($P < 0.01$; **Figure 5**). Further, compared to the control group, the expression of METTL3 in the cortex and the hippocampus in AD mice was significantly higher ($P < 0.05$). However, no significant difference in the expression of METTL3 in the cerebellum was found between the two groups. Additionally, the level of the demethylase FTO in the hippocampus of AD mice was lower than that of control mice ($P < 0.05$), while no significant differences were observed in its expression in the cortex and the cerebellum (**Figure 6**).

The Levels of Aβ Deposition and Synaptophysin Expression Were Different in the Two Groups of Mice

The deposition of Aβ was significantly increased in AD mice, while the opposite trend occurred for synaptophysin ($P < 0.01$). The results were consistent between the cortex and the hippocampus (**Figures 7A,B**).

At Different Levels of m6A RNA, Methylation and Quantity of Gene Expression Were Different

The results of high-throughput sequencing analysis showed that the methylation degree of AMPA was increased in the AD group compared to that in the control group, and its gene expression by qRT-PCR was decreased in the AD group. The trend of NMDA was the same as that of AMPA; however, in the AD group, the level of SEMA gene methylation decreased, and the amount of gene expression by qRT-PCR increased (**Figures 8A,B**).

DISCUSSION

APP/PS1 double transgenic mouse models are often used as a simulation of AD animal models. The advantage lies in the combination of APP and PS1, two susceptibility genes, which makes up for the defects of relatively single pathological changes caused by a single mutated gene and which can

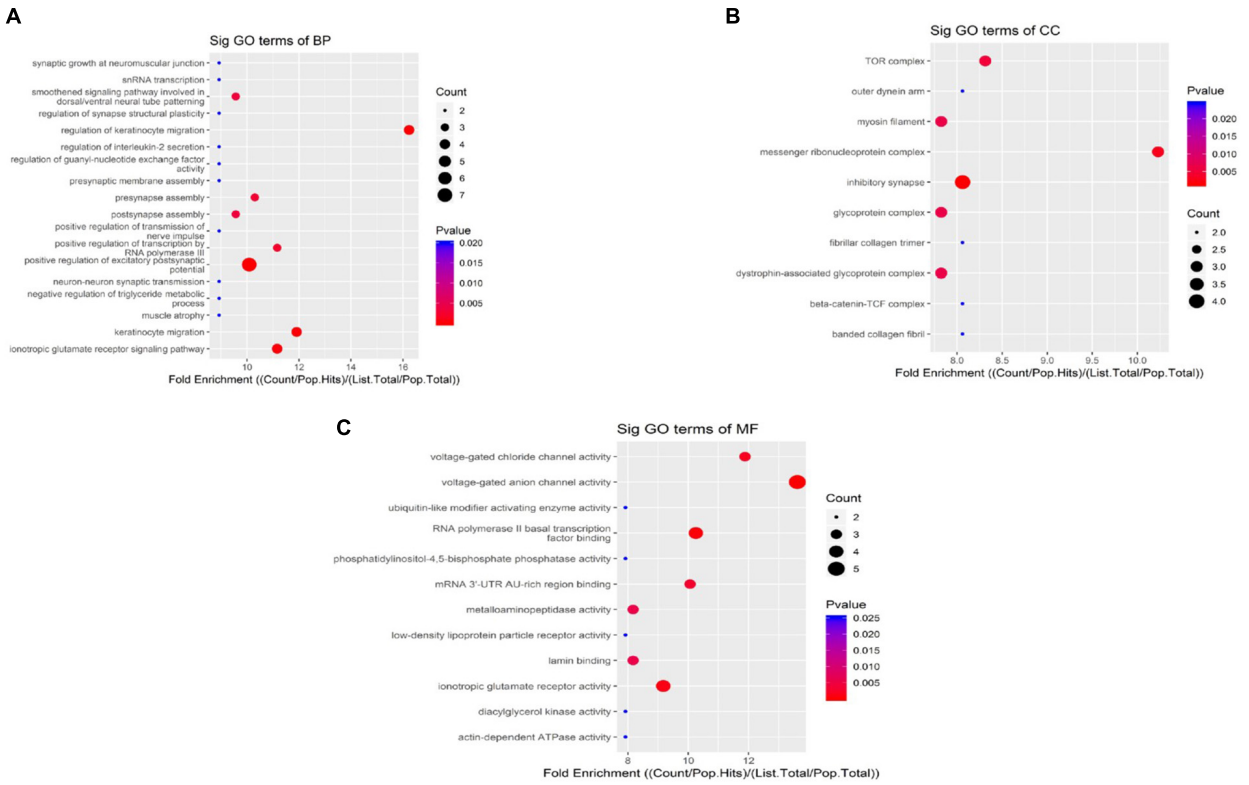

FIGURE 3 | Kyoto Encyclopedia of Genes and Genomes pathway analysis of genes with differentially expressed m6A RNA methylation, showing the top 18 enrichment scores. Analysis predicted the pathways affected by the variation of mRNAs in AD brain samples; biological processes **(A)**, cell components **(B)**, and molecular functions (**C**) show their own pathways. The enrichment score was calculated as –log10 (*P*-value).

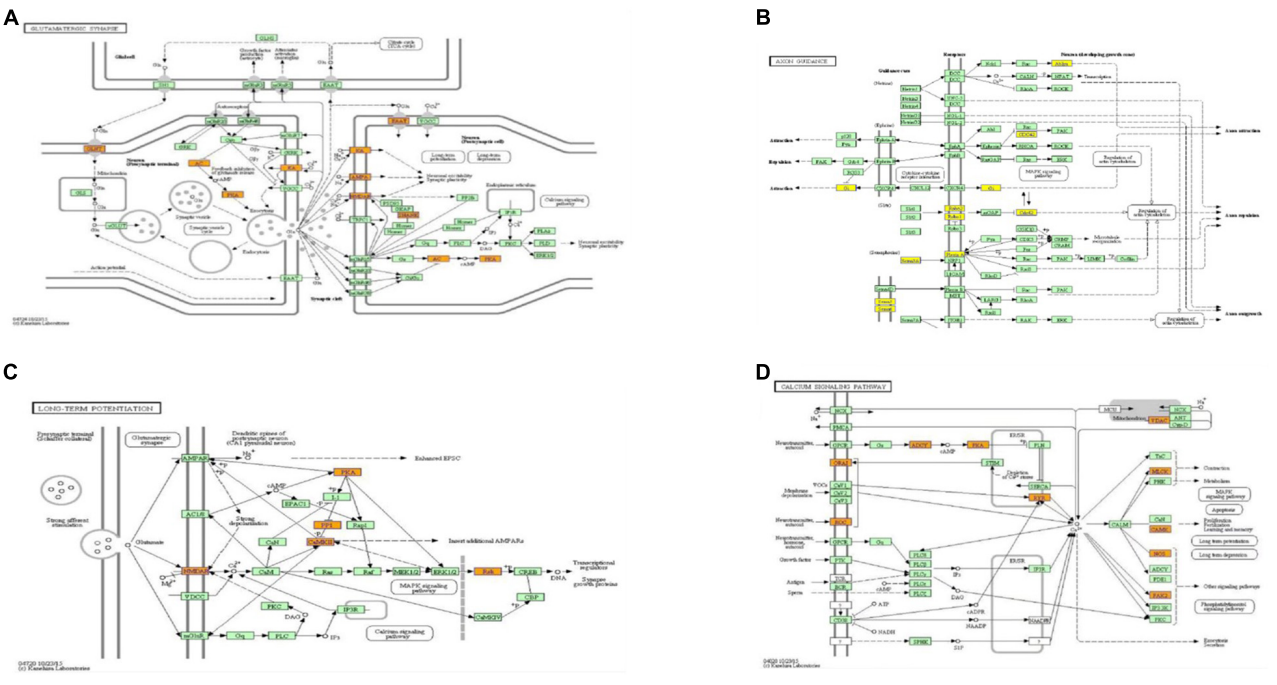

FIGURE 4 | Pathways associated with synaptic function, from which genes to be studied were selected. Glutamatergic synapse **(A)**, axon guidance **(B)**, long-term potentiation **(C)**, and calcium signaling pathway **(D)**.

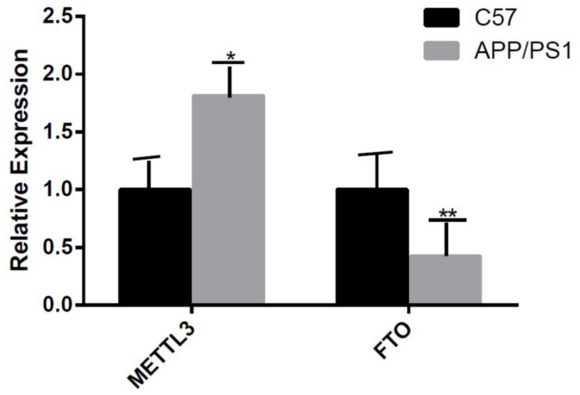

FIGURE 5 | The expression of METTL3 gene is increased and that of FTO gene is decreased in the AD group. Student's *t*-test was used to detect differences between the two groups, and data are presented as mean ± SEM; $n = 5$ per group, $^{*}P < 0.05$, $^{**}P < 0.01$.

better simulate the pathological features and the behavior changes of AD. Similar AD animal models have been used to study the role of RNA demethylase in the pathogenesis of AD, for which triple transgenic mice were used as the AD model (Li et al., 2018). Meanwhile, a large number of studies have shown that the Aβ burden, pathological changes, and cognitive functions of 9-month-old APP/PS1 mice are notably different from those of non-transgenic mice of the same age (Xiong et al., 2011; Izco et al., 2014). In this study, we used the APP/PS1 animal model and verified its pathological changes, which are consistent with those of other studies.

A large number of studies have shown that m6A RNA methylation is related to the occurrence of tumor diseases, such as breast cancer and lung cancer (Kaklamani et al., 2011; Li et al., 2019), while relatively few studies focused on the relationship between m6A RNA methylation and the brain. In 2017, Chang and colleagues performed a transcriptome-wide methylation analysis with mouse brain samples and identified RNA m6A methylation as a new element in the region-specific gene regulatory network (Chang et al., 2017). A study by Ke et al. (2015) indicated that the m6A density peaks early in the 3′ UTR and that the brain transcripts preferentially use distal polyA sites among transcripts with alternative polyA usage in the brain, and a higher proximal m6A density was observed in the last exons. However, no study has reported the role of m6A RNA methylation in AD.

In this study, we found that there was a difference in the m6A levels between AD and control mice, and the m6A methylation genes in the AD group were related to the presynaptic membrane, the postsynaptic membrane, and the synaptic growth, altogether suggesting that m6A may indeed be involved in the occurrence of AD.

Some studies have suggested that METTL3 is related to hippocampal memory function (Zhang et al., 2018), while another study showed that in brain tissues, FTO has a wide variety of physiological and pathological functions (Li et al., 2018). In addition, one study found that METTL14, another important m6A RNA methyltransferase, is critical for the transcriptional regulation of striatum function and learning epitopes (Koranda et al., 2018). Still other studies have suggested that m6A RNA methylation is related to the development of the cerebellum (Ma et al., 2018). More interestingly, one study found that m6A methylation changes dynamically with age in the brains of mice. For that study, total RNA was isolated from mice at different ages, including 18-day-old mouse embryos, at birth, 14 days after birth, and during adulthood. Western blot analysis was then performed to detect the levels of transcription containing m6A methylation. The results showed that the expression level of m6A in mRNA was low throughout embryogenesis but increased significantly in adulthood, showing that m6A methylation has dynamic characteristics in the different stages of neural development (Meyer et al., 2012).

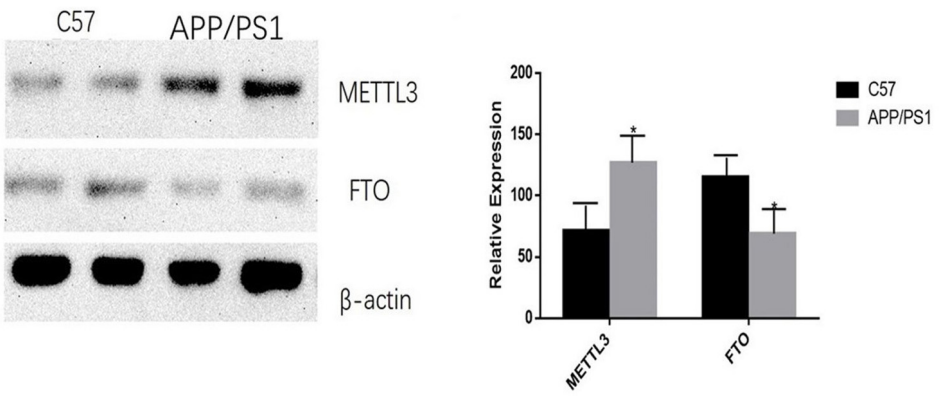

FIGURE 6 | AD group transplantation versus the control group. Expression of METTL3 and FTO enzymes in the brains of AD mice is different from that in the control group. The relative densities of all proteins bands are normalized to β-actin. Student's *t*-test was used to detect differences between the two groups, and data are presented as mean ± SEM; $n = 6$ per group, $^{*}P < 0.05$.

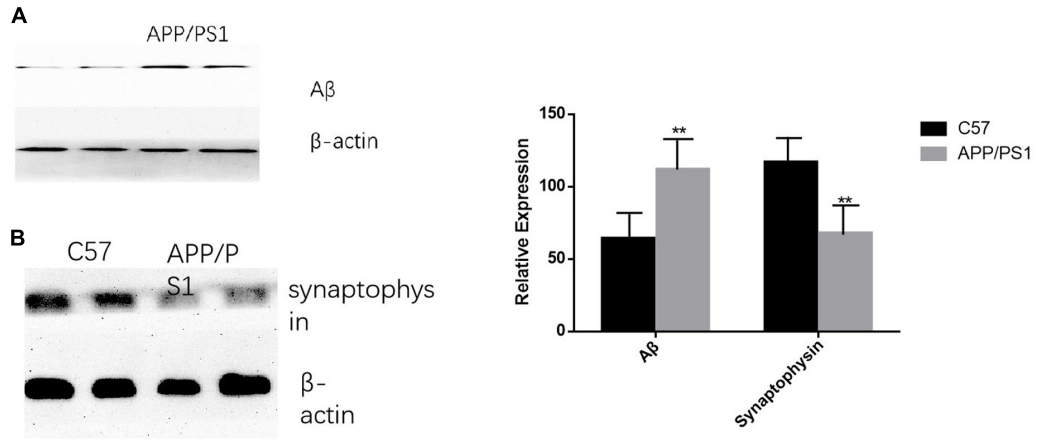

FIGURE 7 | AD animal model validation results. **(A)** The expression level of Aβ in APP/PS1 mice is significantly increased compared with that of the control group, while synaptophysin is decreased in AD animal models **(B)**. Student's *t*-test was used to detect differences between the two groups, and data are presented as mean ± SEM; $n = 6$ per group, $^{**}P < 0.01$.

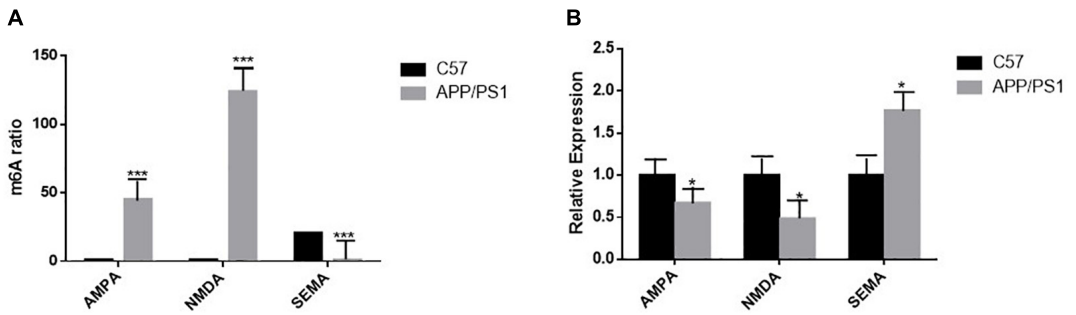

FIGURE 8 | (A) High-throughput sequencing analysis shows statistically significant differences in m6A RNA methylation of AMPA, NMDA, and SEMA in the hippocampus of the two groups of mice; $n = 3$ per group, $^{***}P < 0.001$. **(B)** The mRNA levels of AMPA and NMDA in the brains of AD mice were reduced by quantitative RT-PCR, and that of SEMA is the opposite. β-actin was measured as the reference gene; $n = 5$ per group. Student's *t*-test was used to detect differences between the two groups; data are presented as mean ± SEM; $^{*}P < 0.05$.

Among the methyltransferases, METTL3 is the core catalyst of m6A methylation. The determination of the degree of methylation between the two groups and the verification by Western blot reached the same conclusion – that the expression of METTL3 increased in the AD group.

Some studies imply that FTO is one of the main demethylases in m6A methylation, that it is abundant in the brain, and that it regulates dopaminergic signaling and adult neurogenesis (Jia et al., 2011; Hess et al., 2013; Zhao et al., 2014). In this study, Western blot and qRT-PCR showed that the expression of FTO in the AD group decreased compared to that in the control group, which was consistent with the result of increased methylation in the AD group.

Changes in synaptic function are considered to be the main mechanism of AD (Henstridge et al., 2016). At the same time, some studies have pointed out that mRNA m6A modification plays a key role in synaptic function (Weng et al., 2018; Fu et al., 2019). In our study, among the two groups of genes with changes in m6A RNA methylation levels, GO analysis results and pathway diagrams revealed several genes related to synaptic function. Differences in their expression between the two groups were further verified by qRT-PCR.

The hippocampus and the cortex are the main sections involved in AD pathogenesis, and some studies have pointed out that the development of the cerebellum is also related to m6A methylation (Ma et al., 2018). Therefore, cerebellar tissues were isolated separately in this study and compared between the two groups. The results revealed that there were no significant differences in the levels of methylation, methyltransferase, or demethylase in the cerebellum samples from the two groups, which is consistent with the fact that the main pathogenic sites of AD are located in the cerebral cortex and the hippocampus. Unfortunately, we did not compare the different brain tissues in the same group; since our mice were of the same age, a comparison of mice of different ages in the group might reveal something new. It would be interesting to analyze the m6A RNA methylation at different time points, including the time before the onset of clinical symptoms, during the development of clinical symptoms, and at

the peak of misfolding protein aggregation in the animal model. Together with the results from previous studies, our results suggest that methylase and demethylase are potential targets for the treatment of AD; however, more research is needed to support these conclusions.

DATA AVAILABILITY STATEMENT

All datasets generated for this study are included in the article/supplementary material.

ETHICS STATEMENT

The animal study was reviewed and approved by Ethical Committee for Animal Experiments of Shandong University.

AUTHOR CONTRIBUTIONS

YW, JB, and MH designed the research. MH performed the experiments. ZL, YX, and XL provided technical support and isolated the mouse tissue samples. XL, DW, and FL analyzed the data. YW and MH wrote the manuscript. All authors approved the manuscript for publication.

FUNDING

The study was supported by the fund of the National Natural Science Foundation of China (81870848), the Key Research and Development Program of Shandong Province (2017GSF218046), and the Medical Science and Technology Development Plan of Shandong Province (2014WS0158).

REFERENCES

Bateman, R. J., Xiong, C., Benzinger, T. L. S., Fagan, A. M., Goate, A., Fox, N. C., et al. (2012). Clinical and biomarker changes in dominantly inherited Alzheimer's disease. *N. Engl. J. Med.* 367, 795–804. doi: 10.1056/NEJMoa1202753

Chang, M., Lv, H., Zhang, W., Ma, C., He, X., Zhao, S., et al. (2017). Region-specific RNA m6A methylation represents a new layer of control in the gene regulatory network in the mouse brain. *Open Biol.* 7:170166. doi: 10.1098/rsob.170166

Fu, Y., Zorman, B., Sumazin, P., Sanna, P. P., and Repunte-Canonigo, V. (2019). Epitranscriptomics: correlation of N6-methyladenosine RNA methylation and pathway dysregulation in the hippocampus of HIV transgenic rats. *PLoS One* 14:e0203566. doi: 10.1371/journal.pone.0203566

Henstridge, C. M., Pickett, E., and Spires-Jones, T. L. (2016). Synaptic pathology: a shared mechanism in neurological disease. *Ageing Res. Rev.* 28, 72–84. doi: 10.1016/j.arr.2016.04.005

Hess, M. E., Hess, S., Meyer, K. D., Verhagen, L. A., Koch, L., Brönneke, H. S., et al. (2013). The fat mass and obesity associated gene (Fto) regulates activity of the dopaminergic midbrain circuitry. *Nat. Neurosci.* 16, 1042–1048. doi: 10.1038/nn.3449

Izco, M., Martínez, P., Corrales, A., Fandos, N., García, S., and Insua, D. (2014). Changes in the brain and plasma ab peptide levels with age and its relationship with cognitive impairment in theappswe/ps1de9 mouse model of Alzheimer's disease. *Neuroscience* 263, 269–279. doi: 10.1016/j.neuroscience.2014.01.003

Jia, G., Fu, Y., Zhao, X., Dai, Q., Zheng, G., Yang, Y., et al. (2011). N6-methyladenosine in nuclear RNA is a major substrate of the obesity-associated FTO. *Nat. Chem. Biol.* 7, 885–887. doi: 10.1038/nchembio.687

Kaklamani, V., Yi, N., Sadim, M., Siziopikou, K., Zhang, K., Xu, Y., et al. (2011). The role of the fat mass and obesity associated gene (FTO) in breast cancer risk. *BMC Med. Genet.* 12:52. doi: 10.1186/1471-2350-12-52

Ke, S., Alemu, E. A., Mertens, C., Gantman, E. C., Fak, J. J., Mele, A., et al. (2015). A majority of m6A residues are in the last exons, allowing the potential for 3' UTR regulation. *Genes Dev.* 29, 2037–2053. doi: 10.1101/gad.269415.115

Koranda, J. L., Dore, L., Shi, H., Patel, M. J., Vaasjo, L. O., Rao, M. N., et al. (2018). Mettl14 is essential for epitranscriptomic regulation of striatal function and learning. *Neuron* 99, 283–292. doi: 10.1016/j.neuron.2018.06.007

Li, H., Ren, Y., and Mao, K. (2018). FTO is involved in Alzheimer's disease by targeting TSC1-mTOR-Tau signaling. *Biochem. Biophys. Res. Commun.* 498, 234–239. doi: 10.1016/j.bbrc.2018.02.201

Li, J., Han, Y., Zhang, H., and Qian, Z. (2019). The m6A demethylase FTO promotes the growth of lung cancer cells by regulating the m6A level of USP7 mRNA. *Biochem. Biophys. Res. Commun.* 512, 479–485. doi: 10.1016/j.bbrc.2019.03.093

Li, L., Zang, L., Zhang, F., Chen, J., Shen, H., Shu, L., et al. (2017). Fat mass and obesity-associated (FTO) protein regulates adult neurogenesis. *Hum. Mol. Genet.* 26, 2398–2411. doi: 10.1093/hmg/ddx128

Liu, J., Yue, Y., Han, D., Wang, X., Fu, Y., Zhang, L., et al. (2014). A METTL3-METTL14 complex mediates mammalian nuclear RNA N6-adenosine methylation. *Nat. Chem. Biol.* 10, 93–95. doi: 10.1038/nchembio.1432

Livak, K. J., and Schmittgen, T. D. (2001). Analysis of relative gene expression ata using real-time quantitative PCR and the 2−ΔΔCT method. *Methods* 25, 402–408. doi: 10.1006/meth.2001.1262

Ma, C., Chang, M., and Lv, H. (2018). RNA m6A methylation participates in regulation of postnatal development of the mouse cerebellum. *Genome Biol.* 19:68. doi: 10.1186/s13059-018-1435-z

Meyer, K. D., Saletore, Y., Zumbo, P., Elemento, O., Mason, C. E., and Jaffrey, S. R. (2012). Comprehensive analysis of mRNA methylation reveals enrichment in 3'UTRs and near stop codons. *Cell* 149, 1635–1646. doi: 10.1016/j.cell.2012.05.003

Mucke, L., and Selkoe, D. J. (2012). Neurotoxicity of amyloid β-protein: synaptic and network dysfunction. *Cold Spring Harb. Perspect. Med.* 2:a006338. doi: 10.1101/cshperspect.a006338

Niu, Y., Zhao, X., Wu, Y. S., Li, M. M., Wang, X. J., and Yang, Y. G. (2013). N6-methyl-adenosine (m6A) in RNA: an old modification with a novel epigenetic function. *Genom. Proteom. Bioinform.* 11, 8–17. doi: 10.1016/j.gpb.2012.12.002

Vu, L. P., Pickering, B. F., Cheng, Y., Zaccara, S., Nguyen, D., Minuesa, G., et al. (2017). The N6-methyladenosine (m6A)-forming enzyme METTL3 controls myeloid differentiation of normal hematopoietic and leukemia cells. *Nat. Med.* 23, 1369–1376. doi: 10.1038/nm.4416

Wang, Y., and Zhao, J. C. (2016). Update: mechanisms underlying N6-methyladenosine modification of eukaryotic mRNA. *Trends Genet.* 32, 763–773. doi: 10.1016/j.tig.2016.09.006

Weng, Y. L., Wang, X., An, R., Cassin, J., Vissers, C., Liu, Y., et al. (2018). Epitranscriptomic m6A regulation of axon regeneration in the adult mammalian nervous system. *Neuron* 97, 313–325. doi: 10.1016/j.neuron.2017.12.036

Widagdo, J., Zhao, Q.-Y., Kempen, M. J., Tan, M. C., Ratnu, V. S., Wei, W., et al. (2016). Experience-dependent accumulation of N6-methyladenosine in the prefrontal cortex is associated with memory processes in mice. *J. Neurosci. Off. J. Soc. Neurosci.* 36, 6771–6777. doi: 10.1523/JNEUROSCI

Xiong, H., Callaghan, D., Wodzinska, J., Xu, J., Premyslova, M., Liu, Q. Y., et al. (2011). Biochemical and behavioral characterization of the double transgenic mouse model (APPswe/PS1dE9) of Alzheimer's disease. *Neurosci. Bull.* 27, 221–232. doi: 10.1007/s12264-011-1015-7

Zhang, Z., Wang, M., and Xie, D. (2018). METTL3-mediated N6-methyladenosine mRNA modification enhances long-term memory consolidation. *Cell Res.* 28, 1050–1061. doi: 10.1038/s41422-018-0092-9

Zhao, X., Yang, Y., Sun, B.-F., Shi, Y., Yang, X., Xiao, W., et al. (2014). FTO-dependent demethylation of N6-methyladenosine regulates mRNA splicing and is required for adipogenesis. *Cell Res.* 24, 1403–1419. doi: 10.1038/cr.2014.151

Zhou, J., Wan, J., Gao, X., Zhang, X., Jaffrey, S. R., Qian, S. P., et al. (2015). Dynamicm6A mRNA methylation directs translational control of heat shock response. *Nature* 526, 591–594. doi: 10.1038/nature 15377

Conflict of Interest: The authors declare that the research was conducted in the absence of any commercial or financial relationships that could be construed as a potential conflict of interest.

frontiers in Neuroscience

ORIGINAL RESEARCH
published: 15 April 2020
doi: 10.3389/fnins.2020.00333

Activated Protein C Attenuates Experimental Autoimmune Encephalomyelitis Progression by Enhancing Vascular Integrity and Suppressing Microglial Activation

*Ravi Kant, Sebok K. Halder, Jose A. Fernández, John H. Griffin and Richard Milner**

Department of Molecular Medicine, The Scripps Research Institute, La Jolla, CA, United States

Background: Activated protein C (APC), a serine protease with antithrombotic effects, protects in animal models of ischemic stroke by suppressing inflammation and enhancing vascular integrity, angiogenesis, neurogenesis and neuroprotection. A small number of animal studies suggest it might also have therapeutic potential in multiple sclerosis (MS), though results have been mixed. Based on these conflicting data, the goals of this study were to clarify the therapeutic potential of APC in the experimental autoimmune encephalomyelitis (EAE) model of MS and to determine mechanistically how APC mediates this protective effect.

Methods: The protective potential of APC was examined in a chronic progressive model of EAE. Vascular breakdown, tight junction protein expression and vascular expression of fibronectin and α5β1 integrin as well as vascularity and glial activation were analyzed using immunofluorescence (IF) of spinal cord sections taken from mice with established EAE. The direct influence of APC on microglial activation was evaluated *in vitro* by a combination of morphology and MMP-9 expression.

Results: APC attenuated the progression of EAE, and this was strongly associated at the histopathological level with reduced levels of leukocyte infiltration and concomitant demyelination. Further analysis revealed that APC reduced vascular breakdown which was associated with maintained endothelial expression of the tight junction protein zonula occludens-1 (ZO-1). In addition, APC suppressed microglial activation in this EAE model and *in vitro* studies revealed that APC strongly inhibited microglial activation at both the morphological level and by the expression of the pro-inflammatory protease MMP-9.

Conclusion: These findings build on the work of others in demonstrating strong therapeutic potential for APC in the treatment of inflammatory demyelinating disease and suggest that enhancement of vascular integrity and suppression of microglial activation may be important mediators of this protection.

Keywords: activated protein C, experimental autoimmune encephalomyelitis, microglia, blood-brain barrier, vascular, matrix metalloproteinase-9

OPEN ACCESS

Edited by:
David Pozo,
University of Seville, Spain

Reviewed by:
Elena Gonzalez-Rey,
Instituto de Parasitología y Biomedicina López-Neyra (IPBLN), Spain
Ainhoa Plaza-Zabala,
Achucarro Basque Center for Neuroscience, Spain

***Correspondence:**
Richard Milner
rmilner@sdbri.org

Specialty section:
This article was submitted to Neurodegeneration, a section of the journal Frontiers in Neuroscience

Received: *01 October 2019*
Accepted: *20 March 2020*
Published: *15 April 2020*

Citation:
Kant R, Halder SK, Fernández JA, Griffin JH and Milner R (2020) Activated Protein C Attenuates Experimental Autoimmune Encephalomyelitis Progression by Enhancing Vascular Integrity and Suppressing Microglial Activation. Front. Neurosci. 14:333. doi: 10.3389/fnins.2020.00333

INTRODUCTION

Multiple sclerosis (MS) is an autoimmune disease of the central nervous system (CNS) and is the most common neurological disease in the young to middle age population, affecting more than 400,000 people in the United States (Wingerchuk and Carter, 2014; Doshi and Chataway, 2017). While the precise trigger of MS is unknown, it typically presents with a spectrum of neurological symptoms that include blindness, altered sensation, weakness and eventually paralysis and cognitive defects. At the pathological level, MS is characterized by infiltration of inflammatory lymphocytes directed against myelin antigens into the CNS (brain and spinal cord), which establishes a chronic inflammatory response, resulting in stripping of the myelin sheath from myelinated axons (demyelination) and ultimately, axonal degeneration (ffrench-Constant, 1994; Lassmann, 1998). Because MS is such a common disease that strikes relatively early in life, the last 30 years has witnessed intensive research activity seeking to understand disease pathogenesis. This activity has generated a large number of disease-modifying therapies (DMTs), several of which are effective at suppressing the inflammatory aspect of MS. To date, most of these drugs have been designed to target cells of the immune system, suppressing their activation, proliferation, or egression from peripheral lymph nodes or their transmigration into the CNS. It should be noted that while each of the drugs offer significant benefits in certain sub-populations of MS patients, because of the heterogeneity of the disease, none of the drugs is effective in all patients, and in some types of MS, particularly the chronic progressive form, few therapeutic options are currently available (Wingerchuk and Carter, 2014; Doshi and Chataway, 2017).

Activated protein C (APC) is a homeostatic serine protease that was first defined as an antithrombotic on the basis of inactivation of the clotting factors Va and VIIIa (Mosnier et al., 2007; Rezaie, 2011; Esmon, 2012). Studies in animal models of neurological disease, particularly ischemic stroke, have shown that in addition to its natural antithrombotic actions, APC also triggers a number of protective actions that include attenuation of neuroinflammation and promotion of vascular integrity, angiogenesis, neurogenesis, and neuroprotection (Joyce et al., 2001; Cheng et al., 2003; Guo et al., 2004; Fernandez et al., 2005; Mosnier and Griffin, 2007; Thiyagarajan et al., 2008; Petraglia et al., 2010; Guo et al., 2013; Wang et al., 2013a,b). Sophisticated molecular dissection studies have shown that the antithrombotic and neuroprotective influences reside in separate domains of the APC protein structure and this has led to the generation of different APC variants that lack these specific activities (Mosnier et al., 2004, 2007). Of particular clinical interest is the 3K3A-APC variant which retains neuroprotective actions but lacks antithrombotic activity, thus avoiding the unwanted side-effect of excess bleeding (Mosnier et al., 2007). Encouraged by a large number of studies demonstrating that APC protects in animal models of ischemic stroke, 3K3A-APC is currently being evaluated in an NIH-funded phase 2 clinical trial of ischemic stroke (RHAPSODY).

Interestingly, a small number of studies in the experimental autoimmune encephalomyelitis (EAE) mouse model of MS have suggested that APC might also hold therapeutic potential in the treatment of MS, though to date, results have been conflicting. Specifically, while approaches designed to increase endogenous APC levels protected against EAE (Verbout et al., 2015; Wolter et al., 2016), surprisingly, antibody neutralization of endogenous APC achieved the same outcome (Alabanza et al., 2013). Furthermore, while exogenous APC demonstrated protection in the relapsing-remitting form of EAE (Han et al., 2008), its effect in the chronic progressive form of EAE has yet to be assessed. Based on this incomplete and at times conflicting data, we embarked on the current study with the objective of clarifying whether APC protects against demyelinating disease, as well as seek to define the molecular mechanisms underlying this protection. In particular, in light of the importance of vascular breakdown and remodeling in the pathogenesis of EAE (Gay and Esiri, 1991; Kirk et al., 2003; Roscoe et al., 2009; Seabrook et al., 2010), and our recent finding that APC promotes physiological cerebrovascular remodeling (Burnier et al., 2016), we specifically wanted to examine whether APC protects in EAE via promotion of vascular remodeling. Thus, this study had the following specific goals: (i) evaluate the therapeutic potential of APC in the chronic progressive form of EAE, and (ii) examine how APC influences pathogenic events at the cellular level, paying particular attention to its effects on vascular breakdown and remodeling, leukocyte infiltration, loss of endothelial tight junction proteins, and glial activation.

Abbreviations: APC, Activated protein C; BBB, Blood-brain barrier; BEC, Brain endothelial cells; CFA, Complete Freund's adjuvant; CNS, Central nervous system; Dual-IF, Dual-immunofluorescence; EAE, Experimental autoimmune encephalomyelitis; ECM, Extracellular matrix; FOV, Field of view; MOG, Myelin Oligodendrocyte Glycoprotein; MS, Multiple sclerosis; PAR-1, Protease activated receptor; SEM, Standard error of the mean; TNF-α, Tumor necrosis factor-alpha; WT, Wild-type; ZO-1, Zonula occludens-1.

MATERIALS AND METHODS

Animals

The studies described have been reviewed and approved by The Scripps Research Institute (TSRI) Institutional Animal Care and Use Committee. Wild-type female C57BL6/J mice were obtained from the TSRI rodent breeding colony and maintained under pathogen-free conditions in the closed breeding colony of TSRI.

Experimental Autoimmune Encephalomyelitis (EAE)

EAE was performed using a protocol and materials provided by Hooke Laboratories (Lawrence, MA). Briefly, 10-week old C57BL/6 female mice were immunized subcutaneously with 200 μl of 1 mg/ml MOG_{35-55} peptide emulsified in complete Freud's adjuvant (CFA) containing 2 mg/ml Mycobacterium tuberculosis in both the base of the tail and upper back. In addition, on days 0 and 1, mice also received an intraperitoneal injection of 200 ng pertussis toxin. In WT mice this protocol leads to robust induction of clinical EAE on days 12–14 following immunization (Crocker et al., 2006; Milner et al., 2007). Animals

were monitored daily for clinical signs and scored as follows: 0-no symptoms; 1-flaccid tail; 2-paresis of hind limbs; 3-paralysis of hind limbs; 4-quadriplegia; 5-death. When mice reached a clinical score of 2 (equivalent to hindlimb weakness), they were randomly allocated to one of two different treatment groups: to receive twice-daily intraperitoneal injections of PBS vehicle or recombinant murine 3K3A-APC (0.2 mg/kg re-suspended in PBS pH 7.4 buffer, 100 μl) which was produced and purified as previously described (Fernandez et al., 2005). This treatment was maintained for the duration of the experiment (2 weeks) and mice were clinically evaluated and scored daily. Mice were euthanized at different time-points of EAE, including day 0 (disease-free control) and 25 days post-immunization (peak disease) to obtain tissue for histological studies.

Immunohistochemistry and Antibodies

Immunohistochemistry was performed as described previously (Milner and Campbell, 2002b). Briefly, 10 μm frozen sections of cold phosphate buffer saline (PBS) perfused spinal cord tissues mounted on glass slides were fixed for 5 min in acetone/methanol (1:1) and washed thoroughly in PBS before non-specific binding was blocked in antibody diluent (Cell Signaling Technology, Danvers, MA, United States) for 30 min at 4°C. The following primary antibodies were diluted in antibody diluent and incubated overnight at 4°C: rat monoclonals reactive to CD31 (MEC13.3; 1:500), α5 integrin (5H10-27 (MFR5); 1:100), CD45 (1:300), MECA-32 (1:100), and Mac-1 (M1/70; 1:100), all from BD Pharmingen (La Jolla, CA, United States); mouse monoclonal anti-GFAP-Cy3 conjugate (1:2000; Sigma-Aldrich, St. Louis, MO, United States), hamster monoclonal reactive for CD31 (2H8; 1:500) from Abcam (Cambridge, MA, United States), rabbit polyclonals reactive to fibronectin (1:1000; Sigma-Aldrich), and ZO-1 (1:1500) and fibrinogen (1:2000) (both from Millipore, Temecula, CA, United States). Fluoromyelin-red (1:50) was obtained from Invitrogen (Carlsbad, CA, United States). After several rounds of washing with PBS, tissues were further incubated with the following secondary antibodies diluted in antibody diluent and incubated for 2 h at 4°C: Cy3-conjugated anti-rat and anti-rabbit from Jackson Immunoresearch (West Grove, PA), and Alexa Fluor 488-conjugated anti-rat and anti-hamster from Invitrogen (all secondaries at 1:500). Slides were then washed and mounted in mounting medium containing DAPI (Sigma-Aldrich). Labeling with rat IgG control antibody demonstrated lack of vessel autofluorescence (see **Supplementary Material**).

Image Analysis

Images were acquired using a 2X, 10X, or 20X objective on a Keyence 710 fluorescent microscope. All analysis was performed in the lumbar spinal cord. For each antigen, images of at least three randomly selected areas were taken at 10X or 20X magnification per tissue section and three sections per spinal cord analyzed to calculate the mean for each animal (n = 4 mice per group). For each antigen in each experiment, exposure time was set to convey the maximum amount of information without saturating the image and was maintained constant for each antigen across the different experimental groups. Vascular integrity was evaluated by measuring extravascular leakage of fibrinogen, as measured by the total area of fibrinogen staining per field of view (FOV). Total vascular area (CD31), vascular expression of α5 integrin and fibronectin and leukocyte infiltration as indicated by levels of CD45 and Mac-1 and extent of myelination by fluoromyelin was evaluated by measuring the total area of fluorescence for each marker per FOV. Vascular density was evaluated by counting all the vessels per FOV. The number of MECA-32-positive vessels per FOV was counted in four randomly selected areas in images captured at 10X or 20X magnification per tissue section and three sections per spinal cord analyzed to calculate the mean for each animal (n = 4 mice per group). The percentage of vessels expressing ZO-1 was quantified in a similar manner by counting the number of ZO-1 + vessels/total number of vessels. All data analysis was performed using NIH Image J software. This analysis was performed using four animals per condition per experiment, and the results expressed as the mean ± SEM.

Cell Culture

Pure cultures of mouse microglia were obtained by mechanical shaking of mixed glial cultures (MGC) as described previously (Milner and Campbell, 2002a). Briefly, forebrains from post-natal mice (days 0–2) were stripped of meninges, chopped into small chunks and dissociated in papain before cultured for ∼10 days on ploy-D-lysine (Sigma-Aldrich)-coated T75 tissue culture flasks (Falcon, Franklin, NJ) in DMEM (Sigma) supplemented with 10% fetal bovine serum (Sigma). After establishment of the astrocyte monolayer (7–10 days), the flasks were shaken for 1 h to obtain the loosely adherent microglia. Microglia were counted by hemocytometer and plated at a density of 5×10^4 cells/well in uncoated 24-well plates (Nunc, Naperville, IL, United States) and maintained in the same medium the MGC were cultured in. The purity of these microglial cultures was >99% as determined by Mac-1 positivity in fluorescent immunocytochemistry. Microglia were cultured overnight, then switched to serum-free N2 medium (DMEM supplemented with N2 (Sigma) and grown in the presence or absence of 10 ng/ml TNF-α (R&D) and 15 nM recombinant murine 3K3A-APC that was produced and purified as previously described (Fernandez et al., 2005). After 4 h incubation, 4–6 phase pictures were taken of each condition using a Zeiss Axio Observer microscope. As previously described (Milner and Campbell, 2002a), under basal N2 conditions, microglia displayed two types of morphology: either round (amoeboid) or elongated spindle-shaped cells with one long process extended at both ends. In contrast, cultures treated with APC contained a much higher % of cells displaying a more complex arborized form (ramified). To quantify this marked switch in morphology, we counted the number of cells per FOV that displayed more than 4 process extensions and presented or data as the% of cells with a ramified morphology. Counts were *manually performed* with 4 FOVs analyzed per condition within each experiment and 4 separate experiments performed. The percentage of ramified microglia was quantified and data expressed as the mean ± SD.

Gel Zymography

Gelatin zymography to detect MMP-9 activity was performed as previously described (Heo et al., 1999). Microglial cells were plated at a density of 5×10^4 cells/well in uncoated 24-well plates and cultured in the presence or absence of 10 ng/ml TNF-α (R&D) and different concentrations of recombinant murine 3K3A-APC (0, 3, 15, and 75 nM). After 2 days culture, microglial supernatants were collected and analyzed for gelatinolytic activity. Positive controls for MMP-9 (obtained from R&D) were included. For quantification, gels were scanned using a Bio-Rad VersaDoc imaging system (Hercules, CA, United States) and band intensities quantified using NIH Image J software. Each experiment was repeated a minimum number of four times and the data expressed as mean ± SD.

Statistical Analysis

To measure the impact of APC on clinical score, data were analyzed using one-way analysis of variance (ANOVA) followed by *post hoc* Student's "*t*"-test, in which $p < 0.05$ was defined as statistically significant ($n = 19$ mice per group). In histological studies, all analyses were performed with NIH Image J software, using four animals per condition per experiment, and the results expressed as the mean ± SEM. Statistical significance of histological data was assessed using one-way analysis of variance (ANOVA) followed by Tukey's multiple comparison *post hoc* test, in which $p < 0.05$ was defined as statistically significant. For analysis of the impact of APC on microglial morphological phenotype or MMP-9 expression *in vitro*, experiments were repeated a minimum number of four times and the data expressed as the mean ± SD. Statistical significance was assessed using ANOVA followed by the Student's paired "*t*"-test, in which $p < 0.05$ was defined as statistically significant.

RESULTS

APC Suppressed the Progression of EAE Both at the Clinical and Histopathological Levels

The protective potential of APC was evaluated in the chronic EAE model of MS, in which C57BL/6 mice were immunized with the MOG_{35-55} peptide as previously described (Crocker et al., 2006; Milner et al., 2007). As shown in **Figure 1A**, mice began developing signs of clinical disease between 12 and 14 days post-immunization. When each mouse reached a clinical score of 2 (equivalent to hindlimb weakness), they were randomly allocated to one of two different treatment groups: to receive daily intraperitoneal injections of recombinant murine 3K3A-APC (0.2 mg/kg) or PBS vehicle. Rather than use native wild-type APC, in this study we opted to use the 3K3A-APC variant (for simplicity referred to as APC from hereon) that has three point mutations switching lysine for alanine in the protease domain, because this variant retains cytoprotective properties but has lost the majority of its antithrombotic activity, thus minimizing the potential deleterious side-effect of bleeding (Mosnier et al., 2004, 2007). As shown in **Figure 1A**, after four days of treatment, APC markedly suppressed the clinical progression of EAE at all time-points for the duration of treatment (2 weeks). As the most severe disease in this EAE model occurs in the dorsal end of the spinal cord, we next examined sections of lumbar spinal cord for evidence of neuroinflammation. Histopathological assessment of lumbar spinal cord tissue at the peak of EAE disease (between 21 and 25 days post-immunization) with the pan-leukocyte marker CD45 and the myelin marker fluoromyelin (CD45/fluoromyelin dual-IF) revealed that compared to vehicle-treated controls, APC-treated mice showed marked reduction in the extent of CD45 + leukocyte infiltration into the spinal cord (10.42 ± 0.73 vs. 37.82 ± 2.71% total CD45 + area/FOV under vehicle control conditions, $p < 0.01$) and this was associated with preservation of myelin (89.15 ± 2.09 vs. 72.71 ± 3.81% of fluoromyelin area/FOV under vehicle control conditions, $p < 0.01$) (**Figures 1B–D**). This demonstrates that APC suppressed EAE progression, both at the clinical and histopathological levels.

APC Suppresses Vascular Breakdown and Induction of Endothelial MECA-32 Expression

Previous studies have shown that APC promotes vascular integrity in animal models of ischemic stroke (Mosnier et al., 2007; Guo et al., 2009). To examine how APC influences vascular integrity in this EAE model, we performed dual-IF using CD31 as an endothelial cell marker CD31 and extravascular fibrinogen leak as a marker of vascular breakdown (**Figures 2A,B**). This revealed that while spinal cords of control mice (EAE without APC treatment) had extensive fibrinogen leakage, most notably in spinal cord white matter, mice treated with APC showed reduced levels of fibrinogen leak in their spinal cords (**Figure 2A**). Quantification revealed that fibrinogen leakage was significantly reduced in mice receiving APC compared to vehicle controls (9.26 ± 2.78 compared to 22.43 ± 4.36% total fibrinogen area/FOV under normoxic conditions, $p < 0.01$) (**Figure 2B**). Next, in an alternative approach to examine if blood vessels in APC-treated mice have improved barrier properties we examined vascular expression of MECA-32, a protein that is expressed at high levels on endothelial cells in the developing CNS, but then disappears as CNS endothelium matures (Hallman et al., 1995). Interestingly, MECA-32 is re-expressed in adult CNS blood vessels during inflammatory, hypoxic and ischemic conditions (Engelhardt et al., 1994; Sparks et al., 2000; Li et al., 2012), implying that MECA-32 re-expression on CNS blood vessels occurs when vascular integrity is compromised. Our staining revealed that while no MECA-32 staining was detected in disease-free spinal cord, MECA-32 expression was induced on a sub-population of spinal cord blood vessels in vehicle-treated EAE controls (**Figures 2C,D**), but of note, significantly less MECA-32 expression was detected on blood vessels in mice treated with APC (0.22 ± 0.19 compared to 2.55 ± 0.38 MECA-32 + vessels/FOV, $p < 0.01$). Taken together, these two lines of data demonstrate that

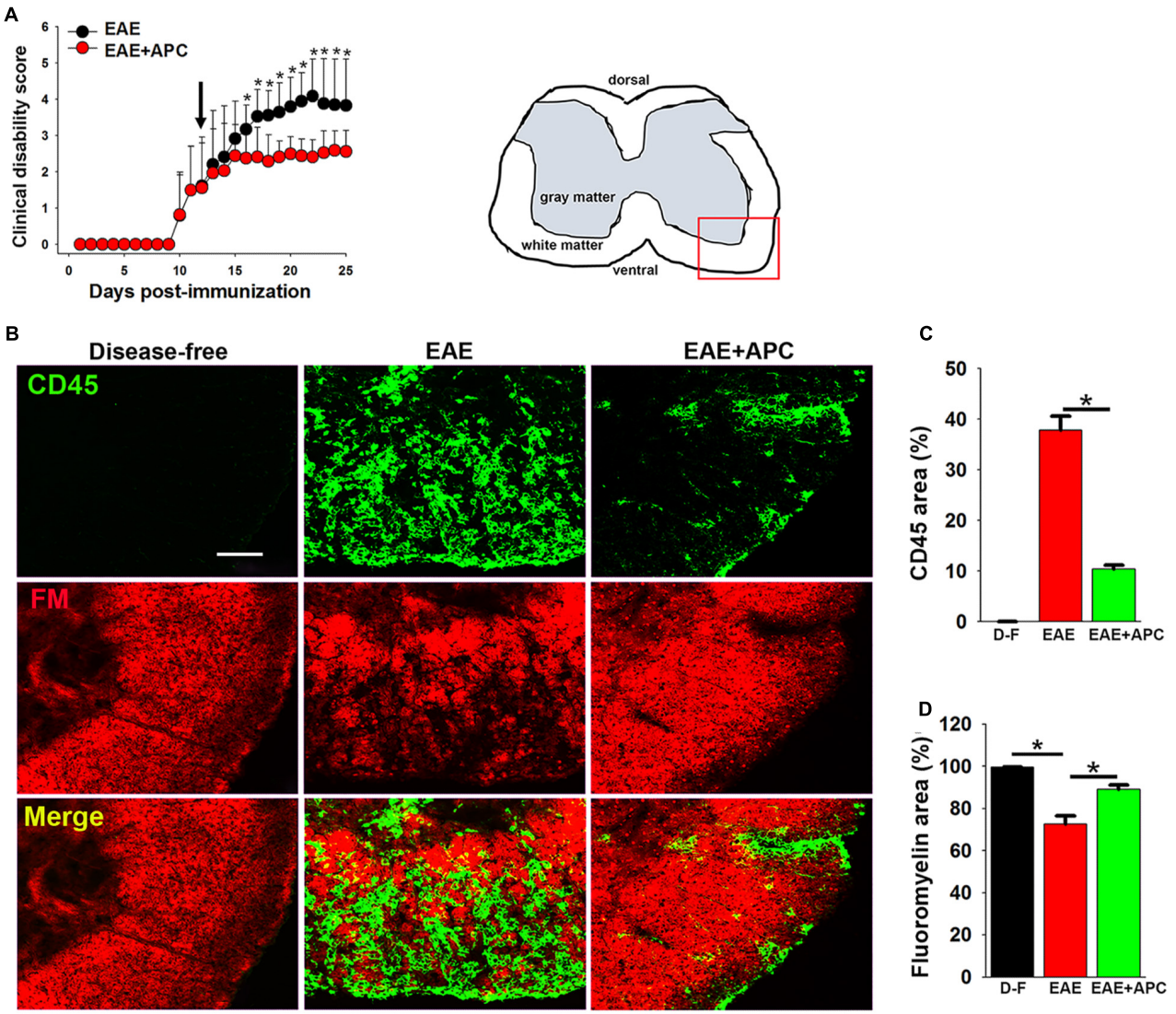

FIGURE 1 | APC suppressed the progression of EAE, both clinically and histopathologically. **(A)** The impact of APC on EAE clinical severity. Once mice acquired a clinical score of 2 they received daily injections of vehicle (EAE) or APC (EAE + APC) as indicated by the arrow, and clinical scores subsequently evaluated at daily intervals. All points represent the mean ± SD (n = 19 mice per group in 3 separate experiments). Note that compared to vehicle controls, after 4 days treatment, APC suppressed the progression of clinical score at all time-points for the duration of the experiment. *$p < 0.05$. **(B)** Frozen sections of lumbar spinal cord taken from disease-free, EAE-vehicle control or EAE + APC mice at the peak phase of EAE were stained for the inflammatory leukocyte marker CD45 (AlexaFluor-488) and fluoromyelin-red (FM). Images were captured in the ventral region as depicted by the red box in the schematic image. Scale bar = 100 μm. **(C,D)** Quantification of CD45 **(C)** and fluoromyelin **(D)** fluorescent signal under disease-free (D–F), or at peak phase of EAE in mice receiving vehicle (EAE) or APC (EAE + APC). Results are expressed as the mean ± SEM (n = 4 mice/group). Note that APC markedly suppressed CD45 + leukocyte infiltration and protected against demyelination. *$p < 0.05$.

spinal cord blood vessels in APC-treated mice show less vascular breakdown.

APC Attenuates Loss of the Endothelial Tight Junction Protein ZO-1 During EAE

Vascular integrity of CNS blood vessels is highly dependent on endothelial expression of tight junction proteins such as ZO-1 which serve to form tight connections between adjacent endothelial cells (Huber et al., 2001; Wolburg and Lippoldt, 2002; Ballabh et al., 2004). The importance of these proteins is illustrated by the finding that endothelial expression of tight junction proteins at cell-cell borders is disrupted both in MS and in EAE (Kirk et al., 2003; Bennett et al., 2010; Errede et al., 2012). To examine how APC influences endothelial expression of ZO-1 in EAE, we performed dual-IF of CD31/ZO-1 on spinal cord sections taken from mice at the peak stage of EAE that had been treated with APC or vehicle controls. As expected, under disease-free conditions, ZO-1 co-localized tightly with the endothelial cell marker CD31 on all spinal cord blood

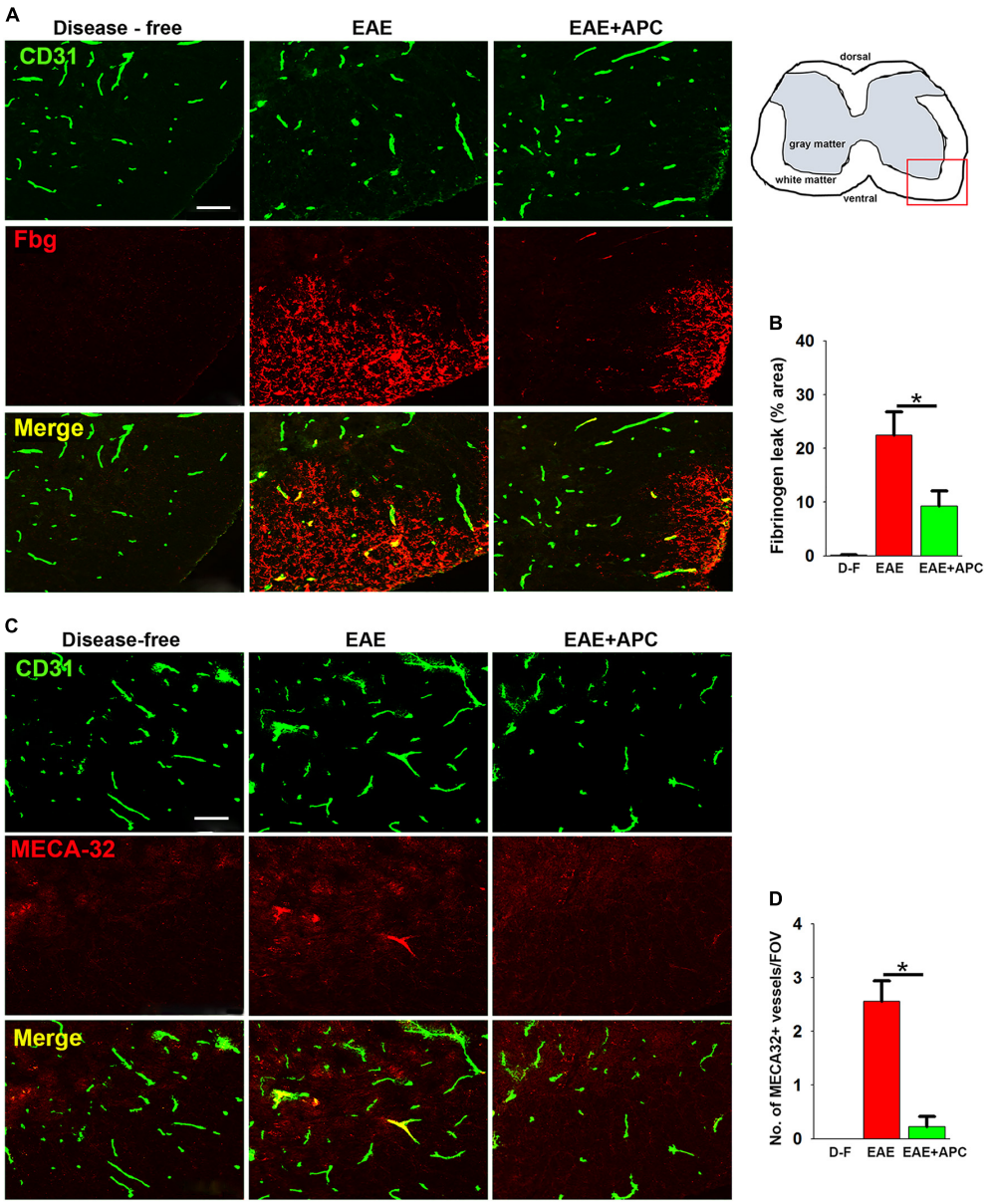

FIGURE 2 | APC protects against loss of vascular integrity during EAE progression. **(A,C)** Frozen sections of lumbar spinal cord taken from disease-free, EAE-vehicle control or EAE + APC mice at the peak phase of EAE were stained for CD31 (AlexaFluor-488) and fibrinogen (Fbg) (Cy-3) in panel A or CD31 (AlexaFluor-488) and MECA-32 (Cy-3) in **(C)**. Images were captured in the ventral region as depicted by the red box in the schematic image. Scale bar = 100 μm. **(B,D)** Quantification of fibrinogen leakage **(B)** and MECA-32 expression **(D)** under disease-free (D–F), or at peak phase of EAE in mice receiving vehicle (EAE) or APC (EAE + APC). Results are expressed as the mean ± SEM (n = 4 mice/group). Note that APC markedly suppressed fibrinogen leakage as well as endothelial expression of MECA-32. *$p < 0.05$.

vessels (**Figure 3A**). However, during the peak stage of EAE, a significant number of blood vessels showed total or partial loss of ZO-1 expression (reduced to 62.69 ± 8.89% of ZO-1 + vessels compared to 97.75 ± 2.45% of ZO-1 + vessels under disease-free conditions, $p < 0.01$). In contrast, blood vessels in APC-treated mice largely maintained expression of ZO-1 such that the proportion of vessels expressing ZO-1 in APC-treated mice was significantly higher than vehicle controls (92.57 ± 2.09% vs. 62.69 ± 8.89%, $p < 0.01$). This demonstrates that APC prevented loss of the endothelial tight junction protein ZO-1 during EAE pathogenesis.

APC Treatment Has No Discernible Influence on Angiogenic Remodeling in EAE

In recent studies we found that a marked angiogenic remodeling response occurs during the pre-symptomatic phase of EAE

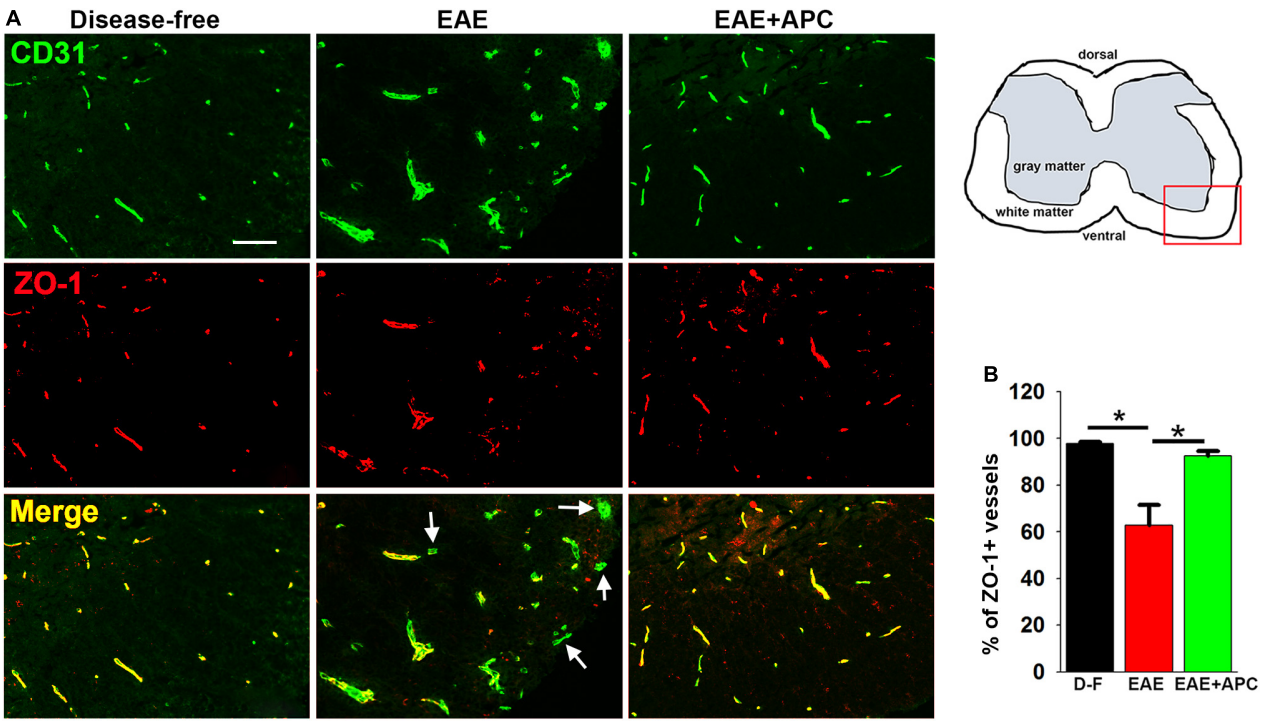

FIGURE 3 | APC protects against loss of the endothelial tight junction protein ZO-1 during EAE. **(A)** Frozen sections of lumbar spinal cord taken from disease-free, EAE-vehicle control or EAE + APC mice at the peak phase of EAE were stained for CD31 (AlexaFluor-488) and ZO-1 (Cy-3). Images were captured in the ventral region as depicted by the red box in the schematic image. Scale bar = 100 μm. **(B)** Quantification of the % of vessels expressing ZO-1. Results are expressed as the mean ± SEM (n = 4 mice/group). Note that under disease-free (D–F) conditions, all blood vessels co-expressed ZO-1 as confirmed by the yellow color in the merged image. In contrast, at the peak of EAE disease, many of the blood vessels in the vehicle control group lacked ZO-1 expression (marked by arrows) and illustrated by the green color in the merge image. In contrast to vehicle control mice, APC protected against loss of ZO-1. *$p < 0.05$.

and that this is associated with upregulated expression of fibronectin and its receptor α5β1 integrin on spinal cord blood vessels (Boroujerdi et al., 2013). In a different model, we showed that chronic mild hypoxia stimulates angiogenic remodeling and interestingly found that APC appears to plays a key role in mediating this response, as functional blockade of APC prevented both upregulation of the fibronectin-α5β1 integrin axis and the associated angiogenic response, while in contrast, exogenous APC enhanced this response (Burnier et al., 2016). In light of these findings, we wondered if the protective effect of APC in EAE might be due to enhanced fibronectin-α5β1 integrin signaling driving a stronger angiogenic response. To examine this concept, we performed dual-IF of CD31/fibronectin and CD31/α5 integrin on spinal cord sections taken from mice at the peak stage of EAE that had received APC or vehicle controls. Consistent with previous reports (Boroujerdi et al., 2013), this showed that EAE was strongly associated with upregulation of both fibronectin (3.97 ± 0.67 vs. 1.71 ± 0.29% fibronectin area/FOV under disease-free conditions, $p < 0.05$), and α5 integrin expression (4.12 ± 0.50 vs. 1.15 ± 0.15% α5 integrin area/FOV under disease-free conditions, $p < 0.05$) (**Figures 4A–D**). Surprisingly however, compared with vehicle control mice, APC showed no discernible increase in either fibronectin expression (3.19 ± 0.64 vs. 3.97 ± 0.67% fibronectin area/FOV under vehicle conditions), or α5 integrin expression (3.40 ± 0.90 vs. 4.12 ± 0.50% α5 integrin area/FOV under vehicle conditions). To examine whether APC could be enhancing angiogenic remodeling via another mechanism, we next examined whether APC influenced vascular density and total vascular area at the peak stage of EAE disease. This showed that while spinal cords of mice with peak EAE disease displayed higher vessel density (75.00 ± 9.60 vs. 47.11 ± 5.11 vessels/FOV under disease-free conditions) and higher total vascular area (4.79 ± 0.65 vs. 2.09 ± 0.15% vascular area/FOV under disease-free conditions) compared to disease-free controls, surprisingly, compared with vehicle controls, APC showed no discernible increase in either vessel density (61.67 ± 11.89 vs. 75.00 ± 9.60 vessels/FOV under vehicle conditions) or total vascular area (4.22 ± 0.51 vs. 4.79 ± 0.65% vascular area/FOV under vehicle conditions). Taken together, these data argue against the notion that APC protects against EAE progression by enhancing angiogenic remodeling.

APC Suppresses Microglial Activation in EAE

Because microglia, the primary immune effector cells resident in the CNS, are thought to play a pivotal role both in the initiation and maintenance of chronic inflammation in

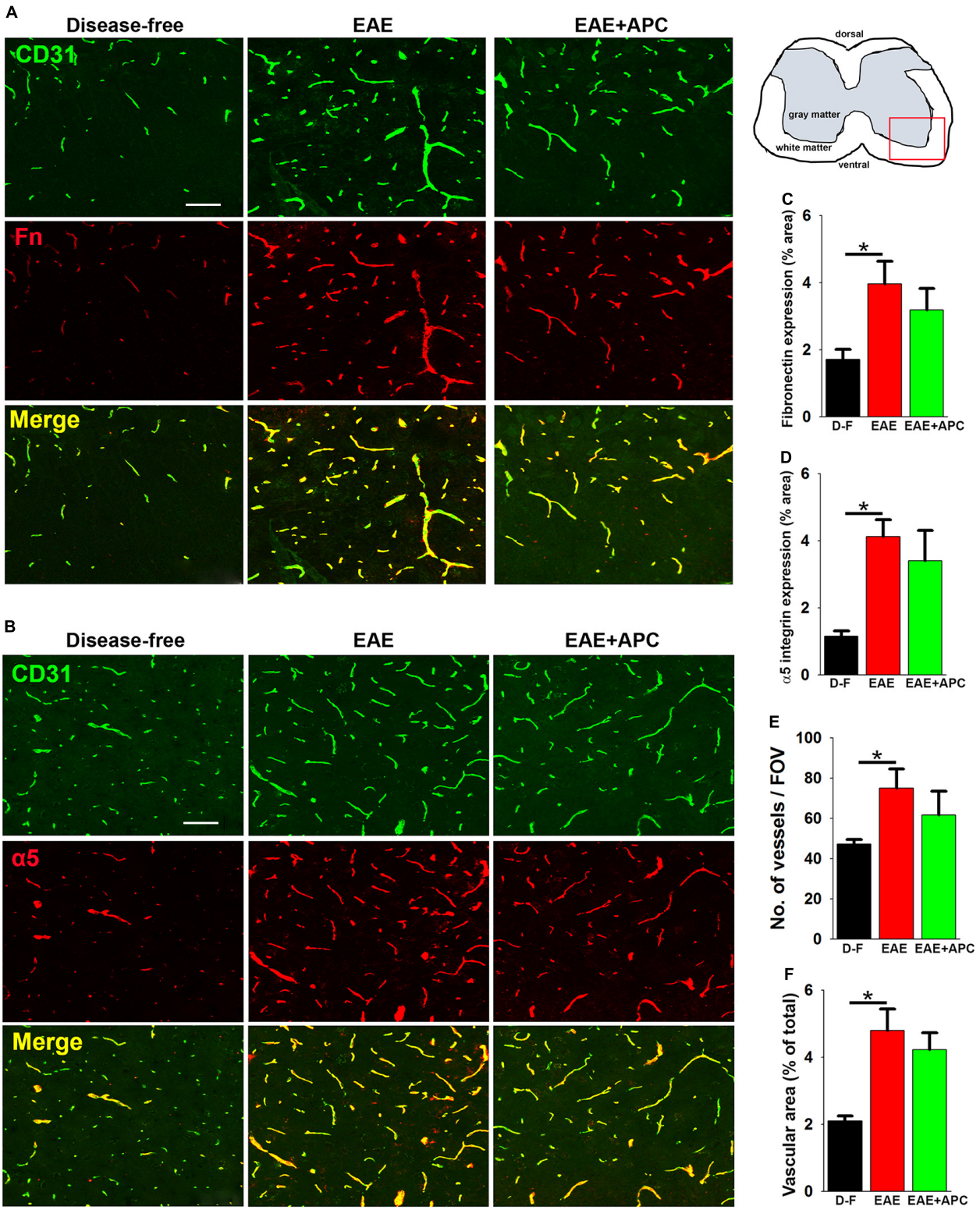

FIGURE 4 | The impact of APC on vascular remodeling during EAE progression. **(A,B)** Frozen sections of lumbar spinal cord taken from disease-free, EAE-vehicle control or EAE + APC mice at the peak phase of EAE were stained for CD31 (AlexaFluor-488) and fibronectin (Fn) (Cy-3) in panel A or CD31 (AlexaFluor-488) and α5 integrin (Cy-3) in **(B)**. Images were captured in the ventral region as depicted by the red box in the schematic image. Scale bar = 100 μm. **(C,D)** Quantification of fibronectin **(C)** and α5 integrin expression **(D)**. **(E,F)** Quantification of vessel density **(E)** and vascular area **(F)**. All results are expressed as the mean ± SEM ($n = 4$ mice/group). Note that compared to disease-free conditions, blood vessels in the EAE-vehicle control group showed increased expression of fibronectin and α5 integrin, which was associated with enhanced vascular density and area, but of note, APC had no significant impact on these changes. *$p < 0.05$.

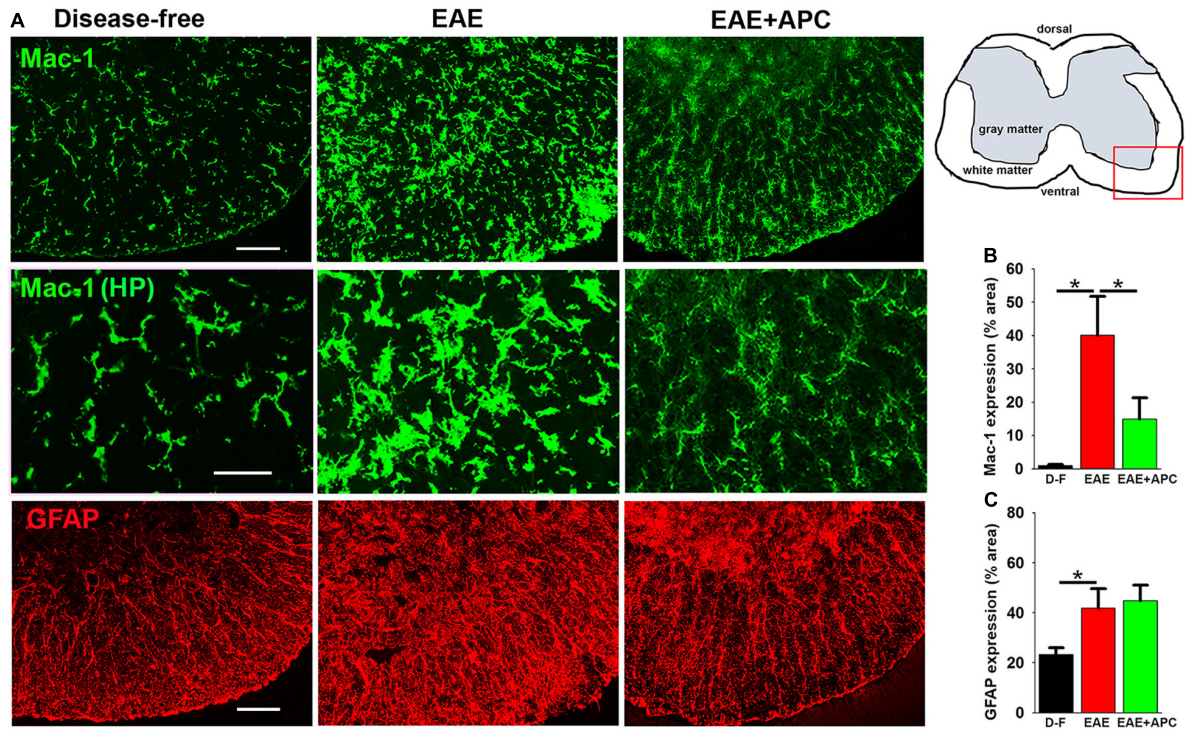

FIGURE 5 | APC suppresses microglial activation during EAE. **(A)** Frozen sections of lumbar spinal cord taken from disease-free, EAE-vehicle control or EAE + APC mice at the peak phase of EAE were stained for Mac-1 (AlexaFluor-488) and GFAP (Cy-3). Images were captured in the ventral region as depicted by the red box in the schematic image. Scale bar = 100 μm except for the high-power images in the middle row = 50 μm. **(B,C)** Quantification of Mac1 **(B)** and GFAP **(C)** expression. Results are expressed as the mean ± SEM (n = 4 mice/group). In the higher magnification images (middle row), note that microglia in vehicle-treated EAE mice displayed large cell bodies and much higher Mac-1 expression, typical of highly activated microglia while in contrast, microglia in APC-treated mice showed highly ramified morphology with small cell bodies and low Mac-1 expression, typical of less activated microglia and more similar to those present in disease-free mice. In addition, GFAP levels in EAE mice were strongly enhanced over disease-free conditions but APC had no discernible effect on this expression. *$p < 0.05$.

MS (Ransohoff, 1999; Trapp et al., 1999), we next examined the influence of APC on microglial activation. As Mac-1 expression levels correlate with degree of microglial activation, we first examined this *in vivo* using Mac-1/GFAP dual-IF. As shown in **Figure 5**, spinal cords of EAE mice showed strongly elevated levels of microglial Mac-1 expression (40.05 ± 11.74 vs. 0.95 ± 0.36% Mac-1 area/FOV under disease-free conditions, $p < 0.05$), but interestingly, Mac-1 levels in APC-treated mice were markedly lower than vehicle-treated controls (14.90 ± 6.48 vs. 40.05 ± 11.74% Mac-1 area/FOV under vehicle-EAE conditions, $p < 0.05$). Strikingly, compared to disease-free conditions, microglia in vehicle-treated EAE mice displayed large cell bodies and much higher Mac-1 expression, typical of highly activated microglia (see high magnification images in the middle row of **Figure 5A**). In contrast, microglia in APC-treated mice showed highly ramified morphology with small cell bodies and lower levels of Mac-1 expression, typical of less activated microglia and similar to those present in disease-free mice. Examination of astrocyte activation by GFAP IF revealed that GFAP levels in the spinal cords of mice with established EAE were enhanced over disease-free conditions (41.82 ± 8.07 vs. 23.51 ± 2.81% Mac-1 area/FOV under disease-free conditions, $p < 0.05$), but treatment with APC had no significant effect on the overall level of GFAP expression (**Figure 5C**).

APC Also Suppresses Microglial Activation and MMP-9 Expression *in vitro*

While our *in vivo* data show that APC suppresses neuropathology and microglial activation in the EAE model, it is difficult to know whether the effect we observe on microglial activation is a direct or secondary response. Therefore, in order to examine if APC directly influences microglial activation, we studied this process in pure cultures of primary mouse microglia, which were derived by mechanical separation from MGC set up from post-natal mice brains, as previously described (Milner and Campbell, 2002a). Following separation from MGC, microglia were cultured overnight, then switched to serum-free N2 medium and stimulated with APC. After 4 h stimulation with 15 nM APC, clear morphological changes in microglia became evident (**Figure 6A**), with cells switching from a predominantly flattened morphology under control conditions to ramified cells having multiple fine cytoplasmic extensions in the presence of APC. In addition, while the pro-inflammatory cytokine TNF-α enhanced cell flattening and the appearance of an amoeboid morphology typical of the activated phenotype, APC prevented

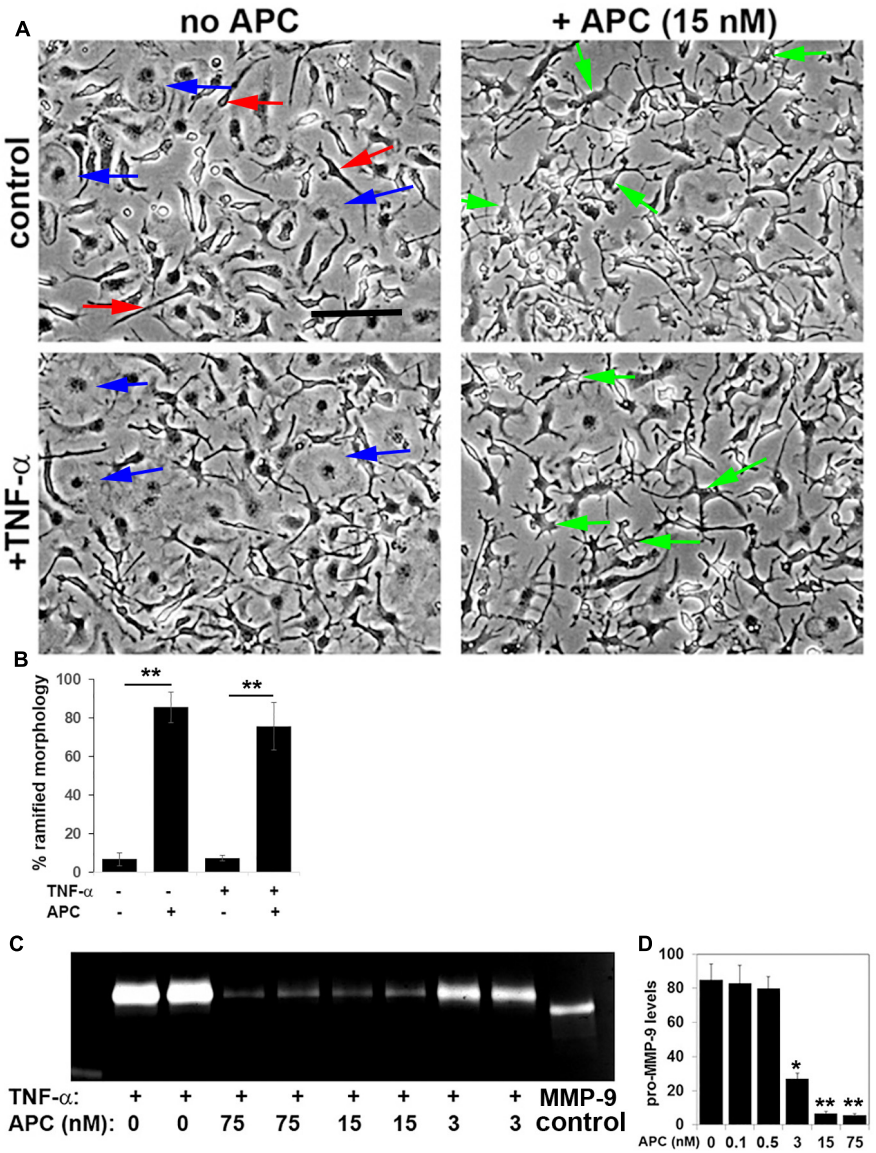

FIGURE 6 | APC suppresses microglial activation and MMP-9 expression *in vitro*. **(A)** Pure cultures of microglia were cultured in the presence or absence of 10 ng/ml TNF-α and/or 15 nM APC. Under control conditions, microglia occupied a mix of amoeboid (blue arrows) and elongated spindle-shaped cells (red arrows). Note that TNF-α promoted the amoeboid phenotype, typical of activated cells, but APC promoted a morphological transformation of microglia into ramified highly arborized cells (green arrows), typical of quiescent microglia. **(B)** Quantification of the percentage of microglia with a ramified morphology under different conditions. Results are expressed as the mean ± SEM (n = 4 images per condition and 4 experiments). $^{**}p < 0.01$. **(C)** Gel zymography of cell culture supernatants taken from microglia that had been treated with TNF-α in the presence of different doses of APC. **(D)** Quantification of MMP-9 levels. Results are expressed as the mean ± SEM (n = 2 samples per condition and 4 experiments). Note that at doses of 75 or 15 nM, APC almost completely blocked TNF-α induction of microglial MMP-9 expression. $^{*}p < 0.05$, $^{**}p < 0.01$.

this transformation and maintained the majority of microglia in the ramified morphology, typical of quiescent microglia. As MMP-9 levels are strongly upregulated upon microglial activation (Kauppinen and Swanson, 2005; Milner et al., 2007; Crocker et al., 2008) and are known to play important pathogenic roles in degrading vascular basement membrane extracellular matrix proteins as well as myelin proteins of oligodendrocytes, we next examined how APC regulates microglial MMP-9 expression. Pure microglia were stimulated with TNF-α to promote microglial activation, then co-incubated with different doses of APC. Two days later, MMP-9 levels within supernatants were analyzed by gel zymography (**Figures 6C,D**). This showed that consistent with previous findings, TNF-α strongly stimulated microglial MMP-9 expression (Crocker et al., 2008). Interestingly, at doses of 75 or 15 nM, APC almost completely blocked TNF-α induction of microglial MMP-9. This inhibition was still evident at the reduced dose of 3 nM APC but diminished at lower doses. Taken together, these *in vitro* studies demonstrate that a dose of

15 nM, APC effectively blocks microglial activation as assessed both at the morphological level and expression of MMP-9. These findings demonstrate that APC directly suppresses microglial activation, though it does not exclude the possibility that some of the anti-inflammatory actions of APC seen *in vivo* may also be secondary, such as prevention of BBB disruption.

DISCUSSION

Inspired by the beneficial effect of APC in stroke models (Thiyagarajan et al., 2008; Wang et al., 2013a,b), recent studies have investigated APC's therapeutic potential in the mouse model of MS, experimental autoimmune encephalomyelitis (EAE), though outcomes have been mixed. Interestingly, while enhancement of APC levels either directly by administration of exogenous APC or via stimulation of the thrombomodulin pathway, conferred protection against EAE (Han et al., 2008; Verbout et al., 2015; Wolter et al., 2016), surprisingly, antibody neutralization of endogenous APC also achieved the same result (Alabanza et al., 2013). Based on this apparent contradiction, the goals of the current study were to clarify the therapeutic potential of APC in the chronic progressive form of EAE, and to determine mechanistically how APC mediates its protective effects. The main findings from our studies were as follows: (1) APC suppressed the progression of EAE, both at the clinical and pathological level, resulting in reduced levels of leukocyte infiltration and concomitant protection against loss of myelin, (2) while APC had no effect on angiogenic remodeling in the EAE model, it prevented loss of vascular integrity which was concomitant with maintained endothelial expression of the tight junction protein ZO-1, and (3) APC suppressed microglial activation both *in vivo* and *in vitro*. These findings build on the work of others in demonstrating strong therapeutic potential for APC in the treatment of inflammatory demyelinating disease and suggest that enhancement of vascular integrity and suppression of microglial activation may be important mediators of this protection.

The Impact of APC on Vascular Protection

One of the major findings of our study was that APC significantly reduced the extent of vascular breakdown in the EAE model, as shown by reduced degree of fibrinogen leak into the parenchyma and suppression of MECA-32 induction on endothelial cells. These findings support the work of others who have demonstrated that APC is vasculoprotective in animal models of ischemic stroke and sepsis (Mosnier and Griffin, 2007; Mosnier et al., 2007; Schuepbach et al., 2009), as well as in cell culture models of human endothelial cell monolayers (Feistritzer and Riewald, 2005; Finigan et al., 2005). Recent work has shed light on the signaling mechanisms underpinning APC's vasculoprotective influence by revealing that APC promoted vascular integrity of an endothelial monolayer *in vitro* and that infusion of APC enhanced vascular barrier integrity in a sepsis model in wild-type mice but not in transgenic mice deficient in protease activated receptor-1 (PAR-1) mice (Schuepbach et al., 2009). In future studies we plan to examine whether APC's protective influence on EAE disease progression is lost in PAR-1 KO mice.

Based on our previous findings that during the pre-symptomatic phase of EAE, a marked vascular remodeling response occurs (Boroujerdi et al., 2013), and that APC plays a key role in mediating cerebrovascular remodeling in response to chronic mild hypoxia (Burnier et al., 2016), we wondered if the protective effect of APC in EAE might, in part, be the result of upregulated fibronectin-α5β1 integrin signaling driving an enhanced angiogenic response. However surprisingly, APC-treated mice showed no appreciable differences in their vascular expression of fibronectin or α5β1 integrin or their overall level of vascularity, compared to vehicle-treated control mice. One possibility is that because such a strong vascular remodeling response occurs during the development of EAE (Boroujerdi et al., 2013), perhaps vascular remodeling is running at near-maximal level, precluding further enhancement of this process.

The Impact of APC on Microglial Activation

Another important finding of our study was that APC suppressed microglial activation both *in vivo* and *in vitro*. Once stimulated, microglia are activated into migratory phagocytic cells that orchestrate the influx of infiltrating leukocytes via cytokine and chemokine communication (Hanisch and Kettenmann, 2007). However if persistently activated, microglia induce excessive tissue damage, and the current consensus is that microglia play a critical role both in the initiation and maintenance of MS pathogenesis (Ransohoff, 1999; Trapp et al., 1999). Our observation that APC suppresses microglial activation *in vivo* suggests two possibilities; either APC is directly suppressing microglial activation *per se*, or this is an indirect consequence of APC reducing BBB breakdown, resulting in less influx of microglial-activating factors such as fibrinogen, fibronectin or vitronectin (Adams et al., 2007; Milner et al., 2007), or via activation of other CNS cell types, such as astrocytes. Interestingly, while the increase in total GFAP levels induced by EAE disease were not affected by APC, we did observe some localized differences in GFAP expression and organization in APC treated mice, suggesting that the impact on APC on glial cells in the CNS might not be entirely microglial-selective. While it is hard to determine whether APCs effects on microglial suppression *in vivo* are primary or secondary, our *in vitro* studies demonstrated that APC directly suppressed microglial activation because it promoted morphological transformation of microglia from the classic activated amoeboid morphology into the ramified form, typical of quiescent microglia, and also suppressed expression of the pro-inflammatory protease MMP-9. These data are consistent with previous findings that APC suppressed microglial activation in an animal model of amyotrophic lateral sclerosis (ALS), a protective effect that was shown to correlate with downregulation of superoxide dismutase-1 (SOD-1) in both microglial cells and neurons (Zhong et al., 2009). Taken together, our findings demonstrate that APC directly suppress microglial activation, though it does not exclude the possibility that some

of the anti-inflammatory actions of APC seen in the EAE model *in vivo* may also be secondary to other effects, such as prevention of BBB disruption.

CONCLUSION

The goals of this study were to evaluate the therapeutic potential of APC in the chronic progressive form of EAE and determine mechanistically how APC mediates protection. We found that APC suppressed the clinical progression of EAE, both at the clinical and pathological level, resulting in reduced levels of leukocyte infiltration and concomitant demyelination. IF analysis revealed that APC reduced vascular breakdown which was associated with maintained endothelial expression of the tight junction protein ZO-1. In addition, APC suppressed microglial activation both *in vivo* and *in vitro*. These findings build on the work of others in demonstrating strong therapeutic potential for APC in the treatment of inflammatory demyelinating disease and suggest that enhancement of vascular integrity and suppression of microglial activation are key mediators of this protection.

DATA AVAILABILITY STATEMENT

The datasets generated for this study are available on request to the corresponding author.

ETHICS STATEMENT

The studies described have been reviewed and approved by The Scripps Research Institute Institutional Animal Care and Use Committee.

AUTHOR CONTRIBUTIONS

RK and SH performed the EAE studies, analyzed clinical EAE progression, and performed the histological analysis. JF and JG provided the APC used in this study. RM established the microglial cell cultures and performed the gel zymography. RM and JG conceived of the study and drafted the manuscript. All authors read and approved the final manuscript.

FUNDING

This work was supported by the NIH R21 grant NS096524 (RM) and RO1 HL052246 and RO1 HL142975 (JG).

SUPPLEMENTARY MATERIAL

The Supplementary Material for this article can be found online at: https://www.frontiersin.org/articles/10.3389/fnins.2020.00333/full#supplementary-material

REFERENCES

Adams, R. A., Bauer, J., Flick, M. J., Sikorski, S. L., Nuriel, T., Lassmann, H., et al. (2007). The fibrin-derived Gamma377-395 peptide inhibits microglia activation and suppresses relapsing paralysis in central nervous system autoimmune disease. *J. Exp. Med.* 204, 571–582. doi: 10.1084/jem.20061931

Alabanza, L. M., Esmon, N. L., Esmon, C. T., and Bynoe, M. S. (2013). Inhibition of endogenous activated Protein C attenuates experimental autoimmune encephalomyelitis by inducing Myeloid-derived suppressor cells. *J. Immunol.* 191, 3764–3777. doi: 10.4049/jimmunol.1202556

Ballabh, P., Braun, A., and Nedergaard, M. (2004). The blood-brain barrier: an overview. structure, regulation and clinical implications. *Neurobiol. Dis.* 16, 1–13.

Bennett, J., Basivreddy, J., Kollar, A., Biron, K. E., Reickmann, P., Jefferies, W. A., et al. (2010). Blood-brain barrier disruption and enhanced vascular permeability in the multiple sclerosis model eae. *J. Neuroimmunol.* 229, 180–191. doi: 10.1016/j.jneuroim.2010.08.011

Boroujerdi, A., Welser-Alves, J., and Milner, R. (2013). Extensive vascular remodeling in the spinal cord of pre-symptomatic experimental autoimmune encephalomyelitis mice. increased vessel expression of fibronectin and the A5β1 integrin. *Exp. Neurol.* 250, 43–51. doi: 10.1016/j.expneurol.2013.09.009

Burnier, L., Boroujerdi, A., Fernandez, J. A., Welser-Alves, J., Griffin, J. H., and Milner, R. (2016). Physiological cerebrovascular remodeling in response to chronic mild Hypoxia: a role for activated protein C. *Exp. Neurol.* 283, 396–403. doi: 10.1016/j.expneurol.2016.07.004

Cheng, T., Liu, D., Griffin, J. H., Fernandez, J. A., Castellino, F., Rosen, E. D., et al. (2003). Activated protein C Blocks P53-mediated apoptosis in ischemic human brain endothelium and is neuroprotective. *Nat. Med.* 9, 338–342. doi: 10.1038/nm826

Crocker, S. J., Frausto, R. F., Whitton, J. L., and Milner, R. (2008). A novel method to establish microglia-free astrocyte cultures: comparison of matrix metalloproteinase expression profiles in pure cultures of Astrocytes and Microglia. *Glia* 56, 1187–1198. doi: 10.1002/glia.20689

Crocker, S. J., Whitmire, J. K., Frausto, R. F., Chertboonmuang, P., Soloway, P. D., Whitton, J. L., et al. (2006). Persistent macrophage/microglial activation and myelin disruption after experimental autoimmune encephalomyelitis in tissue inhibitor of Metalloproteinase-1-Deficient mice. *Am. J. Pathol.* 169, 2104–2116. doi: 10.2353/ajpath.2006.060626

Doshi, A., and Chataway, J. (2017). Multiple sclerosis, a treatable disease. *Clin. Med.* 17, 530–536. doi: 10.7861/clinmedicine.17-6-530

Engelhardt, B., Conley, F. K., and Butcher, E. C. (1994). Cell adhesion molecules on vessels during neuroinflammation in the mouse central nervous system. *J. Neuroimmunol.* 51, 199–208. doi: 10.1016/0165-5728(94)90082-5

Errede, M., Girolamo, F., Ferrara, G., Stripploi, M., Morando, S., Boldrin, V., et al. (2012). Blood-brain barrier alterations in the cerebral cortex in experimental autoimmune Encephalomyelitis. *J. Neuropath. Exp. Neurol.* 71, 840–854. doi: 10.1097/nen.0b013e31826ac110

Esmon, C. T. (2012). Protein C anticoagulant system–anti-inflammatory effects. *Semin. Immunopathol.* 34, 127–132. doi: 10.1007/s00281-011-0284-6

Feistritzer, C., and Riewald, M. (2005). Endothelial barrier protection by activated protein C through Par1-dependent Sphingosine 1-Phosphate Receptor-1 Crossactivation. *Blood* 105, 3178–3184. doi: 10.1182/blood-2004-10-3985

Fernandez, J. A., Xu, X., Liu, D., Zlokovic, B. V., and Griffin, J. H. (2005). Recombinant murine-activated protein C is neuroprotective in a murine ischemic stroke model. *Blood Cells Mol. Dis.* 30, 271–276. doi: 10.1016/s1079-9796(03)00034-2

ffrench-Constant, C. (1994). Pathogenesis of multiple sclerosis. *Lancet* 343, 271–275.

Finigan, J. H., Dudek, S. M., Singleton, P. A., Chiang, E. T., Jacobson, J. R., Camp, S. M., et al. (2005). Activated protein C mediates novel lung endothelial barrier enhancement: role of Sphingosine 1-Phosphate receptor transavtivation. *J. Biol. Chem.* 280, 17286–17293. doi: 10.1074/jbc.m412427200

Gay, D., and Esiri, M. (1991). Blood-brain barrier damage in acute multiple sclerosis plaques. *Brain* 114, 557–572. doi: 10.1093/brain/114.1.557

Guo, H., Liu, D., Gelbard, H., Cheng, T., Insalaco, R., Fernandez, J. A., et al. (2004). Activated protein C prevents neuronal apoptosis via protease activated receptors 1 and 3. *Neuron* 41, 563–572. doi: 10.1016/s0896-6273(04)00019-4

Guo, H., Singh, I., Wang, Y., Deane, R., Barrett, T., Fernandez, J. A., et al. (2009). Neuroprotective activities of activated protein c mutant with reduced anticoagulant activity. *Eur. J. Neurosci.* 29, 1119–1130. doi: 10.1111/j.1460-9568.2009.06664.x

Guo, H., Zhao, Z., Yang, Q., Wang, M., Bell, R. D., Wang, S., et al. (2013). An activated protein C analog stimulates neuronal production by human neural progenitor cells via a Par1-Par3-S1pr1-Akt pathway. *J. Neurosci.* 33, 6181–6190. doi: 10.1523/JNEUROSCI.4491-12.2013

Hallman, R., Mayer, D. N., Berg, E. L., Broermann, R., and Butcher, E. C. (1995). Novel mouse endothelial cell surface marker is suppressed during differentiation of the blood brain barrier. *Dev. Dyn.* 202, 325–332. doi: 10.1002/aja.1002020402

Han, M. H., Hwang, S. I., Roy, D. B., Lundgren, D. H., Price, J. V., Ousman, S. S., et al. (2008). Proteomic analysis of active multiple sclerosis lesions reveals therapeutic targets. *Nature* 451, 1076–1081. doi: 10.1038/nature06559

Hanisch, U. K., and Kettenmann, H. (2007). Microglia: active sensor and versatile effector cells in the normal and pathologic brain. *Nat. Neurosci.* 10, 1387–1394. doi: 10.1038/nn1997

Heo, J. H., Lucero, J., Abumiya, T., Koziol, J. A., Copeland, B. R., and Del Zoppo, G. J. (1999). Matrix metalloproteinases increase very early during experimental focal cerebral ischemia. *J. Cereb. Blood Flow Metab.* 19, 624–633. doi: 10.1097/00004647-199906000-00005

Huber, J. D., Egleton, R. D., and Davis, T. P. (2001). molecular physiology and pathophysiology of tight junctions in the blood-brain barrier. *Trends Neurosci.* 24, 719–725. doi: 10.1016/s0166-2236(00)02004-x

Joyce, D. E., Gelbert, L., Ciaccia, A., Dehoff, B., and Grinnell, B. W. (2001). Gene Expresion profile of antithrombotic protein C defines new mechansims modulating inflammation and apoptosis. *J. Biol. Chem.* 276, 11199–11203. doi: 10.1074/jbc.c100017200

Kauppinen, T. M., and Swanson, R. A. (2005). Poly (Adp-Ribose) Polymerase-1 promotes microglial activation, proliferation and matrix metalloproteinase-9-mediated neuron death. *J. Immunol.* 174, 2288–2296. doi: 10.4049/jimmunol.174.4.2288

Kirk, J., Plumb, J., Mirakhur, M., and Mcquaid, S. (2003). Tight junction abnormality in multiple sclerosis white matter affects all calibres of vessel and is associated with blood-brain barrier leakage and active demyelination. *J. Pathol.* 201, 319–327. doi: 10.1002/path.1434

Lassmann, H. (1998). "Multiple sclerosis pathology," in *McAlpine's Multiple Sclerosis*, 3rd Edn, ed. A. Compston (London: Churchill Livingstone), 323–358.

Li, L., Liu, F., Welser-Alves, J. V., Mccullough, L. D., and Milner, R. (2012). Upregulation of fibronectin and the A5β1 and Avβ3 integrins on blood vessels within the cerebral ischemic penumbra. *Exp. Neurol.* 233, 283–291. doi: 10.1016/j.expneurol.2011.10.017

Milner, R., and Campbell, I. L. (2002a). Cytokines regulate microglial adhesion to laminin and astrocyte extracellular matrix via protein kinase C-Dependent Activation of the A6β1 integrin. *J. Neurosci.* 22, 1562–1572. doi: 10.1523/jneurosci.22-05-01562.2002

Milner, R., and Campbell, I. L. (2002b). Developmental regulation of B1 integrins during angiogenesis in the central nervous system. *Mol. Cell Neurosci.* 20, 616–626. doi: 10.1006/mcne.2002.1151

Milner, R., Crocker, S. J., Hung, S., Wang, X., Frausto, R. F., and Del Zoppo, G. J. (2007). Fibronectin- and vitronectin-induced microglial activation and matrix Metalloproteinase-9 expression is mediated by integrins A5β1 and Avβ5. *J. Immunol.* 178, 8158–8167. doi: 10.4049/jimmunol.178.12.8158

Mosnier, L. O., Gale, A. J., Yegneswaran, S., and Griffin, J. H. (2004). Activated protein C variants with normal cytoprotective but reduced anticoagulant activity. *Blood* 104, 1740–1744. doi: 10.1182/blood-2004-01-0110

Mosnier, L. O., and Griffin, J. H. (2007). The cytoproective protein C pathway. *Blood* 109, 3161–3172.

Mosnier, L. O., Yang, X. V., and Griffin, J. H. (2007). Activated protein c mutant with minimal anticoagulant activity, normal cytoprotective activity, and preservation of thrombin activable fibrinolysis inhibitor-dependent cytoprotective functions. *J. Biol. Chem.* 282, 33022–33033. doi: 10.1074/jbc.m705824200

Petraglia, A. L., Marky, A. H., Walker, C., Thiyagarajam, M., and Zlokovic, B. V. (2010). Activated protein C is neuroprotective and mediates new blood vessel formation and neurogenesis after controlled cortical impact. *Neurosurgery* 66, 165–171. doi: 10.1227/01.NEU.0000363148.49779.68

Ransohoff, R. M. (1999). Mechanisms of inflammation in ms tissue: adhesion molecules and chemokines. *J. Neuroimmunol.* 98, 57–68. doi: 10.1016/s0165-5728(99)00082-x

Rezaie, A. R. (2011). The occupancy of endothelial protein c receptor by its ligand modulates the Par-1 dependent signaling specificity of coagulation proteases. *IUBMB Life* 63, 390–396. doi: 10.1002/iub.447

Roscoe, W. A., Welsh, M. E., Carter, D. E., and Karlik, S. J. (2009). Vegf and angiogenesis in acute and chronic Mog (35-55) peptide induced Eae. *J. Neuroimmunol.* 209, 6–15. doi: 10.1016/j.jneuroim.2009.01.009

Schuepbach, R. A., Feistritzer, C., Fernandez, J. A., Griffin, J. H., and Riewald, M. (2009). Protcetion of vascular barrier integrity by activated protein c in murine models depends on protease-activated Receptor-1. *Thromb. Haemost.* 101, 724–733. doi: 10.1160/th08-10-0632

Seabrook, T. J., Littlewood-Evans, A., Brinkmann, V., Pollinger, B., Schnell, C., and Hiestand, P. C. (2010). Angiogenesis is present in experimental autoimmune encephalomyelitis and pro-angiogenic factors are increased in multiple sclerosis lesions. *J. Neuroinflam.* 7:95. doi: 10.1186/1742-2094-7-95

Sparks, D. L., Kuo, Y. M., Roher, A., Martin, T., and Lukas, R. J. (2000). Alterations of Alzheimer's disease in the cholesterol-fed rabbit, including vascular inflammation. preliminary observations. *Ann. N. Y. Acad. Sci.* 903, 335–344. doi: 10.1111/j.1749-6632.2000.tb06384.x

Thiyagarajan, M., Fernandez, J. A., Lane, S. M., Griffin, J. H., and Zlokovic, B. V. (2008). Activated protein C promotes neovascularization and neurogenesis in postischemic brain via protease-activated receptor 1. *J. Neurosci.* 28, 12788–12797. doi: 10.1523/JNEUROSCI.3485-08.2008

Trapp, B. D., Bo, L., Mork, S., and Chang, A. (1999). Pathogenesis of tissue injury in Ms Lesions. *J. Neuroimmunol.* 98, 49–56. doi: 10.1016/s0165-5728(99)00081-8

Verbout, N. G., Yu, X., Healy, L. D., Philips, K. G., Tucker, E. I., Gruber, A., et al. (2015). Thrombin mutant W215a/E217a treatment improves neurological outcome and attenuates central nervous system damage in Experimental Autoimmune Encephalomyelitis. *Metab. Brain Dis.* 30, 57–65. doi: 10.1007/s11011-014-9558-8

Wang, Y., Zhao, Z., Chow, N., Ali, T., Griffin, J. H., and Zlokovic, B. V. (2013a). Activated protein C analog promotes neurogenesis and improves neurological outcome after focal ischemic stroke in mice via protease activated receptor 1. *Brain Res* 1507, 97–104. doi: 10.1016/j.brainres.2013.02.023

Wang, Y., Zhao, Z., Chow, N., Rajput, P. S., Griffin, J. H., Lyden, P. D., et al. (2013b). Activated protein C analog protects from ischemic stroke and extends the therapeutic window of Tissue-Type Plasminogen activator in aged female mice and hypertensive rats. *Stroke* 44, 3529–3536. doi: 10.1161/STROKEAHA.113.003350

Wingerchuk, D. M., and Carter, J. L. (2014). Multiple sclerosis: current and emerging disease-modifying therapies and treatment strategies. *Mayo Clin. Proc.* 89, 225–240. doi: 10.1016/j.mayocp.2013.11.002

Wolburg, H., and Lippoldt, A. (2002). Tight junctions of the Blood-Brain barrier; development, composition and regulation. *Vasc. Pharmacol.* 38, 323–337.

Wolter, J., Schild, L., Bock, F., Hellwig, A., Gadi, I., Al-Dabet, M. M., et al. (2016). Thrombodmodulin-dependent protein C activation is required for mitochondrial function and Myelination in the central nervous system. *J. Throm. Haem.* 14, 2212–2226. doi: 10.1111/jth.13494

Zhong, Z., Ilieva, H., Hallagan, L., Bell, R., Singh, I., Paquette, N., et al. (2009). Activated Protein C therapy slows als-like disease in mice by transcriptionally inhibiting sod1 in motor neurons and microglia cells. *J. Clin. Invest.* 119, 3437–3449. doi: 10.1172/JCI38476

Conflict of Interest: The authors declare that the research was conducted in the absence of any commercial or financial relationships that could be construed as a potential conflict of interest.

frontiers in Neuroscience

REVIEW
published: 05 June 2020
doi: 10.3389/fnins.2020.00522

Non-invasive Transcranial Electrical Stimulation in Movement Disorders

*Jacky Ganguly, Aditya Murgai, Soumya Sharma, Dorian Aur and Mandar Jog**

Movement Disorder Centre, London Health Sciences Centre, The University of Western Ontario, London, ON, Canada

Dysfunction within large-scale brain networks as the basis for movement disorders is an accepted hypothesis. The treatment options for restoring network function are limited. Non-invasive brain stimulation techniques such as repetitive transcranial magnetic stimulation are now being studied to modify the network. Transcranial electrical stimulation (tES) is also a portable, cost-effective, and non-invasive way of network modulation. Transcranial direct current stimulation and transcranial alternating current stimulation have been studied in Parkinson's disease, dystonia, tremor, and ataxia. Transcranial pulsed current stimulation and transcranial random noise stimulation are not yet studied enough. The literature in the use of these techniques is intriguing, yet many unanswered questions remain. In this review, we highlight the studies using these four potential tES techniques and their electrophysiological basis and consider the therapeutic implication in the field of movement disorders. The objectives are to consolidate the current literature, demonstrate that these methods are feasible, and encourage the application of such techniques in the near future.

Keywords: non-invasive brain stimulation (NIBS), transcranial electrical stimulation (tES), transcranial direct current stimulation (tDCS), transcranial alternating current stimulation (tACS), transcranial pulsed current stimulation (tPCS), transcranial random noise stimulation (tRNS)

OPEN ACCESS

Edited by:
Francesca Trojsi, University of Campania Luigi Vanvitelli, Italy

Reviewed by:
Andrea Pilotto, University of Brescia, Italy
Giovanni Di Pino, Campus Bio-Medico University, Italy

***Correspondence:**
Mandar Jog
Mandar.Jog@lhsc.on.ca

Specialty section:
This article was submitted to Neurodegeneration, a section of the journal Frontiers in Neuroscience

Received: *21 October 2019*
Accepted: *27 April 2020*
Published: *05 June 2020*

Citation:
Ganguly J, Murgai A, Sharma S, Aur D and Jog M (2020) Non-invasive Transcranial Electrical Stimulation in Movement Disorders. Front. Neurosci. 14:522. doi: 10.3389/fnins.2020.00522

INTRODUCTION

In movement disorders, non-invasive brain stimulation (NIBS) is an evolving therapeutic strategy. There is emerging evidence of network-level dysfunction in many neurological disorders. Movement disorders such as Parkinson's disease (PD) (de Schipper et al., 2018), dystonia (Schirinzi et al., 2018), tremor (Benito-León et al., 2015), and ataxia (Falcon et al., 2016; Wu et al., 2018) may fit very well within this construct of network dysfunction to explain the pathophysiology and phenotypes. This paradigm shift of suggesting that the movement disorders are a result of dysfunction in multilevel, interconnected complex cortico-subcortical network rather than only being restricted to the basal ganglia has opened the possibility of modifying that network non-invasively by delivering electromagnetic stimulation. In addition, such an approach extends the neurophysiological substrate of movement disorders beyond chemical dysfunction or intracellular mechanisms. The concept that transcranial stimulation modifies surface and deep brain electrical networks is not intuitive due to the obvious question of penetration of such currents through the scalp and bone. However, interestingly, the current literature is suggesting that NIBS can modulate the complexity of the neural network and alter neural excitability potentially in cortical and deep brain structures. Since movement disorders involve structures at all these levels to potentially generate a disease phenotype, the application of NIBS to these conditions may be of particular interest. This intriguing new technology can not only help us to understand the pathophysiology of the movement disorders with a newer outlook but also be a new armamentarium in our therapeutic strategy for these disorders.

Repetitive transcranial magnetic stimulation (rTMS) has been studied most extensively in this regard. It has been evaluated in PD, dystonia, essential tremor, Huntington's chorea, and chronic tic disorders like Tourette syndrome (Latorre et al., 2019). Four additional methods of NIBS, with transcranial electrical stimulation (tES), are also being evaluated as potential therapeutic options in neurodegenerative disorders—transcranial direct current stimulation (tDCS), transcranial alternating current stimulation (tACS), transcranial pulsed current stimulation (tPCS), and transcranial random noise stimulation (tRNS). The technique of tES involves the delivery of current to an individual's scalp usually *via* two sponge electrodes. The current penetrates the scalp and is conducted to the brain area of interest, where it can alter neuronal excitability. In tDCS, a constant direct current of 0.5–2 mA is delivered for around 20 min. Depending upon the parameters of the stimulation, rTMS and tDCS can increase or decrease cortical excitability and can cause neuroplastic effects. While low-frequency rTMS inhibits cortical neuronal activity, high-frequency rTMS facilitates cortical excitability. Similarly, anodal tDCS increases neuronal excitability by reducing the resting membrane threshold of cortical neurons, while cathodal tDCS decreases neuronal excitability. In contrast, tACS delivers a rhythmic current flow that can entrain pathological brain oscillations (Ingrid et al., 2014; Teo et al., 2017). In tACS, biphasic sinusoidal alternating current is used. However, in tPCS, unidirectional monophasic (although it can be bidirectional/biphasic) rectangular pulses of current are delivered. Thus, in tPCS, the stimulation is interrupted at regular intervals, defining the pulse duration, frequency, and inter-pulse intervals (IPI) of stimulation (Fitzgerald, 2014). Finally, tRNS uses an alternate current of random and constantly changing amplitude and frequency (Ingrid et al., 2014) (**Figure 1**).

This review highlights the application of tES specifically in movement disorders (**Table 1**). As the literature on tES is segregated, a heterogenous patient population has been studied, and diverse protocols have been followed (**Table 2**), it is difficult to write a systemic review. Despite that, we have searched for peer-reviewed articles using PubMed, BioMed Central, Cochrane Library, and ScienceDirect databases to consolidate the literature on the use of different modes of tES in the field of movement disorders. We have explained their electrophysiological basis and also highlighted the unmet needs for promoting tES as a new therapeutic intervention.

TRANSCRANIAL DIRECT CURRENT STIMULATION

Idiopathic Parkinson's Disease

(a) Effect on Gait and Balance

Studies have demonstrated the altered excitability of primary motor cortex (M1) in idiopathic PD patients. The low dopaminergic state of the basal ganglia may facilitate an adaptive beneficial increase of cortical excitability to compensate for the underactive pallido-thalamo-cortical drive. Enhancing the cortical excitability by tDCS may further increase this compensatory mechanism and improve motor function. Anodal tDCS may also induce dopamine release in the basal ganglia by the activation of glutamatergic corticostriatal fibers (Siebner et al., 1999; Fregni et al., 2006; Valentino et al., 2014). Studies have been done by targeting either the motor cortex (M1, 1–2 mA, 13–30 min) (Verheyden et al., 2013; Kaski et al., 2014b; Mak and Yu, 2014; Valentino et al., 2014; Costa-Ribeiro et al., 2016, 2017; Schabrun et al., 2016; Fernandez-Lago et al., 2017; da Silva et al., 2018; Yotnuengnit et al., 2018) or the dorsolateral prefrontal cortex (DLPFC, 2 mA, 7–20 min) (Manenti et al., 2014; Lattari et al., 2017). At post-stimulation, a short-term benefit in gait was noted in most of these studies.

The role of fronto-striatal circuits has been studied in freezing of gait (FOG) in PD (Lewis and Barker, 2009). The motor, the cognitive, and the limbic circuits all converge in common output nuclei globus pallidus interna/substantia nigra pars reticulata to disinhibit pedunculopontine nucleus for locomotion. In PD, there is impaired motor and cognitive processing in the cortico-striatal parallel circuits and the intra-striatal integrative circuits (Helmich et al., 2010; Alamos et al., 2019). During walking, patients with PD are more dependent on the DLPFC for cognitive control to compensate their deficit in locomotion, and more challenging walking like dual tasking needs more DLPFC activation (Maidan et al., 2016; Stuart et al., 2018). So, targeting multiple brain regions, like the prefrontal cortex along with the motor cortex, may provide better results for the gait of PD patients (Lee et al., 2019). Multitarget tDCS may reduce decoupling between the motor network and the cognitive network, improve connectivity between the prefrontal cortex, the motor cortex, and the subcortical structures and may also increase extra-striatal dopamine release (Dagan et al., 2018). Studies with multitargeting have been done with tDCS to the bilateral premotor cortex (PMC) and M1 (1 mA, 20 min) (Alizad et al., 2019), the bilateral PMC and M1 or the prefrontal cortex (PFC) separately (2 mA, 20 min) (Benninger et al., 2010), the bilateral DLPFC (2 mA, 20 min) (Swank et al., 2016; Criminger et al., 2018), the bilateral PFC separately (2 mA, 20 min) (Capecci et al., 2014), and M1 and the left DLPFC (20 min) (Dagan et al., 2018).

Postural imbalance and falls impair the quality of life of PD patients and increase the overall health cost burden. Anodal tDCS to the left DLPFC (2 mA, 20 min) has been noted to improve balance and functional mobility. The increased excitability of DLPFC may enhance visuo-spatial processing, which is responsible for improved balance and functional mobility (Lattari et al., 2017). The beneficial effect of DLPFC tDCS (2 mA, 7 min; two sessions—left and right DLPFC) in timed up and go task has also been observed in another study (Manenti et al., 2014). A single session of anodal tDCS (1.5 mA for 20 min) over the left DLPFC improved step length, stride velocity, and double support time during obstacle negotiation task (Putzolu et al., 2019).

With anodal tDCS to M1 (2 mA, 20 min) (Schabrun et al., 2016) or to bilateral DLPFC tDCS (left anodal, right cathodal; 2 mA, 20 min) (Swank et al., 2016), no significant benefit was noted in dual-task gait in PD, but tDCS has been shown to influence task prioritization on dual-task walking (Criminger

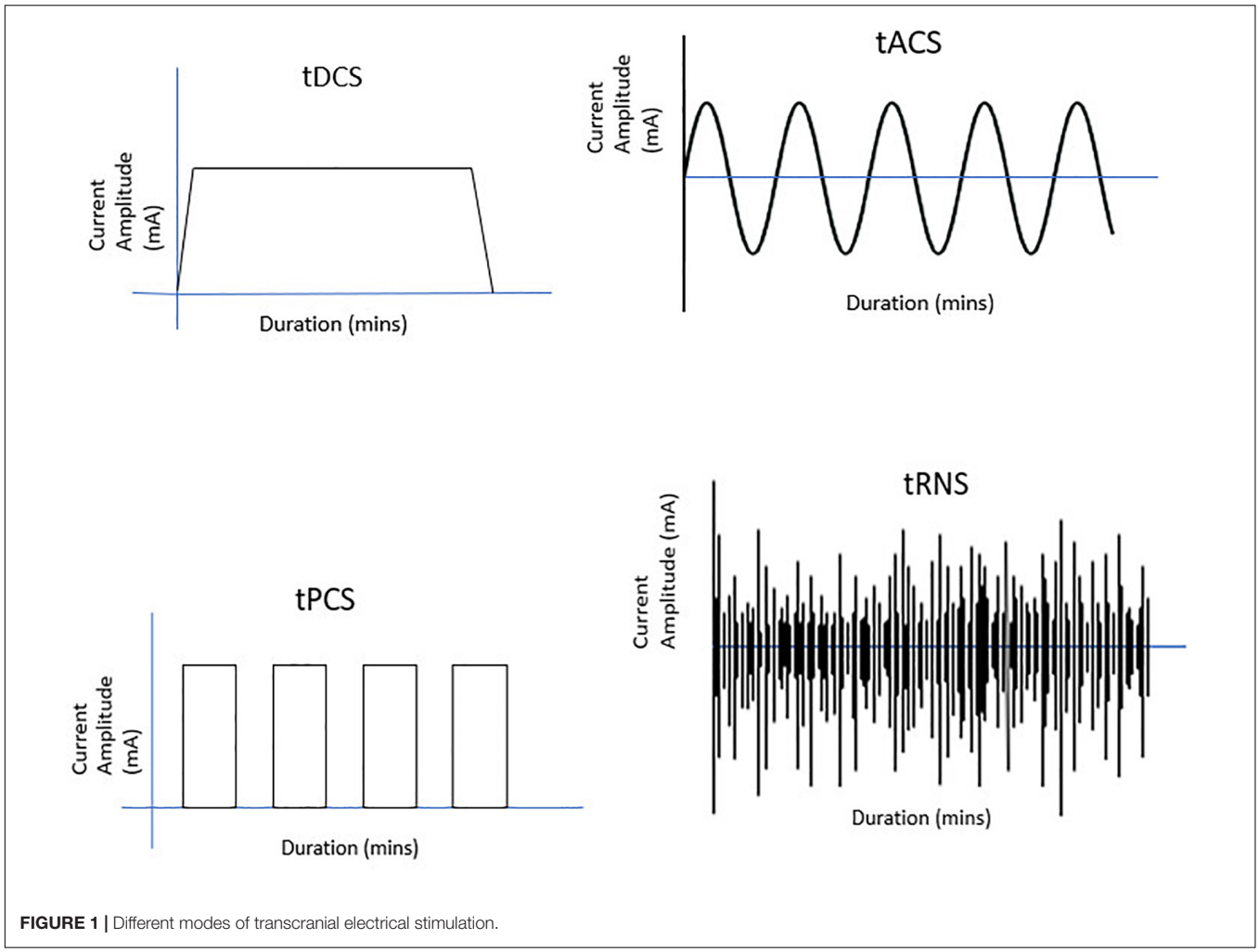

FIGURE 1 | Different modes of transcranial electrical stimulation.

et al., 2018). Anodal tDCS over the supplementary motor area (SMA, 2 mA, 13 min) prolonged the effects of cued gait training on functional mobility independent of dopaminergic medication state (Costa-Ribeiro et al., 2016).

A beneficial effect of combining tDCS (over primary motor and PMC, 2 mA, 15 min) with physical training has been demonstrated on gait velocity and balance. tDCS can lower the threshold of physical training to normalize cortical excitability in M1 (Valentino et al., 2014). A single case study showed the benefit of primary and PMC anodal tDCS on trunk peak velocity and average trunk sway during tango dancing (Kaski et al., 2014a). Combined sessions of exercise-based video gaming (exergaming) and anodal tDCS over M1 (2 mA, 20 min/session, two sessions/week for 12 weeks) improved the static and the dynamic balance in PD patients. Exercise combined with tDCS may help in motor learning and consolidation of long-term motor skill retention in PD patients (Harris et al., 2018).

(b) Effect on Upper Limb Motor Function

In PD, there is progressive involvement of upper limb function, mostly asymmetric to start with, manifested by impaired dexterity, abnormal force generation, and poor bimanual coordination (Ingvarsson et al., 1997; Ponsen et al., 2006; Vanbellingen et al., 2011). An improvement was noted in upper limb motor sequencing and finger tapping after anodal/cathodal tDCS over the more affected/less affected M1 (2 mA, 20 min), respectively, by Cosentino et al. (2017). On the contrary, Salimpour et al. (2015) noted an increase in force assignment to the more affected hand after bilateral tDCS with the cathode over the more affected hand and with the anode over the less affected M1 (2 mA, 25 min). A significant improvement in upper limb motor sequencing was also noted by Benninger et al. (2010) in multi-session anodal tDCS (8 sessions, 2 mA, 20 min) to bilateral M1/PMC or PFC that lasted during 3 months of follow-up. Stimulation to SMA (2 mA, 13 min) (Costa-Ribeiro et al., 2016) or DLPFC (10 sessions, 2 mA, 20 min) (Doruk et al., 2014) revealed no significant benefit.

Broeder et al. (2019) noted an increase in writing amplitude with anodal tDCS to M1 (1 mA, 20 min). Fregni et al. (2006) also noted some benefit in Purdue pegboard task with anodal tDCS to M1 (1 mA, 20 min), but other studies found no significant benefit in dexterity tasks with single- or multi-session tDCS to the fronto-polar area (five sessions, 1 mA, 15 min) (Ishikuro et al., 2018) or DLPFC (10 sessions, 2 mA, 20 min) (Doruk et al., 2014).

Upper limb reaction time improved with anodal tDCS to M1 (1 mA, 20 min) in the study by Fregni et al. (2006), but there was no significant change in reaction time noted in other studies with tDCS to M1 (nine sessions, 2 mA, 20 min) (Schabrun et al., 2016), bilateral M1 and PMC or bilateral PFC (eight sessions, 2 mA, 20 min) (Benninger et al., 2010), DLPFC (10 sessions, 2 mA, 20 min) (Doruk et al., 2014), and bilateral cerebellum (five sessions, 2 mA, 20 min) (Ferrucci et al., 2016).

Thus, the most improvement with M1 tDCS has been noted in simple motor tasks, but in complex task processing, tDCS may not be that beneficial. In complex tasks, where more cognitive load is there along with motor manipulation, stimulating DLPFC along with M1 is more rational, but for a long-term effect, multisession tDCS is needed.

(c) Effect on Cognition

Cognitive dysfunction is one of the most common non-motor symptoms in PD patients. Dysfunction in frontostriatal circuitry involving DLPFC and dorsal caudate, due to dopaminergic depletion, is mainly responsible for the executive dysfunction in PD (de la Fuente-Fernández, 2012). tDCS to the left dorsolateral prefrontal cortex (LDLPFC) has shown an improvement in working memory performance by enhancing the local cortical excitability. A beneficial effect of anodal tDCS has been noted in both, during the task (online effect, 2 mA, 20 min, to the left DLPFC) (Boggio et al., 2006) and after the task (offline effect, 2mA, 20 min to left/right DLPFC) (Doruk et al., 2014). While the online effects of tDCS are due to changes in polarization in neural membranes, the offline effects are related to long-term potentiation, long-term depression, and thus long-term synaptic plasticity (Nitsche et al., 2005).

In patients with Parkinson's disease dementia (PDD), a single session of anodal tDCS to the left DLPFC (current density of 0.08 mA/cm^2 for 20 min) failed to show any benefit in attentional tasks. Multiple stimulation sessions are likely needed to modify complex attentional network in PDD (Elder et al., 2017).

A beneficial effect of tDCS to LDLPFC (1.5–2 mA, 20 min/session, 1–4 days/week for 4 weeks) has been noted in PD with mild cognitive impairment (PD-MCI), with concurrent cognitive training (Biundo et al., 2015; Lawrence et al., 2018) and physiotherapy (anodal tDCS, 2 mA for 25 min/session, five sessions/week for 2 weeks) (Manenti et al., 2016). In PD-MCI, tDCS over the medial frontal cortex (anode over Fpz, cathode between inion and oz, 1.5 mA for 6 min, current density 0.043 mA/cm^2) enhanced the Theory of Mind, i.e., the ability to understand and predict other people's behaviors as assessed by the Attribution of Intentions task (Adenzato et al., 2019).

(d) Effect on Impulsive Pathological Gambling Behavior

Pathological gambling is one of the major side effects of dopamine agonist therapy in PD patients. The dysfunction of the orbitofrontal-ventrostriatal circuitry is likely responsible for such a risky and impulsive behavior (Gatto and Aldinio, 2019). An improvement in decision making was noted in Iowa Gambling Task with cathodal tDCS over the right DLPFC (single session,

TABLE 1 | Summary on the use of transcranial electrical stimulation (tES) in movement disorders.

Mode of tES	Used in
Transcranial direct current stimulation	1. Parkinson's disease • Gait and balance (Benninger et al., 2010; Verheyden et al., 2013; Capecci et al., 2014; Kaski et al., 2014a; Mak and Yu, 2014; Manenti et al., 2014; Valentino et al., 2014; Costa-Ribeiro et al., 2016, 2017; Schabrun et al., 2016; Swank et al., 2016; Fernandez-Lago et al., 2017; Lattari et al., 2017; Criminger et al., 2018; da Silva et al., 2018; Dagan et al., 2018; Harris et al., 2018; Yotnuengnit et al., 2018; Alizad et al., 2019; Putzolu et al., 2019) • Upper limb function (Fregni et al., 2006; Benninger et al., 2010; Doruk et al., 2014; Salimpour et al., 2015; Costa-Ribeiro et al., 2016; Ferrucci et al., 2016; Schabrun et al., 2016; Cosentino et al., 2017; Ishikuro et al., 2018; Broeder et al., 2019) • Cognition (Nitsche et al., 2005; Boggio et al., 2006; Biundo et al., 2015; Manenti et al., 2016; Elder et al., 2017; Lawrence et al., 2018; Adenzato et al., 2019) • Impulsive pathological gambling behavior (Benussi et al., 2017a) • Speech (Pereira et al., 2013) • Sleep (Hadoush et al., 2018) • Fatigue (Forogh et al., 2017) • Dyskinesia (Kishore and Popa, 2014) 2. Multisystem atrophy-Parkinsonian type (motor disability and bradykinesia) (Alexoudi et al., 2018) 3. Corticobasal syndrome (language) (Manenti et al., 2015) 4. Progressive supranuclear palsy (language) (Madden et al., 2019; Valero-Cabré et al., 2019; Cotelli et al., 2020; de Aguiar et al., 2020) 5. Lewy body dementia (Elder et al., 2016, 2019) 6. Focal hand dystonia (Quartarone et al., 2005; Buttkus et al., 2010, 2011; Benninger et al., 2011; Furuya et al., 2014; Sadnicka et al., 2014; Bradnam et al., 2015; Rosset-Llobet et al., 2015; Marceglia et al., 2017) 7. Cervical dystonia (McCambridge and Bradnam, 2018; Summers et al., 2018) 8. Cerebellar ataxia (Grimaldi and Manto, 2013; Grimaldi et al., 2014b; Benussi et al., 2015, 2017b, 2018; Bodranghien et al., 2017; Hulst et al., 2017; John et al., 2017; Maas et al., 2019; Pilloni et al., 2019; Vavla et al., 2019) 9. Essential tremor (Gironell et al., 2014; Helvaci et al., 2016) 10. Orthostatic tremor (Lamy et al., 2018) 11. Huntington's disease (cognitive dysfunction) (Eddy et al., 2017)
Transcranial alternating current stimulation	1. Parkinson's disease (motor and cognitive) (Brittain et al., 2013; Krause et al., 2013; Del Felice et al., 2019) 2. Enhanced physiological tremor (Mehta et al., 2014; Ahmad et al., 2018) 3. Cervical dystonia (Zaghi et al., 2010; Angelakis et al., 2013)
Transcranial pulsed current stimulation	Parkinson's disease (gait and balance) (Alon et al., 2012)
Transcranial random noise stimulation	Parkinson's disease (cognition) and multisystem atrophy-Parkinsonian type (autonomic dysfunction) (Yamamoto et al., 2005)

TABLE 2 | Summary on the studies of transcranial electrical stimulation in movement disorders along with the protocol used and the proposed electrophysiological basis of each of them.

Stimulation method	Proposed mechanism	Tested in	Beneficial effects seen with the protocol
Transcranial direct current stimulation	• Anodal transcranial direct current stimulation: 1. reduces the resting membrane threshold of cortical neurons, resulting in an increase in neuronal excitability 3. may induce dopamine release in the basal ganglia by activation of glutamatergic corticostriatal fibers • Cathodal transcranial direct current stimulation decreases the neuronal excitability.	1. Parkinson's disease • Gait and balance (Benninger et al., 2010; Verheyden et al., 2013; Capecci et al., 2014; Kaski et al., 2014a; Mak and Yu, 2014; Manenti et al., 2014; Valentino et al., 2014; Costa-Ribeiro et al., 2016, 2017; Schabrun et al., 2016; Swank et al., 2016; Fernandez-Lago et al., 2017; Lattari et al., 2017; Criminger et al., 2018; da Silva et al., 2018; Dagan et al., 2018; Harris et al., 2018; Yotnuengnit et al., 2018; Alizad et al., 2019; Putzolu et al., 2019)	• Anodal current of 1–2 mA for 7–20 min/session for two to five sessions over M1/left dorsolateral prefrontal cortex/combined, multitargeting; some with physiotherapy
		• Upper limb function (Fregni et al., 2006; Benninger et al., 2010; Doruk et al., 2014; Salimpour et al., 2015; Costa-Ribeiro et al., 2016; Ferrucci et al., 2016; Schabrun et al., 2016; Cosentino et al., 2017; Ishikuro et al., 2018; Broeder et al., 2019)	• Anodal transcranial direct current stimulation to M1/bilateral M1/premotor cortex or prefrontal cortex 1–2 mA current for 20–25 min, single/multiple sessions
		• Cognition (Nitsche et al., 2005; Boggio et al., 2006; Biundo et al., 2015; Manenti et al., 2016; Elder et al., 2017; Lawrence et al., 2018; Adenzato et al., 2019)	• Anodal current of 1–2 mA for 20–25 min/session for 10–16 sessions over the left dorsolateral prefrontal cortex
		• Impulsive pathological gambling behavior (Benussi et al., 2017a)	• Cathodal transcranial direct current stimulation over the right dorsolateral prefrontal cortex (single session, 2 mA for 10 min starting 2 min before and covering all of the task, current density 0.057 mA/cm^2)
		• Speech (Pereira et al., 2013)	• Increased connectivity in verbal fluency network by anodal transcranial direct current stimulation to the left dorsolateral prefrontal cortex (2 mA, 20 min)
		• Sleep (Hadoush et al., 2018)	• Bilateral anodal transcranial direct current stimulation simultaneously over the left and the right prefrontal and motor areas (10 sessions, 20 min each, five per week)
		• Fatigue (Forogh et al., 2017)	• Left anodal and right cathodal current of 0.06 mA/cm^2 to dorsolateral prefrontal cortex for 20 min/session for eight sessions
		• Dyskinesia (Kishore and Popa, 2014)	• Anodal current of 2 mA to cerebellum and M1 for 20 min/session for five sessions
		2. Multisystem atrophy-Parkinsonian type (motor disability and bradykinesia) (Alexoudi et al., 2018)	• Anodal current of 2 mA to M1 and premotor cortex for 30 min/session for 10 sessions
		3. Corticobasal syndrome (language) (Manenti et al., 2015)	• Anodal current of 2 mA to the left parietal cortex for 7 min, single session
		4. Progressive supranuclear palsy (language) (Madden et al., 2019; Valero-Cabré et al., 2019; Cotelli et al., 2020; de Aguiar et al., 2020)	• Anodal current of 1.5 mA to the left dorsolateral prefrontal cortex or cathodal current to the right dorsolateral prefrontal cortex for 20 min for one to four sessions
		5. Lewy body dementia (Elder et al., 2016, 2019)	• Improvement in attentional tasks noted with anodal transcranial direct current stimulation over the left dorsolateral prefrontal cortex (single 20-min session)
		6. Focal hand dystonia (Quartarone et al., 2005; Buttkus et al., 2010, 2011; Benninger et al., 2011; Furuya et al., 2014; Sadnicka et al., 2014; Bradnam et al., 2015; Rosset-Llobet et al., 2015; Marceglia et al., 2017)	• Cathodal current to bilateral M1-premotor cortex/anodal current to cerebellum/cathodal current to affected motor cortex and anodal to unaffected/cathodal current to left parietal cortex and anodal current to right parietal cortex; 2 mA current for 20–24 min/session for 5 to 10 sessions
		7. Cervical dystonia (McCambridge and Bradnam, 2018; Summers et al., 2018)	• Insufficient data; ongoing studies with anodal current to the cerebellum

(Continued)

TABLE 2 | Continued

Stimulation method	Proposed mechanism	Tested in	Beneficial effects seen with the protocol
		8. Cerebellar ataxia (Grimaldi and Manto, 2013; Grimaldi et al., 2014b; Benussi et al., 2015, 2017b, 2018; Bodranghien et al., 2017; Hulst et al., 2017; John et al., 2017; Maas et al., 2019; Pilloni et al., 2019; Vavla et al., 2019)	• Anodal current of 1–2 mA to the cerebellum/cerebellum and motor cortex for 20 min, single or multiple sessions; anodal cerebellar and cathodal spinal stimulation for 2 weeks; some combined with physiotherapy
		9. Essential tremor (Gironell et al., 2014; Helvaci et al., 2016)	• Anodal current of 2 mA to dorsolateral prefrontal cortex and cathodal current to cerebellum for 20 min/session for 15 sessions
		10. Orthostatic tremor (Lamy et al., 2018)	• Single session of anodal trans-spinal transcranial direct current stimulation (at the 11th thoracic vertebra level, 2.5 mA, 20 min)
		11. Huntington's disease (cognitive dysfunction) (Eddy et al., 2017)	• Single session of anodal transcranial direct current stimulation (1.5 mA, 15 min) over the left dorsolateral prefrontal cortex combined with cognitive training
Transcranial alternating current stimulation	Interact with or even entrain spontaneous brain oscillations in a frequency-specific manner	1. Parkinson's disease (Brittain et al., 2013; Krause et al., 2013; Del Felice et al., 2019)	• Phase-locked stimulation/in 10–20 Hz frequency/according to the higher power spectra band in the electroencephalograph/stimulation for 15 min over M1/chronic stimulation for 2 weeks
		2. Enhanced physiological tremor (Mehta et al., 2014; Ahmad et al., 2018)	• At peak tremor frequency over M1
		3. Cervical dystonia (Zaghi et al., 2010; Angelakis et al., 2013)	• Cathodal transcranial direct current stimulation (1.5 mA, 15 min, five sessions) followed by transcranial alternating current stimulation (two sessions of 15 min stimulation with 1.5 mA at 5–15 Hz and subsequently five daily sessions of 20 min each with 1.5 mA at 15 Hz)
Transcranial pulsed current stimulation	• Tonic effect due to induced net direct current component. Neuronal excitability is modified by tonic depolarization of the resting membrane potential. • Phasic effects by the on/off nature of pulsatile currents	Parkinson's disease (gait and balance) (Alon et al., 2012)	• Anodal current over M1 with monophasic (unidirectional) waveform with pulse duration of 33.3 μs and an interpulse interval of 33.3 μs
Transcranial random noise stimulation	• Boosting synaptic signals, stochastic resonance, inducing long-term potentiation *via* modifying *N*-methyl-D-aspartate receptor efficacy, activation of sodium channels, neuroplasticity effects • Can possibly interfere with ongoing oscillations	Parkinson's disease (cognition) and multisystem atrophy-Parkinsonian type (autonomic dysfunction) (Yamamoto et al., 2005)	• Noisy current alternating in duration and frequency over M1 (for Parkinson's disease), over mastoid (galvanic stimulation for autonomic dysfunction in multisystem atrophy-Parkinsonian type)

2 mA for 10 min, starting 2 min before and covering all of the tasks, current density 0.057 mA/cm^2). Cathodal tDCS over the right DLPFC likely reduced the pathological overdrive in frontostriatal circuitry (Benussi et al., 2017a).

(e) Effect on Speech

Parkinson's disease is associated with deficits in phonemic and semantic fluency due to frontal and temporal lobar dysfunction. Modulation of verbal and phonemic fluency was noted by

anodal tDCS to the left DLPFC (2 mA, 20 min) compared to the left temporo-parietal cortex. DLPFC tDCS increased the functional connectivity in verbal fluency networks involving frontal, parietal, and fusiform areas (Pereira et al., 2013).

(f) Effect on Sleep, Fatigue, and Daytime Sleepiness

Sleep disturbance is a common non-motor symptom in patients with PD, adversely affecting their overall quality of life and promoting neuropsychiatric complications like depression (Kay et al., 2018). Bilateral anodal tDCS simultaneously over the left and the right prefrontal and motor areas (10 sessions, 20 min each, five sessions per week) improved their Pittsburgh Sleep Quality Index total score, sleep latency sub-score, Geriatric Depression Scale total score, and physical and mental component scores of the health-related quality-of-life questionnaire (SF-36) (Hadoush et al., 2018).

A beneficial effect of bilateral DLPFC tDCS (eight sessions, 0.06 mA/cm^2 current, 20 min/session) on fatigue in PD patients, using left anodal and right cathodal stimulation, has been shown by Forogh et al. (2017) when combined with occupational therapy. No significant effect was seen on daytime sleepiness. The effect on fatigue could have been due to an improvement in mood and depressive symptoms.

(g) Effect on Dyskinesia

An involvement of the cerebello-thalamo-cortical circuit and its aberrant plasticity has been noted in L-dopa-induced dyskinesia (LID) (Yoo et al., 2019). An improvement in LID has been shown with a combined effect of increased cerebellar inhibition (CBI) by cerebellar anodal tDCS (2 mA for 20 min/day for five consecutive days) and modulation of motor cortical excitability by M1 tDCS (Ferrucci et al., 2016). Cerebellar stimulation may help in restoring the cerebellar and the basal ganglionic control over the non-salient inputs to the motor areas during pulsatile dopaminergic surges (Kishore and Popa, 2014).

So, there is a huge scope of exploring tDCS in PD. Even with the best use of dopaminergic drugs, symptoms like FOG, non-motor symptoms, and drug-induced dyskinesia are difficult to manage. tDCS is affordable, portable, cost-effective, and well tolerated. The unmet need is to have a clearer idea of the site of stimulation (M1/DLPFC/cerebellum) and the necessary parameters of stimulation (intensity, duration) from rigorous blinded studies in larger datasets.

Parkinson's Plus Syndromes

Parkinson's plus syndromes unlike idiopathic PD do not respond well to levodopa. Evaluating a new therapeutic intervention, such as NIBS, is worthwhile to provide some symptomatic benefit in these disabling disorders.

A lasting beneficial effect on walking speed and leg bradykinesia was noted with anodal tDCS to the motor and the pre-motor cortex (2 mA, 30 min, in 10 sessions over 2 weeks) in a patient with multisystem atrophy-Parkinsonian type (MSA-P) (Alexoudi et al., 2018).

The effect of anodal tDCS over the bilateral parietal cortex on naming performance was evaluated in corticobasal syndrome (CBS) with linguistic deficits. A shortening of action naming latency was observed only after anodal stimulation over the left parietal cortex (Manenti et al., 2015).

Anodal tDCS over the left DLPFC (in four sessions) was used to improve non-fluent aphasia in the case of progressive supranuclear palsy (PSP). An improved performance was seen in phonemic fluency, action naming, and speech production (Madden et al., 2019). Recently, tDCS has been further explored on language processing in PSP by its ability to modulate prefrontal brain networks. Valero-Cabré et al. (2019) has shown a short-term improvement of semantic (category judgment) and lexical (letter fluency) skills by a single session of right cathodal tDCS and left anodal tDCS to the DLPFC, respectively. A combined effect of tDCS and language training has improved naming performance in primary progressive aphasia (PPA) (Cotelli et al., 2020). In PPA, the brain volumes of specific anatomic areas influenced the beneficial effect of anodal tDCS over the left inferior frontal gyrus when combined with written naming/spelling therapy (de Aguiar et al., 2020).

In Lewy body dementia (LBD), an improvement in attentional tasks (choice reaction time and digit vigilance) was noted with anodal tDCS over the left DLPFC (single 20-min session, 0.08 mA/cm^2), but not in visuoperceptual task performance (Elder et al., 2016). Repeated consecutive sessions (two consecutive 20-min sessions, 0.048 mA/cm^2, for 5 days) of parietal anodal tDCS and occipital cathodal tDCS failed to improve visual hallucination, visuoperceptual function, or occipital cortex excitability in LBD (Elder et al., 2019).

Presently, PD plus syndromes are difficult to manage. Neither dopaminergic drugs nor deep brain stimulation (DBS) is a useful option. Data using non-invasive stimulation methods for treatment are minimal. Collaborative studies using standardized protocols are now needed to explore these options.

Dystonia

The excessive and inappropriate muscle activation patterns in dystonia reflect the disinhibition of cortical–subcortical motor circuits, which is a consequence of abnormal sensorimotor integration and maladaptive plasticity (Hallett, 2006). A deficiency in short intracortical inhibition, likely a GABAergic effect, has been demonstrated in some studies, with paired-pulse stimulation (Hallett, 2011). Thus, the down-regulation of cortical excitability by cathodal tDCS seems to be a good therapeutic option in dystonia.

Beneficial effects were noted with bilateral cathodal tDCS (2 mA, 20 min/day for five consecutive days) over the motor–premotor cortex in musicians with focal hand dystonia. Bilateral cathodal tDCS could have downregulated the cortical excitability responsible for excessive excitation and near-synchronous co-contractions of agonists and antagonists (Marceglia et al., 2017).

The cerebellum has been another target for modulation in dystonia due to its inhibitory effect over the motor cortex. Anodal tDCS over the cerebellar hemispheres (2 mA, 20 min) has been shown to reduce the average pen pressure and modify the mean stroke frequency during handwriting and fast cyclic drawing in patients with focal hand dystonia

(Bradnam et al., 2015). There are also some studies of cerebellar anodal tDCS in cervical dystonia (CD), but with insufficient data for therapeutic use (McCambridge and Bradnam, 2018; Summers et al., 2018).

On the contrary, some studies have shown no benefit of tDCS in dystonia. The permanent maladaptive plasticity in chronic dystonia may be responsible for the irreversible changes and loss of efficacy of tDCS (Quartarone et al., 2005).

A study by Benninger et al. (2011) of the contralateral primary motor cortex cathodal stimulation (2 mA, 20 min, three sessions within 1 week) in writer's cramp patients failed to show any improvement. When anodal cerebellar tDCS (ctDCS; 2 mA, 15 min) was tried simultaneously with paired associative stimulation *via* transcranial magnetic stimulation (TMS) in patients with writing dystonia/writers' cramp, the clinical symptoms were unchanged (Sadnicka et al., 2014).

Combining tDCS with neurorehabilitation is another approach. tDCS may prime the central somatosensory pathways, promote their plasticity, and facilitate surrounding inhibition in the hyperactive areas, rendering them more responsive to neurorehabilitation.

When tDCS to bilateral motor cortices (cathodal to affected cortex, anodal to unaffected cortex; 2 mA, 24 min) was tried in pianists with focal dystonia, improvement was seen in the rhythmic accuracy of sequential finger movements only when concurrent motor training was done. Fine motor control of the hand affected by focal dystonia can thus be improved by (i) facilitation of the transcallosal inhibitory input into the affected cortex by activating the unaffected motor cortex by anodal stimulation and (ii) suppression of abnormal hyperactivity in the affected motor cortex by cathodal stimulation (Furuya et al., 2014).

In a study on musician's focal dystonia, retraining with slow, voluntarily controlled movements on the piano was combined with tDCS (2 mA, 20 min) to contralateral primary motor cortex (C3). No beneficial effect was noted with single-session tDCS. However, a single retraining session of 20 min with tDCS may not be sufficient to modify the sensorimotor learning of a highly skilled task like in musician's dystonia (Buttkus et al., 2011). In another similar study by the same group, some improvement was seen in one of the 10 patients with atypical arm dystonia rather than focal hand dystonia (Buttkus et al., 2010).

A significant improvement in dystonia severity score was noted with a 2-week combined therapy of neurorehabilitation by sensory motor retuning (SMR) and biparietal tDCS (cathode over the left and anode over the right; 2 mA for 20 min/session for the first 30 min of the 1-h daily SMR session) (Rosset-Llobet et al., 2015).

In summary, tDCS by itself or in combination with rehabilitation therapy can be an effective way to modulate the dysfunctional network of dystonia. Cathodal stimulation seems more rational. Parameters like site of stimulation (M1/SMA/cerebellum), duration, and sustainability of stimulation are to be evaluated in further research. Unlike Parkinsonian syndromes, dystonia can be focal or generalized. It is likely that the site of stimulation and the effects would be substantially different in focal *versus* generalized dystonia. A careful mapping of these abnormalities to differentiate the syndromes physiologically would be required.

Cerebellar Ataxia

Cerebellar tDCS can modulate the excitability of Purkinje cells in the cerebellar cortex and hence modify the cerebellar output *via* the cerebello-thalamo-cortical pathway. A polarity-specific effect has been shown in different studies. Anodal ctDCS increases the excitability of Purkinje cells of the cerebellar cortex, augmenting the inhibitory effects of the cerebellar cortex on the deep cerebellar nuclei and, hence, reducing the cerebello-thalamic facilitatory drive to the cortical areas (Grimaldi et al., 2014a, 2016; Maas et al., 2020).

An initial study by Grimaldi and Manto (2013) failed to show any significant effect of cerebellar anodal tDCS on upper limb coordination and posture. However, anodal ctDCS (1 mA, 20 min) reduced the amplitudes of long-latency stretch reflexes. Subsequently, in a separate study by the same group, a beneficial effect of the cerebello-cerebral tDCS (tCCDCS; 1 mA, 20 min on each site) has been demonstrated on upper limb tremor (postural and action) by power spectral density analysis. tCCDCS reduced the onset latency of the antagonist activity associated with fast goal-directed movements toward three aimed targets (Grimaldi et al., 2014b). Hence, tCCDCS modified the delayed-onset braking action of antagonist activity that results in hypermetria in cerebellar ataxia.

A transient beneficial effect of single-session ctDCS (2 mA, 20 min) on degenerative cerebellar ataxia has been demonstrated by Benussi et al. (2015). Subsequently, in a different crossover study by the same group, they have demonstrated long-term effects of anodal ctDCS using stimulation for 5 days/week for 2 weeks (Benussi et al., 2017b). Recently, they have also used cerebello-spinal tDCS with anodal cerebellar and cathodal spinal stimulation. CBI was measured using TMS. Statistically significant beneficial effects were seen in short term (2 weeks) and long term (3 months). The benefit is likely due to the combined effect of CBI by anodal ctDCS and influence on the ascending and the descending spinal pathways on spinal reflex excitability and functional neuroplastic changes by spinal cathodal tDCS (Benussi et al., 2018). The results of a similar trial with 2 weeks of anodal ctDCS in patients with spinocerebellar ataxia type 3 are awaited (Maas et al., 2019). An improvement of marked postural tremor in cerebellar ataxia associated with ANO10 mutation was noted with cerebello-cerebral stimulation (anode over cerebellum and cathode over M1, 1.5 Ma, 20 min) (Bodranghien et al., 2017). No significant beneficial effect was noted with anodal tDCS to the cerebellum or the motor cortex in grip force control (2 mA, 25 min) (John et al., 2017) or force-field reaching adaptation (2 mA, 22 min) (Hulst et al., 2017) in patients with cerebellar ataxia.

A beneficial effect of combined intensive rehabilitation program (IRP) and cerebello-cerebral tDCS was seen in patients with Friedreich's ataxia. IRP consisted of two sessions/day for 5 weeks, and tDCS (2 mA, 20 min) was applied once/day for 2 weeks. tDCS can facilitate the rehabilitative interventions, likely by improving the recruitment activity at the pyramidal cell layer on the M1 with subsequent neural network function

recovery (Vavla et al., 2019). A similar positive effect was noted in home-based chronic stimulation with remotely supervised anodal ctDCS (2.5 mA, 20 min, 60 sessions) with cognitive and physiotherapy in an elderly female with progressive cerebellar ataxia (Pilloni et al., 2019).

We believe that there is a huge scope of using tDCS in degenerative cerebellar ataxia where practically no therapeutic options are available. Isolated cerebellar stimulation, or in combination (cerebello-cerebral and cerebello-spinal), can be offered in ataxic patients. A concurrent rehabilitation program may boost the therapeutic benefit.

Essential Tremor

There are two circuits implicated in tremor generation: (de Schipper et al., 2018) the cortico-ponto-cerebello-thalamo-cortical loop and (Schirinzi et al., 2018) the Guillain–Mollaret triangle circuit. The two circuits interact in the cerebellum (Dietrich and Hallett, 2018). In essential tremor (ET) patients, decreased functional connectivity was noted between the cerebellar cortex and the dentate nucleus, with an increase of functional connectivity between the cerebellar cortex and the thalamus (Buijink et al., 2015; Gallea et al., 2015; Maas et al., 2020).

In ET patients, by anodal tDCS to dorsolateral prefrontal areas (Cz and F4) and cathodal stimulation to inion (2 mA, 20 min/session, total of 15 sessions), a significant improvement is seen in the Essential Tremor Rating Assessment Scale and the Activities of Daily Living scores (Helvaci et al., 2016), although in another study in ET patients, using cathodal tDCS to both cerebellar hemispheres and anode over both prefrontal areas (2 mA, 20 min/session, 10 sessions), no significant improvement occurred (Gironell et al., 2014).

The effects of tDCS on tremor may not be noticed acutely and may require a long follow-up period to appreciate. Further studies with larger sample sizes to evaluate the efficacy of tDCS in ET in the short and the long term are needed.

Orthostatic Tremor

Classic > 13 Hz orthostatic tremor (OT) in the legs is believed to be due to a deficit in proprioceptive feedback to the sensory–motor cortex, where medications are of limited value. DBS to caudal zona incerta and spinal cord stimulation are newer options targeting that defective sensory feedback (Krauss et al., 2006; Gilmore et al., 2019). Lamy et al. (2018) noted an improvement in the amplitude of tremor and instability in OT patients with a single session of anodal trans-spinal tDCS (2.5 mA, 20 min).

Huntington's Disease

Cognitive impairment, especially deficit in working memory, may precede motor impairment in Huntington's disease (HD). A reduced activation of the left DLPFC has been noted in HD (Georgiou-Karistianis et al., 2013). A single session of anodal tDCS (1.5 mA, 15 min) over the left DLPFC combined with cognitive training improved the patients' performance on a working memory task (digit reordering task) (Eddy et al., 2017).

Abnormal cortical excitability and plasticity have been demonstrated in the early phase of HD and in asymptomatic HD carriers. A study with low-frequency (1 Hz) rTMS to the SMA improved chorea in HD (Brusa et al., 2005). Like in L-dopa induced dyskinesia, modulation of cortical excitability with tDCS can be tried in HD chorea.

Overall, the transcranial delivery of anodal tDCS can excite the underlying hypoactive brain region, and cathodal tDCS can suppress the hyperactivity. So, the efficacy of tDCS depends on the right choice of the polarity of tDCS based on the hypo- or hyper-activity of the underlying brain network.

TRANSCRANIAL ALTERNATING CURRENT STIMULATION

Parkinson's Disease

Studies using electrophysiological recordings in cortico-basal ganglia circuits have demonstrated that the loss of dopamine in PD increases the sensitivity of the basal ganglia-thalamo-cortical network to rhythmic oscillatory inputs. This possible cortically originating rhythm leads to pathological oscillatory synchronization and thus interferes with the processing of movement-related signals, resulting in motor deficits. Bradykinesia and rigidity in PD are likely related to increased oscillatory beta band synchronization (Feurra et al., 2011; Weinberger and Dostrovsky, 2011). Cross-frequency phase-amplitude coupling between amplitude of slow high frequency oscillation (200–300 Hz) and phase of low-beta (13–22 Hz) has been noted in the OFF phase of PD (López-Azcárate et al., 2010). tACS has been proposed to interact with or even entrain spontaneous brain oscillations in a frequency-dependent manner by the subthreshold modulation of membrane potentials (Teo et al., 2017).

An improvement in motor and cognitive performance in PD was noted with individualized tACS and physiotherapy, where the frequency of tACS was set according to the higher-power spectra band in the electroencephalograph (EEG; 4 Hz tACS if beta excess on EEG map; 30 Hz tACS if theta excess, 5 days/week for 2 weeks) (Del Felice et al., 2019). Brittain et al. (2013) have studied the role of tACS in suppressing rest tremor in 12 PD patients by applying a phase cancellation technique. At first, they identified the timing of cortical oscillations responsible for the rest tremor by delivering tremor-frequency stimulation over M1—the rhythms drift in and out of phase alignment with one another. tACS was delivered at these specified phase alignments to demonstrate around 50% suppression of the ongoing resting tremor amplitude.

In a different study, the effects of 10 and 20 Hz tACS over M1 (1 mA, 15 min, current density 0.0286 mA/cm^2, sinusoidal waveform) have been evaluated on magnetoencephalographic recording during isometric contraction of the forearm muscles (corticomuscular coupling, CMC) and motor tasks (fast finger tapping and wrist pronation–supination) in PD patients. Decreased beta band CMC and variability of fast distal movements were noted with M1 tACS at 20 Hz in PD patients,

possibly because of pathological beta synchronization of the motor cortex in PD (Krause et al., 2013).

Recently, cross-frequency phase-amplitude coupling between phase of theta–alpha (4–12 Hz) and amplitude of fast high frequency oscillation (300–400 Hz) has been demonstrated in the ON state of PD with dyskinesia (Ozturk et al., 2020). So, there is a scope of tACS to evaluate its role also in the ON state of dyskinesia.

Enhanced Physiological Tremor

Mehta et al. (2015) have highlighted the importance of montage selection for entraining physiological tremor. The montage with active electrode over M1 and extracephalic reference electrode contralateral to M1 significantly entrained the physiological tremor. tACS was delivered at the participant's peak tremor frequency. In a different study, they have evaluated the effect of tACS (delivered at the task-dependent peak frequency of tremor) on the postural and the kinetic type of physiological tremor. M1 stimulation gave rise to phase entrainment of postural, but not kinetic, tremor, whereas cerebellar stimulation increased entrainment in both cases. However, tACS had no effect on the amplitude of physiological tremor, which may be because of a dominant role of factors further downstream of the central oscillators in the modulation of tremor amplitude (Mehta et al., 2014). It has been shown that focused M1 tACS caused a significant phase entrainment of the tremor, and the subjects with higher phase entrainment showed more tremor amplitude modulation (Ahmad et al., 2018).

Cervical Dystonia

Transcranial alternating current stimulation (tACS) over the motor cortex is noted to significantly decrease the amplitude of motor-evoked potentials and decreased intracortical facilitation. tACS (15 Hz, 20 min) may have a dampening effect on the cortical networks, and it likely interferes with the temporo-spatial summation of weak subthreshold electric potentials (Zaghi et al., 2010).

With stimulation of the motor cortex by cathodal tDCS (1.5 mA, 15 min, five sessions) followed by tACS (two sessions of 15-min stimulation with 1.5 mA at 5–15 Hz and subsequently five daily sessions of 20 min each with 1.5 mA at 15 Hz), a 54% reduction in the Toronto Western Spasmodic Torticollis Rating Scale (TWSTRS) and a 75% reduction in the TWSTRS Pain Scale was noted in a patient of idiopathic cervical dystonia, and the effects persisted at 30 days of follow-up (Angelakis et al., 2013).

Neural entrainment and plasticity are mainly suggested to mediate the effects of tACS, and there is potential scope for using it as a possible treatment for disorders related to malfunctioned brain oscillations. Frequency, intensity, and duration of stimulation are yet to be standardized.

TRANSCRANIAL PULSED CURRENT STIMULATION

While anodal-tDCS modifies neuronal excitability by tonic depolarization of the resting membrane potential, anodal-tPCS (a-tPCS) modifies neuronal excitability by a combination of tonic and phasic effects. The tonic effects of a-tPCS are related to the net direct current component, leading to the tonic depolarization of the resting membrane potential. The phasic effects of a-tPCS are due to the on/off nature of pulsatile currents. In tPCS, the current flows in unidirectional pulses separated by an IPI, in contrast to the continuous flow of direct current in tDCS (Fitzgerald, 2014; Jaberzadeh et al., 2015). tPCS can be applied with short inter-pulse intervals (tPCSSIPI) or long inter-pulse intervals (tPCSLIPI).

Jaberzadeh et al. (2014) tested four testing conditions: a-tDCS, a-tPCSSIPI (IPI 50 ms), a-tPCSLIPI (IPI 650 ms), and sham a-tPCSSIPI. They have noted that only anodal tDCS and anodal tPCSSIPI over M1 increase the corticospinal excitability in healthy individuals, lasting for at least 30 min. The increase in CSE was larger with a-tPCSSIPI.

The effect of tPCS (with a commercially available tPCS device—Fisher Wallace model FW 100-C, New York) with treadmill walk has been evaluated in PD patients, with focus on gait and balance. The tPCS session increased gait velocity and stride length significantly compared with treadmill or tPCS + treadmill. The number of steps needed to recover balance decreased after tPCS and tPCS + treadmill (Alon et al., 2012).

The intensity-specific modulation of cortical excitability by tPCS has been addressed recently by Ma et al. (2019). Enhancement of cortical excitability by low-intensity anodal tPCS is likely related to astrocytic Ca^{2+} elevations due to the noradrenergic activation of alpha-1 adrenergic receptors, but high-intensity anodal tPCS decrease cortical excitability with excessive calcium activity in neurons.

The role of tPCS in other disorders like ataxia, where gait and balance are predominantly affected, has not been studied to date.

TRANSCRANIAL RANDOM NOISE STIMULATION

The newest mode of NIBS is tRNS. tRNS over M1 has been shown to enhance corticospinal excitability both during and after stimulation in the healthy human brain. The main advantage of tRNS is the direction insensitivity of the stimulation. Boosting synaptic signals, stochastic resonance, activation of sodium channels, and inducing long-term potentiation *via* modifying *N*-methyl-D-aspartate receptor efficacy are likely responsible for the neuroplasticity effects. tRNS, like tACS, can possibly interfere with ongoing oscillations and neuronal activity in the brain (Terney et al., 2008).

Yamamoto et al. (2005) have evaluated the effect of 24-h noisy galvanic vestibular stimulation (GVS) on long-term heart rate dynamics in patients with multisystem atrophy (MSA) and on daytime trunk activity dynamics in patients with PD. They have noted improved autonomic, especially parasympathetic, responsiveness by noisy GVS. The cognitive performance in those PD patients has also been evaluated by means of a continuous performance test. The mean reaction time of the continuous performance test was significantly decreased by the noisy GVS, suggesting improved motor execution during the cognitive task.

Motor cortex plasticity in PD patients has been studied with tRNS and intermittent theta-burst stimulation (iTBS). The plasticity-inducing effect of iTBS was absent in PD patients, but tRNS reduced cortical excitability as compared to pre-stimulation baseline, which is in contrast to the results on healthy subjects (Stephani et al., 2011). Recently, Moret et al. (2019) has noted that, for inducing a significant and persistent increase in cortical excitability, a large amount of noise with a wide range of frequencies (100–700 Hz) is needed.

The altered cortical plasticity in PD patients should be evaluated further. On the other hand, in dystonia, there is definite evidence of maladaptive cortical plasticity and defective sensory–motor integration. Exploring the role of tRNS in these disorders of altered cortical plasticity will be an important next step.

CONCLUSION

The results of tES studies in movement disorders are encouraging, but their utility in the mainstream treatment of movement disorders is still limited. Because of the heterogeneity of patient population and the diversity of the protocols used in these studies, it is hard to do a systemic review and to quantify the actual therapeutic benefit of different modes of tES. The majority of trials are not double-blinded and the level of evidence of efficacy and safety is unknown. These are the major limitations for reviewing different modes of tES. So far, tDCS is the most commonly used technique. In the field of movement disorders, tDCS has been tested mostly for different aspects of PD (22 studies targeting gait and balance, 10 studies evaluating upper limb motor function, seven studies for cognitive function, and one study each for pathological gambling, speech, sleep, fatigue, and dyskinesia). The efficacy of tDCS has also been tested in dystonia and cerebellar ataxia (11 studies for each), but the number of studies for other movement disorders like ET, OT, HD, MSA, PSP, and CBS is quite less. Anodal tDCS over motor cortex in PD, over cerebellum in ataxia (±simultaneous cathodal spinal stimulation) and cathodal tDCS over motor cortex in dystonia, has shown beneficial results. Modifying a complex dysfunctional network by acute stimulation seems unlikely. Chronic stimulation for at least 2 weeks seems to be a safe and rational approach. Other techniques like tACS, tPCS, and tRNS are less well studied in movement disorders. As tACS has been proposed to entrain brain oscillations, it can be used as a tool to assess and modulate the complex tremor network. Recently, cross-frequency phase-amplitude coupling is an evolving pathophysiology for the OFF and the ON state of PD, which further expands the scope of tACS in PD. So far, tACS has been evaluated in PD (three studies), enhanced physiological tremor (two studies), and cervical dystonia (two studies). In contrast, tPCS and tRNS are relatively new in the field of movement disorders. Due to its combined phasic and tonic effects, tPCS can be an effective and more tolerable therapy in PD or ataxia. The role of tRNS with a wide range of frequency should also be evaluated further in movement disorders.

Newer technologies like quantitative electroencephalography, better circuit design for stimulation devices, and programmability of stimulation parameters are all necessary to move this field forward. Elucidating the precise patterns of network dysfunction in a highly connected system is another important engineering problem that has to be directly tackled by novel signal processing methods. It may only then be possible to target the precise individualized sites in specific patients with specific diseases for stimulation. Considered together, this emerging field of individualized dysfunction measurement and device optimization for portable non-invasive stimulation for movement disorders will be the next frontier of tES.

In the literature, there are mostly segregated case reports and reviews on tES. In them, mostly tDCS has been focused, while other modes are neglected. There is no literature combining all the modes of tES together so far. In this review, we have highlighted the basic concept of the different modes of tES and have summarized the studies done so far on the therapeutic benefit of tES in movement disorders. We have also tried to find out the electro-physiological basis of the effect of each of these techniques. There still remain some unanswered questions: (de Schipper et al., 2018). What are the detailed electrophysiological bases of the different modes of tES and are they sufficient enough to alter the complex brain network of movement disorders? (Schirinzi et al., 2018). Are there any methods like quantitative EEG, ligand-bound imaging, *etc*., to probe into the network for planning individualized tES? (Benito-León et al., 2015). Is there any threshold of neurodegeneration beyond which applying tES is not reasonable? (Wu et al., 2018). What would be the realistic expectation after tES? (Falcon et al., 2016). How long does the effect of stimulation last? (Latorre et al., 2019). How feasible is supervised home-based chronic stimulation by patients themselves and is there any scope of adaptive tES as per patient need? Large clinical trials with each of the stimulation technique, precisely targeting the individualized brain network, may help us to find some of the answers and thus will help to set up a standardized protocol for each of them.

Take-Home Message

1. Non-invasive tES may be a safe and cost-effective way to alter cortical excitability.
2. Anodal tDCS over motor cortex in PD, over cerebellum in ataxia (± simultaneous cathodal stimulation over spinal cord), and cathodal tDCS over motor cortex in dystonia have shown beneficial results.
3. While acute stimulation may cause a transient effect, for sustained benefit, chronic stimulation for at least 2 weeks may be required.
4. tACS can entrain pathological brain oscillations.
5. More trials with tPCS and tRNS are needed to evaluate their efficacy.

AUTHOR CONTRIBUTIONS

JG wrote the first draft of the manuscript. AM, SS, and DA contributed to the review and critique. MJ contributed to the conception of the work, review, and critique.

REFERENCES

Adenzato, M., Manenti, R., Enrici, I., Gobbi, E., Brambilla, M., Alberici, A., et al. (2019). Transcranial direct current stimulation enhances theory of mind in Parkinson's disease patients with mild cognitive impairment: a randomized, double-blind, sham-controlled study. *Transl. Neurodegener.* 8:1. doi: 10.1186/s40035-018-0141-9

Ahmad, K., Breukers, J., Op de Beeck, S., Nica, I. G., Aerts, J.-M., Seynaeve, L., et al. (2018). Using high-amplitude and focused transcranial alternating current stimulation to entrain physiological tremor. *Sci. Rep.* 8:8221. doi: 10.1038/s41598-018-26013-3

Alamos, M. F., Sharma, S., Kumar, N., and Jog, M. S. (2019). 'Cognitive freezing': a newly recognized episodic phenomenon in Parkinson's disease. *Parkinsonism Relat. Disord.* 65, 49–54. doi: 10.1016/j.parkreldis.2019.06.004

Alexoudi, A., Patrikelis, P., Fasilis, T., Deftereos, S., Sakas, D., and Gatzonis, S. (2018). Effects of anodal tDCS on motor and cognitive function in a patient with multiple system atrophy. *Disabil. Rehabil.* 21, 1–5. doi: 10.1080/09638288.2018.1510043

Alizad, V., Meinzer, M., Frossard, L., Polman, R., Smith, S., and Kerr, G. (2019). Gait speed after applying anodal-transcranial direct current stimulation in people with Parkinson's disease? *Brain Stimulat.* 12:571. doi: 10.1016/j.brs.2018.12.892

Alon, G., Yungher, D. A., Shulman, L. M., and Rogers, M. W. (2012). Safety and immediate effect of noninvasive transcranial pulsed current stimulation on gait and balance in Parkinson disease. *Neurorehabil Neural Repair.* 26, 1089–1095. doi: 10.1177/1545968312448233

Angelakis, E., Liouta, E., Andreadis, N., Leonardos, A., Ktonas, P., Stavrinou, L. C., et al. (2013). Transcranial alternating current stimulation reduces symptoms in intractable idiopathic cervical dystonia: a case study. *Neurosci. Lett.* 533, 39–43. doi: 10.1016/j.neulet.2012.11.007

Benito-León, J., Louis, E. D., Romero, J. P., Hernández-Tamames, J. A., Manzanedo, E., Álvarez-Linera, J., et al. (2015). Altered functional connectivity in essential tremor: a resting-state fMRI study. *Medicine* 94:e1936. doi: 10.1097/MD.0000000000001936

Benninger, D. H., Lomarev, M., Lopez, G., Pal, N., Luckenbaugh, D. A., and Hallett, M. (2011). Transcranial direct current stimulation for the treatment of focal hand dystonia. *Mov. Disord.* 26, 1698–1702. doi: 10.1002/mds.23691

Benninger, D. H., Lomarev, M., Lopez, G., Wassermann, E. M., Li, X., Considine, E., et al. (2010). Transcranial direct current stimulation for the treatment of Parkinson's disease. *J. Neurol. Neurosurg. Psychiatry* 81, 1105–1111. doi: 10.1136/jnnp.2009.202556

Benussi, A., Alberici, A., Cantoni, V., Manenti, R., Brambilla, M., Dell'Era, V., et al. (2017a). Modulating risky decision-making in Parkinson's disease by transcranial direct current stimulation. *Eur. J. Neurol.* 24, 751–754. doi: 10.1111/ene.13286

Benussi, A., Dell'Era, V., Cotelli, M. S., Turla, M., Casali, C., Padovani, A., et al. (2017b). Long term clinical and neurophysiological effects of cerebellar transcranial direct current stimulation in patients with neurodegenerative ataxia. *Brain Stimul.* 10, 242–250. doi: 10.1016/j.brs.2016.11.001

Benussi, A., Dell'Era, V., Cantoni, V., Bonetta, E., Grasso, R., Manenti, R., et al. (2018). Cerebello-spinal tDCS in ataxia: a randomized, double-blind, sham-controlled, crossover trial. *Neurology* 91, e1090–e1101. doi: 10.1212/WNL.0000000000006210

Benussi, A., Koch, G., Cotelli, M., Padovani, A., and Borroni, B. (2015). Cerebellar transcranial direct current stimulation in patients with ataxia: a double-blind, randomized, sham-controlled study. *Mov. Disord.* 30, 1701–1705. doi: 10.1002/mds.26356

Biundo, R., Weis, L., Fiorenzato, E., Gentile, G., Giglio, M., Schifano, R., et al. (2015). Double-blind randomized trial of tDCS versus sham in parkinson patients with mild cognitive impairment receiving cognitive training. *Brain Stimul.* 8, 1223–1225. doi: 10.1016/j.brs.2015.07.043

Bodranghien, F., Oulad Ben Taib, N., Van Maldergem, L., and Manto, M. (2017). A Postural tremor highly responsive to transcranial cerebello-cerebral DCS in ARCA3. *Front. Neurol.* 8:71. doi: 10.3389/fneur.2017.00071

Boggio, P. S., Ferrucci, R., Rigonatti, S. P., Covre, P., Nitsche, M., Pascual-Leone, A., et al. (2006). Effects of transcranial direct current stimulation on working memory in patients with Parkinson's disease. *J. Neurol. Sci.* 249, 31–38. doi: 10.1016/j.jns.2006.05.062

Bradnam, L. V., Graetz, L. J., McDonnell, M. N., and Ridding, M. C. (2015). Anodal transcranial direct current stimulation to the cerebellum improves handwriting and cyclic drawing kinematics in focal hand dystonia. *Front. Hum. Neurosci.* 9:286. doi: 10.3389/fnhum.2015.00286

Brittain, J. S., Probert-Smith, P., Aziz, T. Z., and Brown, P. (2013). Tremor suppression by rhythmic transcranial current stimulation. *Curr. Biol.* 23, 436–440. doi: 10.1016/j.cub.2013.01.068

Broeder, S., Heremans, E., Pinto Pereira, M., Nackaerts, E., Meesen, R., Verheyden, G., et al. (2019). Does transcranial direct current stimulation during writing alleviate upper limb freezing in people with Parkinson's disease? A pilot study. *Hum. Mov. Sci.* 65, S0167–S9457. doi: 10.1016/j.humov.2018.02.012

Brusa, L., Versace, V., Koch, G., Bernardi, G., Iani, C., Stanzione, P., et al. (2005). Improvement of choreic movements by 1 Hz repetitive transcranial magnetic stimulation in Huntington's disease patients. *Ann. Neurol.* 58, 655–656. doi: 10.1002/ana.20613

Buijink, A. W., van der Stouwe, A. M., Broersma, M., Sharifi, S., Groot, P. F., Speelman, J. D., et al. (2015). Motor network disruption in essential tremor: a functional and effective connectivity study. *Brain* 138(Pt 10), 2934–2947. doi: 10.1093/brain/awv225

Buttkus, F., Baur, V., Jabusch, H. C., de la Cruz Gomez-Pellin, M., Paulus, W., Nitsche, M. A., et al. (2011). Single-session tDCS-supported retraining does not improve fine motor control in musician's dystonia. *Restor. Neurol. Neurosci.* 29, 85–90. doi: 10.3233/RNN-2011-0582

Buttkus, F., Weidenmüller, M., Schneider, S., Jabusch, H. C., Nitsche, M. A., Paulus, W., et al. (2010). Failure of cathodal direct current stimulation to improve fine motor control in musician's dystonia. *Mov. Disord.* 25, 389–394. doi: 10.1002/mds.22938

Capecci, M., Andrenelli, E., Orni, C., and Ceravolo, M. G. (2014). Bilateral prefrontal transcranial direct current stimulation (tDCS) in Parkinson's disease: a placebo controlled trial. *Mov. Disord.* 29, S229–S230.

Cosentino, G., Valentino, F., Todisco, M., Alfonsi, E., Davì, R., Savettieri, G., et al. (2017). Effects of More-Affected vs. Less-Affected Motor Cortex tDCS in Parkinson's Disease. *Front. Hum. Neurosci.* 11:309. doi: 10.3389/fnhum.2017.00309

Costa-Ribeiro, A., Maux, A., Bosford, T., Aoki, Y., Castro, R., Baltar, A., et al. (2017). Transcranial direct current stimulation associated with gait training in Parkinson's disease: a pilot randomized clinical trial. *Dev. Neurorehabil.* 20, 121–128. doi: 10.3109/17518423.2015.1131755

Costa-Ribeiro, A., Maux, A., Bosford, T., Tenorio, Y., Marques, D., Carneiro, M., et al. (2016). Dopamine-independent effects of combining transcranial direct current stimulation with cued gait training on cortical excitability and functional mobility in Parkinson's disease. *J. Rehabil. Med.* 48, 819–823. doi: 10.2340/16501977-2134

Cotelli, M., Manenti, R., Ferrari, C., Gobbi, E., Macis, A., and Cappa, S. F. (2020). Effectiveness of language training and non-invasive brain stimulation on oral and written naming performance in Primary Progressive Aphasia: a meta-analysis and systematic review. *Neurosci. Biobehav. Rev.* 108, 498–525. doi: 10.1016/j.neubiorev.2019.12.003

Criminger, C., Swank, C., Almutairi, S., and Mehta, J. (2018). Transcranial direct current stimulation plus concurrent activity may influence task prioritization during walking in people with Parkinson's disease - initial findings. *J. Parkinsonism Restl.* 8, 25–32. doi: 10.2147/JPRLS.S161740

da Silva, D. C. L., Laa, T., Daa, S. F. A., Horsczaruk, C. H. R., Pedron, C. A., Rodrigues, E. D. C., et al. (2018). Effects of acute transcranial direct current stimulation on gait kinematics of individuals with Parkinson disease. *Top. Geriatr. Rehabil.* 34, 262–268. doi: 10.1097/TGR.0000000000000203

Dagan, M., Herman, T., Harrison, R., Zhou, J., Giladi, N., Ruffini, G., et al. (2018). Multitarget transcranial direct current stimulation for freezing of gait in Parkinson's disease. *Mov. Disord.* 33, 642–646. doi: 10.1002/mds.27300

de Aguiar, V., Zhao, Y., Faria, A., Ficek, B., Webster, K. T., Wendt, H., et al. (2020). Brain volumes as predictors of tDCS effects in primary progressive aphasia. *Brain Lang.* 200:104707. doi: 10.1016/j.bandl.2019.104707

de la Fuente-Fernández, R. (2012). Frontostriatal cognitive staging in Parkinson's disease. *Parkinsons Dis.* 2012:561046. doi: 10.1155/2012/561046

de Schipper, L. J., Hafkemeijer, A., van der Grond, J., Marinus, J., Henselmans, J. M. L., and van Hilten, J. J. (2018). Altered whole-brain and network-based functional connectivity in Parkinson's disease. *Front. Neurol.* 9:419. doi: 10.3389/fneur.2018.00419

Del Felice, A., Castiglia, L., Formaggio, E., Cattelan, M., Scarpa, B., Manganotti, P., et al. (2019). Personalized transcranial alternating current stimulation (tACS) and physical therapy to treat motor and cognitive symptoms in Parkinson's disease: a randomized cross-over trial. *Neuroimage Clin.* 22:101768. doi: 10.1016/j.nicl.2019.101768

Dietrich, H., and Hallett, M. (2018). Essential tremor. *N. Engl. J. Med.* 378, 1802–1810. doi: 10.1056/NEJMcp1707928

Doruk, D., Gray, Z., Bravo, G. L., Pascual-Leone, A., and Fregni, F. (2014). Effects of tDCS on executive function in Parkinson's disease. *Neurosci. Lett.* 582, 27–31. doi: 10.1016/j.neulet.2014.08.043

Eddy, C. M., Shapiro, K., Clouter, A., Hansen, P. C., and Rickards, H. E. (2017). Transcranial direct current stimulation can enhance working memory in Huntington's disease. *Prog. Neuropsychopharmacol. Biol. Psychiatry* 77, 75–82. doi: 10.1016/j.pnpbp.2017.04.002

Elder, G. J., Ashcroft, J., da Silva Morgan, K., Umme Kulsum, M., Banerjee, R., Chatterjee, P., et al. (2017). Transcranial direct current stimulation in Parkinson's disease dementia: a randomised double-blind crossover trial. *Brain Stimul.* 10, 1150–1151. doi: 10.1016/j.brs.2017.07.012

Elder, G. J., Colloby, S. J., Firbank, M. J., McKeith, I. G., and Taylor, J. P. (2019). Consecutive sessions of transcranial direct current stimulation do not remediate visual hallucinations in Lewy body dementia: a randomised controlled trial. *Alzheimers Res. Ther.* 11:9. doi: 10.1186/s13195-018-0465-9

Elder, G. J., Firbank, M. J., Kumar, H., Chatterjee, P., Chakraborty, T., Dutt, A., et al. (2016). Effects of transcranial direct current stimulation upon attention and visuoperceptual function in Lewy body dementia: a preliminary study. *Int. Psychogeriatr.* 28, 341–347. doi: 10.1017/S1041610215001180

Falcon, M. I., Gomez, C. M., Chen, E. E., Shereen, A., and Solodkin, A. (2016). Early cerebellar network shifting in spinocerebellar ataxia Type 6. *Cereb. Cortex.* 26, 3205–3218. doi: 10.1093/cercor/bhv154

Fernandez-Lago, H., Bello, O., Mora-Cerda, F., Montero-Camara, J., and Fernandez-del-Olmo, M. A. (2017). Treadmill walking combined with anodal Transcranial direct current stimulation in Parkinson disease: a pilot study of kinematic and neurophysiological effects. *Am. J. Phys. Med. Rehabil.* 96, 801–808. doi: 10.1097/PHM.0000000000000751

Ferrucci, R., Cortese, F., Bianchi, M., Pittera, D., Turrone, R., Bocci, T., et al. (2016). Cerebellar and motor cortical transcranial stimulation decrease levodopa-induced dyskinesias in Parkinson's disease. *Cerebellum* 15, 43–47. doi: 10.1007/s12311-015-0737-x

Feurra, M., Bianco, G., Santarnecchi, E., Del Testa, M., Rossi, A., and Rossi, S. (2011). Frequency-dependent tuning of the human motor system induced by transcranial oscillatory potentials. *J. Neurosci.* 31, 12165–12170. doi: 10.1523/JNEUROSCI.0978-11.2011

Fitzgerald, P. B. (2014). Transcranial pulsed current stimulation: a new way forward? *Clin. Neurophysiol.* 125, 217–219. doi: 10.1016/j.clinph.2013.10.009

Forogh, B., Rafiei, M., Arbabi, A., Motamed, M. R., Madani, S. P., and Sajadi, S. (2017). Repeated sessions of transcranial direct current stimulation evaluation on fatigue and daytime sleepiness in Parkinson's disease. *Neurol. Sci.* 38, 249–254. doi: 10.1007/s10072-016-2748-x

Fregni, F., Boggio, P. S., Santos, M. C., Lima, M., Vieira, A. L., Rigonatti, S. P., et al. (2006). Noninvasive cortical stimulation with transcranial direct current stimulation in Parkinson's disease. *Mov. Disord.* 21, 1693–1702. doi: 10.1002/mds.21012

Furuya, S., Nitsche, M. A., Paulus, W., and Altenmüller, E. (2014). Surmounting retraining limits in musicians' dystonia by transcranial stimulation. *Ann. Neurol.* 75, 700–707. doi: 10.1002/ana.24151

Gallea, C., Popa, T., García-Lorenzo, D., Valabregue, R., Legrand, A. P., Marais, L., et al. (2015). Intrinsic signature of essential tremor in the cerebello-frontal network. *Brain* 138(Pt 10), 2920–2933. doi: 10.1093/brain/awv171

Gatto, E. M., and Aldinio, V. (2019). Impulse control disorders in Parkinson's disease. A brief and comprehensive review. *Front. Neurol.* 10:351. doi: 10.3389/fneur.2019.00351

Georgiou-Karistianis, N., Poudel, G. R., Domínguez, D. J. F., Langmaid, R., Gray, M. A., Churchyard, A., et al. (2013). Functional and connectivity changes during working memory in Huntington's disease: 18 month longitudinal data from the IMAGE-HD study. *Brain Cogn.* 83, 80–91. doi: 10.1016/j.bandc.2013.07.004

Gilmore, G., Murgai, A., Nazer, A., Parrent, A., and Jog, M. (2019). Zona incerta deep-brain stimulation in orthostatic tremor: efficacy and mechanism of improvement. *J. Neurol.* 266, 2829–2837. doi: 10.1007/s00415-019-09505-8

Gironell, A., Martinez-Horta, S., Aguilar, S., Torres, V., Pagonabarraga, J., Pascual-Sedano, B., et al. (2014). Transcranial direct current stimulation of the cerebellum in essential tremor: a controlled study. *Brain Stimul.* 7, 491–492. doi: 10.1016/j.brs.2014.02.001

Grimaldi, G., Argyropoulos, G. P., Bastian, A., Cortes, M., Davis, N. J., Edwards, D. J., et al. (2016). Cerebellar transcranial direct current stimulation (ctDCS): a novel approach to understanding cerebellar function in health and disease. *Neuroscientist* 22, 83–97. doi: 10.1177/1073858414559409

Grimaldi, G., Argyropoulos, G. P., Boehringer, A., Celnik, P., Edwards, M. J., Ferrucci, R., et al. (2014a). Non-invasive cerebellar stimulation–a consensus paper. *Cerebellum* 13, 121–138. doi: 10.1007/s12311-013-0514-7

Grimaldi, G., Oulad Ben Taib, N., Manto, M., and Bodranghien, F. (2014b). Marked reduction of cerebellar deficits in upper limbs following transcranial cerebello-cerebral DC stimulation: tremor reduction and re-programming of the timing of antagonist commands. *Front. Syst. Neurosci.* 8:9. doi: 10.3389/fnsys.2014.00009

Grimaldi, G., and Manto, M. (2013). Anodal transcranial direct current stimulation (tDCS) decreases the amplitudes of long-latency stretch reflexes in cerebellar ataxia. *Ann. Biomed. Eng.* 41, 2437–2447. doi: 10.1007/s10439-013-0846-y

Hadoush, H., Al-Sharman, A., Khalil, H., Banihani, S. A., and Al-Jarrah, M. (2018). Sleep quality, depression, and quality of life after bilateral anodal transcranial direct current stimulation in patients with Parkinson's disease. *Med. Sci. Monit. Basic Res.* 24, 198–205. doi: 10.12659/MSMBR.911411

Hallett, M. (2006). Pathophysiology of dystonia. *J. Neural Transm. Suppl.* 70, 485–488. doi: 10.1007/978-3-211-45295-0_72

Hallett, M. (2011). Neurophysiology of dystonia: the role of inhibition. *Neurobiol. Dis.* 42, 177–184. doi: 10.1016/j.nbd.2010.08.025

Harris, D. M., Rantalainen, T., Muthalib, M., Johnson, L., Duckham, R. L., Smith, S. T., et al. (2018). Concurrent exergaming and transcranial direct current stimulation to improve balance in people with Parkinson's disease: study protocol for a randomised controlled trial. *Trials* 19:387. doi: 10.1186/s13063-018-2773-6

Helmich, R. C., Derikx, L. C., Bakker, M., Scheeringa, R., Bloem, B. R., and Toni, I. (2010). Spatial remapping of cortico-striatal connectivity in Parkinson's disease. *Cereb. Cortex* 20, 1175–1186. doi: 10.1093/cercor/bhp178

Helvaci, Y. N., Polat, B., and Hanoglu, L. (2016). Transcranial direct current stimulation in the treatment of essential tremor: an open-label study. *Neurologist* 21, 28–29. doi: 10.1097/NRL.0000000000000070

Hulst, T., John, L., Küper, M., van der Geest, J. N., Göricke, S. L., Donchin, O., et al. (2017). Cerebellar patients do not benefit from cerebellar or M1 transcranial direct current stimulation during force-field reaching adaptation. *J. Neurophysiol.* 118, 732–748. doi: 10.1152/jn.00808.2016

Ingrid, M.-D., Gebodh, N., Schestatsky, P., Guleyupoglu, B., Reato, D., Bikson, M., et al. (2014). *Transcranial Electrical Stimulation: Transcranial Direct Current Stimulation (tDCS), Transcranial Alternating Current Stimulation (tACS), Transcranial Pulsed Current Stimulation (tPCS), and Transcranial Random Noise Stimulation (tRNS). The Stimulated Brain*. Amsterdam: Elsevier, 35–59.

Ingvarsson, P. E., Gordon, A. M., and Forssberg, H. (1997). Coordination of manipulative forces in Parkinson's disease. *Exp. Neurol.* 145, 489–501. doi: 10.1006/exnr.1997.6480

Ishikuro, K., Dougu, N., Nukui, T., Yamamoto, M., Nakatsuji, Y., Kuroda, S., et al. (2018). Effects of Transcranial Direct Current Stimulation (tDCS) over the frontal polar area on motor and executive functions in parkinson's disease; a pilot study. *Front. Aging Neurosci.* 10:231. doi: 10.3389/fnagi.2018.00231

Jaberzadeh, S., Bastani, A., and Zoghi, M. (2014). Anodal transcranial pulsed current stimulation: a novel technique to enhance corticospinal excitability. *Clin. Neurophysiol.* 125, 344–351. doi: 10.1016/j.clinph.2013.08.025

Jaberzadeh, S., Bastani, A., Zoghi, M., Morgan, P., and Fitzgerald, P. B. (2015). Anodal transcranial pulsed current stimulation: the effects of pulse duration on corticospinal excitability. *PLoS One* 10:e0131779. doi: 10.1371/journal.pone.0131779

John, L., Küper, M., Hulst, T., Timmann, D., and Hermsdörfer, J. (2017). Effects of transcranial direct current stimulation on grip force control in patients with cerebellar degeneration. *Cerebellum Ataxias* 4:15. doi: 10.1186/s40673-017-0072-8

Kaski, D., Allum, J., Bronstein, A. M., Dominguez, R, O. (2014a). Applying anodal tDCS during tango dancing in a patient with Parkinson's disease. *Neurosci. Lett.* 568, 39–43. doi: 10.1016/j.neulet.2014.03.043

Kaski, D., Dominguez, R. O., Allum, J. H., Islam, A. F., and Bronstein, A. M. (2014b). Combining physical training with transcranial direct current stimulation to improve gait in Parkinson's disease: a pilot randomized controlled study. *Clin. Rehabil.* 28, 1115–1124. doi: 10.1177/0269215514534277

Kay, D. B., Tanner, J. J., and Bowers, D. (2018). Sleep disturbances and depression severity in patients with Parkinson's disease. *Brain Behav.* 8:e00967. doi: 10.1002/brb3.967

Kishore, A., and Popa, T. (2014). Cerebellum in levodopa-induced dyskinesias: the unusual suspect in the motor network. *Front. Neurol.* 5:157. doi: 10.3389/fneur.2014.00157

Krause, V., Wach, C., Sudmeyer, M., Ferrea, S., Schnitzler, A., and Pollok, B. (2013). Cortico muscular coupling and motor performance are modulated by 20 Hz transcranial alternating current stimulation (tACS) in Parkinson's disease. *Front. Hum. Neurosci.* 7:928. doi: 10.3389/fnhum.2013.00928

Krauss, J. K., Weigel, R., Blahak, C., Bäzner, H., Capelle, H. H., Grips, E., et al. (2006). Chronic spinal cord stimulation in medically intractable orthostatic tremor. *J. Neurol. Neurosurg. Psychiatry* 77, 1013–1016. doi: 10.1136/jnnp.2005.086132

Lamy, J. C., Varriale, P., ApartiS, E., Kosutzka, Z., Roze, E., and Vidailhet, M. (2018). Trans-spinal direct current stimulation for managing primary orthostatic tremor [abstract]. *Mov. Disord.* 33(Suppl. 2):1164.

Latorre, A., Rocchi, L., Berardelli, A., Bhatia, K. P., and Rothwell, J. C. (2019). The use of transcranial magnetic stimulation as a treatment for movement disorders: a critical review. *Mov. Disord.* 34, 769–782. doi: 10.1002/mds.27705

Lattari, E., Costa, S. S., Campos, C., de Oliveira, A. J., Machado, S., and Maranhao Neto, G. A. (2017). Can transcranial direct current stimulation on the dorsolateral prefrontal cortex improves balance and functional mobility in Parkinson's disease? *Neurosci. Lett.* 636, 165–169. doi: 10.1016/j.neulet.2016.11.019

Lawrence, B. J., Gasson, N., Johnson, A. R., Booth, L., and Loftus, A. M. (2018). Cognitive training and transcranial direct current stimulation for mild cognitive impairment in Parkinson's disease: a randomized controlled trial. *Parkinson's Dis.* 2018:4318475. doi: 10.1155/2018/4318475

Lee, H. K., Ahn, S. J., Shin, Y. M., Kang, N., and Cauraugh, J. H. (2019). Does transcranial direct current stimulation improve functional locomotion in people with Parkinson's disease? A systematic review and meta-analysis. *J. Neuroeng. Rehabil.* 16:84. doi: 10.1186/s12984-019-0562-4

Lewis, S. J., and Barker, R. A. (2009). A pathophysiological model of freezing of gait in Parkinson's disease. *Parkinsonism Relat. Disord.* 15, 333–338. doi: 10.1016/j.parkreldis.2008.08.006

López-Azcárate, J., Tainta, M., Rodríguez-Oroz, M. C., Valencia, M., González, R., Guridi, J., et al. (2010). Coupling between beta and high-frequency activity in the human subthalamic nucleus may be a pathophysiological mechanism in Parkinson's disease. *J. Neurosci.* 30, 6667–6677. doi: 10.1523/JNEUROSCI.5459-09.2010

Ma, Z., Du, X., Wang, F., Ding, R., Li, Y., Liu, A., et al. (2019). Cortical plasticity induced by anodal transcranial pulsed current stimulation investigated by combining two-photon imaging and electrophysiological recording. *Front. Cell Neurosci.* 13:400. doi: 10.3389/fncel.2019.00400

Maas, R. P. P. W. M., Helmich, R. C. G., and van de Warrenburg, B. P. C. (2020). The role of the cerebellum in degenerative ataxias and essential tremor: insights from noninvasive modulation of cerebellar activity. *Mov. Disord.* 35, 215–227. doi: 10.1002/mds.27919

Maas, R. P. P. W. M., Toni, I., Doorduin, J., Klockgether, T., Schutter, D. J. L. G., and van de Warrenburg, B. P. C. (2019). Cerebellar transcranial direct current stimulation in spinocerebellar ataxia type 3 (SCA3-tDCS): rationale and protocol of a randomized, double-blind, sham-controlled study. *BMC Neurol.* 19:149. doi: 10.1186/s12883-019-1379-2

Madden, D. L., Sale, M. V., O'Sullivan, J., and Robinson, G. A. (2019). Improved language production with transcranial direct current stimulation in progressive supranuclear palsy. *Neuropsychologia* 127, 148–157. doi: 10.1016/j.neuropsychologia.2019.02.022

Maidan, I., Nieuwhof, F., Bernad-Elazari, H., Reelick, M. F., Bloem, B. R., Giladi, N., et al. (2016). The role of the frontal lobe in complex walking among patients with Parkinson's disease and healthy older adults: an fNIRS study. *Neurorehabil. Neural Repair.* 30, 963–971. doi: 10.1177/1545968316650426

Mak, M., and Yu, L. (2014). Effects of transcranial direct current stimulation on dual-task gait performance in patients with Parkinson's disease. *Clin. Neurophysiol.* 125:S127.

Manenti, R., Bianchi, M., Cosseddu, M., Brambilla, M., Rizzetti, C., Padovani, A., et al. (2015). Anodal transcranial direct current stimulation of parietal cortex enhances action naming in Corticobasal Syndrome. *Front. Aging Neurosci.* 7:49. doi: 10.3389/fnagi.2015.00049

Manenti, R., Brambilla, M., Benussi, A., Rosini, S., Cobelli, C., Ferrari, C., et al. (2016). Mild cognitive impairment in Parkinson's disease is improved by transcranial direct current stimulation combined with physical therapy. *Mov. Disord.* 31, 715–724. doi: 10.1002/mds.26561

Manenti, R., Brambilla, M., Rosini, S., Orizio, I., Ferrari, C., Borroni, B., et al. (2014). Time up and go task performance improves after transcranial direct current stimulation in patient affected by Parkinson's disease. *Neurosci. Lett.* 580, 74–77. doi: 10.1016/j.neulet.2014.07.052

Marceglia, S., Mrakic-Sposta, S., Fumagalli, M., Ferrucci, R., Mameli, F., Vergari, M., et al. (2017). Cathodal Transcranial direct current stimulation improves focal hand dystonia in musicians: a two-case study. *Front. Neurosci.* 11:508. doi: 10.3389/fnins.2017.00508

McCambridge, A. B., and Bradnam, L. V. (2018). Cerebellar stimulation for adults with cervical dystonia: a tDCS study. *Clin. Neurophysiol.* 129:e165. doi: 10.1016/j.clinph.2018.04.423

Mehta, A. R., Brittain, J. S., and Brown, P. (2014). The selective influence of rhythmic cortical versus cerebellar transcranial stimulation on human physiological tremor. *J. Neurosci.* 34, 7501–7508. doi: 10.1523/JNEUROSCI.0510-14.2014

Mehta, A. R., Pogosyan, A., Brown, P., and Brittain, J. S. (2015). Montage matters: the influence of transcranial alternating current stimulation on human physiological tremor. *Brain Stimul.* 8, 260–268. doi: 10.1016/j.brs.2014.11.003

Moret, B., Donato, R., Nucci, M., Cona, G., and Campana, G. (2019). Transcranial random noise stimulation (tRNS): a wide range of frequencies is needed for increasing cortical excitability. *Sci. Rep.* 9:15150. doi: 10.1038/s41598-019-51553-7

Nitsche, M. A., Seeber, A., Frommann, K., Klein, C. C., Rochford, C., Nitsche, M. S., et al. (2005). Modulating parameters of excitability during and after transcranial direct current stimulation of the human motor cortex. *J. Physiol.* 568, 291–303. doi: 10.1113/jphysiol.2005.092429

Ozturk, M., Abosch, A., Francis, D., Wu, J., Jimenez-Shahed, J., and Ince, N. F. (2020). Distinct subthalamic coupling in the ON state describes motor performance in Parkinson's disease. *Mov. Disord.* 35, 91–100. doi: 10.1002/mds.27800

Pereira, J. B., Junqué, C., Bartrés-Faz, D., Martí, M. J., Sala-Llonch, R., Compta, Y., et al. (2013). Modulation of verbal fluency networks by transcranial direct current stimulation (tDCS) in Parkinson's disease. *Brain Stimul.* 6, 16–24. doi: 10.1016/j.brs.2012.01.006

Pilloni, G., Shaw, M., Feinberg, C., Clayton, A., Palmeri, M., Datta, A., et al. (2019). Long term at-home treatment with transcranial direct current stimulation (tDCS) improves symptoms of cerebellar ataxia: a case report. *J. Neuroeng. Rehabil.* 16:41. doi: 10.1186/s12984-019-0514-z

Ponsen, M. M., Daffertshofer, A., van den Heuvel, E., Wolters, E. C., Beek, P. J., and Berendse, H. W. (2006). Bimanual coordination dysfunction in early, untreated Parkinson's disease. *Parkinson Relat. Disord.* 12, 246–252. doi: 10.1016/j.parkreldis.2006.01.006

Putzolu, M., Ogliastro, C., Lagravinese, G., Bonassi, G., Trompetto, C., Marchese, R., et al. (2019). Investigating the effects of transcranial direct current stimulation on obstacle negotiation performance in Parkinson disease with freezing of gait: a pilot study. *Brain Stimul.* 12, 1583–1585. doi: 10.1016/j.brs.2019.07.006

Quartarone, A., Rizzo, V., Bagnato, S., Morgante, F., Sant'Angelo, A., Romano, M., et al. (2005). Homeostatic-like plasticity of the primary motor hand area is impaired in focal hand dystonia. *Brain* 128(Pt 8), 1943–1950. doi: 10.1093/brain/awh527

Rosset-Llobet, J., Fàbregas-Molas, S., and Pascual-Leone, Á (2015). Effect of transcranial direct current stimulation on neurorehabilitation of task-specific dystonia: a double-blind, randomized clinical trial. *Med. Probl. Perform. Art.* 30, 178–184. doi: 10.21091/mppa.2015.3033

Sadnicka, A., Hamada, M., Bhatia, K. P., Rothwell, J. C., and Edwards, M. J. (2014). Cerebellar stimulation fails to modulate motor cortex plasticity in writing dystonia. *Mov. Disord.* 29, 1304–1307. doi: 10.1002/mds.25881

Salimpour, Y., Mari, Z. K., and Shadmehr, R. (2015). Altering effort costs in Parkinson's disease with noninvasive cortical stimulation. *J. Neurosci.* 35, 12287–12302. doi: 10.1523/JNEUROSCI.1827-15.2015

Schabrun, S. M., Lamont, R. M., and Brauer, S. G. (2016). Transcranial direct current stimulation to enhance dual-task gait training in Parkinson's disease: a pilot RCT. *PLoS One* 11:e0158497. doi: 10.1371/journal.pone.0158497

Schirinzi, T., Sciamanna, G., Mercuri, N. B., and Pisani, A. (2018). Dystonia as a network disorder: a concept in evolution. *Curr. Opin. Neurol.* 31, 498–503. doi: 10.1097/WCO.0000000000000580

Siebner, H. R., Mentschel, C., Auer, C., and Conrad, B. (1999). Repetitive transcranial magnetic stimulation has a beneficial effect on bradykinesia in Parkinson's disease. *Neuroreport* 10, 589–594. doi: 10.1097/00001756-199902250-00027

Stephani, C., Nitsche, M. A., Sommer, M., and Paulus, W. (2011). Impairment of motor cortex plasticity in Parkinson's disease, as revealed by theta-burst-transcranial magnetic stimulation and transcranial random noise stimulation. *Parkinsonism Relat. Disord.* 17, 297–298. doi: 10.1016/j.parkreldis.2011.01.006

Stuart, S., Vitorio, R., Morris, R., Martini, D. N., Fino, P. C., and Mancini, M. (2018). Cortical activity during walking and balance tasks in older adults and in people with Parkinson's disease: a structured review. *Maturitas* 113, 53–72. doi: 10.1016/j.maturitas.2018.04.011

Summers, R., Chen, M., MacKinnon, C., Kimberley, T. (2018). Effect of cerebellar transcranial direct current stimulation in cervical dystonia. *Brain Stimulat.* 12, 463–464. doi: 10.1016/j.brs.2018.12.508

Swank, C., Mehta, J., and Criminger, C. (2016). Transcranial direct current stimulation lessens dual task cost in people with Parkinson's disease. *Neurosci. Lett.* 626, 1–5. doi: 10.1016/j.neulet.2016.05.010

Teo, W. P., Hendy, A. M., Goodwill, A. M., and Loftus, A. M. (2017). Transcranial alternating current stimulation: a potential modulator for pathological oscillations in Parkinson's disease? *Front. Neurol.* 8:185. doi: 10.3389/fneur.2017.00185

Terney, D., Chaieb, L., Moliadze, V., Antal, A., and Paulus, W. (2008). Increasing human brain excitability by transcranial high-frequency random noise stimulation. *J. Neurosci.* 28, 14147–14155. doi: 10.1523/JNEUROSCI.4248-08.2008

Valentino, F., Cosentino, G., Brighina, F., Pozzi, N. G., Sandrini, G., Fierro, B., et al. (2014). Transcranial direct current stimulation for treatment of freezing of gait: a cross-over study. *Mov. Disord.* 29, 1064–1069. doi: 10.1002/mds.25897

Valero-Cabré, S. C. II, Godard, J., Fracchia, O., Dubois, B., Levy, R., Truong, D. Q., et al. (2019). Language boosting by transcranial stimulation in progressive supranuclear palsy. *Neurology* 93, e537–e547. doi: 10.1212/wnl.0000000000007893

Vanbellingen, T., Kersten, B., Bellion, M., Temperli, P., Baronti, F., Müri, R., et al. (2011). Impaired finger dexterity in Parkinson's disease is associated with praxis function. *Brain Cogn.* 77, 48–52. doi: 10.1016/j.bandc.2011.06.003

Vavla, M., Gabriella, P., Vasco, M., Jimmy, C., Jennifer, P., and Andrea, M. (2019). Combining transcranial direct current stimulation and intensive physiotherapy in patients with Friedreich's ataxia: a pilot study. *Acta Sci. Neurol.* 2.1, 03–10.

Verheyden, G., Purdey, J., Burnett, M., Cole, J., and Ashburn, A. (2013). Immediate effect of transcranial direct current stimulation on postural stability and functional mobility in Parkinson's disease. *Mov. Disord.* 28, 2040–2041. doi: 10.1002/mds.25640

Weinberger, M., and Dostrovsky, J. O. (2011). A basis for the pathological oscillations in basal ganglia: the crucial role of dopamine. *Neuroreport* 22, 151–156. doi: 10.1097/WNR.0b013e328342ba50

Wu, Y. T., Huang, S. R., Jao, C. W., Soong, B. W., Lirng, J. F., Wu, H. M., et al. (2018). Impaired efficiency and resilience of structural network in Spinocerebellar Ataxia type 3. *Front. Neurosci.* 12:935. doi: 10.3389/fnins.2018.00935

Yamamoto, Y., Struzik, Z. R., Soma, R., Ohashi, K., and Kwak, S. (2005). Noisy vestibular stimulation improves autonomic and motor responsiveness in central neurodegenerative disorders. *Ann. Neurol.* 58, 175–181. doi: 10.1002/ana.20574

Yoo, H. S., Choi, Y. H., Chung, S. J., Lee, Y. H., Ye, B. S., Sohn, Y. H., et al. (2019). Cerebellar connectivity in Parkinson's disease with levodopa-induced dyskinesia. *Ann. Clin. Transl. Neurol.* 6, 2251–2260. doi: 10.1002/acn3.50918

Yotnuengnit, P., Bhidayasiri, R., Donkhan, R., Chaluaysrimuang, J., and Piravej, K. (2018). Effects of Transcranial direct current stimulation plus physical therapy on gait in patients with Parkinson disease: a randomized controlled trial. *Am. J. Phys. Med. Rehabil.* 97, 7–15. doi: 10.1097/PHM.0000000000000783

Zaghi, S., de Freitas Rezende, L., de Oliveira, L. M., El-Nazer, R., Menning, S., Tadini, L., et al. (2010). Inhibition of motor cortex excitability with 15Hz transcranial alternating current stimulation (tACS). *Neurosci. Lett.* 479, 211–214. doi: 10.1016/j.neulet.2010.05.060

Conflict of Interest: The authors declare that the research was conducted in the absence of any commercial or financial relationships that could be construed as a potential conflict of interest.

Advantages of publishing in Frontiers

OPEN ACCESS
Articles are free to read for greatest visibility and readership

FAST PUBLICATION
Around 90 days from submission to decision

HIGH QUALITY PEER-REVIEW
Rigorous, collaborative, and constructive peer-review

TRANSPARENT PEER-REVIEW
Editors and reviewers acknowledged by name on published articles

Frontiers
Avenue du Tribunal-Fédéral 34
1005 Lausanne | Switzerland

Visit us: www.frontiersin.org
Contact us: frontiersin.org/about/contact

REPRODUCIBILITY OF RESEARCH
Support open data and methods to enhance research reproducibility

DIGITAL PUBLISHING
Articles designed for optimal readership across devices

FOLLOW US
@frontiersin

IMPACT METRICS
Advanced article metrics track visibility across digital media

EXTENSIVE PROMOTION
Marketing and promotion of impactful research

LOOP RESEARCH NETWORK
Our network increases your article's readership